FLUID MECHANICS

FOR CIVIL ENGINEERS

Bruce Hunt
Department of Civil Engineering
University Of Canterbury
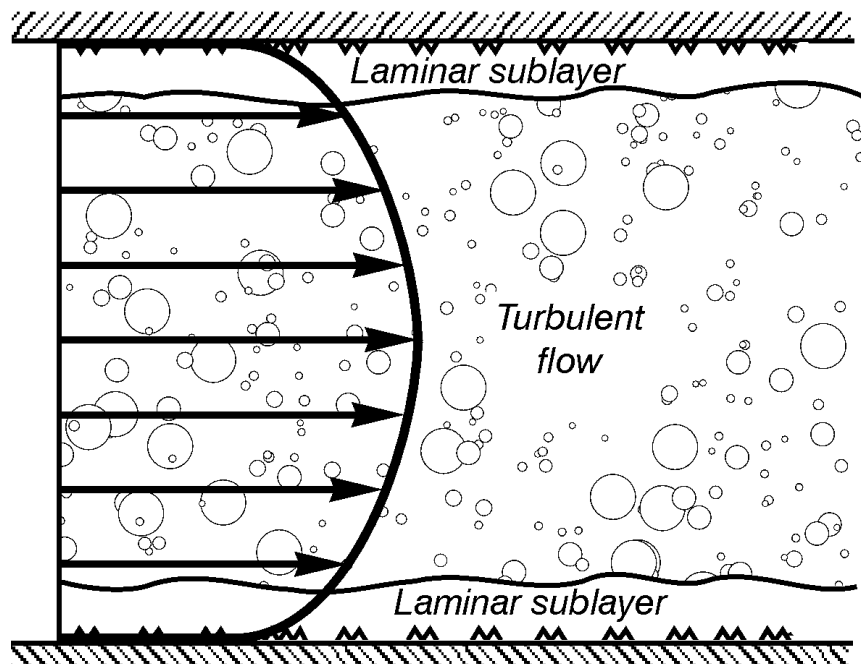**Christchurch, New Zealand**

Table of Contents

Preface

Fluid mechanics is a traditional cornerstone in the education of civil engineers. As numerous books on this subject suggest, it is possible to introduce fluid mechanics to students in many ways. This text is an outgrowth of lectures I have given to civil engineering students at the University of Canterbury during the past 24 years. It contains a blend of what most teachers would call basic fluid mechanics and applied hydraulics.

Chapter 1 contains an introduction to fluid and flow properties together with a review of vector calculus in preparation for chapter 2, which contains a derivation of the governing equations of fluid motion. Chapter 3 covers the usual topics in fluid statics – pressure distributions, forces on plane and curved surfaces, stability of floating bodies and rigid body acceleration of fluids. Chapter 4 introduces the use of control volume equations for one-dimensional flow calculations. Chapter 5 gives an overview for the problem of solving partial differential equations for velocity and pressure distributions throughout a moving fluid and chapters 6–9 fill in the details of carrying out these calculations for irrotational flows, laminar and turbulent flows, boundary-layer flows, secondary flows and flows requiring the calculation of lift and drag forces. Chapter 10, which introduces dimensional analysis and model similitude, requires a solid grasp of chapters 1–9 if students are to understand and use effectively this very important tool for experimental work. Chapters 11–14 cover some traditionally important application areas in hydraulic engineering. Chapter 11 covers steady pipe flow, chapter 12 covers steady open channel flow, chapter 13 introduces the method of characteristics for solving waterhammer problems in unsteady pipe flow, and chapter 14 builds upon material in chapter 13 by using characteristics to attack the more difficult problem of unsteady flow in open channels. Throughout, I have tried to use mathematics, experimental evidence and worked examples to describe and explain the elements of fluid motion in some of the many different contexts encountered by civil engineers.

The study of fluid mechanics requires a subtle blend of mathematics and physics that many students find difficult to master. Classes at Canterbury tend to be large and sometimes have as many as a hundred or more students. Mathematical skills among these students vary greatly, from the very able to mediocre to less than competent. As any teacher knows, this mixture of student backgrounds and skills presents a formidable challenge if students with both stronger and weaker backgrounds are all to obtain something of value from a course. My admittedly less than perfect approach to this dilemma has been to emphasize both physics and problem solving techniques. For this reason, mathematical development of the governing equations, which is started in Chapter 1 and completed in Chapter 2, is covered at the beginning of our first course without requiring the deeper understanding that would be expected of more advanced students.

A companion volume containing a set of carefully chosen homework problems, together with corresponding solutions, is an important part of courses taught from this text. Most students can learn problem solving skills only by solving problems themselves, and I have a strongly held belief that this practice is greatly helped when students have access to problem solutions for checking their work and for obtaining help at difficult points in the solution process. A series of laboratory experiments is also helpful. However, courses at Canterbury do not have time to include a large amount of experimental work. For this reason, I usually supplement material in this text with several of Hunter Rouse's beautifully made fluid-mechanics films.

Chapter 1

Introduction

A fluid is usually defined as a material in which movement occurs continuously under the application of a tangential shear stress. A simple example is shown in Figure 1.1, in which a timber board floats on a reservoir of water.

Figure 1.1 Use of a floating board to apply shear stress to a reservoir surface.

If a force, F, is applied to one end of the board, then the board transmits a tangential shear stress, τ, to the reservoir surface. The board and the water beneath will continue to move as long as F and τ are nonzero, which means that water satisfies the definition of a fluid. Air is another fluid that is commonly encountered in civil engineering applications, but many liquids and gases are obviously included in this definition as well.

You are studying fluid mechanics because fluids are an important part of many problems that a civil engineer considers. Examples include water resource engineering, in which water must be delivered to consumers and disposed of after use, water power engineering, in which water is used to generate electric power, flood control and drainage, in which flooding and excess water are controlled to protect lives and property, structural engineering, in which wind and water create forces on structures, and environmental engineering, in which an understanding of fluid motion is a prerequisite for the control and solution of water and air pollution problems.

Any serious study of fluid motion uses mathematics to model the fluid. Invariably there are numerous approximations that are made in this process. One of the most fundamental of these approximations is the assumption of a continuum. We will let fluid and flow properties such as mass density, pressure and velocity be continuous functions of the spacial coordinates. This makes it possible for us to differentiate and integrate these functions. However an actual fluid is composed of discrete molecules and, therefore, is not a continuum. Thus, we can only expect good agreement between theory and experiment when the experiment has linear dimensions that are very large compared to the spacing between molecules. In upper portions of the atmosphere, where air molecules are relatively far apart, this approximation can place serious limitations on the use of mathematical models. Another example, more relevant to civil engineering, concerns the use of rain gauges for measuring the depth of rain falling on a catchment. A gauge can give an accurate estimate only if its diameter is very large compared to the horizontal spacing between rain droplets. Furthermore, at a much larger scale, the spacing between rain gauges must be small compared to the spacing between rain clouds. Fortunately, the assumption of a continuum is not usually a serious limitation in most civil engineering problems.

Fluid Properties

The mass density, ρ, is the fluid mass per unit volume and has units of kg/m^3. Mass density is a function of both temperature and the particular fluid under consideration. Most applications considered herein will assume that ρ is constant. However, incompressible fluid motion can occur in which ρ changes throughout a flow. For example, in a problem involving both fresh and salt water, a fluid element will retain the same constant value for ρ as it moves with the flow. However, different fluid elements with different proportions of fresh and salt water will have different values for ρ, and ρ will not have the same constant value throughout the flow. Values of ρ for some different fluids and temperatures are given in the appendix.

The dynamic viscosity, μ, has units of $kg/(m-s) = N - s/m^{2\,*}$ and is the constant of proportionality between a shear stress and a rate of deformation. In a Newtonian fluid, μ is a function only of the temperature and the particular fluid under consideration. The problem of relating viscous stresses to rates of fluid deformation is relatively difficult, and this is one of the few places where we will substitute a bit of hand waving for mathematical and physical logic. If the fluid velocity, u, depends only upon a single coordinate, y, measured normal to u, as shown in Figure 1.2, then the shear stress acting on a plane normal to the direction of y is given by

$$\tau = \mu \frac{du}{dy} \tag{1.1}$$

Figure 1.2 A velocity field in which u changes only with the coordinate measured normal to the direction of u.
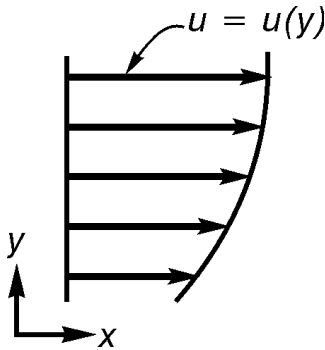
Later in the course it will be shown that the velocity in the water beneath the board in Figure 1.1 varies linearly from a value of zero on the reservoir bottom to the board velocity where the water is in contact with the board. Together with Equation (1.1) these considerations show that the shear stress, τ, in the fluid (and on the board surface) is a constant that is directly proportional to the board velocity and inversely proportional to the reservoir depth. The constant of proportionality is μ. In many problems it is more convenient to use the definition of kinematic viscosity

$$\nu = \mu/\rho \tag{1.2}$$

in which the kinematic viscosity, ν, has units of m^2/s. Values of μ and ν for some different fluids and temperatures are given in the appendix.

---

*   A Newton, N, is a derived unit that is related to a kg through Newton's second law, $F = ma$. Thus, $N = kg - m/s^2$.

Surface tension, σ, has units of $N/m = kg/s^2$ and is a force per unit arc length created on an interface between two immiscible fluids as a result of molecular attraction. For example, at an air-water interface the greater mass of water molecules causes water molecules near and on the interface to be attracted toward each other with greater forces than the forces of attraction between water and air molecules. The result is that any curved portion of the interface acts as though it is covered with a thin membrane that has a tensile stress σ. Surface tension allows a needle to be floated on a free surface of water or an insect to land on a water surface without getting wet.
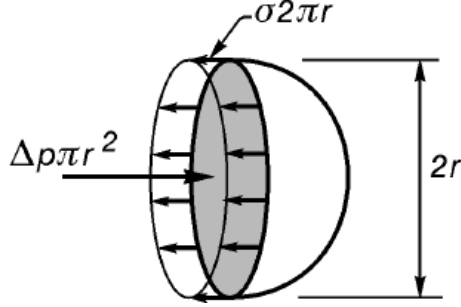
Figure 1.3 Horizontal pressure and surface tension force acting on half of a spherical rain droplet.

For an example, if we equate horizontal pressure and surface tension forces on half of the spherical rain droplet shown in Figure 1.3, we obtain

$$\Delta p \, \pi r^2 = \sigma 2\pi r \tag{1.3}$$

in which Δp = pressure difference across the interface. This gives the following result for the pressure difference:

$$\Delta p = \frac{2\sigma}{r} \tag{1.4}$$

If instead we consider an interface with the shape of a half circular cylinder, which would occur under a needle floating on a free surface or at a meniscus that forms when two parallel plates of glass are inserted into a reservoir of liquid, the corresponding force balance becomes

$$\Delta p \, 2r = 2\sigma \tag{1.5}$$

which gives a pressure difference of

$$\Delta p = \frac{\sigma}{r} \tag{1.6}$$

A more general relationship between Δp and σ is given by

$$\Delta p = \sigma \left(\frac{1}{r_1} + \frac{1}{r_2} \right) \tag{1.7}$$

in which r_1 and r_2 are the two principal radii of curvature of the interface. Thus, (1.4) has $r_1 = r_2 = r$ while (1.6) has $r_1 = r$ and $r_2 = \infty$. From these examples we conclude that (a) pressure differences increase as the interface radius of curvature decreases and (b) pressures are always greatest on the concave side of the curved interface. Thus, since water in a capillary tube has the concave side facing upward, water pressures beneath the meniscus are below atmospheric pressure. Values of σ for some different liquids are given in the appendix.

Finally, although it is not a fluid property, we will mention the "gravitational constant" or "gravitational acceleration", g, which has units of m/s². Both these terms are misnomers because

g is not a constant and it is a particle acceleration only if gravitational attraction is the sole force acting on the particle. (Add a drag force, for example, and the particle acceleration is no longer g.) The definition of g states that it is the proportionality factor between the mass, M, and weight, W, of an object in the earth's gravitational field.

$$W = Mg \tag{1.8}$$

Since the mass remains constant and W decreases as distance between the object and the centre of the earth increases, we see from (1.8) that g must also decrease with increasing distance from the earth's centre. At sea level g is given approximately by

$$g = 9.81 \ \text{m/s}^2 \tag{1.9}$$

which is sufficiently accurate for most civil engineering applications.

Flow Properties

Pressure, p, is a normal stress or force per unit area. If fluid is at rest or moves as a rigid body with no relative motion between fluid particles, then pressure is the only normal stress that exists in the fluid. If fluid particles move relative to each other, then the total normal stress is the sum of the pressure and normal viscous stresses. In this case pressure is the normal stress that would exist in the flow if the fluid had a zero viscosity. If the fluid motion is incompressible, the pressure is also the average value of the normal stresses on the three coordinate planes.

Pressure has units of $N/m^2 = Pa$, and in fluid mechanics a positive pressure is defined to be a compressive stress. This sign convention is opposite to the one used in solid mechanics, where a tensile stress is defined to be positive. The reason for this convention is that most fluid pressures are compressive. However it is important to realize that tensile pressures can and do occur in fluids. For example, tensile stresses occur in a water column within a small diameter capillary tube as a result of surface tension. There is, however, a limit to the magnitude of negative pressure that a liquid can support without vaporizing. The vaporization pressure of a given liquid depends upon temperature, a fact that becomes apparent when it is realized that water vaporizes at atmospheric pressure when its temperature is raised to the boiling point.

Pressure are always measured relative to some fixed datum. For example, absolute pressures are measured relative to the lowest pressure that can exist in a gas, which is the pressure in a perfect vacuum. Gage pressures are measured relative to atmospheric pressure at the location under consideration, a process which is implemented by setting atmospheric pressure equal to zero. Civil engineering problems almost always deal with pressure differences. In these cases, since adding or subtracting the same constant value to pressures does not change a pressure difference, the particular reference value that is used for pressure becomes immaterial. For this reason we will almost always use gage pressures.[*]

---

[*]   One exception occurs in the appendix, where water vapour pressures are given in kPa absolute. They could, however, be referenced to atmospheric pressure at sea level simply by subtracting from each pressure the vapour pressure for a temperature of $100\,°C$ (101.3 kPa).

If no shear stresses occur in a fluid, either because the fluid has no relative motion between particles or because the viscosity is zero, then it is a simple exercise to show that the normal stress acting on a surface does not change as the orientation of the surface changes. Consider, for example, an application of Newton's second law to the two-dimensional triangular element of fluid shown in Figure 1.4, in which the normal stresses σ_x, σ_y and σ_n have all been assumed to have different magnitudes. Thus $\Sigma F_x = m a_x$ gives

$$\sigma_x \Delta y \;-\; \sigma_n \sqrt{\Delta x^2 + \Delta y^2} \, \cos\theta \;=\; \frac{\rho}{2} \, \Delta x \Delta y \, a_x \tag{1.10}$$

in which a_x = acceleration component in the x direction. Since the triangle geometry gives

$$\cos\theta \;=\; \frac{\Delta y}{\sqrt{\Delta x^2 + \Delta y^2}} \tag{1.11}$$

we obtain after inserting (1.11) in (1.10) for $\cos\theta$ and dividing by Δy

$$\sigma_x \;-\; \sigma_n \;=\; \frac{\rho}{2} \, \Delta x \, a_x \tag{1.12}$$
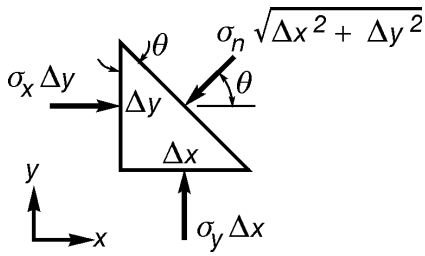
Thus, letting $\Delta x \to 0$ gives

$$\sigma_x \;=\; \sigma_n \tag{1.13}$$

A similar application of Newton's law in the y direction gives

Figure 1.4 Normal stress forces acting on a two-dimensional triangular fluid element.

$$\sigma_y \;=\; \sigma_n \tag{1.14}$$

Therefore, if no shear stresses occur, the normal stress acting on a surface does not change as the surface orientation changes. This result is not true for a viscous fluid motion that has finite tangential stresses. In this case, as stated previously, the pressure in an incompressible fluid equals the average value of the normal stresses on the three coordinate planes.
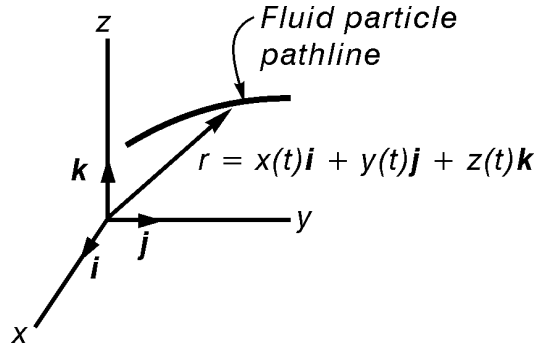
Figure 1.5 The position vector, **r**, and pathline of a fluid particle.

Let $t = $ time and $\mathbf{r}(t) = x(t)\mathbf{i} + y(t)\mathbf{j} + x(t)\mathbf{k}$ be the position vector of a moving fluid particle, as shown in Figure 1.5. Then the particle velocity is

$$\mathbf{V} = \frac{d\mathbf{r}}{dt} = \frac{dx}{dt}\mathbf{i} + \frac{dy}{dt}\mathbf{j} + \frac{dz}{dt}\mathbf{k} \tag{1.15}$$

If we define the velocity components to be

$$\mathbf{V} = u\mathbf{i} + \mathrm{v}\mathbf{j} + w\mathbf{k} \tag{1.16}$$

then (1.15) and (1.16) give

$$u = \frac{dx}{dt}$$

$$\mathrm{v} = \frac{dy}{dt} \tag{1.17 a, b, c}$$

$$w = \frac{dz}{dt}$$

If $\mathbf{e}_t = $ unit tangent to the particle pathline, then the geometry shown in Figure 1.6 allows us to calculate

$$\mathbf{V} = \frac{d\mathbf{r}}{dt} = \frac{\mathbf{r}(t + \Delta t) - \mathbf{r}(t)}{\Delta t} = \frac{\Delta s\, \mathbf{e}_t}{\Delta t} = V\mathbf{e}_t \tag{1.18}$$

in which $s = $ arc length along the pathline and $V = ds/dt = |\mathbf{V}| = $ particle speed. Thus, the velocity vector is tangent to the pathline as the particle moves through space.
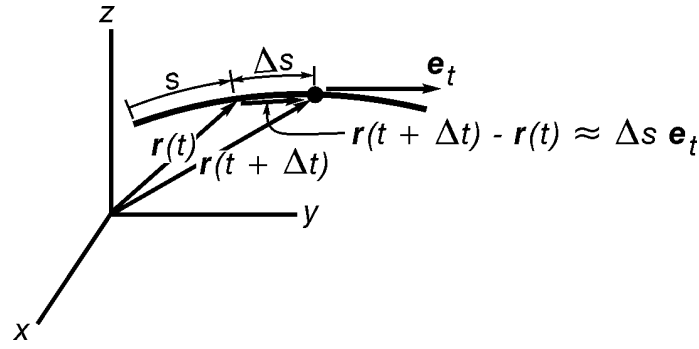
Figure 1.6 Relationship between the position vector,
arc length and unit tangent along a pathline.

It is frequently helpful to view, at a particular value of t, the velocity vector field for a collection of fluid particles, as shown in Figure 1.7.
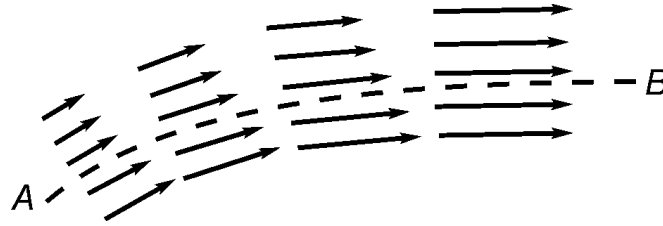
Figure 1.7 The velocity field for a collection of fluid particles at one instant in time.

In Figure 1.7 the lengths of the directed line segments are proportional to $|V| = V$, and the line segments are tangent to the pathlines of each fluid particle at the instant shown. A streamline is a continuous curved line that, at each point, is tangent to the velocity vector V at a fixed value of t. The dashed line AB is a streamline, and, if dr = incremental displacement vector along AB, then

$$V = \lambda \, dr \tag{1.19}$$

in which $dr = dx \, i + dy \, j + dz \, k$ and λ is the scalar proportionality factor between $|V|$ and $|dr|$. [Multiplying the vector dr by the scalar λ does not change the direction of dr, and (1.19) merely requires that V and dr have the same direction. Thus, λ will generally be a function of position along the streamline.] Equating corresponding vector components in (1.19) gives a set of differential equations that can be integrated to calculate streamlines.

$$\frac{dx}{u} = \frac{dy}{v} = \frac{dz}{w} \quad \left(= \frac{1}{\lambda} \right) \tag{1.20}$$

There is no reason to calculate the parameter λ in applications of (1.20). Time, t, is treated as a constant in the integrations.

Steady flow is flow in which the entire vector velocity field does not change with time. Then the streamline pattern will not change with time, and the pathline of any fluid particle coincides with the streamline passing through the particle. In other words, streamlines and pathlines coincide in steady flow. This will not be true for unsteady flow.

The acceleration of a fluid particle is the first derivative of the velocity vector.

$$\boldsymbol{a} = \frac{d\boldsymbol{V}}{dt} \tag{1.21}$$

When $\boldsymbol{V}$ changes both its magnitude and direction along a curved path, it will have components both tangential and normal to the pathline. This result is easily seen by differentiating (1.18) to obtain

$$\boldsymbol{a} = \frac{dV}{dt}\boldsymbol{e}_t + V\frac{d\boldsymbol{e}_t}{dt} \tag{1.22}$$

The geometry in Figure 1.8 shows that

$$\frac{d\boldsymbol{e}_t}{dt} = \frac{\boldsymbol{e}_t(t + \Delta t) - \boldsymbol{e}_t(t)}{\Delta t} = \frac{1}{R}\frac{\Delta s}{\Delta t}\boldsymbol{e}_n = \frac{V}{R}\boldsymbol{e}_n \tag{1.23}$$

in which R = radius of curvature of the pathline and $\boldsymbol{e}_n$ = unit normal to the pathline (directed through the centre of curvature). Thus, (1.22) and (1.23) give

$$\boldsymbol{a} = \frac{dV}{dt}\boldsymbol{e}_t + \frac{V^2}{R}\boldsymbol{e}_n \tag{1.24}$$

Equation (1.24) shows that $\boldsymbol{a}$ has a tangential component with a magnitude equal to dV/dt and a normal component, V^2/R, that is directed through the centre of pathline curvature.
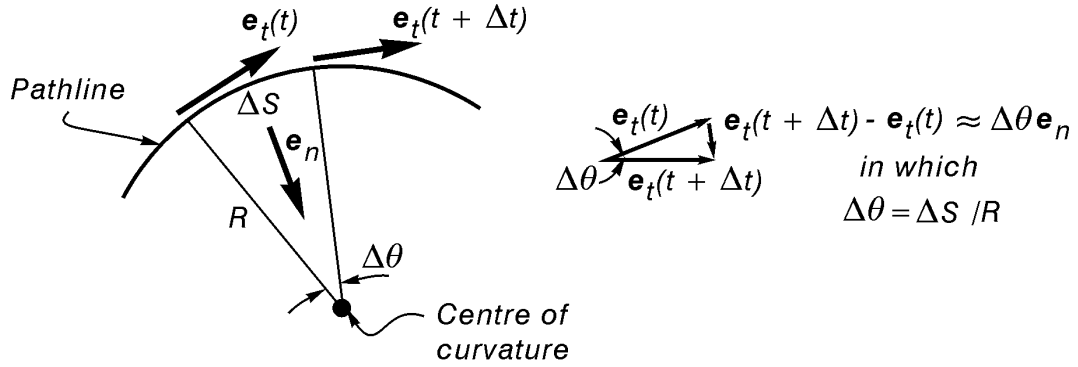
Figure 1.8 Unit tangent geometry along a pathline.

$$\left[\,\left|\,e_t(t + \Delta t)\,\right|\; =\; \left|\,e_t(t)\,\right|\; =\; 1\; \text{ so that }\; \left|\,e_t(t + \Delta t) - e_t(t)\,\right|\; \approx\; 1\,\Delta\theta\,\right]$$

Review of Vector Calculus

When a scalar or vector function depends upon only one independent variable, say t, then a derivative has the following definition:

$$\frac{dF(t)}{dt}\; =\; \frac{F(t + \Delta t) - F(t)}{\Delta t}\quad \text{as}\quad \Delta t \to 0 \tag{1.25}$$

However, in almost all fluid mechanics problems p and V depend upon more than one independent variable, say x, y, z and t. [x, y, z and t are independent if we can change the value of any one of these variables without affecting the value of the remaining variables.] In this case, the limiting process can involve only one independent variable, and the remaining independent variables are treated as constants. This process is shown by using the following notation and definition for a partial derivative:

$$\frac{\partial F(x, y, z, t)}{\partial y}\; =\; \frac{F(x, y + \Delta y, z, t) - F(x, y, z, t)}{\Delta y}\quad \text{as}\quad \Delta y \to 0 \tag{1.26}$$

In practice, this means that we calculate a partial derivative with respect to y by differentiating with respect to y while treating x, z and t as constants.

The above definition has at least two important implications. First, the order in which two partial derivatives are calculated will not matter.

$$\frac{\partial^2 F}{\partial x \partial y}\; =\; \frac{\partial^2 F}{\partial y \partial x} \tag{1.27}$$

Second, integration of a partial derivative

$$\frac{\partial F(x, y, z, t)}{\partial y} = G(x, y, z, t)$$
(1.28)

in which G is a specified or given function is carried out by integrating with respect to y while treating x, z and t as constants. However, the integration "constant", C, may be a function of the variables that are held constant in the integration process. For example, integration of (1.28) would give

$$F(x, y, z, t) = \int G(x, y, z, t)\, dy + C(x, z, t)$$
(1.29)

in which integration of the known function G is carried out by holding x, z and t constant, and $C(x, z, t)$ is an unknown function that must be determined from additional equations.

There is a very useful definition of a differential operator known as *del*:

$$\nabla = i\, \frac{\partial}{\partial x} + j\, \frac{\partial}{\partial y} + k\, \frac{\partial}{\partial z}$$
(1.30)

Despite the notation, *del* (∇) is not a vector because it fails to satisfy all of the rules for vector algebra. Thus, operations such as dot and cross products cannot be derived from (1.30) but must be defined for each case.

The operation known as the gradient is defined as

$$\nabla \phi = i\, \frac{\partial \phi}{\partial x} + j\, \frac{\partial \phi}{\partial y} + k\, \frac{\partial \phi}{\partial z}$$
(1.31)

in which ϕ is any ***scalar function***. The gradient has several very useful properties that are easily proved with use of one form of a very general theorem known as the ***divergence theorem***

$$\int_{\forall} \nabla \phi \, d\forall = \int_{S} \phi\, e_n \, dS$$
(1.32)

in which $\forall$ is a volume enclosed by the surface S with an outward normal e_n.
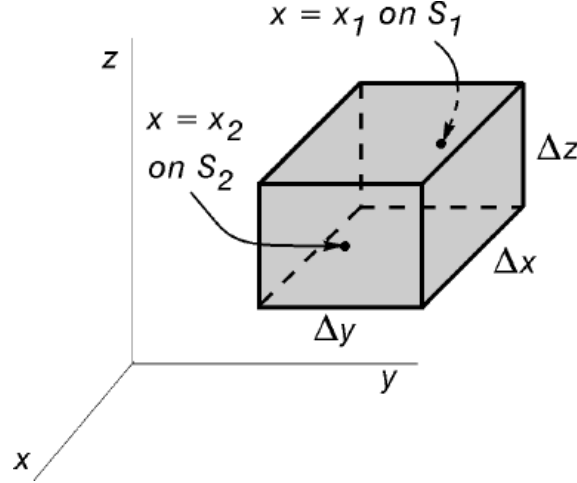
Figure 1.9 Sketch used for derivation of Equation (1.32).

A derivation of (1.32) is easily carried out for the rectangular prism shown in Figure 1.9.

$$\int_{\forall} i \frac{\partial \phi}{\partial x} \, d\forall \;=\; \int\int i \int_{x_1}^{x_2} \frac{\partial \phi}{\partial x} \, dx \, dy \, dz \;=\; \int\int_{S_2} i \, \phi\left(x_2, y, z\right) dy \, dz$$
$$-\; \int\int_{S_1} i \, \phi\left(x_1, y, z\right) dy \, dz \tag{1.33}$$

Since i is the outward normal on S_2 and $-i$ on S_1, (1.33) becomes

$$\int_{\forall} i \frac{\partial \phi}{\partial x} \, d\forall \;=\; \int_{S_2} \phi e_n \, dS \;+\; \int_{S_1} \phi e_n \, dS \tag{1.34}$$

Similar results are obtained for the components of (1.31) in the j and k directions, and adding the three resulting equations together gives

$$\int_{\forall} \nabla \phi \, d\forall \;=\; \sum_{i=1}^{6} \int_{S_i} \phi e_n \, dS \;=\; \int_{S} \phi e_n \, dS \tag{1.35}$$

in which S is the sum of the six plane surfaces that bound $\forall$. Finally, if a more general shape for $\forall$ is subdivided into many small rectangular prisms, and if the equations for each prism are added together, then (1.32) results in which S is the external boundary of $\forall$. (Contributions from the adjacent internal surfaces S_i and S_j cancel in the sum since $\phi_i = \phi_j$ but $e_{n_i} = -e_{n_j}$.)

One easy application of (1.32) is the calculation of the pressure force, F_p, on a tiny fluid element. Since p = normal stress per unit area and is positive for compression, we calculate

$$F_p \;=\; -\int_{S} p \, e_n \, dS \tag{1.36}$$

However, use of (1.32) with p substituted for ϕ gives

$$\boldsymbol{F}_p = -\int_\forall \nabla p \, d\forall \approx -\forall \nabla p$$

(1.37)

Thus, $-\nabla p$ is the pressure force per unit volume acting on a tiny fluid element.
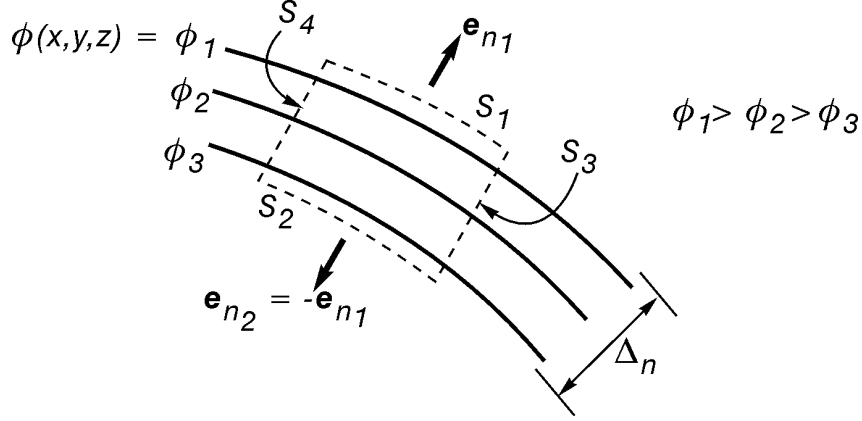
Figure 1.10 A volume chosen for an application of (1.32) in which all surfaces are either parallel or normal to surfaces of constant ϕ.

Further progress in the interpretation of $\nabla\phi$ can be made by applying (1.32) to a tiny volume whose surfaces are all either parallel or normal to surfaces of constant ϕ, as shown in Figure 1.10. Since ϕ has the same distribution on S_3 and S_4 but $\boldsymbol{e}_{n_3} = -\boldsymbol{e}_{n_4}$, contributions from S_3 and S_4 cancel and we obtain

$$\forall \nabla \phi = \phi_1 S_1 \boldsymbol{e}_{n_1} + \phi_2 S_2 \boldsymbol{e}_{n_2}$$

(1.38)

But $S_1 = S_2$ and $\boldsymbol{e}_{n_2} = -\boldsymbol{e}_{n_1}$ so that (1.38) becomes

$$\forall \nabla \phi = S_1 \boldsymbol{e}_{n_1} \left(\phi_1 - \phi_2 \right)$$

(1.39)

Since $\forall = S_1 \Delta n$ in which $\Delta n =$ thickness of $\forall$ in the direction perpendicular to surfaces of constant ϕ, division of (1.39) by $\forall$ gives

$$\nabla \phi = \boldsymbol{e}_{n_1} \frac{\phi_1 - \phi_2}{\Delta n} = \boldsymbol{e}_{n_1} \frac{d\phi}{dn}$$

(1.40)

> Thus, $\nabla\phi$ has a magnitude equal to the maximum spacial derivative of ϕ and is perpendicular to surfaces of constant ϕ in the direction of ***increasing*** ϕ.

Application of the preceding result to (1.37) shows that the pressure force per unit volume, ∇p, has a magnitude equal to the maximum spacial derivative of p. (The derivative of p in the direction normal to surfaces of constant pressure.) Furthermore, because of the negative sign on the right side of (1.37), this pressure force is perpendicular to the surfaces of constant pressure and is in the direction of ***decreasing*** pressure.

Finally, a simple application of (1.40) using the geometry shown in Figure 1.11 will be used to derive a relationship known as the directional derivative. Equation (1.40) applied to Figure 1.11 gives the result

$$\bar{\nabla}\phi = \hat{e}_n \frac{d\phi}{dn} = \hat{e}_n \frac{\phi_1 - \phi_3}{\Delta n} \tag{1.41}$$
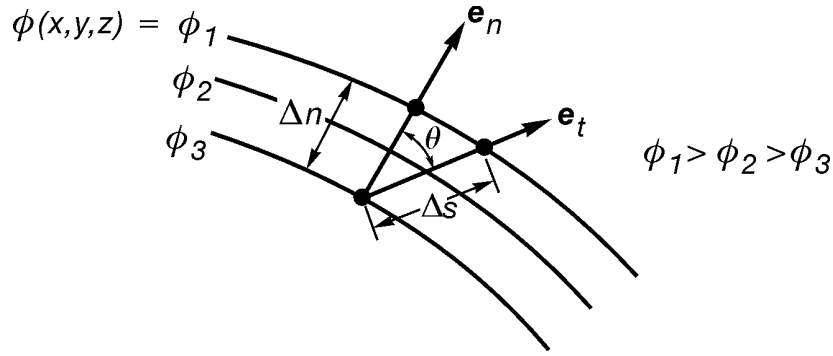
Figure 1.11 Geometry used for the calculation of the directional derivative.

If $\boldsymbol{e}_t$ is a unit vector that makes an angle θ with $\boldsymbol{e}_n$, then dotting both sides of (1.41) with $\boldsymbol{e}_t$ gives

$$\boldsymbol{e}_t \cdot \nabla\phi = \boldsymbol{e}_t \cdot \boldsymbol{e}_n \frac{\phi_1 - \phi_3}{\Delta n} = \cos\theta \frac{\phi_1 - \phi_3}{\Delta n} \tag{1.42}$$

However $\Delta n = \Delta s \cos\theta$, and (1.42) gives the result

$$\boldsymbol{e}_t \cdot \nabla\phi = \frac{\phi_1 - \phi_3}{\Delta s} = \frac{d\phi}{ds} \tag{1.43}$$

In words, (1.43) states that the derivative of ϕ with respect to arc length in any direction is calculated by dotting the gradient of ϕ with a unit vector in the given direction.

Equation (1.43) has numerous applications in fluid mechanics, and we will use it for both control volume and differential analyses. One simple application will occur in the study of irrotational flow, when we will assume that the fluid velocity can be calculated from the gradient of a velocity potential function, ϕ.

$$\boldsymbol{V} = \nabla \phi \tag{1.44}$$

Thus, (1.44) and (1.40) show that $\boldsymbol{V}$ is perpendicular to surfaces of constant ϕ and is in the direction of increasing ϕ. Since streamlines are tangent to $\boldsymbol{V}$, this means that streamlines are perpendicular to surfaces of constant ϕ, as shown in Figure 1.12. If $\boldsymbol{e}_t$ is a unit vector in any direction and s is arc length measured in the direction of $\boldsymbol{e}_t$, then (1.44) and (1.43) give

$$\boldsymbol{e}_t \cdot \boldsymbol{V} = \frac{d\phi}{ds} \tag{1.45}$$

Thus, the component of $\boldsymbol{V}$ in any direction can be calculated by taking the derivative of ϕ in that direction. If $\boldsymbol{e}_t$ is tangent to a streamline, then $d\phi/ds$ is the velocity magnitude, V. If $\boldsymbol{e}_t$ is normal to a streamline, then $d\phi/ds = 0$ along this normal curve (which gives another proof that ϕ is constant along a curve perpendicular to the streamlines). If $\boldsymbol{e}_t$ makes any angle between 0 and $\pi/2$ with a streamline, then (1.45) allows us to calculate the component of $\boldsymbol{V}$ in the direction of $\boldsymbol{e}_t$.
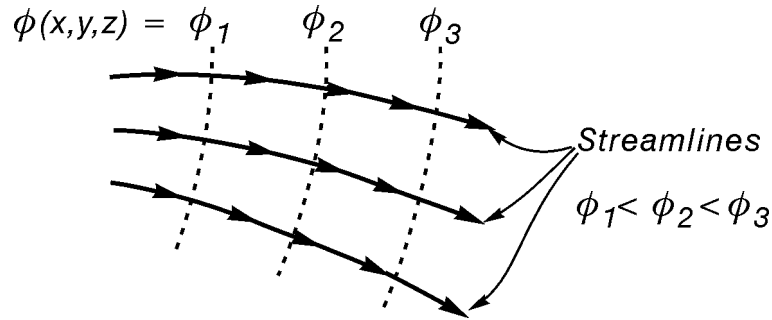
Figure 1.12 Streamlines and surfaces of constant potential for irrotational flow.

The divergence of a vector function is defined for (1.30) in a way that is analogous to the definition of the dot product of two vectors. For example, the divergence of V is

$$\nabla \cdot V = \left(i \frac{\partial}{\partial x} + j \frac{\partial}{\partial y} + k \frac{\partial}{\partial z} \right) \cdot \left(u i + v j + w k \right) = \frac{\partial u}{\partial x} + \frac{\partial v}{\partial y} + \frac{\partial w}{\partial z} \tag{1.46}$$

There is another definition we will make that allows ∇ to be dotted from the left with a vector:

$$V \cdot \nabla = \left(u i + v j + w k \right) \cdot \left(i \frac{\partial}{\partial x} + j \frac{\partial}{\partial y} + k \frac{\partial}{\partial z} \right) = u \frac{\partial}{\partial x} + v \frac{\partial}{\partial y} + w \frac{\partial}{\partial z} \tag{1.47}$$

Equations (1.46) and (1.47) are two entirely different results, and, since two vectors A and B must satisfy the law $A \cdot B = B \cdot A$, we now see that ∇ fails to satisfy one of the fundamental laws of vector algebra. Thus, as stated previously, results that hold for vector algebra cannot automatically be applied to manipulations with *del*.

The definition (1.46) can be interpreted physically by making use of a second form of the ***divergence theorem***:

$$\int_{\forall} \nabla \cdot V \, d\forall = \int_{S} V \cdot e_n \, dS \tag{1.48}$$

in which $\forall$ is a volume bounded externally by the closed surface S, e_n is the outward normal on S and V is any vector function. If V is the fluid velocity vector, then $V \cdot e_n$ gives the component of V normal to S with a sign that is positive when V is out of $\forall$ and negative when V is into $\forall$. The product of this normal velocity component with dS gives a volumetric flow rate with units of m³/s. Thus, the right side of (1.48) is the net volumetric flow rate out through S since outflows are positive and inflows negative in calculating the sum represented by the surface integral. If (1.48) is applied to a small volume, then the divergence of V is given by

$$\nabla \cdot V = \frac{1}{\forall} \int_{S} V \cdot e_n \, dS \tag{1.49}$$

Equation (1.49) shows that the divergence of V is the net volumetric outflow per unit volume through a small closed surface surrounding the point where $\nabla \cdot V$ is calculated. If the flow is incompressible, this net outflow must be zero and we obtain the "continuity" equation

$$\nabla \cdot V = \frac{\partial u}{\partial x} + \frac{\partial v}{\partial y} + \frac{\partial w}{\partial z} = 0 \tag{1.50}$$

A derivation of (1.48) can be obtained by using Figure 1.9 to obtain

$$\int_\forall \frac{\partial u}{\partial x} \, d\forall = \int\int_{x_1}^{x_2}\int \frac{\partial u}{\partial x} \, dx \, dy \, dz = \int\int_{S_2} u\left(x_2, y, z\right) dy \, dz - \int\int_{S_1} u\left(x_1, y, z\right) dy \, dz \qquad (1.51)$$

But $i \cdot e_n = 1$ on S_2 and $i \cdot e_n = -1$ on S_1 since e_n is the outward normal. Thus, (1.51) becomes

$$\int_\forall \frac{\partial u}{\partial x} \, d\forall = \int_{S_2} u\,i \cdot e_n \, dS + \int_{S_1} u\,i \cdot e_n \, dS = \int_S u\,i \cdot e_n \, dS \qquad (1.52)$$

in which use has been made of the fact that $i \cdot e_n = 0$ on every side of the prism except S_1 and S_2.

Similar results can be obtained for $\int_\forall \partial v / \partial y \, d\forall$ and $\int_\forall \partial w / \partial z \, d\forall$, and adding the resulting three equations together gives

$$\int_\forall \left(\frac{\partial u}{\partial x} + \frac{\partial v}{\partial y} + \frac{\partial w}{\partial z} \right) d\forall = \int_S \left(u\,i + v\,j + w\,k\right) \cdot e_n \, dS \qquad (1.53)$$

Equation (1.53) holds for arbitrary functions u, v and w and is clearly identical with (1.48). The extension to a more general volume is made in the same way that was outlined in the derivation of (1.32).

In analogy with a cross product of two vectors the curl of a vector is defined in the following way:

$$\nabla \times V = \begin{vmatrix} i & j & k \\ \dfrac{\partial}{\partial x} & \dfrac{\partial}{\partial y} & \dfrac{\partial}{\partial z} \\ u & v & w \end{vmatrix} = \begin{aligned} &\left(\frac{\partial w}{\partial y} - \frac{\partial v}{\partial z} \right) i - \left(\frac{\partial w}{\partial x} - \frac{\partial u}{\partial z} \right) j \\ &+ \left(\frac{\partial v}{\partial x} - \frac{\partial u}{\partial y} \right) k \end{aligned} \qquad (1.54)$$

If we let V be the fluid velocity vector, then a physical interpretation of (1.54) can be made with the use of Figure 1.13. Two line segments of length Δx and Δy are in a plane parallel to the x, y plane and have their initial locations shown with solid lines. An instant later these lines have rotated in the counterclockwise direction and have their locations shown with dashed lines. The angular velocity of the line Δx in the k direction is

$$\frac{\partial v}{\partial x} k = \frac{v_2 - v_1}{\Delta x} k = \omega_z k \qquad (1.55)$$
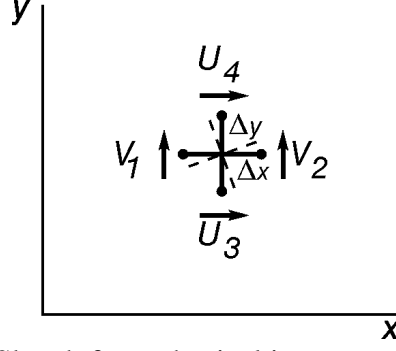
Figure 1.13 Sketch for a physical interpretation of $\nabla \times V$.

and the angular velocity of the line Δy in the k direction is

$$- \frac{\partial u}{\partial y} k \;=\; - \frac{u_4 - u_3}{\Delta y} k \;=\; \frac{u_3 - u_4}{\Delta y} k \;=\; \omega_z k \tag{1.56}$$

in which the right sides of (1.55) and (1.56) are identical if the fluid rotates as a rigid body. Thus, the k component in (1.54) becomes

$$\left(\frac{\partial v}{\partial x} - \frac{\partial u}{\partial y} \right) k \;=\; 2\, \omega_z k \tag{1.57}$$

if rigid-body rotation occurs. Similar interpretation can be made for i and j components of (1.54) to obtain

$$\nabla \times V \;=\; 2\, \boldsymbol{\omega} \tag{1.58}$$

in which $\boldsymbol{\omega}$ is the angular velocity vector. Often $\nabla \times V$ is referred to in fluid mechanics as the vorticity vector.

A very useful model of fluid motion assumes that $\nabla \times V = 0$. Equation (1.58) shows that this is equivalent to setting $\boldsymbol{\omega} = 0$, which gives rise to the term "irrotational" in describing these flows. In an irrotational flow, if the line Δx in Figure 1.13 has an angular velocity in the counterclockwise direction, then the line Δy must have the same angular velocity in the clockwise direction so that $\omega_z = 0$. Many useful flows can be modelled with this approximation.

Some other applications of the curl come from the result that the curl of a gradient always vanishes,

$$\nabla \times \nabla \phi \;=\; 0 \tag{1.59}$$

in which ϕ is any scalar function. Equation (1.59) can be proved by writing

$$\nabla \times \nabla \phi = \begin{vmatrix} \boldsymbol{i} & \boldsymbol{j} & \boldsymbol{k} \\ \dfrac{\partial}{\partial x} & \dfrac{\partial}{\partial y} & \dfrac{\partial}{\partial z} \\ \dfrac{\partial \phi}{\partial x} & \dfrac{\partial \phi}{\partial y} & \dfrac{\partial \phi}{\partial z} \end{vmatrix} = \left(\dfrac{\partial^2 \phi}{\partial y \partial z} - \dfrac{\partial^2 \phi}{\partial z \partial y} \right) \boldsymbol{i} - \left(\dfrac{\partial^2 \phi}{\partial x \partial z} - \dfrac{\partial^2 \phi}{\partial z \partial x} \right) \boldsymbol{j} + \left(\dfrac{\partial^2 \phi}{\partial x \partial y} - \dfrac{\partial^2 \phi}{\partial y \partial x} \right) \boldsymbol{k} \tag{1.60}$$

Since x, y and z are independent variables, (1.60) and (1.27) can be used to complete the proof of (1.59).

When velocities are generated from a potential function, as shown in (1.44), then taking the curl of both sides of (1.44) gives

$$\nabla \times \boldsymbol{V} = \nabla \times \nabla \phi \tag{1.61}$$

Thus, (1.58), (1.59) and (1.61) show that the angular velocity vanishes for a potential flow, and a potential flow is irrotational.

For another application, consider the equation that we will derive later for the pressure variation in a motionless fluid. If $\boldsymbol{k}$ points upward, this equation is

$$\nabla p = -\rho g \boldsymbol{k} \tag{1.62}$$

Equations (1.40) and (1.62) show that surfaces of constant pressure are perpendicular to $\boldsymbol{k}$ and that pressure increases in the $-\boldsymbol{k}$ direction. Equation (1.62) gives three scalar partial differential equations for the calculation of p. However, there is a compatibility condition that must be satisfied, or else these equations will have no solution for p. Since $\nabla \times \nabla p = 0$, taking the curl of both sides of (1.62) shows that this compatibility condition is

$$0 = \nabla \times \left(-\rho g \boldsymbol{k} \right) = -g \frac{\partial \rho}{\partial y} \boldsymbol{i} + g \frac{\partial \rho}{\partial x} \boldsymbol{j} \tag{1.63}$$

Dotting both sides of (1.63) with $\boldsymbol{i}$ gives

$$\frac{\partial \rho}{\partial y} = 0 \tag{1.64}$$

and dotting both sides of (1.63) with $\boldsymbol{j}$ gives

$$\frac{\partial \rho}{\partial x} = 0 \tag{1.65}$$

Equations (1.64) and (1.65) show that ρ cannot change with x and y if (1.62) is to have a solution for p. Thus, ρ may be a constant or may vary with z and/or t, and a solution of (1.62) for p will exist.

Chapter 2

The Equations of Fluid Motion

In this chapter we will derive the general equations of fluid motion. Later these equations will be specialized for the particular applications considered in each chapter. The writer hopes that this approach, in which each specialized application is treated as a particular case of the more general equations, will lead to a unified understanding of the physics and mathematics of fluid motion.

There are two fundamentally different ways to use the equations of fluid mechanics in applications. The first way is to assume that pressure and velocity components change with more than one spacial coordinate and to solve for their variation from point to point within a flow. This approach requires the solution of a set of partial differential equations and will be called the "differential equation" approach. The second way is to use an integrated form of these differential equations to calculate average values for velocities at different cross sections and resultant forces on boundaries without obtaining detailed knowledge of velocity and pressure distributions within the flow. This will be called the "control volume" approach. We will develop the equations for both of these methods of analysis in tandem to emphasize that each partial differential equation has a corresponding control volume form and that both of these equations are derived from the same principle.

Continuity Equations

Consider a volume, $\forall$, bounded by a fixed surface, S, in a flow. Portions of S may coincide with fixed impermeable boundaries but other portions of S will not. Thus, fluid passes freely through at least some of S without physical restraint, and an incompressible flow must have equal volumetric flow rates entering and leaving $\forall$ through S. This is expressed mathematically by writing

$$\int_S \boldsymbol{V} \cdot \boldsymbol{e}_n \, dS = 0 \tag{2.1}$$

in which $\boldsymbol{e}_n$ = outward normal to S. Thus, (2.1) states that the net volumetric outflow through S is zero, with outflows taken as positive and inflows taken as negative. Equation (2.1) is the control volume form of a continuity equation for incompressible flow.

The partial differential equation form of (2.1) is obtained by taking $\forall$ to be a very small volume in the flow. Then an application of the second form of the divergence theorem, Eq. (1.49), allows (2.1) to be rewritten as

$$\int_\forall \nabla \cdot \boldsymbol{V} \, d\forall = 0 \tag{2.2}$$

Since $\forall$ can always be chosen small enough to allow the integrand to be nearly constant in $\forall$, Eq. (2.2) gives

$$\nabla \cdot \boldsymbol{V} = 0 \tag{2.3}$$

for the partial differential equation form of (2.1). If we set $\boldsymbol{V} = u\boldsymbol{i} + v\boldsymbol{j} + w\boldsymbol{k}$, then the unabbreviated form of (2.1) is

$$\frac{\partial u}{\partial x} + \frac{\partial v}{\partial y} + \frac{\partial w}{\partial z} = 0 \tag{2.4}$$

A conservation of mass statement for the same control volume used to derive (2.1) states that the net mass flow rate out through S must be balanced by the rate of mass decrease within $\forall$.

$$\int_S \rho\,\boldsymbol{V} \cdot \boldsymbol{e}_n\,dS = -\frac{d}{dt}\int_\forall \rho\,d\forall \tag{2.5}$$

Equation (2.5) is a control volume equation that reduces to (2.1) when ρ is everywhere equal to the same constant. However, as noted in the previous chapter, some incompressible flows occur in which ρ changes throughout $\forall$.

The partial differential equation form of (2.5) follows by applying (2.5) and the divergence theorem to a small control volume to obtain

$$\int_\forall \left[\nabla \cdot (\rho\,\boldsymbol{V}) + \frac{\partial \rho}{\partial t} \right] d\forall = 0 \tag{2.6}$$

in which the ordinary time derivative in (2.5) must be written as a partial derivative when moved within the integral. ($\int_\forall \rho\,d\forall$ is a function of t only, but ρ is a function of both t and the spacial coordinates.) Since (2.6) holds for an arbitrary choice of $\forall$, we obtain the following partial differential equation form of (2.5):

$$\nabla \cdot (\rho\,\boldsymbol{V}) + \frac{\partial \rho}{\partial t} = 0 \tag{2.7}$$

The unabbreviated form of (2.7) is

$$\frac{\partial (\rho u)}{\partial x} + \frac{\partial (\rho v)}{\partial y} + \frac{\partial (\rho w)}{\partial z} + \frac{\partial \rho}{\partial t} = 0 \tag{2.8}$$

Again we see that (2.7) reduces to (2.3) if ρ is everywhere equal to the same constant.

Now we can consider the consequence of applying (2.3) and (2.7) simultaneously to an incompressible heterogeneous flow, such as a flow involving differing mixtures of fresh and salt water. Expansion of $\nabla \cdot (\rho \boldsymbol{V})$ in either (2.7) or (2.8) gives

$$\rho(\nabla \cdot \boldsymbol{V}) + \boldsymbol{V} \cdot \nabla\rho + \frac{\partial\rho}{\partial t} = 0 \tag{2.9}$$

The first term in (2.9) vanishes by virtue of (2.3), and use of (1.17 a, b, c) in (2.9) gives

$$0 = \boldsymbol{V} \cdot \nabla\rho + \frac{\partial\rho}{\partial t} = \frac{dx}{dt}\frac{\partial\rho}{\partial x} + \frac{dy}{dt}\frac{\partial\rho}{\partial y} + \frac{dz}{dt}\frac{\partial\rho}{\partial z} + \frac{\partial\rho}{\partial t} \tag{2.10}$$

The four terms on the right side of (2.10) are the result of applying the chain rule to calculate $d\rho/dt$ in which $\rho = \rho(x, y, z, t)$ with $x(t)$, $y(t)$ and $z(t)$ equal to the coordinates of a moving fluid particle. This time derivative following the motion of a fluid particle is called either the substantial or material derivative and is given the special notation

$$\frac{D}{Dt} = \boldsymbol{V} \cdot \nabla + \frac{\partial}{\partial t} \tag{2.11}$$

Thus, (2.9) can be written in the compact form

$$\boxed{\frac{D\rho}{Dt} = 0} \tag{2.12}$$

or in the unabbreviated form

$$u\frac{\partial\rho}{\partial x} + \mathrm{v}\frac{\partial\rho}{\partial y} + w\frac{\partial\rho}{\partial z} + \frac{\partial\rho}{\partial t} = 0 \tag{2.13}$$

Equation (2.12), or (2.13), states that the mass density of a fluid particle does not change with time as it moves with an incompressible flow. Equation (2.5) is the only control volume form of (2.12), and the partial differential equations (2.3), (2.7) and (2.12) contain between them only two independent equations. An alternative treatment of this material is to derive (2.7) first, then postulate (2.12) as "obvious" and use (2.7) and (2.12) to derive (2.3).[*]

In summary, a homogeneous incompressible flow has a constant value of ρ everywhere. In this case, (2.1) and (2.3) are the only equations needed since all other continuity equations either reduce to these equations or are satisfied automatically by ρ = constant. A heterogeneous incompressible flow has $\rho = \rho(x, y, z, t)$. In this case, (2.1) and (2.3) are used together with either (2.5) and (2.7) or (2.5) and (2.12).

---

[*]   It has been assumed in deriving (2.3), (2.7) and (2.12) that $\bar{V}$ is the same velocity in all three equations. In other words, it has been assumed that mass and material velocities are identical. In mixing problems, such as problems involving the diffusion of salt or some other contaminant into fresh water, mass and material velocities are different. In these problems (2.3) is used for incompressible flow and (2.7) and (2.12) are replaced with a diffusion or dispersion equation. Yih (1969) gives a careful discussion of this subtle point.

Momentum Equations

The various forms of the momentum equations all originate from Newton's second law, in which the resultant of external forces on a moving element of fluid equals the product of the mass and acceleration. The acceleration was defined in Eq. (1.21) as the time derivative of the velocity vector of a moving fluid particle. Since the x, y and z coordinates of this particle are all functions of t, and since $V = V(x, y, z, t)$, an application of the chain rule gives

$$a = \frac{dV}{dt} = \frac{dx}{dt}\frac{\partial V}{\partial x} + \frac{dy}{dt}\frac{\partial V}{\partial y} + \frac{dz}{dt}\frac{\partial V}{\partial z} + \frac{\partial V}{\partial t} \tag{2.14}$$

Thus, (2.14) and (1.17a, b, c) show that a is calculated from the material derivative of V.

$$a = u\frac{\partial V}{\partial x} + v\frac{\partial V}{\partial y} + w\frac{\partial V}{\partial z} + \frac{\partial V}{\partial t} = (V \cdot \nabla)V + \frac{\partial V}{\partial t} = \frac{DV}{Dt} \tag{2.15}$$

Since Newton's law will be applied in this case to the movement of a collection of fluid particles as they move with a flow, we must choose the surface of $\forall$ a little differently. We will let S deform with t in a way that ensures that the same fluid particles, and only those particles, remain within $\forall$ over an extended period of time. This is known in the literature as a system volume, as opposed to the control volume that was just used to derive the continuity equations. The mass of fluid within this moving system volume does not change with time.

If we include pressure, gravity and viscous forces in our derivation, then an application of Newton's second law to a tiny system volume gives

$$-\int_S p\,e_n\,dS + \int_\forall \rho g\,d\forall + \int_\forall f\rho\,d\forall = \int_\forall \frac{DV}{Dt}\rho\,d\forall \tag{2.16}$$

in which the pressure force $p\,dS$ creates a force in the negative e_n direction for $p > 0$, g is a vector directed toward the centre of the earth with a magnitude of $g\,(= 9.81\text{ m/s}^2$ at sea level) and f = viscous force per unit mass. An application of the first form of the divergence theorem, Eq. (1.32) with $\phi = p$, to the first term of (2.16) gives

$$-\int_\forall \nabla p\,d\forall + \int_\forall \rho g\,d\forall + \int_\forall f\rho\,d\forall = \int_\forall \rho\frac{dV}{Dt}\,d\forall \tag{2.17}$$

Since $\forall$ can be chosen to be very small, (2.17) gives a partial differential equation form of the momentum equation:

$$-\nabla p + \rho g + \rho f = \rho\frac{DV}{Dt} \tag{2.18}$$

A relatively complicated bit of mathematical analysis, as given for example by Yih (1969) or Malvern (1969), can be used to show that an incompressible Newtonian flow has

$$\boldsymbol{f} = \nu \nabla^2 \boldsymbol{V} = \nu \left(\frac{\partial^2 \boldsymbol{V}}{\partial x^2} + \frac{\partial^2 \boldsymbol{V}}{\partial y^2} + \frac{\partial^2 \boldsymbol{V}}{\partial z^2} \right) \qquad (2.19)$$

in which ν = kinematic viscosity defined by (1.2). Thus, inserting (2.19) into (2.18) and dividing by ρ gives

$$-\frac{1}{\rho} \nabla p + \boldsymbol{g} + \nu \nabla^2 \boldsymbol{V} = \frac{D\boldsymbol{V}}{Dt} \qquad (2.20)$$

Equation (2.20), which applies to both homogeneous and heterogeneous incompressible flows, is a vector form of the Navier-Stokes equations that were first obtained by the French engineer Marie Henri Navier in 1827 and later derived in a more modern way by the British mathematician Sir George Gabriel Stokes in 1845.

Equation (2.20) can be put in a simpler form for homogeneous incompressible flows. Since ρ is everywhere equal to the same constant value in these flows, the first two terms can be combined into one term in the following way:

$$-\frac{1}{\rho} \nabla p + \boldsymbol{g} = -g \left[\nabla \left(\frac{p}{\rho g} \right) - \frac{\boldsymbol{g}}{g} \right] = -g \nabla h \qquad (2.21)$$

in which the piezometric head, h, is defined as

$$h = \frac{p}{\rho g} - \boldsymbol{e}_g \cdot \boldsymbol{r} \qquad (2.22)$$

The vector $\boldsymbol{e}_g = \boldsymbol{g}/g$ = unit vector directed through the centre of the earth, and $\boldsymbol{r}$ = position vector defined by

$$\boldsymbol{r} = x\boldsymbol{i} + y\boldsymbol{j} + z\boldsymbol{k} \qquad (2.23)$$

Thus, $\boldsymbol{e}_g \cdot \boldsymbol{r}$ is a gravitational potential function that allows h to be written for any coordinate system. For example, if the unit vector $\boldsymbol{j}$ points upward, then $\boldsymbol{e}_g = -\boldsymbol{j}$ and

$$h = \frac{p}{\rho g} + y \qquad (2.24)$$

If the unit vector $\boldsymbol{k}$ points downward, then $\boldsymbol{e}_g = \boldsymbol{k}$ and

$$h = \frac{p}{\rho g} - z \tag{2.25}$$

In open channel flow calculations it is customary to let $\boldsymbol{i}$ point downstream along a channel bed that makes an angle θ with the horizontal, as shown in Figure 2.1. Then $\boldsymbol{e}_g = \boldsymbol{i} \sin\theta - \boldsymbol{j} \cos\theta$ and

$$h = \frac{p}{\rho g} - x \sin\theta + y \cos\theta \tag{2.26}$$

Note that (2.26) reduces to (2.24) when $\theta = 0$.
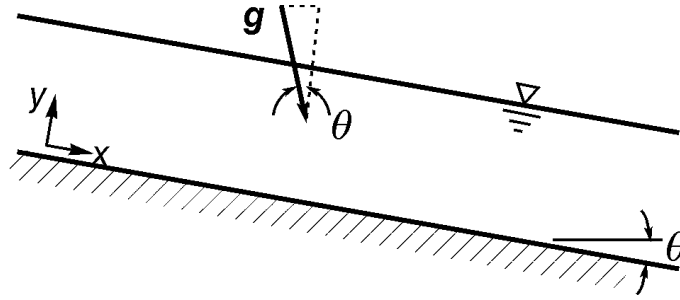
Figure 2.1 Coordinate system used for an open-channel flow.

The introduction of (2.21) into (2.20) gives a form of the Navier-Stokes equations for homogeneous incompressible flows:

$$-g \, \nabla h + \nu \nabla^2 V = \frac{DV}{Dt} \tag{2.27}$$

Equation (2.27) is a vector equation that gives the following three component equations:

$$-g \frac{\partial h}{\partial x} + \nu \left(\frac{\partial^2 u}{\partial x^2} + \frac{\partial^2 u}{\partial y^2} + \frac{\partial^2 u}{\partial z^2} \right) = u \frac{\partial u}{\partial x} + \nu \frac{\partial u}{\partial y} + w \frac{\partial u}{\partial z} + \frac{\partial u}{\partial t}$$

$$-g \frac{\partial h}{\partial y} + \nu \left(\frac{\partial^2 v}{\partial x^2} + \frac{\partial^2 v}{\partial y^2} + \frac{\partial^2 v}{\partial z^2} \right) = u \frac{\partial v}{\partial x} + \nu \frac{\partial v}{\partial y} + w \frac{\partial v}{\partial z} + \frac{\partial v}{\partial t} \qquad \textbf{(2.28 a, b, c)}$$

$$-g \frac{\partial h}{\partial z} + \nu \left(\frac{\partial^2 w}{\partial x^2} + \frac{\partial^2 w}{\partial y^2} + \frac{\partial^2 w}{\partial z^2} \right) = u \frac{\partial w}{\partial x} + \nu \frac{\partial w}{\partial y} + w \frac{\partial w}{\partial z} + \frac{\partial w}{\partial t}$$

Thus for homogeneous incompressible flows, Eqs. (2.3) and (2.27) give four scalar equations for the four unknown values of h, u, v and w. For an inhomogeneous incompressible flow, ρ becomes a fifth unknown, and Eq. (2.27) must be replaced with Eq. (2.20). Then the system of equations is closed by using either (2.7) or (2.12) to obtain a fifth equation.

The control volume form of the momentum equation is obtained by integrating (2.18) throughout a control volume of finite size. In contrast to the system volume that was used to derive (2.18), the control volume is enclosed by a fixed surface. Parts of this surface usually coincide with physical boundary surfaces, while other parts allow fluid to pass through without physical restraint. Since the three terms on the left side of (2.18) are forces per unit volume from pressure, gravity and viscosity, respectively, integration throughout a control volume gives

$$\boldsymbol{F} = \int_\forall \rho \, \frac{D\boldsymbol{V}}{Dt} \, d\forall \tag{2.29}$$

in which $\boldsymbol{F}$ = resultant external force on fluid within the control volume. In general, this will include the sum of forces from pressure, gravity and boundary shear.

The right side of (2.29) can be manipulated into the sum of a surface integral and volume integral by noting that

$$\frac{\partial(\rho u \boldsymbol{V})}{\partial x} + \frac{\partial(\rho v \boldsymbol{V})}{\partial y} + \frac{\partial(\rho w \boldsymbol{V})}{\partial z} + \frac{\partial(\rho \boldsymbol{V})}{\partial t} = \left[\nabla \cdot (\rho \boldsymbol{V}) + \frac{\partial \rho}{\partial t} \right] \boldsymbol{V} + \rho \left[(\boldsymbol{V} \cdot \nabla) \boldsymbol{V} + \frac{\partial \boldsymbol{V}}{\partial t} \right] \tag{2.30}$$

The first term on the right side of (2.30) vanishes by virtue of (2.7), and the last term is the product of ρ with the material derivative of Therefore,

$$\rho \, \frac{D\boldsymbol{V}}{Dt} = \frac{\partial(\rho u \boldsymbol{V})}{\partial x} + \frac{\partial(\rho v \boldsymbol{V})}{\partial y} + \frac{\partial(\rho w \boldsymbol{V})}{\partial z} + \frac{\partial(\rho \boldsymbol{V})}{\partial t} \tag{2.31}$$

Integrating both sides of (2.31) throughout $\forall$ and using the same techniques that were used to derive Eq. (1.48) [see, for example, Eq. (1.52)] leads to the result

$$\int_\forall \rho \, \frac{D\boldsymbol{V}}{Dt} \, d\forall = \int_S \rho \boldsymbol{V}(\boldsymbol{V} \cdot \boldsymbol{e}_n) \, dS + \int_\forall \frac{\partial(\rho \boldsymbol{V})}{\partial t} \, d\forall \tag{2.32}$$

Placing the partial derivative in front of the integral in the last term of (2.32) allows the partial derivative to be rewritten as an ordinary derivative since integrating $\rho \boldsymbol{V}$ throughout $\forall$ gives a result that is, at most, a function only of t. Thus, (2.32) and (2.29) together give the following control volume form for the momentum equation:

$$\boldsymbol{F} = \int_S \rho \boldsymbol{V}(\boldsymbol{V} \cdot \boldsymbol{e}_n) \, dS + \frac{d}{dt} \int_\forall \rho \boldsymbol{V} \, d\forall \tag{2.33}$$

This very general equation holds for all forms of incompressible flow and even for compressible flow. It states that the resultant of all external forces on a control volume is balanced by the sum of the net flow rate (flux) of momentum out through S and the time rate of increase of momentum without $\forall$. The last term in (2.33) vanishes when the flow is steady.

Another equation that is often used in control volume analysis is obtained from (2.27) by neglecting viscous stresses $(\nu = 0)$ and considering only steady flow $(\partial V / \partial t = 0)$. Then (2.27) reduces to

$$- g \nabla h = (V \cdot \nabla) V \tag{2.34}$$

If we dot both sides of (2.34) with the unit tangent to a streamline

$$e_t = \frac{V}{V} \tag{2.35}$$

we obtain

$$- g\, e_t \cdot \nabla h = \frac{V}{V} \cdot (V \cdot \nabla) V \tag{2.36}$$

The scalar $V = |V|$ may be moved under the brackets in the denominator on the right side of (2.36) to obtain

$$- g\, e_t \cdot \nabla h = V \cdot \left(\frac{V}{V} \cdot \nabla \right) V = V \cdot (e_t \cdot \nabla) V \tag{2.37}$$

But Eq. (1.44) can be used to write $e_t \cdot \nabla = d/ds$ in which s = arc length in the direction of e_t (i.e. s = arc length measured along a streamline). Thus, (2.37) becomes

$$- g \frac{dh}{ds} = V \cdot \frac{dV}{ds} = \frac{d}{ds} \left(\frac{1}{2} V \cdot V \right) = \frac{d}{ds} \left(\frac{1}{2} V^2 \right) \tag{2.38}$$

Dividing both sides of (2.38) by g and bringing both terms to the same side of the equation gives

$$\frac{d}{ds} \left(h + \frac{V^2}{2g} \right) = 0 \tag{2.39}$$

Equation (2.39) states that the sum of the piezometric head and velocity head does not change along a streamline in steady inviscid flow, and it is usually written in the alternative form

$$h_1 + \frac{V_1^2}{2g} = h_2 + \frac{V_2^2}{2g} \tag{2.40}$$

in which points 1 and 2 are two points on the *same* streamline. Since streamlines and pathlines coincide in steady flow, and since ρ is seen from (2.12) to be constant for any fluid particle following along a streamline, a similar development starting from (2.20) rather than (2.27) can be used to show that (2.40) holds also for the more general case of heterogeneous incompressible flow. Equation (2.40) is one form of the well known Bernoulli equation.

Finally, although we will be concerned almost entirely with incompressible flow, this is an opportune time to point out modifications that must be introduced when flows are treated as compressible. Since volume is not conserved in a compressible flow, Eq. (2.3) can no longer be used. Equations (2.7) and (2.18) remain valid but Eq. (2.19) is modified slightly to

$$\boldsymbol{f} = \nu\nabla^2\boldsymbol{V} + \frac{\nu}{3}\nabla\left(\nabla\cdot\boldsymbol{V}\right) \tag{2.41}$$

Equation (2.7) and the three scalar components of the Navier-Stokes equations that result when (2.41) is substituted into (2.18) contain five unknowns: the pressure, three velocity components and the mass density. This system of equations is then "closed" for a liquid or gas flow of constant temperature by assuming a relationship between p and ρ. However, for a gas flow in which the temperature also varies throughout the flow, it must be assumed that a relationship exists between p, ρ and the temperature, T. For example, an ideal gas has the equation

$$p = \rho RT \tag{2.42}$$

in which p = absolute pressure, ρ = mass density, T = absolute temperature and R = gas constant. Equation (2.42) is the fifth equation, but it also introduces a sixth unknown, T, into the system of equations. The system of equations must then be closed by using thermodynamic considerations to obtain an energy equation, which closes the system with six equations in six unknowns. Both Yih (1969) and Malvern (1969) give an orderly development of the various equations that are used in compressible flow analysis.

References

Malvern, L.E. (1969) *Introduction to the mechanics of a continuous medium*, Prentice-Hall, Englewood Cliffs, N.J., 713 p.

Yih, C.-S. (1969) *Fluid mechanics*, McGraw-Hill, New York, 622 p.

Chapter 3

Fluid Statics

In this chapter we will learn to calculate pressures and pressure forces on surfaces that are submerged in reservoirs of fluid that either are at rest or are accelerating as rigid bodies. We will only consider homogeneous reservoirs of fluid, although some applications will consider systems with two or more layers of fluid in which ρ is a different constant within each layer. We will start by learning to calculate pressures within reservoirs of static fluid. This skill will be used to calculate pressure forces and moments on submerged plane surfaces, and then forces and moments on curved surfaces will be calculated by considering forces and moments on carefully chosen plane surfaces. The stability of floating bodies will be treated as an application of these skills. Finally, the chapter will conclude with a section on calculating pressures within fluid that accelerates as a rigid body, a type of motion midway between fluid statics and the more general fluid motion considered in later chapters.

Fluid statics is the simplest type of fluid motion. Because of this, students and instructors sometimes have a tendency to treat the subject lightly. It is the writer's experience, however, that many beginning students have more difficulty with this topic than with any other part of an introductory fluid mechanics course. Because of this, and because much of the material in later chapters depends upon mastery of portions of this chapter, students are encouraged to study fluid statics carefully.

Pressure Variation

A qualitative understanding of pressure variation in a constant density reservoir of motionless fluid can be obtained by setting $V = 0$ in Eq. (2.20) to obtain

$$\nabla p = \rho \boldsymbol{g} \tag{3.1}$$

Since $\boldsymbol{g}$ points downward through the centre of the earth, and since ∇p is normal to surfaces of constant p and points in the direction of increasing p, Eq. (3.1) shows that surfaces of constant pressure are horizontal and that pressure increases in the downward direction.

Quantitative calculations of pressure can only be carried out by integrating either (3.1) or one of its equivalent forms. For example, setting $V = 0$ in (2.27) gives

$$- g \, \nabla h = 0 \tag{3.2}$$

which leads to the three scalar equations

$$\frac{\partial h}{\partial x} = 0$$

$$\frac{\partial h}{\partial y} = 0 \qquad\qquad\qquad \textbf{(3.3 a, b, c)}$$

$$\frac{\partial h}{\partial z} = 0$$

Equation (3.3a) shows that h is not a function of x, (3.3b) shows that h is not a function of y and (3.3c) shows that h is not a function of z. Thus, we must have

$$h = h_0 \qquad\qquad\qquad \textbf{(3.4)}$$

in which h_0 is usually a constant, although h_0 may be a function of t under the most general circumstances. If we use the definition of h given by (2.22), Eq. (3.4) can be put in the more useful form

$$p = p_0 + \rho \boldsymbol{g} \cdot \boldsymbol{r} \qquad\qquad\qquad \textbf{(3.5)}$$

in which $p_0 = \rho g h_0 =$ pressure at $|\boldsymbol{r}| = r = 0$ and $\boldsymbol{g} = g\,\boldsymbol{e}_g =$ gravitational vector defined following Eq. (2.16). Since $\boldsymbol{g} \cdot \boldsymbol{r} = g r \cos\theta = g$ multiplied by the projections of $\boldsymbol{r}$ along $\boldsymbol{g}$, the geometry in Figure (3.1) shows that

$$\boxed{p = p_0 + \rho g\, \xi} \qquad\qquad \textbf{(3.6)}$$

in which $p_0 =$ pressure at $\xi = 0$ and ξ is a vertical coordinate that is positive in the downward direction and negative in the upward direction.
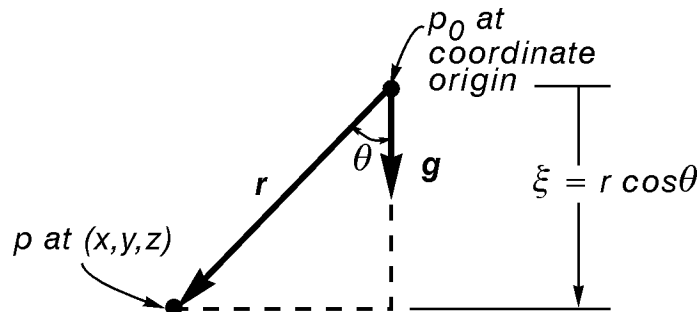
Figure 3.1 Geometry for the calculation of $\boldsymbol{g} \cdot \boldsymbol{r}$ in (3.5).

Equation (3.6) also shows that p is constant in the horizontal planes ξ = constant and that p increases in the downward direction as ξ increases. An alternative interpretation of (3.6) is that the pressure at any point in the fluid equals the sum of the pressure at the origin plus the weight per unit area of a vertical column of fluid between the point (x, y, z) and the origin. Clearly, the choice of coordinate origin in any problem is arbitrary, but it usually is most convenient to choose the origin at a point where p_0 is known. Examples follow.

Example 3.1
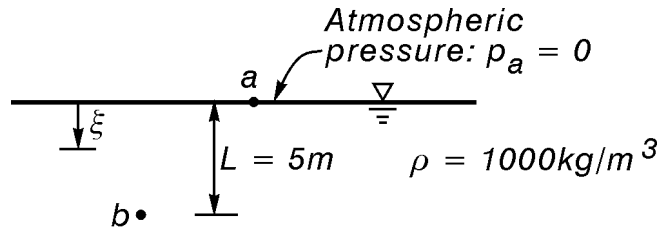
Given: ρ and L.

Calculate: p at point b in gage pressure.

Solution: Whenever possible, the writer prefers to work a problem algebraically with symbols before substituting numbers to get the final answer. This is because (1) mistakes are less apt to occur when manipulating symbols, (2) a partial check can be made at the end by making sure that the answer is dimensionally correct and (3) errors, when they occur, can often be spotted and corrected more easily.

By measuring ξ from the free surface, where $p = 0$, we can apply (3.6) between points a and b to obtain

$$p_b = 0 + \rho g L = \boxed{\rho g L}$$

Units of p_b are $\left(\text{kg/m}^3\right)\left(\text{m/s}^2\right)(\text{m}) = \text{kg/m} - \text{s}^2 = \text{N/m}^2$, so the units are units of pressure, as expected. Substitution of the given numbers now gives

$$p_b = (1000)(9.81)(5) = 49{,}050 \text{ N/m}^2 = \boxed{49.05 \text{ kN/m}^2}$$

Example 3.2

Water: ρ = 1000 kg/m^3 at 5°C
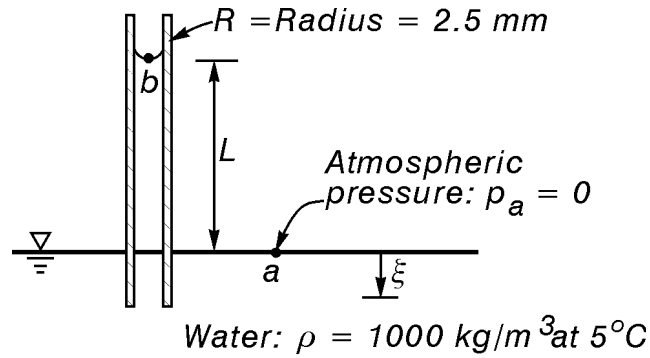
Given: ρ and R.

Calculate: The height, L, of water rise in the tube if the meniscus has a radius of curvature equal to the tube radius, R.

Solution: Applying (3.6) between points a and b gives

$$p_b = 0 + \rho g(-L) = -\rho g L$$

Thus, the pressure is negative at b. If R = tube radius, and if the meniscus has the same spherical radius as the tube, Eq. (1.4) or (1.7) gives

$$p_b = -\frac{2\sigma}{R}$$

Elimination of p_b from these two equations gives

$$L = \frac{2\sigma}{\rho g R}$$

A check of units gives $L = (N/m) \div (kg/m^3) \times \left(\dfrac{m}{s^2}\right) \times m = \dfrac{N - s^2}{kg} = m$, which is correct.

After obtaining σ from the appendix, substituting numbers gives

$$L = \frac{2(7.54 \times 10^{-2})}{(1000)(9.81)(.0025)} = 0.00615 \text{ m} = \boxed{6.15 \text{ mm}}$$

This value of L has been calculated by using σ for distilled water in air. Impurities in tap water decrease σ, and some additives, such as dish soap, also decrease σ. It is common practice in laboratories, when glass piezometer tubes are used to measure pressure, to use as large diameter tubes as possible, which reduces L by increasing R. If capillarity is still a problem, then L is reduced further by using additives to decrease σ.

Example 3.3
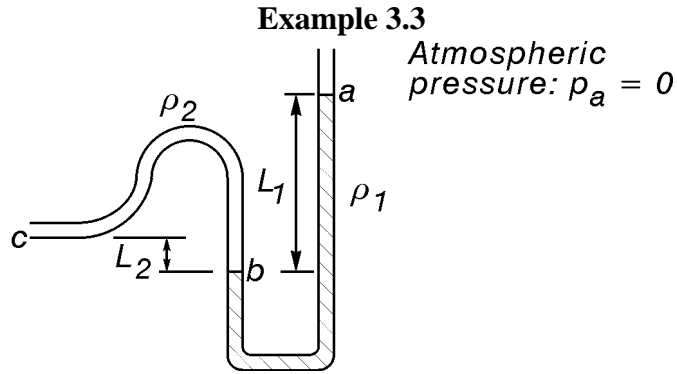
Given: ρ_1, ρ_2, L_1 and L_2.

Calculate: p_c if surface tension effects at a and b are negligible.

Solution: Applying (3.6) from a to b gives

$$p_b = p_a + \rho_1 g L_1 = 0 + \rho_1 g L_1$$

Applying (3.6) from c to b gives

$$p_b = p_c + \rho_2 g L_2$$

Elimination of p_b gives

$$\rho_1 g L_1 = p_c + \rho_2 g L_2$$

or
$$p_c = \boxed{\rho_1 g L_1 - \rho_2 g L_2}$$

This calculation can be done in one step by writing the pressure at a and then adding $\rho g \Delta \xi$ when going down or subtracting $\rho g \Delta \xi$ when going up to eventually arrive at c.

$$0 + \rho_1 g L_1 - \rho_2 g L_2 = p_c$$

The next example also illustrates this technique.

Example 3.4
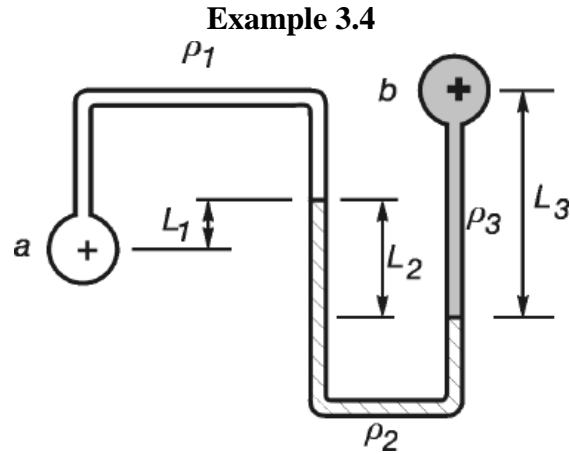
Given: ρ_1, ρ_2, ρ_3, L_1, L_2 and L_3.

Calculate: $p_a - p_b$.

Solution:

$$p_a - \rho_1 g L_1 + \rho_2 g L_2 - \rho_3 g L_3 = p_b$$

$$\therefore \quad p_a - p_b = \boxed{\rho_1 g L_1 - \rho_2 g L_2 + \rho_3 g L_3}$$

Area Centroids

There are certain area integrals that arise naturally in the derivation of formulae for calculating forces and moments from fluid pressure acting upon plane areas. These integrals have no physical meaning, but it is important to understand their definition and to know how to calculate their value. Therefore, we will review portions of this topic before considering the problem of calculating hydrostatic forces on plane areas.

The area centroid coordinates, (x_c, y_c), are given by the following definitions:

$$x_c A = \int_A x \, dx \, dy$$

$$y_c A = \int_A y \, dx \, dy$$

(3.7 a, b)

The integrals on the right side of (3.7 a, b) are sometimes referred to as the first moments of the area, and (x_c, y_c) can be thought of as average values of (x, y) within the plane area, A. When $x_c = y_c = 0$, then (3.7 a, b) show that

$$\int_A x \, dx \, dy \ = \ 0$$

$$\int_A y \, dx \, dy \ = \ 0$$

(3.8 a, b)

In this case, the coordinate origin coincides with the area centroid.
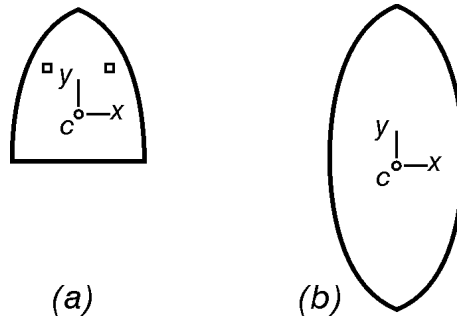
Figure 3.2 Two geometries considered in the calculation of area centroids.

In many applications, one or both of the centroidal coordinates can be found through considerations of symmetry. In Figure 3.2 a, for example, c lies along a line of symmetry since corresponding elements on opposite sides of the y axis (the line of symmetry) cancel out in the sum

$$x_c \ = \ \frac{1}{A} \int_A x \, dA \ \approx \ \frac{1}{A} \sum_{i=1}^{N} x_i \, \Delta A_i \ = \ 0$$

(3.9)

The y_c coordinate in Figure 3.2 a must be determined from an evaluation of the integral in (3.7 b). When two orthogonal lines of symmetry exist, as in Figure 3.2 b, then the area centroid coincides with the intersection of the lines of symmetry. Locations of centroids are given in the appendix for a few common geometries.

Moments and Product of Inertia

The moments and product of inertia for a plane area in the (x, y) plane are defined as

$$I_x = \int_A y^2 \, dA$$

$$I_y = \int_A x^2 \, dA$$

(3.10 a, b, c)

$$I_{xy} = \int_A xy \, dA$$

in which I_x and I_y are moments of inertia about the x and y axes, respectively, and I_{xy} is the product of inertia. Again, these integrals have no physical meaning but must often be calculated in applications. These integrals are sometimes referred to as second moments of the area.

If one, or both, of the coordinate axes coincides with a line of symmetry, as in Figures 3.2 a and 3.2 b, then the product of inertia vanishes.

$$\int_A xy \, dA \approx \sum_{i=1}^{N} x_i y_i \, \Delta A_i = 0$$

(3.11)

When this happens, the coordinate axes are called "principal axes". Frequently, principal axes can be located from considerations of symmetry. In other cases, however, they must be located by solving an eigenvalue problem to determine the angle that the coordinate axes must be rotated to make the product of inertia vanish. We will only consider problems in which principal axes can be found by symmetry. Moments and products of inertia for some common geometries are given in the appendix.

Forces and Moments on Plane Areas

Consider the problem of calculating the pressure force on a plane area, such as one of the areas shown in Figure 3.2. The pressure at the area centroid, c, can be calculated from an application of (3.6), and pressures on the surface are given by (3.5) after setting $p_0 = p_c$, $\boldsymbol{g} = g_x \boldsymbol{i} + g_y \boldsymbol{j} + g_z \boldsymbol{k}$ and $\boldsymbol{r} = x\boldsymbol{i} + y\boldsymbol{j}$ (since $z = 0$ on A).

$$p = p_c + \rho g_x x + \rho g_y y$$

(3.12)

The coordinate origin coincides with the area centroid, and the pressure force on the area is given by the integral of p over A:

$$\boldsymbol{F} = -\boldsymbol{k} \int_A p \, dA$$

(3.13)

Inserting (3.12) in (3.13) and making use of (3.8 a, b) gives

$$\boldsymbol{F} = -p_c A \boldsymbol{k} \tag{3.14}$$

> Equation (3.14) shows that the force on a plane area equals the product of the area with the pressure at the area centroid.

Frequently we need to calculate both the pressure force and the moment of the pressure force. The moment of the pressure force about the centroid, c, is

$$\boldsymbol{M} = \int_A \boldsymbol{r} \times (-p \boldsymbol{k} \, dA) = -\boldsymbol{i} \int_A y \, p \, dA + \boldsymbol{j} \int_A x \, p \, dA \tag{3.15}$$

On a plane area there is one point, called the centre of pressure and denoted by cp, where the force $p_c A$ can be applied to give exactly the same moment about c as the moment calculated from (3.15). Thus, the moment about c is then

$$\boldsymbol{M} = \boldsymbol{r}_{cp} \times (-p_c A \boldsymbol{k}) = -\boldsymbol{i} \, y_{cp} \, p_c A + \boldsymbol{j} \, x_{cp} \, p_c A \tag{3.16}$$

in which x_{cp} and y_{cp} are the coordinates of the centre of pressure. The corresponding $\boldsymbol{i}$ and $\boldsymbol{j}$ components of (3.15) and (3.16) give

$$
\begin{aligned}
x_{cp} &= \frac{1}{p_c A} \int_A x \, p \, dA \\
y_{cp} &= \frac{1}{p_c A} \int_A y \, p \, dA
\end{aligned}
\tag{3.17 a, b}
$$

When the pressure, p, is plotted as a function of x and y over a plane surface area, A, we obtain a three-dimensional volume known as the pressure prism. Equations (3.17 a, b) show that the centre of pressure has the same x and y coordinates as the volumetric centroid of the pressure prism. There is a very important case in which the centroid of the pressure prism is used directly to locate the centre of pressure. This occurs when a constant width plane area intersects a free surface, as shown in Figure 3.3. Then the pressure prism has a cross section in the shape of a right triangle, and the centre of pressure is midway between the two end sections at a point one third of the distance from the bottom to the top of the prism.
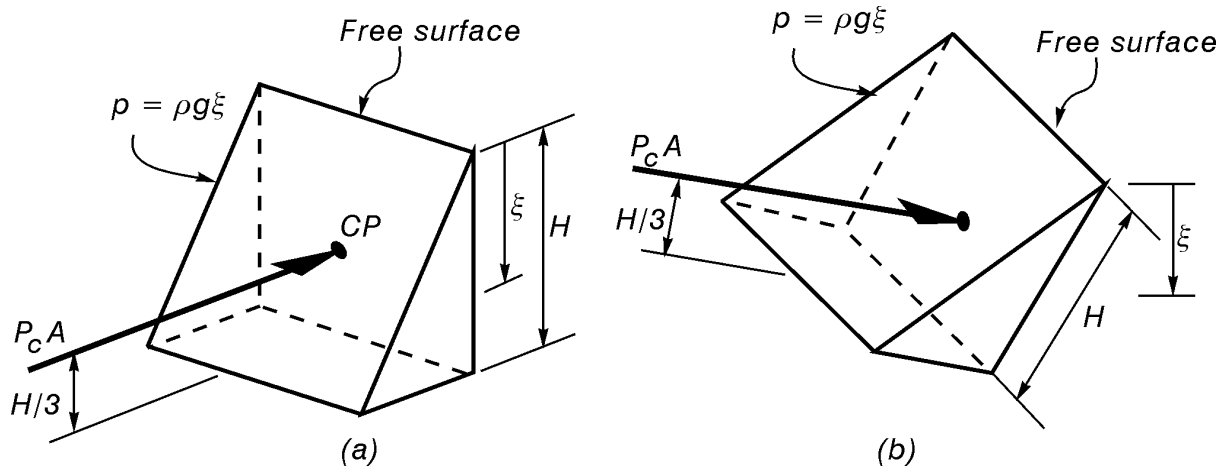
Figure 3.3 Pressure prisms and centres of pressure when a plane area intersects a free surface for (a) a vertical area and (b) a slanted area.

For more general cases when the plane area either is not rectangular or does not intersect a free surface, the centre of pressure is usually located by substituting (3.12) into (3.17 a, b) to obtain

$$x_{cp} = \frac{\rho}{p_c A}\left(g_x I_y + g_y I_{xy}\right)$$

$$y_{cp} = \frac{\rho}{p_c A}\left(g_x I_{xy} + g_y I_x\right)$$

(3.18 a, b)

in which g_x and g_y are the x and y components of the vector $\mathbf{g}$ and I_x, I_y and I_{xy} are the moments and products of inertia defined by (3.10 a, b, c). In most applications a set of principal axes is located by symmetry and used so that $I_{xy} = 0$.

Example 3.5
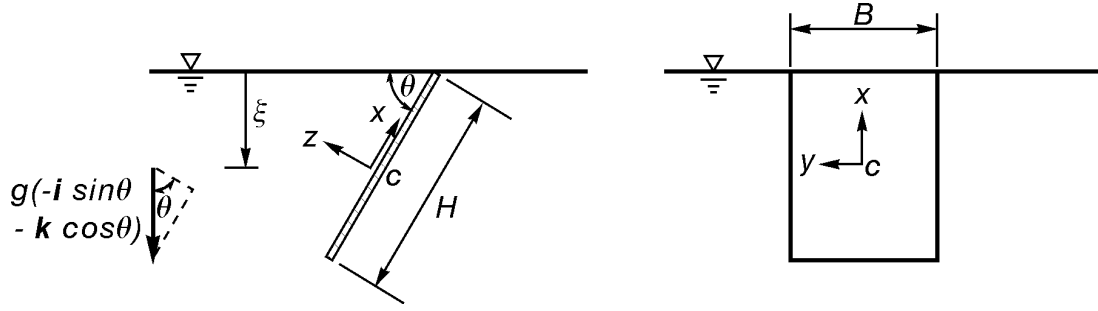
Given: ρ, θ, H and B.

Calculate: The pressure force and $\boldsymbol{r}_{cp} = x_{cp}\boldsymbol{i} + y_{cp}\boldsymbol{j}$.

Solution: The pressure force is given by

$$\boldsymbol{F} = -p_c A \boldsymbol{k} = -\rho g \xi_c A \boldsymbol{k} = \boxed{-\rho g \frac{H}{2} \sin\theta \, (BH)\boldsymbol{k}}$$

The area centroid, c, has been located by symmetry at the midpoint of the rectangle, and considerations of symmetry also show that the coordinate axes have been oriented so that $I_{xy} = 0$. Thus, a set of principal axes is being used and (3.18 a, b) reduce to

$$x_{cp} = \frac{\rho}{p_c A} g_x I_y \quad \text{and} \quad y_{cp} = \frac{\rho}{p_c A} g_y I_x$$

In these equations we have $g_x = -g\sin\theta$, $g_y = 0$, $A = BH$, $I_y = bH^3/12$ and $I_x = B^3H/12$. Thus, we obtain

$$x_{cp} = \frac{\rho}{\left(\rho g \dfrac{H}{2}\sin\theta\right)(BH)} (-g\sin\theta)\frac{BH^3}{12} = \boxed{-\frac{H}{6}}$$

$$y_{cp} = \frac{\rho}{\left(\rho g \dfrac{H}{2}\sin\theta\right)(BH)} (0)\frac{B^3H}{12} = \boxed{0}$$

The distance from the plate bottom to the centre of pressure is $H/2 - H/6 = H/3$, which agrees with the result noted in the discussion of the volume centroid of the pressure prism shown in Figure 3.3(b). As a partial check, we also notice that the dimensions of the expressions for $\boldsymbol{F}$, x_{cp} and y_{cp} are correct.

Example 3.6
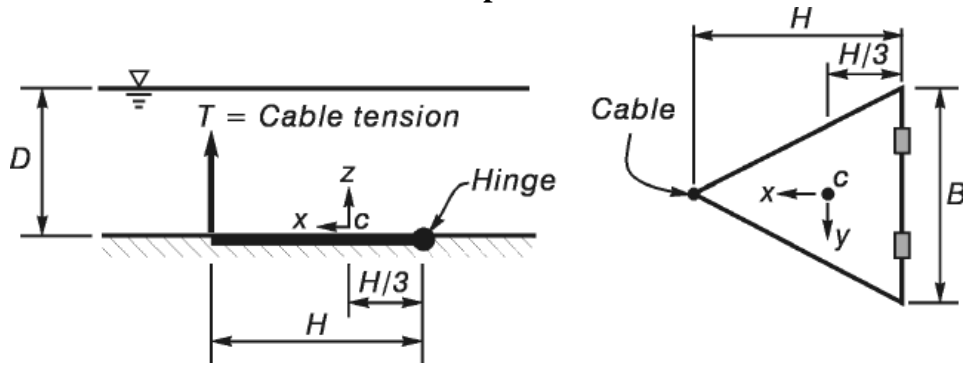
Given: ρ, D, B and H.

Calculate: The tension, T, in the cable that is just sufficient to open the gate.

Solution: When the gate starts to open, the reservoir bottom and the gate edge lose contact. Thus, the only forces on the gate are the cable tension, the water pressure force on the top of the gate surface and the hinge reaction when T is just sufficient to open the gate. We will assume that the hinges are well lubricated and that atmospheric pressure exists on the lower gate surface. A free body diagram of the gate is shown below.

Setting the summation of moments about the hinge equal to zero gives

$$TH - p_c A \left(H/3 + x_{cp} \right) = 0$$

$$\therefore \quad T = \left(1/3 + x_{cp}/H \right) p_c A$$

Since $\boldsymbol{g} = -g\boldsymbol{k}$, we have $g_x = g_y = 0$ and, therefore, $x_{cp} = y_{cp} = 0$ from (3.18 a, b).[*]

We also have $p_c = \rho g D$ and $A = BH/2$.

$$\therefore \quad T = 1/3 \left(\rho g D \right) \left(BH/2 \right) = \boxed{\dfrac{\rho g D B H}{6}}$$
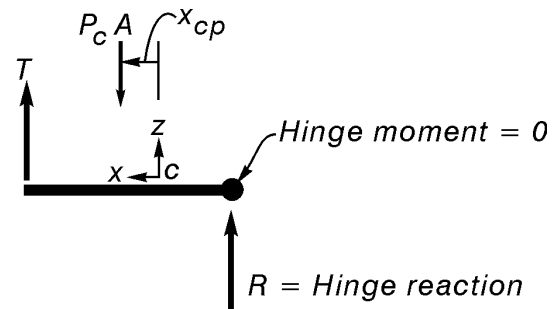
The hinge reaction force could be found by setting the vector sum of forces equal to zero.

---

[*]   This result could have been found more efficiently by noting that the pressure distribution over the gate is uniform. Thus, a line normal to the gate and passing through the area centroid also passes through the volume centroid of the pressure prism.

Example 3.7

View E-E'

Given: ρ, ξ_c, B, H, α, and β.
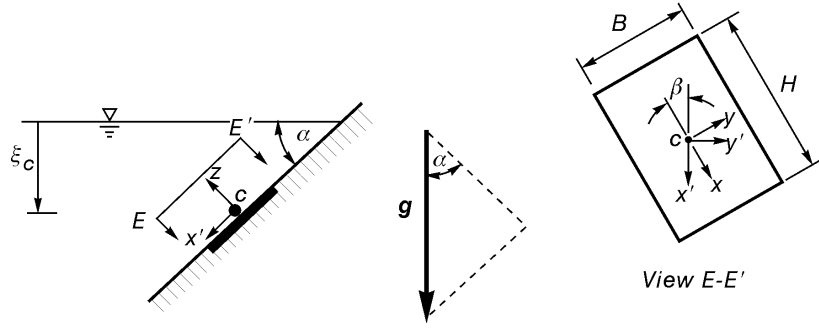
Calculate: x_{cp} and y_{cp} for the rectangular gate.

Solution: The zx' plane is vertical, and the angle between the x' and x axis is β. The xy and $x'y'$ are both in the plane of the gate. The most difficult part of the problem is writing g as a vector in the xy system of coordinates, which is a set of principal axes for the rectangular gate. This can be done by writing g as a vector in both the $zx'y'$ and zxy coordinate systems:

$$g = g\left(i' \sin\alpha - k \cos\alpha\right) = g_x i + g_y j + g_z k$$

Since k is perpendicular to i', dotting both sides with k gives

$$-g\cos\alpha = g_z$$

Dotting both sides with i gives

$$g\, i \cdot i' \sin\alpha = g_x$$

But

$$i \cdot i = \cos\left(i, i'\right) = \cos\beta$$

$$\therefore \quad g_x = g\sin\alpha \cos\beta$$

Dotting both sides with j gives

$$g\, j \cdot i' \sin\alpha = g_y$$

But

$$j \cdot i' = \cos\left(j, i'\right) = \cos\left(\pi/2 + \beta\right) = -\sin\beta$$

$$\therefore \quad g_y = -g\sin\alpha \sin\beta$$

Since $p_c = \rho g \xi_c$, $I_{xy} = 0$, $I_y = BH^3/12$, $I_x = B^3H/12$ and $A = BH$, we obtain from (3.18 a, b)

$$x_{cp} = \frac{\rho}{\rho g \xi_c(BH)}\left(g\sin\alpha \cos\beta\right)\left(BH^3/12\right) = \boxed{\frac{H^2}{12\xi_c}\sin\alpha \cos\beta}$$

$$y_{cp} = \frac{\rho}{\rho g \xi_c(BH)}\left(-g\sin\alpha \sin\beta\right)\left(B^3H/12\right) = \boxed{-\frac{B^2}{12\xi_c}\sin\alpha \sin\beta}$$

Several partial checks can be made on these answers. First, the dimensions are correct. Second, if we set $\beta = 0$ and $\xi_c = (H/2)\sin\alpha$, we get $y_{cp} = 0$ and $x_{cp} = H/6$, which agrees with the result obtained for Example 3.5. Finally, if we set $\beta = \pi/2$ and $\xi_c = (B/2)\sin\alpha$, we get $x_{cp} = 0$ and $y_{cp} = -B/6$, which also agrees with the result obtained for Example 3.5. Also note that x_{cp} and y_{cp} both vanish as ξ_c becomes infinite.

Forces and Moments on Curved Surfaces

The problem of calculating forces and moments on a curved surface can always be reduced to an equivalent system consisting of a vertical force acting through the centroid of a volume and vertical and horizontal forces on plane areas acting through the centre of pressure for each plane area. For example, consider the problem of calculating the force and moment from the pressure acting on the left side of the curved area shown in Figure 3.4(a).
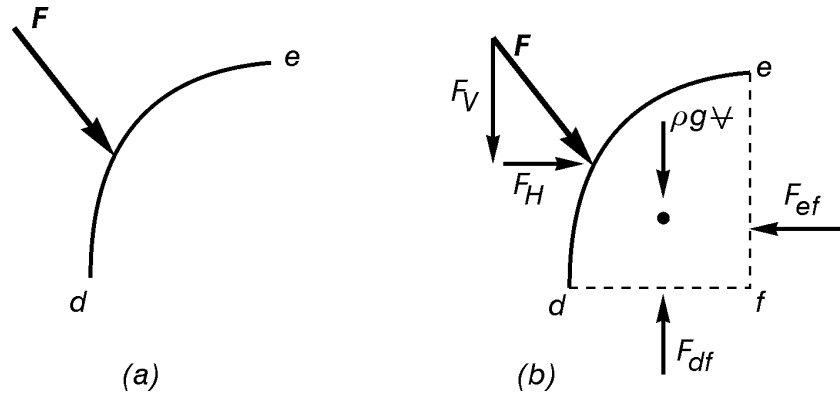
Figure 3.4 Calculation of forces and moments on the left side of the curved surface de.

Figure 3.4(b) shows an imaginary closed surface def within the same fluid, which is everywhere at rest. The pressure forces on the curved surfaces de in Figures 3.4(a) and 3.4(b) will obviously be identical provided that the surface de has the same geometry and orientation and is located at the same depth in both cases. However, if in Figure 3.4(b) we consider the closed surface def, we must have both the summation of external forces and the summation of moments equal to zero since the fluid within def is in equilibrium. The external forces consist of (a) the vertical and horizontal components, F_V and F_H, of the pressure force on de, (b) the weight of fluid $\rho g \forall$ within def that acts through the volume centroid of def, (c) the horizontal pressure force F_{ef} that acts through the centre of pressure of the vertical plane surface ef and (d) the vertical pressure force F_{df} that acts through the centre of pressure of the horizontal plane surface df. Summing horizontal forces gives

$$F_H = F_{ef} \tag{3.19}$$

and summing vertical forces gives

$$F_V = F_{df} - \rho g \forall \tag{3.20}$$

The line of action of the horizontal force F_H can be found by considering horizontal forces F_1 and F_2 on the horizontal element shown in Figure 3.5.

Since the sum of horizontal forces on this element must vanish, F_1 and F_2 must be equal. When we consider the contributions of all horizontal elements that occur in *def*, it becomes evident that the horizontal pressure forces F_H and F_{ef} create moments about any point in space that are equal in magnitude but opposite in direction. Therefore, we conclude that the horizontal forces F_H and F_{ef} in Figure 3.4(b) have the same magnitude and line of action but opposite directions.
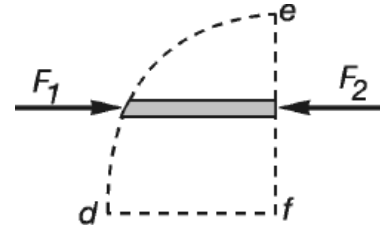
Figure 3.5 Horizontal forces F_1 and F_2 on a horizontal fluid element in Figure 3.4(b).

Since the horizontal forces F_H and F_{ef} have the same magnitude and line of action, and since the summation of all moments acting on *def* must vanish, it is evident that the line of action of F_V must be such that the moment created about any point in space by the vertical forces must vanish. When three vertical forces are involved, as in Figure 3.4(b), these three forces will not be collinear. However, if the horizontal surface coincides with a free surface, as shown in Figure 3.6, then only two forces are involved and they must be collinear. Thus, in Figure 3.6 the vertical force F_V and the weight of fluid $\rho g \forall$ must both pass through the volumetric centroid of *defh*.
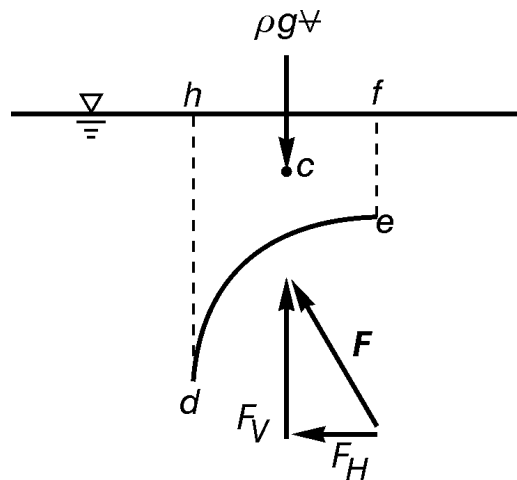
Figure 3.6 Calculation of F_v and its line of action when the horizontal surface *hf* coincides with a free surface.

If the volume *defh* in Figure 3.6 is also used to calculate the horizontal force F_H, then F_H will equal the difference between the horizontal forces on *hd* and *ef*. However, summing moments to determine a line of action for either F_V or F_H can always be avoided, if desired, by choosing different geometries for the calculation of F_V and F_H. For example Figure 3.4(b) could be used to calculate F_H and its line of action, and Figure 3.6 could be used to calculate F_V and its line of action. In fact, the geometry of Figure 3.6 can always be used to calculate F_V and its line of action, even if a free surface does not exist in the stated problem. In this case, an equivalent problem is used with a free surface placed at an elevation that creates the same pressures on the curved surface as existed in the original problem. The extension of these ideas to three dimensions is obvious and will not be discussed.

Example 3.8
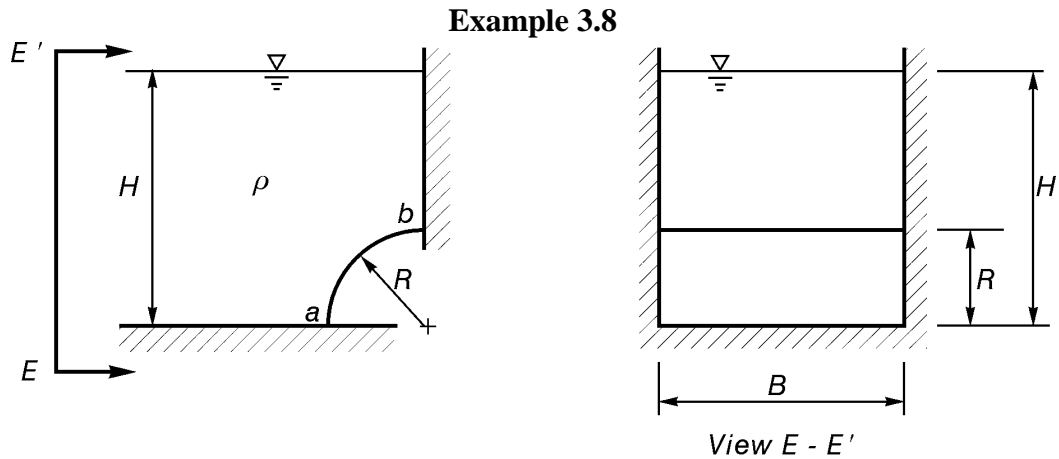
Given: ρ, R, H, and B.

Calculate: The vertical and horizontal pressure forces and their lines of action for the quarter circular cylinder ab.

Solution: We will solve this problem by considering the following problem:
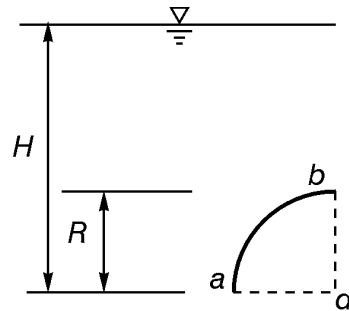
The forces acting on abd are as follows:
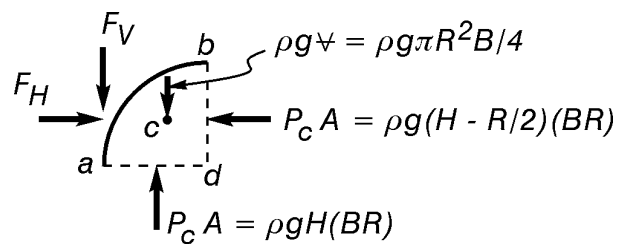
The forces F_H and $\rho g(H - R/2)(BR)$ have the same line of action, which can be calculated from Eq. (3.18 a, b).
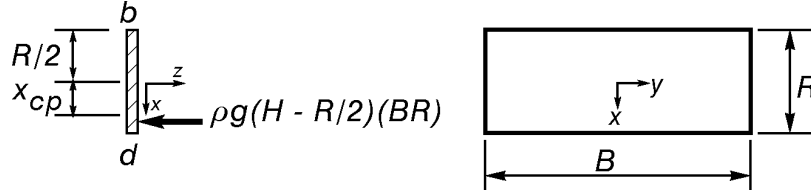
$$I_y = \frac{1}{12} BR^3, \ I_{xy} = 0, \ g_x = g, \ g_y = 0$$

$$\therefore \quad \boxed{y_{cp} = 0} \quad \text{and} \quad x_{cp} = \frac{\rho}{p_c A} g_x I_y = \frac{\rho g \left(BR^3/12\right)}{\rho g \left(H - R/2\right)\left(BR\right)} = \boxed{\frac{R^2}{12 \left(H - R/2\right)}}$$
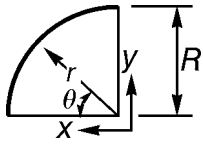
Calculation of the x coordinate of the volume centroid for abd follows:

$$x_c \forall = \int_\forall x \, d\forall \quad \therefore \quad x_c \left(\pi R^2/4\right) B = \int_A x \left(B \, dA\right) = B \int_A x \, dA$$

The constant values of B cancel, and switching to polar coordinates in which $x = r \cos \theta$ gives

$$x_c \left(\pi R^2/4\right) = \int_0^{\frac{\pi}{2}} \int_0^R \left(r \cos \theta\right)\left(r \, dr \, d\theta\right) = \int_0^{\frac{\pi}{2}} \cos \theta \, d\theta \int_0^R r^2 \, dr$$

Calculation of the integrals gives

$$x_c = \frac{4}{3\pi} R$$

Since the pressure distribution over ad is uniform, the volumetric centroid of the pressure prism is easily located by symmetry midway between points a and d. Thus, the vertical forces have the following magnitudes and lines of action:
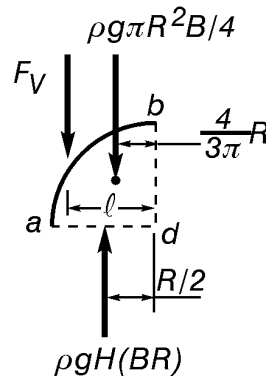
Summing forces in the vertical direction gives

$$- F_V - \rho g \pi R^2 B/4 + \rho g H B R = 0$$

$$\therefore \quad F_V = \boxed{\rho g B R\left(H - \pi R/4\right)}$$

Summing moments about d gives, since moments of the horizontal forces cancel,

$$\rho g H(BR)(R/2) - \rho g \pi R^2(B/4)\left(\frac{4}{3\pi}R\right) - \ell F_V = 0$$

Substituting the calculated value of F_V and solving for ℓ gives

$$\ell = \boxed{\left(\frac{\dfrac{H}{2} - \dfrac{R}{3}}{H - \dfrac{\pi R}{4}}\right) R}$$

The expressions for all forces and lengths have the correct dimensions, which gives a partial check on the calculations.

Example 3.9

Check the calculations for the vertical force F_V in Example 3.8 by using the volume shown below:
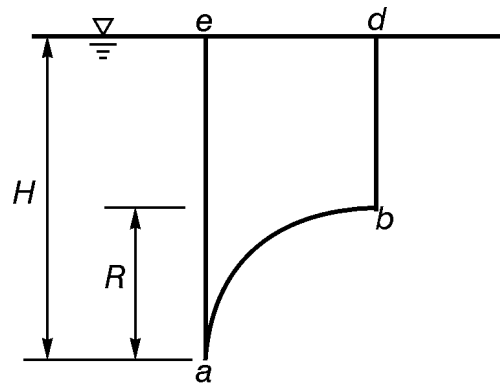
The only vertical forces acting on $abde$ are the weight of fluid within $abde$ and the vertical component of force on ab. Thus, these two forces have the same magnitude since the sum of vertical forces must vanish.

$$\therefore \quad F_V = \rho g \forall = \rho g B\left(H R - \pi R^2/4\right) = \boxed{\rho g B R\left(H - \pi R/4\right)}$$

This agrees with the result calculated previously in Example 3.8.

Since all moments created by the horizontal forces cancel, the moment of the vertical forces must also cancel. Since only two forces act in the vertical direction, they must have the same line of action through the volume centroid of $abde$.
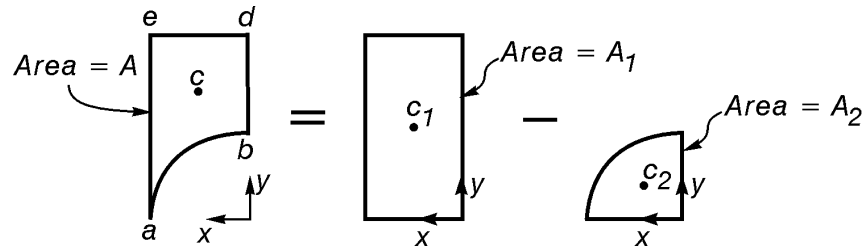
The width B is constant and cancels out in the calculation of x_c, so that x_c is identical with the x coordinate of the area centroid of $abde$.

$$x_c A \;=\; \int\limits_{A=A_1-A_2} x\,dA \;=\; \int\limits_{A_1} x\,dA \;-\; \int\limits_{A_2} x\,dA \;=\; x_{c_1} A_1 \;-\; x_{c_2} A_2$$

$$\therefore \quad x_c\left(HR - \pi R^2/4\right) \;=\; (R/2)(HR) \;-\; \left(\frac{4}{3\pi}R\right)\left(\pi R^2/4\right)$$

Solution for x_c gives

$$x_c \;=\; \left(\frac{\dfrac{H}{2} - \dfrac{R}{3}}{H - \dfrac{\pi R}{4}}\right) R$$

This value agrees with the value calculated previously for ℓ in Example 3.8.

Buoyancy Forces

A buoyancy force is defined to be the net force from fluid pressure acting on the surface of an object that is either completely or partially submerged in a fluid at rest. The buoyancy force and its line of action can always be found by the principles just introduced for the calculation of forces on curved surfaces. For example, if the object is completely submerged so that its entire surface is wetted, then we consider a body of fluid at rest that is submerged at the same depth and that has the same geometry and orientation as the surface of the submerged body. The fluid body has only two external forces acting upon it: its weight, which acts downward through its mass centroid, and the pressure or buoyancy force acting on its surface. Since the vector sum of these external forces must vanish, and since the fluid weight is in the vertical direction, the buoyancy force must have zero horizontal components and a vertical component equal to the weight of fluid displaced by the physical object (Archimedes' buoyancy principle). Since there are only two forces acting on the body of fluid, and since these two external forces must create a zero net moment, these forces must also be collinear. If the fluid is homogeneous so that ρ is constant everywhere, then the mass centroid and volume centroid of the body of fluid coincide. In conclusion, this means that the net buoyancy or pressure force on a submerged physical object is vertical with a magnitude equal to the weight of displaced fluid and has a line of action that passes through the volume centroid of the displaced fluid. This result is shown in Figure 3.7.
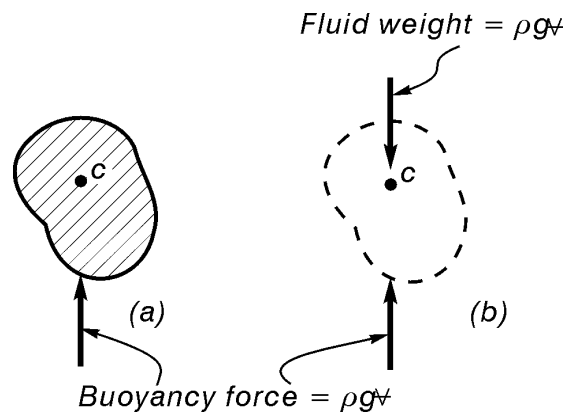
Figure 3.7 Buoyancy forces on (a) a submerged physical object and (b) a volume of fluid with the same pressure distribution around its surface.

An equilibrium configuration or position for the submerged object is determined by considering all of the external forces acting on the object. These forces include the buoyancy force (which is upward with a vertical line of action that passes through the volume centroid of the displaced fluid), the object weight (which is downward with a vertical line of action that passes through the mass centroid, cg, of the object) plus all other external forces acting on the object. If the system of forces is statically determinate, then setting the sum of forces and moments equal to zero will be sufficient to determine all unknown forces plus the body orientation in equilibrium. If the system is statically indeterminate, then elastic considerations must be used to close the system of equations. An example is shown in Figure 3.8, where an object is tethered by a single rope. Since the rope is capable of carrying only a single tensile force in the direction of its longitudinal axis, the tensile force in the rope must equal the difference between the upward buoyancy force and the downward object weight. All three of these forces are vertical (the rope force must be vertical since the weight and buoyancy force are both vertical), and setting the summation of moments equal to zero will give the relative positions of c, cg and the point at which the rope is attached to the body. For instance, if the object is homogeneous, then c and cg and the point of rope attachment all lie along the same vertical line.
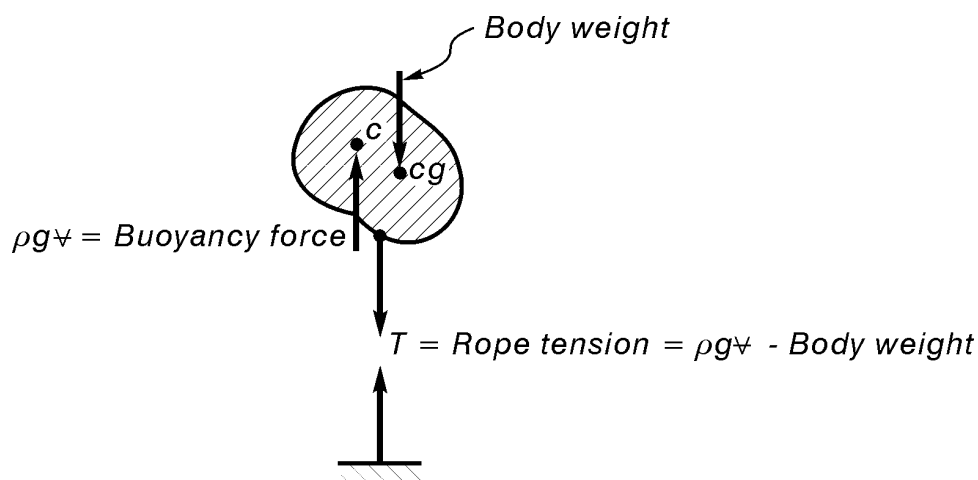
Figure 3.8 Forces acting on an object tethered by a single rope.

The problem for an object floating on a free surface differs from the problem for a completely submerged object in two ways. First, the object weight and the buoyancy force are usually the only two external forces acting on the floating body. This means that these two forces must be equal in magnitude, opposite in direction and have the same line of action in order to ensure that the resultant force and moment both vanish. Second, the volume of fluid that is used to calculate the buoyancy force and its line of action has the same geometry as the wetted surface of the floating object when closed with a plane of zero fluid pressure that coincides with the free surface. An example is shown in Figure 3.9.
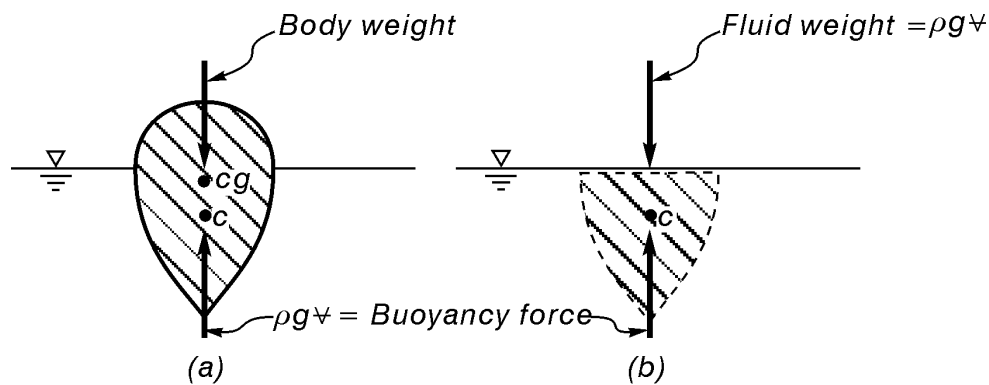
Figure 3.9 Forces on (a) a floating object and (b) the volume of fluid used to calculate the corresponding buoyancy force on the floating object.

Example 3.10

It is believed that Archimedes discovered the buoyancy laws about 200 B.C. when asked by King Hiero of Syracuyse to determine if his new crown contained the stipulated amount of gold. Show how this could be done for pure gold by first weighing the crown in air, which has a density small enough relative to gold to be neglected, and then in water, which has a density relative to gold of 0.052.

Solution: The weight of the crown in any fluid is identical with the tension in a string when the crown is suspended in the fluid by the string. If we denote the string tension in air and water by T_a and T_w, respectively, and if we consider the buoyancy force in air small enough to be neglected, then free body diagrams for the crown in air and water are as follows:
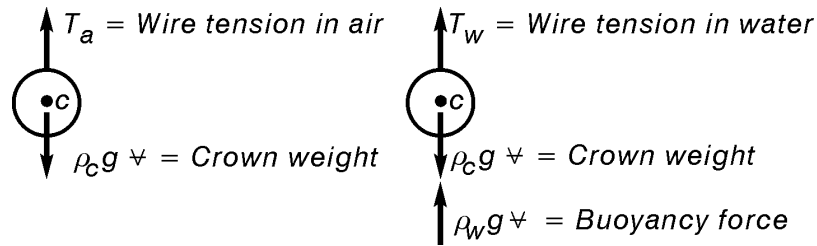
Summing forces in air and then in water gives

$$T_a = \rho_c \, g \, \forall$$

$$T_w = \rho_c \, g \, \forall - \rho_w \, g \, \forall$$

Elimination of $g\forall$ from these two equations gives

$$\boxed{\frac{T_w}{T_a} = 1 - \frac{\rho_w}{\rho_c}}$$

Thus, a measured value of T_w/T_a allows the calculation of ρ_w/ρ_c, which could then be compared with the value of 0.052 that is known for gold.

Example 3.11

Given: ρ, ρ_c, a and H.
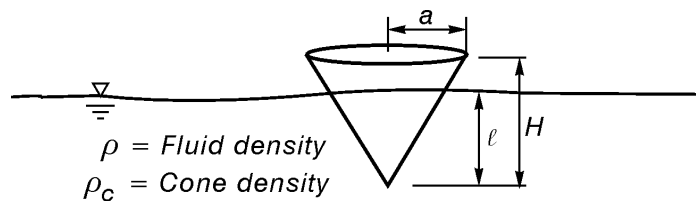
Calculate: ℓ

Solution: Since the volume of a right circular cone with a base radius r and height h is $\pi r^2 h/3$, and since the buoyancy is calculated by using a cone of height ℓ while the cone weight is calculated for a cone of height H, we obtain the following free body diagram:

$$\rho_c \, g \, \pi a^2 H/3 = \text{Cone weight}$$

$$\rho g \, \pi \left(\tfrac{a}{H} \ell\right)^2 \ell/3 = \text{Buoyancy force}$$
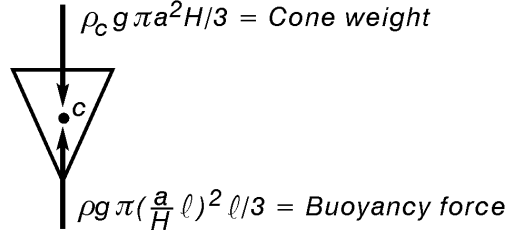
where $a\ell/H$ is the cone radius in the plane of the free surface.

Summing forces in the vertical direction gives

$$\rho g \pi \left(\frac{a}{H} \ell \right)^2 \ell/3 \;=\; \rho_c \, g \pi a^2 H /3$$

from which we calculate

$$\ell \;=\; \boxed{\left(\rho_c / \rho\right)^{1/3} H}$$

We will see in the next section that the cone may or may not be stable in this position.

Stability of Floating Bodies

Not all equilibrium configurations are stable. As in all stability theory, the stability of a floating body is tested by subjecting the body to a small disturbance. This disturbance, which takes the form of a small rotation, creates a change in the system of forces acting on the body. If this new system of forces acts to force the body back into its initial configuration, then the initial configuration is said to be stable. However, if the new system of forces acts to further increase the disturbance, then the initial configuration is unstable.
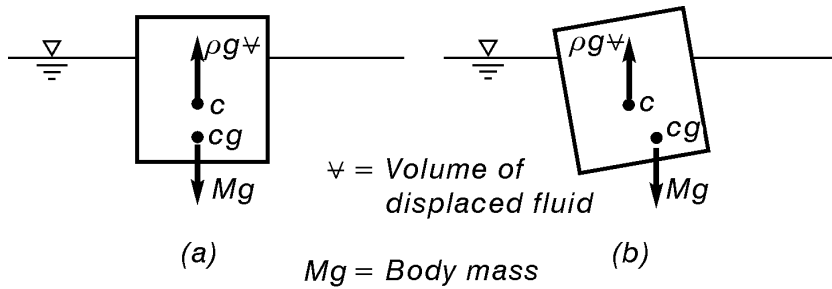
Figure 3.10 An example of stable equilibrium.

As an example of stable equilibrium, consider the body shown in Figure 3.10(a). The volume centroid of the displaced fluid, c, has the force $\rho g \forall$ acting through it. This is the resultant of pressure stresses acting over the wetted surface area of the body and is the buoyancy force. The mass centroid, cg, of the floating body has the body weight, Mg, acting through it. Both c and cg lie along the same vertical line, and, since $\rho g \forall = Mg$, Figure 3.10(a) is an equilibrium configuration.

To test the configuration in Figure 3.10(a) for stability, the body is given a small angular displacement, as shown in Figure 3.10(b). The mass centroid, cg, is fixed in the body and, therefore, rotates with it. However, the volume centroid, c, of the displaced fluid moves leftward as a result in the change in geometry of $\forall$. The resulting couple from the forces shown in Figure 3.10(b) would act to cause the body to rotate in the clockwise direction back toward the initial configuration shown in Figure 3.10(a). Thus, Figure 3.10(a) shows an example of stable equilibrium. In general, any floating object that has cg below c will be in stable equilibrium.
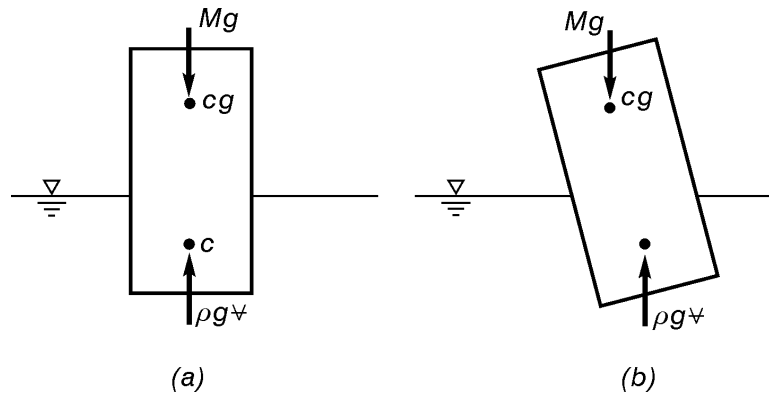
Figure 3.11 An example of unstable equilibrium.

An example of unstable equilibrium is shown in Figure 3.11. An equilibrium configuration is shown in Figure 3.11(a) since c and cg lie along the same vertical line and since $\rho g \forall = Mg$. In this case, a small rotation creates the force system shown in Figure 3.11(b). Since c lies to the right of cg in Figure 3.11(b), the couple created by $\rho g \forall$ and Mg is in the counterclockwise direction and acts to cause the body to rotate further from the equilibrium configuration shown in Figure 3.11(a). Thus, Figure 3.11(a) shows an unstable equilibrium configuration.
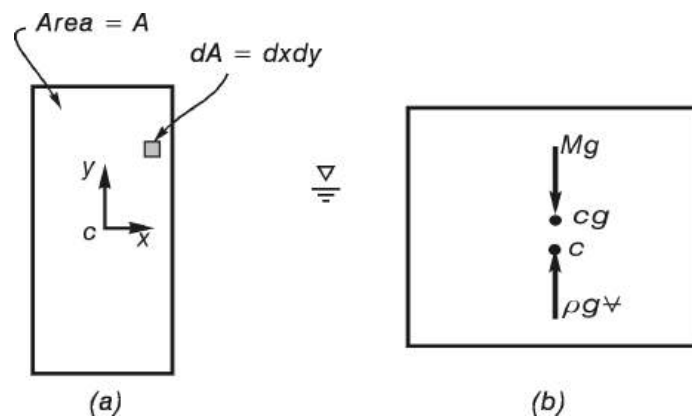
Figure 3.12 A floating body shown (a) in plan view and (b) in elevation view.

The example considered in Figure 3.11 might tempt a student to conclude that all equilibrium configurations in which cg lies above c are unstable. Figures 3.12 and 3.13, however can be used to show that this is incorrect. Figure 3.12 shows a floating body in which cg lies above c. Figure 3.13 shows the same body after being rotated a small angle, θ. If c lies to the left of cg when the rotation is counterclockwise, as shown in Figure 3.13(a), then the resulting couple will be in the clockwise direction and the equilibrium configuration shown in Figure 3.12(b) will be stable. This is quantified by calculating the distance ℓ in Figure 3.13(a) and comparing ℓ with the vertical distance between cg and c in Figure 3.12(b).
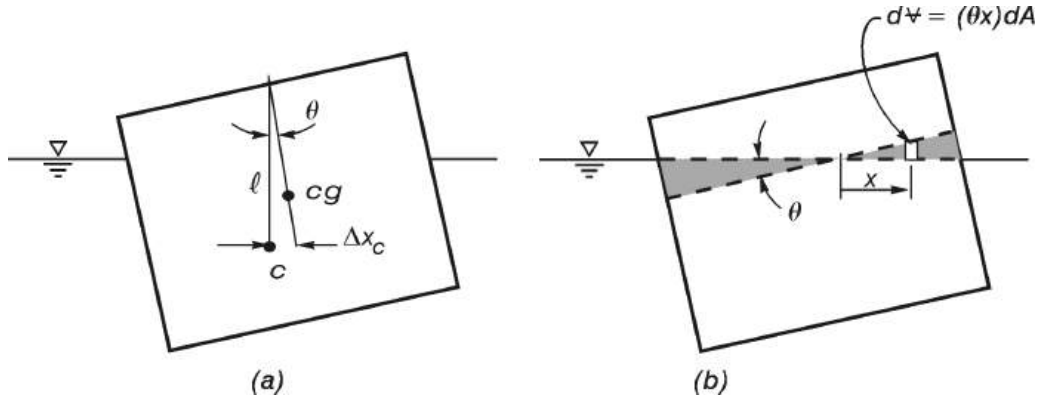
Figure 3.13 The object in Figure 3.12 after rotating a small angle, θ.

The difference between ℓ and the vertical distance between cg and c is called the metacentric height. A positive metacentric height indicates stability, and a negative metacentric height indicates instability.

Since θ is very small, the distance Δx_c that the volume centroid, c, moves when the body is rotated is seen from Figure 3.13(a) to be

$$\Delta x_c = \ell\theta \tag{3.21}$$

But Δx_c can also be calculated by considering the location of c before and after rotation. Before rotation, c coincides with the coordinate origin in Figure 3.12 and

$$0 = \int_{\forall_1} x \, d\forall \tag{3.22}$$

in which $\forall_1$ = volume of displaced fluid before rotation. After rotation, Δx_c in Figure 3.13(a) is the new x coordinate of c in the displaced fluid and is given by

$$\forall_2 \, \Delta x_c = \int_{\forall_2} x \, d\forall \tag{3.23}$$

in which $\forall_2$ = volume of displaced fluid after rotation. Subtracting (3.22) from (3.23) gives

$$\forall_2 \Delta x_c = \int_{\forall_2} x \, d\forall - \int_{\forall_1} x \, d\forall = \int_{\forall_2 - \forall_1} x \, d\forall \tag{3.24}$$

in which $\forall_2 - \forall_1$ is the shaded region near the free surface that is shown in Figure 3.13(b). In this region $d\forall$ is given by

$$d \forall = (\theta x) dA \qquad (3.25)$$

in which dA is the area of a small element in the (x, y) plane that is shown in Figures 3.12(a) and 3.13(b). Substituting (3.25) into (3.24) and then eliminating Δx_c between the result and (3.21) gives

$$\ell = \frac{1}{\forall_2} \int_A x^2 \, dA \qquad (3.26)$$

Although $\forall_1$ and $\forall_2$ have different geometries, their magnitudes are identical. Furthermore, the integral in (3.26) is the moment of inertia denoted by I_y. Therefore (3.26) can be written more compactly as

$$\ell = I_y / \forall \qquad (3.27)$$

where I_y is calculated in the plane of the free surface when $\theta = 0$.

If δ = vertical distance between c and cg, then the metacentric height, m_c, is given by

$$m_c = \ell - \delta = I_y / \forall - \delta \qquad (3.28)$$

A positive value for m_c denotes stability, and a negative value denotes instability.

The (x, y) plane, which is the plane in which I_y is calculated in (3.28), coincides with the plane of the free surface, and the value of m_c calculated from (3.28) is a quantitative measure of the stability of a floating body for a small rotation about the y axis. However, there was nothing in the derivation of (3.28) which determined the direction that the y axis must point. Clearly, the worst case occurs when the y axis points in a direction that makes I_y a minimum. The moments and product of inertia are components of a two-dimensional matrix or tensor, I.

$$I = \begin{bmatrix} I_x & I_{xy} \\ I_{xy} & I_y \end{bmatrix} \qquad (3.29)$$

A mathematical development like the one used by Fung (1969) for the two-dimensional stress matrix can be used to show that I_y has its minimum value when (1) the (x, y) axes are a set of principal axes so that $I_{xy} = 0$ and (2) the y axis parallels the direction of the largest dimension of A. Then (3.28) will give the smallest value for m_c.

Example 3.12
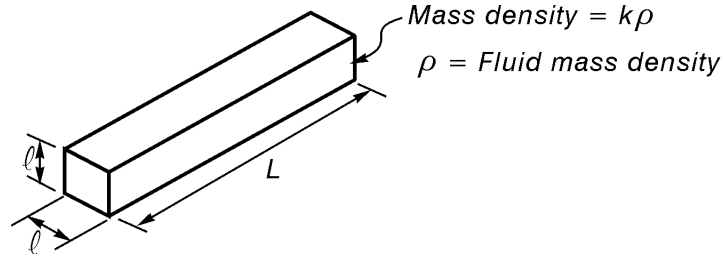
The homogeneous body shown above has a mass density $\kappa\rho$ in which ρ = fluid mass density. If ρ and the dimensions ℓ and L are given, calculate the range of values for κ that will allow the body to float with its lateral faces vertical.
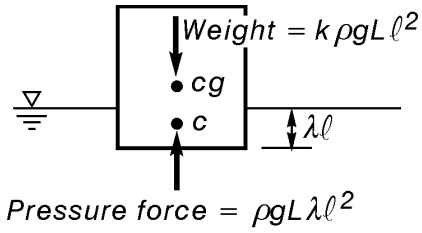
Solution: If the bottom of the body is a depth $\lambda\ell$ below the free surface, then equating the object weight to the pressure force gives

$$\kappa\rho g L \ell^2 \;=\; \rho g L \lambda \ell^2$$

$$\therefore \quad \lambda \;=\; \kappa$$

From this we see that the volume of displaced fluid is

$$\forall \;=\; L\ell(\lambda\ell) \;=\; \kappa L \ell^2$$

The body will be stable if $m_c > 0$. Thus, (3.28) gives

$$I_y/\forall \,-\, \delta \,>\, 0$$

Since δ = vertical distance between cg and c, we have

$$\delta \;=\; \ell/2 \,-\, \lambda\ell/2 \;=\; \ell/2 \,-\, \kappa\ell/2 \;=\; (1-\kappa)\ell/2$$

$$\therefore \quad I_y \;>\; \forall\delta \;=\; (\kappa L \ell^2)(1-\kappa)\ell/2$$

We want the minimum value for I_y. This means that we must choose a set of centroidal axes with the y axis parallel to the direction of largest dimension of the A, as shown below.
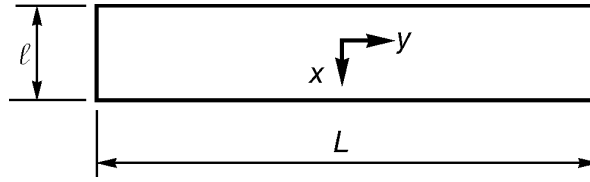
$$I_y = \int_A x^2\, dA = \frac{1}{12} L\, \ell^3$$

$$\therefore \quad \frac{1}{12} L\, \ell^3 > \kappa L\, \ell^3 (1 - \kappa)/2$$

Dividing an inequality by a positive constant does not change its sense. Thus, dividing by $L\, \ell^3/2$ gives

$$\frac{1}{6} > \kappa(1 - \kappa)$$

Since the body will only float if its density is less than the fluid density, we must also have the restriction

$$0 < \kappa < 1$$

Simultaneous solution of these inequalities gives

$$\boxed{0 < \kappa < \frac{1}{2}\left(1 - \frac{1}{\sqrt{3}}\right)} \quad \text{and} \quad \boxed{\frac{1}{2}\left(1 + \frac{1}{\sqrt{3}}\right) < \kappa < 1}$$

Thus, the body will only float with its lateral faces vertical for values of κ in either of the ranges $0 < \kappa < 0.211$ or $0.789 < \kappa < 1$. For values of κ in the range $0.211 < \kappa < 0.789$ the equilibrium configuration under consideration is unstable, and some other configuration will occur. An experimental confirmation of this result is shown in Figure 3.14.
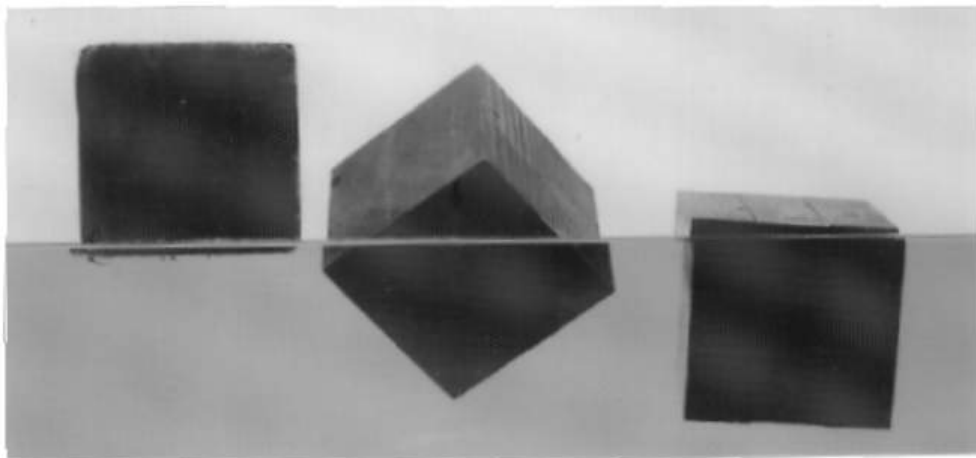
Figure 3.14 Three floating cubes. Values of κ, from left to right, are 0.03, 0.39 and 0.82. The cubes were originally constructed for teaching purposes by Professor Frank Henderson.

Example 3.13

Calculate the relationship between ρ_c and ρ for the cone in Example 3.11 that must be satisfied in order that the equilibirum configuration shown in Example 3.11 be stable.

Solution: Equation (3.28) gives the requirement for stability as

$$I_y / \forall - \delta > 0$$

I_y and $\forall$ are given by

$$I_y = \pi r^4 / 4 = \pi \left(\frac{a}{H} \ell \right)^4 \Big/ 4$$

$$\forall = \pi r^2 h / 3 = \pi \left(\frac{a}{H} \ell \right)^2 \ell / 3$$

The mass centroid of a right circular cone of height H is a distance $H/4$ above its base. Thus, δ is given by

$$\delta = \left(H - \ell + \ell/4 \right) - H/4 = 3(H - \ell)/4$$

Substituting I_y, $\forall$ and δ in the inequality gives

$$\frac{3}{4} \left(\frac{a}{H} \ell \right)^2 \frac{1}{\ell} - \frac{3}{4}(H - \ell) > 0$$

This inequality can be manipulated into the form

$$\frac{\ell}{H} > \frac{1}{1 + (a/H)^2}$$

Inserting the solution for ℓ/H from Example 3.11 gives

$$\frac{\rho_c}{\rho} > \frac{1}{\left[1 + (a/H)^2 \right]^3}$$

Since the cone will only float if $\rho_c / \rho < 1$, we have the stability requirement

$$\boxed{\frac{1}{\left[1 + (a/H)^2 \right]^3} < \frac{\rho_c}{\rho} < 1}$$

Thus, a cone that is too light will violate this inequality, and a different (stable) equilibrium configuration will be found. Also note that a light cone can be made stable by increasing a/H to a sufficiently large value.

Rigid Body Fluid Acceleration

When a container of fluid is accelerated so that no relative motion occurs between fluid particles, we say that the fluid is being accelerated as a rigid body. In this case the viscous stress vector, $\boldsymbol{f}$, vanishes in Eq. (2.18) to give

$$- \nabla p \; + \; \rho \boldsymbol{g} \; = \; \rho \boldsymbol{a} \tag{3.30}$$

in which $\boldsymbol{a} \; = \; D\boldsymbol{V}/Dt = $ fluid acceleration. We will consider two cases. When the container is moving along a straight line, $\boldsymbol{a}$ will be given as the same constant vector for every fluid particle. When the container is rotated about a fixed axis, $\boldsymbol{a}$ will be given as the vector $-r\,\omega^2 \boldsymbol{e}_n$ in which r = radical coordinate, ω = angular velocity of rotation and $\boldsymbol{e}_n$ = unit vector normal to the circular pathlines and pointing toward the axis of rotation, as defined in Eq. (1.24). In either case, the vector $\boldsymbol{a}$ in (3.30) is specified, and (3.30) can be put in the form

$$\nabla p \; = \; \rho \boldsymbol{G} \tag{3.31}$$

in which the vector $\boldsymbol{G}$ is given by

$$\boldsymbol{G} \; = \; \boldsymbol{g} \; - \; \boldsymbol{a} \tag{3.32}$$

If $\boldsymbol{g} \; = \; g_x \boldsymbol{i} \; + \; g_y \boldsymbol{j} \; + \; g_z \boldsymbol{k}$ and $\boldsymbol{a} \; = \; a_x \boldsymbol{i} \; + \; a_y \boldsymbol{j} \; + \; a_z \boldsymbol{k}$, then (3.32) gives

$$G \; = \; |\boldsymbol{G}| \; = \; \sqrt{\left(g_x - a_x\right)^2 \; + \; \left(g_y - a_y\right)^2 \; + \; \left(g_z - a_z\right)^2} \tag{3.33}$$

In applications it will be more convenient to calculate $\boldsymbol{G}$ directly from (3.32) rather than (3.33) since numerous components of $\boldsymbol{g}$ and $\boldsymbol{a}$ are usually zero.

Since ∇p is normal to surfaces of constant p and points in the direction of increasing p, Eq. (3.31) shows that surfaces of constant p are normal to $\boldsymbol{G}$ and that p increases in the direction of $\boldsymbol{G}$. When motion is along a straight line and $\boldsymbol{a}$ is the same constant vector for every fluid particle, then $\boldsymbol{G}$ is a constant vector and surfaces of constant p are ***planes*** perpendicular to $\boldsymbol{G}$. In this case (3.31) and (3.1) are identical if we substitute $\boldsymbol{G}$ for $\boldsymbol{g}$. This means that pressure variations and pressure forces on plane and curved surfaces can be calculated by using the same results obtained for a static fluid reservoir provided that $\boldsymbol{G}$ and G are substituted for $\boldsymbol{g}$ and g and provided that ξ in (3.6) is measured perpendicular to surfaces of constant p in the direction of $\boldsymbol{G}$.

When the container of fluid is rotated about a fixed axis with a constant angular velocity ω, we have $V \; = \; r\,\omega$ and Eq. (1.24) shows that $\boldsymbol{G}$ is a function of r. In this case surfaces of constant p will no longer be plane surfaces, and pressures and forces within the fluid must be calculated by integrating (3.31).

Example 3.14
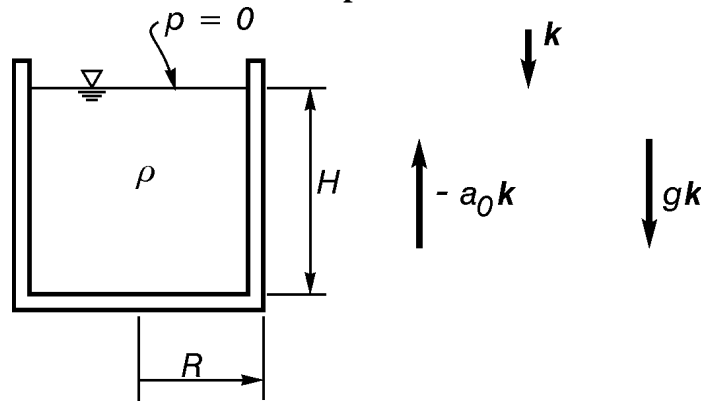
A cylindrical container of liquid (mass density $= \rho$) has a radius R and fluid depth H. Calculate the pressure force on the container bottom if the container is given an acceleration a_0 in the upward direction.

Solution: If k is a unit vector in the downward direction, then $a = -a_0 k$ and $g = g k$.

$$\therefore \quad G = g - a = \left(g + a_0\right)k$$

Surfaces of constant p are normal to G and, therefore, are horizontal surfaces. Since ξ in (3.6) is measured perpendicular to these surfaces and in the direction of G, we will measure ξ downward from the horizontal free surface. Since the equations of statics apply if we replace g with $G = \left(g + a_0\right)$, we obtain

$$p_c = \rho\left(g + a_0\right)H$$

for the pressure at the area centroid of the circular container bottom. The resulting force is

$$F = p_c A k = \boxed{\rho\left(g + a_0\right)H\,\pi R^2 k}$$

In this particular case a_0 may vary with t without changing the essentially rigid body motion of the fluid.

Example 3.15
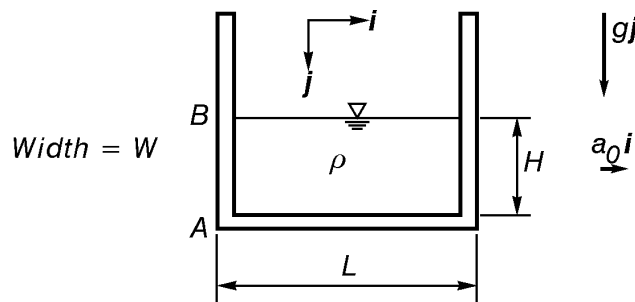
The rectangular container of liquid shown above is given a constant horizontal acceleration $a_0 \boldsymbol{i}$. Calculate the depth of the liquid along AB, to ensure that liquid is not lost, and the force created on AB if the tank has a width W.

Solution: Using the unit base vectors $\boldsymbol{i}$ and $\boldsymbol{j}$ shown in the sketch, we obtain

$$\boldsymbol{G} = \boldsymbol{g} - \boldsymbol{a} = g\boldsymbol{j} - a_0\boldsymbol{i} \text{ and } G = \sqrt{g^2 + a_0^2}$$

Surfaces of constant p are perpendicular to $\boldsymbol{G}$ and are shown in the following sketch with dashed lines:
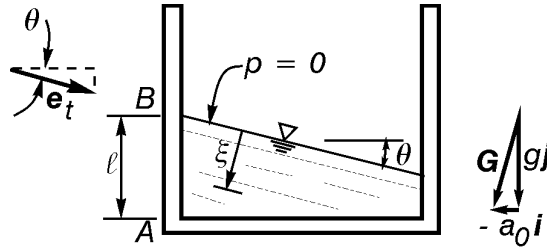
A vector tangent to surfaces of constant p is

$$\boldsymbol{e}_t = \boldsymbol{i} \cos\theta + \boldsymbol{j} \sin\theta$$

Since we must have $\boldsymbol{G} \cdot \boldsymbol{e}_t = 0$, we obtain

$$- a_0\cos\theta + g \sin\theta = 0$$

or

$$\boxed{\tan\theta = \frac{a_0}{g}}$$

The configuration shown in the sketch only applies if $\tan\theta = a_0/g \leq \ell/L$. In this case, since we must always have the same volume of fluid that we started with, and since the free surface tilts as a plane surface, the distance ℓ between A and B is

$$\ell = H + (L/2)\tan\theta = \boxed{H + (L/2)(a_0/g)}$$

The pressure on the area centroid of AB is

$$p_c = \rho G \xi_c = \rho\sqrt{g^2 + a_0^2}\ (\ell/2)\cos\theta$$

But $\cos\theta = g \Big/ \sqrt{g^2 + a_0^2}$
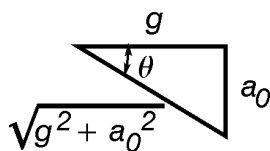
$$\therefore \quad p_c = \rho g\, \ell/2 = \rho g\big[H + (L/2)(a_0/g)\big]/2$$

$$\boldsymbol{F}_{AB} = -p_c A\boldsymbol{i} = -p_c \ell W\boldsymbol{i} = \boxed{-\rho g W\big[H + (L/2)(a_0/g)\big]^2 \Big/ 2}$$
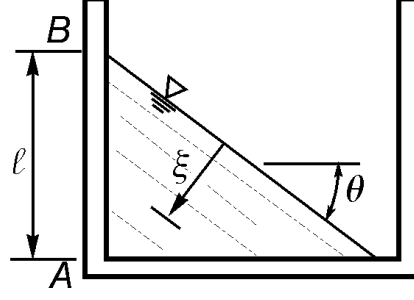
When accelerations are large enough to satisfy $\tan\theta = a_0/g \geq \ell/L$, the geometry of the free surface and surfaces of constant pressure change to those shown in the sketch. In this case, equating the volume of accelerated liquid to its volume at rest gives

$$\frac{1}{2}\, \frac{\ell^2 W}{\tan\theta} = HLW$$

$$\therefore \quad \ell = \sqrt{2HL\tan\theta} = \boxed{\sqrt{2HLa_0/g}}$$

As before, the pressure on the area centroid is

$$p_c = \rho\, G\, \xi_c = \rho\sqrt{g^2 + a_0^2}\, (\ell/2)\cos\theta$$

in which

$$\cos\theta = g\bigg/\sqrt{g^2 + a_0^2}$$

$$\therefore \quad p_c = \rho g \ell/2$$

$$\boldsymbol{F}_{AB} = -p_c A\boldsymbol{i} = -p_c \ell W \boldsymbol{i} = -\left(\rho g W \ell^2/2\right)\boldsymbol{i}$$

$$\therefore \quad \boldsymbol{F}_{AB} = \boxed{-\rho\, WHL\, a_0\, \boldsymbol{i}}$$

This result is not surprising. Since *AB* is the only vertical surface that can create a force in the $\boldsymbol{i}$ direction on the fluid, this pressure force is simply the product of the total mass of fluid with its horizontal acceleration.

Example 3.16

$p = p_0$

$a_0 i$

$g j$
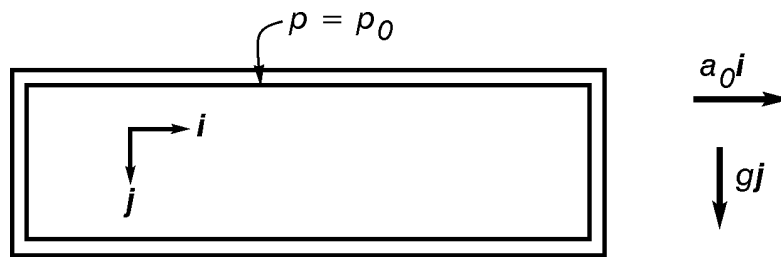
An enclosed tank of liquid has $p = p_0$ at its top when the tank and fluid are motionless. Give a qualitative description of the pressure distribution after the tank is given a horizontal acceleration $a = a_0 i$.

Solution: Since $G = g - a = -a_0 i + g j$, surfaces of constant pressure are as shown in the following sketch:

$p = constant$

$-a_0 i$

g

G
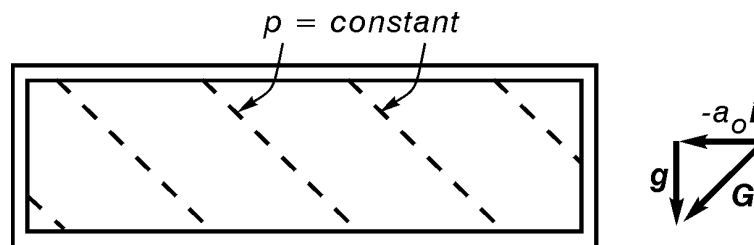
Since pressures increase in the direction of G, pressures are a minimum at the upper right-hand corner and a maximum at the lower left-hand corner. The integration of (3.31) to calculate unique values for pressures requires specification of pressure as a function of time at one point in the fluid. This is accomplished in most instances by either including a free surface or else by venting the tank to the atmosphere at one point. If no free surface or vent exists, a unique answer for the pressure distribution can be calculated only by including elastic effects in the fluid and tank walls. This procedure, which is carried out in Chapter 13 for unsteady pipe flow, introduces time derivatives of pressure into the problem and allows future pressure distributions to be calculated from specification of the initial hydrostatic distribution that exists when motion starts.

Example 3.17

ω

ρ

H

R
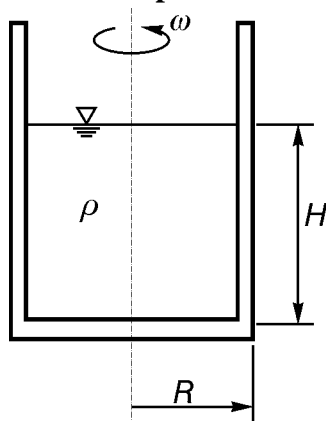
A cylindrical tank of liquid is spun with a constant angular velocity, ω, about a vertical axis through its centre. Calculate the equation of the free surface and the pressure distribution within the tank if the fluid rotates with the tank as a rigid body $(V = r\omega)$.

Solution:

z

e_z

e_θ

r

θ

e_r

y

x
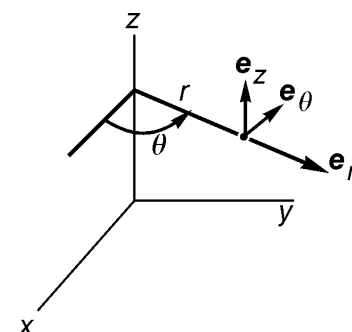
If we use the cylindrical coordinate system shown in the sketch, then Eq. (1.24) gives

$$\mathbf{a} = -\frac{V^2}{r}\mathbf{e}_r = -r\omega^2\mathbf{e}_r$$

$$\therefore \quad \mathbf{G} = \mathbf{g} - \mathbf{a} = -g\mathbf{e}_z - \left(-r\omega^2\mathbf{e}_r\right) = r\omega^2\mathbf{e}_r - g\mathbf{e}_z$$

The components of ∇p in cylindrical coordinates are shown by Hildebrand (1976) to be

$$\nabla p = \frac{\partial p}{\partial r}\mathbf{e}_r + \frac{1}{r}\frac{\partial p}{\partial\theta}\mathbf{e}_\theta + \frac{\partial p}{\partial z}\mathbf{e}_z$$

Since $\mathbf{G} = \mathbf{G}(r)$, surfaces of constant p are not plane surfaces. Putting the equations for $\mathbf{G}$ and ∇p into Eq. (3.31) and dotting both sides of the equation with $\mathbf{e}_r$, $\mathbf{e}_\theta$ and $\mathbf{e}_z$ gives three scalar equations.

$$\frac{\partial p}{\partial r} = \rho r\omega^2$$

$$\frac{1}{r}\frac{\partial p}{\partial\theta} = 0$$

$$\frac{\partial p}{\partial z} = -\rho g$$

The second equation shows that $p = p(r, z)$ only, and the first and second equations have a solution for p since

$$\frac{\partial^2 p}{\partial z\partial r} = \frac{\partial^2 p}{\partial r\partial z}$$

This condition is identical with the compatibility requirement that $\nabla\times\nabla p = 0$, as discussed at the end of Chapter 1.

Integration of the first equation gives

$$p = \frac{\rho}{2}r^2\omega^2 + F(z)$$

Substitution of this result for p into the third equation gives an equation for $F(z)$.

$$\frac{dF(z)}{\partial z} = -\rho g$$

$$\therefore \quad F(z) = -\rho g z + C$$

and
$$\boxed{p = \frac{\rho}{2}r^2\omega^2 - \rho g z + C}$$

The equation of the free surface is obtained by setting $p = 0$.

$$0 = \frac{\rho}{2} r^2 \omega^2 - \rho g z + C$$

Thus, the free surface is a parabola of revolution, and C is determined by requiring that the volumes in the motionless and spinning fluid be identical.

$$\pi R^2 H = \int_0^{2\pi} \int_0^R \int_0^{z(r)} dz \, r \, dr \, d\theta$$

in which $z(r) = \dfrac{C}{\rho g} + \dfrac{r^2 \omega^2}{2g}$. Integration gives

$$\pi R^2 H = \left(\frac{CR^2}{2\rho g} + \frac{R^4 \omega^2}{8g} \right) 2\pi$$

$$\therefore \quad C = \rho g H - \frac{\rho}{4} R^2 \omega^2$$

References

Fung, Y.C. 1969. *A first course in continuum mechanics*, Prentice-Hall, Englewood Cliffs, N.J., pp. 70-73.

Hildebrand, F.B. 1976. *Advanced calculus for applications*, second edition, Prentice-Hall, Englewood Cliffs, N.J., p. 312.

Chapter 4

Control Volume Methods

This chapter uses control volume forms of the governing equations to solve problems involving fluid motion. These equations are relatively few in number and include the continuity equation, (2.1),

$$\int_S V \cdot e_n \, dS = 0 \tag{4.1}$$

the momentum equation, (2.33),

$$F = \int_S \rho V(V \cdot e_n) \, dS + \frac{d}{dt} \int_\forall \rho V \, d\forall \tag{4.2}$$

and the Bernoulli equation, (2.40),

$$h_1 + \frac{V_1^2}{2g} = h_2 + \frac{V_2^2}{2g} \tag{4.3}$$

in which the piezometric head, $h,$ is defined by (2.22) and Figure 3.1 to be

$$h = \frac{p}{\rho g} - e_g \cdot r = \frac{p}{\rho g} - \xi \tag{4.4}$$

The variable ξ is a vertical coordinate that is positive in the downward direction. If it is decided instead to define ξ as positive in the upward direction, then the minus sign in front of ξ in (4.4) must be replaced with a plus sign. In many texts k points upward and h becomes $p/\rho g + z.$

Although the equations that are used in control volume analysis are few in number, the effective use of these equations in applications requires a subtle blend of mathematical skill and physical insight. This combination of talents, which makes the study of fluid mechanics both interesting and challenging, is probably best taught by using a combination of worked examples and student homework problems. However, there are a few general points that can be discussed before working a series of specific examples.

We will only apply control volume equations to problems in steady flow. It was pointed out in Chapter 1 that steady flow occurs when the vector velocity field does not change with time. One consequence of this assumption, which has already been made in the derivation of (4.3), is that streamlines and fluid particle pathlines coincide. The $V \cdot e_n$ terms that appear in both (4.1) and (4.2) vanish along any portions of S that coincide with streamlines or stream surfaces (since V is tangent to these lines and surfaces). A second important consequence is that the last term in (4.2) vanishes, and the momentum equation reduces to

$$ F = \int_S \rho V \left(V \cdot e_n \right) dS $$

(4.5)

One of the keys to developing skill in working control volume problems is to make a neat and qualitatively correct sketch of both the control volume and internal streamline pattern. The control volume boundary, S, is often chosen so that it is a combination of streamlines or stream surfaces, along which $V \cdot e_n = 0$, and surfaces normal to the streamlines in regions of uniform flow, where V can be approximated with a vector that has both a constant magnitude and direction. An example of this is shown in Figure 4.2. Furthermore, since the acceleration is shown by (1.24) to have a zero component normal to streamlines in uniform flow, dotting both sides of (2.27) with e_n and using the directional derivative (1.44) shows that

$$ -g \frac{dh}{dn} = 0 $$

(4.6)

in which n = arc length normal to the streamlines in a region of uniform flow. Thus, h is not changing in the direction of n when streamlines have zero curvature. In other words, pressures are distributed hydrostatically across streamlines in regions of uniform flow, and the principles that were covered in Chapter 3 can be used to calculate pressure forces on portions of S that lie within these regions.

The deceptively simple looking Bernoulli equation, (4.3), has sometimes been described as the most misused equation in fluid mechanics. Its derivation, which was given in Chapter 2, assumes that the flow is steady and that points 1 and 2 lie on the same streamline. One classical case of its correct use is shown in Figure 4.1, in which a Pitot tube is used to measure the velocity at point 1.
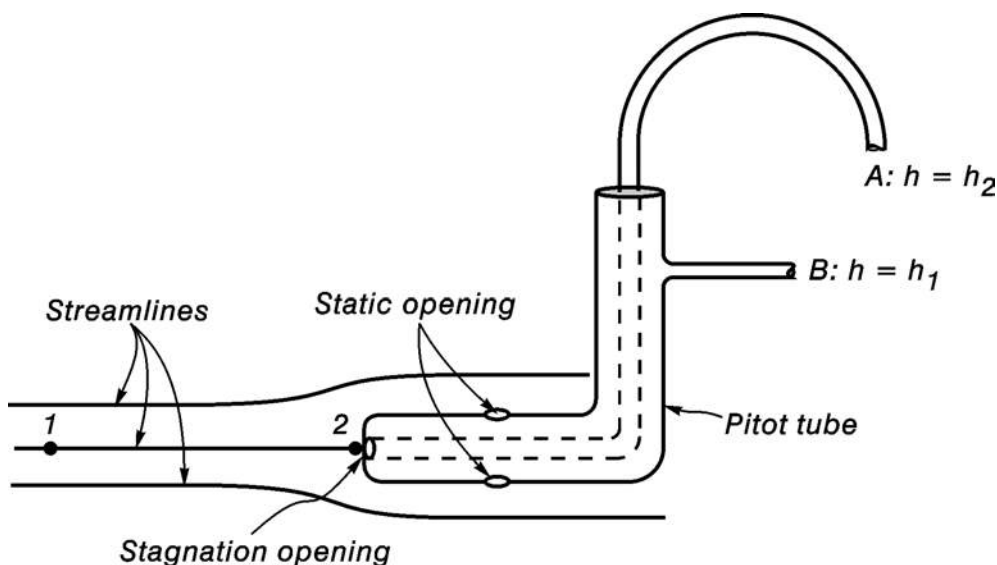
Figure 4.1 A sketch of a Pitot tube and surrounding streamlines.

Point 2 lies on the same streamline as point 1 and is directly in front of the stagnation opening, where the velocity is zero. (The flow on the Pitot tube nose is radial and away from point 2, and symmetry requires that the velocity stagnate or vanish at point 2.) Thus, an application of (4.3) with $V_2 = 0$ gives

$$V_1 = \sqrt{2g(h_2 - h_1)} \tag{4.7}$$

The static openings are located far enough downstream from the Pitot tube nose to be in a region of uniform flow. Therefore, (4.6) applies and the value of h at the static opening equals the value of h in the undisturbed flow. Thus, the static tube measures h_1, and connecting the stagnation tube, A, and the static tube, B, to piezometers allows $h_2 - h_1$ to be measured and inserted in (4.7) to calculate V_1. This principle is probably the simplest, most direct, most accurate and most used method for measuring flow velocities. For example, stagnation tubes are sometimes placed in low speed airplanes for measuring air speeds. In this case, a flow that is unsteady when viewed from a fixed point on the ground becomes steady when viewed from the moving cockpit, where the stagnation and static values of h are read.

By substituting (4.4) into (4.3) and multiplying both sides of the resulting equation by ρg we obtain the following alternative form of the Bernoulli equation:

$$p_1 - \rho g \xi_1 + \frac{\rho}{2} V_1^2 = p_2 - \rho g \xi_2 + \frac{\rho}{2} V_2^2 \tag{4.8}$$

In many flows gravity is neglected $(g = 0)$ by omitting the $\rho g \xi$ terms in (4.8). Formal justification for this can be obtained by manipulating (4.8) into the following form:

$$\frac{p_1 - p_2}{\rho V_1^2 / 2} = \left(\frac{V_2}{V_1} \right)^2 - 1 + \frac{2g(\xi_1 - \xi_2)}{V_1^2} \tag{4.9}$$

The last two terms in (4.9) show that we may omit the term containing g if, and only if,

$$\frac{2g |\xi_1 - \xi_2|}{V_1^2} << 1 \tag{4.10}$$

This usually occurs for high speed flows of a gas or liquid when changes in ξ are not too large. For example, along a free streamline of a high speed jet we might have $|\xi_1 - \xi_2| = 0.1$ m and $V_1 = 10$ m/s. Then we calculate

$$\frac{2g |\xi_1 - \xi_2|}{V_1^2} = \frac{2(9.81)(0.1)}{(10)^2} = 0.0196 \tag{4.11}$$

Since this number is small compared with unity, we would be justified in setting $g = 0$ in either (4.8) or (4.9). Since pressures are also constant along a free streamline (a line or surface of atmospheric pressure), either (4.8) or (4.9) shows that velocities are constant along a free streamline $(V_2 = V_1)$ when gravity is neglected. This approximation is often made in working control volume problems involving high speed liquid jets.
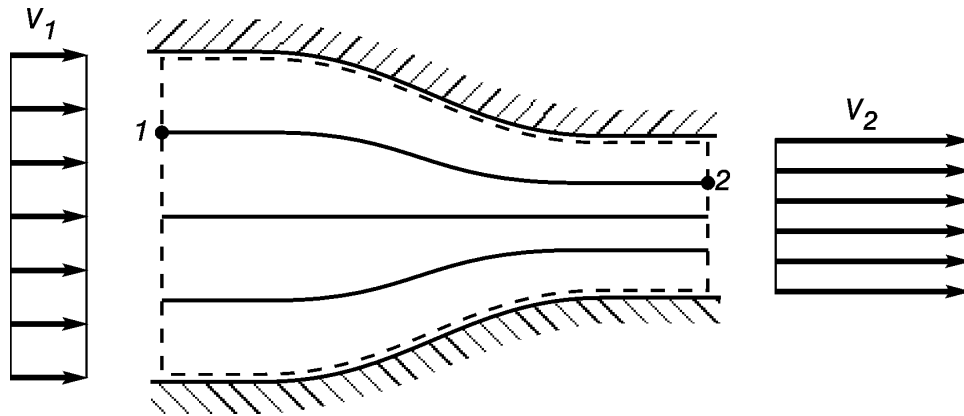
Figure 4.2 Flow in a streamlined constriction. The control volume surface, S, is shown with a dashed line.

Flow through the streamlined constriction shown in Figure 4.2 is a simple but typical example of a flow in which control volume methods are used routinely. Boundary surfaces of the control volume either coincide with streamlines or are located at the two end sections in regions of uniform flow, where the streamlines are straight and parallel. Equation (4.6) shows that hydrostatic pressure distributions occur at each of the two end cross sections. Therefore, the pressure force on each end cross section is the product of the centreline pressure [p_c in Eq. (3.14)] with the area of the cross section. We also assume constant, or uniform, velocity distributions at each of these two end cross sections, an approximation that is often called a "one-dimensional flow approximation". Thus, since h and V are both constant across each cross section located in uniform flow, the application of (4.3) along any of the streamlines joining these two cross sections gives exactly the same result. If instead we apply (4.8), then p will vary across each cross section as $\rho g \xi$ varies, but the sum $p - \rho g \xi$ will be the same constant for any point in the cross section because of the hydrostatic pressure distribution indicated by Eq. (4.6).

Finally, it remains to discuss the occurrence of energy losses in flows. Equations (4.3) and (4.8) can be described as work-energy equations in which the sum of work done by pressure and gravity in moving a fluid particle from point 1 to point 2 equals the change in kinetic energy between these same two points. Work done by tangential stresses has been ignored. Thus, if work done by tangential stresses becomes relatively large, then Eqs. (4.3) and (4.8) either cannot be used or else must be modified to account for this work. These modifications take the following forms:

$$h_1 + \frac{V_1^2}{2g} = h_2 + \frac{V_2^2}{2g} + H_L \qquad\qquad (4.12)$$

$$p_1 - \rho g \xi_1 + \frac{\rho}{2} V_1^2 = p_2 - \rho g \xi_2 + \frac{\rho}{2} V_2^2 + E_L \qquad\qquad (4.13)$$

in which H_L and $E_L = \rho g H_L$ are described as a head-loss term and an energy-loss term, respectively. Point 2 is downstream from point 1, so that H_L and E_L are always positive. This is because the tangential stresses being considered are passive stresses that can only subtract energy from a flow as it proceeds downstream.

There are two instances in which H_L and E_L often become too large to ignore. In the first instance, tangential stresses may be small but the work done by these stresses accumulates to a sizeable value within a control volume that has a large length to width ratio. Examples of this occur in flow through pipes and flow in rivers and canals where control volume length to width ratios may be of the order of 100, 1000 or more. The second instance usually occurs in decelerating flow, where streamlines diverge and flow separation and highly turbulent flow exist. For example, if the direction of flow in Figure 4.2 is reversed, flow is likely to separate from the diverging boundaries and the flow tends to become highly turbulent,[*] as shown in Figure 4.3. A transfer of energy from the main flow into the many vortices creates an energy loss in the main flow. These energy losses, which occur over relatively short distances, are often called "local" or "minor" losses. (Although they may not be minor in the sense of being relatively small.) The first type of loss, which occurs within relatively long control volumes, is often referred to either as a "resistance" or "friction" loss.
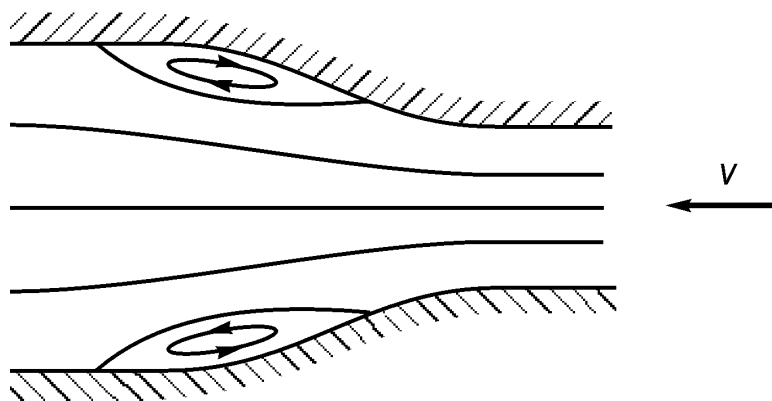
Figure 4.3 Flow in an expansion.

Energy losses do not have a direct influence upon the use of either the continuity equation, (4.1), or the momentum equation, (4.2). In fact we will use these two equations to calculate energy losses in a few flows. However, energy losses can have an indirect influence on the accuracy of approximation when the continuity and momentum equations are applied. This is because large local losses invariably occur as a result of fluid decelerations, and fluid decelerations usually cause increased departures from the one-dimensional velocity distributions that are assumed in evaluating the surface integrals in (4.1) and (4.2). For example, behaviours for experimental velocity distributions in Figures 4.2 and 4.3 are shown in Figures 4.4 and 4.5, respectively. In these sketches it is seen that the rapid accelerations that occur in Figure 4.4 create a downstream velocity distribution that is relatively close to the one-dimensional approximation pictures in Figure 4.2. The decelerating flow in Figure 4.5, however, has a downstream velocity distribution that departs much more markedly from its one-dimensional approximation.

---

[*]   Turbulence is a highly disorganized state of flow that occurs when a flow becomes unstable. Looked at closely, it consists of many vortices of differing sizes and intensities superimposed on the main flow pattern. The net effect of turbulence is to create both lateral mixing of the flow and energy dissipation. Turbulence will be studied in more detail later in the text.
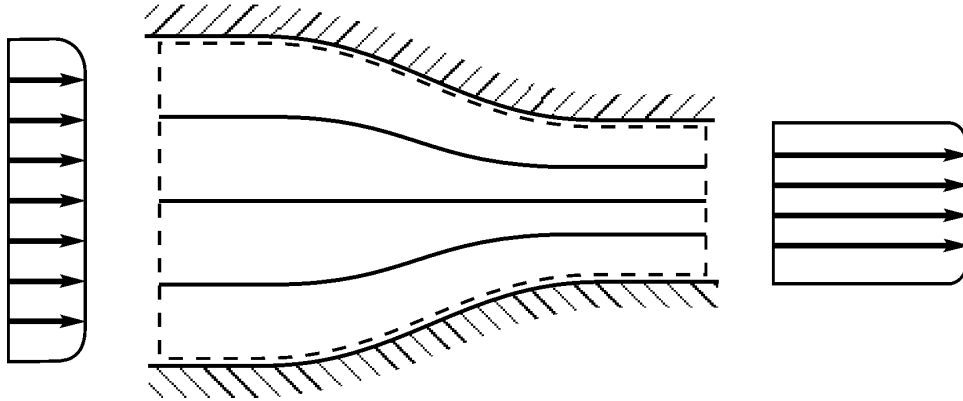
Figure 4.4 A sketch of experimental velocity distributions that occur for highly accelerated flow through a streamlined constriction.
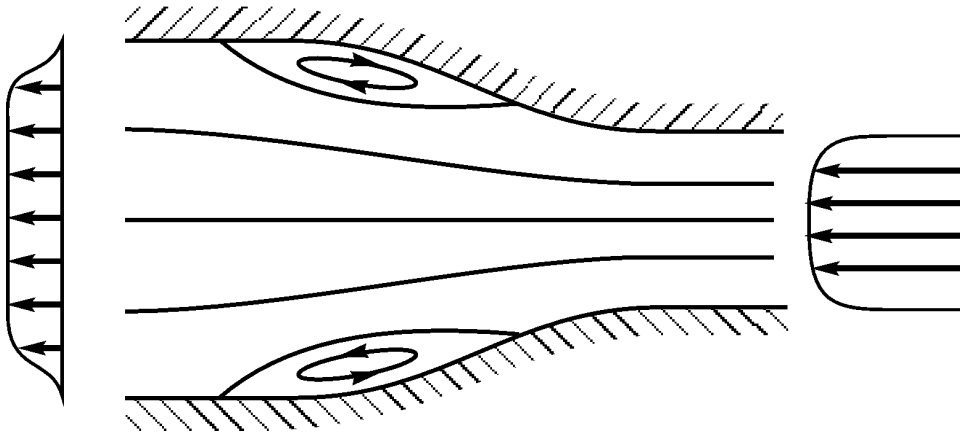
Figure 4.5 A sketch of experimental velocity distributions that occur for decelerated flow through an expansion.

Example 4.1

Suppose that the flow in Figure 4.2 has known values for the flow rate, Q, the cross sectional areas A_1 and A_2 and the pressure p_{c_1} at the intersection of the centre streamline with the area A_1. We will calculate the velocities V_1 and V_2, the pressure p_{c_2} at the intersection of the centre streamline with the area A_2 and the force that the conduit walls exert upon the flow. This force, of course, is equal in magnitude and opposite in direction to the force that the flow exerts upon the conduit walls, and the conduit walls and joints must be designed to withstand the stresses created by this force.

Solution: Since $\mathbf{V} \cdot \mathbf{e}_n = 0$ along the conduit boundary, and since $\mathbf{V} \cdot \mathbf{e}_n = -V_1$ on A_1 and $\mathbf{V} \cdot \mathbf{e}_n = V_2$ on A_2, an application of the continuity equation (4.1) to the control volume shown with a dashed line in Figure 4.2 gives

$$- A_1 V_1 + A_2 V_2 = 0$$

Since the flow rate, Q, is the product of an area with the velocity component normal to the area, this equation can be written as

$$A_1 V_1 = A_2 V_2 = Q$$

from which we obtain

$$\boxed{V_1 = \frac{Q}{A_1}} \text{ and } \boxed{V_2 = \frac{Q}{A_2}}$$

in which Q is the known flow rate that is usually measured in units of m^3/s.

We will assume that the centre streamline passes through the area centroids of A_1 and A_2, which will be true if the conduit is either an axisymmetric pipe or a rectangular duct. Then p_{c_1} and p_{c_2} are pressures at two points of the same streamline, and an application of the Bernoulli equation, (4.3) or (4.8), gives

$$p_{c_1} + \rho \frac{V_1^2}{2} = p_{c_2} + \rho \frac{V_2^2}{2}$$

in which it has been assumed either that the conduit is horizontal, in which case the gravitational potential terms $-\rho g \xi$ cancel on both sides of the equation, or else that velocities are so large that gravity can be neglected, as illustrated by (4.10). In either case, the pressure p_{c_1} is given by

$$\boxed{p_{c_2} = p_{c_1} + \rho \frac{V_1^2}{2} - \rho \frac{V_2^2}{2}}$$

in which all quantities on the right side have either been given or calculated previously.

Since the momentum equation, (4.2) or (4.5), requires a sum of forces on its left side, use of the momentum equation should ***always*** be preceded by a sketch of a free body diagram of the control volume and coordinate system, as shown next.
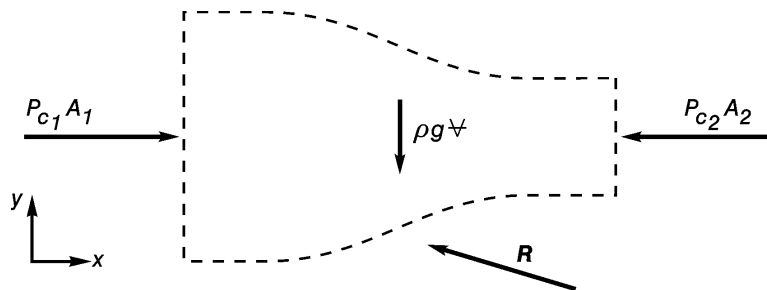
Since the end sections A_1 and A_2 are in regions of uniform flow, where streamlines have zero curvature, pressures are distributed hydrostatically across the streamlines and pressure forces are given by the product of pressures at area centroids with the corresponding areas.

The curved streamlines along the conduit boundaries have rapidly varying, non-hydrostatic pressure distributions, and we can only replace the integral of these pressures with the unknown resultant force, $\boldsymbol{R}$. The weight of fluid in the control volume, $\rho g \forall$, is important only for low speed flows in which the pressure forces and fluid weight are of comparable magnitude. An application of (4.5) to the control volume shown both in Figure 4.2 and in the free body diagram gives the following result:

$$p_{c_1} A_1 \boldsymbol{i} - p_{c_2} A_2 \boldsymbol{i} - \rho g \forall \boldsymbol{j} + \boldsymbol{R} = \rho \left(V_2 \boldsymbol{i} \right)\left(V_2 A_2 \right) + \rho \left(V_1 \boldsymbol{i} \right)\left(-V_1 A_1 \right)$$

Solution for the unknown value of $\boldsymbol{R}$ gives

$$\boxed{\boldsymbol{R} = \left(-p_{c_1} A_1 + p_{c_2} A_2 + \rho V_2^2 A_2 - \rho V_1^2 A_1 \right) \boldsymbol{i} + \rho g \forall \boldsymbol{j}}$$

in which all values on the right side have either been given or calculated previously.

Example 4.2
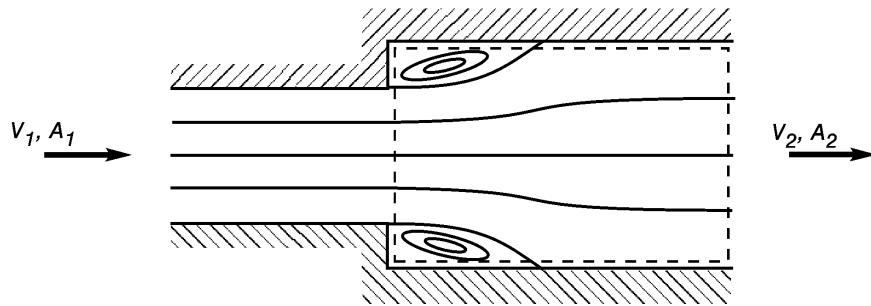
Flow in the abrupt expansion shown in the sketch has relatively large energy losses as a result of flow separation and turbulence. We will neglect gravity to calculate an expression for this energy loss.

Solution: Students should form the habit of sketching streamlines within control volumes when solving problems. This shows regions of uniform and curvilinear flow and helps immensely in selecting boundary locations for control volume analysis. It also helps locate regions of diverging streamlines and separated flow, where energy losses become relatively large and one-dimensional velocity approximations become less accurate. Streamlines for this flow are shown in the sketch.

Control volume boundaries for this problem are shown with a dashed line in the sketch. An application of the continuity equation (4.1) gives

$$- V_1 A_1 + V_2 A_2 = 0$$

and an application of the Bernoulli equation with an energy loss term and zero gravitational potential, (4.13), gives

$$p_1 + \rho \frac{V_1^2}{2} = p_2 + \rho \frac{V_2^2}{2} + E_L$$

This last equation can be solved for E_L.

$$E_L = (p_1 - p_2) + \rho \frac{V_1^2}{2} - \rho \frac{V_2^2}{2}$$

The pressure difference, $p_1 - p_2$, can be calculated by an application of the momentum equation. A free body diagram for the control volume follows:
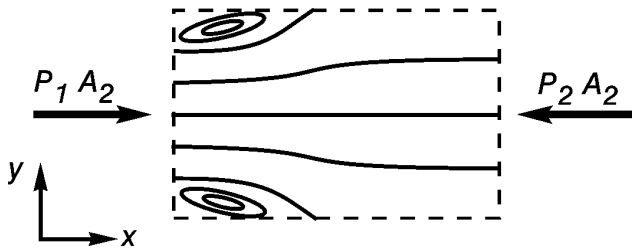
Notable points about this free body diagram are that (1) the net boundary pressure force in a direction normal to the axis of symmetry is zero because of symmetry and the neglect of gravity and (2) the pressure force on the upstream cross section is calculated over the area A_2 rather than A_1. This is possible because pressures are distributed hydrostatically over the entire upstream cross section. (Pressures across A_1 are hydrostatic since the streamlines there have no curvature, and velocities and accelerations within any zone of separated flow are known from experimental evidence to be small enough to give hydrostatic pressure distributions across the separated flow region.) Thus, an application of (4.2) or (4.5) gives

$$p_1 A_2 \boldsymbol{i} - p_2 A_2 \boldsymbol{i} = \rho (V_2 \boldsymbol{i})(V_2 A_2) + \rho (V_1 \boldsymbol{i})(-V_1 A_1)$$

Dotting both sides of this vector equation with $\boldsymbol{i}$ and solving the resulting scalar equation for $p_1 - p_2$ gives

$$(p_1 - p_2) = \rho V_2^2 - \rho V_1^2 \frac{A_1}{A_2}$$

Substituting this expression for $p_1 - p_2$ into the expression for E_L gives

$$E_L = \rho V_2^2 - \rho V_1^2 \frac{A_1}{A_2} + \rho \frac{V_1^2}{2} - \rho \frac{V_2^2}{2}$$

The result from the continuity equation can be used to put the expression for E_L in any one of the following three forms:

$$E_L = \rho \frac{(V_1 - V_2)^2}{2} = \left(1 - \frac{A_1}{A_2}\right)^2 \rho \frac{V_1^2}{2} = \left(\frac{A_2}{A_1} - 1\right)^2 \rho \frac{V_2^2}{2}$$

Decelerating flow within the control volume creates larger differences between experimental and one-dimensional velocity approximations at the downstream cross section than for the accelerated flow considered in Example 1. Thus, the results from Example 1 can be expected to describe experimental flows more closely than the results from Example 2. Nevertheless, the results from Example 2 are useful and are the basis for representing local or minor energy losses for less mathematically tractable flows in any one of the following forms:

$$E_L = K_1 \rho \frac{(V_1 - V_2)^2}{2} = K_2 \rho \frac{V_1^2}{2} = K_3 \rho \frac{V_2^2}{2}$$

in which values for the loss coefficients, K_i, are determined experimentally.

Example 4.3
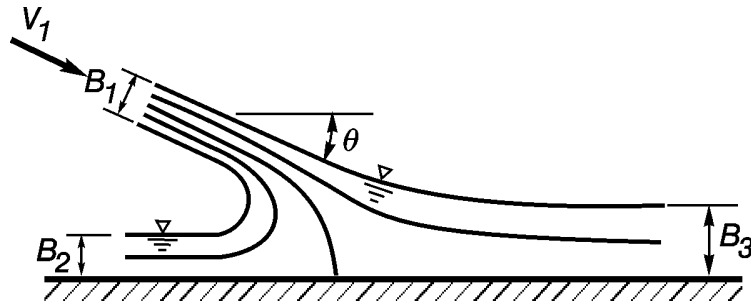
The high-speed two-dimensional jet shown in the sketch strikes a rigid horizontal surface and divides in two. The velocity V_1, the jet dimension, B_1 and the angle θ are known. We will calculate the depths B_2 and B_3 and the force per unit width that the rigid surface exerts against the jet. Both gravity and tangential boundary stresses will be neglected.

Solution: Since velocities are assumed to be large, application of the Bernoulli equation along each of the two free streamlines shows that the velocity magnitude equals V_1 at every point on both free streamlines, as explained following equation (4.8). Thus, the uniform velocities at cross sections 2 and 3 both have magnitudes of V_1, and an application of the continuity equation to a unit width control volume gives

$$- V_1 B_1 + V_1 B_2 + V_1 B_3 = 0$$

Division by V_1 gives the following equation with unknown values of B_2 and B_3 :

$$B_2 + B_3 = B_1$$

Since gravity has been neglected, we can dot both sides of (2.20) with e_n in the regions of uniform flow that exist at cross sections 1, 2 and 3 to obtain

$$- \frac{1}{\rho} e_n \cdot \nabla p = 0$$

in which e_n is normal to the straight, parallel streamlines. Thus, the directional derivative (1.44) allows this result to be written as

$$\frac{dp}{dn} = 0$$

Since this shows that p is not changing in a direction normal to the streamlines, and since $p = 0$ on each of the two free streamlines, we see that $p = 0$ across each of the three cross sections 1, 2 and 3. Thus, the only force acting on the control volume of fluid is a normal pressure force exerted by the rigid horizontal surface, as shown in the following free body diagram:
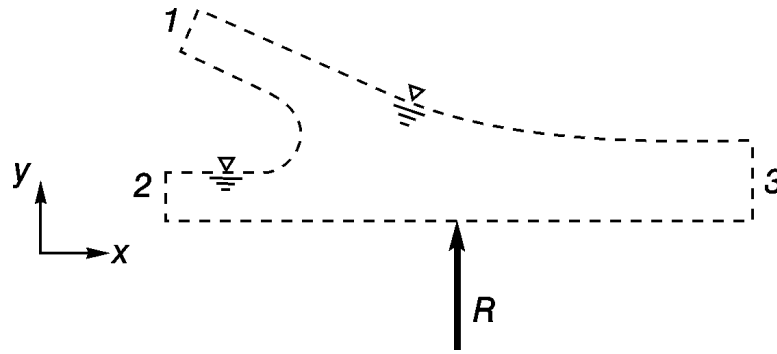
An application of the momentum equation gives

$$R\boldsymbol{j} = \rho\left(V_1\cos\theta\,\boldsymbol{i} - V_1\sin\theta\,\boldsymbol{j}\right)\left(-V_1 B_1\right)$$

$$+ \rho\left(-V_1\,\boldsymbol{i}\right)\left(V_1 B_2\right) + \rho\left(V_1\,\boldsymbol{i}\right)\left(V_1 B_3\right)$$

Dotting both sides of this vector equation with $\boldsymbol{i}$ and then $\boldsymbol{j}$ gives the following two scalar equations:

$$0 = -\rho V_1^2 B_1\cos\theta - \rho V_1^2 B_2 + \rho V_1^2 B_3$$

$$\boxed{R = \rho V_1^2 B_1\sin\theta}$$

The second equation gives the required force per unit width, and the first equation can be solved simultaneously with $B_2 + B_3 = B_1$ to obtain

$$\boxed{\begin{aligned} B_2 &= \left(1 - \cos\theta\right)B_1/2 \\ B_3 &= \left(1 + \cos\theta\right)B_1/2 \end{aligned}}$$

For a partial check on these results, we see that $B_2 = B_3 = B_1/2$ when $\theta = \pi/2$ (which must be true from considerations of symmetry) and that $B_2 = 0$ and $B_3 = B_1$ when $\theta = 0$.

Example 4.4
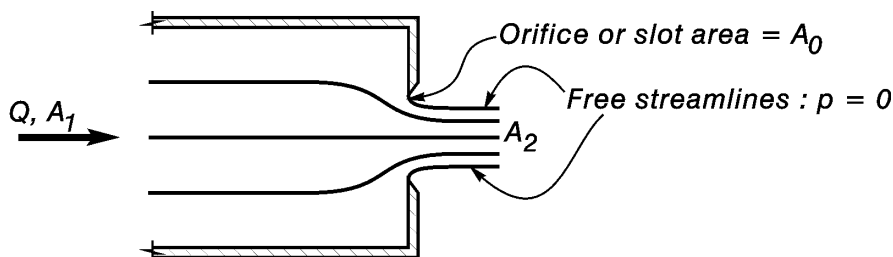
Flow exits with a high velocity through either a circular orifice or a slot in a plate covering the end of either a pipe or two-dimensional conduit. The jet downstream from the orifice or slot contracts so that its cross sectional area, A_2, is less than the orifice or slot area, A_0. The contraction coefficient, C_c, is defined to be the ratio of jet to orifice or slot areas.

$$C_c = \frac{A_2}{A_0} \quad , \quad \left(C_c < 1 \right)$$

It will be shown in a later chapter that C_c is a function of A_0/A_1, and values of C_c will be given in that chapter for axisymmetric and two-dimensional high speed jets. In this problem we will assume that A_1, A_0 and C_c are known, and this will allow us to calculate a relationship between the pressure p_1 and the flow rate Q and also an expression for the pressure force that the orifice plate exerts upon the flow. Gravity and tangential boundary stresses will be neglected.

Solution: An application of the continuity equation between cross sections 1 and 2 gives

$$- A_1 V_1 + C_c A_0 V_2 = 0$$

which can be rewritten in terms of the flow rate, Q.

$$A_1 V_1 = C_c A_0 V_2 = Q$$

Since the jet has high enough velocities to allow the neglect of gravity, the discussion in Example 3 with regard to the lateral pressure gradient in regions of uniform flow applies to this problem as well. Thus, the pressure across A_2 is zero, and the pressure across A_1 is a positive constant. This means that application of (4.8), with $g = 0$, along any streamline that connects A_1 and A_2 gives

$$p_1 + \rho \frac{V_1^2}{2} = \rho \frac{V_2^2}{2}$$

The continuity result can be used to rewrite V_1 and V_2 in terms of Q, and solution of the resulting equation for Q gives

$$Q = \sqrt{\frac{2p_1}{\rho \left(\dfrac{1}{C_c^2 A_0^2} - \dfrac{1}{A_1^2} \right)}}$$

This result is often used to measure flow rates in civil engineering applications.
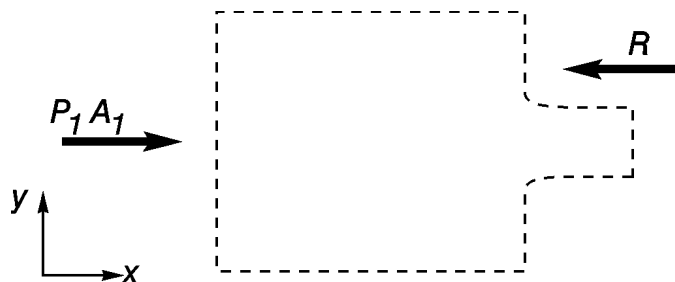
The free body diagram has only a horizontal pressure force over the area A_1 and a horizontal pressure force, R, exerted by the orifice plate upon the flow. The resultant pressure force normal to the axis of symmetry vanishes since gravity has been neglected. Thus, the momentum equation gives

$$p_1 A_1 \, \boldsymbol{i} \, - \, R \, \boldsymbol{i} \, = \, \rho \left(V_1 \, \boldsymbol{i} \right)\left(- V_1 A_1 \right) \, + \, \rho \left(V_2 \, \boldsymbol{i} \right)\left(V_2 \, C_c \, A_0 \right)$$

Dotting both sides of this equation with $\boldsymbol{i}$ gives

$$p_1 A_1 \, - \, R \, = \, - \rho \, A_1 \, V_1^2 \, + \, \rho \, C_c \, A_0 \, V_2^2$$

The Bernoulli equation can be used to eliminate p_1 to obtain

$$R \, = \, A_1 \left(\rho \, \frac{V_2^2}{2} \, - \, \rho \, \frac{V_1^2}{2} \right) \, + \, \rho \, A_1 \, V_1^2 \, - \, \rho \, C_c \, A_0 \, V_2^2$$

and use of the continuity equation to rewrite V_1 **and** V_2 in terms of Q ultimately leads to the result

$$\boxed{R \, = \, \frac{\rho \, Q^2}{2 A_1} \left(1 \, - \, \frac{A_1}{C_c \, A_0} \right)^2}$$

The orifice plate and welds must be strong enough to withstand the force R.

Example 4.5
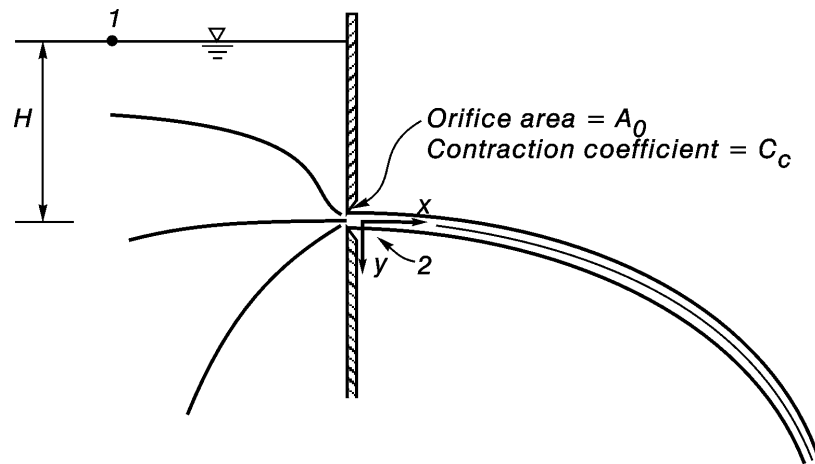
Water flows through an orifice in the side of a large reservoir. The orifice centreline is a vertical distance H below the reservoir free surface. Calculate the flow rate through the orifice and the jet trajectory if the orifice area, A_0, and contraction coefficient, C_c, are known. The downward curvature of the free jet is caused by gravity, so that gravity will be included in our calculations.

Solution: The Bernoulli equation, (4.3), can be applied along a streamline that starts on the reservoir free surface, where $V \to 0$, and passes through the free surface in the contracted part of the jet to obtain

$$H = \frac{V_0^2}{2g}$$

in which V_0 = free surface velocity at the jet vena contracta. If H is large compared to the orifice diameter, then the velocity distribution in the vena contracta is nearly uniform and the flow rate is given by

$$\boxed{Q = C_c A_0 V_0 = C_c A_0 \sqrt{2gH}}$$

since the area of the contracted jet cross section is $C_c A_0$.

Downstream from the vena contracta pressures are atmospheric throughout the jet. Thus, if tangential stresses on the jet free surface are neglected, and if the jet does not break apart into droplets of spray from turbulence, then a free body diagram of a fluid particle in the jet has its weight, mg, as the only external force.

Newton's second law, $F = mDV/Dt$, gives

$$mg\boldsymbol{j} = m\left(\frac{d^2x}{dt^2}\boldsymbol{i} + \frac{d^2y}{dt^2}\boldsymbol{j} \right)$$

Dotting both sides with $\boldsymbol{i}$ and $\boldsymbol{j}$ gives two scalar equations.

$$\frac{d^2x}{dt^2} = 0$$

$$\frac{d^2y}{dt^2} = g$$

Integrating each equation once gives

$$\frac{dx}{dt} = C_1 = V_0 = \sqrt{2gH}$$

$$\frac{dy}{dt} = gt + C_2 = gt$$

in which $C_1 = V_0$ and $C_2 = 0$ were determined by requiring $dx/dt = V_0$ and $dy/dt = 0$ in the vena contracta at $x = y = t = 0$. A second integration gives

$$x = t\sqrt{2gH} + C_3 = t\sqrt{2gH}$$

$$y = \frac{1}{2}gt^2 + C_4 = \frac{1}{2}gt^2$$

in which $C_3 = C_4 = 0$ since $x = y = 0$ at $t = 0$ in the vena contracta. Time, t, plays the role of a parameter in these equations, and elimination of this parameter by solving the first equation for t and substituting the result into the second equation gives an equation for the jet trajectory.

$$y = \frac{1}{2}g\left(\frac{x}{\sqrt{2gH}}\right)^2$$

This equation can be put in the following dimensionless form:

$$\left(\frac{y}{H}\right) = \frac{1}{4}\left(\frac{x}{H}\right)^2$$

This is the equation of a parabola with its vertex at the coordinate origin in the vena contracta.

If a number of orifices with different values for H are present in the reservoir side walls, as shown in the following sketch, then points in an experimental plot of y/H versus x/H for each jet should all lie along the same curve, which is obtained from a plot of $(y/H) = (1/4)(x/H)^2$. This type of solution, in which results for a number of different experiments collapse onto a single curve, is often encountered in fluid mechanics and is known as a similarity solution. A plot of some experimental data obtained by students in an actual laboratory exercise is also shown.

$$\frac{y}{H} = \frac{1}{4}\left(\frac{x}{H}\right)^2$$

	H/D
+	33
□	61
▲	94
○	124
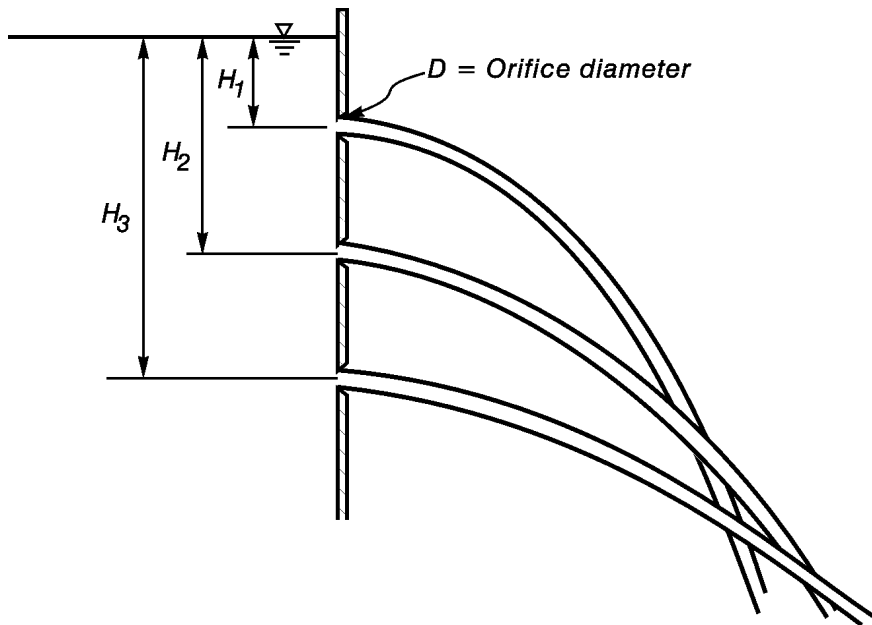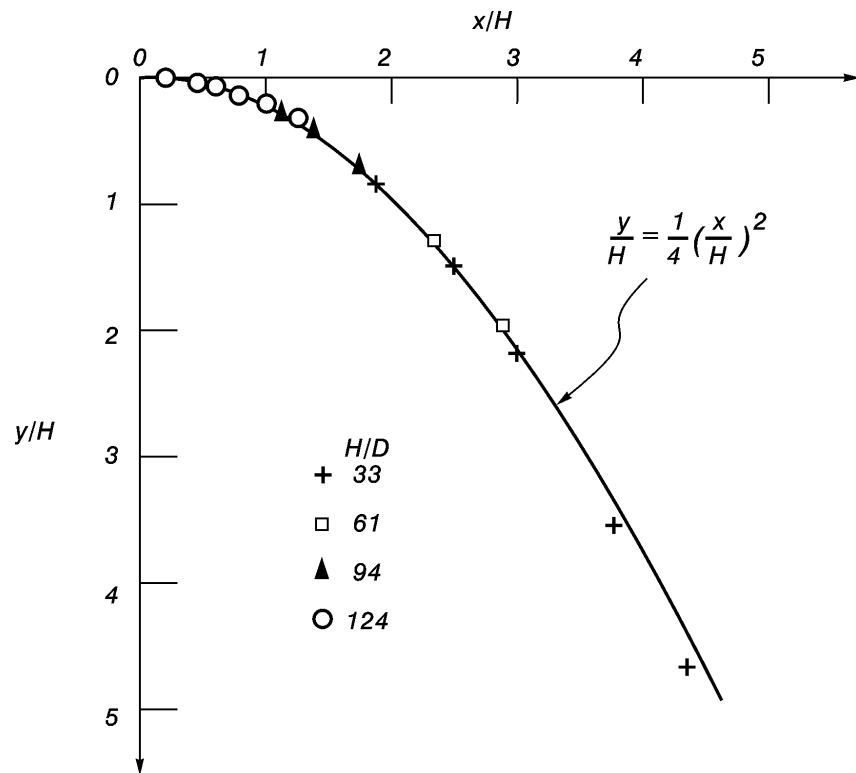
Example 4.6
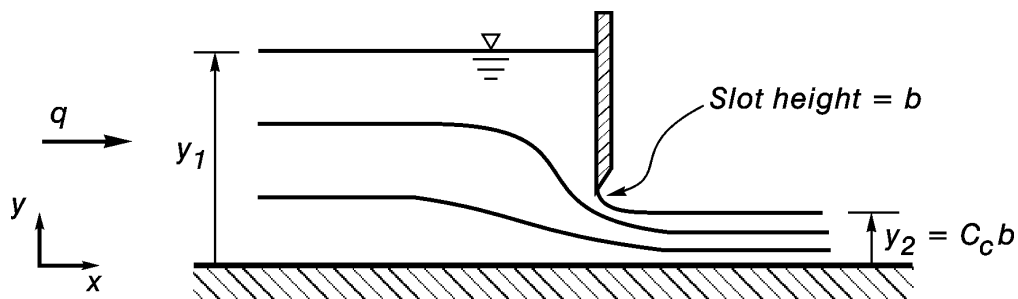
Flow in an open channel exits beneath a sluice gate, which has an opening or slot height of b. The initial depth, y_1, slot height, b, and contraction coefficient, C_c, are known. We will calculate the flow rate per unit width, q (in units of m²/s), and the pressure force exerted by the gate upon the flow. Values of C_c for a sluice gate of this type will be given in a later chapter.

Solution: Since cross sections 1 and 2 are in regions of uniform flow, an application of the continuity equation to a flow of unit width gives

$$V_2 C_c b - V_1 y_1 = 0$$

This equation can be rewritten as

$$V_2 C_c b = V_1 y_1 = q$$

in which q = flow rate per unit width.

An application of the Bernoulli equation, (4.3), between points on the free surface at cross sections 1 and 2 (both points are on the same streamline) gives

$$y_1 + \frac{V_1^2}{2g} = C_c b + \frac{V_2^2}{2g}$$

in which h in (4.4) has been used in the form $h = p/\rho g + y$. Substitution for V_1 **and** V_2 in terms of q from the continuity result gives

$$y_1 + \frac{q^2}{2gy_1^2} = C_c b + \frac{q^2}{2gC_c^2 b^2}$$

This equation can be solved for q in the following form:

$$q = \sqrt{\frac{2g(y_1 - C_c b)}{\dfrac{1}{C_c^2 b^2} - \dfrac{1}{y_1^2}}} = C_c b y_1 \sqrt{\frac{2g}{y_1 + C_c b}}$$

Velocities in this type of flow are too small to allow the neglect of gravity. However, the control volume is relatively short so that tangential boundary forces are small compared with normal pressure forces. Thus, a free body diagram includes only pressure forces on the two end sections, the gate and the channel bottom together with the weight of fluid in the control volume.
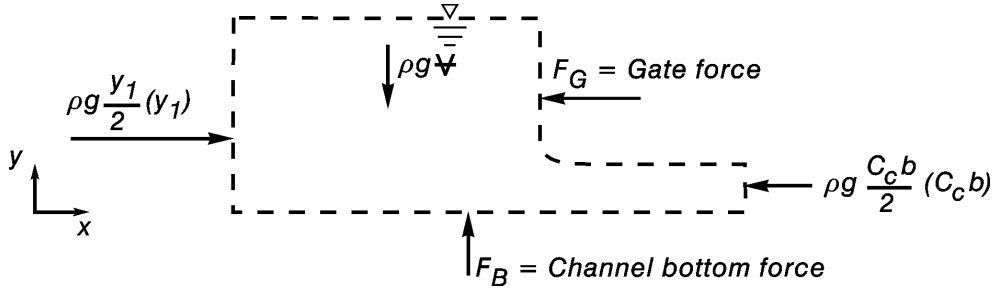
Since uniform flow exists at cross sections 1 and 2, Eq. (4.6) shows that pressures are distributed hydrostatically in the vertical direction at each end cross section. Thus, hydrostatic pressure forces at the end cross sections are the products of pressures at area centroids with cross sectional areas. Use of the momentum equation, (4.2) or (4.5), gives

$$\left(\rho g \frac{y_1^2}{2} - \rho g \frac{C_c^2 b^2}{2} - F_G \right) \boldsymbol{i} + \left(F_B - \rho g \forall \right) \boldsymbol{j} = \rho \left(V_2 \boldsymbol{i} \right) \left(V_2 C_c b \right)$$

$$+ \rho \left(V_1 \boldsymbol{i} \right) \left(-V_1 y_1 \right)$$

Dotting both sides of this vector equation with $\boldsymbol{i}$ and $\boldsymbol{j}$ gives two scalar component equations.

$$\rho g \frac{y_1^2}{2} - \rho g \frac{C_c^2 b^2}{2} - F_G = \rho V_2^2 C_c b - \rho V_1^2 y_1$$

$$F_B - \rho g \forall = 0$$

The second equation states that the pressure force on the channel bottom equals the weight of fluid in the control volume. If V_2 **and** V_1 are written in terms of q from the continuity equation, the first equation gives the gate force as

$$F_G = \rho g \frac{y_1^2}{2} - \rho g \frac{C_c^2 b^2}{2} + \rho \frac{q^2}{y_1} - \rho \frac{q^2}{C_c b}$$

Use of the previously calculated expression for q and a bit of algebra allows this to be simplified.

$$\boxed{F_G = \frac{\rho g (y_1 - C_c b)^3}{2(y_1 + C_c b)}}$$

Example 4.7
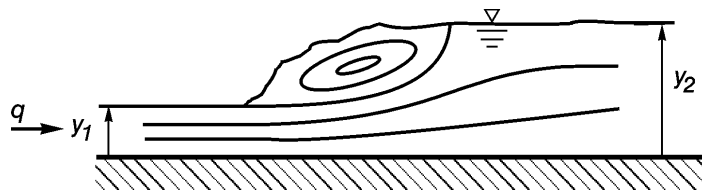
A hydraulic jump often forms downstream from structures such as dam spillways or sluice gates. In these flows a high velocity flow with a relatively small depth suddenly increases its depth with a corresponding decrease in velocity. When changes in depth and velocity are relatively large, the jump contains a great deal of turbulence and a large roller, as shown in the sketch. Thus, energy losses can be considerable and should not be ignored. In this example we will calculate expressions for the change in depth and the head loss across the jump.

Solution: An application of the continuity equation to a flow of unit width gives

$$- V_1 y_1 + V_2 y_2 = 0$$

which can be rewritten in terms of the flow rate per unit width, q.

$$V_1 y_1 = V_2 y_2 = q$$

An application of the Bernoulli equation with a head-loss term gives

$$y_1 + \frac{V_1^2}{2g} = y_2 + \frac{V_2^2}{2g} + H_L$$

Use of the continuity result allows this to be rewritten in terms of q.

$$H_L = (y_1 - y_2) + \frac{q^2}{2g}\left(\frac{1}{y_1^2} - \frac{1}{y_2^2}\right)$$

A free body diagram for the control volume contains pressure forces at the two end cross sections and along the channel bottom together with the weight of fluid within the control volume.
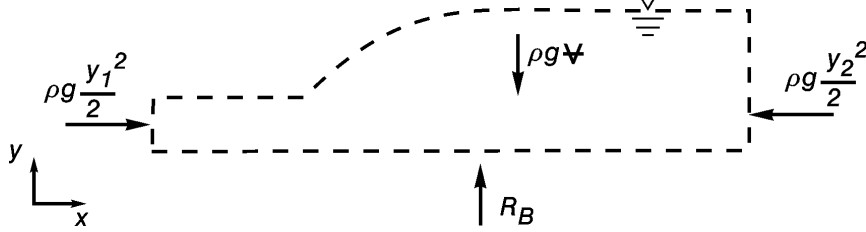
This allows application of the momentum equation to obtain

$$\left(\rho g \frac{y_1^2}{2} - \rho g \frac{y_2^2}{2}\right) \boldsymbol{i} + \left(R_B - \rho g \forall\right)\boldsymbol{j} = \rho\left(V_2 \boldsymbol{i}\right)\left(V_2 y_2\right) + \rho\left(V_1 \boldsymbol{i}\right)\left(-V_1 y_1\right)$$

The $\boldsymbol{i}$ and $\boldsymbol{j}$ components of this equation give

$$\rho g \frac{y_1^2}{2} - \rho g \frac{y_2^2}{2} = \rho V_2^2 y_2 - \rho V_1^2 y_1$$

$$R_B - \rho g \forall = 0$$

The second equation states that the pressure force on the channel bottom equals the weight of fluid within the control volume. The first equation, however, leads to a more interesting result that can be obtained by rewriting V_1 and V_2 in terms of q.

$$\frac{g}{2}\left(y_1^2 - y_2^2\right) = q^2\left(\frac{1}{y_2} - \frac{1}{y_1}\right) = q^2 \frac{y_1 - y_2}{y_1 y_2}$$

Since $y_1 = y_2$ is not a root that is of interest, division by $(y_1 - y_2)$ gives

$$\frac{g}{2}\left(y_1 + y_2\right) = \frac{q^2}{y_1 y_2}$$

This equation is a quadratic equation for y_2 that has the classical solution

$$\boxed{\frac{y_2}{y_1} = \left(-1 + \sqrt{1 + 8F_1^2}\right)\Big/ 2}$$

in which the Froude number, F_1, is defined as

$$\boxed{F_1 = \frac{q}{\sqrt{gy_1^3}} = \frac{V_1}{\sqrt{gy_1}}}$$

The Froude number is dimensionless and has great significance in open channel flow calculations.

If the expression for q^2 is substituted into the expression for the head loss, H_L, we obtain

$$H_L = \left(y_1 - y_2\right) + \frac{1}{4}\left(y_1 y_2\right)\left(y_1 + y_2\right)\left(\frac{1}{y_1^2} - \frac{1}{y_2^2}\right)$$

This result can be manipulated into a much simpler and more significant form.

$$H_L = \frac{\left(y_2 - y_1\right)^3}{4 y_1 y_2}$$

Since $H_L > 0$, this result shows that y_2 must be greater than y_1. (Only an increase in depth across a jump is possible.) It also shows that H_L increases as $\left(y_2 - y_1\right)$ increases, and the expression for y_2/y_1 shows that this is caused by an increase in F_1. In other words, an increase in Froude number for the approaching flow increases both the change in depth and the energy loss across the jump. Engineers often design stilling basins below spillways so that hydraulic jumps form within these basins. This is to ensure that high velocity flows from the lower part of the spillway exit from the stilling basin with a smaller velocity and larger depth in order to prevent erosion near the spillway base.

In some design problems the upstream depth must be calculated for a given downstream depth and Froude number. In that case the solution can be written in the following form:

$$\frac{y_1}{y_2} = \left(-1 + \sqrt{1 + 8F_2^2}\right)\bigg/2$$

The following figure, which has been replotted from a figure in Rouse (1946), shows a comparison between calculated and measured depths in a hydraulic jump together with a curve that gives the length, *L,* of the jump. This curve, which was obtained from laboratory measurements, is useful when designing the length of a stilling basin.
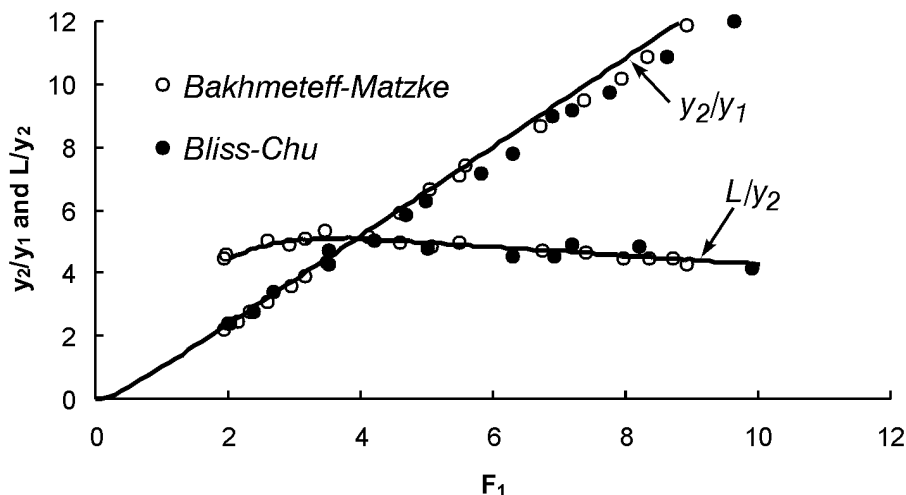
Extensions for Control Volume Applications

The methods that we have used so far can be extended in two different ways. First, techniques used in the study of particle and rigid body dynamics can be used to obtain equations for moving control volumes that are both translating and rotating. Second, moment of momentum equations can be obtained for both stationary and moving control volumes. Applications of these equations include fluid motion through rotating machinery, such as pumps and turbines, and calculation of lines of action for control volume forces. Shames (1962) gave what was probably the first and most complete derivation of these equations. We will consider only the relatively simple case of a translating control volume.
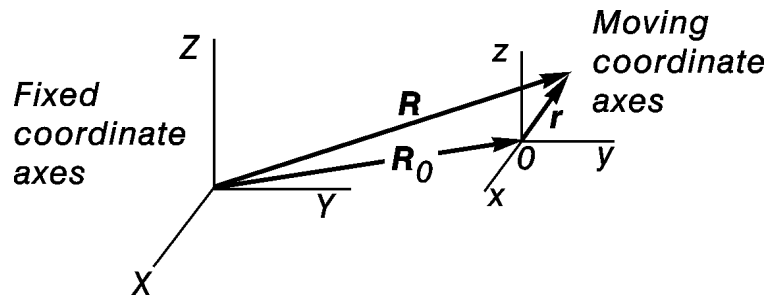
Figure 4.6   Position vectors in a moving (x, y, z) coordinate system and a fixed (X, Y, Z) coordinate system.

Figure 4.6 shows an (X, Y, Z) coordinate system that is fixed in space and an (x, y, z) coordinate system that is translating. Since the moving coordinate system is not rotating, we can use the same base vectors (i, j, k) for both coordinate systems by choosing the coordinate axes of the two systems to be parallel. Thus, if R is the position vector of a fluid particle relative to the fixed coordinate system, we can write

$$R = R_0 + r \tag{4.14}$$

in which

$$R = Xi + Yj + Zk \tag{4.15}$$

$$R_0 = X_0 i + Y_0 j + Z_0 k \tag{4.16}$$

$$r = xi + yj + zk \tag{4.17}$$

Equation (4.14) shows that the position of the fluid particle relative to the fixed coordinate system equals the sum of the position vector of the translating origin and the position of the fluid particle relative to the translating coordinate system. Since the (i, j, k) base vectors are not rotating, they have zero time derivatives. Thus, differentiation of (4.14) gives

$$\frac{d\mathbf{R}}{dt} = \frac{d\mathbf{R}_0}{dt} + \frac{d\mathbf{r}}{dt} \tag{4.18}$$

in which

$$\frac{d\mathbf{R}_0}{dt} = \frac{dX_0}{dt}\mathbf{i} + \frac{dY_0}{dt}\mathbf{j} + \frac{dZ_0}{dt}\mathbf{k} = U_0\mathbf{i} + V_0\mathbf{j} + W_0\mathbf{k} \tag{4.19}$$

$$\frac{d\mathbf{r}}{dt} = \frac{dx}{dt}\mathbf{i} + \frac{dy}{dt}\mathbf{j} + \frac{dz}{dt}\mathbf{k} = u\mathbf{i} = \mathbf{v}\mathbf{j} + w\mathbf{k} \tag{4.20}$$

Equations (4.18) – (4.20) show that the absolute velocity of the fluid particle equals the vector sum of the absolute velocity of the translating origin and the velocity relative to the moving coordinate system.

Newton's second law is only valid for the absolute acceleration of a particle, and differentiation of (4.18) to obtain this absolute acceleration gives

$$\frac{d^2\mathbf{R}}{dt^2} = \frac{d^2\mathbf{R}_0}{dt^2} + \frac{d^2\mathbf{r}}{dt^2} \tag{4.21}$$

in which

$$\frac{d^2\mathbf{R}_0}{dt^2} = \frac{dU_0}{dt}\mathbf{i} + \frac{dV_0}{dt}\mathbf{j} + \frac{dW_0}{dt}\mathbf{k} \tag{4.22}$$

$$\frac{d^2\mathbf{r}}{dt^2} = \frac{Du}{Dt}\mathbf{i} + \frac{D\mathbf{v}}{Dt}\mathbf{j} + \frac{Dw}{Dt}\mathbf{k} \tag{4.23}$$

Equations (4.21) – (4.23) show that the absolute acceleration of the fluid particle equals the vector sum of the absolute acceleration of the translating origin and the acceleration relative to the moving coordinate system.

The equations of motion in the translating coordinate system can be obtained by substituting $d^2\mathbf{R}/dt^2$ in (4.21) for $D\mathbf{V}/Dt$ in (2.18). The end result is that $\mathbf{V}$ in all of the governing equations, including the continuity equations, is the velocity relative to the moving coordinate system, and a term $d^2\mathbf{R}_0/dt^2$ given by the right side of (4.22) must be added to (2.20) and (2.27). Since this additive term is a function of t but not of the spacial coordinates, the control volume form of the momentum equation contains a corresponding function of time added to the right side of (2.33).

$$\boxed{\boldsymbol{F} = \rho \forall \frac{d^2 \boldsymbol{R}_0}{dt^2} + \int_S \rho \boldsymbol{V}\left(\boldsymbol{V}\cdot \boldsymbol{e}_n\right)ds + \frac{\partial}{\partial t}\int_\forall \rho \boldsymbol{V}\partial\forall} \qquad (4.24)$$

If the flow is steady when viewed from the moving coordinate system, then (2.34) becomes

$$-g\nabla h = \left(\boldsymbol{V}\cdot\nabla\right)\boldsymbol{V} + \frac{d^2 \boldsymbol{R}_0}{dt^2} \qquad (4.25)$$

in which the last term is a function only of t. The sketch shown in Figure 1.6 can be used to show that

$$\boldsymbol{e}_t = \frac{d\boldsymbol{r}}{ds} \qquad (4.26)$$

so that a series of steps similar to those followed in the derivation of (2.40) shows that (2.39) is replaced with

$$\frac{d}{ds}\left(h + \frac{V^2}{2g} + x\frac{dU_0}{dt} + y\frac{dV_0}{dt} + z\frac{dW_0}{dt}\right) = 0 \qquad (4.27)$$

and (2.40) is replaced with

$$\boxed{\begin{aligned} h_1 + \frac{V_1^2}{2g} + x_1\frac{dU_0}{dt} + y_1\frac{dV_0}{dt} + z_1\frac{dW_0}{dt} = \\[2mm] h_2 + \frac{V_2^2}{2g} + x_2\frac{dU_0}{dt} + y_2\frac{dV_0}{dt} + z_2\frac{dW_0}{dt} \end{aligned}} \qquad (4.28)$$

in which V_1 and V_2 are velocities relative to the moving coordinate system. The question of whether it is possible to have a flow that appears steady in a coordinate system that is accelerating will not be discussed.

We will only consider applications in which the moving control volume and coordinate system are translating with a constant velocity. Then $dU_0/dt = dV_0/dt = dW_0/dt = d^2\boldsymbol{R}_0/dt^2 = 0$, and all of the governing equations become identical with the equations for a fixed control volume **except** that velocities are now measured relative to the translating coordinate system. The following examples should help make this clear.

Example 4.8

If an obstruction, such as a sluice gate, is suddenly lowered into an open channel flow, a shock or surge will move upstream with a constant speed that we will call c. (The c stands for celerity.) This surge has the appearance of the hydraulic jump considered in Example 4.7 except that it is moving upstream, as shown in the following sketch:
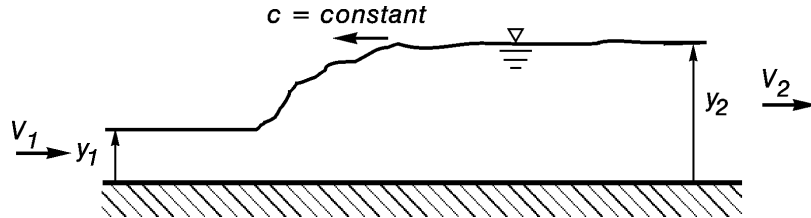
in which V_1 and V_2 are absolute velocities. If we choose a control volume and coordinate system that move with the surge and write velocities relative to the moving control volume, we obtain the result shown in the following sketch:
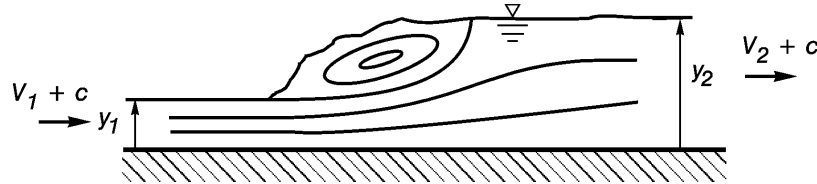
This flow, from the viewpoint of an observer in the translating control volume and coordinate system, appears to be the same steady flow considered in Example 4.7 except that V_1 and V_2 are replaced with the relative velocities $V_1 + c$ and $V_2 + c$. Thus, from the results calculated in Example 4.7, we have

$$\frac{y_2}{y_1} = \left(-1 + \sqrt{1 + 8F_1^2}\right) \Big/ 2$$

in which

$$F_1 = \frac{V_1 + c}{\sqrt{gy_1}}$$

In addition, the continuity equation gives

$$(c + V_1)y_1 = (c + V_2)y_2$$

The two circled equations contain five variables: y_1, y_2, V_1, V_2 and c. Any three of these variables can be specified, and the remaining two can be found from these equations. For example, if a sluice gate is lowered all the way to the channel floor, then $V_2 = 0$ and V_1 and y_1 would be the known velocity and depth that existed before the gate entered the flow. Then these two equations could be solved for c and y_2. For a second example, we might generate the surge

in a reservoir of still water by moving the sluice gate leftward with a specified velocity. Then $V_1 = 0$, y_1 is the undisturbed water depth and V_2 is a negative number equal to the speed at which the sluice gate moves. Again, the circled equations could be solved for c and y_2.

Surges exist naturally in some river estuaries as a result of an interaction between the river flow and a rising tide. They can also occur in rivers as a result of blockage by an avalanche, or they can travel down a river as a result of a sudden increase in flow caused, for example, by a dam bursting or a sudden release of flow from a reservoir.

Example 4.9
A high speed jet directed against a moving curved blade is often used as the basis for
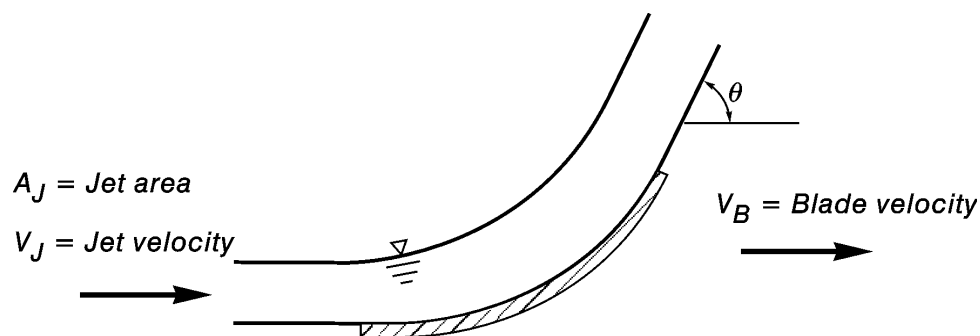
understanding the fluid mechanics of a Pelton wheel. (The Pelton wheel is an impulse turbine in which curved blades or buckets are mounted along the periphery of a large diameter wheel. A high speed water jet directed against the blades, tangential to the wheel periphery, spins the wheel. The spinning wheel is used either to generate electric power or to do other useful work.) We will assume that A_J, V_J, V_B and θ are known, and this will allow us to calculate the force vector that the moving blade exerts on the flow, the absolute velocity vector for the flow as it leaves the blade and the power extracted from the flow by the moving blade.

Solution: We will choose a control volume and coordinate system that moves with the blade. Since the flow is steady when viewed from this moving control volume, and since the jet speed is large enough to allow us to neglect gravity, the relative flow speed on the free surface is constant. Thus, streamlines and relative velocities are as shown in the following sketch:
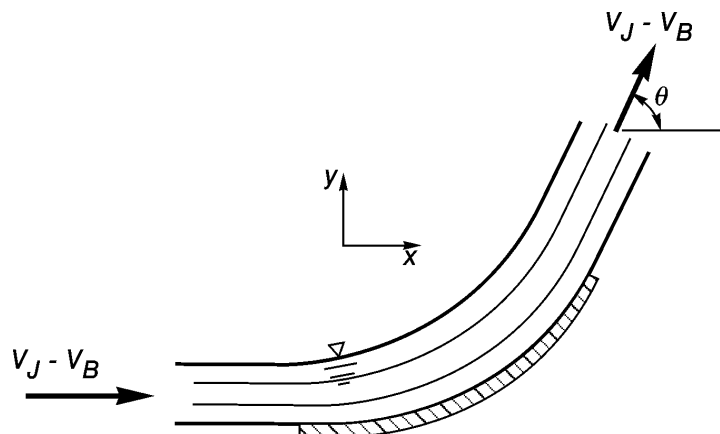
Since pressures are atmospheric on the free surfaces and across uniform flow streamlines at the entrance and exit of the control volume, and since the weight of fluid within the control volume is relatively small, a free body diagram of the control volume has the pressure force between the blade surface and fluid as the only external force.
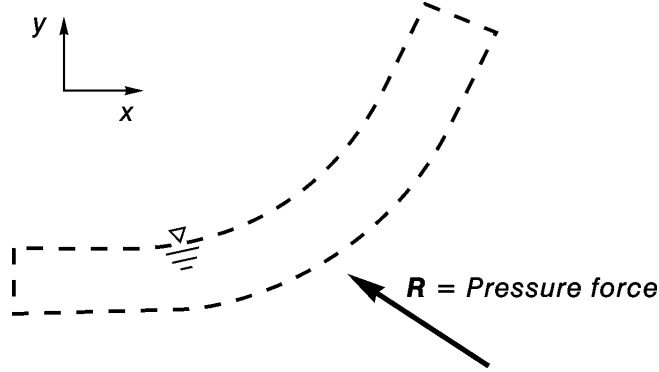
Equation (4.18) shows that the absolute velocity at the control volume exit is the sum of the control volume velocity and the relative velocity.

$$V = V_B i + (V_J - V_B)(\cos\theta\, i + \sin\theta\, j)$$

The force exerted by the blade on the flow can be calculated from the momentum equation,

$$R = \rho\left[(V_J - V_B)i\right]\left[-(V_J - V_B)A_J\right]$$
$$+ \rho\left[(V_J - V_B)(i\cos\theta + j\sin\theta)\right]\left[(V_J - V_B)A_J\right]$$

in which use has been made of the continuity equation to show that the cross sectional areas of the jet at its exit and entrance are both equal to A_J. The expression for R simplifies to

$$R = \rho A_J(V_J - V_B)^2\left[-(1 - \cos\theta)i + \sin\theta\, j\right]$$

Power has units of $N-m/s = $ ***Watt,*** abbreviated W, and is computed from the dot product of a force with the velocity at the point of force application. (If the velocity is the product of an angular velocity with a radial distance from a centre of rotation to the point of force application, this dot product also equals the product of the angular velocity with the torque or moment created by the force about the centre of rotation.) Thus, since the force exerted by the fluid upon the blade is $-R$, the power imparted to the blade is

$$P = (V_B i)\cdot(-R) = \rho A_J V_B (V_J - V_B)^2(1 - \cos\theta)$$

This shows that the fluid imparts zero power to the blade if $V_B = 0$, $V_B = V_J$ or $\theta = 0$. This suggests that the power reaches a maximum when V_B is somewhere in the range $0 < V_B < V_J$. Differentiation of P with respect to V_B gives

$$\frac{dP}{dV_B} = \rho A_J (1 - \cos\theta)\left[(V_J - V_B)^2 - 2V_B(V_J - V_B)\right]$$

Thus, $dp/V_B = 0$ when $V_J - V_B = 0$, which is not of interest since P attains a minimum value of zero then, and when

$$\boxed{V_J = 3V_B}$$

This gives a maximum power extraction of

$$P_{\text{max}} = 4\rho A_J V_B^3 (1 - \cos\theta) = 4\rho A_J V_J^3 (1 - \cos\theta)\big/27$$

When viewed as a function of θ, the power extraction is also maximized by making $\theta = \pi$.

References

Rouse, H. (1946) *Elementary Mechanics of Fluids*, John Wiley & Sons, Inc, New York, p. 146.

Shames, I.H. (1962) *Mechanics of Fluids*, McGraw-Hill Book Co., New York, pp. 109-114, 123-140.

Chapter 5

Differential Equation Methods

Pressure and velocity variations at points within a control volume can be found only from the solution of the partial differential equations of fluid motion. An example of this has already occurred in Chapter 3 when we integrated these equations to calculate pressures in motionless bodies of fluid. Now we will be concerned with integrating the equations for problems involving fluid motion. This chapter will give a general overview of the problem, and the following chapters will fill in more details.

The governing equations for homogeneous, incompressible, steady, two-dimensional flow are the continuity equation, (2.4),

$$\frac{\partial u}{\partial x} + \frac{\partial v}{\partial y} = 0 \tag{5.1}$$

and two components of the Navier-Stokes equations, (2.20),

$$-\frac{1}{\rho}\frac{\partial p}{\partial x} + \nu\left(\frac{\partial^2 u}{\partial x^2} + \frac{\partial^2 u}{\partial y^2}\right) = u\frac{\partial u}{\partial x} + v\frac{\partial u}{\partial y}$$

$$-\frac{1}{\rho}\frac{\partial p}{\partial y} + \nu\left(\frac{\partial^2 v}{\partial x^2} + \frac{\partial^2 v}{\partial y^2}\right) = u\frac{\partial v}{\partial x} + v\frac{\partial v}{\partial y} \tag{5.2 a, b}$$

in which gravity has been neglected. If gravity is included, then (2.28) shows that p/ρ is replaced with gh.

The exact solution of (5.1) – (5.2) is extremely difficult, largely because of the nonlinear acceleration terms on the right side of (5.2). Numerical techniques considerably increase the number of problems for which (5.1) – (5.2) can be solved, but even then there remain many problems for which neither mathematical nor numerical solutions of (5.1) – (5.2) are possible. Thus, in many problems it becomes necessary to use mathematical and physical insight to obtain approximate solutions of (5.1) – (5.2).

The most important technique for finding approximate solutions of (5.1) – (5.2) uses order of magnitude estimates for terms that appear in these equations. An order of magnitude is a factor of ten. Thus, two orders of magnitude are 100, three orders of magnitude are 1000, etc. To say that a term is of order 1 does not mean that its magnitude is exactly 1. Rather, it means that its absolute magnitude is not likely to exceed 1, 2 or 3 rather than 10, 20 or 30. The technique consists of choosing suitable estimates for maximum values of terms in Eqs. (5.1) – (5.2). Then the relative importance of terms are compared to see which, if any, are small enough to be neglected.

For example, if maximum changes in u and v are denoted by U and V, respectively, and if these changes occur over distances ℓ_x and ℓ_y in the x and y directions, respectively, then order of magnitude estimates for $\partial u/\partial x$ and $\partial v/\partial y$ are given by

$$\frac{\partial u}{\partial x} \sim \frac{U}{\ell_x}$$

$$\frac{\partial v}{\partial y} \sim \frac{V}{\ell_y}$$

(5.3 a, b)

in which ~ is read "of the order of". If either (5.3 a) or (5.3 b) is known to be nonzero, then (5.1) shows that

$$\frac{U}{\ell_x} \sim \frac{V}{\ell_y}$$

(5.4)

(Signs do not matter in scale analysis.) Thus, (5.4) gives an estimate for V if U, ℓ_x and ℓ_y are known.

$$V \sim \frac{\ell_y}{\ell_x} U$$

(5.5)

If P is an estimate for the maximum change in p, then using P, U, ℓ_x, ℓ_y and the estimate for V from (5.5) gives the following estimates for terms in (5.2):

$$\frac{P}{\rho \ell_x} + \nu \left(\frac{U}{\ell_x^2} + \frac{U}{\ell_y^2} \right) \sim \frac{U^2}{\ell_x} + \frac{U^2}{\ell_x}$$

$$\frac{P}{\rho \ell_y} + \nu \left(\frac{U \ell_y}{\ell_x^3} + \frac{U}{\ell_x \ell_y} \right) \sim \frac{U^2 \ell_y}{\ell_x^2} + \frac{U^2 \ell_y}{\ell_x^2}$$

(5.6 a, b)

Division of (5.6 a) by U^2/ℓ_x and (5.6 b) by U^2/ℓ_y gives dimensionless estimates for the relative magnitude of each term.

$$\frac{P}{\rho U^2} + \frac{\nu}{U \ell_x} \left[1 + \left(\frac{\ell_x}{\ell_y} \right)^2 \right] \sim 1 + 1$$

$$\frac{P}{\rho U^2} + \frac{\nu}{U \ell_x} \left[\left(\frac{\ell_y}{\ell_x} \right)^2 + 1 \right] \sim \left(\frac{\ell_y}{\ell_x} \right)^2 + \left(\frac{\ell_y}{\ell_x} \right)^2$$

(5.7 a, b)

The dimensionless ratios $P/(\rho U^2)$ and $U\ell_x/\nu$ are important parameters in fluid mechanics and are known as an Euler number and Reynolds number, respectively. Because of the way in which the Euler and Reynolds numbers were obtained in (5.7), authors frequently state that Euler and Reynolds numbers are dimensionless ratios of a pressure force to an acceleration and an acceleration to a viscous force, respectively. The reader is cautioned, however, that this physical interpretation is not always possible. For example, the Reynolds number also makes its appearance when considering flow resistance and energy losses for fully-developed laminar pipe flow. Velocity distributions in this flow do not change from one cross section to the next. Thus, fluid accelerations are zero everywhere, yet the Reynolds number still appears in the expression for the Darcy-Weisbach friction factor.
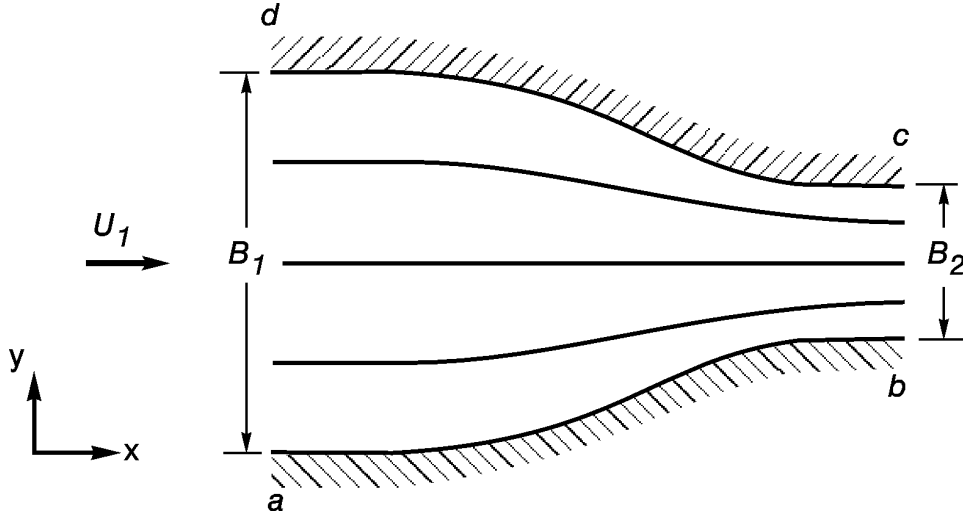
Figure 5.1 Flow through a streamlined constriction.

Consider flow through the streamlined constriction shown in Figure 5.1. The boundary geometry and velocity U_1 would be specified for this two-dimensional flow, and control volume techniques would allow us to calculate $U = U_2 - U_1$. In this case we take $\ell_x \sim \ell_y \sim B_1$, and (5.7) becomes

$$\frac{P}{\rho U^2} + \frac{\nu}{U B_1}\left[1 + 1\right] \sim 1 + 1$$

$$\frac{P}{\rho U^2} + \frac{\nu}{U B_1}\left[1 + 1\right] \sim 1 + 1$$

(5.8 a, b)

If, for example, the fluid is oil with $\nu \sim 10^{-5}$ m^2/s, $U \sim 2$ mm/s and $B_1 \sim 5$ mm, then

$$\frac{\nu}{U B_1} \sim 1 \tag{5.9}$$

In this case all terms are of equal importance, and the following estimate is obtained for P:

$$P \sim \rho U^2 \tag{5.10}$$

More importantly, all terms in (5.1) – (5.2) would have to be retained, and it would be necessary to impose the following boundary conditions:

$$u = v = 0 \quad \text{on} \quad ab \quad \text{and} \quad cd \tag{5.11}$$

$$u = U_1(y) \quad \text{and} \quad v = 0 \quad \text{on} \quad ad \tag{5.12}$$

$$u = U_2(y) \quad \text{and} \quad v = 0 \quad \text{on} \quad bc \tag{5.13}$$

$$p = p_1 \quad \text{for one point in the flow} \tag{5.14}$$

The requirement that u and v be specified on all boundaries is equivalent to specifying **both** normal and tangential velocity components and is necessary in order that the solution of (5.1) – (5.2) be unique. The solution would undoubtedly have to be obtained by using numerical techniques, and the flow would be described as viscous and laminar, a topic that will be discussed briefly in a following chapter.

In a more likely civil engineering application involving the flow of water, we could take $v \sim 10^{-6} \text{ m}^2/\text{s}$, $U \sim 1$ m/s and $B_1 \sim 100$ mm to obtain

$$\frac{v}{U B_1} \sim 10^{-5} \tag{5.15}$$

In this case (5.8) shows that the viscous terms are negligible, and an estimate for P is again given by (5.10). This flow would be termed inviscid, and (5.1) – (5.2) would be approximated with

$$\frac{\partial u}{\partial x} + \frac{\partial v}{\partial y} = 0$$

$$-\frac{1}{\rho} \frac{\partial p}{\partial x} = u \frac{\partial u}{\partial x} + v \frac{\partial v}{\partial y} \tag{5.16 a, b, c}$$

$$-\frac{1}{\rho} \frac{\partial p}{\partial y} = u \frac{\partial v}{\partial x} + v \frac{\partial v}{\partial y}$$

Since the second derivatives in (5.2) have been dropped, uniqueness requires that only **normal** velocity components be specified around the boundary.

$$\mathbf{V} \cdot \mathbf{e}_n = 0 \quad \text{on} \quad ab \quad \text{and} \quad cd$$

$$= U_1(y) \quad \text{on} \quad ad \tag{5.17}$$

$$= U_2(y) \quad \text{on} \quad bc$$

$$p = p_1 \quad \text{for one point in the flow} \tag{5.18}$$

Since the tangential component of V cannot be specified (because of the loss of second derivatives of u and v in the approximation), the flow will slip along boundaries ab and cd. A particular type of inviscid flow, known as either potential or irrotational flow, will be discussed at length in the following chapter.

The inviscid flow just described would be a good description of experiment throughout most of the control volume. However, slippage of the flow along boundaries ab and cd is unrealistic, and the inviscid flow approximation breaks down near these boundaries. The reason for this is that our scaling estimates were incorrect for the boundary region. This boundary region in which an inviscid flow approximation breaks down along a physical boundary is called a boundary layer. If we denote its thickness by $\ell_y = \delta$ in which x and y are now coordinates measured along and normal, respectively, to the physical boundary, then a boundary layer is characterised by the statement

$$\frac{\delta}{\ell_x} \ll 1 \tag{5.19}$$

In this case the largest viscous term in (5.7 a) must be of order one (since at least one viscous term must be retained if we want to specify both normal and tangential velocity components on the boundary), and we obtain the estimate

$$\frac{\nu}{U\ell_x}\left(\frac{\ell_x}{\delta}\right)^2 \sim 1 \tag{5.20}$$

which becomes

$$\left(\frac{\delta}{\ell_x}\right)^2 \sim \frac{\nu}{U\ell_x} \tag{5.21}$$

Using our estimates of $\nu \sim 10^{-6}$ m^2/s, $U \sim 1$ m/s and $B_1 \sim 100$ mm with $\ell_x \sim B_1$ gives $(\delta/B_1) \sim 0.003$, which suggests that the boundary layer is so thin compared to control volume dimensions that an accurate numerical solution of (5.1) – (5.2) for the entire control volume would be impossible to obtain.

Using (5.21) to eliminate the Reynolds number from (5.7) gives

$$\frac{P}{\rho U^2} + \left[\left(\frac{\delta}{\ell_x}\right)^2 + 1\right] \sim 1 + 1$$
$$\frac{P}{\rho U^2} + \left(\frac{\delta}{\ell_x}\right)^2\left[\left(\frac{\delta}{\ell_x}\right)^2 + 1\right] \sim \left(\frac{\delta}{\ell_x}\right)^2 + \left(\frac{\delta}{\ell_x}\right)^2 \tag{5.22}$$

Since $\delta/\ell_x \ll 1$, comparison of (5.2) and (5.22) shows that the boundary layer equations are

$$\frac{\partial u}{\partial x} + \frac{\partial v}{\partial y} = 0$$

$$-\frac{1}{\rho}\frac{\partial p}{\partial x} + \nu\frac{\partial^2 u}{\partial y^2} = u\frac{\partial u}{\partial x} + v\frac{\partial u}{\partial y} \qquad\qquad \textbf{(5.23 a, b, c)}$$

$$-\frac{1}{\rho}\frac{\partial p}{\partial y} = 0$$

in which x and y are now curvilinear coordinates measured along and normal to the boundary, as shown in Figure 5.2. Equation (5.23 c) shows that p does not change across the boundary layer, and this very important result means that p is first calculated along the boundary from the inviscid solution of (5.16) – (5.18) and then substituted into the first term of (5.23 b) to calculate velocities and shear stresses near boundaries ab and cd. This boundary layer approximation was first suggested by the German engineer L. Prandtl in 1904, and it marks a milestone in the understanding of both fluid mechanics and applied mathematics. Boundary layer flows will be treated at some length in a later chapter.
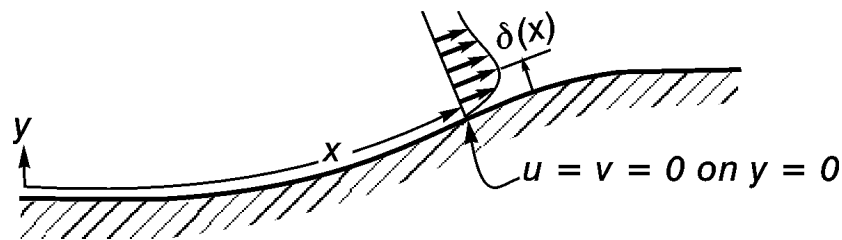
Figure 5.2 Boundary layer development along boundary ab of Figure 5.1.

The only remaining topic to mention is turbulence. Turbulence appears in flows when a disturbance, in the form of a small vortex, becomes amplified into an unsteady pattern of large and small vortices superimposed upon both themselves and the main flow pattern. This is flow instability in which an otherwise one or two-dimensional steady flow suddenly becomes three-dimensional and unsteady. A mathematical or numerical solution of a problem involving turbulence requires the solution of the unsteady, three-dimensional form of the Navier-Stokes equations with extremely small spacial and time resolutions. This has never been accomplished. Thus, the study of turbulence relies heavily upon laboratory observation and ad hoc hypotheses and theories that have little hope of being useful for general applications. We will discuss turbulence briefly in one of the following chapters.

In summary, order of magnitude estimates have been used to suggest that all terms multiplied by the kinematic viscosity, ν, in Eqs. (5.2a, b) can be neglected throughout most of the flow when Reynolds numbers are large. This inviscid flow approximation works well for many civil engineering applications, although it is not valid when flows are highly turbulent or when Reynolds numbers are of order one or smaller (for example, submerged turbulent jets, groundwater flow or very fine sediment particles falling slowly through water). The most commonly used inviscid flow approximation is called irrotational flow and is discussed in chapter 6. Examples of flows that are closely approximated with irrotational flow include flow under sluice gates, free jets exiting through orifices, flow over spillways and weirs and unsteady wave motion. However, at large Reynolds numbers, all inviscid flow approximations break down in very thin regions next to boundaries. In these regions, which are called boundary layers, pressures are calculated from an inviscid flow approximation but velocities and tangential stresses are calculated by including one of the viscous terms on the left side of Eq. (5.2a). Boundary-layer approximations are discussed in chapter 8. Finally, some very important engineering applications that require an understanding of both irrotational flow and boundary-layer approximations are covered in chapter 9, which is concerned with drag and lift forces on objects that are submerged in flows.

Chapter 6

Irrotational Flow

In this chapter we will consider the inviscid flow approximation that is known as either irrotational or potential flow. This approximation assumes that Reynolds numbers are sufficiently large to allow the neglect of all viscous terms in the Navier-Stokes equations. It also assumes that boundary layer thicknesses along physical boundaries are small relative to control volume dimensions. In general, boundary layer thicknesses remain small when Reynolds numbers are large and when fluid particles are highly accelerated as they move with the flow. In steady flow this requirement means that streamlines must converge rapidly in the direction of motion.

The governing equations for an inviscid, incompressible flow are the continuity equation, (2.3),

$$\nabla \cdot V = 0 \tag{6.1}$$

and the inviscid form of the Navier-Stokes equations, (2.27)

$$-g \nabla h = \frac{DV}{Dt} \tag{6.2}$$

The three scalar components of (6.2) are usually referred to as Euler's equations.

Circulation and the Velocity Potential Function

Not all inviscid flows are irrotational, and it is important to understand when a flow can be approximated as both inviscid and irrotational. Further understanding can be obtained by introducing the definition of circulation,[*] Γ,

$$\Gamma = \int_a^b V \cdot dr \tag{6.3}$$

in which dr = displacement vector along a path or curved line joining points a and b. The integrand $V \cdot dr$ in (6.3) is the projection of the velocity vector, V, upon dr multiplied by $|dr| = ds$ and can be written as

$$V \cdot dr = V \cdot e_t ds \tag{6.4}$$

in which e_t = unit tangent to the curve joining points a and b.

---

[*] The discussion in this section parallels similar arguments that are often made in particle dynamics when introducing the concept of work done on a particle by conservative forces.

If Γ is calculated along a material curve that is defined by joining the same fluid particles as they move with the flow, then $d\boldsymbol{r} = d\boldsymbol{r}(t)$ and the time derivative of (6.3) is

$$\frac{d\Gamma}{dt} = \int_a^b \left[\frac{d\boldsymbol{V}}{dt} \cdot d\boldsymbol{r} + \boldsymbol{V} \cdot d\left(\frac{d\boldsymbol{r}}{dt} \right) \right] \tag{6.5}$$

But $d\boldsymbol{r}/dt = \boldsymbol{V}$, and $d\boldsymbol{V}/dt = D\boldsymbol{V}/Dt$ can be replaced with the left side of (6.2) to obtain

$$\frac{d\Gamma}{dt} = \int_a^b \left[-g\nabla h \cdot d\boldsymbol{r} + \boldsymbol{V} \cdot d\boldsymbol{V} \right] \tag{6.6}$$

Since g is a constant, the integrand of (6.6) can be written as an exact differential.

$$\frac{d\Gamma}{dt} = \int_a^b \left[\nabla(-gh) \cdot d\boldsymbol{r} + d(\boldsymbol{V} \cdot \boldsymbol{V}/2) \right]$$
$$= \int_a^b d\left(-gh + V^2/2 \right) \tag{6.7}$$

Thus, if the integration path is closed so that points a and b coincide, and if we only consider flows in which h and V are single valued, we obtain a result known as Kelvin's circulation theorem.

$$\frac{d\Gamma}{dt} = \left(-gh + V^2/2 \right)_b - \left(-gh + V^2/2 \right)_a = 0 \tag{6.8}$$

Equation (6.8) shows that the circulation calculated around a closed material path of fluid particles remains constant with time as this path moves with the flow provided that the flow is inviscid.

There are two very important cases in which the constant value of Γ for a closed material path is zero. The first case is when the material path starts from rest. Then $V = 0$ at $t = 0$, and the constant value of Γ computed from (6.3) at $t = 0$ obviously vanishes. The second case occurs when $\boldsymbol{V} = $ constant vector at $t = 0$. Then

$$\Gamma_{t=0} = \boldsymbol{V} \cdot \int_a^b d\boldsymbol{r} = \boldsymbol{V} \cdot \left[\boldsymbol{r}(b) - \boldsymbol{r}(a) \right] = 0 \tag{6.9}$$

since points a and b coincide. Thus, any closed material path that starts out either in a region of zero motion or of uniform flow will have a zero value for Γ as the path moves with the flow.

Now consider a third point, c, on a closed material path that has a zero circulation, as shown in Figure 6.1.

Then (6.3) gives

$$\Gamma = 0 = \int_a^b \boldsymbol{V} \cdot d\boldsymbol{r} = \int_a^c \boldsymbol{V} \cdot d\boldsymbol{r} + \int_c^b \boldsymbol{V} \cdot d\boldsymbol{r} \qquad \textbf{(6.10)}$$
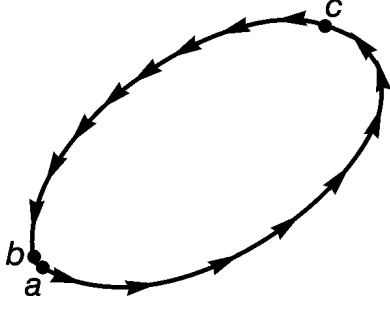
Figure 6.1 Circulation calculated around a closed material path for an inviscid flow.

Since points a and b coincide, and since reversing the order of limits reverses the sign in front of an integral, (6.10) is equivalent to

$$\int_a^c \boldsymbol{V} \cdot d\boldsymbol{r} = \int_b^c \boldsymbol{V} \cdot d\boldsymbol{r} \qquad \textbf{(6.11)}$$

Equation (6.11) shows that the circulation calculated along all paths joining points a and c is exactly the same, and this is only possible if $\boldsymbol{V} \cdot d\boldsymbol{r}$ is the exact differential of a scalar function that we will call ϕ.

$$\boldsymbol{V} \cdot d\boldsymbol{r} = d\phi = \nabla\phi \cdot d\boldsymbol{r} \qquad \textbf{(6.12)}$$

Since (6.12) must hold for an arbitrary choice for $d\boldsymbol{r}$, Eq. (6.12) shows that the velocity vector must be calculated from the gradient of a potential function, ϕ.

$$\boxed{\boldsymbol{V} = \nabla\phi} \qquad \textbf{(6.13)}$$

Clearly, we could have placed a minus sign in front of $d\phi$ and $\nabla\phi$ on the right side of (6.12) and (6.13), and some authors choose to do so. The potential function, ϕ, has no physical meaning beyond the fact that its first derivatives give velocity components in the three coordinate directions.

$$u = \frac{\partial\phi}{\partial x}$$

$$\mathrm{v} = \frac{\partial\phi}{\partial y} \qquad \textbf{(6.14 a, b, c)}$$

$$w = \frac{\partial\phi}{\partial z}$$

In summary, we can now say that any highly accelerated flow in which motion starts either from a state of rest or a state of uniform flow can be approximated with a velocity field generated from the gradient of a potential function. Since this velocity field is shown by Equation (1.59) to have a zero curl, and since the average angular velocity of a fluid element is shown by Equation (1.58) to be proportional to the curl of **V**, we also see that a potential flow is irrotational.
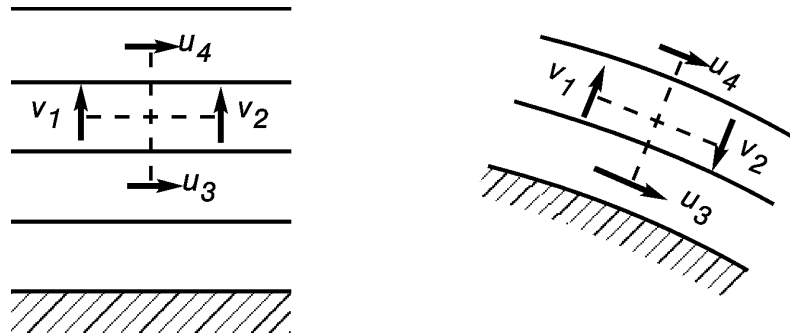
Figure 6.2 Vorticity for irrotational motion in (a) uniform flow and (b) curvilinear flow.

It is now worth reviewing the physical interpretation of vorticity and irrotationality that was introduced in the first chapter. If we consider the uniform flow shown in Figure 6.2(a), then the angular velocities of the two dashed lines must be equal in magnitude and opposite in direction. Since $v_1 = v_2 = 0$, this means that $u_4 = u_3$. Thus, velocities parallel to the physical boundary must remain constant all the way to the boundary, and there can be no boundary layer. The curvilinear flow in Figure 6.2(b) has $v_2 = -v_1$. This means that the dashed line parallel to the curved boundary has an angular velocity in the clockwise direction. Thus, the dashed line normal to the boundary must have the same angular velocity in the counterclockwise direction, which means that $u_3 > u_4$. In other words, the irrotational velocity must increase as we move toward the centre of curvature, and this rate of velocity increase must be maintained right to the physical boundary. Again, we see that fluid must slip along the physical boundary in irrotational flow, and no boundary layer can exist. This means that the definitions of a streamline and a fixed physical boundary are identical for steady irrotational motion: the normal velocity component, and only the normal velocity component, vanishes along both surfaces.

Thus, any streamline in steady irrotational flow can be replaced with a fixed physical boundary, and vice versa.

Simplification of the Governing Equations

Equations (6.1) – (6.2) simplify considerably with the introduction of (6.13). For example, substitution for **V** from (6.13) in (6.1) shows that ϕ satisfies the Laplace equation.

$$\nabla^2 \phi = 0 \tag{6.15}$$

The unabbreviated form of (6.15) is

$$\frac{\partial^2 \phi}{\partial x^2} + \frac{\partial^2 \phi}{\partial y^2} + \frac{\partial^2 \phi}{\partial z^2} = 0 \tag{6.16}$$

This effectively uncouples (6.1) - (6.2) since (6.16) contains ϕ as its only unknown. Furthermore, (6.15) is linear with constant coefficients and is one of the simplest and most studied partial differential equations in mathematical physics.

Boundary conditions for (6.15) require that we specify normal velocity components along all boundaries. Thus, if we replace e_t and s in (1.45) with e_n and n, respectively, then boundary conditions take the form

$$\frac{d\phi}{dn} = \boldsymbol{V} \cdot \boldsymbol{e}_n = F \tag{6.17}$$

in which n = arc length normal to a boundary and F is a prescribed function that may or may not be zero. For example, $F = 0$ along boundaries ab and cd in Figure 5.1. However, F would be non-zero constants along ad and bc given by $F = U_1$ and $F = U_1 B_1 / B_2$ for ad and bc, respectively. Thus, the function F cannot be prescribed in a completely arbitrary way on all boundaries of a flow region; it must be constant along boundaries that lie in uniform flow, and it must also satisfy the control volume form of the continuity equation, (3.1).

Equations (6.15) and (6.17) can be solved for ϕ, and ϕ can in turn be used to calculate $\boldsymbol{V}$ in any part of the flow. The remaining unknown, the pressure, p, or the piezometric head, h, (knowledge of h gives p, and vice versa), must then be found by integration (6.2). However, this can be done, once and for all, in a very general way. In particular, because of the identities

$$\frac{\partial u}{\partial y} = \frac{\partial}{\partial y}\left(\frac{\partial \phi}{\partial x}\right) = \frac{\partial}{\partial x}\left(\frac{\partial \phi}{\partial y}\right) = \frac{\partial v}{\partial x}$$

$$\frac{\partial u}{\partial z} = \frac{\partial}{\partial z}\left(\frac{\partial \phi}{\partial x}\right) = \frac{\partial}{\partial x}\left(\frac{\partial \phi}{\partial z}\right) = \frac{\partial w}{\partial x} \tag{6.18 a, b, c}$$

$$\frac{\partial u}{\partial t} = \frac{\partial}{\partial t}\left(\frac{\partial \phi}{\partial x}\right) = \frac{\partial}{\partial x}\left(\frac{\partial \phi}{\partial t}\right)$$

the acceleration component in the $\boldsymbol{i}$ direction can be rewritten as

$$u\frac{\partial u}{\partial x} + v\frac{\partial u}{\partial y} + w\frac{\partial u}{\partial z} + \frac{\partial u}{\partial t} = u\frac{\partial u}{\partial x} + v\frac{\partial v}{\partial x} + w\frac{\partial w}{\partial x} + \frac{\partial}{\partial x}\left(\frac{\partial \phi}{\partial t}\right)$$

$$= \frac{\partial}{\partial x}\left[\left(u^2 + v^2 + w^2\right)\big/2 + \frac{\partial \phi}{\partial t}\right] \tag{6.19}$$

Similar expressions can be obtained for the j and k acceleration components, and this allows (6.2) to be rewritten as

$$\nabla\left(gh + \mathbf{V} \cdot \mathbf{V}\big/2 + \frac{\partial \phi}{\partial t} \right) = 0 \qquad\qquad \textbf{(6.20)}$$

After dividing by g, Eq. (6.20) gives the following three component equations:

$$\frac{\partial}{\partial x}\left(h + \frac{V^2}{2g} + \frac{1}{g}\frac{\partial \phi}{\partial t} \right) = 0$$

$$\frac{\partial}{\partial y}\left(h + \frac{V^2}{2g} + \frac{1}{g}\frac{\partial \phi}{\partial t} \right) = 0 \qquad\qquad \textbf{(6.21 a, b, c)}$$

$$\frac{\partial}{\partial z}\left(h + \frac{V^2}{2g} + \frac{1}{g}\frac{\partial \phi}{\partial t} \right) = 0$$

Since the bracketed terms in (6.21) are not functions of x, y and z, the most general solution of (6.21) is

$$\boxed{h + \frac{V^2}{2g} + \frac{1}{g}\frac{\partial \phi}{\partial t} = H} \qquad\qquad \textbf{(6.22)}$$

in which H is a function of t. However, $\mathbf{V}$ is calculated from the spacial derivatives of ϕ, and neither ϕ nor its time derivative have any physical meaning in this problem. Thus, we can always include in the definition of ϕ an added function of t that has been determined so that its time derivative gives $gH(t)$.

$$\phi(x, y, z, t) = \phi'(x, y, z, t) + \int_0^t gH(t)\, dt \qquad\qquad \textbf{(6.23)}$$

Then ϕ is replaced with ϕ' in (6.15), (6.17) and (6.22), and H on the right side of (6.22) is replaced with a zero.[*] ***This means that H in Eq. (6.22) can always be chosen to be either zero or a constant, and we will always do so***.

Equation (6.22) is a general form of the Bernoulli equation that differs in two very important respects from the Bernoulli equation (4.3) that we used for control volume analysis. First, it can be used for unsteady as well as steady flow. Second, the sum of terms on the left side of (6.22) is constant for each and every point in the flow and not just for points along the same streamline.

---

[*]   This argument fails in steady flow, where variables do not depend upon time. In this case, H in (6.22) is a constant that must be calculated for each problem.

Basic Irrotational Flow Solutions

Known solutions and solution techniques for the Laplace equation cover a vast quantity of material. Therefore, we will limit our consideration to steady flow in two dimensions. Then the Laplace equation has the form

$$\frac{\partial^2 \phi}{\partial x^2} + \frac{\partial^2 \phi}{\partial y^2} = 0 \tag{6.24}$$

which can also be written in the following polar coordinate form:

$$\frac{1}{r}\frac{\partial}{\partial r}\left(r\frac{\partial \phi}{\partial r} \right) + \frac{1}{r^2}\frac{\partial^2 \phi}{\partial \theta^2} = 0 \tag{6.25}$$

Velocity vectors in these coordinate systems are calculated from

$$\boldsymbol{V} = \boldsymbol{i}\,\frac{\partial \phi}{\partial x} + \boldsymbol{j}\,\frac{\partial \phi}{\partial y} = \boldsymbol{e}_r\,\frac{\partial \phi}{\partial r} + \boldsymbol{e}_\theta\,\frac{1}{r}\,\frac{\partial \phi}{\partial \theta} \tag{6.26}$$

A sketch of these two coordinate systems is shown in Figure 6.3.
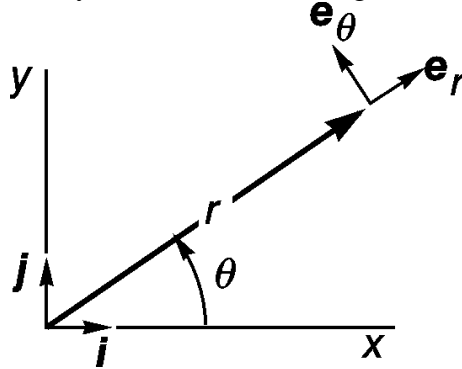
Figure 6.3 Coordinates and unit base vectors in the Cartesian and polar coordinate systems.

Uniform flow in the positive x direction has the potential

$$\phi = Ux \quad , \quad \left(U = \text{constant} \right) \tag{6.27}$$

in which U is positive for flow in the $\boldsymbol{i}$ direction and negative for flow in the $-\boldsymbol{i}$ direction. Direct substitution of (6.27) into (6.24) shows that (6.27) satisfies the Laplace equation, and substitution into (6.26) gives the corresponding velocity field.

$$\boldsymbol{V} = U\boldsymbol{i} \tag{6.28}$$

A solution of (6.25) with radial symmetry is easily seen to be given by

$$\phi = \frac{q}{2\pi} \ln(r) \quad , \quad (q = \text{constant})$$

(6.29)

Substitution of (6.29) into (6.26) gives

$$V = \frac{q}{2\pi r} \, \boldsymbol{e}_r$$

(6.30)

Equation (6.30) shows that V is radially outward for $q > 0$ and inward for $q < 0$. Since $|V| = |q|/(2\pi r)$, and since $2\pi r = $ circumference of a circle of radius r, we see that $q = $ flow rate per unit width emitted by a source $(q > 0)$ or absorbed by a sink $(q < 0)$. Note that V becomes singular as $r \to 0$.

Since (6.25) contains only a second derivative with respect to θ, a solution of (6.25) is also given by a linear function of θ.

$$\phi = \frac{\Gamma_0}{2\pi} \theta \quad , \quad \left(\Gamma_0 = \text{constant}\right)$$

(6.31)

Substitution of (6.31) into (6.26) gives

$$V = \frac{\Gamma_0}{2\pi r} \, \boldsymbol{e}_\theta$$

(6.32)

Since V is in the $\boldsymbol{e}_\theta$ direction and changes only with r, (6.31) is the solution for an irrotational vortex. As noted earlier, $|V|$ increases as r decreases, and we see again the V becomes singular as $r \to 0$. The velocity is in the $\boldsymbol{e}_\theta$ direction for $\Gamma_0 > 0$ and in the $-\boldsymbol{e}_\theta$ direction for $\Gamma_0 < 0$. Furthermore, calculation of the circulation around any closed path that includes $r = 0$ in its interior shows that the constant Γ_0 in (6.31) - (6.32) is the circulation Γ defined in (6.3). The circulation calculated from (6.3) for any closed path that does not include the point $r = 0$ in its interior can also be shown to be zero. (This does not violate Kelvin's constant circulation theorem since any closed material path that surrounds $r = 0$ at $t = 0$ will also include $r = 0$ at later times. Thus, the circulation will remain constant for any closed material path.)

The easiest way to calculate the circulation from (6.3) for any irrotational flow is to substitute (6.13) into (6.3) to obtain

$$\Gamma = \int_a^b V \cdot dr = \int_a^b \nabla \phi \cdot dr = \int_a^b d\phi = \phi_b - \phi_a$$

(6.33)

Thus, (6.31) and (6.33) show for an irrotational vortex that the circulation about any closed path that surrounds the origin, since $\theta_b - \theta_a = 2\pi$, is

$$\Gamma = \frac{\Gamma_0}{2\pi}\left(\theta_b - \theta_a\right) = \Gamma_0 \qquad\qquad (6.34)$$

and that any closed path that excludes $r = 0$ from its interior has $\theta_b = \theta_a$ so that

$$\Gamma = \frac{\Gamma_0}{2\pi}\left(\theta_b - \theta_a\right) = 0 \qquad\qquad (6.35)$$

Since the coefficients in (6.24) are constant, replacing x and y in any solution of (6.24) with $x - \xi$ and $y - \eta$ will still give a solution of (6.24) provided that ξ and η do not depend upon x and y. Thus, in any of our basic solutions we can replace r and θ with

$$r = \sqrt{(x - \xi)^2 + (y - \eta)^2} \qquad\qquad (6.36)$$

$$\theta = \tan^{-1}\left(\frac{y - \eta}{x - \xi}\right) \qquad\qquad (6.37)$$

in which r and θ now have the interpretations of radial distance and angular displacement in a local coordinate system with its origin at the point (ξ, η). Since (6.24) is also linear, we can add or subtract any number of these basic solutions to obtain other solutions. This is a process known as superposition.

An example of the superposition process can be used to obtain the basic potential for flow from a doublet. If a source and sink are placed at points 2 and 1, respectively, in Figure 6.4, the potential is

$$\phi = \frac{q}{2\pi}\ln(r_2) - \frac{q}{2\pi}\ln(r_1) \qquad (6.38)$$
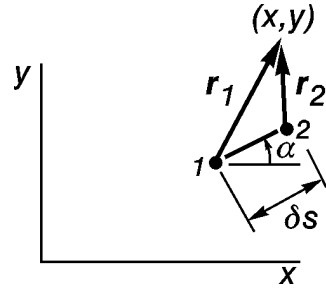
Multiplying the right side of (6.38) by $\delta s/\delta s$ in which δs = distance between points 1 and 2 gives

$$\phi = \frac{q\,\delta s}{2\pi}\,\frac{\ln(r_2) - \ln(r_1)}{\delta s} \qquad (6.39)$$

Figure 6.4 Superposition of a source at point 2 and a sink at point 1 to obtain a doublet.

If we now set $q\,\delta s = \Delta$ = constant and take the limit $\delta s \to 0$ we obtain

$$\phi = \frac{\Delta}{2\pi}\,\frac{d}{ds}\ln(r) = \frac{\Delta}{2\pi}\,\nabla_{\xi,\eta}\ln(r)\cdot e_t \qquad\qquad (6.40)$$

in which $\nabla_{\xi,\eta}$ is the gradient calculated with respect to the (ξ,η) coordinates and $\boldsymbol{e}_t$ = unit vector along the doublet axis 1 - 2. Since r is given by (6.36), the gradients with respect to (ξ,η) and (x, y) differ by a minus sign. Thus, we can set $\nabla_{\xi,\nabla} = -\nabla_{x,y}$ and use the polar coordinate form of (6.26) to calculate $\nabla_{x,y}$. This gives

$$\phi = -\frac{\Delta}{2\pi r}\, \boldsymbol{e}_r \cdot \boldsymbol{e}_t = -\frac{\Delta}{2\pi r}\cos(\theta - \alpha) \tag{6.41}$$

The velocity field calculated from (6.26) and (6.41) is

$$V = \frac{\Delta}{2\pi r^2}\left[\cos(\theta - \alpha)\,\boldsymbol{e}_r + \sin(\theta - \alpha)\,\boldsymbol{e}_\theta\right] \tag{6.42}$$

The superposition principle applies not only to velocity potential functions but also to velocity vector fields generated from the potentials. Streamline geometries for uniform flow, a source and sink, a vortex and a doublet are shown in Figure 6.5.

$V = U_0\boldsymbol{i}$
$\phi = U_0 x$
$\psi = U_0 y$

Uniform flow

$V = \dfrac{q}{2\pi}\dfrac{1}{r}\boldsymbol{e}_r$

$\phi = \dfrac{q}{2\pi}\ln(r)$

$\psi = \dfrac{q}{2\pi}\theta$

Source (q>0)   *Sink (q<0)*

$V = \dfrac{\Gamma_0}{2\pi}\dfrac{1}{r}\boldsymbol{e}_\theta$

$\phi = \dfrac{\Gamma_0}{2\pi}\theta$

$\psi = -\dfrac{\Gamma_0}{2\pi}\ln(r)$

Vortex ($\Gamma_0 > 0$)

$V = \dfrac{\Delta}{2\pi}\dfrac{1}{r^2}[\cos(\theta\text{-}\alpha)\boldsymbol{e}_r + \sin(\theta\text{-}\alpha)\boldsymbol{e}_\theta]$

$\phi = -\dfrac{\Delta}{2\pi}\dfrac{\cos(\theta\text{-}\alpha)}{r}$

$\psi = \dfrac{\Delta}{2\pi}\dfrac{\sin(\theta\text{-}\alpha)}{r}$
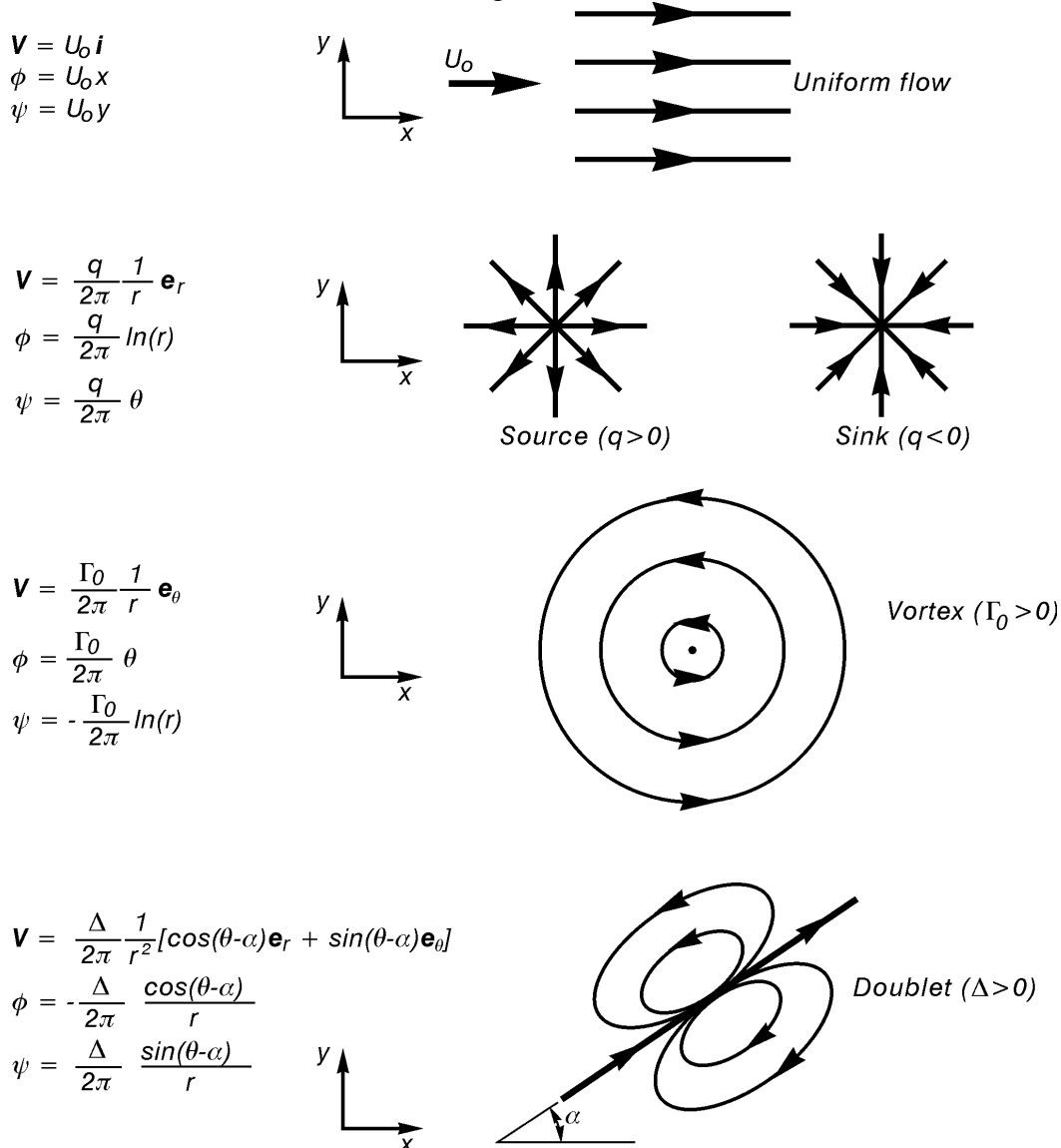
Doublet ($\Delta > 0$)

Figure 6.5 Streamline patterns for some basic flows.

Example 6.1
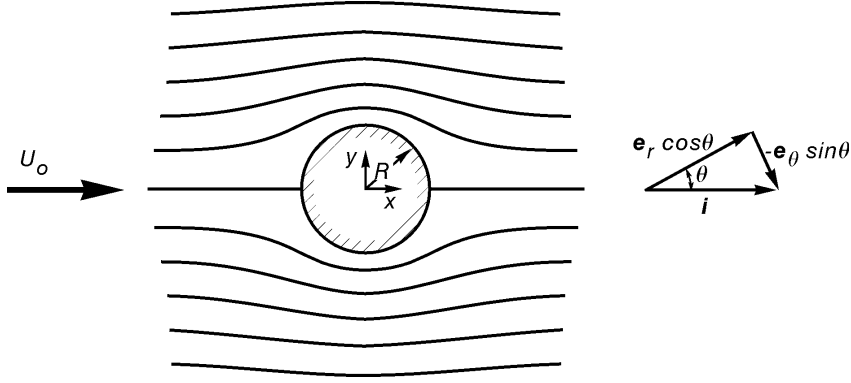
Flow past a circle of radius R surrounding the origin can be obtained by adding the potentials and velocity fields for uniform flow and a doublet at the origin with $\alpha = \pi$.

$$\phi = U_0 x + \frac{\Delta}{2\pi r} \cos\theta$$

$$V = U_0 i + \frac{\Delta}{2\pi r^2}\left(-\cos\theta\, e_r - \sin\theta\, e_\theta\right)$$

Set $i = \cos\theta\, e_r - \sin\theta\, e_\theta$ in the expression for V to obtain

$$V = \left(U_0 - \frac{\Delta}{2\pi r^2}\right)\cos\theta\, e_r - \left(U_0 + \frac{\Delta}{2\pi r^2}\right)\sin\theta\, e_\theta$$

Since the normal velocity component must vanish on the cylinder surface $r = R$, we must set

$$U_0 - \frac{\Delta}{2\pi R^2} = 0$$

to obtain $\Delta = 2\pi R^2 U_0$ and

$$V = U_0\left[1 - \left(\frac{R}{r}\right)^2\right]\cos\theta\, e_r - U_0\left[1 + \left(\frac{R}{r}\right)^2\right]\sin\theta\, e_\theta$$

At $r = \infty$ we see that $V = U_0 \cos\theta\, e_r - U_0 \sin\theta\, e_\theta = U_0 i$, and on $r = R$ we have $V \cdot e_r = 0$, which proves that this is the solution for flow past the circular cylinder. On the cylinder surface the tangential velocity vector is

$$V = -2U_0 \sin\theta\, e_\theta$$

The pressure on the cylinder surface is calculated from the Bernoulli equation

$$p + \rho V^2\big/2 = \text{constant} = \rho U_0^2\big/2$$

in which we have neglected gravity and the integration constant has been evaluated at infinity, where $V^2 = U_0^2$ and $p = 0$. Setting $V^2 = 4U_0^2 \sin^2\theta$ on the cylinder surface gives

$$p_{r=R} = \left(1 - 4\sin^2\theta\right)\rho \, U_0^2 \Big/ 2$$

A dimensionless plot of this pressure distribution is shown below.
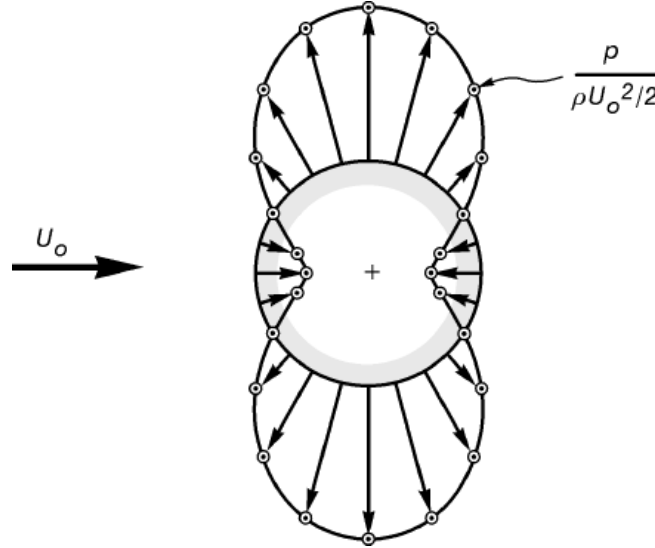
It is evident from the symmetry of pressure distribution that there is no net pressure force on the cylinder in any direction. The fact that the drag force (the force in the direction of the approaching flow) is zero is known as D'Alembert's paradox, a result that is true for any object submerged in an irrotational flow without separation.

Example 6.2

Since an irrotational vortex has a zero radial component of velocity and an e_θ velocity component that vanishes as $r \to \infty$, we can add the potential and velocity fields for a vortex to the potential and velocity fields in Example 6.1 to obtain a solution for flow past a cylinder with circulation.

$$\phi = U_0\left(x + \frac{R^2}{r}\cos\theta\right) + \frac{\Gamma_0}{2\pi}\theta$$

$$V = U_0\left[1 - \left(\frac{R}{r}\right)^2\right]\cos\theta \, e_r - U_0\left[1 + \left(\frac{R}{r}\right)^2\right]\sin\theta \, e_\theta + \frac{\Gamma_0}{2\pi r}e_\theta$$

Since velocity vector components add near the cylinder bottom and subtract near the top, this increases V and decreases p near the bottom and decreases V and increases p near the top. A sketch of the streamline pattern is shown below.
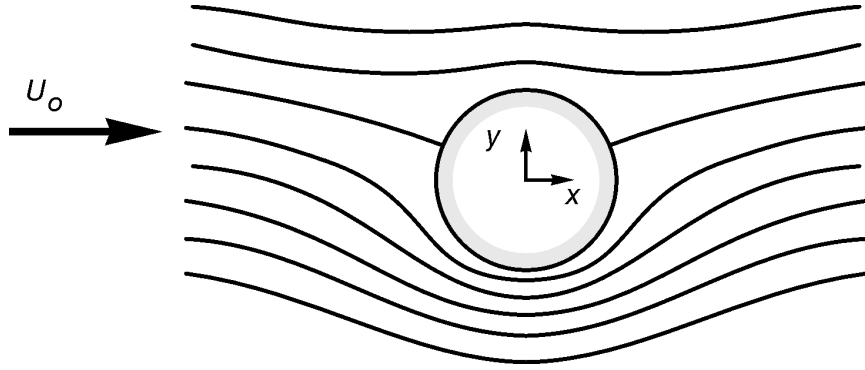
Symmetry shows that the drag force is still zero, but the increased pressures on top and decreased pressures below obviously lead to a downward "lift" force. Since V^2 on the cylinder surface is given by

$$V^2 = \left(-2U_0 \sin\theta + \frac{\Gamma_0}{2\pi R} \right)^2$$

the pressure on the cylinder surface is

$$p = \rho U_0^2 / 2 - \rho \left(-2U_0 \sin\theta + \frac{\Gamma}{2\pi R} \right)^2 / 2$$

The pressure force on the cylinder is

$$\boldsymbol{F} = -\int p\,\boldsymbol{e}_r\,ds = -\int_{-\pi}^{\pi} p\,(\boldsymbol{i}\cos\theta + \boldsymbol{j}\,\sin\theta)\,R\,d\theta$$

Substitution for p and integration gives

$$\boldsymbol{F} = -\rho U_0 \Gamma_0 \boldsymbol{j}$$

It can be shown that this expression for a lift force holds for irrotational flow past any object. An approximation to this flow field can be generated in the laboratory by placing a spinning cylinder in a uniform flow. In this case viscosity forces the fluid to "stick" to the spinning boundary and generates a circulation pattern around the cylinder. In three dimensions this same process creates the side thrust that causes a spinning golf ball, tennis ball, cricket ball or baseball to curve.

Example 6.3

The previous two examples were concerned with flow exterior to the surface of a circular cylinder $(r > R)$. However, a mathematical flow also occurs within the cylinder boundary even though the region $r < R$ lies outside the region of physical interest for this particular application. A sketch of the internal streamline pattern for Example 6.1 is shown below:
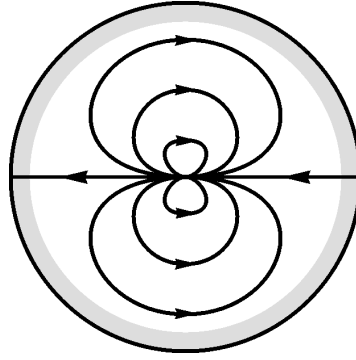
Thus, a streamline has been used to replace a physical boundary.

Flow past a circular cylinder was generated in Examples 6.1 and 6.2 by placing singularities within the circular streamline that modelled the boundary. This suggests that flow past more generally shaped boundaries might be modelled by adding potential and velocity fields for numerous sources, sinks, doublets and vortices that have been placed within the streamline that coincides with the physical boundary. For example, the following velocity potential

$$\phi = Ux + \frac{q}{2\pi} \ln\left(r_1\right) - \frac{q}{2\pi} \ln\left(r_2\right)$$

might be used to approximate flow past the elliptical boundary shown below.
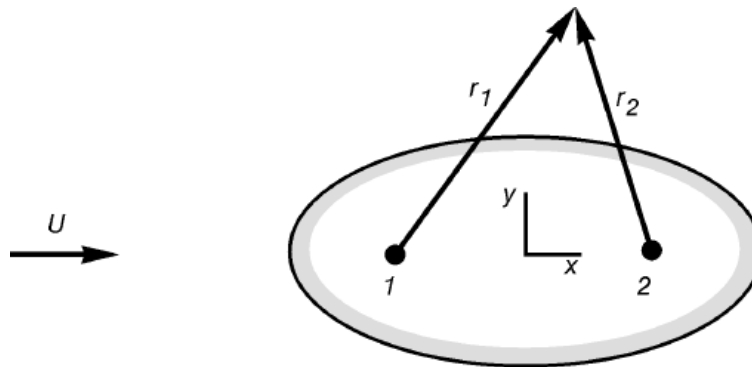
The potential function is the sum of the potentials for uniform flow, a source of strength q at point 1 and a sink of strength q at point 2. The source and sink must be of equal strength since no flow can pass through the closed streamline that models the physical boundary, and the undetermined constant q can be found by requiring that the normal velocity component vanish at one point on the boundary streamline.

A better approximation for this flow could be obtained by placing a number of sources along the x axis and determining the strengths of these singularities by requiring zero normal velocity components at a number of different points along the boundary. In particular, we might set

$$\phi = Ux + \sum_{i=1}^{N} \frac{q_i}{2\pi} \ln\left(r_i\right)$$

and determine the constants q_i by requiring

$$0 = \nabla \phi \cdot e_n = U \frac{dx_j}{dn} + \sum_{i=1}^{N} \frac{q_i}{2\pi} \left[\left(x_j - x_i \right) \frac{dx_j}{dn} + y_j \frac{dy_j}{dn} \right] \Big/ r_{ij}^2$$

in which $\left(x_j, y_j \right)$ is a point on the ellipse boundary, $\left(x_i, 0 \right)$ is a point on the x axis inside the ellipse boundary, $r_{ij} =$ distance between points $\left(x_i, 0 \right)$ and $\left(x_j, y_j \right)$ and

$$e_n = \frac{dx_j}{dn} i + \frac{dy_j}{dn} j$$

is the boundary unit normal at $\left(x_j, y_j \right)$. By choosing point j at N different points along the boundary we could obtain N simultaneous equations to solve for the N unknown values of q_i. Solution of these equations would give positive values for some q_i's and negative values for others. In general, we would find that

$$\sum_{i=1}^{N} q_i = 0$$

since no flow passes through the boundary. The use of doublets instead of sources would obviate this last requirement since a doublet is the result of combining a source and sink of equal strength.

Even more accurate results could be obtained by using definite integrals to distribute singular solutions over the boundary surface. This method leads to the solution of singular integral equations, a technique that is known in most present day engineering literature as the boundary element method.

Stream functions

In many applications it is helpful to be able to plot streamlines for a flow. This can be done relatively easily for two-dimensional and axisymmetric flows by introducing a stream function, which we will denote by ψ. For example, in two dimensions the continuity equation

$$\frac{\partial u}{\partial x} + \frac{\partial v}{\partial y} = 0 \tag{6.43}$$

can be satisfied for all flows, inviscid or viscid, by calculating u and v from the following equations:

$$u = \frac{\partial \psi}{\partial y}$$

$$v = -\frac{\partial \psi}{\partial x} \tag{6.44 a, b}$$

Substitution of (6.44) into (6.43) shows that all choices for ψ will generate values for u and v that satisfy (6.43).

If we also require that a flow be irrotational (i.e. flow generated from a velocity potential function, ϕ), then (6.14) and (6.44) require that

$$\frac{\partial \phi}{\partial x} = \frac{\partial \psi}{\partial y}$$

$$\frac{\partial \phi}{\partial y} = -\frac{\partial \psi}{\partial x}$$

(6.45 a, b)

Elimination of ϕ from (6.45) gives

$$0 = \frac{\partial}{\partial y}\left(\frac{\partial \phi}{\partial x}\right) - \frac{\partial}{\partial x}\left(\frac{\partial \phi}{\partial y}\right) = \frac{\partial}{\partial y}\left(\frac{\partial \psi}{\partial y}\right) - \frac{\partial}{\partial x}\left(-\frac{\partial \psi}{\partial x}\right)$$

(6.46)

This shows that the stream function, ψ, is also a solution of the Laplace equation.[*]

$$\frac{\partial^2 \psi}{\partial x^2} + \frac{\partial^2 \psi}{\partial y^2} = 0$$

(6.47)

The physical significance of ψ is found by substituting for u and v from (6.44) into the equation for a streamline, which is given by Eq. (1.20).

$$0 = -v\,dx + u\,dy = \frac{\partial \psi}{\partial x}\,dx + \frac{\partial \psi}{\partial y}\,dy = d\psi$$

(6.48)

> Thus, integration of (6.48) shows that the equation of a streamline is obtained by setting ψ equal to a constant.

$$\psi(x, y) = \text{constant}$$

(6.49)

Every streamline in a flow will have a different value for the integration constant in (6.49).

The integration constant in (6.49) has a very important physical meaning that can be found by calculating the flow rate contained between any two streamlines. For example, the flow rate passing through any line parallel to the y axis that connects point 1 on the streamline $\psi(x, y) = \psi_1$ with point 2 on the streamline $\psi(x, y) = \psi_2$ is

$$q = \int_1^2 u\,dy = \int_1^2 \frac{\partial \psi}{\partial y}\,dy = \psi_2 - \psi_1$$

(6.50)

---

[*] Do not try to extrapolate this result to axisymmetric flows. A similar procedure for axisymmetric flows easily leads to the equation satisfied by ψ, but it is ***not*** the Laplace equation.

Equation (6.50) shows that the difference between two numerical values of ψ on any two streamlines gives the flow rate contained between the two streamlines. Of course there is also a sign associated with q in (6.50), and this sign will depend upon whether u is in the direction $\boldsymbol{i}$ or $-\boldsymbol{i}$ and whether $y_2 > y_1$ or $y_2 < y_1$. The same result can be obtained by integrating along a line parallel to the x axis, and a little more effort can produce the same result by integrating along any curved line joining points 1 and 2. ***One important consequence of (6.50) is that the integration constant in (6.49) may be chosen arbitrarily on one streamline in a flow, and numerical values for the remaining constants will be fixed by (6.50) for all other streamlines.***

The stream function for a uniform flow in the x direction is obtained by using (6.27) and (6.45).

$$\frac{\partial \psi}{\partial y} = \frac{\partial \phi}{\partial x} = U$$

$$\frac{\partial \psi}{\partial x} = -\frac{\partial \phi}{\partial y} = 0$$

(6.51 a, b)

Integration of (6.51 b) gives

$$\psi = f(y) \tag{6.52}$$

and substitution of (6.52) into (6.51 a) gives an ordinary differential equation for $f(y)$.

$$\frac{df(y)}{dy} = U \tag{6.53}$$

Integration of (6.53) and substitution of the result into (6.52) gives

$$\psi = Uy + C \tag{6.54}$$

Choosing $\psi = 0$ on the streamline $y = 0$ gives $C = 0$. Thus, the stream function for uniform flow in the x direction is

$$\psi = Uy \tag{6.55}$$

Since streamlines for this flow are shown by (6.55) to be lines of constant y, it is obvious that (6.55) satisfies (6.50).

Stream functions for the remaining basic solutions are most easily obtained by writing the polar coordinate form of (6.45).

$$\frac{\partial \phi}{\partial r} = \frac{1}{r}\frac{\partial \psi}{\partial \theta}$$

$$\frac{1}{r}\frac{\partial \phi}{\partial \theta} = -\frac{\partial \psi}{\partial r}$$

(6.56 a, b)

Thus, the stream function for a source is found from (6.28) and (6.56) as the integral of

$$\frac{\partial \psi}{\partial \theta} = \frac{q}{2\pi}$$

$$\frac{\partial \psi}{\partial r} = 0$$

(6.57 a, b)

The solution of (6.57) is

$$\psi = \frac{q}{2\pi} \theta$$

(6.58)

with $q > 0$ for a source and $q < 0$ for a sink. Equation (6.58) shows that streamlines for a source are the radial lines θ = constant. Since numerical values of θ on two adjacent streamlines differ by 2π after one complete circuit about the source, (6.58) also shows that q is the flow rate emitted by the source.

The stream function for a vortex is

$$\psi = -\frac{\Gamma_0}{2\pi} \ln(r)$$

(6.59)

in which $\Gamma_0 > 0$ for counterclockwise circulation. The stream function for a doublet is

$$\psi = \frac{\Delta}{2\pi} \frac{\sin(\theta - \alpha)}{r}$$

(6.60)

Streamlines for a vortex are seen from (6.58) to be circles about the vortex centre, while streamlines for a doublet have a more complicated geometry that has been sketched in Figure 6.5 and Example 6.3.

The stream function, ψ, satisfies a linear equation, (6.47). Thus, stream functions can also be superimposed by the algebraic addition and subtraction of stream functions for different flows. For example, the stream function for Example 6.1 is

$$\psi = U_0 y - \frac{\Delta}{2\pi} \frac{\sin\theta}{r} \quad , \quad \left(\Delta = 2\pi R^2 U_0\right)$$

(6.61)

Streamlines are most conveniently plotted from (6.61) by setting $y = r \sin\theta$ to obtain

$$\psi = U_0 \left(r - \frac{R^2}{r} \right) \sin\theta$$

(6.62)

In other problems it is sometimes easier to use Cartesian coordinates or to mix Cartesian and polar coordinates in the same expression for ψ. The values of ψ calculated in this section are summarized in Figure 6.5.

Example 6.4

Flow past a half body is obtained by placing a source in a uniform flow. A sketch of the flow pattern is shown below.
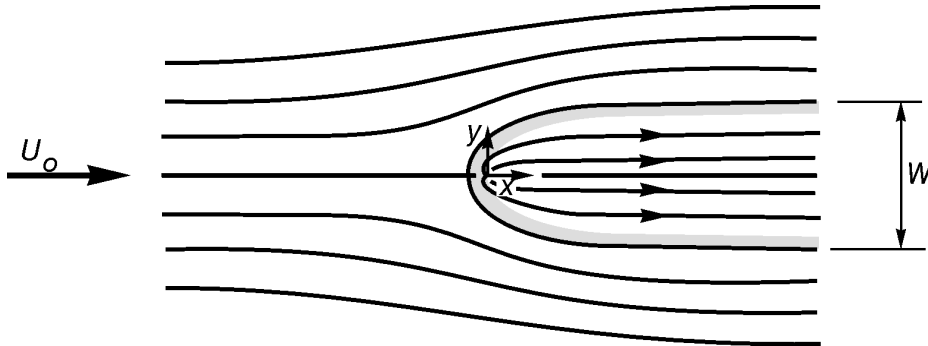
Since all velocities, both within and outside the half body, approach U_0 as $r \to \infty$, the flow rate emitted by the source at the coordinate origin is calculated at $x = \infty$ within the half body as

$$q = U_0 W$$

which determines q in terms of the approach velocity and the asymptotic width. The potential function, stream function and velocity field for this flow are

$$\phi = U_0 x + \frac{q}{2\pi} \ln(r)$$

$$\psi = U_0 y + \frac{q}{2\pi} \theta$$

$$V = U_0 i + \frac{q}{2\pi} \frac{e_r}{r}$$

Flow past the rear half of a half body is obtained by placing a sink in a uniform flow field. The flow pattern is identical with the above sketch except that both U_0 and the x axis have their directions reversed.

Example 6.5

Steady groundwater flow is a very important application area for potential flow in civil and environmental engineering. If an aquifer is homogeneous, and if streamlines are horizontal, then these flows are solutions of a continuity equation

$$\frac{\partial u}{\partial x} + \frac{\partial v}{\partial y} = 0$$

and Darcy's law

$$u = \frac{\partial \phi}{\partial x} \quad \text{and} \quad v = \frac{\partial \phi}{\partial y} \quad \text{with} \quad \phi = -Kh$$

in which K = coefficient of permeability and h = piezometric head = water table elevation if the aquifer is unconfined. These equations are identical with the equations used to treat two-dimensional irrotational flow. Thus, a stream function can be defined in the same way and solutions for irrotational flow can be used for groundwater flow.

The half body solution considered in Example 6.4 is important in groundwater pollution problems since it describes the streamlines for flow from a point source of contamination. If contaminant scattering is neglected, then the contaminant is contained entirely within the half body boundary. Flow past the rear half of the half body becomes important if a well is placed downstream from a contaminated area to abstract the contaminated groundwater for treatment. Then the half body interior becomes what is known as the "zone of capture". If the well abstracts a total flow of Q m^3/s, and if the aquifer has a saturated thickness of B, then $q = Q/B$. Thus, if the polluted area has a horizontal width W across the streamlines, then the well must abstract a minimum flow of

$$Q = B U_0 W$$

in order to keep the polluted area entirely within the zone of capture. A sketch of this case is shown below.
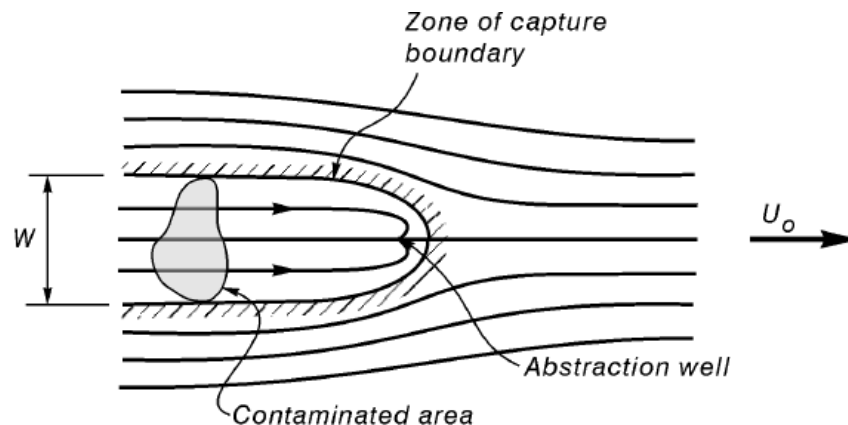
Flow Net Solutions

Flow nets provide a graphical technique for solving steady two-dimensional problems. Numerical techniques, such as the boundary element method mentioned at the end of Example 6.3, are considerably more accurate, efficient and versatile and are used for almost all modern applications of irrotational flow theory. Flow nets, however, have one great advantage over any other solution technique: they provide an easily grasped method for obtaining a physical understanding of irrotational flow behaviour. For this reason it can be argued that flow net methods are more important for an introductory course on fluid mechanics than the method of superposition of basic flows, which forms the basis for boundary element techniques.
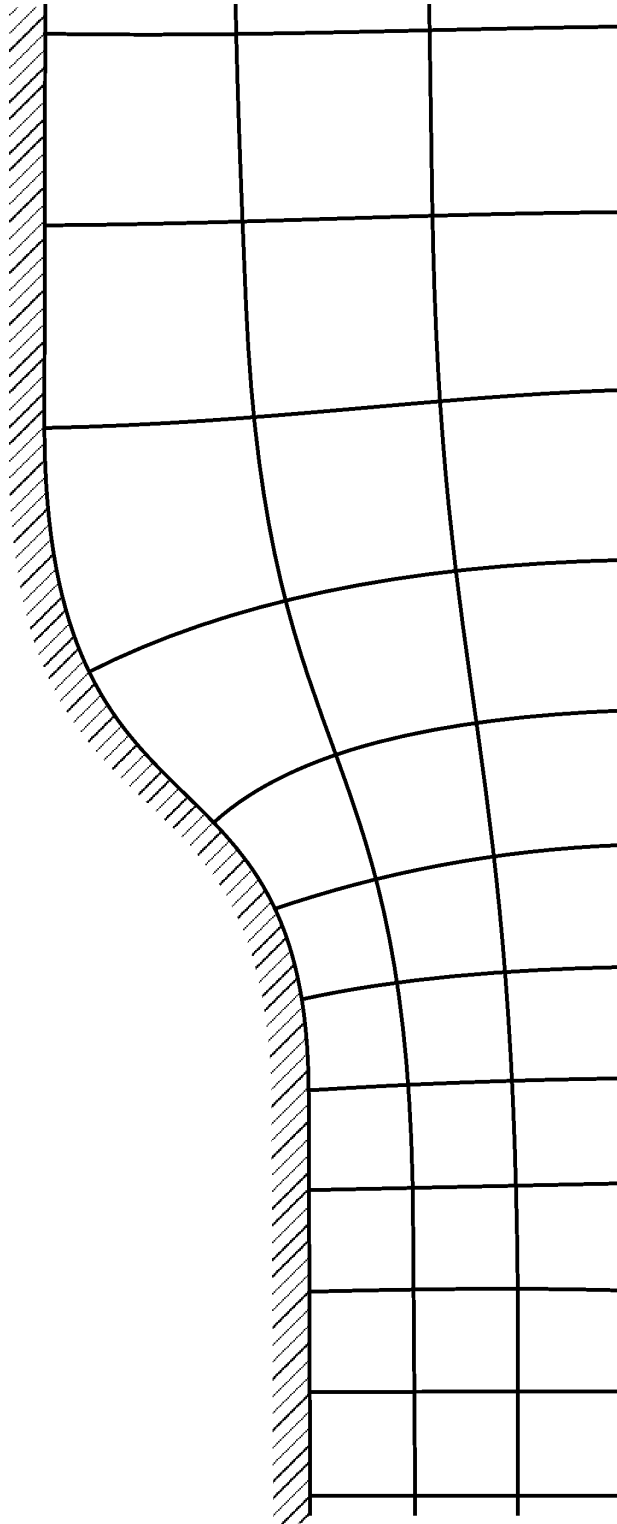
Figure 6.6 A flow net for the lower half of the flow shown in Figure 4.2.

It was explained in Chapter One, following Eq. (1.44), that the velocity vector is perpendicular to curves of constant ϕ. Since curves of constant ψ were shown by Eq. (6.49) to be tangent to the velocity vector, we immediately see that the curves $\phi(x, y) = $ constant and $\psi(x, y) = $ constant meet at right angles. This is true for all points in a flow except at isolated points where $\nabla\phi$ either vanishes or becomes infinite. A flow net is simply a freehand sketch of these curves of constant ϕ and ψ. An example is shown in Figure 6.6 for flow through the streamlined constriction shown in Figure 4.2. Since flow in Figure 4.2 is symmetrical about the conduit centreline, and since any streamline can be replaced with a boundary in irrotational flow, the flow net in Figure 6.6 has been drawn only for the lower half of the flow shown in Figure 4.2.

Flow net construction starts by sketching a guessed pattern of streamlines. Then the potential lines are sketched in at right angles to check the guessed streamline pattern. The check is accomplished by ensuring that the continuity equation is satisfied at each point in the flow. More specifically, along any streamtube bounded by two successive streamlines we can calculate the flow rate

$$\Delta q = \int_1^2 \boldsymbol{V} \cdot \boldsymbol{e}_t \, dn \tag{6.63}$$

in which $\boldsymbol{e}_t$ is tangent to both $\boldsymbol{V}$ and the streamlines, $n = $ distance normal to the streamlines, Δq = flow rate through the streamtube and points 1 and 2 are points on the two streamlines that bound the streamtube. Since $\Delta q = \psi_2 - \psi_1 = \Delta\psi$ from (6.50), and since $\boldsymbol{V} \cdot \boldsymbol{e}_t = d\phi/ds$ from (1.45), (6.63) becomes

$$\Delta\psi = \int_1^2 \frac{d\phi}{ds} \, dn \tag{6.64}$$

A finite-difference approximation for the integral in (6.64) gives

$$\Delta\psi = \frac{\Delta\phi}{\Delta s} \, \Delta n \tag{6.65}$$

in which $\Delta\phi$ = change in ϕ across two successive curves of constant ϕ, Δs = distance between these two curves measured across the element mid-point, $\Delta\psi$ = change in ψ across two successive curves of constant ψ and Δn = distance between these two curves measured across the element mid-point. A sketch of the geometry used to obtain (6.65) from (6.64) is shown in Figure 6.7. Equation (6.65) is the basic equation that is used to see if a flow net has been sketched so that continuity is satisfied across the mid-point of each flow net element.
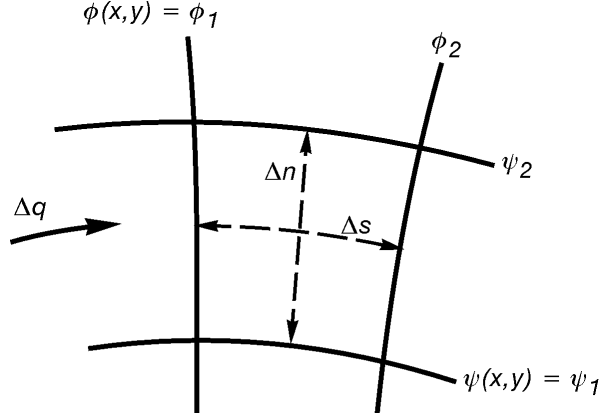
Figure 6.7 Geometry for a flow net element.

The usual practice when sketching flow nets is to choose $\Delta n = \Delta s$ across the mid-point of every flow net element and to refer to these elements as curvilinear squares. Then (6.65) shows that across each element

$$\Delta\psi \ = \ \Delta\phi \tag{6.66}$$

Along a stream tube, however, $\Delta\psi$ is the same constant for every element. Consequently, (6.66) shows that $\Delta\phi$ must also be the same constant across every element in that stream tube. Similarly, along a potential tube[*] $\Delta\phi$ is a constant, and (6.66) shows that $\Delta\psi$ is the same constant for every element in the potential tube. ***The end result is that by choosing $\Delta n = \Delta s$ in a flow net we ensure that $\Delta\psi$ is the same constant for all stream tubes, that $\Delta\phi$ is the same constant for all potential tubes and that $\Delta\psi = \Delta\phi$ for all elements in the flow net.***

The velocity at any point in a flow can be calculated by using a finite-difference approximation of Eq. (1.45)

$$V = \boldsymbol{V} \cdot \boldsymbol{e}_t = \frac{\Delta\phi}{\Delta s} \tag{6.67}$$

in which V = velocity at the mid-point of Δs. Equation (6.67) can be written for two different points in the flow net, and, since $\Delta\phi$ is the same constant at each point, the ratio of these two equations gives

$$\frac{V_b}{V_a} = \frac{\Delta s_a}{\Delta s_b} \tag{6.68}$$

Equation (6.68) allows velocities at points in the flow to be calculated in terms of one reference velocity, say V_a in (6.68). Then specification of that single reference velocity will determine all other velocities in the flow.

---

[*]   We define a potential tube to be the region between two successive curves of constant ϕ.

Students often make the mistake of thinking that Δs in (6.67) and (6.68) must be measured across the mid-point of a fluid element. ***This is not a requirement.*** In fact, most applications require the calculation of velocities and pressures on a physical boundary. In this case Δs is measured along the boundary between two curves of constant ϕ to obtain the velocity on the boundary mid-way between these two equi-potential curves. The geometry for this type of calculation is shown in Figure 6.8.
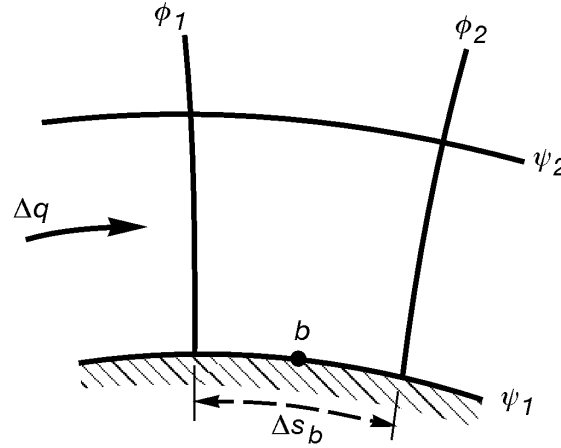
Figure 6.8 Geometry used for the calculation of the velocity on a boundary.

If (6.22) is applied between points a and b in steady flow, we obtain

$$h_b + \frac{V_b^2}{2g} = h_a + \frac{V_a^2}{2g} \tag{6.69}$$

Manipulations identical with those used to obtain Eq. (4.9) allow (6.69) to be rewritten in the following dimensionless form:

$$\frac{h_a - h_b}{V_a^2 \big/ (2g)} = \left(\frac{V_b}{V_a}\right)^2 - 1 \tag{6.70}$$

If gravity is neglected, then we obtain

$$\frac{p_a - p_b}{\rho V_a^2 \big/ 2} = \left(\frac{V_b}{V_a}\right)^2 - 1 \tag{6.71}$$

Since (6.68) gives a way of calculating the right side of either (6.70) or (6.71), we see that a flow net enables us to calculate velocities and pressures at points throughout the flow once the velocity and pressure are specified at one point in the flow. If a more general solution is desired in which V_a and h_a or p_a are not specified in advance, then (6.68) can be used to calculate distributions of the dimensionless term on the left side of (6.70) or (6.71). This is done in Figure 6.9 for the flow net shown in Figure 6.6.

$$\frac{p-p_a}{\rho V_a^2/2} = -3.53$$

$$\frac{p-p_a}{\rho V_a^2/2} = 0.5$$

Point a
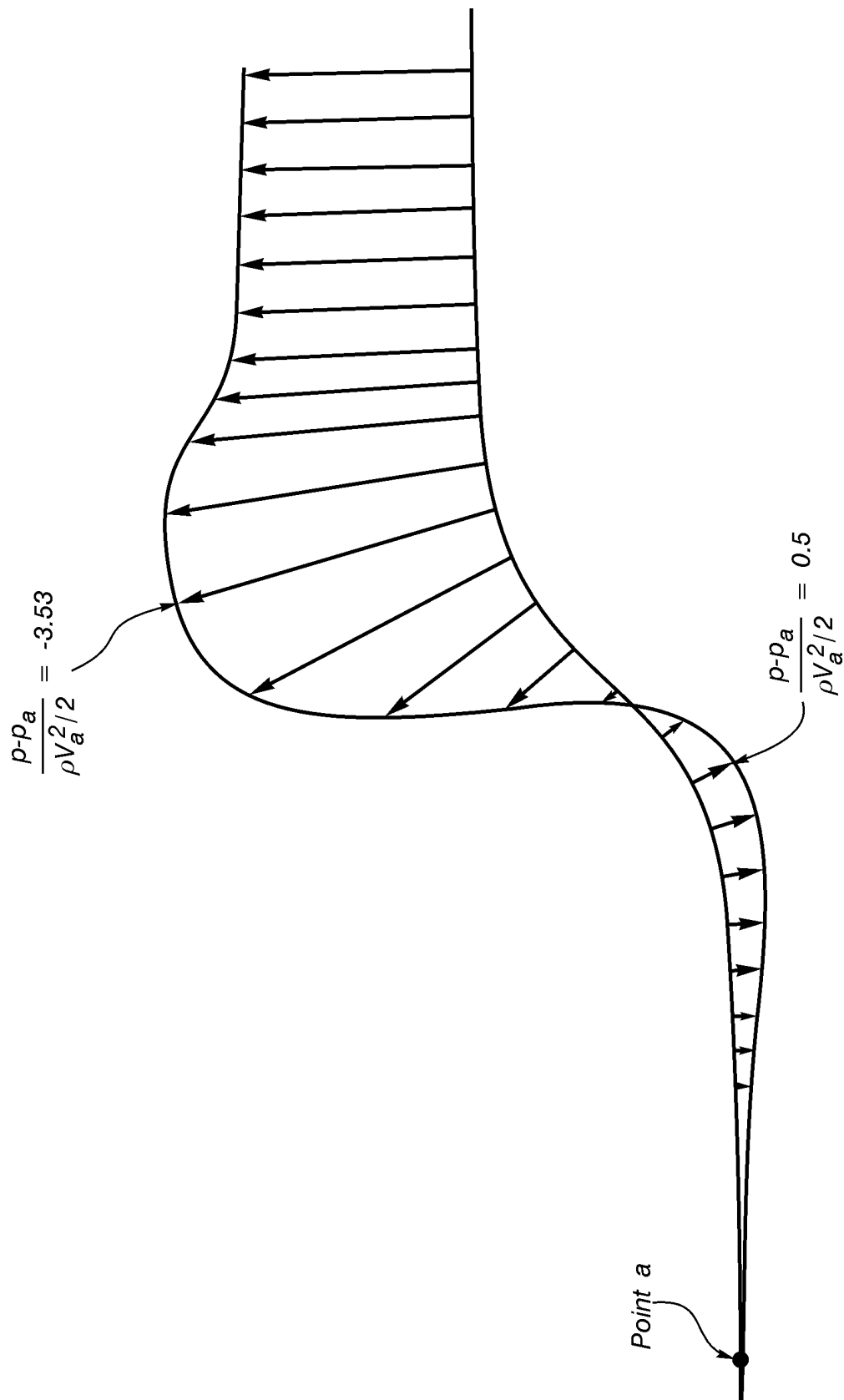
Figure 6.9 Dimensionless boundary pressures calculated from the flow net in Figure 6.6 and plotted normal to the boundary.

It is worth commenting now on the requirements for a unique irrotational flow solution. A unique velocity distribution for a given boundary geometry can be calculated if normal velocity components are specified along all boundaries of the flow region. There are, however, some restrictions on the way in which these normal velocity components can be specified: they must be uniform distributions across regions in which streamlines are straight and parallel, and they must satisfy the control volume form of the continuity equation. In addition to these requirements, a unique calculation of h or p requires that h or p be specified at one point in the flow.

The only exception to the orthogonality requirement for lines of constant ϕ and ψ occurs at points where streamlines form sharp corners. Examples of this are shown in Figure 6.10. In Figure 6.10 a the interior angle, α, is in the range $0 < \alpha < \pi$, and the sharp corner is a point of stagnation where $|V| = 0$. In Figure 6.10 b the interior angle is in the range $\pi < \alpha < 2\pi$, and the sharp corner is a singularity where $|V| \to \infty$. The velocity remains finite, and lines of constant ϕ and constant ψ are orthogonal, only when $\alpha = \pi$.
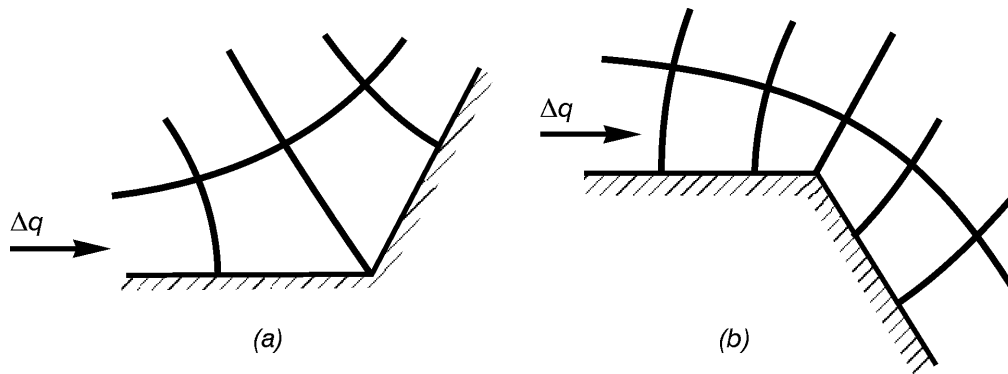
Figure 6.10 Flow net construction where streamlines form sharp corners.

The behaviour of velocities at sharp corners can be shown rigorously by considering flow in the sharp corner shown in Figure 6.11. The stream function for this flow must satisfy the Laplace equation and be a constant, say zero, on the boundary. In polar coordinates these requirements become

$$\frac{1}{r} \frac{\partial}{\partial r} \left(r \frac{\partial \psi}{\partial r} \right) + \frac{1}{r^2} \frac{\partial^2 \psi}{\partial \theta^2} = 0 \qquad \textbf{(6.72)}$$

$$\psi(r, 0) = 0 \quad \text{for} \quad 0 < r < \infty \qquad \textbf{(6.73)}$$

$$\psi(r, \alpha) = 0 \quad \text{for} \quad 0 < r < \infty \qquad \textbf{(6.74)}$$

A solution of (6.72) - (6.74) is readily seen to be given by

$$\psi = A\, r^{\pi/\alpha} \sin\!\left(\pi\theta/\alpha\right) \tag{6.75}$$

in which A is an undetermined constant. The velocity vector is obtained in polar coordinates from

$$V = \frac{1}{r}\frac{\partial\psi}{\partial\theta}\, e_r - \frac{\partial\psi}{\partial r}\, e_\theta \tag{6.76}$$

which gives the result

$$V = A\left[\cos\!\left(\pi\theta/\alpha\right) e_r - \sin\!\left(\pi\theta/\alpha\right) e_\theta\right](\pi/\alpha)\, r^{(\pi/\alpha)-1} \tag{6.77}$$

The velocity magnitude in (6.77) is zero, finite or infinite as $r \to 0$ when the exponent of r is positive, zero or negative, respectively. Thus, (6.77) gives the final result

$$
\begin{aligned}
|V| &\to 0 && \text{if} \quad 0 < \alpha < \pi \\
&= \text{Finite Number} && \text{if} \quad \alpha = \pi \\
&\to \infty && \text{if} \quad \pi < \alpha < 2\pi
\end{aligned}
\tag{6.78}
$$
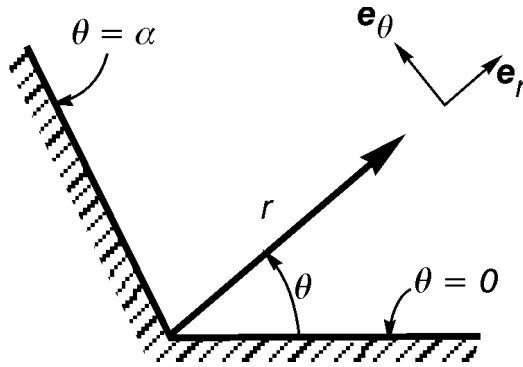
Figure 6.11 Irrotational flow in a sharp corner.

An example of flow net construction with sharp corners is shown in Figure 6.12. Since a streamline and a physical boundary can be interchanged in irrotational flow, this flow net can be used to model either flow over a fence or the top half of flow past a flat plate. Points of stagnation occur at points A and C, and a singularity occurs at point B. A viscid flow would not tolerate either the infinite velocity or the corresponding negatively infinite pressure at point B. Thus, a viscid flow separates at point B, as shown in Figure 6.13 for flow past a flat plate.
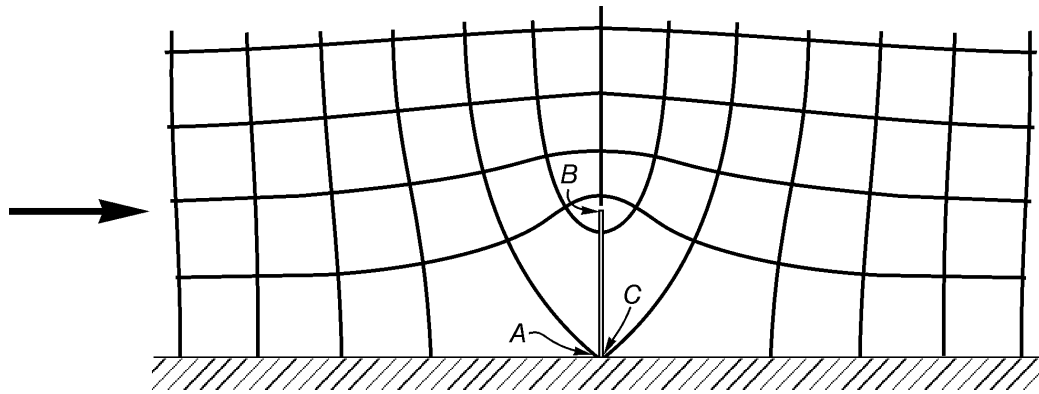
Figure 6.12 Irrotational flow over a fence.
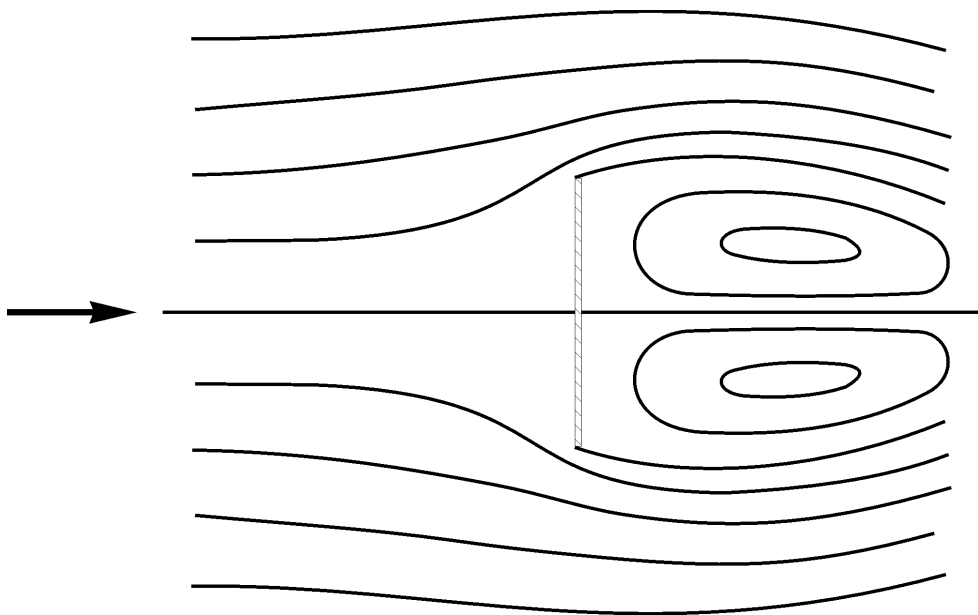
Figure 6.13 Viscid flow past a flat plate.

Free Streamline Problems

There are two important reasons for an engineer to study irrotational flow. First, irrotational flow provides a basic foundation for the study of boundary layer theory. Second, irrotational flow solutions give a close approximation for a number of flows that occur in practice. Many of the problems in this category are problems that have free surfaces. Examples include free jet flows through orifices and slots and open channel flows beneath sluice gates and over spillways and weirs.

A free surface or free streamline has an unknown geometry that must be calculated as part of a problem solution. This means that two boundary conditions must be prescribed along a free streamline. The first boundary condition requires that the normal velocity component vanish along the free streamline, which is equivalent to requiring that the free streamline be a line of constant ψ. The second boundary condition requires that the pressure be constant, say zero,

along the free streamline. When dealing with a high speed jet in which gravity may be neglected, this second requirement is shown by Eq. (6.71) to be equivalent to requiring a constant velocity along the free streamline, as pointed out previously in Chapter 4. In open channel flows where gravity cannot be neglected, Eq. (6.70) shows that a constant pressure along a free streamline requires that

$$\frac{y_a - y_b}{V_a^2 / (2g)} = \left(\frac{V_b}{V_a} \right)^2 - 1 \tag{6.79}$$

in which points a and b are on the same free streamline.

Complex variable methods have been used to calculate a few exact free streamline solutions for problems in which gravity can be neglected. In most other problems, though, numerical solutions have been calculated by using a method of trial and error. (An optimist would describe the procedure as one of successive approximation!) This procedure consists of calculating the irrotational flow solution for a guessed free streamline geometry. Then velocities are calculated along the free streamline and used to see if pressures remain constant. It not, then the free streamline geometry is adjusted and the procedure is repeated.

Tables and figures on the following pages give contraction coefficients and discharge coefficients for some free streamline problems. The degree of approximation in these types of problems may be judged by observing the comparison between calculated and measured free surface coordinates for the axisymmetric jet shown in Figure 6.14. These measurements were made for a jet leaving a 100 mm diameter orifice, and it is seen that the experimental jet diameter is slightly larger than the irrotational jet diameter. This small difference is believed to be the result of a thin boundary layer along the free surface. A boundary layer develops along the plate boundary before the jet exits from the orifice. Although relatively thin in such a highly accelerated flow, this creates a layer of lower velocity flow on the free surface. The effect of this boundary layer is to move the free streamline radially outward if the discharge is to remain the same for both irrotational and experimental jets. Generally, irrotational flow solutions describe experimental flows better as both the scale and Reynolds number increase. This is because these conditions cause a decrease in the ratio of boundary layer thickness to control volume dimensions, and irrotational flow solutions have zero boundary layer thicknesses.
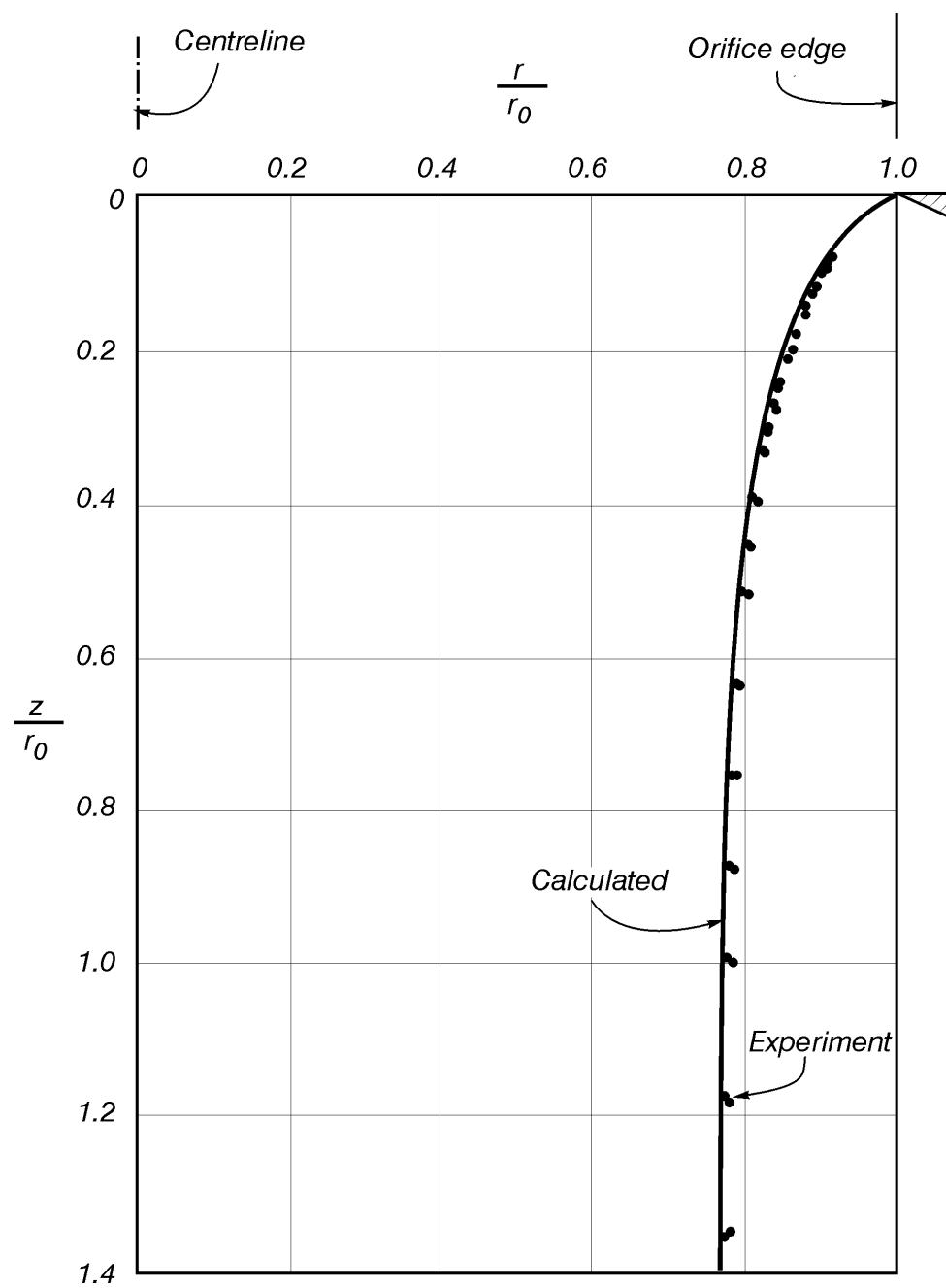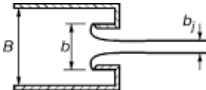
Figure 6.14 Comparison between calculated and measured free streamline geometries for an orifice in the wall of an infinite reservoir.

FLOW THROUGH A SLOT
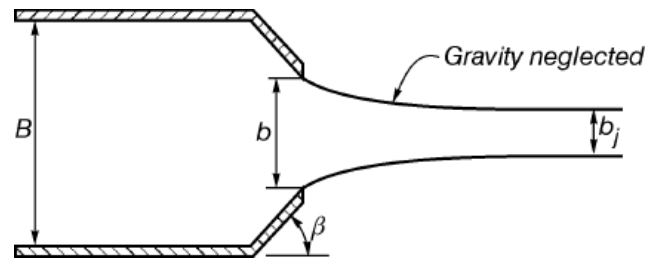
Values of C_c = $A_\text{jet} \big/ A_\text{slot}$ = $b_j \big/ b$				
b/B	β = 45°	β = 90°	β = 135°	β = 180° *
0 †	.746	.611	.537	.500
.1	.747	.612	.546	.513
.2	.747	.616	.555	.528
.3	.748	.622	.566	.544
.4	.749	.631	.580	.564
.5	.752	.644	.599	.586
.6	.758	.662	.620	.613
.7	.768	.687	.652	.646
.8	.789	.722	.698	.691
.9	.829	.781	.761	.760
1.0	1.000	1.000	1.000	1.000

* The limit $\beta \to 180°$ gives "Borda's mouthpiece", shown at left.

† b/B = 0 is interpreted as $B \to \infty$ for a fixed value of b.

Reference

Rouse, H. (1946). *Elementary Mechanics of Fluids*, John Wiley and Sons, New York, p. 57.

AXISYMMETRIC FLOW THROUGH AN ORIFICE

Gravity neglected and $\beta = 90°$	
$\dfrac{A_\text{orifice}}{A_\text{pipe}} = \left(\dfrac{b}{B} \right)^2$	$C_c = \dfrac{A_\text{jet}}{A_\text{orifice}} = \left(\dfrac{b_j}{b} \right)^2$
0	.578
.25	.594
.50	.624
.75	.691
1.00	1.000

Reference

Hunt, B. (1968) Numerical solution of an integral equation for flow from a circular orifice, *Jnl Fluid Mech.*, Vol. 31, Pt. 2, pp. 361-377.

FLOW BENEATH A SLUICE GATE
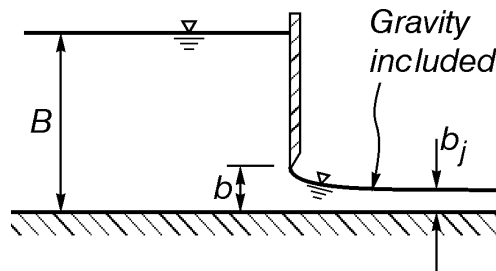
$\dfrac{b}{B}$	$C_c = \dfrac{A_{jet}}{A_{slot}} = \dfrac{b_j}{b}$
0	.611
.1	.605
.2	.600
.4	.595
.6	.594

Reference

Fangmeier, D.D. and T.S. Strelkoff. (1968). Solution for gravity flow under a sluice gate, *Jnl Engrg Mech. Div.*, ASCE, Vol. 94, No. EM1, pp. 153-176.

TWO-DIMENSIONAL SHARP-CRESTED WEIR
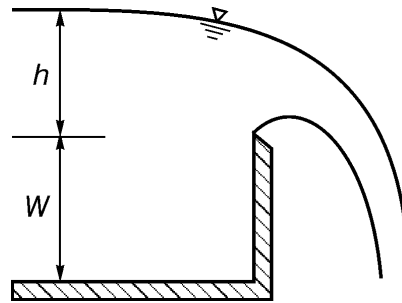
Gravity included. Underside fully ventilated.

$$q = \frac{2}{3} C_d \sqrt{2g h^3}$$

q = flow rate/unit width
C_d = discharge coefficient.

h/W	0	0.1	0.5	1.0	2.0	3.0
C_d	.611	.618	.644	.677	.743	.809

Reference

Strelkoff, T.S. (1964). Solution of highly curvilinear gravity flows, *Jnl Engrg Mech. Div.*, ASCE, Vol. 90, No. EM3, pp. 195-221.

Chapter 6 Summary

This chapter has been concerned with calculating solutions of Eqs. (6.1)–(6.2), which describe inviscid flows. Generally, an inviscid flow approximation is most accurate when moderate to large Reynolds number flows are accelerated rapidly. This is because boundary-layer thicknesses decrease rapidly in accelerated flow, flow separation from boundary-layer development will not occur unless sharp corners exist along boundaries and disturbances present in the flow are damped rather than amplified into full-scale turbulence. Under these circumstances an inviscid-flow approximation can be expected to give velocity distributions that are accurate everywhere except within very thin layers next to physical boundaries, and pressure distributions both along these boundaries and throughout the remainder of the flow field are closely approximated by the inviscid-flow solution.

The irrotational or potential flow approximation is the simplest and most widely used inviscid-flow approximation. Kelvin's circulation theorem, which was proved and discussed in the first part of this chapter, shows that the circulation, Γ, around a closed material path of fluid particles remains constant as this material path is convected with the flow. If this material path starts out from a point where $\Gamma = 0$, such as a point where the flow is either at rest or in a state of uniform motion, then $\Gamma = 0$ for all time around this path and the velocity field is derivable from the gradient of a potential function, as shown by Eq. (6.13). This chapter has been entirely concerned with the treatment of these kinds of flows.

There are some flows for which an inviscid-flow approximation is appropriate but which also have velocity fields that are not derivable from the gradient of a potential function. These are flows that have moderate to large Reynolds numbers and are highly accelerated over relatively short distances, **but motion starts from an approaching velocity field that is non-uniform**. Examples include flow through a streamlined pipe construction when the velocity field of the approaching flow is highly non-uniform, or flow around a building or other structure that lies within an atmospheric boundary layer where the approaching velocity increases with distance above the ground surface. There is no general body of the theory that can be used to treat these kinds of flows, and analysis must usually proceed by obtaining numerical solutions of Eqs. (6.1)–(6.2).

Chapter 7

Laminar and Turbulent Flow

Laminar flow derives its name from the experimental observation that different layers of fluid appear to slide over each other in layers or laminae without the disorderly movement and mixing that is characteristic of turbulent flow. A strict interpretation of this definition would include both low Reynolds number, highly viscous flows and the high Reynolds number, highly accelerated flows that were considered in the previous chapter. However, we will use the term laminar to mean low Reynolds number flows in which viscous effects are important throughout most of the flow region.
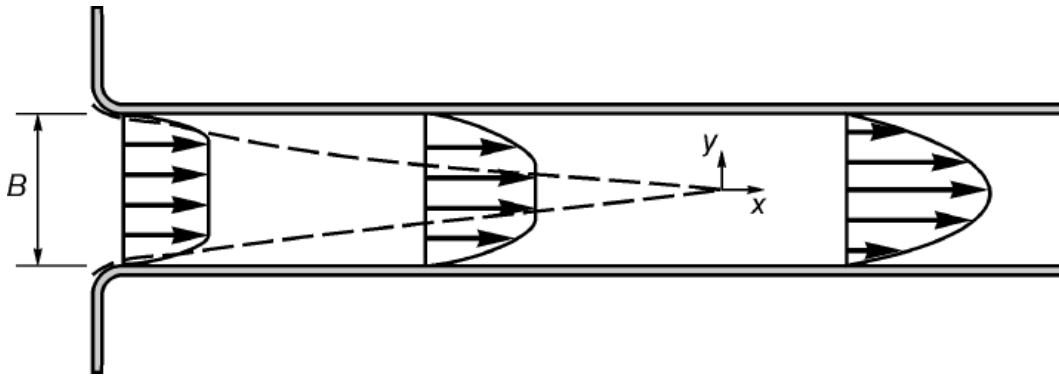
Figure 7.1 Developing and fully developed laminar flow between two flat plates.

Laminar Flow Solutions

Figure 7.1 shows the two-dimensional laminar flow that occurs when fluid from a reservoir enters the region between two parallel flat plates. Boundary layer thicknesses near the entrance are very small compared to the plate spacing, B. As flow proceeds downstream, however, boundary layer thicknesses increase and cause a corresponding increase in uniform flow velocity near the centre since total flow rates at each cross section are identical. At $x = 0$ in Figure 7.1 the top and bottom boundary layers meet, and the flow is said to be fully developed for $x \geq 0$. In this fully developed flow region $v = 0$ and $u = u(y)$. In other words, in the fully developed flow region the velocity vector is parallel to the plate boundaries, and velocity distributions do not change from one cross section to the next.

If we set $v = 0$ and $u = u(y)$ to obtain a solution for fully developed flow, the continuity equation (2.4) reduces to the identity $0 = 0$ and the Navier-Stokes equations (2.28) reduce to

$$-g\ \frac{\partial h}{\partial x}\ +\ \nu\ \frac{d^2 u\,(y)}{dy^2}\ =\ 0$$

$$-g\ \frac{\partial h}{\partial y}\ =\ 0$$

(7.1 a, b)

Equation (7.1 b) shows that $h\ =\ h\,(x)$, and all terms in (7.1 a) can then be written as ordinary derivatives.

$$g\ \frac{dh\,(x)}{dx}\ =\ \nu\ \frac{d^2 u\,(y)}{dy^2}$$

(7.2)

However, x and y are independent variables, which means that one variable can change its value without causing a corresponding change in the other. Thus, Eq. (7.2) only makes sense if each of its two terms equals the same constant, C_0.

$$g\ \frac{dh\,(x)}{dx}\ =\ C_0$$

$$\nu\ \frac{d^2 u(y)}{dy^2}\ =\ C_0$$

(7.3 a, b)

Integration of (7.3) gives

$$h\,(x)\ -\ h\,(0)\ =\ C_0 x\big/g$$

$$u\,(y)\ =\ C_1\ +\ C_2 y\ +\ y^2 C_0\big/(2\nu)$$

(7.4 a, b)

Since $u\ =\ 0$ at $y\ =\ B/2$ and $y\ =\ -B/2$, we obtain $C_2\ =\ 0$ and $C_1\ =\ -\left(B/2\right)^2 C_0/(2\nu)$. Thus, (7.4 b) becomes

$$u\,(y)\ =\ \left[y^2 - \left(B/2\right)^2\right]C_0/(2\nu)$$

(7.5)

If we define a discharge or flux velocity U by

$$UB\ =\ \int_{-B/2}^{B/2} u\,(y)\,dy$$

(7.6)

then inserting (7.5) in the right side of (7.6) allows us to calculate C_0 from

$$U\ =\ -\frac{2}{3}\left(\frac{B}{2}\right)^2 \frac{C_0}{2\nu}$$

(7.7)

Eliminating C_0 between (7.5) and (7.7) gives

$$u(y) = \frac{3}{2}\left[1 - \left(\frac{y}{B/2}\right)^2\right]U \qquad \text{(7.8)}$$

which shows that the velocity distribution is a parabola that is symmetrical about the centreline $y = 0$. Since the maximum velocity, U_{max}, occurs at $y = 0$, setting $y = 0$ in (7.8) gives the relationship between maximum and flux velocities.

$$U_{max} = \frac{3}{2}U \qquad \text{(7.9)}$$

Finally, eliminating C_0 between (7.4 a) and (7.7) gives an expression for the change in piezometric head.

$$h(x) - h(0) = -12\,\frac{\nu x U}{g B^2} \qquad \textbf{(7.10)}$$

Further manipulation can be used to put (7.10) in the following more significant form:

$$h(0) - h(x) = f\,\frac{x}{B}\,\frac{U^2}{2g} \qquad \text{(7.11)}$$

in which the dimensionless friction factor, f, is given by

$$f = \frac{24}{Re} \quad , \quad \left(Re = \frac{UB}{\nu}\right) \qquad \textbf{(7.12)}$$

There are several notable points about this solution. First, since velocities are not changing with x, the change in piezometric head given by the right side of (7.11) is also the change in total head. In other words, (7.11) is an expression for an energy loss, and (7.10) shows that this energy loss increases as ν, x and U increase and B decreases. Second, the Reynolds number, Re, has made its appearance in a flow that is not accelerating, and this is despite the statement that is sometimes made that a Reynolds number is the ratio of an acceleration to a viscous force.

A similar result can be obtained for axisymmetric pipe flow. In this case, the corresponding results are

$$u(r) = 2\left[1 - \left(\frac{r}{D/2}\right)^2\right]U$$

$$U_{max} = 2U$$

$$h(0) - h(x) = f\,\frac{x}{D}\,\frac{U^2}{2g}$$

$$f = \frac{64}{Re} \quad , \quad \left(Re = \frac{UD}{\nu}\right)$$

(7.13 a, b, c, d)

in which D = pipe diameter.

Equation (7.13 a) shows that the velocity distribution is a parabola of revolution, and the results differ from results for the two-dimensional flow only by the magnitude of some of the constants. An experimental verification of (7.13) is shown in Figure 7.2.
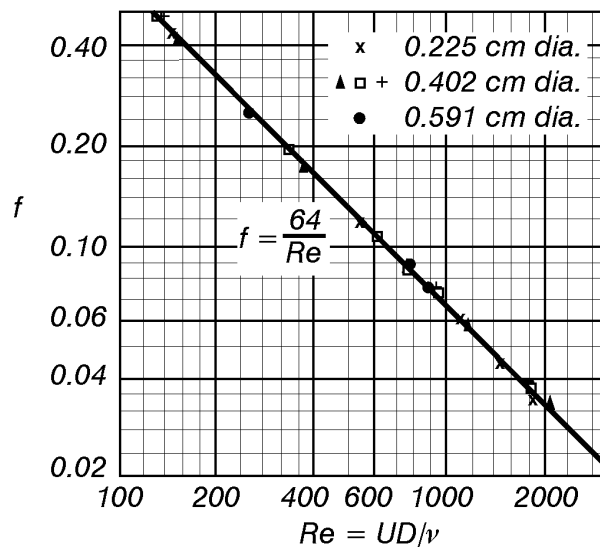
Figure 7.2 Experimental verification of (7.13). [Measurements by Hagen, reproduced from Schlichting (1968).]

An approximate solution for very slow motion past a sphere gives a drag force on the sphere of

$$F = 3\pi\mu D U \qquad\qquad\qquad \textbf{(7.14)}$$

in which D = sphere diameter and U = velocity of the approaching flow or the velocity of the sphere when falling with a constant speed through a motionless fluid. Equation (7.14) can be put in the standard form

$$F = C_D A \rho\,\frac{U^2}{2} \quad , \quad \left(A = \pi D^2/4\right) \qquad\qquad \textbf{(7.15)}$$

in which the dimensionless drag coefficient, C_D, is given by

$$C_D = \frac{24}{Re} \quad , \quad \left(Re = \frac{UD}{\nu} \right) \tag{7.16}$$

Equation (7.14) was first obtained by Stokes in 1851. It neglects accelerations and is a reasonable approximation when $Re < 1$, flows which are sometimes termed "creeping flows". Equations (7.14) - (7.16) find civil engineering applications when calculating fall velocities for very fine particles settling through water in both geomechanics and sediment transport. Experimental verification of (7.16) and drag coefficients for some other axisymmetric bodies are shown in Figure 7.3.
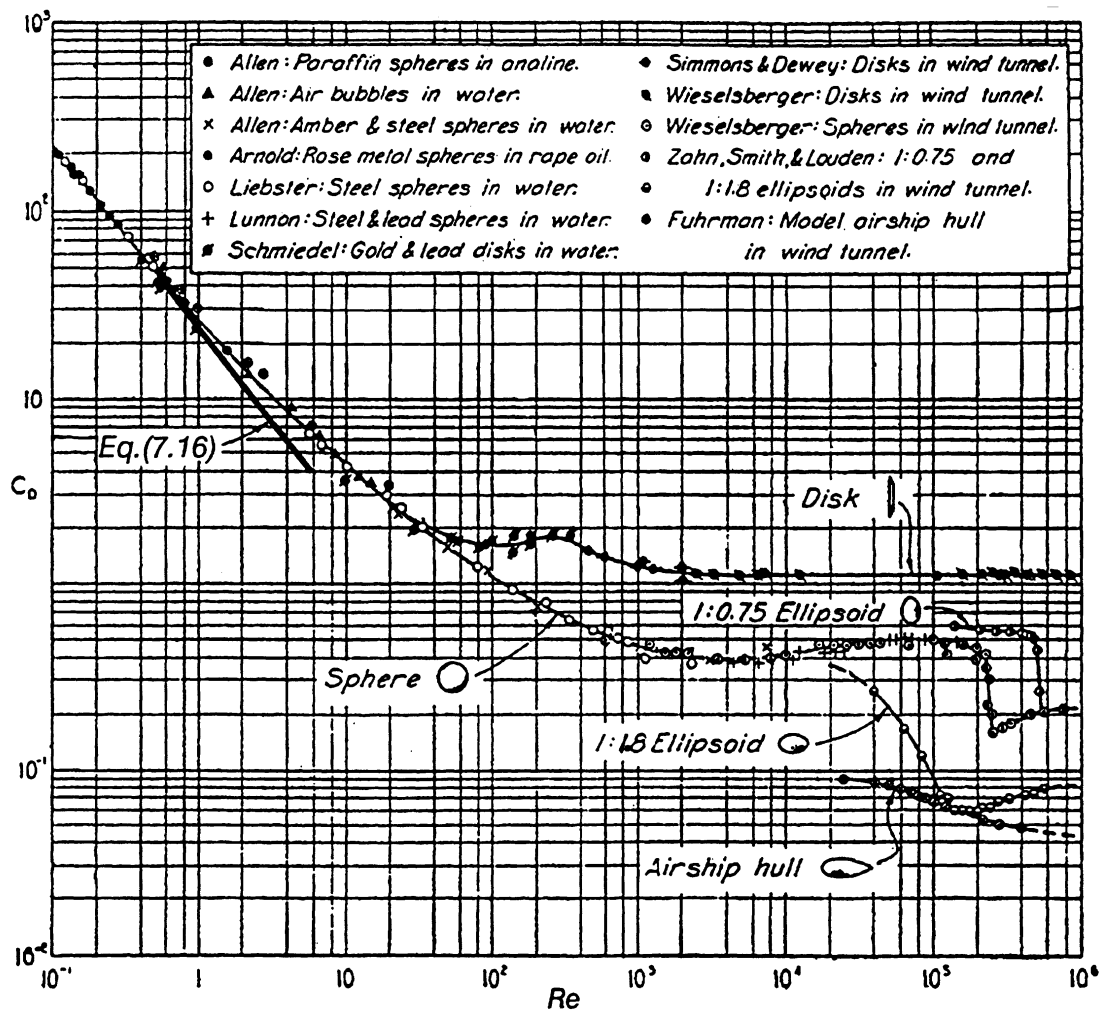
Figure 7.3 Drag coefficients for some axisymmetric bodies. [Reproduced from Rouse (1946).]

It is important to realise that (7.14) - (7.16) all neglect the effect of gravity. This is a valid approximation when the sphere density is much greater than the fluid density. When this is not the case, gravitational effects must be included by adding a vertical hydrostatic buoyancy force. For example, the application of (7.14) to calculate the constant terminal velocity of a spherical body uses the free body diagram shown in Figure 7.4. The only forces acting on the body are the

body weight, the drag force and the hydrostatic buoyancy force. Since the sphere has a zero acceleration, setting the sum of vertical forces equal to zero gives the equation of motion.

$$\rho_s \, g \, \pi D^{\,3}/6 \, - \, \rho_f g \, \pi D^{\,3}/6 \, - \, 3\pi\mu \, D \, U_\infty \, = \, 0 \tag{7.17}$$

in which ρ_f and ρ_s = mass densities of the fluid and sphere, respectively, and U_∞ = sphere terminal velocity. Solution for the terminal velocity gives

$$U_\infty \, = \, \frac{g\left(\rho_s - \rho_f\right)D^{\,2}}{18\mu} \tag{7.18}$$

Equation (7.18) is shown by Figure 7.3 to apply only when Reynolds numbers are less than unity.

An additional force must be considered when a body is accelerating. This force is written as a coefficient, k, multiplied by the displaced mass of fluid and the body acceleration. Because this additional term is traditionally added to the acceleration term in Newton's second law, it is called the "added mass term", and k is called the "added mass coefficient". The value of k computed from irrotational flow theory for a sphere is 0.500, and some values for other bodies are given by Robertson (1965). Although it may be possible to make a physical interpretation of this term, it is probably less confusing to simply think of an added mass term as the difference between drag forces in steady and unsteady flows.

$\rho_s g \pi D^3/6$ = Body weight

$3\pi\mu D U_\infty$ = Drag force

$\rho_f g \pi D^3/6$ = Buoyancy force
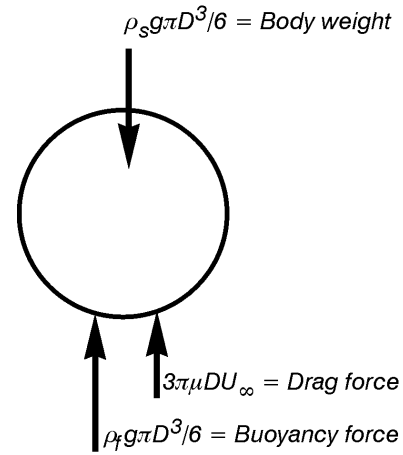
Figure 7.4 The free body diagram for a spherical body falling through a dense fluid with a constant terminal velocity.

If we consider the movement of a spherical body from the time when it is first released from rest, Newton's second law becomes

$$\rho_s g \, \pi D^{\,3}/6 \, - \, \rho_f g \, \pi D^{\,3}/6 \, - \, 3\pi\mu \, D \, U \, = \, \left(\rho_s + k\rho_f\right)\!\left(\pi D^{\,3}/6\right)\!dU/dt \tag{7.19}$$

in which the added mass term has been added to the right side. Equation (7.19) can be simplified by using (7.17) to put it in the form

$$\frac{dU}{dt} \, + \, \frac{18\mu}{\left(\rho_s + k\,\rho_f\right)D^{\,2}} \, \left(U - U_\infty\right) = 0 \tag{7.20}$$

It is easier to interpret the result if U is calculated as a function of distance, x, from the point of release rather than t. This can be done by setting

$$\frac{dU}{dt} = \frac{dx}{dt}\frac{dU}{dx} = U\frac{dU}{dx} \tag{7.21}$$

Inserting (7.21) in (7.20) and separating variables gives

$$\int_0^{U(x)} \frac{U}{U - U_\infty}\, dU = -\frac{18\mu}{\left(\rho_s + k\rho_f\right)D^2}\int_0^x dx \tag{7.22}$$

in which the integration limits have been set by requiring $U(x) = 0$ at $x = 0$. Since $U/\left(U - U_\infty\right) = 1 + U_\infty/\left(U - U_\infty\right)$, a straightforward integration gives

$$U(x) + U_\infty \ln\left[1 - U(x)/U_\infty\right] = -\frac{18\mu x}{\left(\rho_s + k\rho_f\right)D^2} \tag{7.23}$$

Division of both sides of (7.23) by U_∞ gives the following result:

$$\frac{U(x)}{U_\infty} + \ln\left[1 - \frac{U(x)}{U_\infty}\right] = -18\frac{x/D}{\left(\rho_s/\rho_f + k\right)Re} \tag{7.24}$$

in which the Reynolds number is given by

$$Re = \frac{U_\infty D \rho_f}{\mu} = \frac{U_\infty D}{\nu} \tag{7.25}$$

A dimensionless plot of (7.24) in Figure 7.5 shows that the terminal velocity, U_∞, is approached very quickly. For example if $Re = 1$, $k = 0.5$ and $\rho_s/\rho_f = 10$, the sphere reaches 99 per cent of its terminal velocity after moving just over two sphere diameters from its point of release $\left(x/D = 2.10\right)$.

Another civil engineering application of laminar flow occurs when considering seepage of water through the ground. If we assume that control volume dimensions are large compared to soil particle diameters, then we can treat the flow as a continuum and write a continuity equation in the form

$$\nabla \cdot V = 0 \tag{7.26}$$
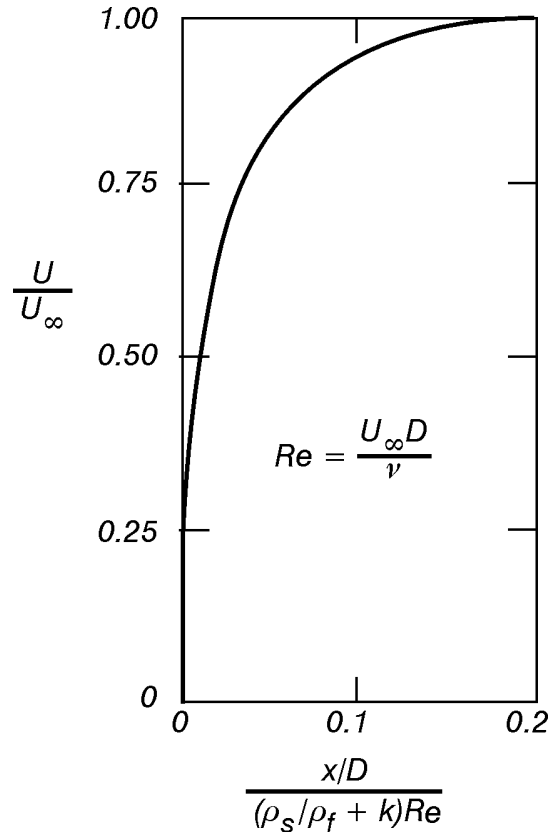
Figure 7.5 The approach to terminal velocity when a sphere is released from rest.

in which V = a flux velocity. (i.e. The product of an area with the normal component of V gives the flow rate through the area. This area includes the sum of the areas of solids and pores.) Since particle diameters are of the order of 1 mm, velocities of the order of 1-10 m/day and the kinematic viscosity for water is of the order of 10^{-6} m^2/s, we see that the Reynolds number has an order of magnitude between 1/100 and 1/10. This suggests, from Eq. (5.8), that viscous terms in the Navier-Stokes equations are 10 to 100 times larger than acceleration terms and, consequently, that acceleration terms can be neglected. Therefore, the momentum equation, (2.18), can be approximated with

$$-\nabla p + \rho g + \rho f = 0 \tag{7.27}$$

in which f = viscous force per unit mass exerted on the fluid. If we assume that the flow is homogeneous and incompressible, Eq. (2.22) allows (7.27) to be written as

$$- g \nabla h + f = 0 \tag{7.28}$$

in which the piezometric head, h, is given by (2.22). However, Stoke's law, (7.14), suggests that the force per unit mass might be approximated with

$$f = - \frac{\mu}{k_0 \rho} V \tag{7.29}$$

in which k_0 = constant of proportionality that has units of m^2. The negative sign on the right side of (7.29) reflects the fact that f and V are in opposite directions. Eliminating f between (7.28) and (7.29) gives Darcy's law,

$$V = - K \nabla h \tag{7.30}$$

in which

$$K = \frac{k_0 \rho g}{\mu} \tag{7.31}$$

The constant k_0 is the intrinsic permeability and is a function only of the porous matrix geometry, and K is the coefficient of permeability with units of a velocity (m/s).

If the aquifer is homogeneous and isotropic, then K is a constant and (7.30) can be written

$$V = \nabla \phi \quad , \quad \left(\phi = - K h \right) \tag{7.32}$$

Equations (7.26) and (7.32) are identical with Eqs. (6.1) and (6.13). This means that the equations that describe groundwater flow, which is a flow dominated by viscous resistance, are identical with the equations that describe inviscid irrotational flow.

Our final application of laminar flow theory will consider the Hele-Shaw approximation. Hele-Shaw flows are very slow (creeping) viscous flows between two parallel plates, as shown in Figure 7.6.
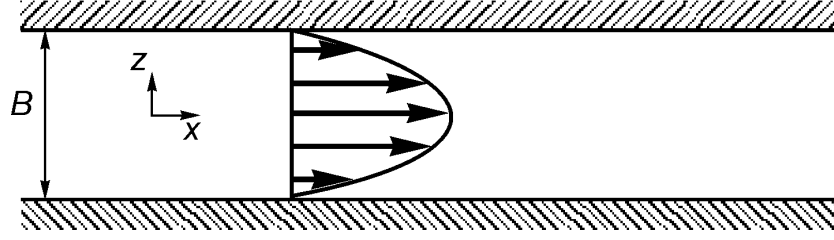
Figure 7.6 A Hele-Shaw flow between two parallel plates.

If we assume that accelerations can be neglected and that all velocities are parallel to the two boundaries, then the Navier-Stokes equations, (2.28), reduce to

$$- g \, \frac{\partial h}{\partial x} + \nu \left(\frac{\partial^2 u}{\partial x^2} + \frac{\partial^2 u}{\partial y^2} + \frac{\partial^2 u}{\partial z^2} \right) = 0$$

$$- g \, \frac{\partial h}{\partial y} + \nu \left(\frac{\partial^2 v}{\partial x^2} + \frac{\partial^2 v}{\partial y^2} + \frac{\partial^2 v}{\partial z^2} \right) = 0 \qquad \textbf{(7.33 a, b, c)}$$

$$- g \, \frac{\partial h}{\partial z} = 0$$

Equation (7.33 c) shows that h does not change with z, and an order of magnitude analysis similar to the one carried out in Chapter 5 can be used to show that the second derivatives of u and v are much larger in the z direction than in the x and y directions. Thus, (7.33) reduces to

$$- g \, \frac{\partial h}{\partial x} + \nu \, \frac{\partial^2 u}{\partial z^2} = 0$$

$$- g \, \frac{\partial h}{\partial y} + \nu \, \frac{\partial^2 v}{\partial z^2} = 0 \qquad \textbf{(7.34 a, b, c)}$$

$$h = h(x, y, t)$$

Finally, Eq. (7.8) suggests that we might approximate u and v with

$$u = \frac{3}{2} \left[1 - \left(\frac{z}{B/2} \right)^2 \right] U(x, y, t)$$

$$v = \frac{3}{2} \left[1 - \left(\frac{z}{B/2} \right)^2 \right] V(x, y, t) \qquad \textbf{(7.35 a, b)}$$

Elimination of u and v from (7.34) - (7.35) gives the end result

$$U = -K \frac{\partial h}{\partial x}$$

(7.36 a, b)

$$V = -K \frac{\partial h}{\partial y}$$

in which U and V are flux velocities in the x and y directions, respectively, and K is given by

$$K = \frac{gB^2}{12\nu}$$

(7.37)

Since U and V are flux velocities, the continuity equation

$$\frac{\partial U}{\partial x} + \frac{\partial V}{\partial y} = 0$$

(7.38)

completes the description of the flow. Equations (7.36) and (7.38), which describe fluid movement in directions parallel to the two plate boundaries in Figure 7.6, are identical with the two-dimensional form of Eqs. (7.26) and either (7.30) or (7.32), which can be used to describe either inviscid irrotational flow or groundwater flow. Thus, a Hele-Shaw experiment is an experimental analogy that can be used to model either of these two types of flow.

Probably the most important practical use of a Hele-Shaw analogue models two-dimensional groundwater flow in a vertical plane. Since h, U and V have the same physical meaning in both model and prototype,[*] boundary conditions for a free surface or an interface between two fluids with different densities are identical for model and prototype ***provided that the groundwater aquifer porosity is taken as unity in the Hele-Shaw model***. Thus, one of the great advantages of a Hele-Shaw experiment is that it locates a free surface or interface experimentally without using the trial and error procedure that is required when numerical methods are used.

Equation (7.37) shows that the "permeability" is directly proportional to the square of the plate spacing. This means that changes in permeability can be modeled by a change in plate spacing, which is easily accomplished by inserting a third plate, with its required thickness calculated from (7.37), between the two boundaries shown in Figure 7.6. For example, if the permeabilities for two different regions in the flow have the ratio $K_1/K_2 = 1/5$, then (7.37) shows that the plate spacings in these two regions must have the ratio $B_1/B_2 = \sqrt{K_1/K_2} = 1/\sqrt{5}$. A reservoir of constant depth is modelled by making B for the reservoir very large compared to the value of B used for the aquifer. One implication that follows from this is that if K_1/K_2 is either very large or very small, say 100 or 1/100, then the region of larger permeability will behave essentially as a reservoir in which velocities are negligible and piezometric heads are nearly constant. In this case it is better to model only the region of smaller permeability and to treat the region of larger permeability as a reservoir.

---

[*]   A prototype is a flow in the field that is approximated with a model flow.
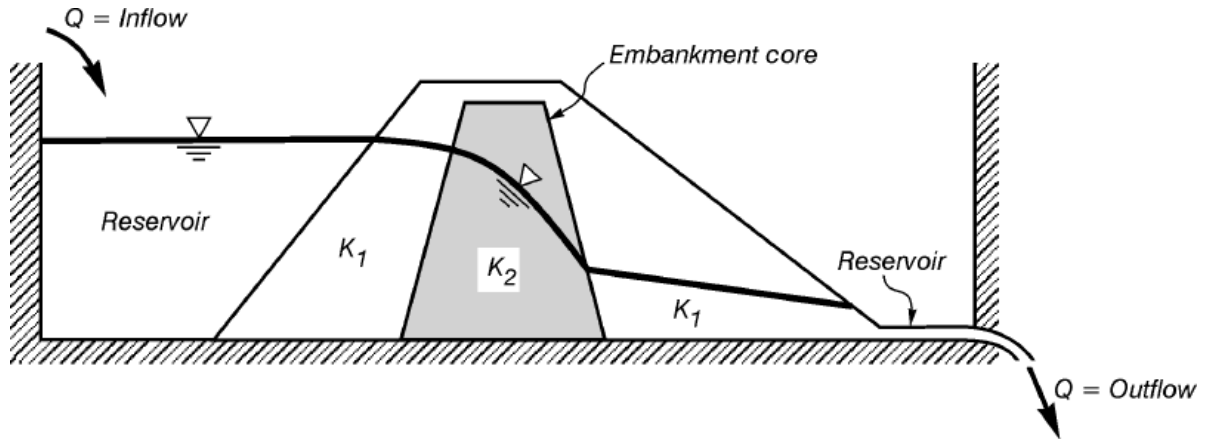
Figure 7.7 A Hele-Shaw model for seepage through a zoned embankment.

An example of a vertical Hele-Shaw experiment used to model seepage through a zoned embankment is shown in Figure 7.7. The embankment core has a low permeability, K_2, to reduce seepage through the embankment. Embankment cores are typically constructed from fine silt or clay, but these materials have very low structural strengths. Consequently, coarser material with a permeability K_1 is placed on both sides of the core to add structural strength and to prevent erosion of the core material from seepage (piping). The two reservoirs have plate spacings, B, which are much larger than plate spacings for the embankment (by a factor of at least 10), and the plate spacing ratio B_1/B_2 is calculated from $B_1/B_2 = \sqrt{K_1/K_2}$. If this ratio is 10 or more, then it would be better to treat the outer material as reservoirs and to only model flow through the homogeneous core. Figure 7.8 shows the flow that would result if $B_1/B_2 \geq 10$ and if this procedure were not followed.
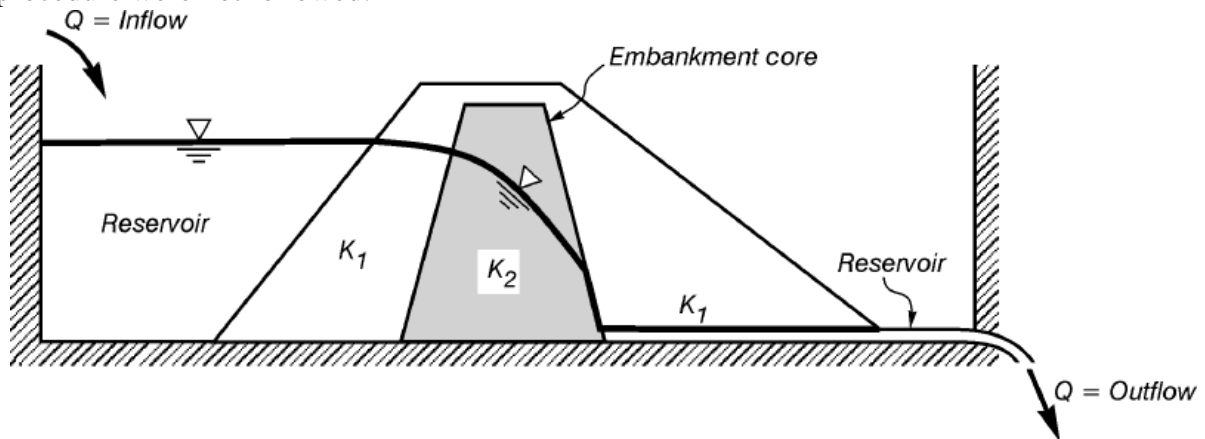
Figure 7.8 The flow that would occur in Figure 7.7 if $K_1/K_2 \geq 100$.

There are several practical problems to consider when constructing Hele-Shaw experiments. First, since K is proportional to B^2, it is very important to keep B constant in regions of constant K. This is normally done by using plates constructed from relatively flexible material, such as Perspex or Lucite, and by inserting numerous spacers throughout the region of flow. These spacers are most conveniently constructed by drilling holes through both plates and inserting small diameter bolts through larger diameter metal sleeves with lengths that have been machined to the same length as the required plate spacing. Flow disturbances caused by these spacers are localised and have negligible effects on the overall flow characteristics.

A second practical consideration concerns the choice of fluid and plate spacing. (The relative plate spacings are determined from the permeability ratios, but a plate spacing must still be chosen for one of the regions of constant K.) Since the Hele-Shaw analogy assumes creeping laminar motion, velocities must be very low. Velocities can be decreased by decreasing the plate spacing and/or increasing the fluid viscosity. However, since a free surface occurs in the experiment, decreasing the plate spacing too much causes errors from capillary climb. This is easily spotted in a model by observing an apparent jump in free surface height where the plate spacing changes. In the writer's experience it is better to keep plate spacings reasonably large to minimize capillary effects and to increase the fluid viscosity to keep velocities at acceptably low values. For example, the writer has used one experiment for a number of years in which oil flows between two Perspex plates with a spacing of 3 mm.

A relatively high fluid viscosity causes the pump that is used to recirculate the oil to heat the oil during the experiment. Since changing the oil temperature affects both the oil viscosity and the permeability given by (7.37), it becomes necessary to know how the permeability varies with oil temperature. This information is obtained by measuring the permeability at a number of different temperatures with a "permeameter" that consists essentially of a vertical free jet between two plates of Perspex, as shown in Figure 7.9. Since streamlines are vertical in this flow, $U = 0$ and (7.36 a) shows that h is a function of y determined by its value along either of the two vertical free streamlines, where $h = y$. Thus, $h = y$ everywhere within the jet, and this result together with Eq. (7.36 b) shows that the vertical flux velocity exactly equals the coefficient of permeability, K. Therefore, the permeability is measured by dividing the total flow rate by the cross sectional area of the jet.

Finally the problem of scaling results from model to prototype needs to be considered. The recommended technique uses results from a dimensional analysis for this purpose. In Figure 7.7, for example, if H is the upstream reservoir depth and if L is a characteristic horizontal dimension of the embankment (say its base width), then the flow rate per unit length of embankment, q, will be a function of the following group of dimensionless variables:

$$\frac{q}{K_2 L} = f\left(\frac{H}{L}, \frac{K_1}{K_2} \right) \qquad \textbf{(7.39)}$$

Figure 7.9 Use of a vertical free jet to measure the permeability in a Hele-Shaw experiment.
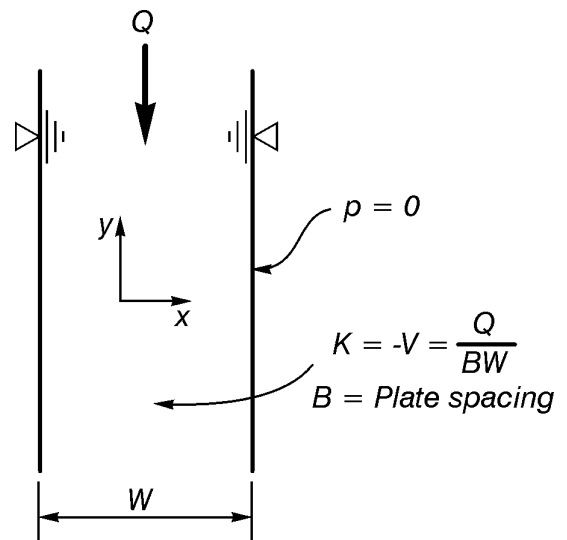
in which model and prototype embankments are geometrically similar. The function f is not known, but it is exactly the same function for both model and prototype. Thus, if we require that

$$\left(\frac{H}{L} \right)_{\text{prototype}} = \left(\frac{H}{L} \right)_{\text{model}} \qquad \textbf{(7.40)}$$

$$\left(\frac{K_1}{K_2} \right)_{prototype} = \left(\frac{K_1}{K_2} \right)_{model} \tag{7.41}$$

then we must also have

$$\left(\frac{q}{K_2 L} \right)_{prototype} = \left(\frac{q}{K_2 L} \right)_{model} \tag{7.42}$$

These three equations can be used to calculate H, K_1/K_2 and q for the prototype from values measured for the model. Dimensional analysis techniques, which are used to obtain Eq. (7.39), will be introduced in a later chapter.

Turbulence

In Chapter 4 it was stated that turbulence is a highly disorganised state of flow that occurs when a flow becomes unstable. In detail, it consists of many vortices of differing sizes and intensities superimposed upon the main flow pattern. This means that a flow that might otherwise be steady and one or two-dimensional becomes unsteady and three-dimensional, although time averages of velocities and pressures may still be steady and one or two-dimensional. For example, a typical velocity measurement at a point in turbulent flow is shown in Figure 7.10, and it is seen in this case that the velocity fluctuations caused by turbulence have a zero time average and instantaneous magnitudes that are small compared to the time averaged velocity.
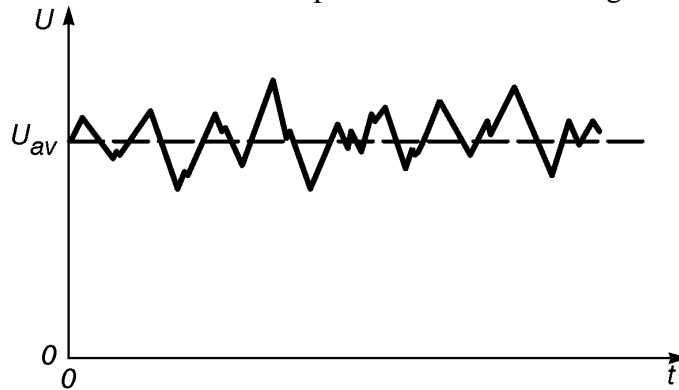
Figure 7.10 Variation of velocity with time at a point in turbulent flow.

All turbulence starts as a disturbance that becomes unstable and is amplified throughout a larger region as time proceeds. A very good example of this is shown in Figure 7.11 for flow along a flat plate. Ludwig Prandtl took these photographs in 1933 by moving a camera with the flow after sprinkling aluminium dust on the free surface to make the flow pattern visible. Osborne Reynolds carried out the first systematic investigation of flow stability in 1883 by injecting a filament of dye into flow through a glass tube. Reynolds defined a stability parameter, now known as the Reynolds number, for these flows by using the average flux velocity and the tube diameter, as shown in Eq. (7.13 d). He initially found that the flow became unstable for $Re \approx 1400$ but later changed this value to $Re \approx 1900 - 2000$.
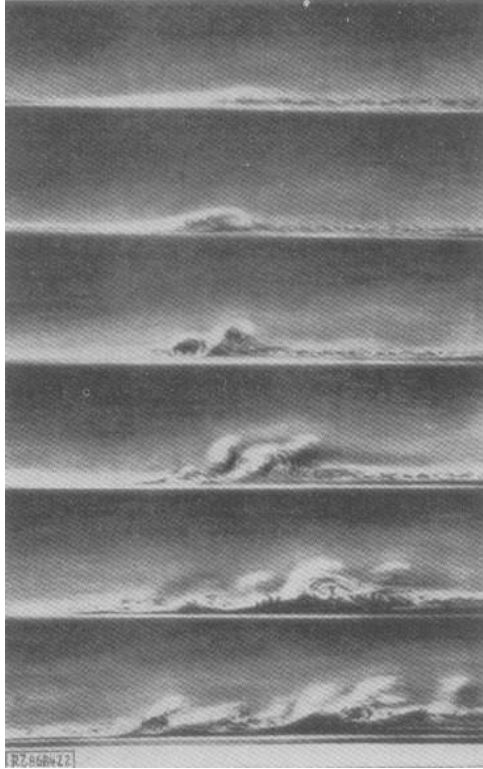
Figure 7.11   The amplification of a disturbance into turbulence for flow along a flat plate. [Photographs by Prandtl, reproduced from Schlichting (1968).]

There is a tendency for students to think that the transition from laminar to turbulent flow depends entirely on the value of a characteristic Reynolds number. Actually, this transition depends upon a number of factors, including the presence of an initial disturbance that has a suitable scale (characteristic linear dimension) and frequency, a large enough Reynolds number, whether the flow is being accelerated or decelerated and the presence or absence of steep lateral velocity gradients. Each of these factors will be discussed now in more detail.

Schlichting (1968) gives a brief discussion of early experimental evidence which indicated that the transition to turbulence can be delayed by reducing the amount of disturbance present in a flow. For example, V.W. Ekman in 1910 conducted experiments similar to Reynolds' experiments in which laminar flow occurred for Reynolds numbers as high as 40,000. This was accomplished by avoiding, as far as possible, the introduction of disturbances in the flow. Thus, the figure of 2,000 must be regarded as a lower limit of the Reynolds number for flow through a pipe. Furthermore, Tollmien in 1929 showed mathematically that whether or not a disturbance is amplified as time proceeds also depends upon both the wave length, or scale, and the frequency of an introduced disturbance. This analysis was carried out by introducing a mathematical disturbance into the Navier-Stokes equations and then determining values for parameters in the resulting equation that allow this disturbance to grow with time. The curve of neutral stability, which is the boundary between regions of stable and unstable flow, is shown in Figure 7.12 for flow along a flat plate. (β_r is the disturbance frequency, U_∞ is the velocity at infinity, ν is the kinematic viscosity and δ_1 is the boundary-layer displacement thickness for a laminar boundary layer — about one third of the total boundary layer thickness.) Experimental confirmation of this result was not obtained until 1943 when H.L. Dryden, G.B. Schubauer and H.K. Skramstad of the U.S. National Bureau of Standards succeeded in constructing a wind tunnel with an extremely low turbulence intensity in the approaching flow. Their experimental data is also shown in Figure 7.12.

Figure 7.12 shows that all flows along a flat plate with $Re < 400$ will be laminar, which confirms the intuitive notion that increases in viscosity tend to damp disturbances while increases in either scale lengths or velocities hasten the approach to instability. For $Re > 400$, flow along a flat plate may be either laminar or turbulent — depending upon the disturbance frequency. Since the disturbance frequency can be replaced with a velocity divided by the disturbance scale, it can be concluded that disturbance scale also affects the transition to turbulence.

It must not be concluded from this discussion that the same critical Reynolds number applies for all flows. As illustrated by Eqs. (7.12), (7.13 d), (7.16) and Fig. 7.12, Reynolds numbers are defined with different characteristic velocities and length scales for different flows. As far as the writer knows, there is no way that different stability limits for *Re* in different flows can be related, and it must be accepted that the transition to turbulence will occur at different values of *Re* for different flows.

Fluid accelerations tend to damp disturbances, while decelerations rapidly amplify disturbances for flows with moderate to large Reynolds numbers. In steady flow this means that flows with rapidly converging streamlines are likely to remain laminar, and flows with diverging streamlines are likely to

Figure 7.12 The curve of neutral stability for flow along a flat plate predicted from theory by Tollmien in 1929 and verified with experiment by Schubauer and Skramstad in 1943. [Reproduced from Schlichting (1968).]

be turbulent. As an example, a key feature of the low turbulence-intensity wind tunnel that was used to obtain the experimental data in Figure 7.12 was a very large contraction ratio for the approaching flow.

Steep lateral velocity gradients are seen from Eq. (1.1) to create large tangential stresses in a flow. These tangential stresses introduce many disturbances, decelerate the flow and, at high enough Reynolds numbers, lead to highly turbulent flows. The classic example of this type of flow occurs where a submerged jet enters a reservoir of otherwise motionless fluid, as shown in Figure 7.13. A free shear layer of highly turbulent flow starts at the nozzle edge, where the lateral gradient of the velocity is nearly infinite. This free shear layer expands rapidly in size as it extends further into the reservoir of fluid, and the rapidly decelerated flow becomes highly turbulent. Other examples of this nature occur in wakes behind bluff bodies and along interfaces between two fluids with different densities and velocities. An atmospheric example of this latter type of flow is shown in Figure 7.14, in which clouds show the development of vortices along the boundary between relatively dense fluid in a cold front below lighter warm air above.

Turbulence has two important effects on any flow: *energy dissipation and mixing*. The fact that energy dissipation occurs at a greatly increased rate in turbulent flow as the result of energy transfer from the main flow into the vortices has already been pointed out in Chapter 4. Ultimately this transferred energy is dissipated in the form of heat, although temperature rises are so small as to be almost unmeasurable. The submerged jet in Figure 7.13 provides an outstanding example

of energy dissipation in a highly turbulent flow. It is an experimental fact that piezometric heads are constant throughout a submerged jet if the reservoir of motionless receiving fluid is large compared to the nozzle diameter, D. It is also an experimental fact that centreline velocities decay to zero as z/D becomes large. Thus, the Bernoulli sum $h + V^2/(2g)$ along the centre streamline decays from its maximum value at $z = 0$ to its minimum value of h at $z = \infty$, in which h is the same constant throughout the flow. In other words, the head loss and energy loss are exactly $V^2/(2g)$ and $\rho V^2/2$, respectively.
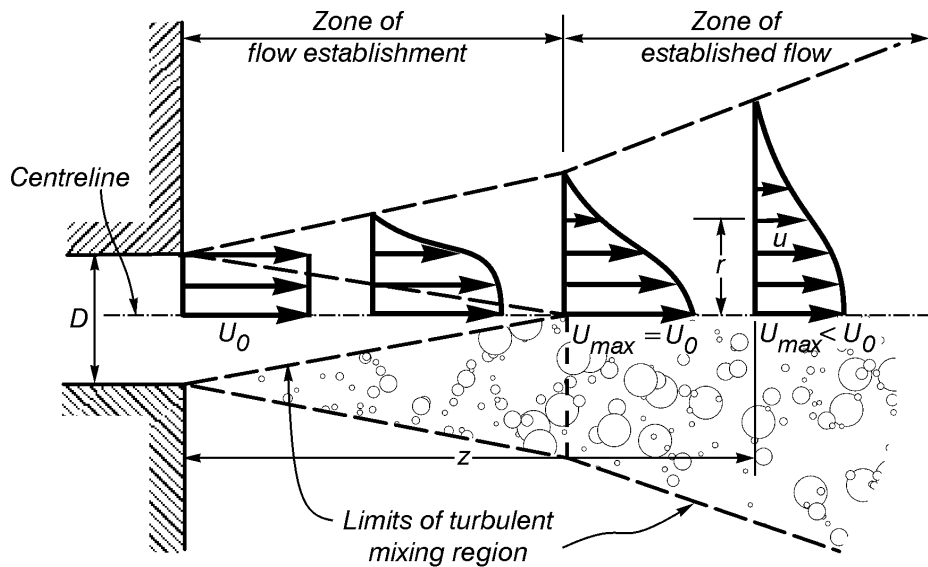
Figure 7.13   Velocity distributions and the turbulent mixing region in a submerged jet. [Reproduced from Albertson, Dai, Jensen and Rouse (1948).]
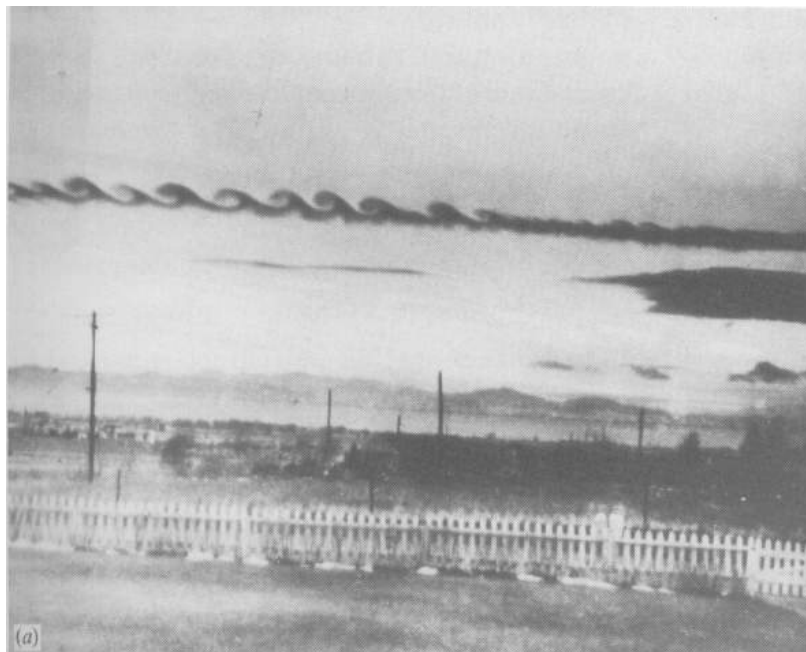
Figure 7.14 A free shear flow along the interface between cold and warm air in the atmosphere. [Photograph by Paul E. Branstine, reproduced from Drazin and Reid (1981).]

The effects of turbulent mixing are usually most noticeable in directions that are normal to the direction of main flow. This lateral mixing, which transports high velocity particles into regions of lower velocity and vice versa, creates a redistribution of average longitudinal velocity and also mixes or spreads contaminants and tracers across time averaged streamlines. For example, Figure 7.13 shows that the lateral width of the central core of uniform velocity in the zone of flow establishment is rapidly reduced through turbulent mixing to a value of zero at the start of the zone of established flow. This occurs at just over six nozzle diameters from the point where the jet first enters the reservoir. This lateral mixing then continues to spread the longitudinal velocity distribution in the zone of established flow, and the longitudinal velocities are ultimately reduced to zero everywhere as they are spread over larger and larger radial distances. If the jet contains a contaminant or tracer, such as smoke, that is not present in the undisturbed receiving reservoir of fluid, this tracer is mixed and spread laterally in the same way.

A second example of lateral mixing caused by turbulence concerns fully developed flow in pipes. Laminar pipe flow with an average or flux velocity U is seen from (7.13 a) to be a parabola of revolution.

$$\frac{u}{U} = 2\left[1 - \left(\frac{r}{D/2}\right)^2\right] \tag{7.43}$$

An empirical expression that is often used to describe turbulent flow in smooth pipes is given by the following power law:

$$\frac{u}{U_{max}} = \left(\frac{y}{D/2}\right)^{1/n} \tag{7.44}$$

in which y = distance from the pipe wall = $D/2 - r$ and n is an exponent that depends upon Re.

An integration of (7.44) over the pipe cross section gives the following relationship between average and maximum (centreline) velocities:

$$\frac{U}{U_{max}} = \frac{2n^2}{(n+1)(2n+1)} \tag{7.45}$$

Typically, n is taken as 7 and (7.44) is referred to as the one seventh power law.[*] In this case, (7.44) becomes

$$\frac{u}{U} = \frac{60}{49}\left[1 - \left(\frac{r}{D/2}\right)\right]^{1/7} \tag{7.46}$$

---

[*] n actually varies with the Reynolds number in smooth pipes. Schlichting (1968) gives an experimentally measured variation from $n = 6$ at $Re = 4,000$ to $n = 10$ at $Re = 3,2000,000$. The value $n = 7$ holds at $Re = 110,000$.

Since Eqs. (7.43) and (7.46) both measure u relative to the same flux velocity, U, these equations can be plotted upon the same graph and compared, as shown in Figure 7.15. This plot, which keeps the flow rate constant for the two flows, shows that lateral mixing creates a much more uniform velocity distribution in the turbulent flow.
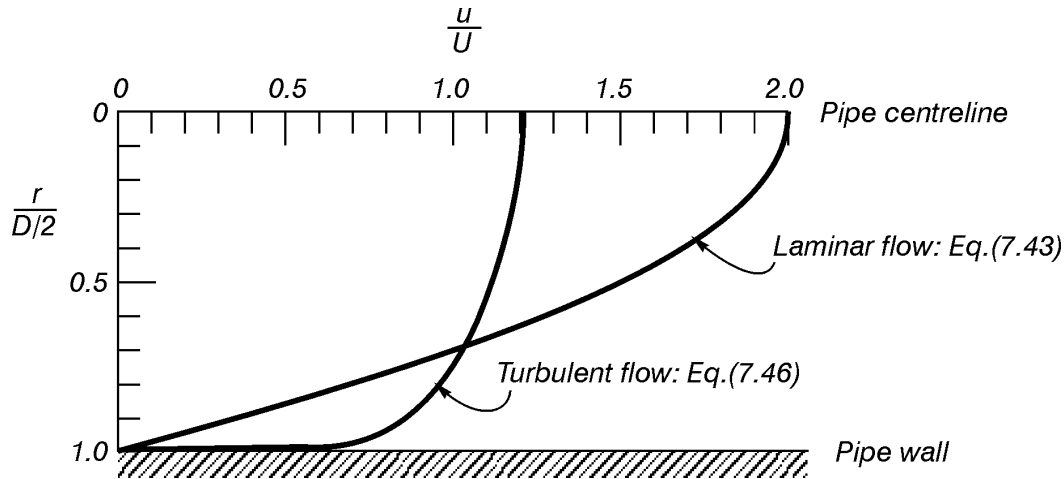
Figure 7.15 Velocity distributions in laminar and turbulent pipe flow.

Turbulence Solutions

There is no general analytical technique that can be used to obtain solutions for problems with turbulent flow. Various methods have been used in the past and have provided some answers for specific types of problems. These include mixing length techniques, statistical methods and more recent $k - \epsilon$ computer modelling methods. None of these techniques, however, are generally applicable, and experimental methods have undoubtedly provided the most useful general method for obtaining turbulent flow solutions. We will consider only two of these solutions: flow in pipes and flow in the submerged jet shown in Figure 7.13.

The solution for laminar pipe flow was given in Eqs. (7.13 a, b, c, d), and it is important to notice that the roughness of the pipe wall boundary does not appear in these equations. Thus, the friction factor, f, in laminar flow depends only upon the Reynolds number and not upon the pipe wall roughness. When turbulence first appears in the flow, it occurs in central portions of the flow away from the boundary, as shown in Figure 7.16. Thus, a layer of laminar flow, called the laminar sublayer, exists next to the boundary. As long as this sublayer has a thickness that is sufficient to submerge the pipe wall roughness, this laminar sublayer will exist and the pipe is described as "hydraulically smooth". This is because boundary shear forces are calculated from Newton's law of viscosity, Eq. (1.1), and boundary roughness has no influence in laminar flow. Thus, boundary shear forces in smooth pipes depend only upon the Reynolds number, but they are considerably larger than corresponding stresses in completely laminar flow because of the much steeper velocity gradient created on the pipe boundary from turbulent mixing in the central portion of the flow.
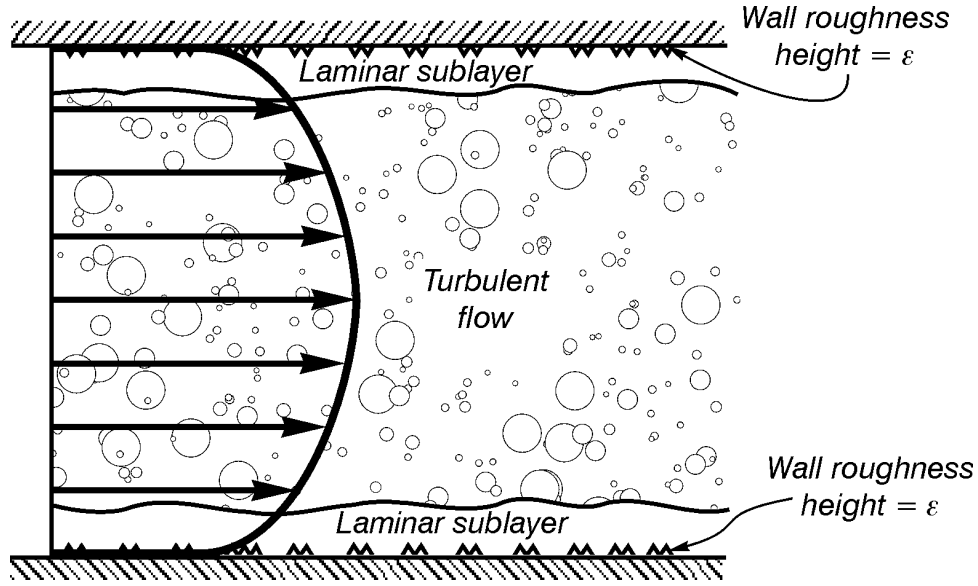
Figure 7.16 Zones occupied by turbulent and laminar flow for turbulent flow through a hydraulically smooth pipe.

The thickness of the laminar sublayer decreases as the Reynolds number increases. When the sublayer thickness decreases to about the same value as the roughness element height, the sublayer disappears and turbulent flow exists all the way to the boundary. At this point the tangential boundary force consists almost entirely of pressure forces acting on the roughness elements (pressure or form drag), and the Bernoulli equation suggests that the tangential boundary stress might be approximated with

$$\tau = \lambda \rho U^2/2 \tag{7.47}$$

in which U is a characteristic velocity that we will take as the flux velocity, Q/A, and λ is an experimental coefficient known as the Fanning friction factor. In this case λ can be expected to depend only upon the relative roughness height, ϵ/D, and not upon the viscosity. The pipe is now described as "hydraulically rough". Thus, the same pipe can be either smooth or rough, depending upon relative dimensions of the roughness elements and laminar sublayer.

A free body diagram showing horizontal control volume forces for fully developed turbulent flow through a horizontal pipe is shown in Figure 7.17. The only horizontal forces are pressure forces on the two end sections and the tangential boundary force given by the product of τ in (7.47) with surface area $P_w L$ in which P_w is the wetted perimeter, πD, and L is the control volume length. Since the fluxes of momentum out of and into the control volume are identical, the momentum equation requires that the sum of these horizontal forces vanish.

$$p_1 A - p_2 A - P_w L \lambda \rho U^2/2 = 0 \tag{7.48}$$
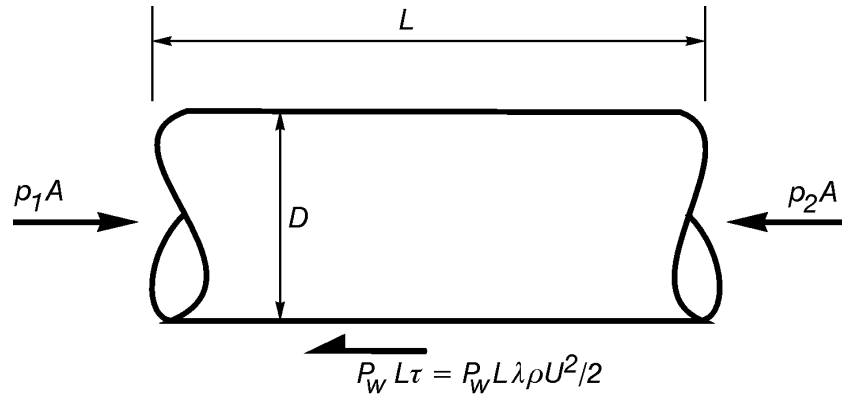
Figure 7.17 Horizontal control volume forces for turbulent flow through a horizontal pipe. (A = cross sectional area and P_w = wetted perimeter.)

Solution of (7.48) for the pressure difference gives

$$p_1 - p_2 = \lambda \, \frac{P_w}{A} \, L \rho \, \frac{U^2}{2} \tag{7.49}$$

The ratio A/P_w is called the "hydraulic radius" and has an important significance for non-circular cross sections and open channel flow. For a pipe, this ratio is $D/4$. Thus, Eq. (7.49) becomes

$$p_1 - p_2 = f \, \frac{L}{D} \, \rho \, \frac{U^2}{2} \tag{7.50}$$

in which f = Darcy-Weisbach friction factor that is related to the Fanning friction factor, λ, by

$$f = 4\lambda \tag{7.51}$$

There are several important points about Eq. (7.50). First, since the flow velocity is the same at both cross sections, Eqs. (4.12) and (4.13) show that head and energy losses are given by

$$H_L = f \, \frac{L}{D} \, \frac{U^2}{2g}$$

$$E_L = f \, \frac{L}{D} \, \rho \, \frac{U^2}{2} \tag{7.52 a, b}$$

in which there has been an obvious switch in notation from V to U for the flux velocity. Second, our development suggests that f depends upon ϵ/D but not Re for completely turbulent flow through a rough pipe but that f depends upon Re and not ϵ/D either for completely laminar flow or for turbulent flow through a smooth pipe. This suggests that a transition zone must exist in which f depends upon both Re and ϵ/D for turbulent flow in a pipe that is neither completely smooth nor completely rough.

All of the features just discussed are illustrated in the Moody diagram for f that is shown in Figure 7.18. This plot, which is essential for the engineering solution of pipe flow problems, shows that f is given by (7.13 d) for $Re < 2000$. A critical zone, shown by cross hatching, exists for $2000 < Re < 4000$. It is in this zone that a disturbance first becomes amplified into turbulence. Turbulent flow in smooth pipes is shown by the bottom curve for $Re > 4000$. Along this curve f depends upon Re but not upon ϵ/D. The horizontal lines to the right of the dashed curve are for complete turbulence in rough pipes, when f depends upon ϵ/D but not upon Re. The curved lines joining the smooth pipe curve to the family of rough pipe curves lie in a transition zone where f depends upon both Re and ϵ/D. Thus, as stated previously, the same pipe may be either smooth or rough, depending upon Re and ϵ/D values — which determine the relative dimensions of the laminar sublayer and roughness heights. At this point the writer suggests that students might profit from rereading this section on turbulence solutions while referring back to Figure 7.18 for an illustration of the various points raised in the discussion.

Problems involving flow through conduits with non-circular cross sections are usually solved with (7.49) and (7.51) provided that cross section width to height ratios are not too different from unity. Thus, head and energy losses for these flows are computed from

$$H_L = \frac{f}{4} \frac{L}{A/P_w} \frac{U^2}{2g}$$

$$E_L = \frac{f}{4} \frac{L}{A/P_w} \rho \frac{U^2}{2}$$

(7.53 a, b)

The Reynolds number and relative roughness for calculation of f in (7.53 a, b) are determined by substituting four times the hydraulic radius, A/P_W, for D. Equations (7.53 a, b) reduce to (7.52 a, b) for circular cross sections.

The turbulent jet shown in Figure 7.13 will be considered in detail in a later chapter on dimensional analysis. Since pressures are known from experimental measurements to be hydrostatic throughout the flow, the momentum flux through any cross section normal to the flow does not change with z. This fact, together with a functional relationship obtained from dimensional analysis, greatly simplify the problem of fitting mathematical equations to experimental data. The end result for an axisymmetric jet follows:
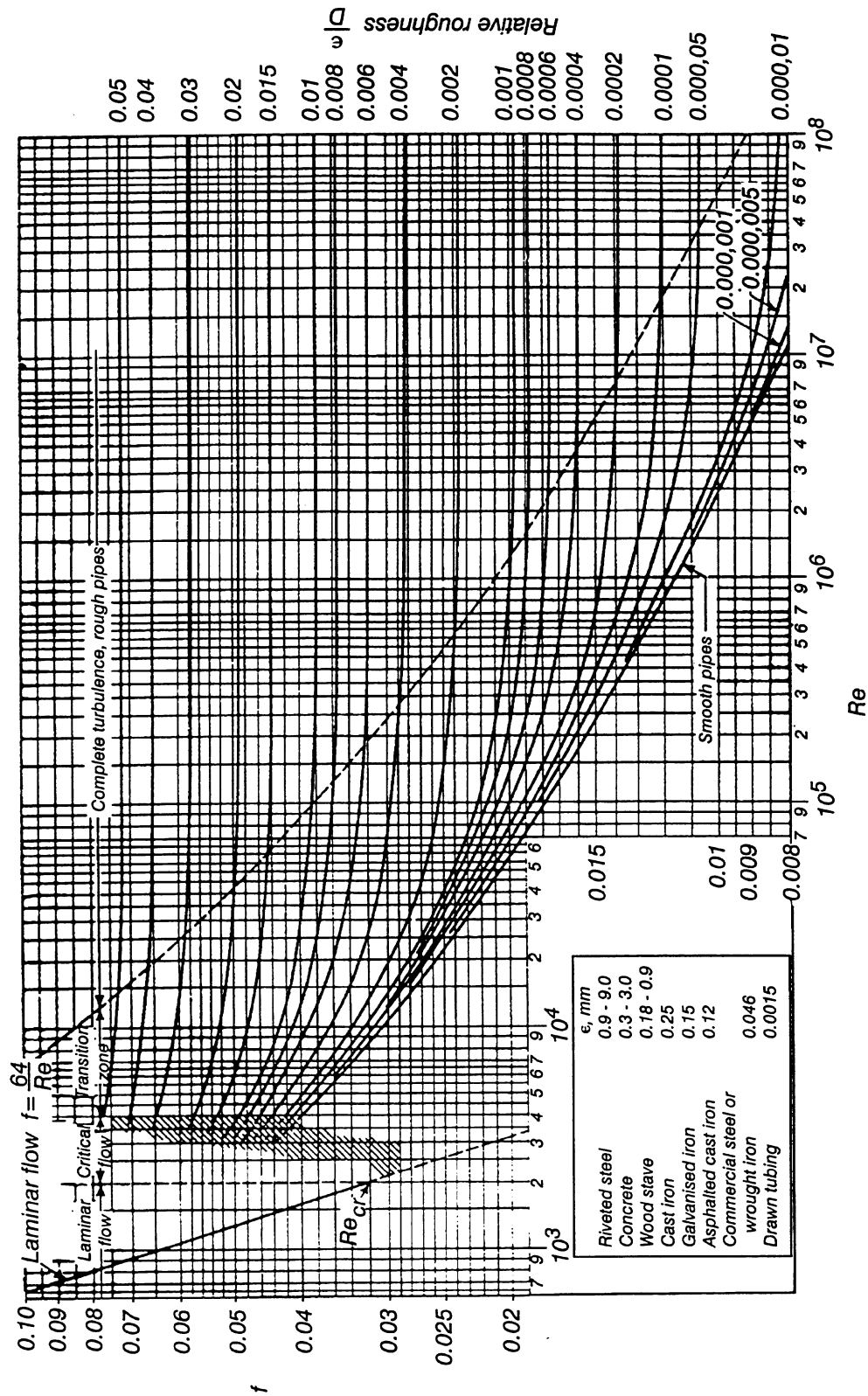
Figure 7.18 The Moody diagram for flow through pipes.

$$\frac{U_{max}}{U_0} = 1 \qquad \text{for} \quad 0 \le z/D \le 6.2$$

$$\qquad\quad = \frac{6.2}{z/D} \quad \text{for} \quad 6.2 \le z/D < \infty \tag{7.54}$$

$$\frac{u}{U_{max}} = e^{-77(r/z)^2} \quad \text{for} \quad 6.2 \le z/D < \infty \tag{7.55}$$

$$\frac{Q}{Q_0} = 0.32 \, \frac{z}{D} \quad \text{for} \quad 6.2 \le z/D < \infty \tag{7.56}$$

$$\frac{C_{max}}{C_0} = 1 \qquad \text{for} \quad 0 \le z/D \le 5.0$$

$$\qquad\quad = \frac{5.0}{z/D} \quad \text{for} \quad 5.0 \le z/D < \infty \tag{7.57}$$

$$\frac{c}{C_{max}} = e^{-62(r/z)^2} \quad \text{for} \quad 5.0 \le z/D < \infty \tag{7.58}$$

in which c, C_0 and C_{max} are concentrations for a neutrally buoyant tracer or contaminant that are usually expressed in units of mg/litre. Corresponding results for the two-dimensional jet (flow from a slot) follow:

$$\frac{U_{max}}{U_0} = 1 \qquad \text{for} \quad 0 \le z/D \le 5.2$$

$$\qquad\quad = \frac{2.28}{\sqrt{z/D}} \quad \text{for} \quad 5.2 \le z/D < \infty \tag{7.59}$$

$$\frac{u}{U_{max}} = e^{-42(y/z)^2} \quad \text{for} \quad 5.2 \le z/D < \infty \tag{7.60}$$

$$\frac{Q}{Q_0} = 0.62\sqrt{\frac{z}{D}} \quad \text{for} \quad 5.2 \le z/D < \infty \tag{7.61}$$

$$\frac{C_{max}}{C_0} = 1 \qquad \text{for} \quad 0 \leq z/D < 5.6$$

$$= \frac{2.38}{\sqrt{z/D}} \quad \text{for} \quad 5.6 \leq z/D < \infty \tag{7.62}$$

$$\frac{c}{C_{max}} = e^{-40(y/z)^2} \quad \text{for} \quad 5.6 \leq z/D < \infty \tag{7.63}$$

in which D = slot width and y replaces the radial coordinate of the axisymmetric jet. Equations (7.54) - (7.56) and (7.59) - (7.61) were obtained by Albertson, Dai, Jensen and Rouse (1948), and (7.57) - (7.58) and (7.62) - (7.63) were abstracted from Fischer, List, Koh, Imberger and Brooks (1979).

Equations (7.54) - (7.63) show that turbulence mixes the time averaged velocity distribution and a tracer in similar, but not completely identical, ways. All velocities decay as $z \rightarrow \infty$, which means that a head loss of $U_0^2/(2g)$ occurs along the centre streamline. Finally, Eqs. (7.56) and (7.61) show that the volume flux past any cross section increases with z as a result of entrainment from turbulent mixing. Entrainment from mixing is another characteristic of highly turbulent flow, and entrainment from turbulent mixing even occurs across an air-water interface in hydraulic jumps or high velocity flows down spillways.

References

Albertson, M.L., Dai, Y.B., Jensen, R.A. and H. Rouse (1948). Diffusion of submerged jets, *ASCE Proceedings*, December, pp. 639-664.

Drazin, P.G. and W.H. Reid (1981) *Hydrodynamic Stability*, Cambridge University Press, Cambridge, p. 21.

Fischer, H.B., List, E.J., Koh, R.C.Y., Imberger, J. and N.H. Brooks (1979) *Mixing in Inland and Coastal Waters*, Academic Press, New York, Ch. 9.

Robertson, J.M. (1965) *Hydrodynamics in Theory and Application*, Prentice-Hall, Inc. Englewood Cliffs, N.J., p. 208.

Rouse, H. (1947) *Elementary Mechanics of Fluids*, John Wiley and Sons, New York, p. 245.

Schlichting, H. (1968) *Boundary-layer Theory*, 6th edition, McGraw-Hill Book Co., New York, pp. 80, 432, 457, 460, 563.

Chapter 8

Boundary-Layer Flow

It was shown in Chapter 5 that many flows with large Reynold numbers have viscous effects that become important only near physical boundaries. If x is a curvilinear coordinate measured along such a boundary from the start of the layer of retarded flow, then Eq. (5.21) estimates that the thickness, δ, of a laminar boundary layer has the following order of magnitude:

$$\frac{\delta}{x} \sim \frac{1}{\sqrt{Re_x}} \quad , \quad \left(Re_x = \frac{Ux}{\nu} \right) \tag{8.1}$$

in which U is the velocity at the outer edge of the boundary layer. Equation (8.1) implies that the relevant Reynolds number for boundary-layer calculations uses the velocity at the outer edge of the boundary layer and distance along the boundary for the characteristic velocity and length in the Reynolds number. It also shows that an increase in the Reynolds number causes a decrease in the relative boundary layer thickness. [The relative thickness, δ/x, is shown by (8.1) to decrease inversely with $\sqrt{x}$. However, the absolute thickness, δ, is shown by this same equation to increase directly with $\sqrt{x}$.] The strict definition of a boundary layer requires that δ/x be very small $(\delta/x << 1)$, which implies that $Re_x >> 1$.
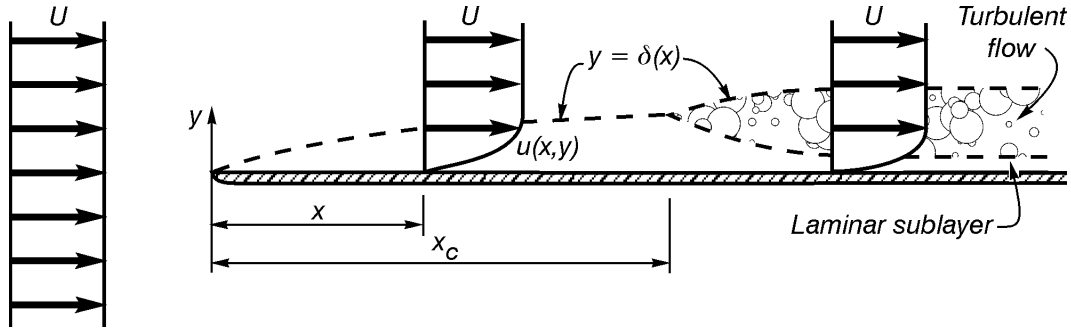
Figure 8.1 Boundary-layer development along a flat plate.

The simplest example of boundary-layer development occurs for flow along a flat plate, which is illustrated in Figure 8.1. The coordinate origin is chosen at the leading edge of the plate, and x is measured along the plate surface in the direction of flow. The plate has a zero thickness, and the boundary-layer thickness, δ, is the y coordinate of the point where the velocity is within one per cent of the approach velocity, U. If the flow were inviscid, the constant velocity U would be maintained all the way to the plate boundary $y = 0$. Thus, $y = \delta(x)$ marks the outer edge of the region which is affected by viscous shear next to the plate surface. The surface $y = \delta(x)$ must not be confused with a streamline, since flow actually crosses through this mathematical surface.

The boundary layer starts with zero thickness at $x = 0$ and increases its thickness with distance downstream. Flow within the boundary layer is initially laminar, and tangential stresses on the plate surface are unaffected by plate roughness. However, the Reynolds number defined in (8.1)

increases its magnitude with distance downstream. Thus, if Re_x becomes large enough, and if a disturbance of the correct magnitude and frequency is present, the boundary layer becomes turbulent at $x = x_c$. Then a viscous sublayer forms next to the boundary, and the plate behaves as a smooth surface provided that the roughness elements are completely submerged in the laminar sublayer. In this case, plate roughness has no effect upon tangential plate stresses. However, if the sublayer thickness and roughness element height have the same order of magnitude, the sublayer vanishes. Then turbulent flow exists right up to the plate surface, and the plate becomes a hydraulically rough surface.

Tangential stresses along a plate surface can, in theory, be calculated from Eq. (1.1) as long as the plate surface remains smooth. Over the front portion of the plate, where the boundary layer is completely laminar, the velocity gradient on the plate surface decreases with x. Thus, tangential stresses decrease with x until $x = x_c$. Downstream from $x = x_c$ turbulent mixing creates much steeper velocity gradients, and tangential stresses on the plate surface increase. If the laminar sublayer vanishes and the plate surface becomes hydraulically rough, pressure drag on the roughness elements becomes the dominant source of tangential stress, a stress that is larger than the tangential boundary stress for either a completely laminar boundary layer or a turbulent boundary layer along a smooth boundary. Thus, tangential boundary stresses increase as flow in the boundary layer goes from completely laminar flow to turbulent flow along a smooth boundary to turbulent flow along a rough boundary.

Boundary Layer Analysis

The fundamental ideas of boundary layer theory were first published by the German engineer Ludwig Prandtl in a paper given at a mathematics conference in Heidelberg, Germany in 1904. Although Prandtl had exceptional insight into the physics of fluid motion and was particularly skilful in applying this insight to remove relatively small terms from the governing partial differential equations, he was unable to solve these equations by himself. The first solution of the boundary layer equations was published in 1908 by Blasius, a young student of Prandtl's. Blasius obtained a mathematical solution of Eqs. (5.23 a, b, c), which describe flow in a laminar boundary layer. However, we will illustrate the fundamental ideas of boundary layer calculations by using an approximate method that was first proposed by K. Pohlhausen in 1921. This method is far simpler than obtaining direct solutions of the partial differential equations for a laminar boundary layer, and it also has the great advantage of providing an approximate method for the calculation of turbulent boundary layers.
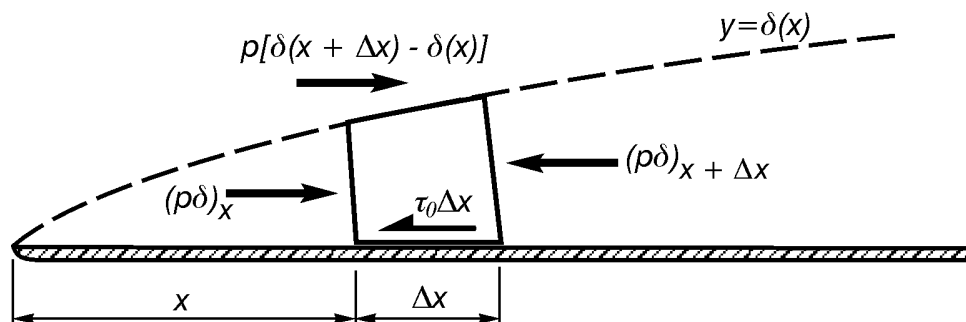
Figure 8.2 Horizontal forces on a control volume in the boundary layer.

The Pohlhausen integral equation can be obtained by applying the horizontal component of the momentum equation to the control volume shown in Figure 8.2. Since $\delta / x \ll 1$, gravitational forces are neglected in boundary layer calculations. Thus, pressure and boundary shear create the only horizontal forces on the control volume. Equation (5.23 c) shows that pressures are constant at any cross section in the boundary layer, which in turn shows that p within a boundary layer is determined from its irrotational value on the boundary. (Since $\delta / x \ll 1$, irrotational flow pressures are calculated along the boundary by neglecting the presence of a boundary layer.) Thus, the momentum equation gives

$$
\begin{aligned}
(p\delta)_x - (p\delta)_{x+\Delta x} &+ p\left[\delta(x + \Delta x) - \delta(x)\right] - \tau_0 \Delta x = \\
&\int_0^{\delta(x+\Delta x)} \rho u^2 \, dy - \int_0^{\delta(x)} \rho u^2 \, dy + \int_{y=\delta(x)} \rho u \left(\mathbf{V} \cdot \mathbf{e}_n\right) ds
\end{aligned}
\tag{8.2}
$$

in which the last integral does not vanish since $\mathbf{V} \cdot \mathbf{e}_n \neq 0$ along $y = \delta(x)$. However, $u = U(x)$ along $y = \delta(x)$ in which $U(x)$ is the irrotational flow velocity on the plate surface, and the last integral can be rewritten as

$$
\int_{y=\delta(x)} \rho u \left(\mathbf{V} \cdot \mathbf{e}_n\right) ds = \rho U \int_{y=\delta(x)} \left(\mathbf{V} \cdot \mathbf{e}_n\right) ds = \rho U \left[\int_0^{\delta(x)} u \, dy - \int_0^{\delta(x+\Delta x)} u \, dy\right]
\tag{8.3}
$$

in which the continuity equation has been used to calculate the flux through $y = \delta(x)$ as the difference between the flux through the cross sections at x and $x + \Delta x$. Substituting (8.3) into (8.2) and dividing by Δx gives

$$
\begin{aligned}
-\frac{(p\delta)_{x+\Delta x} - (p\delta)_x}{\Delta x} &+ p\frac{\delta(x+\Delta x) - \delta(x)}{\Delta x} - \tau_0 = \\
\rho \frac{\displaystyle\int_0^{\delta(x+\Delta x)} u^2 \, dy - \int_0^{\delta(x)} u^2 \, dy}{\Delta x} &- \rho U \frac{\displaystyle\int_0^{\delta(x+\Delta x)} u \, dy - \int_0^{\delta(x)} u \, dy}{\Delta x}
\end{aligned}
\tag{8.4}
$$

Letting $\Delta x \to 0$ in (8.4) gives the end result.

$$
-\frac{d(p\delta)}{dx} + p\frac{d\delta}{dx} - \tau_0 = \rho \frac{d}{dx} \int_0^{\delta} u^2 \, dy - \rho U \frac{d}{dx} \int_0^{\delta} u \, dy
\tag{8.5}
$$

Expansion of the first term and division by the constant $(-\rho)$ puts (8.5) in the following simpler form:

$$
\boxed{\frac{\delta}{\rho}\frac{dp}{dx} + \frac{\tau_0}{\rho} = U\frac{d}{dx}\int_0^{\delta} u \, dy - \frac{d}{dx}\int_0^{\delta} u^2 \, dy}
\tag{8.6}
$$

in which dp/dx and U are functions of x that have been calculated previously from an irrotational flow solution that disregards the presence of the boundary layer.

Equation (8.6) can be shown to be the exact result of integrating the boundary layer equation (5.23 a, b, c), across the boundary. The approximation comes in the method that must be used to solve (8.6). This method uses the following steps:

1 Values of dp/dx and U are calculated from an irrotational flow solution and substituted into (8.6).

2 A physically realistic assumption is made for the variation of u within the boundary layer and is substituted into the integrals on the right side of (8.6).

3 An expression for τ_0 is substituted into the left side of (8.6). For a laminar boundary layer, τ_0 is calculated from Eq. (1.1) and the assumed variation of u. For turbulent boundary layers, empirical pipe flow equations are used to approximate τ_0.

4 The resulting first-order ordinary differential equation for $\delta(x)$ is integrated. The integration constant is calculated by requiring $\delta(0) = 0$.

For the simplest problem of a flat plate of zero thickness aligned with the flow, the irrotational flow solution is U = constant and $dp/dx = 0$. Then (8.6) simplifies to

$$\frac{\tau_0}{\rho} = \frac{d}{dx} \int_0^{\delta} (U - u)\, u \, dy \quad , \quad (U = \text{constant}) \qquad \textbf{(8.7)}$$

The drag force on one side of the plate is obtained from

$$F = \int_0^L \tau_0 \, dx \qquad \textbf{(8.8)}$$

in which L = plate length and the plate has a unit width. Using (8.7) in (8.8) and making use of the initial condition $\delta(0) = 0$ gives

$$F = \rho \int_0^{\delta(L)} (U - u)\, u \, dy \qquad \textbf{(8.9)}$$

in which $u = u(L, y)$ and U = constant.

Example 8.1

We will use (8.7) and (8.9) to calculate the solution for a laminar boundary layer along a flat plate. Since fully developed laminar flow between two flat plates has a velocity distribution given by a parabola, we will assume that

$$u(x, y) = a(x) + b(x)y + c(x)y^2$$

Physics requires the boundary conditions

$$u(x, 0) = 0 \quad , \quad u(x, \delta) = U \quad , \quad \frac{\partial u(x, \delta)}{\partial y} = 0$$

These three equations determine a, b and c and lead to the result

$$u(x, y) = U\left(2\xi - \xi^2\right) \text{ in which } \xi = \frac{y}{\delta(x)}$$

Thus, the integral on the right sides of (8.7) and (8.9) is

$$\int_0^\delta (U - u) u \, dy = U^2 \int_0^\delta \left(1 - 2\xi + \xi^2\right)\left(2\xi - \xi^2\right) dy = U^2 \delta \int_0^1 \left(2\xi - 5\xi^2 + 4\xi^3 - \xi^4\right) d\xi$$

$$= \frac{2}{15} U^2 \delta(x)$$

(The integral on the right side of (8.7) can always be calculated most easily by changing the integration variable from y to ξ.) The shear stress on the left side of (8.7) is calculated by inserting the expression for $u(x, y)$ into Eq. (1.1) to obtain

$$\tau_0 = \mu \frac{\partial u(x, 0)}{\partial y} = \mu \left(\frac{du}{d\xi}\right)_{\xi = 0} \frac{\partial \xi}{\partial y} = \mu \frac{2U}{\delta}$$

Thus, Eq. (8.7) becomes

$$\frac{\mu}{\rho} \frac{2U}{\delta} = \frac{2}{15} U^2 \frac{d\delta}{dx}$$

Separating variables gives

$$\int_0^{\delta(x)} \delta \, d\delta = 15 \frac{\nu}{U} \int_0^x dx$$

and integration gives

$$\frac{1}{2} \delta^2 = 15 \frac{\nu}{U} x$$

This can be written dimensionlessly as

$$\frac{\delta}{x} = \sqrt{\frac{30}{Ux/\nu}} = \frac{5.48}{\sqrt{Re_x}}$$

The force per unit width on one side of the plate is calculated from (8.9).

$$F = \rho \int_0^{\delta(L)} (U - u)\,u\,dy = \rho \frac{2}{15} U^2 \delta(L) = \rho \frac{2}{15} U^2 \frac{5.48}{\sqrt{Re_L}} L$$

This can be put in the more significant form

$$F = C_D A \rho \frac{U^2}{2} \quad , \quad A = L \times 1 \quad , \quad C_D = \frac{1.46}{\sqrt{Re_L}} \quad , \quad Re_L = \frac{UL}{\nu}$$

The exact solution of (5.23 a, b, c) that was obtained by Blasius gave

$$\frac{\delta}{x} = \frac{5.0}{\sqrt{Re_x}} \quad , \quad C_D = \frac{1.33}{\sqrt{Re_L}}$$

Thus, the error of approximation in our solution is about 10 per cent. A comparison between experiment, the approximate solution and the Blasius solution is shown in Figure 8.3 for the velocity distribution within a laminar boundary layer.
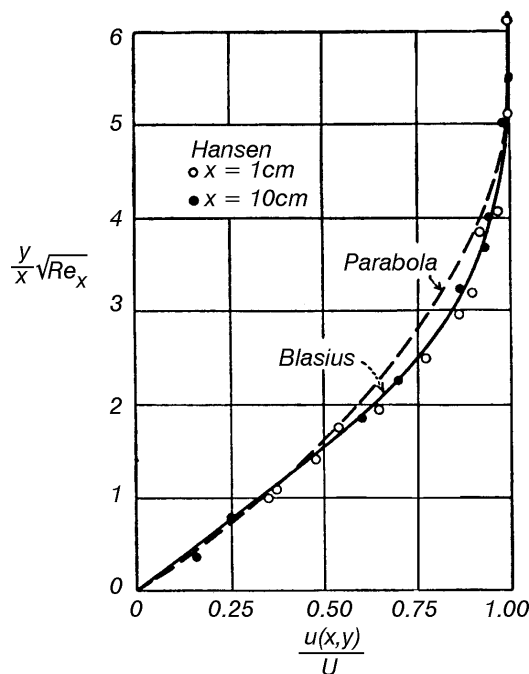
Figure 8.3 Comparison between measured and calculated velocity distributions within a laminar boundary layer on a flat plate. [Measurements by Hansen, reproduced from Rouse (1961).]

Example 8.2

We will use (8.7) and (8.9) to calculate an approximate solution for a turbulent boundary layer along a smooth flat plate. We will use the one seventh power law given by Eq. (7.43)

$$u(x, y) = U\xi^{1/7} \quad , \quad \xi = \frac{y}{\delta(x)}$$

Thus, the integral on the right sides of (8.7) and (8.9) is

$$\int_0^\delta (U - u)u\,dy = U^2\delta \int_0^1 \left(1 - \xi^{1/7}\right)\xi^{1/7}\,d\xi = \frac{7}{72}U^2\delta(x)$$

Although the boundary is covered by a laminar sublayer that allows the use of Eq. (1.1) for calculating τ_0, our assumed velocity distribution is too inaccurate to give a good approximation for τ_0 from (1.1). (In fact, $\partial u/\partial y = \infty$ on $y = 0$ if we use the power law.) Thus, τ_0 must be approximated with an empirical expression from pipe flow measurements. A reasonable approximation has been found to be

$$\tau_0 = 0.0225 \left(\frac{\nu}{U\delta}\right)^{1/4} \rho U^2$$

Thus, (8.7) becomes

$$0.0225 \left(\frac{\nu}{U\delta}\right)^{1/4} U^2 = \frac{7}{72}U^2\frac{d\delta}{dx}$$

Integration of this differential equation gives

$$\frac{\delta}{x} = \frac{0.37}{Re_x^{1/5}}$$

This allows the drag force to be computed from (8.9).

$$F = \rho \int_0^{\delta(L)} (U - u)u\,dy = \rho\frac{7}{72}U^2\delta(L) = \rho\frac{7}{72}U^2\frac{0.37}{Re_L^{1/5}}L$$

This result can be rewritten in the following standard form:

$$F = C_D A\rho\frac{U^2}{2} \quad , \quad A = L \times 1 \quad , \quad C_D = \frac{0.072}{Re_L^{1/5}} \quad , \quad Re_L = \frac{UL}{\nu}$$

In practice, experimental data shows that this holds for $5 \times 10^5 < Re_L < 10^7$ when 0.072 is changed to 0.074 in the formula for C_D.

Example 8.3

The results from examples 8.1 and 8.2 assume that the boundary layer is either entirely laminar or entirely turbulent from the leading edge of the flat plate. More generally, the boundary layer will change from laminar to turbulent at $x = x_c$ when $0 < x_c < L$. It is possible to calculate a solution for this case using the same techniques that were used in examples 8.1 and 8.2. In practice, a simpler approximation suggested by Prandtl is used in which the laminar drag force for $0 < x < x_c$ is added to the turbulent drag force for $x_c < x < L$. Prandtl's approximation assumes that the forces on each of these two intervals are identical with the forces that would occur if the boundary layer were entirely laminar or entirely turbulent, respectively, from the leading edge. Thus, if we set

$$Re_c = \frac{Ux_c}{\nu}$$

then the total drag force is approximated with

$$F = \frac{1.33}{\sqrt{Re_c}} x_c \rho \frac{U^2}{2} + \frac{0.074}{Re_L^{1/5}} L \rho \frac{U^2}{2} - \frac{0.074}{Re_c^{1/5}} x_c \rho \frac{U^2}{2}$$

in which the first term is the laminar drag for $0 < x < x_c$ and the turbulent drag for $x_c < x < L$ is computed from the last two terms by subtracting the turbulent contribution for $0 < x < x_c$ from the turbulent drag for $0 < x < L$. Since $A = L \times 1$, this result can be rewritten in the form

$$F = C_D A \rho \frac{U^2}{2}$$

in which

$$C_D = \frac{1/33}{\sqrt{Re_c}} \frac{x_c}{L} + \frac{0.074}{Re_L^{1/5}} - \frac{0.074}{Re_c^{1/5}} \frac{x_c}{L}$$

However, $x_c/L = Re_c/Re_L$ and this becomes

$$C_D = \frac{0.074}{Re_L^{1/5}} - \frac{C_1}{Re_L}$$

in which

$$C_1 = Re_c \left(\frac{0.074}{Re_c^{1/5}} - \frac{1.33}{\sqrt{Re_c}} \right)$$

An average value of $Re_c = 5 \times 10^5$ is usually used to calculate $C_1 = 1741$ in applications. However, there is always some uncertainty about which value of Re_c to use since the transition to turbulence depends upon more than just a Reynolds number. Therefore, when a more precise value for drag is needed in an experiment, the leading edge of the plate is usually roughened to ensure that the boundary layer is turbulent from the leading edge.

Figure 8.4 shows a plot of the solutions calculated in examples 8.1–8.3 together with some experimental data. The solution for Example 8.2 holds for a more limited range of Re_L than the range shown in Figure 8.4. ***Thus, it is recommended that Figure 8.4 be used to obtain values for C_D in all calculations for either a laminar boundary layer or a turbulent boundary layer along a smooth plate***. This plot makes obvious the fact that, at the same value of Re_L, a turbulent boundary layer creates a much larger drag than a laminar boundary layer.

The similarity between Figure 8.4 and the Moody diagram for pipe flow, Figure 7.18, suggest that another family of curves should be appended to Figure 8.4 for a rough plate. These calculations were published in 1934 by Prandtl and Schlichting and are plotted in Figure 8.5. Values for the roughness height, ϵ, are given in Figure 7.18 for some different surfaces.
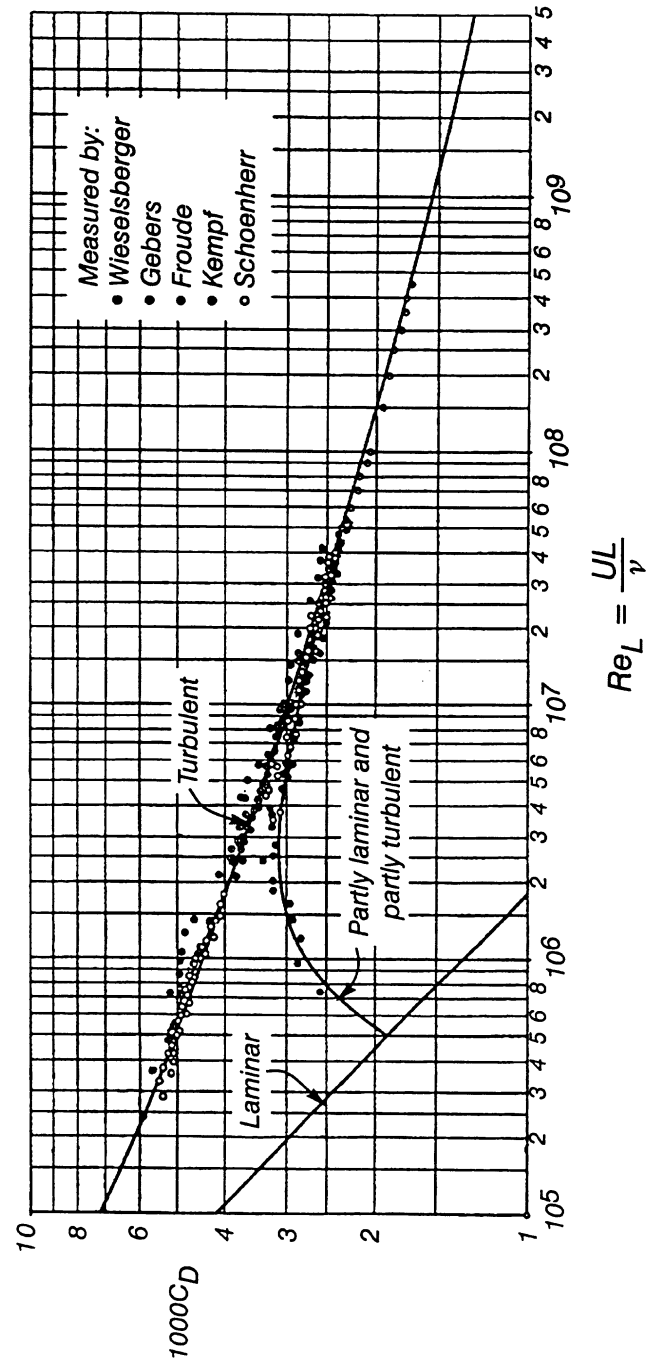
Figure 8.4 The drag coefficient for one side of a flat plate aligned with the flow. [Reproduced from Schlichting (1968).]
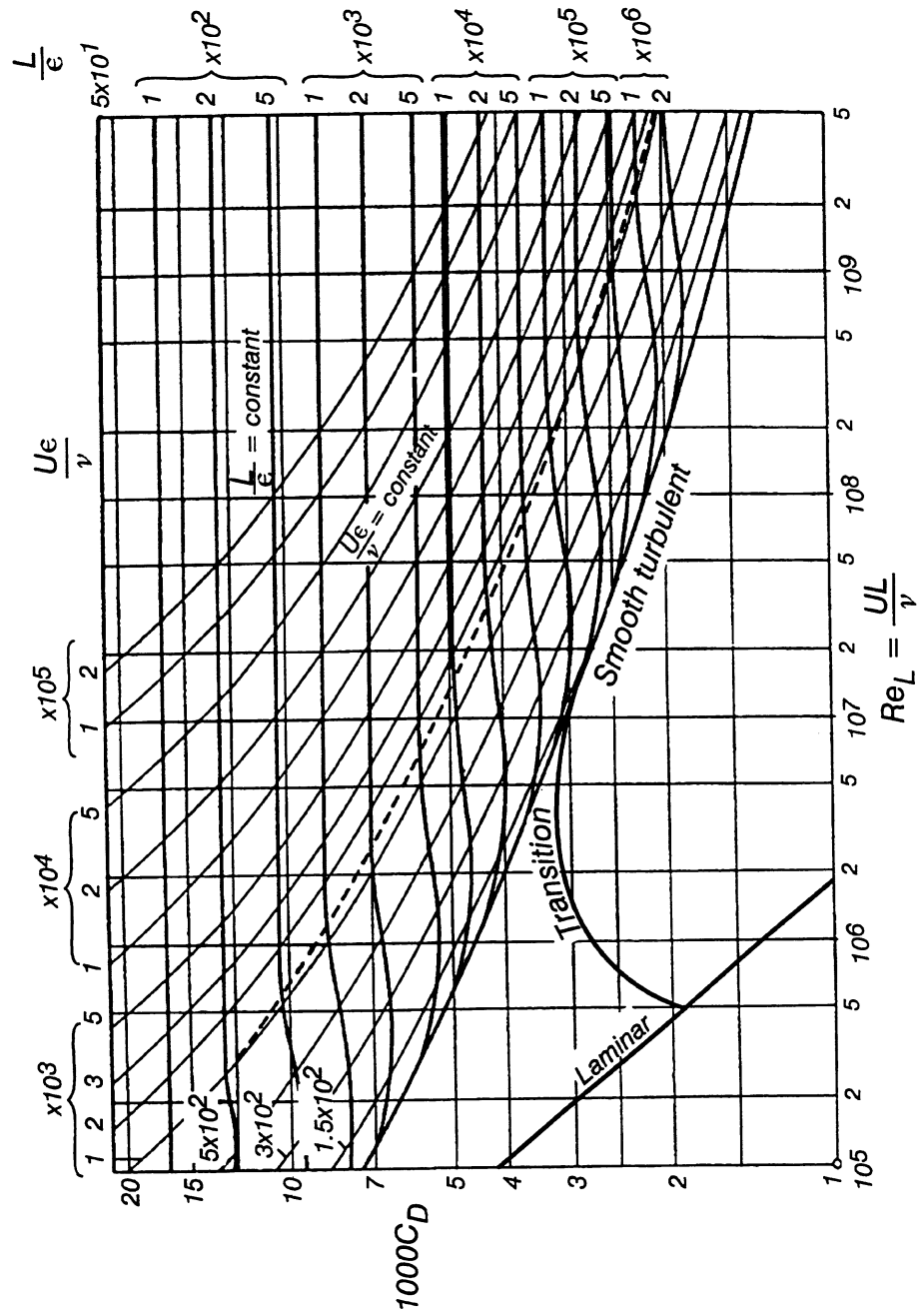
Figure 8.5 The drag coefficient for one side of rough and smooth flat plates aligned with the flow. [Reproduced from Schlichting (1968).]

Example 8.4

Wind blowing across a relatively shallow reservoir of water causes the reservoir free surface to tilt. The increase in water depth at the downwind end of the reservoir is known as "wind setup" and must be considered when determining freeboard requirements for a dam design. For a first approximation, the free surface can be assumed to tilt as a plane, and boundary layer theory can be used to calculate the drag force created on the free surface by the wind. The principal horizontal forces involved are the free surface wind drag and hydrostatic pressure forces on the two end sections, as shown in the following sketch for a cross section of unit width.
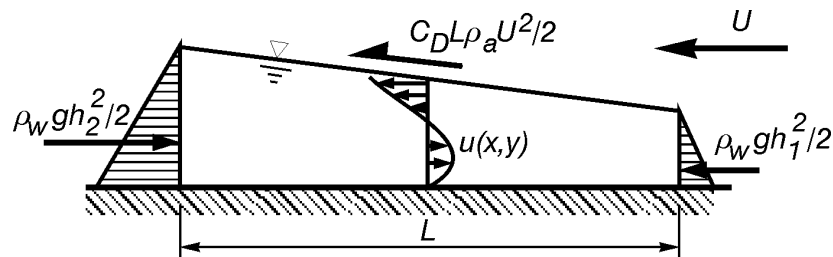
Setting the sum of horizontal forces equal to zero gives

$$\rho_w\, g\, h_2^2 \Big/ 2 \; - \; \rho_w\, g\, h_1^2 \Big/ 2 \; - \; C_D\, L\, \rho_a\, U^2 \Big/ 2 \; = \; 0$$

in which ρ_w and ρ_a are water and air mass densities, respectively.

This equation can be manipulated into the form

$$\frac{1}{2}\left(h_2^2 - h_1^2\right) = \frac{1}{2}\left(h_2 + h_1\right)\left(h_2 - h_1\right) = C_D\, L\, \frac{U^2}{2g}\, \frac{\rho_a}{\rho_w}$$

Since the free surface has been assumed to tilt as a plane,

$$\frac{1}{2}\left(h_2 + h_1\right) = h_0$$

in which h_0 is the depth before the wind started to blow. Thus, the difference in water depth between the two ends is

$$\left(h_2 - h_1\right) = C_D\, \frac{L}{h_0}\, \frac{U^2}{2g}\, \frac{\rho_a}{\rho_w}$$

in which L is known as the "fetch". This shows that wind setup is increased by increasing L/h_0 and U. Thus, wind setup is greatest for shallow reservoirs. Lake Ellesmere, a shallow lake south of Christchurch has a fetch of about 25 km and an average depth of about 2 m. Values of $\left(h_2 - h_1\right)$ of a metre or more often occur on this lake as a result of storms.

Wind stresses on the reservoir free surface create surface water velocities in the downwind direction. However, if the ends are enclosed so that zero flow occurs across both end sections, then the continuity equation requires that there be a zero net flow past any vertical cross section. Thus, a region of return flow near the reservoir bottom must balance the downwind flow near the free surface, as shown with the velocity distribution in the sketch.

Example 8.5

Now consider a three-dimensional flow that results when wind blows across a reservoir that is shallow on one side and deeper on the other, as in the following plan view:
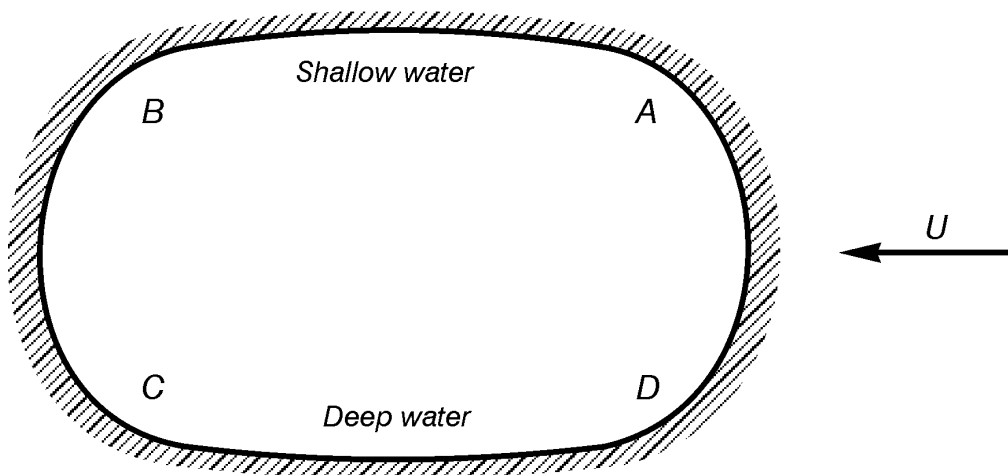
Since wind setup is greater for the shallow side than for the deep side, the free surface elevation at A is lower than at D and the elevation at B is higher than at C. Thus, pressure gradients in the form of a sloping free surface are created in the directions from D to A and from B to C. Since no other horizontal forces occur in these directions, the water must be accelerated from D to A and from B to C and a depth-averaged counterclockwise pattern of circulation must be created, as shown in the following sketch:
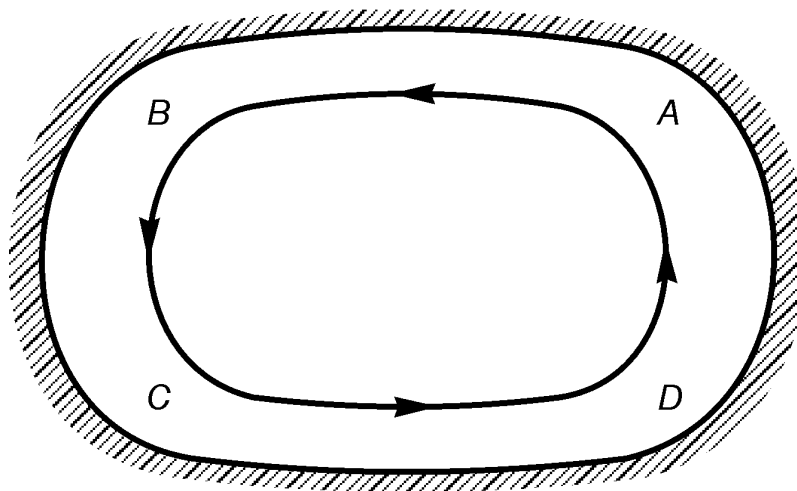
Water velocities near the free surface must all be in the downwind direction, but return flows near the bottom no longer balance with these surface flows since there must be a net flow at any vertical cross section in the direction of the circulation cell. If sides AB and CD are both shallow, and if deeper water occurs in the reservoir centre, then two circulation cells are created, as shown in the sketch. The writer is indebted to Dr R. Spigel for this example.
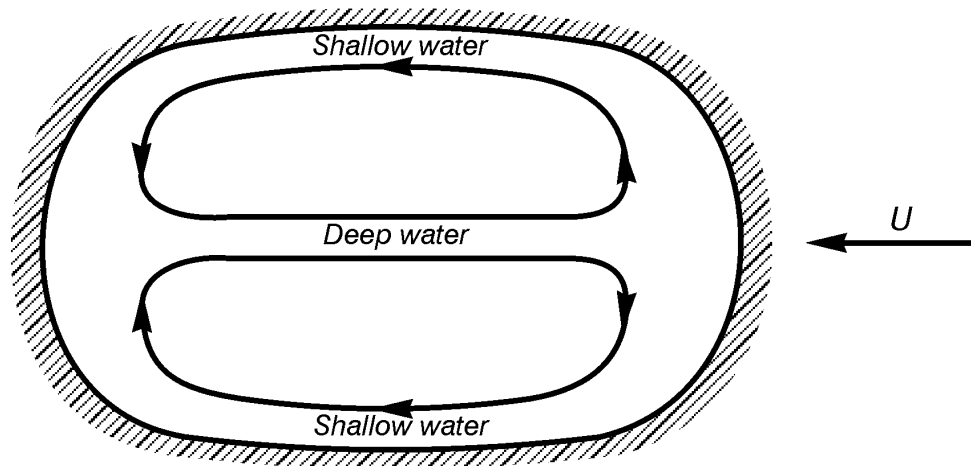
Pressure Gradient Effects in a Boundary Layer

Equation (5.23 c) shows that pressures within a boundary layer are fixed by inviscid flow pressures calculated on the boundary. Thus, flow within a boundary layer reacts to pressure gradients that are imposed externally by an inviscid flow. Boundary layer development along a flat plate was particularly simple to analyse because this pressure gradient is zero. Now we will consider flow along boundaries where pressure gradients are non-zero and can cause important effects.

A pressure gradient causes a net force on a fluid particle in the direction of decreasing pressure. Thus, if pressures decrease in the direction of flow along a boundary, then Newton's law shows that a fluid particle will be accelerated in the direction of motion. This is called a favourable pressure gradient, and it is characterized by irrotational flow streamlines that converge as flow moves along the boundary. If pressures increase in the direction of flow along a boundary, then pressure forces oppose motion and create a deceleration. This is called an adverse pressure gradient, and it is characterized by irrotational flow streamlines that diverge as flow moves along a boundary.

Since a favourable pressure gradient accelerates a fluid particle within a boundary layer, we would expect velocity distributions within the boundary layer to become more uniform when irrotational flow streamlines converge in the direction of flow. Conversely, we would expect an adverse pressure gradient to decelerate flow and create less uniform velocity distributions within a boundary layer when irrotational flow streamlines diverge in the direction of flow. This is shown with sketches in Figure 8.6, in which it is also shown that boundary layer thicknesses decrease with x for a favourable pressure gradient and thicken with x for an adverse pressure gradient.
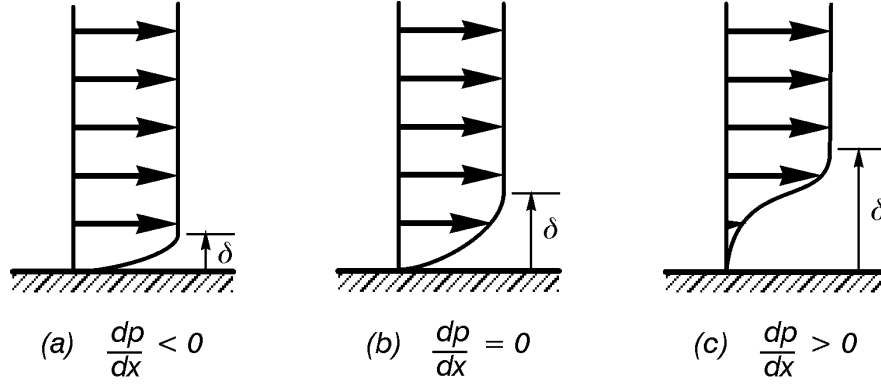
Figure 8.6 Typical velocity distributions and boundary-layer thicknesses that result from (a) favourable, (b) zero and (c) adverse pressure gradients.

Mathematical proof that boundary layers react to pressure gradients in the way shown in Figure 8.6 is provided by the Falkner-Skan laminar boundary-layer solution for flow past a wedge plotted in Figure 8.7. The interior wedge half angle is $\beta\pi/2$, and the inviscid boundary velocity is given by $U(x) = u_1 x^m$ in which u_1 and m are constants and $0 < x < \infty$. This velocity is used to calculate boundary pressures, so that positive and negative values of m correspond to favourable and adverse pressure gradients, respectively, and $m = 0$ corresponds to flow along a flat plate. Boundary-layer thicknesses decrease and velocity gradients on the boundary increase as m increases from 0, while exactly the opposite happens for an adverse pressure gradient as m becomes negative.

Flow in a boundary layer can withstand only a very limited amount of deceleration from an adverse pressure gradient before separating from the boundary. A sketch showing the stream-line pattern and velocity distribution near a point of flow separation is shown in Figure 8.8. The separating streamline is defined as the streamline that leaves the boundary at the point where the boundary shear, τ_0, vanishes. [$\tau_0 = 0$ at this point since velocities and boundary shear forces are in opposite directions on either side of the separation point. In laminar flow Eq. (1.1) shows that this is equivalent to requiring $\partial u(x, 0)/\partial y = 0$ at the separation point.] Flow outside the separating streamline can still be approximated as inviscid, while flow between the boundary and separating streamline is highly rotational. However, calculation of the separating streamline geometry is extremely difficult since its existence modifies the inviscid flow velocity and pressure distribution both upstream and downstream from the separation point, and it is this unknown pressure distribution that must be inserted into the viscous flow equations to determine the point at which $\tau_0 = 0$. Furthermore, the boundary- layer equations are probably invalid near the separation point since the term $\partial^2 u/\partial x^2$ is unlikely to remain negligible there. Thus, the general problem of calculating a mathematical solution that is valid near a point of flow separation has, at present, no satisfactory solution.

Despite the mathematical difficulty of calculating valid solutions near points of flow separation, experimental and mathematical considerations allow us to make several important observations about these flows. First, boundary-layer separation has two important requirements that must both be met before separation can occur: ***the presence of a retarded layer of fluid next to a boundary (a boundary layer) and the presence of an adverse pressure gradient.*** The classical experimental evidence for this conclusion is shown in Figure 8.9, which shows flow normal to a flat plate both without and with a splitter plate extending into the flow on the upstream side of the plate.
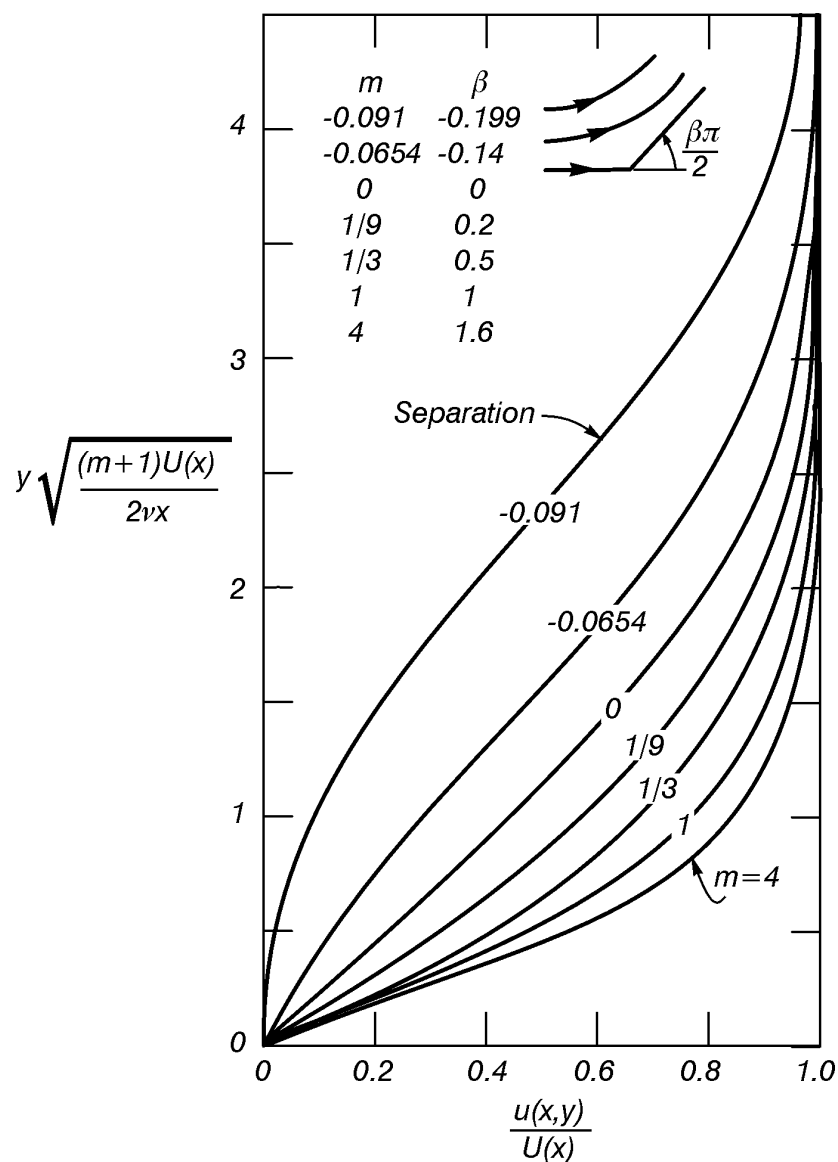
Figure 8.7 The Falkner-Skan solution for flow past a wedge with $U(x) = u_1 x^m$. [Reproduced from Schlichting (1968).]
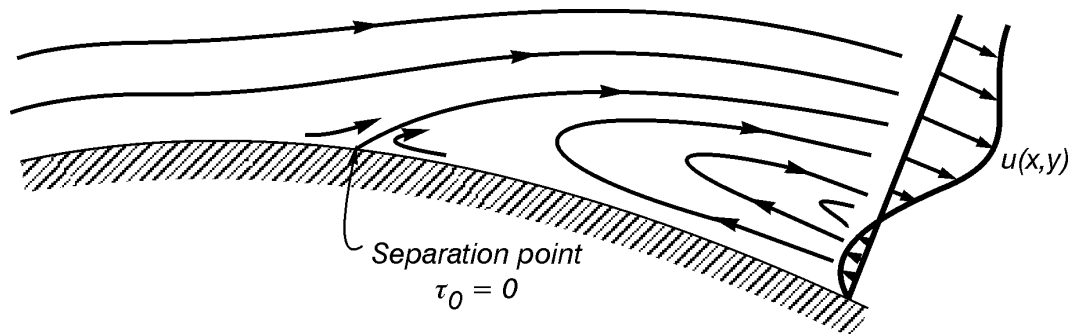
Figure 8.8 Streamline pattern and velocity distribution near a point of flow separation.

The same adverse pressure gradient is present for both flows, but flow separation only occurs with the splitter plate because this also provides a boundary layer for the approaching flow. Similar flows can be observed through the movement of dust in a trapped vortex when a dry hot wind blows against a building corner or in front of a large hill or mountain when flow at low levels in front of the mountain is observed to be in a direction opposite to the approaching flow.
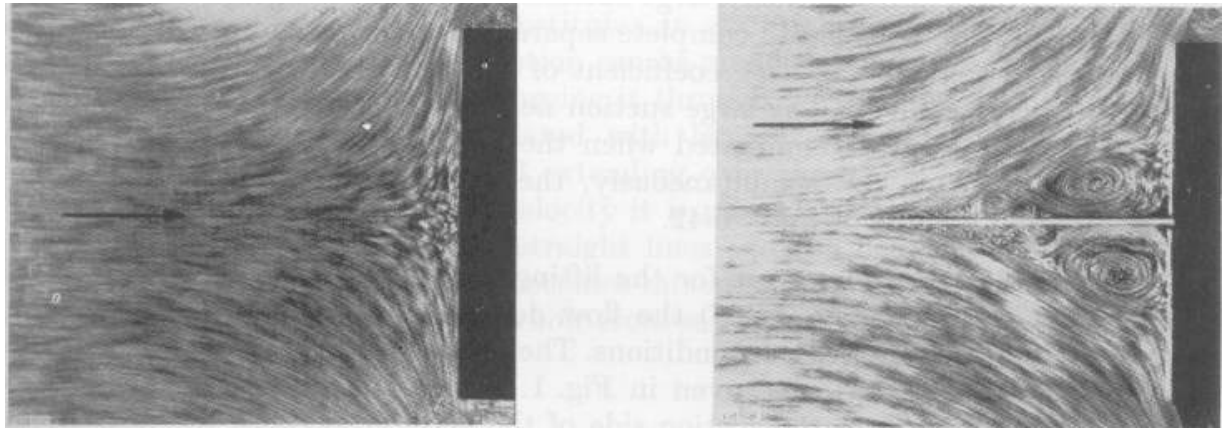
Figure 8.9 Flow normal to a flat plate, (a) without and (b) with a splitter plate. [Photographed by Foettinger, reproduced from Schlichting (1968).]

A second experimentally observed characteristic of flow in zones of flow separation is that pressures, or piezometric heads if gravity is important, remain nearly constant in cross sections normal to the boundary. Thus, flow separation creates large and important modification of boundary pressure distributions. In fact, the net boundary pressure component of a drag force is known to be zero if flow separation is not present in an irrotational flow (D'Alembert's paradox). Thus, control of boundary-layer separation is important if one wants to control the boundary pressure component of a drag force. This control, when practical, is accomplished by speeding up flow within the boundary layer to counteract the effects of an adverse pressure gradient. The most common example uses roughness elements (dimples on a golf ball, roughness elements on top of airplane wings, etc.) to create a turbulent boundary layer, which has higher velocities close to the boundary as a result of turbulent mixing. However, moving a boundary in the direction of flow, injecting higher velocity flow into a boundary layer or sucking lower velocity fluid out of the boundary layer can all be used to speed up flow in the boundary layer and either delay or prevent separation. The two volumes edited by Lachmann give extensive consideration to methods of controlling boundary-layer separation.

Another form of flow separation occurs at sharp corners. The cause of this type of separation can be attributed either to an infinite velocity and negatively infinite pressure calculated from irrotational flow theory, neither of which can be tolerated by a viscous fluid, or else an extreme form of boundary-layer separation, which results from an infinite adverse pressure gradient on the downstream side of the sharp corner. Regardless of which of these two explanations is accepted as a reason, the important fact is that flow separation always occurs at a sharp corner. *Furthermore, while the location of the separation point can, and usually does, change with Reynolds number along a more gently curving boundary, the separation point at a sharp corner remains fixed at the sharp corner for all Reynolds numbers.*
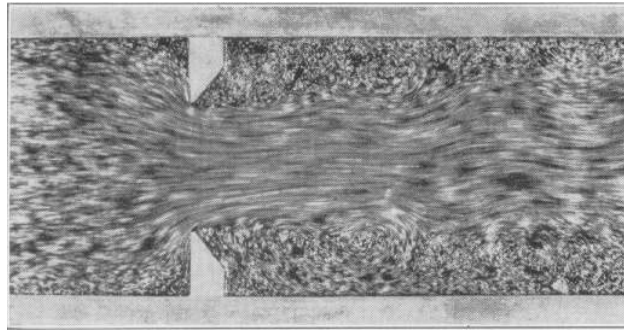
(a)
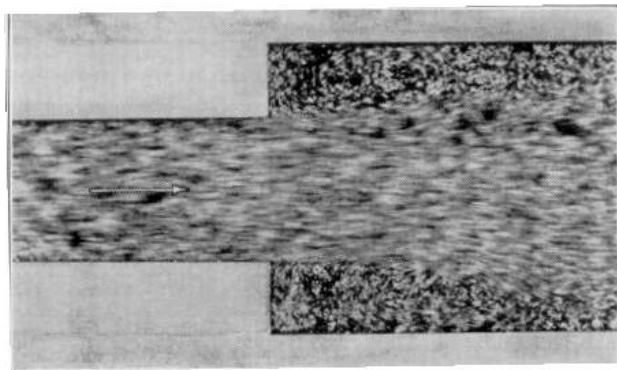
(b)
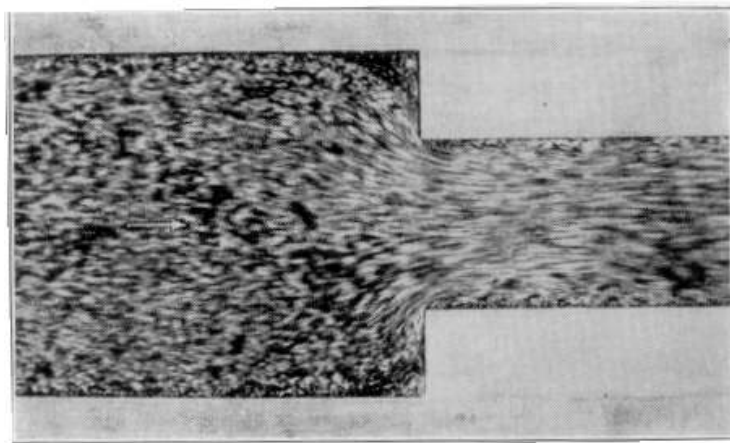
(c)

Figure 8.10   Some additional examples of flow separation. All flows are from left to right. [Reproduced from Rouse (1961).]

Some additional examples of flow separation are shown in Figure 8.10. In Fig. 8.10 a, which resembles flow past an orifice plate inserted in a pipe, separation similar to the separation shown in Fig. 8.9 b occurs in the corner on the upstream side of the plate, and a second separation point occurs at the protruding sharp corner. Figure 8.10 b shows separation at the sharp corner formed by the junction of the two conduits, and Fig. 8.10 c shows separation both in the corner stagnation point and at the protruding sharp corner. Figures 8.10 b and 8.10 c also show the difference between flow patterns in an abrupt expansion and an abrupt contraction. Energy losses from a transfer of energy into the regions of separated flow occur in both instances. Intuition suggests that these losses increase as the size of the zone of separated flow increases, which suggests that losses will be larger for Figure 8.10 b than for Figure 8.10 c.

Secondary Flows

In some instances pressure gradients are at right angles to the direction of primary flow outside the boundary layer, and these transverse pressure gradients cause a component of fluid motion perpendicular to the direction of primary flow. Because of this, the motion is referred to as secondary. In general, secondary flows create energy losses, redistribute longitudinal velocities and cause sediment erosion and transport in erodible channels.
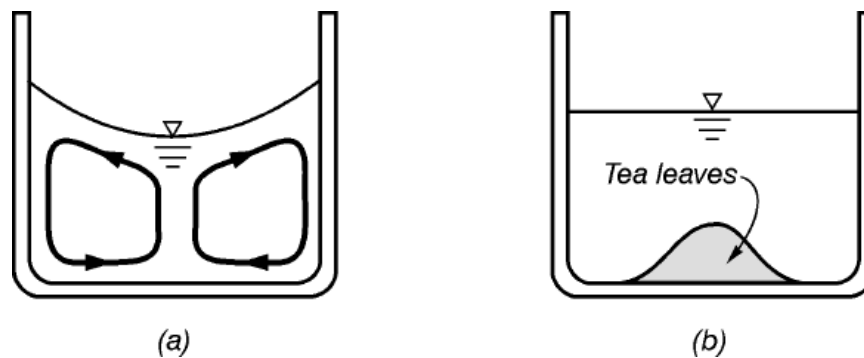
Figure 8.11 Secondary flow currents in a stirred cup of tea (a) immediately after stirring has stopped and (b) after all motion has stopped with tea leaves deposited in the centre by the secondary flow.

A commonly encountered example of secondary flow occurs after a cup of tea has been stirred, as shown in Fig. 8.11 a. Immediately after stirring has stopped, the primary flow has circular streamlines with a centripetal acceleration component, V^2/R, given by the radial component of Eq. (1.24). This radial acceleration is directed toward the vertical axis of symmetry and, from Newton's second law, is accompanied by a pressure gradient that causes pressures to decrease in the same direction. Since vertical accelerations are relatively small, pressures are hydrostatic along vertical lines. Thus, the radial pressure decrease results in a free surface that slopes downward toward the centre of the cup, as shown in Figure 8.11 a. Since this same pressure gradient exists in the boundary layer along the bottom, slowly moving fluid particles on the bottom are accelerated toward the cup centre. This results in the two circulation cells shown in Figure 8.11 a, although the actual motion in these cells is three-dimensional with a velocity component in the e_θ direction as well. The pile of tea leaves deposited in the centre after all motion has ceased gives evidence of the earlier existence of the secondary flow.

The teacup principle just described creates secondary flows in a number of applications that are of interest to civil engineers. One example occurs in pipe flow through a bend, as shown in Figure 8.12. The primary flow has circular streamlines and a radial acceleration, V^2/R, directed toward the centre of streamline curvature at point 0 in Figure 8.12 a. The acceleration is accompanied by a decrease in pressure toward point 0 in both the primary flow and the boundary layer next to the pipe walls. Thus, a convective acceleration is created along the pipe boundaries from a to b and c to d in Figure 8.12 b as a result of the pressure gradient imposed by the primary flow. The circulation cell motion is shown in Figure 8.12 b, but this motion is highly three-dimensional. In fact, streamlines in the boundary layer zone follow the spiral pattern shown in Figure 8.12 a.
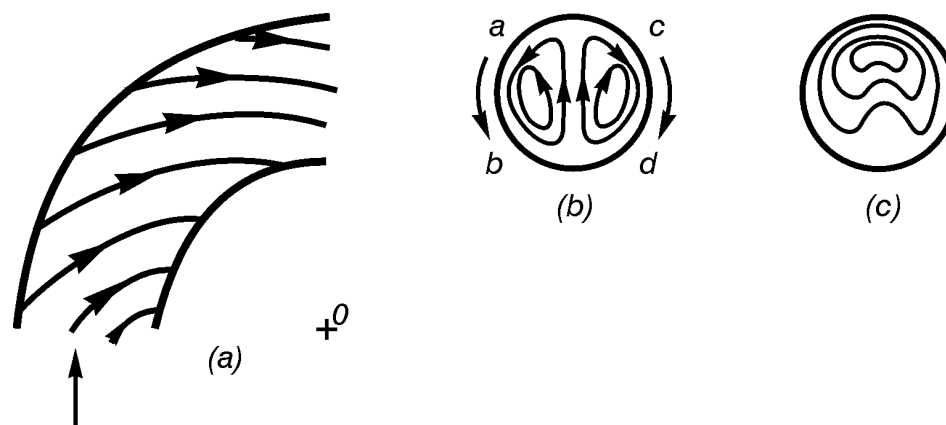
Figure 8.12 Secondary flow in a curved pipe showing (a) streamlines in the boundary layer zone, (b) the circulation cell flow pattern and (c) contours of constant velocity (isovels).

There are two effects caused by the secondary flow shown in Figure 8.12. First, the secondary flow carries low velocity flow from the boundary layer into the primary flow near the inside of the bend and higher velocity flow near the pipe centre toward the pipe boundary on the outside of the bend. This is shown by the isovels or contours of constant velocity sketched in Figure 8.12 c. Therefore, velocities in the primary flow are modified considerably from an irrotational flow distribution, which would have maximum and minimum velocities on the inside and outside of the bend, respectively. Second, the secondary flow creates an energy loss through a transfer of energy from the primary flow into the spiral motion of the secondary flow. If separation also occurs on the inside of the bend, then this energy loss is increased further. Thus, a "minor" or "local" energy loss term of the form

$$E_L = K\rho \frac{U^2}{2} \tag{8.10}$$

is used for bends in the Bernoulli equation when working pipe flow problems. K is a dimensionless experimental coefficient that varies with both the angle of the bend and, to a lesser extent, with the pipe wall roughness.

The teacup principle is also responsible for secondary flow in open channel bends, as shown in Figure 8.13. Since no boundary layer exists along the free surface, only one circulation cell occurs, with flow near the bottom boundary having both radially inward and longitudinal velocity components. The end result, as in flow through a pipe bend, is a spiralled flow superimposed upon the primary flow, increased energy losses and a shift in longitudinal velocity distribution with larger velocities occurring near the outside of the bend and smaller velocities near the inside.

Furthermore, when the open channel is lined with erodible material, larger velocities near the outside of the bend cause erosion that deepens the channel and moves the outer boundary further outward in the horizontal direction. At the same time the inward velocity component near the channel bottom carries sediment toward the inside of the bend and deposits it on the channel bottom in the region of smaller velocity. Thus, water depths become shallower on the inside of the bend, and the inside bend boundary moves horizontally outward. When longitudinal river bed slopes are small enough, this process continues until the bend migrates so far in the outward direction that a flood cuts the bend off on the inside and forms an oxbow lake. This process is sketched in Figure 8.14.
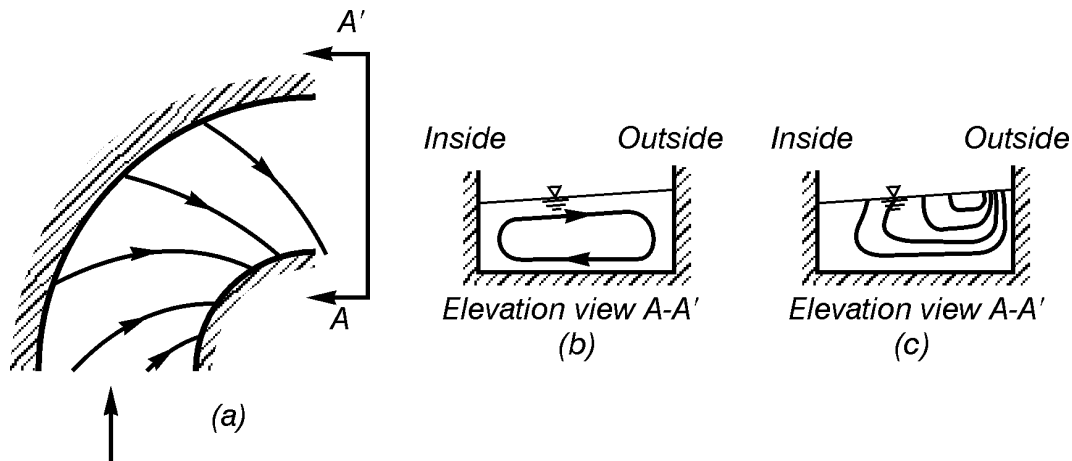
Figure 8.13 Secondary flow in an open channel bend showing (a) streamlines in the bottom boundary layer, (b) the circulation cell pattern and (c) isovel contours.
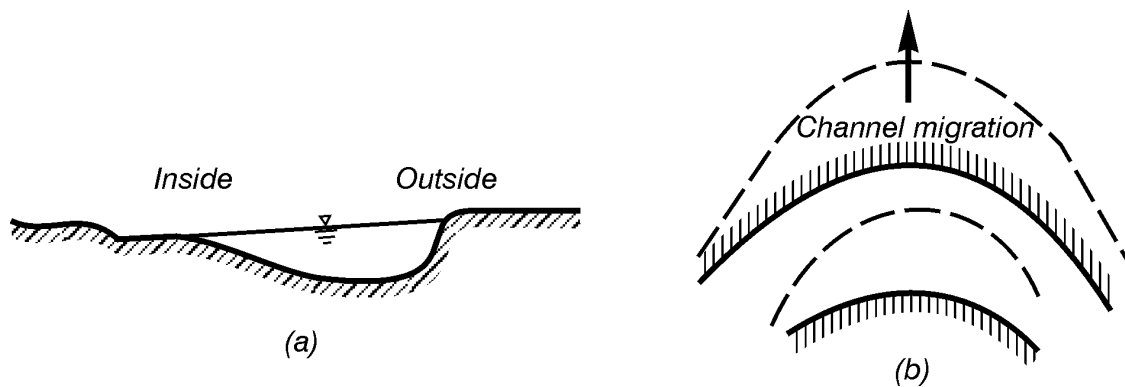
Figure 8.14 River bend geometry in erodible material showing (a) the flow cross section at the bend and (b) the direction of channel migration caused by secondary flow.

Another important example of secondary flow occurs in flow past a bridge pier and is shown schematically in Figure 8.15. Boundary-layer separation occurs on the channel bottom along the stagnation streamline at the front nose of the pier. This forms a vortex in the zone of separated flow that wraps itself around the front of the pier and trails downstream on both sides in the shape of a horseshoe. This horseshoe vortex has large enough velocities to create a scour hole in front of the pier, and many bridge failures have occurred when the scour hole has become deep enough to undermine a pier. There is an equilibrium depth that exists for a scour hole in each particular set of circumstances, and a design engineer must ensure that the bridge pier extends far enough below this equilibrium depth to avoid losing the pier in a flood.
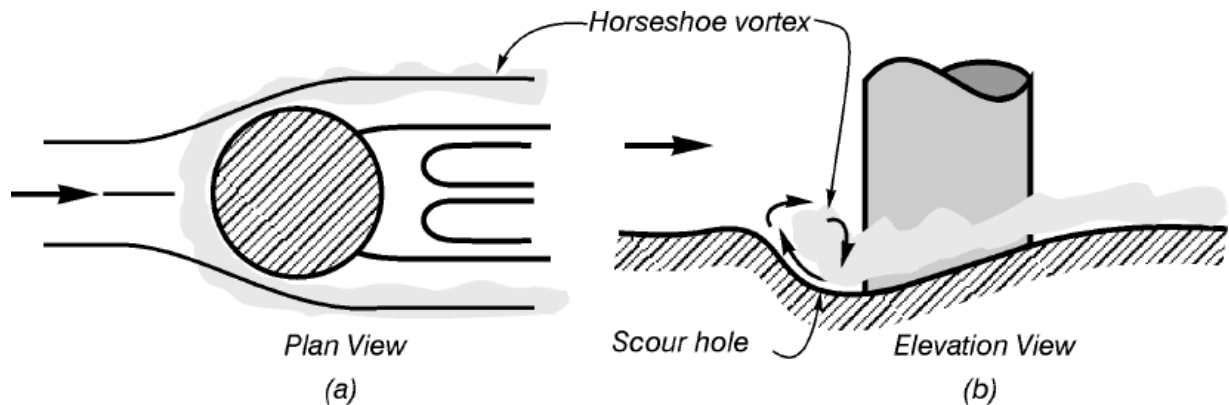
Figure 8.15 Erosion around a bridge pier caused by a horseshoe vortex.

Not all secondary flows are created by boundary-layer pressure gradients that originate from curved streamlines in the primary flow. Figure 8.16 a shows a set of isovels that were determined experimentally by Nikuradse for turbulent flow in a long straight conduit with a rectangular cross section. Intuition suggests that velocities should be relatively small in the corners because of the close proximity of two perpendicular boundaries. However, Fig. 8.16 a shows that isovels are actually pushed into the corners so that longitudinal velocities remain relatively high in the corners. The apparent explanation is that turbulent velocity fluctuations in the primary flow create relatively high corner pressures and the secondary flow patterns shown in Fig. 8.16 b. These secondary flows carry fluid with higher longitudinal velocities from the primary flow into the corner and slower moving fluid from the boundary layer into the primary flow.
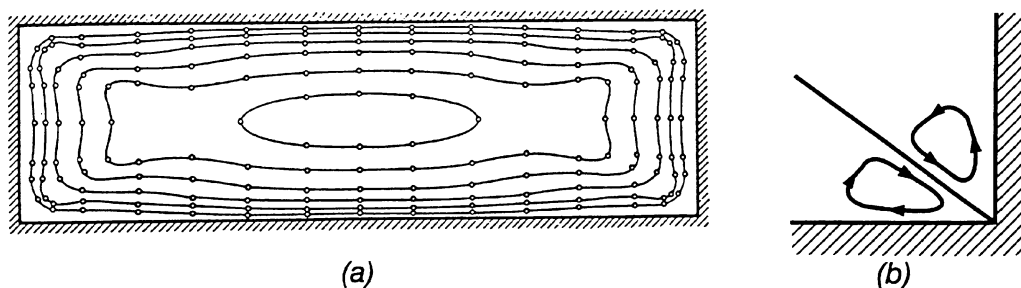
Figure 8.16 Flow in a rectangular conduit showing (a) isovels measured by Nikuradse and (b) secondary flow cells that influence the isovels near a corner. [Measurements by Nikuradse, reproduced from Schlichting (1968).]

References

Lachmann, G.V. (editor) (1961) *Boundary Layer and Flow Control*, Vols. 1 and 2, Pergamon Press, New York, 1260 p.

Rouse, H. (1948) *Elementary Mechanics of Fluids*, John Wiley and Sons, New York, pp. 254, 259.

Rouse, H. (1961) *Fluid Mechanics for Hydraulic Engineers*, Dover Publications, New York, p. 198.

Schlichting, H. (1968) *Boundary Layer Theory*, 6th edition, McGraw-Hill Book Co., New York, pp. 35, 151, 576, 600, 611.

Chapter 9

Drag and Lift

The resultant force that a flow exerts upon a body has, in general, one component parallel and one component normal to the approaching flow. The force component parallel to the approaching flow is called drag, and the normal component is called lift. Drag and lift forces are the result of integrating pressure and shear stresses around the body surface, and an understanding of drag and lift is important for an engineer who wants to design structures that will withstand these forces.

Drag

A drag force is expressed in the following way:

$$F_D = C_D A \rho \frac{U_\infty^2}{2} \tag{9.1}$$

in which C_D = dimensionless drag coefficient, A = area, ρ = fluid mass density and U_∞ = velocity of the approaching flow. The area, A, is usually defined to be the projected area of the body on a plane normal to the approaching flow, although for a flat plate aligned with the flow it becomes the surface area of the plate.

The drag coefficient, C_D, is almost always measured experimentally. (Two exceptions to this occur for a flat plate aligned with the flow and creeping motion past a sphere, which allows the use of Stokes solution.) In the most general case C_D varies with the geometry and orientation of the body, the Reynolds number and the relative surface roughness. In practice, the surface roughness effect tends to be relatively small and is almost always neglected. (The drag on a flat plate aligned with the flow is one example, however, in which surface roughness can be included. See Figure 8.5.) Experimental drag coefficients for some axisymmetric bodies were given previously in Figure 7.3 as a function of body geometry and orientation and the Reynolds number.

A better understanding of drag can be obtained by considering the details of pressure and shear stress distributions around boundary surfaces. Figure 7.3 suggests that C_D is a strong function of the Reynolds number when Reynolds numbers are low. Stokes solution for creeping flow past a sphere gives a pressure drag that is one third of the total drag force and a tangential shear or surface drag contribution that is two thirds of the total drag. (The pressure drag contribution is sometimes called form drag, and surface drag is often called skin friction drag.) At higher Reynolds numbers, however, the surface drag component only becomes important for well streamlined bodies that have large length to width ratios. For this reason, most attempts to reduce drag focus on modification of pressure distributions around bodies.

At larger Reynolds numbers, when boundary layers are thin, pressures around the surface of a body are determined by inviscid flow pressures on the boundary. D'Alembert's paradox states that any body submerged in a steady inviscid flow without separation has a zero drag force. A general proof of this result in two dimensions can be given by using the fact that irrotational flow around any body can be obtained by distributing sources, sinks, doublets and vortices either within or on the boundary surface. Since the net flow emitted and absorbed by all the sources and sinks must be zero for a closed body ($\sum_{i=1}^{N} q_i = 0$, as noted in example 6.3), the velocity on a large circle of radius r that surrounds the body has the asymptotic behaviour

$$V \sim U_\infty i + \frac{\Gamma_0}{2\pi r} e_\theta + 0\left(\frac{1}{r^2}\right) \tag{9.2}$$

in which U_∞ = velocity at infinity, Γ_0 = sum of the circulations from all vortices and $0\left(1/r^2\right)$ means that the next term is bounded by a finite constant divided by r^2 as $r \to \infty$. A sketch of this flow is shown in Figure 9.1.
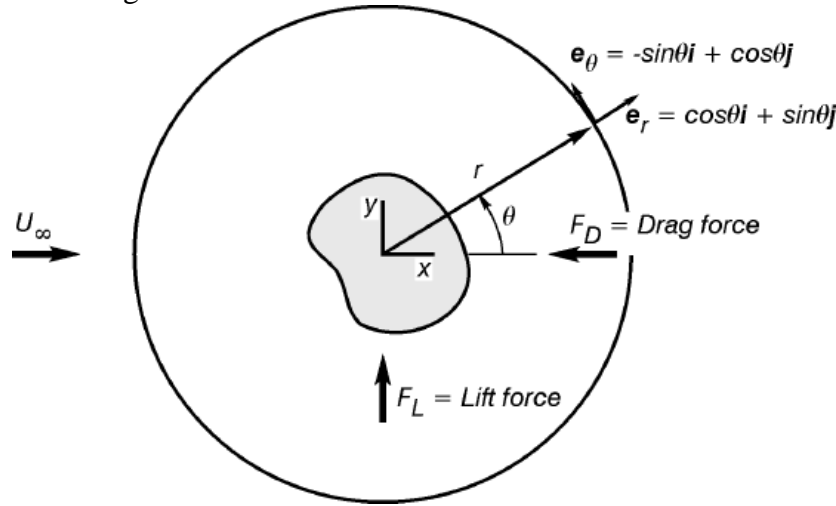
Figure 9.1 Two-dimensional flow past a body.

If gravity is neglected, then the momentum equation applied to Figure 9.1 gives

$$- F_D i + F_L j - \int_{-\pi}^{\pi} p\, e_r (rd\,\theta) = \int_{-\pi}^{\pi} \rho V \left(V \cdot e_r\right)(rd\,\theta) \tag{9.3}$$

The Bernoulli equation gives

$$p = \rho \frac{U_\infty^2}{2} - \rho \frac{V^2}{2} \tag{9.4}$$

in which p and V are the pressure and velocity magnitudes on the large circle and the Bernoulli constant, $\rho U_\infty^2/2$, has been obtained by setting $p = 0$ at infinity. Putting (9.2) and (9.4) into (9.3) gives, after rewriting e_r and e_θ in terms of i and j, (because e_r and e_θ are functions of θ but i and j are constant unit vectors)

$$-F_D \boldsymbol{i} + F_L \boldsymbol{j} - \rho \frac{U_\infty \Gamma_0}{2\pi} \int\limits_{-\pi}^{\pi} \left[\sin\theta (\cos\theta \, \boldsymbol{i} + \sin\theta \, \boldsymbol{j}) + 0\left(\frac{1}{r}\right) \right] d\theta$$

$$= \int\limits_{-\pi}^{\pi} \left[\rho U_\infty^2 \, r \cos\theta + \frac{\rho U_\infty \Gamma_0}{2\pi} (\cos\theta \, \boldsymbol{j} - \sin\theta \, \boldsymbol{i}) \cos\theta + 0\left(\frac{1}{r}\right) \right] d\theta$$

$$\tag{9.5}$$

However, the integrals

$$\int\limits_{-\pi}^{\pi} \cos\theta \, d\theta = \int\limits_{-\pi}^{\pi} \sin\theta \cos\theta \, d\theta = 0 \tag{9.6}$$

allow (9.5) to be simplified to

$$-F_D \boldsymbol{i} + F_L \boldsymbol{j} = \frac{\rho U_\infty \Gamma_0}{2\pi} \boldsymbol{j} \int\limits_{-\pi}^{\pi} \left(\sin^2\theta + \cos^2\theta \right) d\theta + 0\left(\frac{1}{r}\right) \tag{9.7}$$

Since the integrand in (9.7) is unity, letting $r \to \infty$ and evaluating the integral gives the following significant result:

$$F_D = 0$$

$$F_L = \rho U_\infty \Gamma_0$$

$$\textbf{(9.8 a, b)}$$

Equation (9.8) states that the drag force is zero but that a finite lift force exists if the flow is uniform at infinity and if circulation occurs around the body. This same result was obtained in Example 6.2 for the particular case of flow around a circular cylinder.

Since the pressure drag on a body submerged in irrotational flow is zero if no separation occurs, and since pressure distributions on a surface are approximated closely by irrotational flow pressures on the boundary for high Reynolds numbers, it becomes obvious that *significant pressure or form drag forces in high Reynolds number flows must be the result of flow separation*. This is shown very clearly in Figure 9.2 for flow past a sphere. Measured pressures along the forward portion of the sphere boundary are very close to the irrotational flow pressure distribution shown in Figure 9.2 a. However, experimental boundary pressures immediately upstream from the separation point deviate from irrotational flow values, and the nearly constant boundary pressure across the wake is fixed by the negative pressure that occurs at the point of flow separation. This negative wake pressure often makes a larger contribution to the pressure drag than the zone of positive pressure along the front boundary. All of these considerations suggest that *pressure drag at high Reynolds numbers can only be decreased by moving the point of flow separation as far as possible toward the rear of the body*.

(a) Irrotational flow

(b) Re = 162,500
Boundary layer laminar

(c) Re = 435,000
Boundary layer turbulent

Measurements by Flachsbart in air
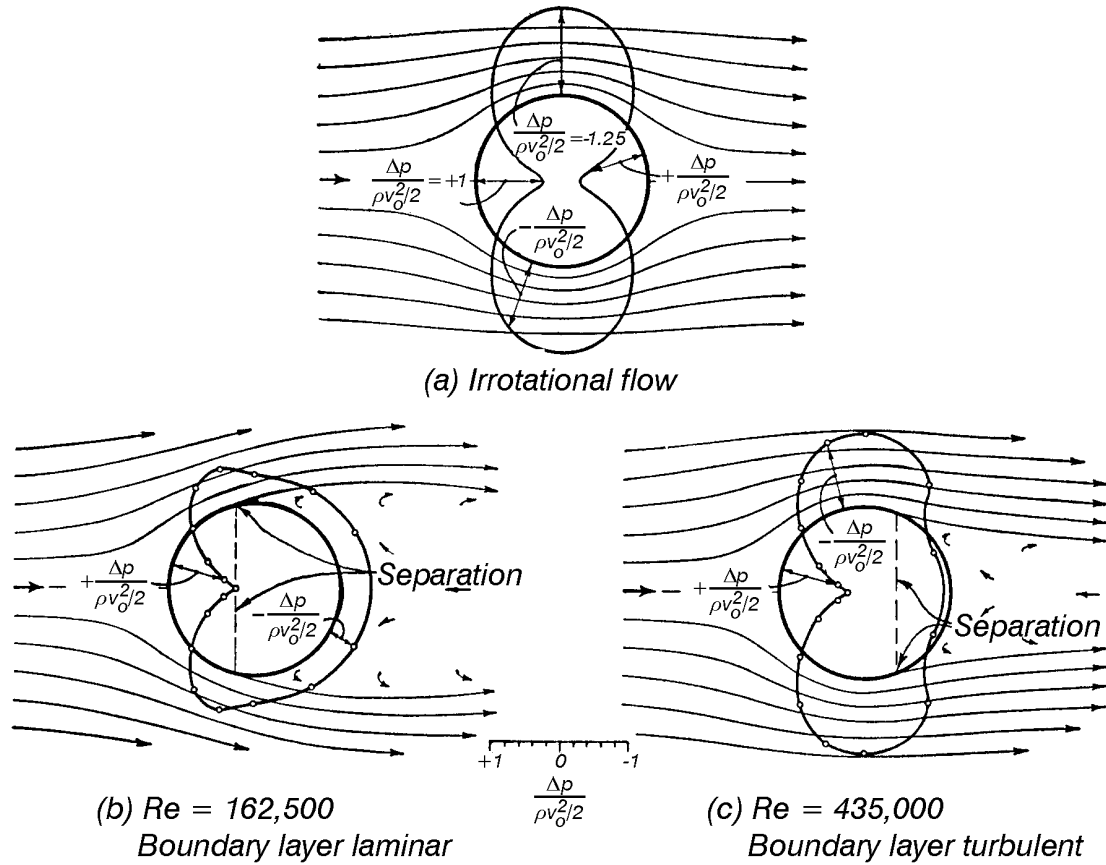
Figure 9.2   Irrotational and measured pressured distributions for flow past a sphere. [Reproduced from Rouse (1948).]
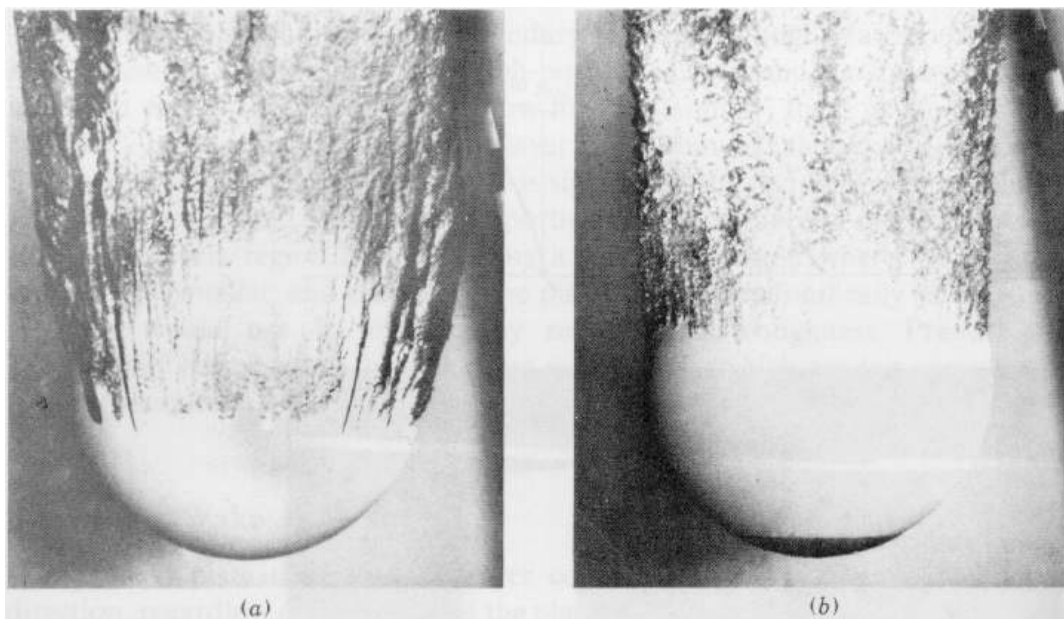
Figure 9.3   The use of turbulence in the boundary layer to delay separation. (U.S. Navy photographs.)

Some of the methods that can be used to delay or prevent boundary-layer separation were discussed in Chapter 8. Probably the most commonly used method is to introduce turbulence into the boundary layer. This increases velocities close to the boundary through turbulent mixing and moves the separation point further downstream. Examples of this are shown in Figures 9.2 b and 9.2 c and in Figure 9.3 for a bowling ball dropped into water. In Figure 9.3 a the ball has a smooth surface with a laminar boundary layer. In Figure 9.3 b the nose of the ball has been covered with sandpaper to create a turbulent boundary layer, and the point of flow separation has been moved further downstream. The end result is that the drag coefficient has been reduced from about 0.5 in Figure 9.3 a to about 0.2 in Figure 9.3 b. Since the terminal velocity is inversely proportional to the square root of C_D, the sphere in Figure 9.3 b should have a terminal velocity about 58 per cent greater than the sphere in Figure 9.3 a. The decrease in drag coefficient that results from turbulence in the boundary layer is shown in Figure 7.3 to occur at a Reynolds number of about 3×10^5 for a sphere, although the presence or lack of a correct disturbance frequency and scale in the boundary layer can change this critical Reynolds number value. Practical applications of this result include dimples on golf balls, roughness elements on the top of airplane wings and the use of upraised seams on cricket balls and baseballs to cause turbulence in the boundary layer on one side of the ball. This leads to an asymmetric pressure distribution and causes the ball to curve during its flight.

When separation point locations are fixed by sharp corners at high Reynolds numbers, drag coefficients become independent of the Reynolds number. This is why tables often give only one value for C_D for unstreamlined angular bodies. Examples include circular disks and flat plates normal to the flow, hemispheres, right circular cones and rods with rectangular cross sections. For lower Reynolds numbers, however, Eqs. (5.7 a, b) show that pressures throughout a flow are influenced by viscosity. This is one reason why drag coefficients in Figure 7.3 vary rapidly with Reynolds numbers for smaller values of Re. Figure 9.4 shows the variation of drag coefficient with Reynolds number for some two-dimensional bodies, and Table 1 lists drag coefficients for various bodies.
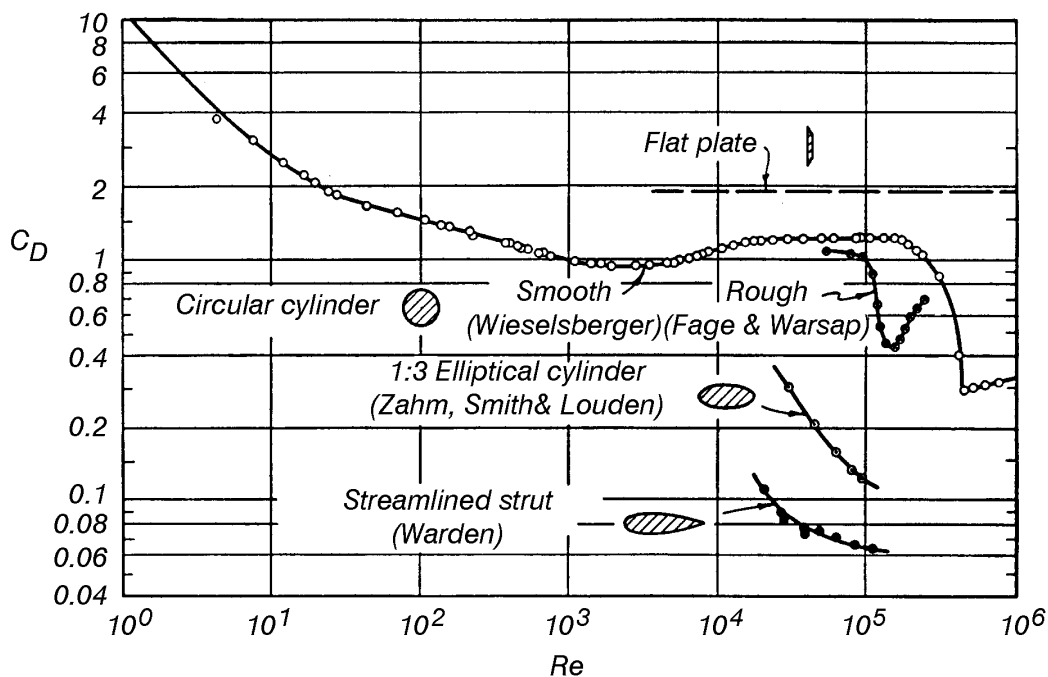
Figure 9.4 Drag coefficients for some two-dimensional bodies. [Reproduced from Rouse (1948).]

Table 9.1 Drag coefficients for various bodies.

Form of Body	L/D	Re	C_D
Circular disk		$> 10^3$	1.12
Tandem disks (L = spacing)	0 1 2 3	$> 10^3$	1.12 0.93 1.04 1.54
Rectangular plate (L = length, D = width)	1 5 20 ∞	$> 10^3$	1.16 1.20 1.50 1.90
Circular cylinder (axis ∥ to flow)	0 1 2 4 7	$> 10^3$	1.12 0.91 0.85 0.87 0.99
Circular cylinder (axis ⊥ to flow)	1 5 20 ∞ 5 ∞	10^5 $> 5 \times 10^5$	0.63 0.74 0.90 1.20 0.35 0.33
Streamlined foil (1:3 airplane strut)	∞	$> 4 \times 10^4$	0.07
Hemisphere: Hollow upstream Hollow downstream		$> 10^3$	1.33 0.34
Sphere		10^5 $> 3 \times 10^5$	0.50 0.20
Ellipsoid (1:2 major axis ∥ to flow)		$> 2 \times 10^5$	0.07
Airship hull (model)		$> 2 \times 10^5$	0.05
Half circular cylinder: Hollow upstream Hollow downstream		$> 10^4$ $> 10^4$	2.30 1.20
Square rod (axis ⊥ to flow, faces ∥ and ⊥ to flow)		$> 10^4$	2.00
Parachute		$> 10^5$	1.20
Cube (faces ∥ and ⊥ to flow)		$> 10^4$	1.10
Right circular cone (apex angle of 60° pointing upstream)		$> 10^4$	0.50

Drag Force in Unsteady Flow

The drag forces considered so far are for steady flow. However, Robertson (1965) notes that it was found as early as 1786 that an additional mass of fluid has to be added to the mass of an oscillating sphere in order to account for experimental differences in drag forces in steady and unsteady flow. This added mass concept was introduced in Chapter 7 when studying the slow movement of a sphere dropped from rest in a fluid. In that case the fluid motion was laminar, but the same concept applies for all unsteady motions of a body through fluid.

Robertson (1965) gives an interesting discussion of the history and application of the added mass concept. Added mass coefficients are usually calculated mathematically by using irrotational flow approximations. However, these coefficients also depend, to a limited extent, upon viscosity and the presence or absence of nearby boundaries. Furthermore, when the moment of momentum equation of rigid body dynamics is applied to rotating bodies, then an added moment of inertia must be used. The calculation of added mass and moment of inertia coefficients is relatively difficult, and we will finish this section by simply stating that the added mass coefficients, k, for a sphere and an infinitely long circular cylinder translating in an unbounded fluid are 0.5 and 1.0, respectively. The added moment of inertia when these bodies are spinning is zero.

<div align="center">

Example 9.1

</div>

Calculate the terminal velocity for a sphere falling through a fluid.

***Solution*:**
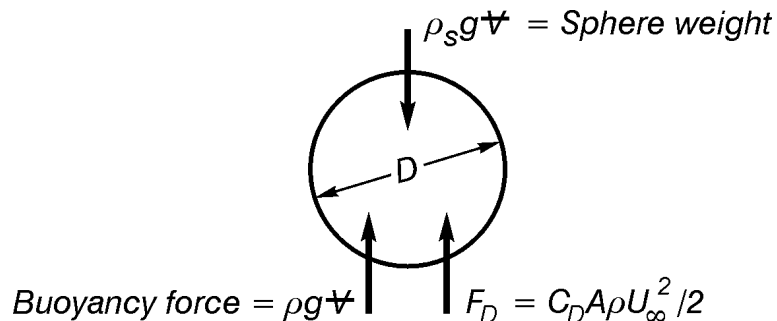
The three forces acting on the sphere are the sphere weight, the buoyancy force (equal to the weight of displaced fluid) and the drag force, as shown in the free body diagram. Since the sphere at terminal velocity is translating with a constant speed, the sphere acceleration is zero. Therefore, setting the sum of vertical forces equal to zero gives

$$- C_D A \rho U_\infty^2/2 \; - \; \rho g \, \forall \; + \; \rho_s g \, \forall \; = \; 0$$

in which

$$A \; = \; \pi D^2/4$$

$$\forall \; = \; \pi D^3/6$$

Solution for U_∞ gives

$$U_\infty = \sqrt{\frac{4}{3} \frac{(\rho_s/\rho - 1)gD}{C_D}}$$

If $\rho_s < \rho$, then the sphere will rise and the direction of the drag force is reversed. This gives a terminal velocity in the upward direction of

$$U_\infty = \sqrt{\frac{4}{3} \frac{(1 - \rho_s/\rho)gD}{C_D}}$$

In general, C_D changes with U_∞. This means that these expressions for U_∞ may have to be solved by successive approximation.

Example 9.2

Calculate the unsteady motion of the sphere in Example 9.1 after it is released from rest. Assume that C_D is constant.

Solution:

Using the free body diagram in Example 9.1, Newton's second law for the sphere becomes

$$- C_D A \rho_f U^2/2 \; - \; \rho_f g \, \forall \; + \; \rho_s g \, \forall \; = \; \left(\rho_s + k \rho_f\right) \forall \; \frac{dU}{dt}$$

in which k = added mass coefficient. The second and third terms on the left side can be rewritten in terms of the terminal velocity from Example 9.1 to obtain

$$- C_D A \, \rho_f \, U^2/2 \; + \; C_D A \, \rho_f \, U_\infty^2/2 \; = \; \left(\rho_s + k \rho_f\right) \forall \; \frac{dU}{dt}$$

Use of the expressions for $\forall$ and A allows this to be rewritten in the following form:

$$\frac{dU}{dt} = \frac{3}{4} \frac{C_D}{\left(\rho_s/\rho_f + k\right)D} \left(U_\infty^2 - U^2\right)$$

Since t does not appear on the right side of this equation, we can calculate U as a function of x by using the chain rule to write

$$\frac{dU}{dt} = \frac{dU}{dx} \frac{dx}{dt} = U \frac{dU}{dx}$$

Substituting the previous expression for dU/dt and separating variables gives

$$\int_0^U \frac{U\,dU}{U_\infty^2 - U^2} = \frac{3}{4}\,\frac{C_D}{\left(\rho_s/\rho_f + k\right)D}\int_0^x dx$$

in which we have required $U = 0$ at $x = 0$ in the corresponding lower integration limits. Integration gives

$$\boxed{-\ln\!\left(1 - U^2/U_\infty^2\right) = \frac{3}{2}\,C_D\,\frac{x/D}{\left(\rho_s/\rho_f + k\right)}}$$

The qualitative behaviour of this solution is similar to the behaviour for the creeping flow case shown in Figure 7.5. By setting $U = 0.99\,U_\infty$ we find that 99 per cent of the terminal velocity is reached at

$$\frac{x/D}{\left(\rho_s/\rho_f + k\right)} = \frac{2.61}{C_D}$$

If we take $C_D = 0.5$, $\rho_s/\rho_f = 10$ and $k = 0.5$, which were used in the numerical example for Stokes solution in Chapter 7, we find that terminal velocity is achieved at $x/D = 54.8$. This compares with the value of $x/D = 2.10$ that we calculated for creeping flow in Chapter 7, and it suggests that creeping flows achieve terminal velocity much more quickly. If we use a value of $C_D = 0.2$ that occurs after the boundary layer becomes turbulent, we find that x/D increases to 137.

Example 9.3

The drag force on a large structure can be measured in a laboratory with a greatly reduced scale model. The model and prototype must be geometrically similar and must be orientated with respect to the flow in the same way. Then the drag coefficient is a function only of the Reynolds number and relative roughness

$$C_D = f\left(\frac{UL}{\nu}\,,\,\frac{\epsilon}{L}\right)$$

in which U = approach velocity, L = characteristic length, ν = kinematic viscosity and ϵ = roughness height. The unknown function f is to be determined from measurements, and it will be the same function for both model and prototype. Thus, if the Reynolds number and relative roughness are the same for model and prototype,

$$\left(\frac{UL}{\nu}\right)_m = \left(\frac{UL}{\nu}\right)_p \quad \text{and} \quad \left(\frac{\epsilon}{L}\right)_m = \left(\frac{\epsilon}{L}\right)_p$$

then C_D will be the same for model and prototype.

$$\left(C_D\right)_m = \left(C_D\right)_p \quad \text{or} \quad \left(\frac{F/A}{\rho U^2/2}\right)_m = \left(\frac{F/A}{\rho U^2/2}\right)_p$$

The Reynolds number similarity requirement can be rewritten in the form

$$\frac{U_m}{U_p} = \frac{L_p}{L_m} \frac{\nu_m}{\nu_p}$$

in which $L_p/L_m > 1$. If the same fluid is used for model and prototype, then $\nu_m/\nu_p = 1$ and we must have

$$\frac{U_m}{U_p} = \frac{L_p}{L_m} > 1$$

This is not usually practical. For example, the drag force on a 50 m high building in a 20 m/s wind could be measured in a wind tunnel with a 0.5 m high model only if
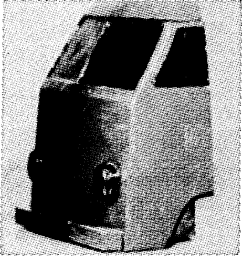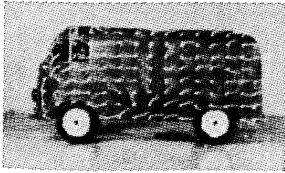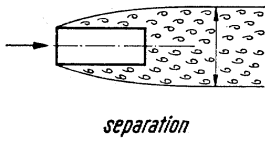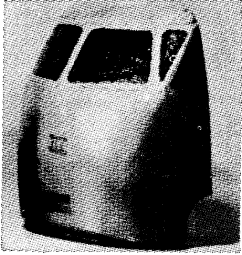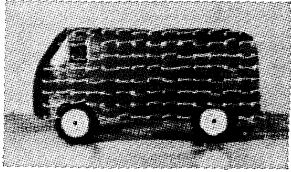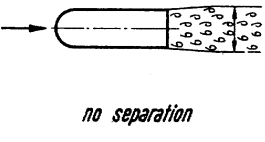
$$U_m = \frac{L_p}{L_m} U_p = \frac{50}{0.5}(20) = 2,000 \text{ m/s}$$

If water is used as the fluid for the model, then $\nu_m/\nu_p \approx 1/10$ and

$$U_m = \frac{L_p}{L_m} \frac{\nu_m}{\nu_p} U_p = \frac{50}{0.5} \frac{1}{10}(20) = 200 \text{ m/s}$$

Neither of these possibilities is practical since the required velocities are too high to achieve. (Even if these velocities could be obtained in a laboratory, fluid compressibility effects would have to be considered for flows with such large velocities.)

Drag forces on buildings are in fact measured in laboratories, but this can only be done if C_D does not change with Reynolds number. The drag force on most buildings is almost entirely pressure or form drag, and points of flow separation are almost always fixed at sharp corners and do not change location with Reynolds number. Thus, C_D does not usually change with Reynolds number in these problems provided that Reynolds numbers are reasonably large.

(a) Angular nose

separation

$C_D =$

0.76

(b) Round nose

no separation

0.42

Example 9.4

The above figure, which is reproduced from Schlichting, shows drag coefficients that were measured by E. Moeller in 1951 for a Volkswagon delivery van. Rounding the front corners of the van moved the points of flow separation to the rear and decreased the drag coefficient by 45 per cent. The power required to overcome a drag force equals the product of the drag force with the velocity. Thus, the power required to overcome wind drag at any particular speed for this van was also decreased by 45 per cent with this simple change in body geometry.

Example 9.5

$u = U(y/\ell)^{1/n}$

ℓ

$2R$

y
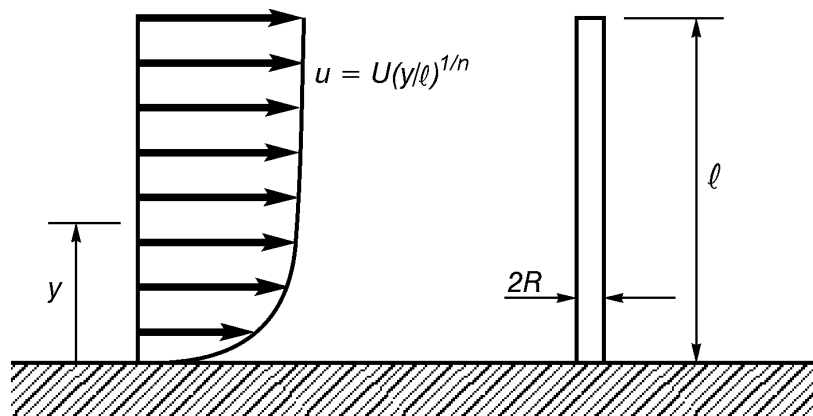
A cylindrical pole of length ℓ and radius R has an approaching wind velocity given by

$$u = U(y/\ell)^{1/n}$$

in which U and n are known constants. If we assume that the flow at any fixed value of y is two dimensional, then the total force and moment about the pole base caused by wind drag are given approximately by

$$F = \int_0^\ell C_D(2R)\rho \frac{u^2}{2} dy$$

$$M = \int_0^\ell y\, C_D(2R)\rho \frac{u^2}{2} dy$$

in which we will take C_D as a constant and assume that u varies with y. Using the power law equation for u and evaluating the integrals gives

$$\boxed{\begin{aligned} F &= C_D\, R\, \ell \rho U^2 \big/ (1 + 1/n) \\ M &= C_D\, R\, \ell^2 \rho\, U^2 \big/ (2 + 1/n) \end{aligned}}$$

An estimate of the degree of approximation can be made for the case of a uniform approach velocity, for which $n = \infty$. Then

$$F = C_D\, R\, \ell \rho U^2$$

in which C_D is given in Table 9.1 as 1.20 for $L/D = \infty$. However, the correct value for C_D when $n = \infty$, which takes into account end effects at the pole top, is also obtained from Table 9.1 by setting $L/D = 2\ell/(2R) = \ell/R$. (We must use $L = 2\ell$ since the ground boundary is a streamline and, therefore, a line of symmetry for a pole of length 2ℓ in an inviscid flow.) Table 9.1 shows how C_D varies with ℓ/R, and the end effect at the pole top is seen to become relatively small as ℓ/R and Re increase.

Lift

Lift is the force component created on a body normal to the direction of an approaching flow. A lift force is usually expressed in the following way:

$$F_L = C_L A\, \rho\, \frac{U_\infty^2}{2} \tag{9.9}$$

in which C_L = lift coefficient, A = area, ρ = fluid mass density and U_∞ = velocity of the approaching flow. The lift coefficient is usually measured experimentally, and the area, A, for an aerofoil is usually defined to be the product of the wing chord with the wing length.

(The wing chord is the maximum straight line distance across the wing, in the direction of flow, at a zero angle of attack.) The lift coefficient is a function of the aerofoil geometry and orientation. Thus, C_L is usually plotted for a given aerofoil as a function of the angle of attack. Typical plots of C_L and C_D for an aerofoil are shown in Figure 9.5.
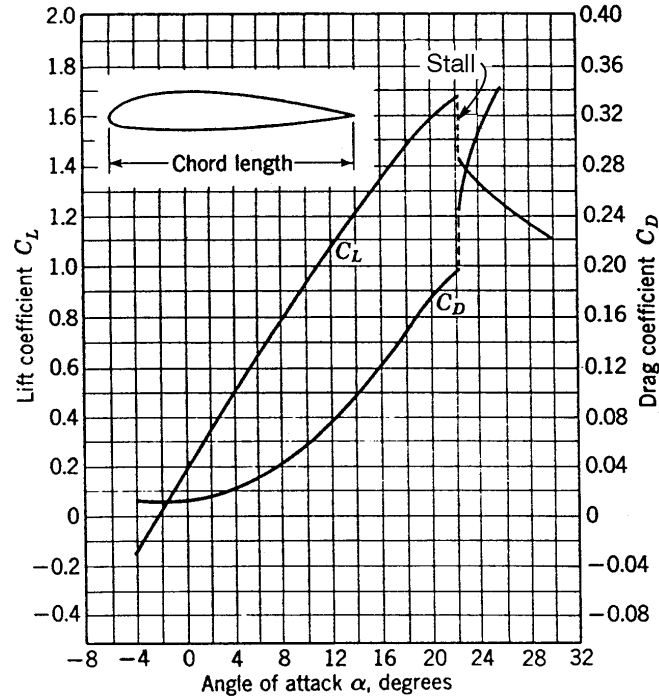
Figure 9.5 Coefficients of lift and drag plotted as a function of attack angle for a typical aerofoil. [Reproduced from Streeter and Wylie (1981).]

A better understanding of lift can be obtained by considering details of flow around an aerofoil. Figure 9.6 shows photographs of two-dimensional flow around an aerofoil (a) at a low angle of attack, when the aerofoil is an efficient lifting device, and (b) at a high angle of attack, when flow separates from the top boundary and stall occurs. As shown in Figure 9.5, C_L increases as the angle of attack increases until the angle of stall is reached. At the angle of stall the flow separation point suddenly moves forward to the leading edge, lift decreases and drag increases. Stall has been responsible for a large number of plane crashes.

The unseparated high Reynolds number flow shown in Figure 9.6 a can be modelled fairly accurately with irrotational flow. It was shown both for a circular cylinder in Example 6.2 and for flow about any two-dimensional body in this chapter that an irrotational lift force is given by Eq. (9.8 b). Equating values of F_L in (9.8 b) and (9.9) gives

$$C_L = \frac{2\Gamma_0}{\ell U_\infty}$$ (9.10)

in which ℓ = chord length for a two-dimensional aerofoil. (We have set $A = \ell$ for a foil of unit length.)
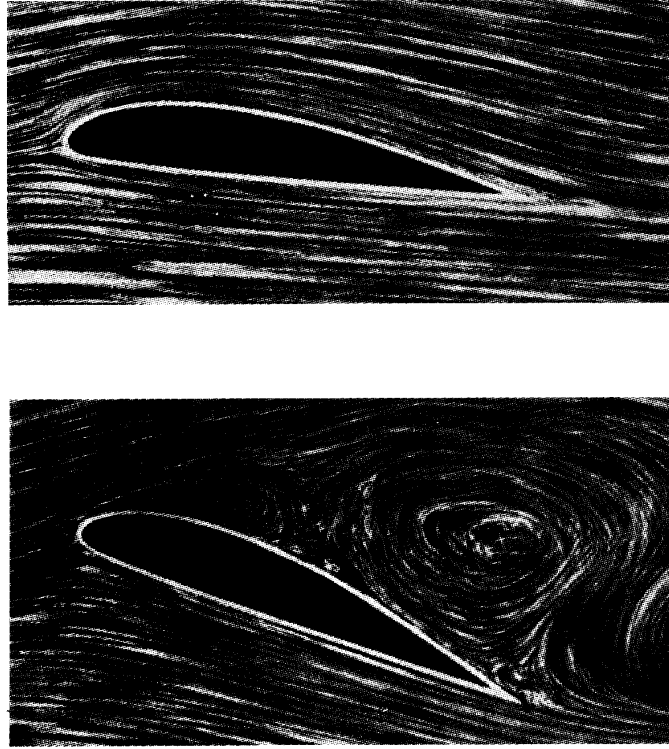
Figure 9.6 Flow past an aerofoil (a) at a low angle of attack and (b) at a high angle of attack with flow separation. [Photograph by Prandtl and Tiejens, reproduced from Schlichting (1968).]
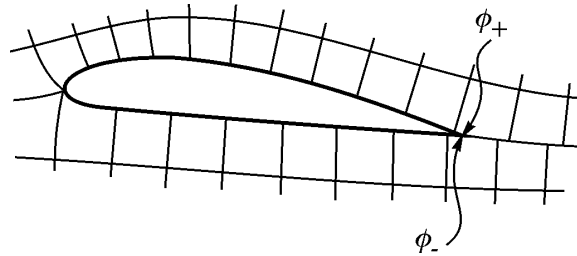
Figure 9.7 A flow net constructed for Figure 9.6 a.

A flow net constructed for the flow in Figure 9.6 a is shown in Figure 9.7. Since

$$\Gamma_0 = \int_-^+ \boldsymbol{V} \cdot d\boldsymbol{r} = \int_-^+ \nabla \phi \cdot d\boldsymbol{r} = \int_-^+ d\phi = \phi_+ - \phi_- \tag{9.11}$$

in which the integration path is any closed curve that starts on the bottom side of the trailing edge, encircles the aerofoil in the clockwise direction and finishes on top of the trailing edge. Since there are 10.1 values of $\Delta\phi$ along the top boundary and 7.2 values of $\Delta\phi$ along the bottom boundary, (9.11) gives

$$\Gamma_0 = 10.1 \Delta\phi - 7.2 \Delta\phi = 2.9 \Delta\phi \tag{9.12}$$

in which $\Delta \phi$ = change in ϕ between any two successive potential lines in Figure 9.7. *Equation (9.12) is significant because it shows that circulation occurs around the aerofoil in irrotational flow, and this result is generally interpreted to mean that circulation occurs about the experimental aerofoil in Figure 9.6 a as well*. Since $\Delta \phi$ in Figure 9.7 can be calculated from the flow net geometry as

$$\Delta \phi \;=\; \Delta \psi \;=\; U_\infty \Delta n_\infty \tag{9.13}$$

in which Δn_∞ = streamtube spacing in the approaching flow, and since direct measurement of the chord length, ℓ, in Figure 9.7 gives

$$\ell \;=\; 7.7 \Delta n_\infty \tag{9.14}$$

where Δn_∞ has been estimated from an upstream portion of the flow net that is not shown in Fig. 9.7, we obtain from (9.10) and (9.12) - (9.14) the following value for C_L:

$$C_L \;=\; \frac{2(2.9)}{7.7} \;=\; 0.75 \tag{9.15}$$

Thus, C_L has been calculated from a flow net whose construction required nothing more than specification of the aerofoil geometry and angle of attack. This is why C_L is normally considered to be a function only of the aerofoil geometry and orientation.

The flow net in Fig. 9.7 has one streamline that leaves the trailing edge of the aerofoil. This requirement, which is necessary if the irrotational flow model is to give a physically realistic description of the actual flow, is known as the *Kutta condition*. If this condition is not imposed, then irrotational flow rounds the sharp trailing edge of the foil with an infinite velocity. The Kutta condition also makes the mathematical solution unique by fixing a numerical value for the circulation, Γ, that is sufficient to move a stagnation point on the top foil surface to the sharp trailing edge.

The previous discussion showed that circulation around an aerofoil exists in steady irrotational flow and, therefore, probably exists for viscid flow. There is also an ingenious argument, based on Kelvin's circulation theorem (proved in Chapter 6), which is used to show how circulation becomes established around an aerofoil as it starts its motion from rest. Consider a large closed material path that surrounds the aerofoil when the fluid and foil are both motionless, as shown in Figure 9.8 a. The circulation around this path is zero before motion starts, and Kelvin's theorem states that the circulation around this path remains constant, and therefore zero, as the aerofoil and fluid start to move. However, experimental observation shows that a large "starting vortex" together with a series of smaller vortices are shed from the trailing edge of the foil as it starts its motion, as shown in Figure 9.8 b. Since each of these shed vortices has a counterclockwise circulation, and since the sum of all circulation within the large material path must be zero, there must be a clockwise circulation around the aerofoil that balances the counterclockwise circulation of the shed vortices. The clockwise circulation around the aerofoil is often referred to as a "bound vortex", and if the experimental foil is suddenly stopped, this bound vortex is released into the flow. A photograph showing this in an experimental flow appears in Figure 9.9.

Material path

Stationary aerofoil

Fluid at rest

(a)

Starting vortex

Bound vortex

(b)
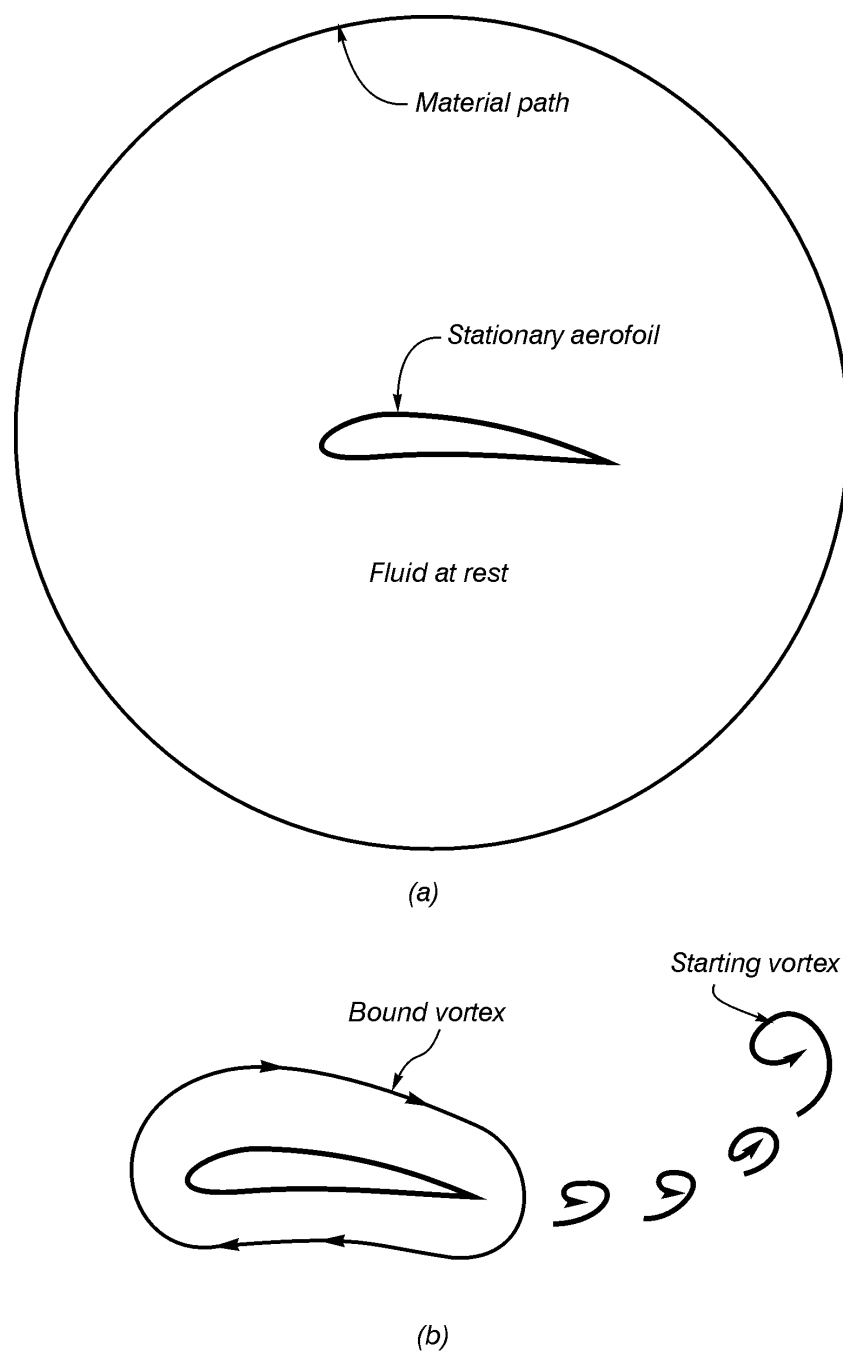
Figure 9.8 The establishment of circulation around an aerofoil as it starts motion.
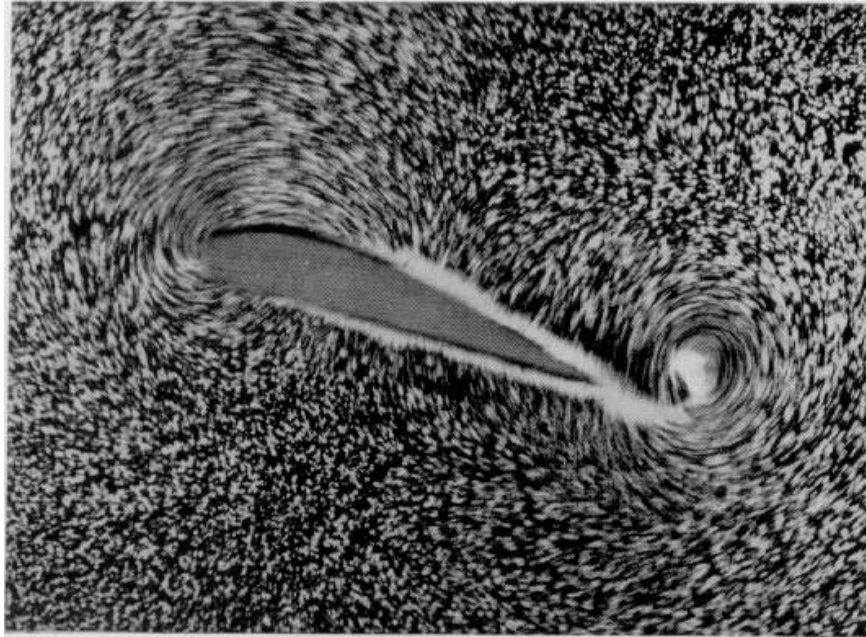
(a)
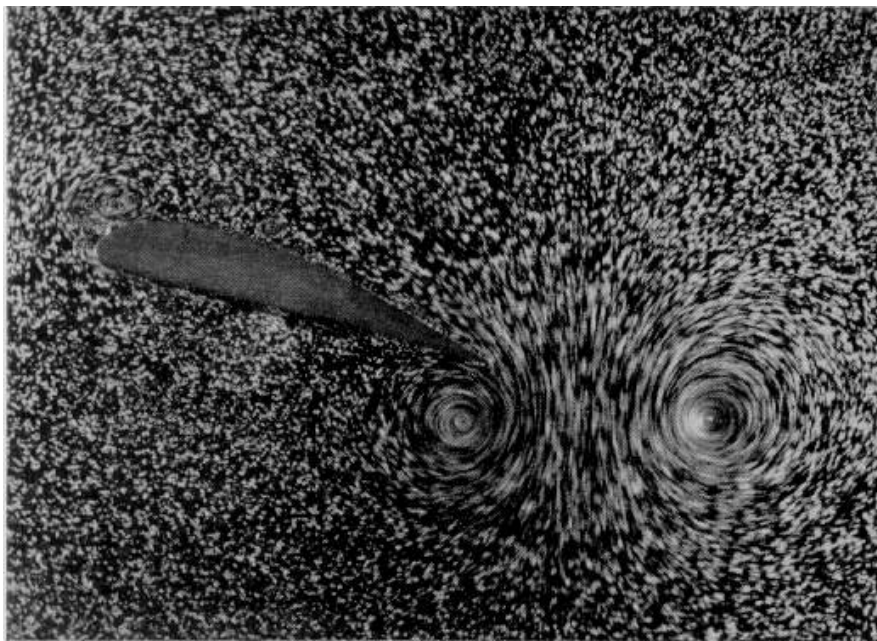
(b)

Figure 9.9 Photographs of (a) a starting vortex shed into the flow as the foil starts motion and (b) a bound vortex shed into the flow beside the starting vortex when the foil suddenly stops motion. [Reproduced from Prandtl and Tietjens (1934).]

A secondary flow, known as a wing-tip vortex, occurs at the end of an aerofoil that has a finite length. Positive pressures occur beneath the foil, and negative pressures occur on top. (Positive and negative meaning pressures that are greater and less, respectively, than the pressure in the undisturbed approaching flow.) At the wing tip the fluid in the high pressure zone beneath the foil moves toward the low pressure zone on top of the foil and creates a vortex that trails from the wing tip, as shown in Figure 9.10. The end result of this three-dimensional effect is that lift is decreased and drag increased from values that would occur for two-dimensional flow. Wing-tip vortices can persist for some minutes after a larger plane has passed, and pilots of smaller planes must be careful not to land too closely behind a larger plane because of the danger of running into a large wing-tip vortex.
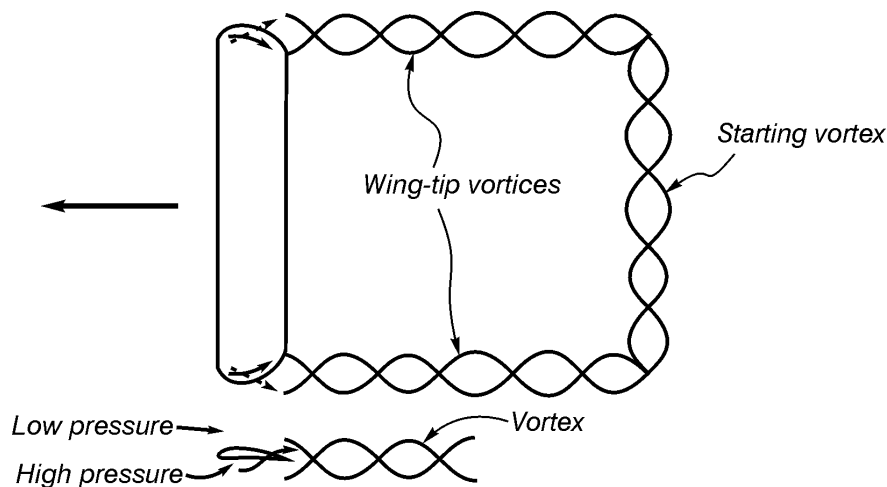
Figure 9.10 The location of wing-tip and starting vortices soon after a plane has started its motion.

There are numerous applications of the principles of lift. Bird wings, sails and kites all act as aerofoils. Airplane propellers have cross sections in the shape of foils. In this case, since the relative speed of the approaching flow changes with distance from the axis of rotation, an efficiently designed propeller has a cross-sectional geometry and angle of attack that change with distance along its length. Hydrofoils can be mounted below a boat to lift its hull out of the water and greatly reduce its drag. Ship propellers, pump impellers and turbine blades are other examples of foils.

Cavitation can become a problem when foils are used in a heavy liquid, such as water. Cavitation occurs in a flow of liquid when the pressure is reduced to the vaporization pressure of the liquid. (The vaporization pressure of a liquid depends upon its temperature, as discussed in the first chapter.) Vaporization causes many small bubbles to form in the flow, and the collapse of these bubbles causes large pressure waves. When a nearby boundary reflects these waves, the boundary is subjected repeatedly to large compressive and tensile stresses and eventually fails from fatigue. In a pump or turbine the top boundaries of the foils are sometimes destroyed from this process. Ship propellers can have cavitation in their wing-tip vortices, as shown in Figure 9.11. This last phenomenon is sometimes prevented by encasing the propeller in a tube.
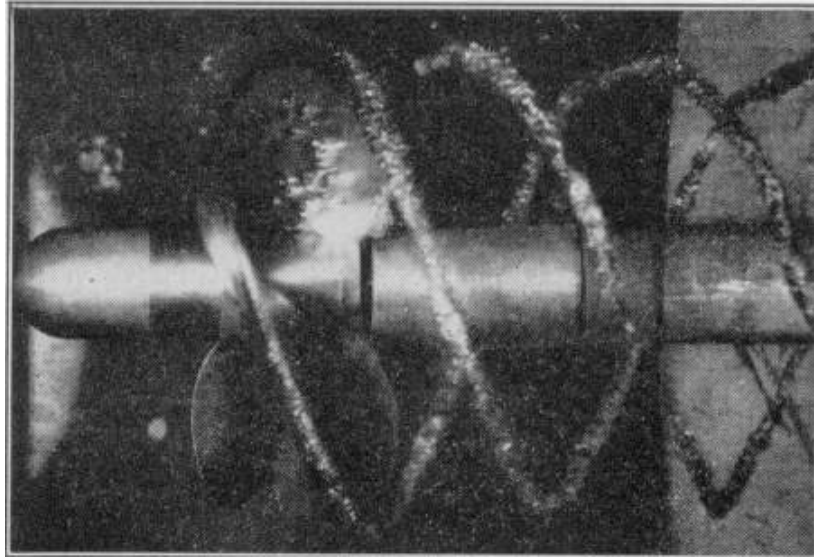
Figure 9.11 Flow cavitating in wing-tip vortices shed from a ship propeller. [U.S. Navy photograph, reproduced from Rouse (1948).]

Oscillating Lift Forces

Oscillating lift forces sometimes create vibrations and even failures in structures. The Tacoma Narrows Bridge failure of 1940 is probably the best known example of a failure caused by oscillating lift forces. However, difficulties from this type of flow behaviour can occur in many structures ranging from long slim bridges to flag poles, smoke stacks and cables. The basic cause of these failures is a matching of the oscillating lift force frequency with one of the natural frequencies of the structure. The lift force itself need not be vertical but may be horizontal or in any direction at right angles to the approaching flow.

An oscillating lift force is caused by a row of vortices that forms in the wake of a body. A picture of such a vortex trail is shown in Figure 9.12. The essential feature of this flow is that vortices, with circulations in opposite directions, are formed and shed periodically on alternate sides behind the body. If a large closed material contour surrounds both the body and vortex trail, then Kelvin's theorem states that the sum of all circulations within this contour must be zero. (Kelvin's theorem was proved in Chapter 6.) However, the total circulation of all vortices in the vortex trail is periodically changing with time as each new vortex is formed and shed into the flow. Thus, there must be circulation around the body that oscillates in direction to balance the constantly changing direction of total circulation in the vortex trail. This creates a lift force on the body that oscillates in direction with the same frequency as the vortex shedding frequency.
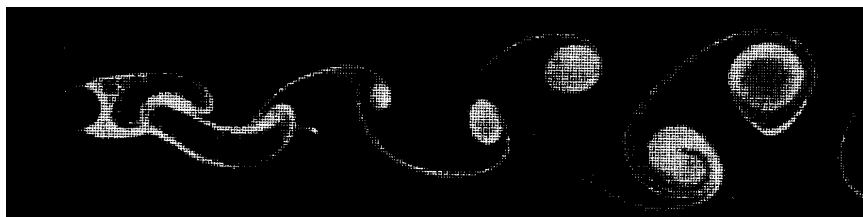
Figure 9.12 The vortex trail behind a circular cylinder. [Reproduced from Schlichting (1968).]
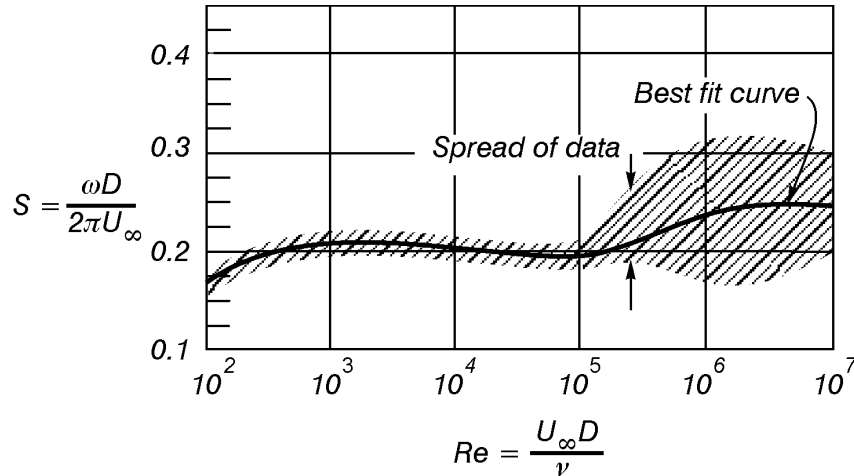
Figure 9.13 The Strouhal number, S, versus Reynolds number for a vortex trail behind a circular cylinder. The frequency, ω, is in radians per second. [Reproduced from Gerhart and Gross (1985).]

Although small structural oscillations can be noisy and troublesome, really large oscillations and structural failure can result if the lift force frequency matches one of the natural frequencies of the structure and causes resonance. Dimensionless values of the vortex frequency, ω, are plotted as a function of the Reynolds number in Figure 9.13 for flow past a circular cylinder. The next section shows how this plot can be used to predict the onset of resonance in structures subjected to oscillating lift forces.

Oscillating Lift Forces and Structural Resonance

As a first example, consider a right circular cylinder suspended horizontally by a system of springs in a flow with an approach velocity U_∞. If y is a coordinate normal to the approaching flow, then the transverse component of Newton's second law of motion becomes

$$M\frac{d^2y}{dt^2} = -Ky + F_0\sin(\omega t) \tag{9.16}$$

where M = cylinder mass, t = time, K = sum of all spring constants, F_0 = lift force amplitude and ω = lift force frequency, which is given as a first approximation by Figure 9.13. The coordinate y is measured from the equilibrium position of the cylinder centre when $U_\infty = 0$. The left side of (9.16) is the product of the cylinder mass and y component of acceleration. The first term on the right side is the spring resistance force, and the last term is the forcing function created by the oscillating life force. Since the system starts from a state of rest, appropriate initial conditions are given by

$$y(0) = 0 \tag{9.17}$$

$$\frac{dy(0)}{dt} = 0 \tag{9.18}$$

which require that the cylinder displacement and velocity be zero at $t = 0$.

The solution of (9.16)–(9.18) is given by

$$y(t) = \frac{F_0/M}{K/M - \omega^2} \left[\sin(\omega t) - \frac{\omega}{\sqrt{K/M}} \sin\left(t\sqrt{K/M}\right) \right] \tag{9.19}$$

where $\sqrt{K/M}$ is the natural frequency of the unforced system. Resonance occurs when $\sqrt{K/M} \to \omega$. Since the right side of (9.19) has the indeterminate form $0/0$, an application of l'Hospital's rule gives

$$\underset{\sqrt{K/M} \to \omega}{\text{Limit}} \quad y(t) = \frac{F_0/M}{2\omega} \left[\frac{1}{\omega} \sin(\omega t) - t\cos(\omega t) \right] \tag{9.20}$$

Equation (9.20) shows that the displacement amplitude at resonance grows linearly with time and that $y \to \infty$ as $t \to \infty$. In practice, the small amplitude approximation that was implicit in modelling both the spring force and wind lift force would invalidate the use of Eq. (9.16) long before this point is reached. It is also worth noting that including a linear damping term in Eq. (9.16) leads to a resonant solution for $y(t)$ that is relatively large but bounded.

The previous example was worked as a particle dynamics problem and gave a single value for the resonant frequency. The remaining examples will model several different structures with continuous distributions of mass. Consequently, these examples will all have an infinite number of resonant frequencies. In these cases, it is frequently the smallest resonant frequency that is of most interest.

Bodies such as smokestacks, flag poles and long slender bridges can be modelled with the equation that describes the lateral vibration of beams. This equation, which is derived by Humar (1990) and numerous other authors, has the form

$$\frac{\partial^2}{\partial x^2}\left(EI \frac{\partial^2 u}{\partial x^2} \right) + m \frac{\partial^2 u}{\partial t^2} = F_0 \sin(\omega t) \tag{9.21}$$

in which u = lateral displacement, E = modulus of elasticity, I = moment of inertia of the cross section, m = mass per unit length, F_0 = lift force amplitude, ω = lift force frequency,

x = distance along the beam and t = time. We will assume that EI, m and F_0 are constants. In this case a solution of (9.21) is given by

$$u(x,t) = \left[C_1\cosh(ax) + C_2\sinh(ax) + C_3\cos(ax) + C_4\sin(ax) - \frac{F_0}{EIa^4} \right]\sin(\omega t) \quad \textbf{(9.22)}$$

in which

$$a = \left(\frac{m\omega^2}{EI} \right)^{1/4} \qquad\qquad \textbf{(9.23)}$$

Equations (9.22) - (9.23) give what is often referred to as the "steady state" solution of (9.21), which is the solution of (9.21) when t has become large enough to disregard the influence of initial conditions on the behaviour of u.

If (9.21) models the behaviour of a smokestack or flag pole, then the correct boundary conditions to determine the C_i's in (9.22) are as follows:

$$u(0, t) = 0 \qquad\qquad \textbf{(9.24)}$$

$$\frac{\partial u(0, t)}{\partial x} = 0 \qquad\qquad \textbf{(9.25)}$$

$$\frac{\partial^2 u(\ell, t)}{\partial x^2} = 0 \qquad\qquad \textbf{(9.26)}$$

$$\frac{\partial^3 u(\ell, t)}{\partial x^3} = 0 \qquad\qquad \textbf{(9.27)}$$

Equations (9.24) and (9.25) require that the beam be clamped at x = 0, and (9.26) and (9.27) require that the free end have a zero moment and shear force, respectively.

Substituting (9.22) into (9.24) - (9.27) and dividing the homogeneous equations by non-zero factors that are common to each term gives the following set of four equations for the unknown constants C_1, C_2, C_3 and C_4:

$$C_1 \quad + \quad C_3 \quad = \frac{F_0}{EIa^4}$$

$$C_2 \quad + \quad C_4 \quad = 0$$

$$C_1 \cosh(a\ell) + C_2 \sinh(a\ell) - C_3 \cos(a\ell) - C_4 \sin(a\ell) = 0$$

$$C \sinh(a\ell) + C_2 \cosh(a\ell) + C_3 \sin(a\ell) - C_4 \cos(a\ell) = 0$$

<div align="right">(9.28 a, b, c, d)</div>

Equation (9.28) will have bounded solutions for C_i unless the determinant of the coefficient matrix vanishes. Thus, setting this determinant equal to zero gives the following requirement for resonance:

$$1 + \cos(a\ell) \cosh(a\ell) = 0 \tag{9.29}$$

Equation (9.29) has an infinite number of real roots that can be found easily by Newton's method. The results are

$$a\ell = 1.19\,\pi/2, \quad 2.99\,\pi/2, \quad 5.00\,\pi/2, \quad 7.00\,\pi/2, \quad \dots \tag{9.30}$$

By using the definition of the Strouhal number to eliminate ω in (9.23), we obtain an expression for $a\ell$.

$$a\ell = \ell \left(\frac{m}{EI} \right)^{1/4} \sqrt{2\pi \frac{SU_\infty}{D}} \tag{9.31}$$

Since resonance cannot occur when $(a\ell)$ is less than the smallest values in (9.30), we see that resonance is not possible if

$$\ell \left(\frac{m}{EI} \right)^{1/4} \sqrt{\frac{SU_\infty}{D}} < 0.75 \tag{9.32}$$

Equation (9.32) shows that long slender beams with large ratios of ℓ/D are most likely to give problems with resonance from oscillating lift forces. Smaller amplitude oscillations may still occur, however, even if resonance is not possible.

Example 9.6

Suppose that a solid steel pole $\left(E = 200 \times 10^9 \text{ N/m}^2 \right)$ of length $\ell = 10$ m is to be designed so that resonance cannot occur with wind speeds up to a maximum value of $U_\infty = 20$ m/s. We will use a Strouhal number from Figure 9.13 of 0.20 and a mass density for steel of 7,860 kg/m³ to calculate the range of pole diameters for which resonance is not possible. The pole will have one end clamped and the other end free.

Solution:

If we let ρ = mass density of steel, then $m = \rho \pi D^2/4$. Since $I = \pi D^4/64$, Eq. (9.32) becomes

$$\ell\left(\frac{16\rho}{ED^2}\right)^{1/4}\sqrt{\frac{SU_\infty}{D}} < 0.75$$

Setting $\ell = 10$ m, $\rho = 7,860$ kg/m^3, $E = 200 \times 10^9$ N/m^2, $U_\infty = 20$ m/s and $S = 0.2$ shows that resonance is not possible if

$$\boxed{D > 0.751 \text{ m}}$$

Example 9.7

Suppose that the solid steel pole in the previous example is replaced with a hollow steel pole that has a wall thickness, T, that is small compared to the outer diameter, D.

Solution:

If T = wall thickness, then $m = \rho(\pi/4)\left[D^2 - (D - 2T)^2\right] \approx \rho\pi DT$ and $I = \dfrac{\pi}{64}\left[D^4 - (D - 2T)^4\right]$ $\approx \pi D^3 T/8$ for $2T/D << 1$. Therefore, Eq. (9.32) becomes

$$\ell\left(\frac{8\rho}{ED^2}\right)^{1/4}\sqrt{\frac{SU_\infty}{D}} < 0.75$$

Setting $\ell = 10$ m, $\rho = 7,860$ kg/m^3, $E = 200 \times 10^9$ N/m^2, $U_\infty = 20$ m/s and $S = 0.2$ shows that resonance is not possible if

$$\boxed{D > 0.632 \text{ m}}$$

It is interesting to notice that T cancels out when calculating the ratio m/I. This means that the wall thickness has no influence on the result provided that $2T/D << 1$. However, T would have to be large enough to withstand bending moments and shear forces created by the wind drag (Example 9.5).

Similar calculations can be carried out for other boundary conditions. For example, if the beam is simply supported at both ends, so that the deflection and moment vanish at each end, then resonance occurs when

$$\ell \left(\frac{m}{EI} \right)^{1/4} \sqrt{2\pi \frac{SU_\infty}{D}} = (2n - 1)\pi \quad \text{for } n = 1, 2, 3, \dots \tag{9.33}$$

This shows that resonance is not possible if

$$\ell \left(\frac{m}{EI} \right)^{1/4} \sqrt{\frac{SU_\infty}{D}} < \sqrt{\frac{\pi}{2}} \tag{9.34}$$

If the beam is clamped at both ends, resonance occurs when

$$\ell \left(\frac{m}{EI} \right)^{1/4} \sqrt{2\pi \frac{SU_\infty}{D}} = 3.01\,\pi/2, \quad 5.00\,\pi/2, \quad 7.00\,\pi/2, \dots \tag{9.35}$$

and resonance is not possible if

$$\ell \left(\frac{m}{EI} \right)^{1/4} \sqrt{\frac{SU_\infty}{D}} < 1.89 \tag{9.36}$$

Vibrations in some structures are described by the wave equation,

$$c^2 \frac{\partial^2 u}{\partial x^2} = \frac{\partial^2 u}{\partial t^2} + \frac{F_0}{m} \sin(\omega t) \tag{9.37}$$

in which c = wave speed in the body. For a tightly stretched cable, c is given by

$$c = \sqrt{P/m} \tag{9.38}$$

in which P = cable tension and m = mass per unit length. Humar (1990) shows that a tall building modelled as a shear beam has

$$c = \sqrt{\frac{12\,\Sigma EI}{mh^2}} \tag{9.39}$$

in which ΣEI = sum of the products of E and I for all columns in the building cross section, m = mass per unit height and h = storey height.

Equation (9.37) is a second order equation and requires only one boundary condition at each end. A cable stretched tightly between two fixed supports has $u = 0$ at each end, and resonance occurs in this case when

$$2\pi \frac{\ell}{D} \frac{U_\infty}{c} S = n\pi \quad \text{for} \quad n = 1, 2, 3, \dots \tag{9.40}$$

Since ℓ/D is very large for a cable, it is virtually impossible to design a cable so that large amplitude oscillations can be avoided under all conditions.

A building has a zero displacement at ground level and a zero shear force at its top. The zero shear force condition is imposed by requiring $\partial u/\partial x = 0$ at the building top and leads to the following requirement for resonance:

$$2\pi \frac{\ell}{D} \frac{U_\infty}{c} S = (2n - 1) \frac{\pi}{2} \quad \text{for} \quad n = 1, 2, 3, \dots \tag{9.41}$$

Thus resonance is not possible if

$$\frac{\ell}{D} \frac{U_\infty}{c} S < \frac{1}{4} \tag{9.42}$$

The ratio $U_\infty/c \approx 1/3$, and $S \approx 0.2$ from Figure 9.13. This suggests that resonance from an oscillating lift force is not possible in a tall building if $\ell/D < 3.75$, which is usually true. Smaller lateral oscillations may occur since the vortex trail and accompanying oscillating lift force are always present. The lateral oscillations, however, are unlikely to become very large.

The preceding analysis neglected damping and the yielding of supports. It also assumed that the structures are elastic. A departure from any one of these assumptions leads to resonant oscillations that remain bounded. In fact, vibration amplitudes are sometimes controlled by inserting damping rather than by changing dimensions of the structures.

References

Gerhart, P.M. and R.J. Gross (1985) *Fundamentals of Fluid Mechanics*, Addison-Wesley Publishing Co., Reading, Massachusetts, p. 555.

Humar, J.L. (1990) *Dynamics of Structures*, Prentice-Hall, Englewood Cliffs, N.J. Ch. 14.

Prandtl, L. and O.G. Tietjens (1934) *Applied Hydro and Aeromechanics*, Translated by J.P. Den Hertog, McGraw-Hill Book Co., New York, p. 301.

Robertson, J.M. (1965) *Hydrodynamics in Theory and Application*, Prentice-Hall, Englewood Cliffs, N.J. pp. 204-211.

Rouse, H. (1948) *Elementary Mechanics of Fluids*, John Wiley and Sons, New York, pp. 237, 247, 293.

Schlichting, H. (1968) *Boundary Layer Theory*, 6th edition, McGraw-Hill Book Co., New York, pp. 18, 35, 36.

Streeter, V.L. and E.B. Wylie (1981) *Fluid Mechanics*, 1st SI edition, McGraw-Hill Ryerson Ltd, New York, p. 224.

Chapter 10

Dimensional Analysis and Model Similitude

Experimental methods have traditionally played a major role in the study of fluid mechanics. Exact mathematical solutions are exceptions rather than the rule, and this means that the end result of different mathematical approximations must be tested with experiment before they can be used with confidence. Experimental methods must be used for some problems, such as flows requiring solutions that depend upon three spacial coordinates, that tax the limits of both modern day computers and specialists in numerical methods who devise and use computer software. Finally, problems involving turbulent flow cannot presently be solved in a general way with either numerical or mathematical methods. At best, approximate methods must be used, and these approximations always require experimental data to determine unknown constants and to ensure that approximations are realistic. *Dimensional analysis provides a basic tool that helps organize an experiment, plot results in a general way and scale results from model to prototype*.

The theory of dimensional analysis requires one basic hypothesis: it must be possible to describe an experiment uniquely with a function that depends upon variables with dimensions. For example, consider the problem of measuring the drag force on an object in a flow. If we consider only objects that are geometrically similar and that have the same orientation in the flow, then the drag force is a unique function of the following variables:

$$F_D = f\left(\rho, \, U_\infty, \, D, \, \nu, \, \epsilon\right) \qquad \textbf{(10.1)}$$

in which F_D = drag force $\left(N = \text{kg} - \text{m/s}^2\right)$, ρ = fluid mass density $\left(\text{kg/m}^3\right)$, U_∞ = approach velocity at infinity (m/s), D = characteristic length (m) that determines the scale of the geometrically similar bodies, ν = kinematic viscosity (m^2/s) and ϵ = absolute roughness height (m). Since ρ has been included, and since the dynamic and kinematic viscosities are related by $\nu = \mu/\rho$, we could replace ν with μ but should not include both μ and ν. In other words, we should include only independent variables on the right side of (10.1).

The following development, although too unwieldy for general use, shows why dimensional analysis can be used for any problem that is described uniquely with a set of variables that has dimensions. If we use M, L and T to represent the fundamental dimensions of mass, length and time, then dimensions of the terms in (10.1) can be represented symbolically in the following way:

$$F_D \sim \frac{ML}{T^2}, \quad \rho \sim \frac{M}{L^3}, \quad U_\infty \sim \frac{L}{T}, \quad D \sim L, \quad \nu \sim \frac{L^2}{T}, \quad \epsilon \sim L \qquad \textbf{(10.2)}$$

in which $\sim$ is read "has dimensions of" rather than indicating orders of magnitude, as in Chapter 5. Dimensions of mass can be removed from F_D by writing

$$F_D = \left(\frac{F_D}{\rho} \right) \rho \qquad\qquad (10.3)$$

If F_D in (10.3) is now regarded as the product of $\left(F_D / \rho \right)$ with ρ, then (10.1) can be rewritten in the equivalent form

$$F_D / \rho = f_1 \left(\rho, U_\infty, D, \nu, \epsilon \right) \qquad\qquad (10.4)$$

in which

$$F_D / \rho \sim \frac{L^4}{T^2} \qquad\qquad (10.5)$$

Since ρ is the only variable in (10.4) that contains dimensions of mass, a change in units for M (say from kg to slugs) will change the numerical magnitude of ρ but will leave the magnitude of all other variables in (10.4) unchanged. However, it is impossible to change the numerical magnitude of just one variable in a functional relationship without changing the magnitude of at least one other variable in the relationship. Thus, (10.4) can be correct only if ρ does not appear by itself in f_1.

$$F_D / \rho = f_1 \left(U_\infty, D, \nu, \epsilon \right) \qquad\qquad (10.6)$$

If we now use U_∞ to eliminate dimensions of time from (10.6) by writing

$$\frac{F_D}{\rho} = \left(\frac{F_D}{\rho U_\infty^2} \right) U_\infty^2 \qquad\qquad (10.7)$$

$$\nu = \left(\frac{\nu}{U_\infty} \right) U_\infty \qquad\qquad (10.8)$$

then (10.6) can be written in the equivalent form

$$\frac{F_D}{\rho U_\infty^2} = f_2 \left(U_\infty, D, \frac{\nu}{U_\infty}, \epsilon \right) \qquad\qquad (10.9)$$

in which

$$\frac{F_D}{\rho U_\infty^2} \sim L^2 \qquad\qquad (10.10)$$

$$\frac{\nu}{U_\infty} \sim L \tag{10.11}$$

Thus, time is contained only in the dimensions of U_∞ in (10.9), and a change in units of time (say from seconds to minutes) will change only the magnitude of U_∞. This is inconsistent with the behaviour of a functional relationship unless U_∞ no longer appears by itself in (10.9).

$$\frac{F_D}{\rho U_\infty^2} = f_2 \left(D, \frac{\nu}{U_\infty}, \epsilon \right) \tag{10.12}$$

Finally, D can be used to eliminate the dimensions of length by writing

$$\frac{F_D}{\rho U_\infty^2} = \left(\frac{F_D/D^2}{\rho U_\infty^2} \right) D^2 \tag{10.13}$$

$$\frac{\nu}{U_\infty} = \left(\frac{\nu}{U_\infty D} \right) D \tag{10.14}$$

$$\epsilon = \left(\frac{\epsilon}{D} \right) D \tag{10.15}$$

This allows (10.12) to be rewritten as

$$\frac{F_D/D^2}{\rho U_\infty^2} = f_3 \left(D, \frac{\nu}{U_\infty D}, \frac{\epsilon}{D} \right) \tag{10.16}$$

in which D has units of length and all other terms are dimensionless. A change in units of length (say from metres to feet) will change only the magnitude of D, which means that D must not appear by itself in (10.16).

$$\frac{F_D/D^2}{\rho U_\infty^2} = f_3 \left(\frac{\nu}{U_\infty D}, \frac{\epsilon}{D} \right) \tag{10.17}$$

Since we are considering drag forces on geometrically similar bodies, specification of D also determines an area, A, which is proportional to D^2. Furthermore, we are free to insert dimensionless constants in any of the terms in (10.17) or to replace any term with another power of itself. Thus, (10.17) can be written in the equivalent form

$$\frac{F_D/A}{\rho U_\infty^2/2} = f_4\left(\frac{U_\infty D}{\nu}, \frac{\epsilon}{D}\right)$$

(10.18)

in which the left side of (10.18) is the drag coefficient, C_D, that we studied in Chapter 9.

Two advantages of using dimensional analysis are that it reduces the amount of experimental work and it allows experimental results to be used to predict results for other similar flows. For example, Equation (10.18) has been used to plot the experimental curves shown in Figure 9.4 for smooth and rough circular cylinders. This is a three-dimensional plot in which C_D is plotted against Re while holding the third dimensionless variable, ϵ/D, constant for each curve. [There are only two curves shown for a circular cylinder in Figure 9.4: one for a smooth surface $(\epsilon/D = 0)$ and one for a rough surface with ϵ/D unspecified. Presumably this is because the drag on a circular cylinder is almost entirely pressure or form drag at large values of Re, and different values of ϵ/D will probably give much the same result provided that ϵ/D is of sufficient size to cause turbulence in the boundary layer.] Furthermore, these plots hold for any other experiment in which Re falls within the range shown in Figure 9.4. This result should be contrasted with the difficulties that would arise if the data were plotted dimensionally according to (10.1): six variables would require the use of a large number of three-dimensional plots, and each plot could be used only for the particular values of dimensional variables that were used in the original experiments.

A dimensional analysis also provides the basis for scaling results from model to prototype in a model study. For example, the function f_4 in (10.18) is the same function for model and prototype. Therefore, if the independent variables are identical for model and prototype, then the dependent variable must also be the same for model and prototype:

$$\left(\frac{U_\infty D}{\nu}\right)_p = \left(\frac{U_\infty D}{\nu}\right)_m$$

(10.19)

$$\left(\frac{\epsilon}{D}\right)_p = \left(\frac{\epsilon}{D}\right)_m$$

(10.20)

$$\left(\frac{F_D/A}{\rho U_\infty^2/2}\right)_p = \left(\frac{F_D/A}{\rho U_\infty^2/2}\right)_m$$

(10.21)

in which the subscripts m and p denote model and prototype, respectively. In the language of hydraulic modelling, Equations (10.19) - (10.21) require Reynolds number similarity, geometric similarity and Euler number similarity, respectively. The direct use of (10.19) - (10.21) for a particular model study merely eliminates the intermediate step of preparing the general dimensionless plot shown in Figure 9.4.

A Streamlined Procedure

The example just considered is useful for showing why dimensional analysis works for any problem that can be described uniquely with a set of variables that has dimensions. In practice, however, the process that was just used to obtain (10.18) can be streamlined by using ρ, U_∞ and D to obtain one dimensionless variable when combined with each of the remaining variables. When ρ, U_∞ and D are combined with F_D, they give

$$F_D \times \frac{1}{\rho} \times \frac{1}{U_\infty^2} \times \frac{1}{D^2} = \frac{F/D^2}{\rho U_\infty^2} \propto \frac{F/A}{\rho U_\infty^2/2} \tag{10.22}$$

$$\frac{ML}{T^2} \times \frac{L^3}{M} \times \frac{T^2}{L^2} \times \frac{1}{L^2} \sim 1 \tag{10.23}$$

in which (10.23) shows the dimensions of each term in (10.22).

When ρ, U_∞ and D are combined with ν, they give

$$\nu \times \frac{1}{U_\infty} \times \frac{1}{D} = \frac{\nu}{U_\infty D} = \frac{1}{Re} \tag{10.24}$$

$$\frac{L^2}{T} \times \frac{T}{L} \times \frac{1}{L} \times \sim 1 \tag{10.25}$$

Finally, combining ρ, U_∞ and D with ϵ gives

$$\epsilon \times \frac{1}{D} = \frac{\epsilon}{D} \tag{10.26}$$

$$L \times \frac{1}{L} \sim 1 \tag{10.27}$$

Thus, (10.22), (10.24) and (10.26) lead to (10.18) with considerably less effort than was required for the first procedure. An observant student, however, will notice that the streamlined procedure merely uses a different order for the same steps that were used in the first procedure.

Steps in the streamlined procedure can be organized in the following general way:

1   Write down the dependent variable and the corresponding list of independent variables, as in Eq. (10.1).

2   Write down the dimensions of each variable, as in Eq. (10.2).

3   Choose as many "repeating variables" as basic dimensions represented in step 2. (Our first example had the three basic dimensions M, L and T represented in (10.2), and we chose the three repeating variables ρ, U_∞ and D. Other examples might have fewer, say L and T, or more, say M, L, T and temperature.) The repeating variables must contain between them all of the basic dimensions present in step 2, and it must not be possible to form a dimensionless variable by using only the repeating variables.

4   Combine the repeating variables with each of the remaining variables to form dimensionless variables, as in (10.22) - (10.27).

Standard Dimensionless Variables

It has already been pointed out that a derived dimensionless variable can always be modified by inserting dimensionless multiplicative constants and by taking the variable to any power other than zero. It is also possible to replace a dimensionless variable by its product with any combination of powers of other dimensionless variables in the problem. For example, if a particular problem has the result

$$\pi_1 = f\left(\pi_2,\ \pi_3,\ \pi_4\right) \tag{10.28}$$

in which dimensionless variables are represented by π_i, then we can always write

$$\pi_2 = \left(\pi_2\ \pi_3^a\ \pi_4^b\right)\Big/\left(\pi_3^a\ \pi_4^b\right) \tag{10.29}$$

Since (10.29) can be viewed as the product of $\left(\pi_2\ \pi_3^a\ \pi_4^b\right)$ with a function of π_3 and π_4, we can replace (10.28) with the following equivalent statement:

$$\pi_1 = f_1\left[\left(\pi_2\ \pi_3^a\ \pi_4^b\right),\ \pi_3,\ \pi_4\right] \tag{10.30}$$

in which a and b are arbitrary numbers. This means, of course, that the result of a dimensional analysis is never unique. In practice, this additional flexibility is used to obtain standardized forms for dimensionless variables whenever possible. Some of these standard dimensionless variables follow:

$$\text{Euler number} = \frac{\Delta p}{\rho U^2/2} \tag{10.31}$$

$$\text{Reynolds number} = \frac{UL}{\nu} \tag{10.32}$$

$$\text{Froude number} = \frac{U}{\sqrt{gL}} \tag{10.33}$$

$$\text{Densimetric Froude number} = \frac{U}{\sqrt{Lg\,\Delta\rho/\rho}} \tag{10.34}$$

$$\text{Strouhal number} = \frac{\omega L}{U} \tag{10.35}$$

$$\text{Weber number} = \frac{U}{\sqrt{\sigma/(\rho L)}} \tag{10.36}$$

in which Δp and $\Delta\rho$ are changes in pressure and mass density, respectively, ω = frequency and σ = surface tension. We see from (10.31) that the drag coefficient given by the left side of (10.18) is actually an Euler number.

Example 10.1

A model study of the spillway shown in the sketch is to be carried out in a laboratory by constructing a geometrically similar model at a reduced scale.
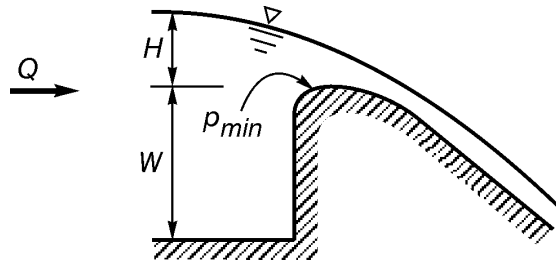
We will use a dimensional analysis to organize the study and to scale results from model to prototype. The dependent variables are the flow rate, Q, over the spillway and the minimum pressure, $p_{\min}$, on the spillway crest. (To save construction costs, designers sometimes reduce the radius of curvature of the spillway crest. Too large a reduction, however, would create sufficiently negative pressures to cause cavitation. Thus, a model study of this nature measures minimum crest pressures to see if cavitation might occur. The relationship between Q and H is important because the dam embankment must not be overtopped when the spillway passes the maximum possible outflow from the reservoir.)

Solution: The flow rate, Q, over the spillway is a function of the following independent variables:

$$Q = f(W, H, g, \epsilon, \nu, \rho)$$

in which W = spillway height, H = reservoir height above the spillway crest, g = gravitational constant, ϵ = spillway surface roughness, ν = kinematic viscosity and ρ = fluid mass density. Dimensions of these variables follow:

$$Q \sim \frac{L^3}{T}, \quad W \sim L, \quad H \sim L, \quad g \sim \frac{L}{T^2}, \quad \epsilon \sim L, \quad \nu \sim \frac{L^2}{T}, \quad \rho \sim \frac{M}{L^3}$$

Since ρ is the only variable that contains M, it cannot combine with any of the other variables. Thus, we will omit ρ from this part of the analysis, which means that two basic dimensions, L and T, occur and that two repeating variables must be chosen. We will choose W and g for repeating variables. This is a suitable choice because they contain between them both basic dimensions of L and T and because W and g cannot form a dimensionless variable by themselves.

Combining W and g with Q gives

$$Q \times \frac{1}{\sqrt{g}} \times \frac{1}{W^{5/2}} = \frac{Q}{W^2\sqrt{gW}}$$

$$\frac{L^3}{T} \times \frac{T}{L^{1/2}} \times \frac{1}{L^{5/2}} \sim 1$$

This dimensionless flow rate is a Froude number. Combining W and g with H obviously gives H/W, and from ϵ we obtain a relative roughness term ϵ/W. The kinematic viscosity can be combined with W and g to obtain

$$\frac{1}{\nu} \times \sqrt{g} \times W^{3/2} = \frac{W\sqrt{gW}}{\nu}$$

$$\frac{T}{L^2} \times \frac{L^{1/2}}{T} \times L^{3/2} \sim 1$$

Since any analysis that contains a viscosity, velocity and length can be expected to yield a Reynolds number, we will replace this last variable by its product with the dimensionless flow rate to obtain

$$\boxed{\frac{Q}{W^2\sqrt{gW}} = f_1\left(\frac{H}{W}, \frac{\epsilon}{W}, \frac{Q}{\nu W}\right)}$$

The result contains both a Froude and Reynolds number, but there is a fundamental difficulty in obtaining both Froude and Reynolds number similarity when the same fluid is used for model and prototype. In particular, this requires

$$\left(\frac{Q}{W^2\sqrt{gW}}\right)_p = \left(\frac{Q}{W^2\sqrt{gW}}\right)_m \quad \text{and} \quad \left(\frac{Q}{\nu W}\right)_p = \left(\frac{Q}{\nu W}\right)_m$$

If g and ν are the same for both model and prototype, this gives two conflicting requirements:

$$\frac{Q_p}{Q_m} = \left(\frac{W_p}{W_m}\right)^{5/2} \quad \text{and} \quad \frac{Q_p}{Q_m} = \frac{W_p}{W_m}$$

This contradiction is resolved by making use of our knowledge of irrotational flow. We know that irrotational flow calculations would give a highly accurate approximation for Q if boundary layer thicknesses are very small compared with flow depths on the spillway crest. This will certainly be true for the prototype, since Reynolds numbers are very large, and it will be approximately true for the model if model surfaces are made very smooth $(\epsilon/D \to 0)$ and if the scale is large enough to have fairly large Reynolds numbers. Nobody knows what this scale ratio must be to ensure relatively small boundary-layer effects, but everyone agrees that it should be as large as practically possible. Under these conditions, the dimensional analysis gives

$$\boxed{\frac{Q}{W^2\sqrt{gW}} = f_1\left(\frac{H}{W}\right)}$$

and similarity requirements become

$$\boxed{\left(\frac{Q}{W^2\sqrt{gW}}\right)_p = \left(\frac{Q}{W^2\sqrt{gW}}\right)_m} \quad \text{and} \quad \boxed{\left(\frac{H}{W}\right)_p = \left(\frac{H}{W}\right)_m}$$

Minimum spillway crest pressures depend upon the following variables:

$$p_{\min} = f(W, H, g, \rho)$$

in which boundary layer effects have been neglected. Dimensions of $p_{\min}$ are

$$p_{\min} \sim \frac{M}{LT^2}$$

and dimensions of the remaining variables have been given previously. This time dimensions of mass appear in both $p_{\min}$ and ρ, which means that ρ cannot be discarded. There are three basic dimensions $(M, L$ and $T)$, and we will choose W, g and ρ as repeating variables. Combining the repeating variables with $p_{\min}$ gives

$$p_{\min} \times \frac{1}{g} \times \frac{1}{\rho} \times \frac{1}{W} = \frac{p_{\min}}{\rho g W}$$

$$\frac{M}{LT^2} \times \frac{T^2}{L} \times \frac{L^3}{M} \times \frac{1}{L} \sim 1$$

Combining W, g and ρ with H gives H/W, and we obtain the following end result:

$$\frac{p_{\min}}{\rho g W} = f\left(\frac{H}{W}\right)$$

Thus, for similarity we have the requirements

$$\left(\frac{p_{\min}}{\rho g W}\right)_p = \left(\frac{p_{\min}}{\rho g W}\right)_m \quad \text{and} \quad \left(\frac{H}{W}\right)_p = \left(\frac{H}{W}\right)_m$$

Example 10.2

Use the results from Example 10.1 to calculate Q, $p_{\min}/(\rho g)$ and h for the prototype if a 1:20 scale model gives values of 0.0225 m³/s, - 0.12 m and 0.15 m, respectively, for a particular run.

Solution: The Froude number similarity requirement gives

$$\left(\frac{Q}{W^2\sqrt{gW}}\right)_p = \left(\frac{Q}{W^2\sqrt{gW}}\right)_m \quad \text{or} \quad Q_p = \left(\frac{W_p}{W_m}\right)^{5/2} Q_m = \left(\frac{20}{1}\right)^{5/2}(0.0225) = \boxed{40.2 \ \text{m}^3/\text{s}}$$

The corresponding reservoir depth is

$$H_p = \frac{W_p}{W_m} H_m = \frac{20}{1}(0.15) = \boxed{3.0 \ \text{m}}$$

and the minimum crest pressure head is

$$\left(\frac{p_{\min}}{\rho g}\right)_p = \frac{W_p}{W_m}\left(\frac{p_{\min}}{\rho g}\right)_m = \frac{20}{1}(-0.12) = \boxed{-2.4 \ \text{m}}$$

This is well above the vaporization pressure head at sea level and 5°C of - 10.2 m (gage pressure).

Selection of Independent Variables

Up to this point we have been concerned entirely with the process of combining dependent and independent variables into dimensionless variables. This is an important step in a dimensional analysis, and it obviously is a step that must be mastered if correct results are to be obtained. However, the most difficult step in an analysis is the first step, the step in which independent variables are chosen. This process frequently requires a combination of mathematical and physical insight that can be learned only through experience. In fact, that is the primary reason for placing this chapter at the end rather than at the beginning of a series of chapters that are concerned with the study of basic fluid mechanics.

Normally, an experimental study hopes to obtain results for a class of flows with geometrically similar geometries. This means that a single geometric length is usually sufficient to characterize the flow geometry, and specification of more than one geometric length would be incorrect since a functional relationship should not have more than one dependent variable. An exception occurs if the orientation of the geometry changes during the experiments. In this case, one or more angles, which are already dimensionless, must be included in the list of independent variables.

It is often necessary to include a velocity in the list of independent variables. For example, the velocity at infinity was included in (10.1) since a change in U_∞, with all other independent variables held constant, would certainly change the drag force, F_D. It would have been incorrect, however, to include a second velocity for any other point in the flow. This is because the flow net and one specified velocity are sufficient to calculate the velocity at all other points in the flow.

Some of the most difficult variables to consider are the mass density, ρ, the viscosity, μ or ν, and the gravitational constant, g. Generally, since the Navier-Stokes equations can be written in the form

$$-\nabla p \; + \; \rho \boldsymbol{g} \; + \; \mu \nabla^2 \boldsymbol{V} \; = \; \rho \; \frac{D\boldsymbol{V}}{Dt} \tag{10.37}$$

it is always possible to divide the pressure, p, into the sum of a hydrostatic pressure, p_s, and a dynamic pressure, p_d.

$$p \; = \; p_s \; + \; p_d \tag{10.38}$$

The hydrostatic pressure satisfies (10.37) when $\boldsymbol{V} \; = \; 0$.

$$-\nabla p_s \; + \; \rho \boldsymbol{g} \; = \; 0 \tag{10.39}$$

Subtraction of (10.39) from (10.37) and use of (10.38) gives

$$-\nabla p_d \; + \; \mu \nabla^2 \boldsymbol{V} \; = \; \rho \; \frac{D\boldsymbol{V}}{Dt} \tag{10.40}$$

Equation (10.40) can be solved simultaneously with the continuity equation

$$\nabla \cdot \boldsymbol{V} = 0 \tag{10.41}$$

for the unknown values of p_d and $\boldsymbol{V}$. After p_d has been calculated from (10.40) - (10.41), p_s can be calculated from the principles of hydrostatics and added to p_d to obtain p in (10.38). We will use (10.40) - (10.41) to show when g and ρ must be included in an analysis.

Since g is missing from (10.40) - (10.41), the solution for p_d and V will not depend upon g unless g enters the problem through a boundary condition on either a free surface or an interface between two fluids with different densities. Along a free surface $p = 0$ and, from (10.38), $p_d = -p_s$. Since p_s is shown from (10.39) to depend upon g, we see that p_d and $\boldsymbol{V}$ will also depend upon g. The only exception occurs when changes in free surface elevation are small compared with $V^2/(2g)$, as shown with Equations (4.9) - (4.10). One common example of this occurs for free jets with extremely large velocities.

Prandtl (1952) points out that constant-density two-layer flows can be simplified if one of the layers has a pressure distribution that is nearly hydrostatic. He gives as an example a layer of cold dense air flowing across a mountain range beneath a relatively thick layer of warmer air. In this case pressures in the upper layer of warm air are nearly hydrostatic. Pressures in the layer with a hydrostatic pressure distribution satisfy

$$-\nabla p_s + \rho_s \boldsymbol{g} = 0 \tag{10.42}$$

Thus, since pressures in the other layer satisfy (10.37), subtraction of (10.42) from (10.37) gives

$$-\nabla p_d + (\rho - \rho_s)\boldsymbol{g} + \mu \nabla^2 \boldsymbol{V} = \rho \frac{D\boldsymbol{V}}{Dt} \tag{10.43}$$

in which ρ and ρ_s are prescribed constants. The dynamic boundary condition along the interface requires that $p_d = 0$, so that (10.43) shows that the interface can be treated as a free surface but with a reduced gravitational term $(\rho - \rho_s)\boldsymbol{g}$. In steady flow this means that if a change in velocity creates a certain depth change in an open channel flow, then the same change in velocity for a two-layer flow has a depth change that is magnified by the ratio $\rho/(\rho - \rho_s)$. In unsteady flow the reduced gravitational term increases the time scale for a problem as $(\rho - \rho_s) \to 0$. In a dimensional analysis for this type of problem we can replace ρ, ρ_s and g with just ρ and $(\rho - \rho_s)g = g\Delta\rho$ in the list of independent variables, a simplification that ultimately leads to the densimetric Froude number defined in Eq. (10.34). If, on the other hand, pressure distributions in one of the layers cannot be described by (10.42), then it becomes necessary to include all three of the variables ρ, ρ_s and g.

The mass density, ρ, is seen from (10.40) - (10.41) to appear in any problem that has non-zero accelerations. For example, Stoke's solution for creeping flow past a sphere neglects accelerations, and Eq. (7.14) shows that ρ does not appear in the expression for the dynamic drag force. (If a buoyancy force must be included as part of the problem, then ρg re-enters the

problem. This is because a buoyancy force is calculated from p_s, which is seen from (10.39) to depend upon ρg. Frequently, however, we study only the dynamic effects of a problem so that g can be omitted.) In another example, fully developed laminar flow in a pipe has zero acceleration everywhere, and Eq. (7.10) shows that the **dynamic** pressure loss is independent of both ρ and g. [If we consider only dynamic pressures, then $h = p_d/(\rho g)$. Since $\nu = \mu/\rho$ on the right side of (7.10), both ρ and g cancel out of the solution for the dynamic pressure loss.] On the other hand, Eq. (7.51) and the Moody diagram, Figure 7.18, show that the dynamic pressure loss in turbulent flow is independent of g but depends upon ρ. [For example, f depends upon ϵ/D but not Re for completely turbulent flow in a rough pipe, and ρ does not cancel out of Eq. (7.51).] This is because highly turbulent flow has instantaneous accelerations that are non-zero, even when time-averaged velocities are not changing with time. ***Thus, ρ must be included in any problem that has non-zero accelerations, and this includes problems in which instantaneous accelerations are caused by turbulence***.

The viscosity can be expected to appear in any problem for which Reynolds numbers are sufficiently small. It will also appear in high Reynolds number flows that have laminar boundary layers or laminar sublayers next to a boundary either (a) if tangential boundary stresses are an important part of the problem or (b) if points of flow separation change location with changes in the Reynolds number. Examples of some of these possibilities are shown in Figure 7.3. In particular, the drag coefficient for a circular disk varies with the Reynolds number for $0 < Re < 10^3$ but remains constant thereafter. Evidently, since flow separates at the sharp disk edge for all but the smallest values of Re, pressures on the disk surface change with viscosity until Reynolds numbers reach about 10^3. The drag coefficient for a sphere varies rapidly with Reynolds number for $0 < Re < 10^3$. Thereafter, C_D remains nearly constant until $Re \approx 3 \times 10^5$, when the pressure distribution is changed abruptly by the onset of turbulence in the boundary layer. The drag coefficient for a flat plate aligned with the flow is seen in Figure 8.5 to depend upon Re, and therefore the viscosity, until the laminar sublayer vanishes and the plate becomes hydraulically rough. Thereafter, the influence of viscosity disappears.

With this background it now becomes easy to see why some variables have been included and others omitted in the problems considered so far. Equation (10.1) contains ρ because the fluid is accelerated as it passes the object, and g was omitted because no free surface is present and we have only considered the dynamic drag force. The viscosity is important if flow occurs at lower Reynolds numbers, if surface drag is a significant part of the total drag force or if points of flow separation change location with Re. The roughness, ϵ, was included because it may create turbulence within the boundary layer at high enough Reynolds numbers and because relative roughness has a strong influence on surface drag when the laminar sublayer vanishes. For relatively short, unstreamlined bodies submerged in moderate to high Reynolds number flows, both ν and ϵ can be omitted if points of flow separation are fixed at sharp corners.

In Example 10.1 g was included because of the presence of a free surface. The mass density, ρ, was included because flow is highly accelerated as it passes over the spillway crest. (ρ later dropped out of the analysis for Q because none of the other variables contained dimensions of mass. However, ρ did combine with the pressure, p, when spillway crest pressures were considered.) Both ν and ϵ were included because boundary layer thicknesses can be a significant portion of flow depths on the crest for small enough Reynolds numbers.

Example 10.3
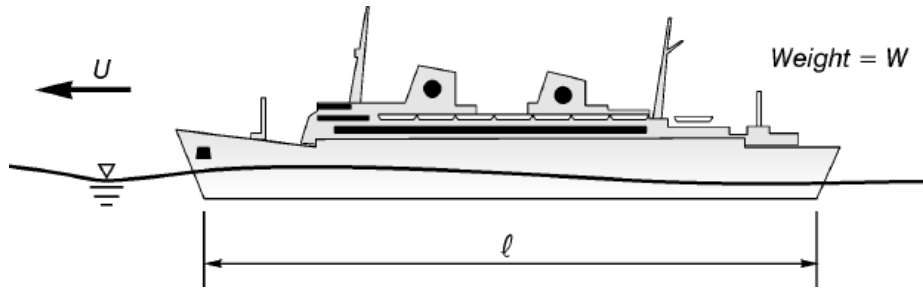
A small scale model is to be used to predict the total drag force on a ship. Carry out a dimensional analysis for this problem.

Solution: The drag force can be expected to be a function of the following variables:

$$F = f\left(U, \ell, \rho, g, \nu, \epsilon, W\right)$$

The ship velocity, U, and hull length, ℓ, are obvious choices for independent variables that influence the magnitude of the drag force, F. The mass density, ρ, is included because fluid accelerations occur. The gravitational constant, g, results from the presence of a free surface. The kinematic viscosity, ν, and relative roughness, ϵ, are included because surface or skin friction drag is a significant portion of the total drag force on a well streamlined ship. Finally, the total weight, W, of the ship and its cargo is included since this will determine the submergence depth of the hull. Dimensions for these variables follow:

$$F \sim \frac{ML}{T^2}, \quad U \sim \frac{L}{T}, \quad \ell \sim L, \quad \rho \sim \frac{M}{L^3}, \quad g \sim \frac{L}{T^2}, \quad \nu \sim \frac{L^2}{T}, \quad \epsilon \sim L, \quad W \sim \frac{ML}{T^2}$$

There are three basic dimensions $(M, L \text{ and } T)$ represented, and we will choose U, ℓ and ρ for repeating variables. This means that 8 - 3 = 5 dimensionless variables will result. Combining U, ℓ and ρ with each of the remaining variables can be carried out either by setting down each group of four variables and using appropriate powers to make units cancel or by making use of past experience to write the end result. (U, ℓ and ρ combined with F will give an Euler number; U, ℓ and ρ combined with g will give a Froude number; U, ℓ and ρ combined with ν will give a Reynolds number; etc.) In either case, an acceptable final result is

$$\boxed{\frac{F/\ell^2}{\rho U^2/2} = f\left(\frac{U}{\sqrt{g\ell}}, \quad \frac{U\ell}{\nu}, \quad \frac{\epsilon}{\ell}, \quad \frac{W}{\rho g \ell^3}\right)}$$

[An observant student will notice that combining U, ρ and ℓ with W gives

$$\frac{W}{\rho \ell^2 U^2}$$

This dimensionless variable was then replaced by its product with $\left(U/\sqrt{g\ell}\right)^2$ to obtain a dimensionless variable, $W/\left(\rho\,g\,\ell^3\right)$, that effectively determines the hull submergence depth when the ship is not moving. This step is not obligatory. It is merely a result of the writer's personal tastes.]

Example 10.4

Discuss difficulties that arise when trying to use the results from Example 10.3 to scale drag forces from model to prototype.

Solution: The end result of Example 10.3 requires both Froude and Reynolds number similarity.

$$\left(\frac{U}{\sqrt{g\ell}}\right)_m = \left(\frac{U}{\sqrt{g\ell}}\right)_p \quad \text{and} \quad \left(\frac{U\ell}{\nu}\right)_m = \left(\frac{U\ell}{\nu}\right)_p$$

If the same fluid is used for model and prototype, this gives conflicting requirements for velocity scales.

$$\frac{U_m}{U_p} = \sqrt{\frac{\ell_m}{\ell_p}} \quad \text{and} \quad \frac{U_m}{U_p} = \frac{\ell_p}{\ell_m}$$

In practice, this difficulty is circumvented by an approximate method that divides the total drag into the sum of pressure drag and surface drag.

$$\boxed{F = F_{\text{pres}} + F_{\text{sur}}}$$

The surface drag is calculated analytically with approximations from boundary layer theory *for both model and prototype*. Then the pressure drag is scaled using experimental results from the model with the following approximation:

$$\boxed{\frac{F_{\text{pres}}/\ell^2}{\rho U^2/2} = f\left(\frac{U}{\sqrt{g\ell}}, \ \frac{W}{\rho g\ell^3}\right)}$$

Both model and prototype are normally considered to have smooth boundaries. However, there is some uncertainty in Figure 8.4 about whether calculations for the model should assume a completely laminar boundary layer, a completely turbulent boundary layer or a boundary layer that is partly laminar and partly turbulent. This problem is usually solved by roughening the leading edge of the model to ensure a completely turbulent boundary layer.

Example 10.5

A 1:100 scale model has a total drag of $F = 0.9$ N when towed at a speed of $U = 1.0$ m/s in fresh water. The smooth hull has its leading edge roughened, a wetted length of 0.60 m and a wetted surface area of 0.10 m^2. Calculate for the prototype in salt water the corresponding speed, total drag force and power required to overcome the drag force.

Solution: The model surface drag calculation requires a Reynolds number.

$$Re = \frac{UL}{\nu} = \frac{(1.0)\,(0.6)}{1.31 \times 10^{-6}} = 4.6 \times 10^5$$

Since the rough leading edge ensures a completely turbulent boundary layer, Figure 8.4 gives

$$C_D = 0.0052$$

This allows an approximate calculation of the model surface drag.

$$F_{sur} = C_D A \rho \frac{U^2}{2} = (0.0052)\,(0.10)\,(1000)\,\frac{(1.0)^2}{2} = 0.26 \text{ N}$$

Thus, the pressure drag for the model is

$$F_{pres} = F - F_{sur} = 0.9 - 0.26 = 0.64 \text{ N}$$

The corresponding prototype speed is obtained by requiring Froude number similarity.

$$\left(\frac{U}{\sqrt{g\ell}}\right)_p = \left(\frac{U}{\sqrt{g\ell}}\right)_m \quad \text{or} \quad U_p = U_m \sqrt{\frac{\ell_p}{\ell_m}} = 1.0\sqrt{\frac{100}{1}} = \boxed{10 \text{ m/s} = 36 \text{ km/hr}}$$

Euler number similarity gives the prototype pressure drag.

$$\left(\frac{F/\ell^2}{\rho U^2/2}\right)_p = \left(\frac{F/\ell^2}{\rho U^2/2}\right)_m \quad \text{or} \quad F_p = F_m \frac{\rho_p}{\rho_m}\left(\frac{U_p}{U_m}\right)^2\left(\frac{\ell_p}{\ell_m}\right)^2$$

Since $U_p/U_m = \sqrt{\ell_p/\ell_m}$, this gives

$$F_p = F_m \frac{\rho_p}{\rho_m}\left(\frac{\ell_p}{\ell_m}\right)^3 = (0.64)\,(1.025)\left(\frac{100}{1}\right)^3 = 6.56 \times 10^5 \text{ N}$$

The prototype Reynolds number is

$$Re = \frac{UL}{\nu} = \frac{(10)\,(0.60 \times 100)}{1.31 \times 10^{-6}} = 4.6 \times 10^8$$

in which L has been computed from the product of the model wetted length with the scale ratio. Figure 8.4 gives

$$C_D = 0.0017$$

Thus, the prototype surface drag is

$$F_{sur} = C_D A \rho \frac{U^2}{2} = (0.0017)\left(0.10 \times 100^2\right)(1,025)\,\frac{10^2}{2} = 8.71 \times 10^4 \text{ N}$$

Adding the prototype surface and pressure drag forces gives the total drag.

$$F = F_{pres} + F_{sur} = 6.56 \times 10^5 + 8.71 \times 10^4 = \boxed{7.43 \times 10^5 \text{ N}}$$

Finally, the power required to overcome this drag is calculated from the product of the drag force and speed.

$$\text{Power} = FU = \left(7.43 \times 10^5\right)(10) = 7.43 \times 10^6 \text{ watts}$$

$$= \boxed{7.43 \text{ megawatts}}$$

Example 10.6

Carry out a dimensional analysis for velocities in the highly turbulent axisymmetric submerged jet shown in Figure 7.13.

Solution: It was pointed out in Chapter 7 that experimental pressures have been found to be hydrostatic throughout a turbulent submerged jet when the receiving reservoir of fluid is relatively large. Therefore, a control volume contained between any two vertical planes in Figure 7.13 has a zero horizontal pressure force, and the horizontal momentum flux through each of the two vertical planes must be identical. In other words, the momentum flux through any vertical plane remains unchanged as the z coordinate of the plane changes, which means that this constant momentum flux can be computed from the momentum flux at the nozzle.

$$M_0 = \rho U_0^2 \pi D^2 / 4$$

In general we would have to expect that the velocity, u, at any point in the flow would depend upon both U_0 and D. However, the preceding comments about momentum flux suggest that it might be possible to combine U_0 and D into the single term M_0 for large enough values of z/D. Experiments have shown that this is possible, and, for large enough values of z/D, the nozzle is referred to as a "point source of momentum". Thus, the following analysis is valid only for the zone of established flow in Figure 7.13.

The time averaged velocity in the zone of established flow is a function of the following variables:

$$u = f\left(M_0, \rho, r, z\right)$$

The mass density, ρ, has been included because accelerations occur both in the mean flow and in the turbulent velocity fluctuations. The gravitational constant, g, has been omitted because there is no free surface, and the viscosity has been omitted because measurements show that changes in viscosity have a negligible effect on time averaged velocities in highly turbulent flow at large Reynolds numbers. Dimensions of these variables follow:

$$u \sim \frac{L}{T}, \quad M_0 \sim \frac{ML}{T^2}, \quad \rho \sim \frac{M}{L^3}, \quad r \sim L, \quad z \sim L$$

Since there are three basic dimensions $\left(M, L \text{ and } T\right)$ represented, we will choose M_0, ρ and z as repeating variables. This will give 5 - 3 = 2 dimensionless variables. Combining M_0, ρ and z with u gives

$$u \times \frac{1}{\sqrt{M_0}} \times \sqrt{\rho} \times z = \frac{uz}{\sqrt{M_0/\rho}}$$

$$\frac{L}{T} \times \frac{T}{\sqrt{ML}} \times \frac{\sqrt{M}}{L^{3/2}} \times L \sim 1$$

Combining M_0, ρ and z with r obviously gives r/z. Thus, we obtain

$$\boxed{\frac{z\,u\left(r, z\right)}{\sqrt{M_0/\rho}} = f\left(\frac{r}{z}\right)}$$

If we set $r = 0$, we get an expression for the maximum velocity at the centreline in the region of fully established flow.

$$\frac{z\,U_{\text{max}}}{\sqrt{M_0/\rho}} = f(0) = C_1$$

The constant C_1 has been determined experimentally to be $C_1 = 7.0$, and substitution for M_0/ρ and C_1 leads to Eq. (7.53).

$$\frac{U_{max}}{U_0} = \frac{6.2}{z/D} \quad \text{for} \quad 6.2 \le z/D < \infty$$

If we divide the first circled equation by the equation for C_1 that follows it, we obtain

$$\frac{u(r,z)}{U_{max}} = \frac{f(r/z)}{C_1} = e^{-C_2 r^2/z^2} \quad \text{for} \quad 6.2 \le z/D < \infty$$

in which the given exponential function has been found empirically to provide a close fit of experimental data. The constant C_2 can be calculated from C_1 by using the constant momentum flux requirement.

$$M_0 = \int_0^\infty \rho u^2(r,z) \, 2\pi r \, dr$$

Substitution for M_0 and $u(r,z)$ gives

$$\rho U_0^2 \pi D^2/4 = 2\pi\rho U_{max}^2 \int_0^\infty e^{-2C_2 r^2/z^2} r \, dr$$

$$= 2\pi\rho \left(\frac{6.2 \, U_0}{z/D}\right)^2 \int_0^\infty e^{-2C_2 r^2/z^2} r \, dr$$

By cancelling terms and changing the integration variable from r to $\xi = r/z$ (with z fixed) we obtain

$$\frac{1}{4} = 2(6.2)^2 \int_0^\infty e^{-2C_2 \xi^2} \xi \, d\xi = 2(6.2)^2 \frac{1}{4C_2}$$

Thus, we calculate for C_2 the value given in Eq. (7.54).

$$C_2 = 2(6.2)^2 = 77$$

The following plot shows the experimental variation of centreline velocity for an axisymmetric jet. [Reproduced from Albertson, Dai, Jensen and Rouse (1948).]
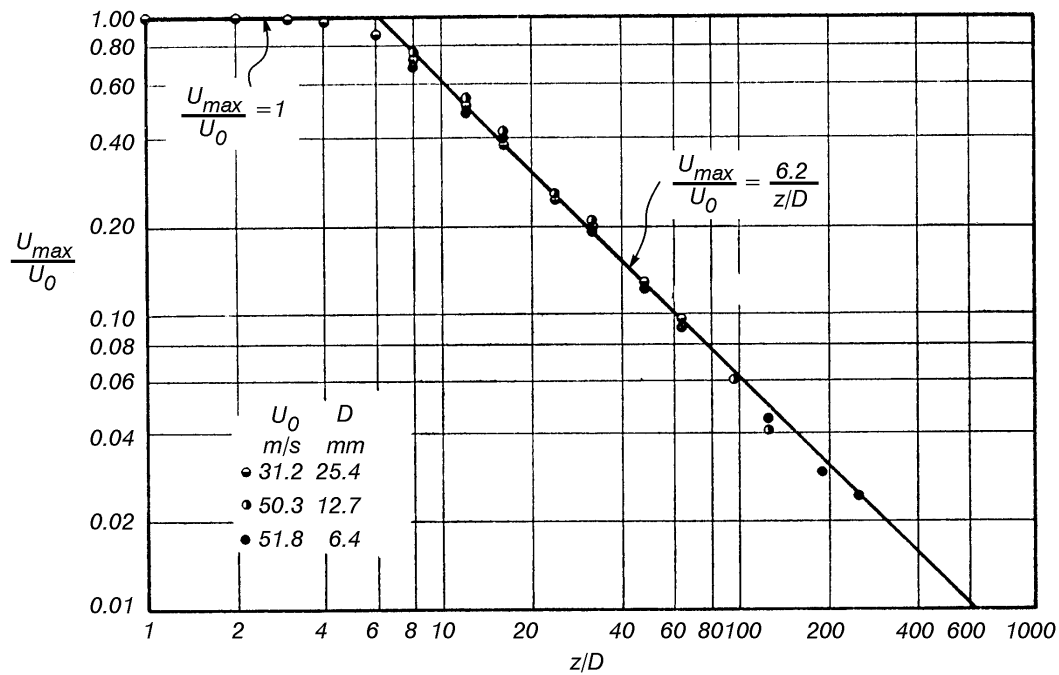
Example 10.7

For a number of years civil engineering students at Canterbury have carried out a laboratory experiment in which spheres are suspended in turbulent jets of air and water, as shown in the following sketch:
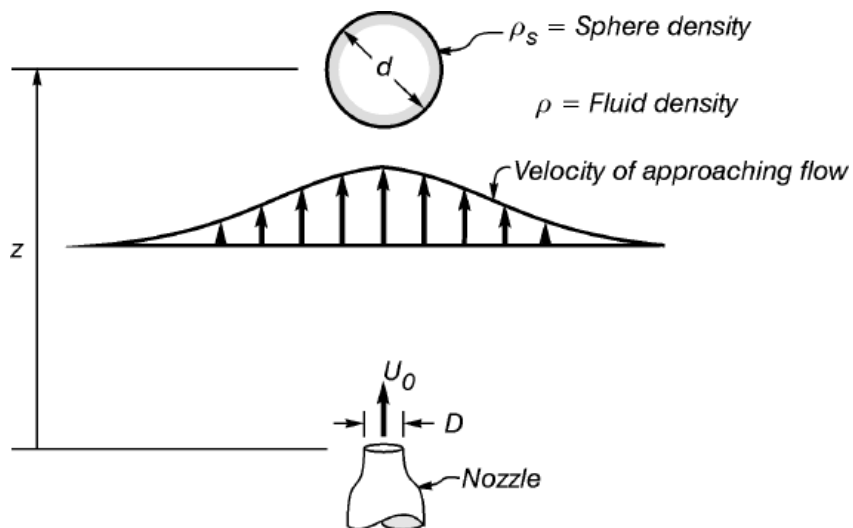
The sphere has an equilibrium position that is stable for small horizontal displacements because of the velocity distribution of the approaching flow. For example, if the sphere is displaced slightly to the right of its pictured position, the bell shaped velocity distribution in the approaching flow creates higher velocities and lower pressures on the left side of the sphere than on the right. As a result, an unsymmetric pressure distribution forces the sphere back towards its original position along the jet centreline.

The vertical elevation, z, of the sphere is a function of the following variables:

$$z = f\left(d, \, g\,\Delta\rho, \, \rho, \, M_0\right)$$

in which d = sphere diameter, g = gravitational constant, ρ = fluid mass density, ρ_s = sphere mass density, $\Delta\rho = \rho_s - \rho$ and $M_0 = \rho\,U_0^2\,\pi D^2/2$ = nozzle momentum flux. Our previous experience with highly turbulent submerged jets suggests that viscosity is unimportant and that the nozzle diameter and flow velocity can be combined into M_0 for a point source of momentum. The fluid mass density, ρ, has been included because fluid accelerations are present, and d is needed to fix the scale of the experiment. Setting the summation of vertical forces equal to zero for the sphere gives

$$g\left(\rho_s - \rho\right)\pi d^3/6 = C_D\left(\pi d^2/4\right)\rho\,U^2/2$$

in which the left side is the difference between the sphere weight and the buoyancy force, and the right side is a drag force calculated from an unknown drag coefficient and characteristic velocity in the approaching flow. Since ρ_s and g appear in the equation only in the form $g\left(\rho_s - \rho\right) = g\,\Delta\rho$, this suggests that ρ, ρ_s and g might be replaced by $g\,\Delta\rho$ and ρ.

Dimensions for the five relevant variables follow:

$$z \sim L, \quad d \sim L, \quad g\,\Delta\rho \sim \frac{M}{T^2L^2}, \quad \rho \sim \frac{M}{L^3}, \quad M_0 \sim \frac{ML}{T^2}$$

Since there are three basic dimensions represented $\left(M, L \text{ and } T\right)$, we will choose $d, g\,\Delta\rho$ and ρ for repeating variables to obtain $5 - 3 = 2$ dimensionless variables. Combining the repeating variables with z gives z/d, and combining the repeating variables with M_0 gives the following result:

$$M_0 \times \frac{1}{g\,\Delta\rho} \times \frac{1}{d^3} = \frac{M_0}{d^3 g\,\Delta\rho}$$

$$\frac{ML}{T^2} \times \frac{T^2L^2}{M} \times \frac{1}{L^3} \sim 1$$

This gives the relationship

$$\frac{z}{d} = f\left(\frac{M_0}{d^3 g\,\Delta\rho}\right)$$

However, since M_0 is proportional to ρU_0^2, we see that the dimensionless momentum flux term is actually a densimetric Froude number. For this reason, we will replace this term with its square root to obtain

$$\frac{z}{d} = f\left(\sqrt{\frac{M_0}{d^3 g \Delta \rho}}\right)$$

Some experimental measurements confirming this result are shown in the following plot:
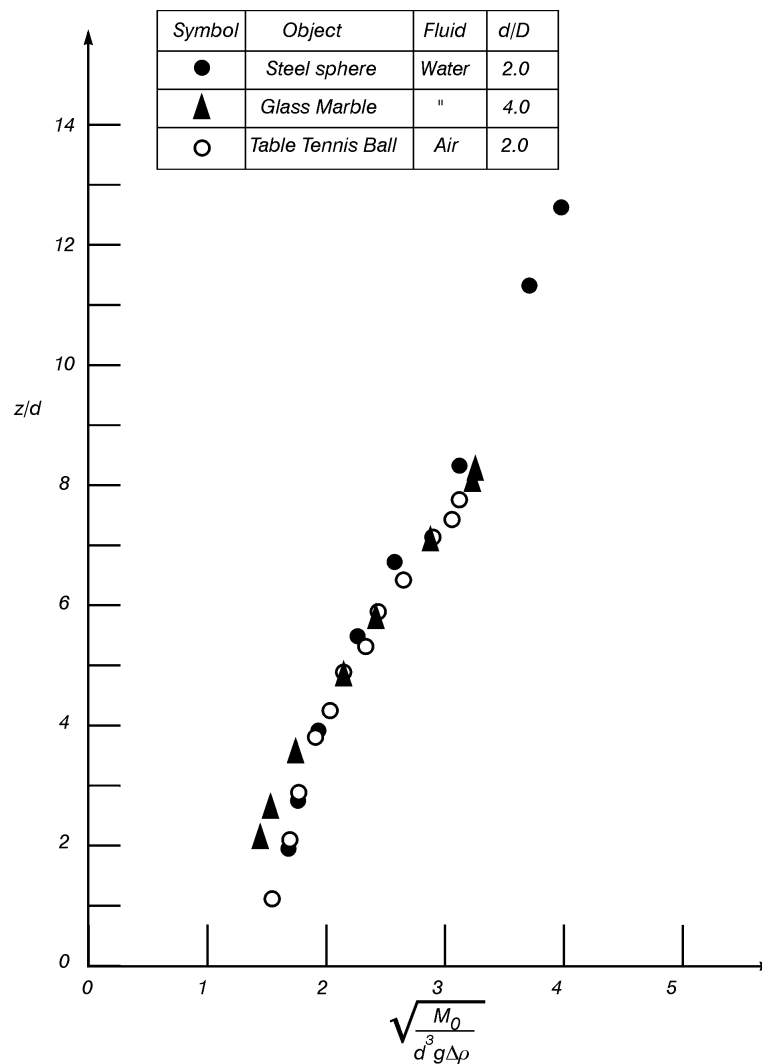
Symbol	Object	Fluid	d/D
●	Steel sphere	Water	2.0
▲	Glass Marble	"	4.0
○	Table Tennis Ball	Air	2.0

References

Albertson, M.L., Dai, Y.B., Jensen, R.A. and H. Rouse (1948) Diffusion of submerged jets, *ASCE Proceedings*, December, 639-664.

Prandtl, L. (1952) *Essentials of Fluid Dynamics*, (Translated edition), Blackie and Son Ltd, London, p. 368.

Chapter 11

Steady Pipe Flow

Pipe-flow problems are important for engineers who design distribution systems for water supply and waste disposal. These are problems in which control volumes have extremely large ratios of length to width. Thus, as explained in Chapter 4, the Bernoulli equation must be modified to account for energy losses that result from work done by tangential stresses. This means that Eq. (4.12)

$$h_1 + \frac{U_1^2}{2g} = h_2 + \frac{U_2^2}{2g} + H_L \tag{11.1}$$

and a one-dimensional form of the continuity equation

$$Q = U_1 A_1 = U_2 A_2 \tag{11.2}$$

are the main tools of analysis. We will let z be a vertical coordinate that is positive in the upward direction, which means that the piezometric head in (11.1) has the following form:

$$h = \frac{p}{\rho g} + z \tag{11.3}$$

The head loss term in (11.1) most generally consists of the sum of friction losses over long lengths of pipe, given by Eq. (7.51 a),

$$H_L = f \frac{L}{D} \frac{U^2}{2g} \tag{11.4}$$

and local or "minor" losses expressed in any one of the three forms suggested in Example 4.2:

$$H_L = K_1 \frac{\left(U_1 - U_2\right)^2}{2g} = K_2 \frac{U_1^2}{2g} = K_3 \frac{U_2^2}{2g} \tag{11.5}$$

in which cross sections 1 and 2 are immediately upstream and downstream, respectively, from the sudden change in pipe geometry that creates the local loss. Local losses are the result of high

levels of turbulence, flow separation and/or secondary flows. These losses occur over relatively short lengths of pipe as a result of pipe expansions and contractions, bends, valves and other pipe fittings. They are usually called "minor" losses because often they are small compared to friction losses. This is not always true, however, and we will prefer to describe these losses as local rather than minor.

Foundations for the use of (11.4) have been given in Chapter 7 and will not be repeated in this chapter. Instead, we will remind readers that L and D are the length and constant diameter, respectively, of the pipe and that the friction factor, f, is a function of the Reynolds number, $Re = UD/\nu$, and relative roughness, ϵ/D. Values of ϵ and f are given in the Moody diagram shown in Fig. 7.18.

With a few exceptions, local loss coefficients are usually determined experimentally. One notable exception occurs for a sudden expansion, for which it was shown in Example 4.2 that

$$K_1 = 1$$

$$K_2 = \left(1 - \frac{A_1}{A_2} \right)^2$$

$$K_3 = \left(\frac{A_2}{A_1} - 1 \right)^2$$

(11.6 a, b, c)

Equations (11.6 a) and (11.6 b) also hold for the limiting case of a submerged pipe discharging into a large reservoir, in which case U_2 vanishes and A_2 is infinite.

Local loss coefficients for sudden contractions are given in Table 11.1, and loss coefficients for some commercial pipe fittings are shown in Table 11.2. Loss coefficients for gradual expansions, bends and various other pipe transition geometries and fittings can be found in other texts, such as Albertson, Barton and Simons (1960).

Table 11.1 Loss coefficients for sudden contractions.

D_2/D_1	K_3
1	0
0.8	0.13
0.6	0.28
0.4	0.38
0.2	0.45
0.0 (reservoir inlet)	0.50

Table 11.2 Loss coefficients for commercial pipe fittings.

Globe valve (fully open)	10
Angle valve (fully open)	5
Swing check valve (fully open)	2.5
Gate valve (fully open)	0.2
Close return bend	2.2
Standard tee	1.8
Standard elbow	0.9
Medium sweep elbow	0.75
Long sweep elbow	0.6

Hydraulic and Energy Grade Lines

Every term in Eqs. (11.1) and (11.3) has dimensions of length. This makes it possible to show in a sketch for any pipe-flow problem the qualitative behaviour of each term in these two equations. The *energy grade line* (abbreviated EGL) shows the magnitude of the Bernoulli sum, $h + U^2/(2g)$. This line is sketched by starting from its known elevation at a point upstream (often a reservoir free surface). Friction losses are shown by (11.4) to cause the EGL to slope downward linearly with distance in the direction of flow, and local losses, given by (11.5), are assumed to create discontinuities in the EGL at the locations of expansions, contractions, bends, valves, etc. The *hydraulic grade line* (abbreviated HGL) shows the magnitude of the piezometric head, h. Since h differs from the Bernoulli sum by the velocity head, $U^2/(2g)$, the HGL is parallel to the EGL and lies below it by an amount $U^2/(2g)$. Since z in (11.3) is the elevation of the pipe centreline, the pressure head, $p/(\rho g)$, is the vertical distance between the HGL and the pipe centreline. ***Therefore pressures in the pipe are positive and negative, respectively, when the HGL lies above and below the pipe centreline***. The following examples should help make these ideas clear.

Example 11.1
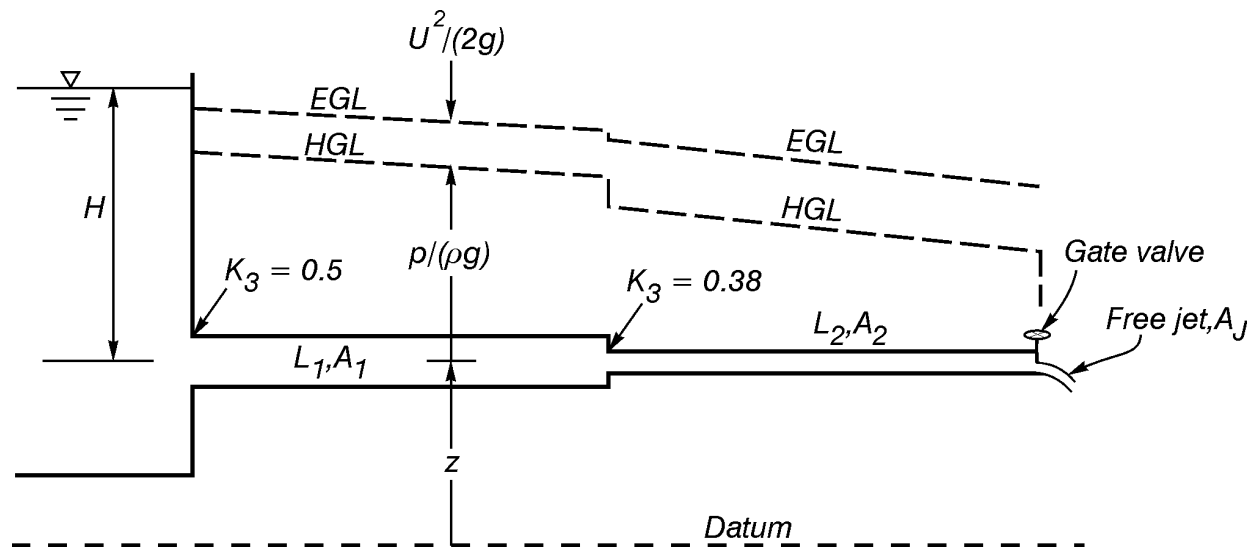
Two pipes, joined in series, allow flow to exit from a reservoir. The loss coefficient for the gate valve is zero since no free shear layer and associated turbulence exist downstream from the valve. Sketch the energy and hydraulic grade lines. Then use symbols to write an equation that could be solved for the flow rate leaving the reservoir.

Solution: The EGL and HGL are shown in the sketch with dashed lines. Since atmospheric pressure exists both on the reservoir free surface and within the free jet, writing (11.1) between these two points gives

$$H = \frac{(Q/A_J)^2}{2g} + f_1 \frac{L_1}{D_1} \frac{(Q/A_1)^2}{2g} + f_2 \frac{L_2}{D_2} \frac{(Q/A_2)^2}{2g}$$
$$+ \, 0.5 \frac{(Q/A_1)^2}{2g} + 0.38 \frac{(Q/A_2)^2}{2g}$$

in which the arbitrary datum has been chosen to coincide with the pipe centreline and the velocity on the reservoir free surface has been taken as zero.

Example 11.2

Suppose that the pipes in Example 11.1 are commercial steel and that the following data applies:

$$H = 10 \text{ m} \qquad\qquad A_J = 0.003 \text{ m}^2$$

$$L_1 = 100 \text{ m} \qquad\qquad L_2 = 10 \text{ m}$$
$$D_1 = 200 \text{ mm} \qquad\qquad D_2 = 80 \text{ mm}$$

Water Temperature $= 10°C$

Calculate the flow rate, Q.

Solution: Calculations give $A_1 = 0.0314 \text{ m}^2$ and $A_2 = 0.0050 \text{ m}^2$. Figure 7.18 gives $\epsilon = 0.046$ mm for commercial steel, which leads to $\epsilon/D_1 = 0.00023$ and $\epsilon/D_2 = 0.00058$. Inserting these numbers in the equation obtained for Example 11.1 gives

$$10 = \left(5{,}663 + 25{,}847 \, f_1 + 251{,}811 \, f_2 + 26 + 766\right) Q^2$$

Solution for Q gives

$$Q = \frac{1}{\sqrt{646 + 2{,}585 f_1 + 25{,}181 f_2}}$$

in which f_1 and f_2 vary with relative roughness and Reynolds number. This means that f_1 and f_2 are functions of Q, and this equation must be solved by successive approximation.

The values of $\epsilon/D_1 = 0.00023$ and $\epsilon/D_2 = 0.00058$, when used with Fig. 7.18, suggest that we might start with $f_1 = 0.0143$ and $f_2 = 0.0178$. This gives

$$Q = 0.0297 \text{ m}^3/\text{s}$$

$$Re_1 = \frac{U_1 D_1}{\nu} = \frac{\left(Q/A_1\right) D_1}{\nu} = \frac{(0.947)(.200)}{1.31 \times 10^{-6}} = 1.45 \times 10^5$$

$$Re_2 = 3.61 \times 10^5$$

These values of Re and ϵ/D give new values of $f_1 = 0.0183$ and $f_2 = 0.0184$. This gives the following second approximation:

$$Q = 0.0294 \text{ m}^3/\text{s}$$
$$Re_1 = 1.43 \times 10^5$$
$$Re_2 = 3.57 \times 10^5$$

Since values for f_1 and f_2 do not change in the next cycle, we have the final result

$$\boxed{Q = 0.0294 \text{ m}^3/\text{s}}$$

Example 11.3
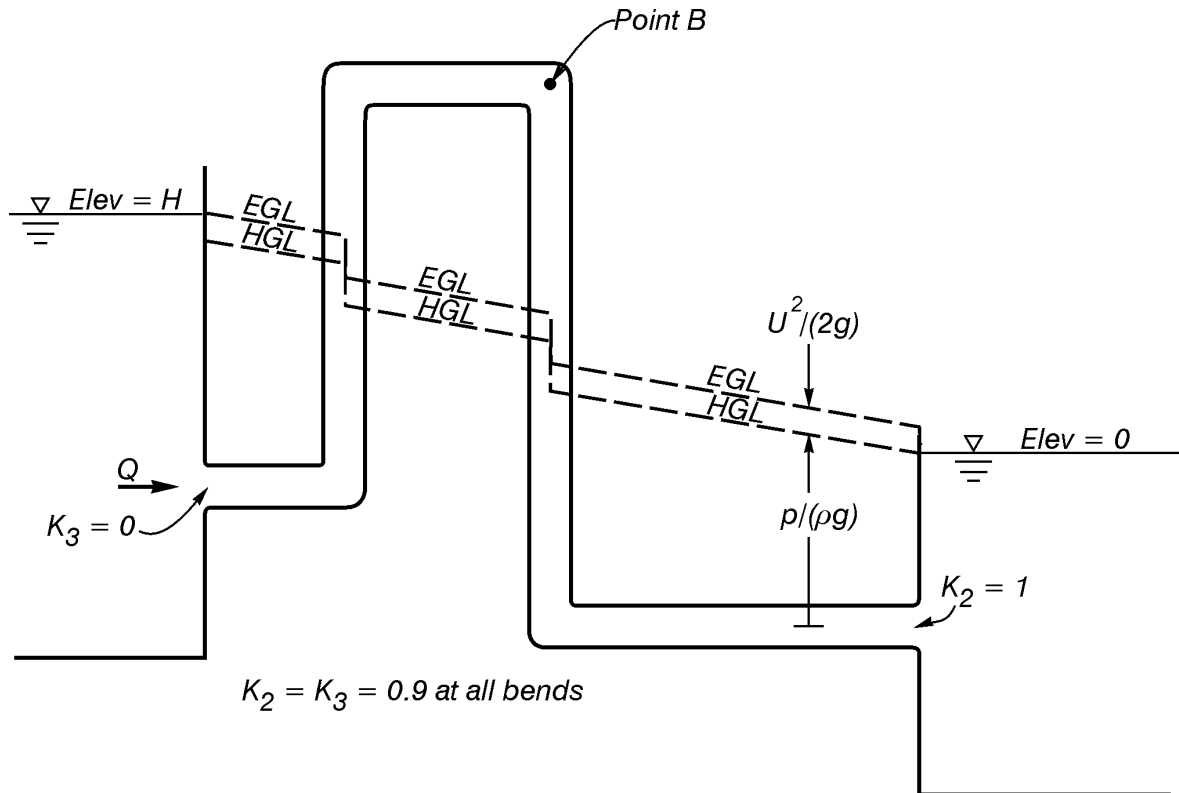
Sketch the EGL and HGL and write an equation that could be solved for the flow rate through the siphon shown in the sketch. Then determine the lowest negative pressure in the pipe.

Solution: The EGL and HGL are shown with dashed lines. Since the pipe entrance is rounded, $K_3 = 0$ and the EGL starts at the free surface elevation in the upstream reservoir. Friction losses in the vertical pipe sections and local losses at the four pipe bends cause vertical discontinuities in the EGL, and EGL slopes are the same for all horizontal sections of pipe since the pipe diameter is constant.

The HGL is parallel to the EGL and lies a vertical distance $U^2/2g$ below it. Furthermore, since pressures are known, from experiment, to be hydrostatic within a submerged jet entering a large reservoir, the HGL meets the free surface in the downstream reservoir. Pipe pressures are negative at points where the pipe centreline lies above the HGL.

Writing (11.1) between points on the free surfaces of the two reservoirs, where $U = 0$, gives the following equation to solve for Q:

$$H = 4(0.9)\frac{(Q/A)^2}{2g} + 1\frac{(Q/A)^2}{2g} + f\frac{L}{D}\frac{(Q/A)^2}{2g}$$

in which z has been measured upward from the downstream reservoir free surface. Since f depends upon Q, the solution of this equation would have to proceed by successive approximation.

Pressures within the pipe can be calculated once Q has been determined. Inspection of the relative elevations of the HGL and pipe centreline shows that the lowest negative pressure will occur either immediately downstream from point B or else further downstream. If p_B and z_B are the pressure and elevation of a point immediately downstream from point B, then an application of (11.1) between this point and a point further downstream in the vertical section of pipe gives

$$\frac{p_B}{\rho g} + z_B + \frac{(Q/A)^2}{2g} = \frac{p}{\rho g} + z + \frac{(Q/A)^2}{2g} + f \frac{(z_B - z)}{D} \frac{(Q/A)^2}{2g}$$

This equation can be put in the following form:

$$\frac{p}{\rho g} = \frac{p_B}{\rho g} + \left[1 - \frac{f}{D} \frac{(Q/A)^2}{2g} \right] (z_B - z)$$

Since p varies linearly with z, there can be no relative minimum for p. If the last term is positive, then an absolute minimum for p occurs when $(z_B - z) = 0$. If the last term is negative, then an absolute minimum occurs where $(z_B - z)$ attains a maximum positive value. However, the circled equation that was written to obtain Q shows that

$$f \frac{L}{D} \frac{(Q/A)^2}{2g} = H - 4(0.9) \frac{(Q/A)^2}{2g} - 1 \frac{(Q/A)^2}{2g} < H$$

This gives the inequality

$$\frac{f}{D} \frac{(Q/A)^2}{2g} < \frac{H}{L}$$

The problem sketch shows that $H/L < 1$, which leads to the following inequality:

$$\left[1 - \frac{f}{D} \frac{(Q/A)^2}{2g} \right] > 0$$

Thus, the minimum value of $p/(\rho g)$ occurs where $(z_B - z) = 0$

$$\boxed{ \text{Min} \left\{ \frac{p}{\rho g} \right\} = \frac{p_B}{\rho g} }$$

An application of (11.1) between a point on the upstream reservoir free surface and the point immediately downstream from point B gives

$$H = \frac{p_B}{\rho g} + z_B + \frac{(Q/A)^2}{2g} + 3\,(0.9)\,\frac{(Q/A)^2}{2g} + f\,\frac{L_B}{D}\,\frac{(Q/A)^2}{2g}$$

in which L_B = pipe length between point B and the upstream reservoir. This equation can be solved for the minimum pipe pressure, p_B. If p_B exceeds the vaporization pressure of water, then cavitation will not occur. (A brief discussion of cavitation is given in Chapter 9 in connection with Fig. 9.11.)

Hydraulic Machinery

A civil engineer sometimes needs to design pipe systems that contain pumps or turbines. The purpose of this section is to acquaint readers with a few of the fundamental ideas that are used to choose pumps or turbines for specific applications. More detailed discussions of hydraulic machinery are given in other texts, such as Streeter and Wiley (1981).

The power delivered to a system by a pump or extracted from a system by a turbine is given by

$$P = \rho g\,Q\,\Delta H_M \tag{11.7}$$

in which P = power in watts $\left(\text{W} = \text{N} - \text{m/s} = \text{kg} - \text{m}^2/\text{s}^3\right)$, ρ = fluid mass density $\left(\text{kg/m}^3\right)$, g = gravitational constant $\left(\text{m/s}^2\right)$, Q = flow rate (m^3/s) and ΔH_M = change in Bernoulli sum across the machine (m). The output power required from a motor to drive a pump shaft is obtained by dividing (11.7) by the pump efficiency, and the power delivered by a turbine is obtained by multiplying (11.7) by the turbine efficiency. Linsley and Franzini (1955) suggest that impulse, Francis, propeller and Kaplan turbines can have efficiencies as high as 80 to 95 per cent. Peak efficiencies for centrifugal pumps are of the order of 80 to 90 per cent.

Equation (11.1) must be modified when hydraulic machinery is present. The modification takes the form

$$h_1 + \frac{U_1^2}{2g} = h_2 + \frac{U_2^2}{2g} + H_L \pm \Delta H_M \tag{11.8}$$

in which the plus and minus signs in front of ΔH_M are used for a turbine and pump, respectively. The correct sign is easily remembered since a turbine subtracts energy from a flow and a pump adds energy. Consequently, when sketching an EGL, a step decrease in elevation of the EGL occurs at a turbine and a step increase at a pump.

Turbines are usually designed individually for each specific application. Pumps, however, are mass produced, and pump manufacturers routinely provide pump characteristic curves for their
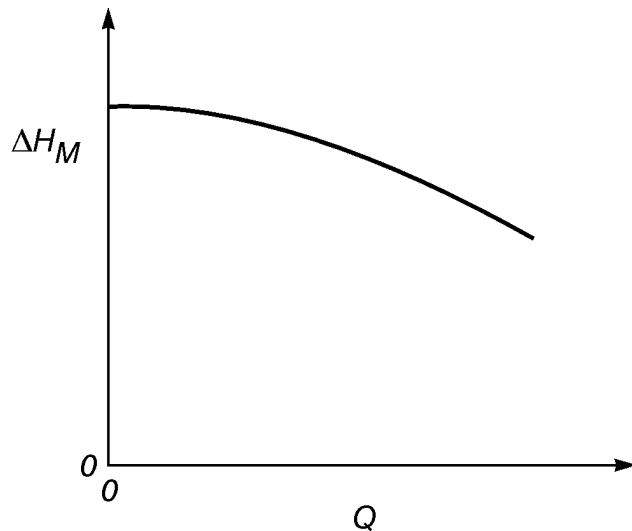
Figure 11.1 A typical characteristic curve for a centrifugal pump.

products.[*] The most important of these curves from our standpoint is a plot of ΔH_M versus Q. An example of a typical characteristic curve for a centrifugal pump is shown in Fig. 11.1.

Sometimes it becomes necessary to connect two or more pumps in either series or parallel. In this case a single equivalent characteristic curve can be constructed from the curves for each pump by remembering that Q is constant and ΔH_M additive for two pumps connected in series, as shown in Fig. 11.2. When pumps are connected in parallel, ΔH_M is constant and Q is additive, as shown in Fig. 11.3.
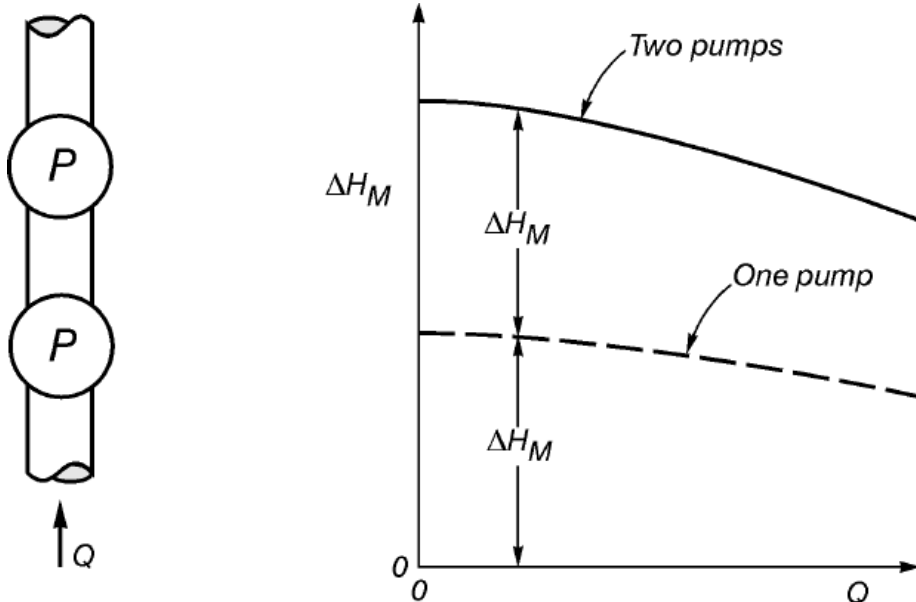
Figure 11.2 An equivalent pump characteristic curve for two pumps connected in series

Choosing a pump to deliver a specified discharge, Q, generally requires the following steps:

1   Apply Eq. (11.8) with the specified Q to calculate ΔH_M.

2   Choose from a set of characteristic curves supplied by a pump manufacturer a pump that will supply the given Q and calculated ΔH_M at a reasonably high efficiency.

3   Choose a motor that will provide sufficient power to turn the pump shaft.

---

[*]   It is possible to use a pump in reverse as a turbine for relatively small applications. Efficiencies are likely to be reduced, however.
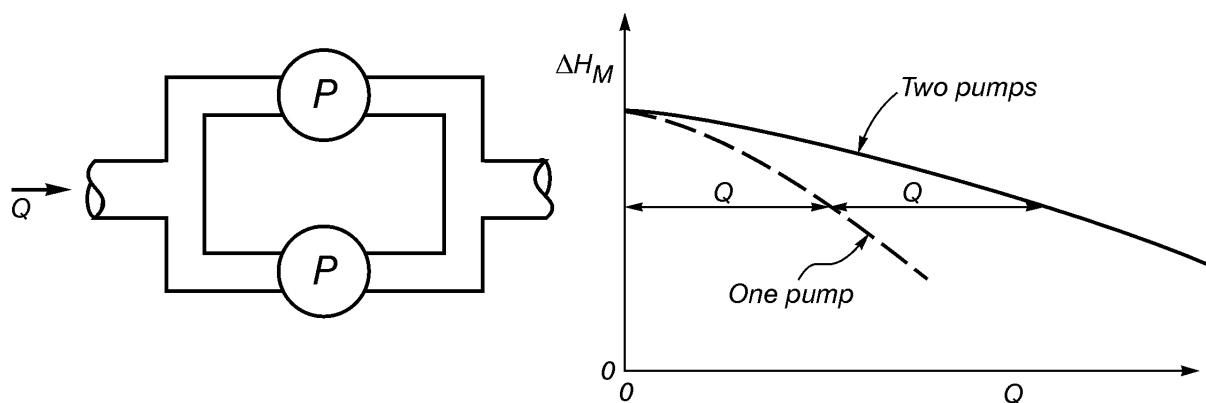
Figure 11.3 An equivalent pump characteristic curve for two pumps connected in parallel.

In some applications it becomes necessary to calculate the flow rate, Q, delivered by a pipe system that has a given pump already in place. This requires the simultaneous solution of Eq. (11.8) and a pump characteristic curve that plots Q versus ΔH_M. The solution is obtained by using (11.8) to calculate and plot ΔH_M for a number of specified values of Q for the pipe system. The intersection of this system curve with the pump characteristic curve gives the operating point, as shown in Fig. 11.4.
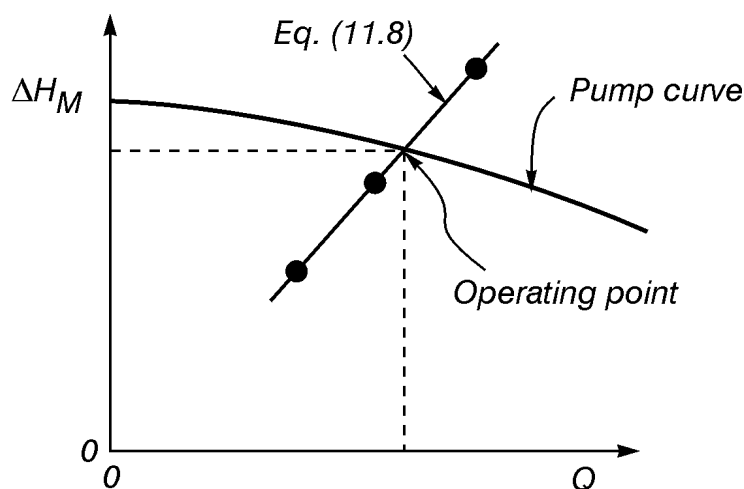
Figure 11.4 Calculation of ΔH_M and Q for a given pump installed in a pipe system.

Example 11.4
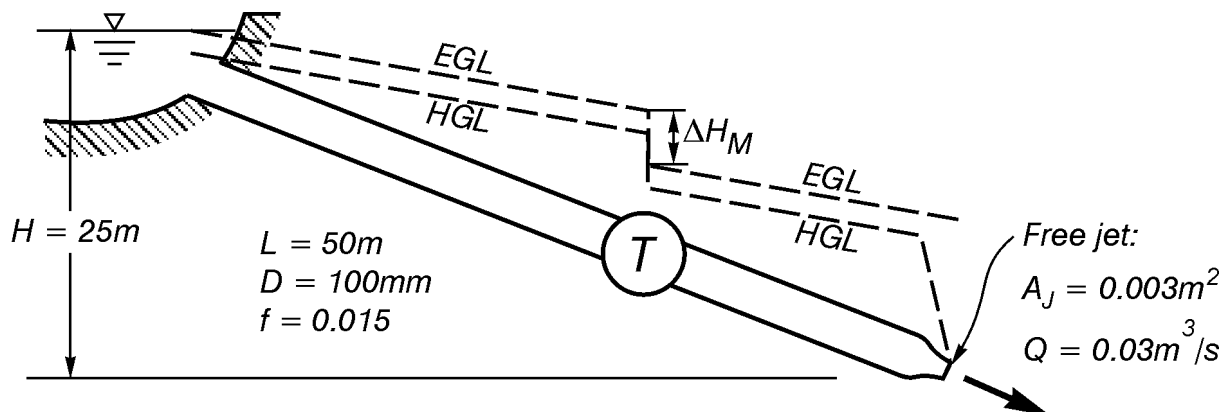
A flow of 0.03 m³/s can be diverted from a small stream through a 50 m length of pipe and discharged as a free jet at a point 25 m below the free surface of the stream intake. Neglect local losses and assume an efficiency of 100 per cent to calculate the maximum amount of power that could be produced by placing a turbine in the pipe line.

Solution: The EGL and HGL are shown in the sketch. A step decrease in elevation of these lines occurs at the turbine location. Application of Eq. 11.8) between a point on the free surface above the intake and a point in the free jet gives the following result:

$$H = \frac{(Q/A_J)^2}{2g} + f\frac{L}{D}\frac{(Q/A)^2}{2g} + \Delta H_M$$

Substitution of the given numbers leads to the result

$$\Delta H_M = 14.3 \text{ m}$$

Equation (11.7) can now be used to calculate the power extracted from the flow, which would also be the power produced by the turbine if it were 100 per cent efficient.

$$P = \rho g Q \, \Delta H_M = (1000)(9.81)(0.03)(14.3) = 4,220 \text{ W}$$

$$\boxed{P = 4.22 \text{ kW}}$$

An 80 per cent efficiency would reduce P to 3.37 kW.

Example 11.5
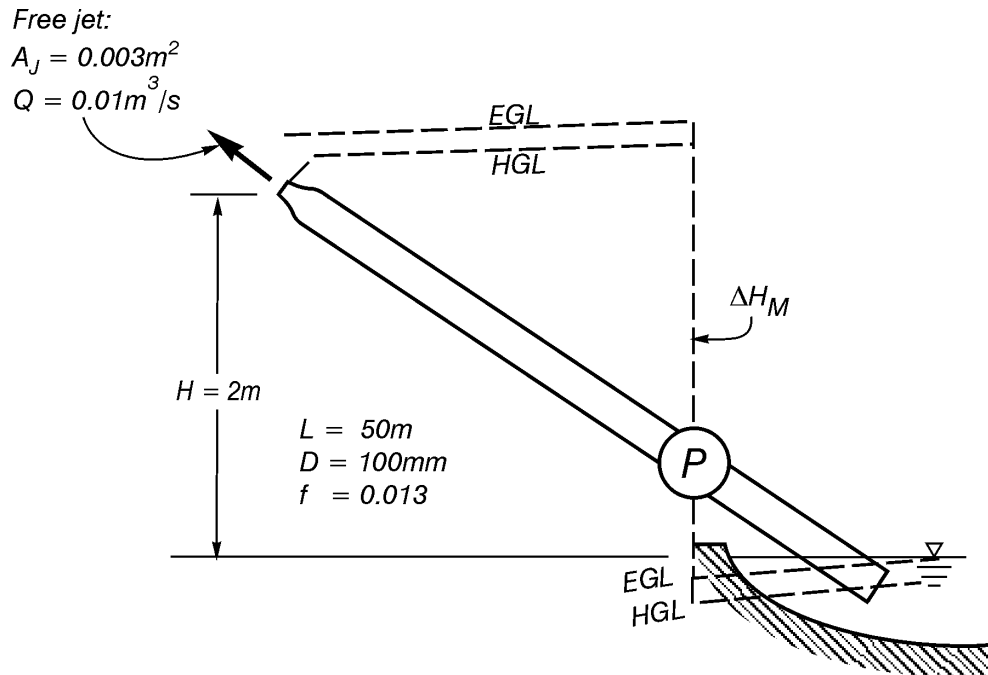
A pump is to be used to force 0.01 m³/s of water through a 50 m length of pipe to a point 2 m above the intake free surface. Calculate the value of ΔH_M that must be supplied by the pump. Then estimate the power that must be used to drive the pump if the pump and motor together are 80 per cent efficient. Neglect all local losses.

Solution: The EGL and HGL are shown in the sketch. A step increase in elevation of these lines occurs at the pump location. Furthermore, the pipe centreline lies above the HGL between the reservoir and pump, which means that pressures in this region are negative. The magnitude of these negative pressures can be reduced by moving the pump to as low an elevation as possible.

If a local loss at the pipe entrance is neglected, Eq. (11.8) can be applied between a point on the intake free surface and a point in the free jet to obtain

$$ 0 \ = \ H \ + \ \frac{\left(Q/A_J\right)^2}{2g} \ + f \ \frac{L}{G} \ \frac{\left(Q/A\right)^2}{2g} \ - \ \Delta H_M $$

Substituting the given numbers leads to the following value of ΔH_M :

$$ \boxed{\Delta H_M \ = \ 3.10 \ \text{m}} $$

The values of ΔH_M and Q could be used with a manufacturer's set of pump characteristic curves to choose a pump and motor for this application. If the pump and motor are 80 per cent efficient, the power required to drive the system can be estimated from Eq. (11.7).

$$P = \frac{\rho g \, Q \, \Delta H_M}{\text{efficiency}} = \frac{(1000)(9.81)(0.01)(3.10)}{(0.80)}$$

$$\boxed{P = 380 \ \text{W} = 0.380 \ \text{kW}}$$

Pipe Network Problems

We will define a pipe network to be any system that contains at least one junction where three or more pipes meet. Some examples are shown in Fig. 11.5. It is normally assumed when working these problems that piezometric head and friction loss terms dominate the Bernoulli equation. This means that Eqs. (11.1) and (11.4) are approximated with

$$h_1 - h_2 = f \frac{L}{D} \frac{(Q/A)^2}{2g} \tag{11.9}$$

and Eq. (11.2) is replaced with the following equation at each junction:

$$\sum_j Q_j = 0 \tag{11.10}$$

in which flows out and into the junction are taken as positive and negative, respectively. When Eq. (11.9) is written for every pipe in the network and Eq. (11.10) for every pipe junction, specification of h at one or more pipe ends or junctions gives enough equations to solve for h at every pipe junction and Q through every pipe.

Pipe network problems can be formulated so that the unknowns are either flow rates or piezometric heads. Since Eq. (11.9) is nonlinear, either method requires the use of successive approximation to solve a set of simultaneous, nonlinear equations. Large pipe networks can contain many pipes, and computers are an essential ingredient in the solution of these problems. In the writer's opinion it is easier to both understand and program the formulation in which piezometric heads are unknowns, and this will be the only formulation that will be considered herein. Readers will find the second formulation, in which flow rates are unknowns, described in most other texts. In either case, solution for one set of unknowns leads to a direct calculation of the other set from Eq. (11.9).

A typical junction in a pipe network is shown in Fig. 11.6. The junction under consideration is labelled 0, and the numbers 1 - 4 denote the other end of pipes meeting at 0. (The number of pipes joined at 0 is arbitrary. There is no particular reason for using four pipes in Fig. 11.6). The external flow at node 0 is denoted by Q_0 and has a sign that is positive for outflow and negative for inflow. The resistances, R_j, for each pipe are defined by the following equation:
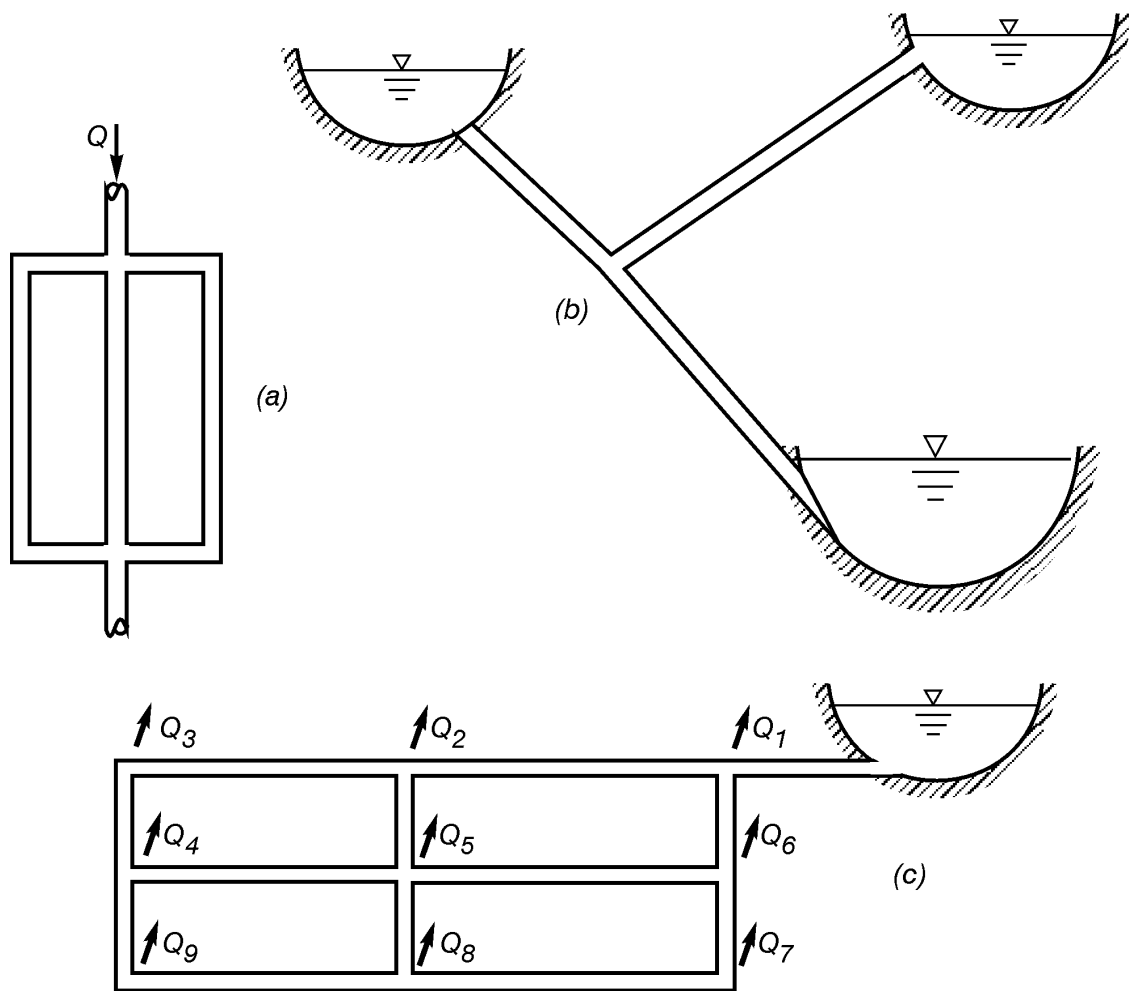
Figure 11.5 Some examples of pipe networks.
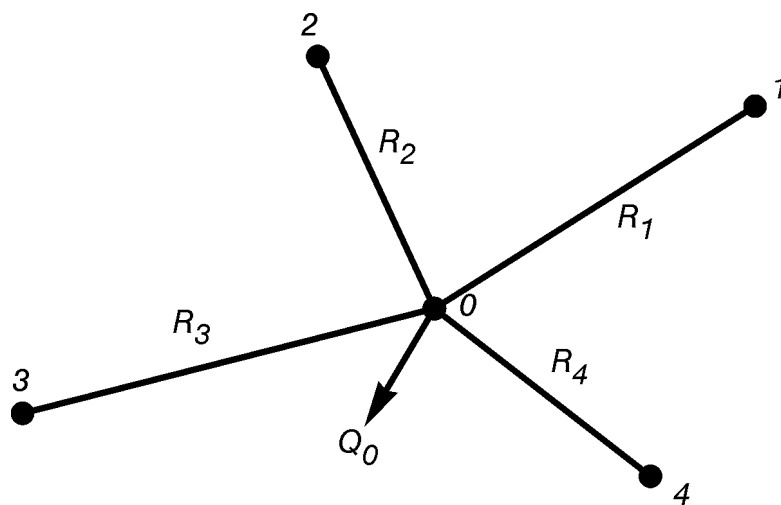
Figure 11.6 A typical junction in a pipe network.

$$Q_j = R_j \left(h_0 - h_j \right) \tag{11.11}$$

in which, since $R_j > 0$, the sign of Q_j is determined by the sign of $\left(h_0 - h_j \right)$. Thus, Q_j is also positive and negative for outflow and inflow, respectively. Expressions for R_j will be given later.

Substituting (11.11) into (11.10) and using the definition of Q_0 gives the following equation, which has values of h at nodes 0 through 4 as its only unknowns:

$$Q_0 + \sum_{j=1}^{4} R_j \left(h_0 - h_j \right) = 0 \tag{11.12}$$

By writing a similar equation for every node at which h is unknown, and by specifying values of h at the remaining nodes, we obtain as many equations as unknown values of h. These equations can be solved by using either a direct method, such as Gaussian elimination, or by an iterative technique, such as the Gauss-Seidel iteration. Iterative techniques are probably easier to program and more efficient for this application. The Gauss-Seidel iteration uses Eq. (11.12) in the following form:

$$h_0 = \frac{-Q_0 + \sum_{j=1}^{N} R_j \, h_j}{\sum_{j=1}^{N} R_j} \tag{11.13}$$

in which the upper limit on the sum has been changed to N to allow any number of pipes to be joined at node 0. The iteration proceeds by using the last approximations for h_j in the right side of (11.13) to calculate the newest approximation for h_0. Calculations terminate when values of h cease to change significantly at all nodes for any two successive cycles in the iteration.

Varga (1962) shows that the Gauss-Seidel iteration will always converge from any starting values of h_i if the governing equations are both linear and irreducibly diagonally dominant. Equation (11.12) satisfies these criteria for laminar flow when h is specified at one or more nodes in the network. In this case Eq. (11.9) and $f = 64/Re$ give the following constant value for R_j:

$$R_j = \frac{\pi}{128} \frac{g D^4}{\nu L} \tag{11.14}$$

In most instances, however, flow is turbulent. Then R_j depends upon h, Eq. (11.12) becomes nonlinear and there are no theorems to guarantee convergence. Nevertheless, Isaacs and Mills (1980) report satisfactory convergence in applications they have considered. Equation (11.9) shows that R_j has the following value for turbulent flow:

$$R_j = \frac{\pi D^2}{4} \sqrt{\frac{2g\,D/L}{f\,|\,h_0 - h_j\,|}} \tag{11.15}$$

Equation (11.15) never gives a singular value for R_j since a small value of $|\,h_0 - h_j\,|$ leads to a small Reynolds number and requires the use of (11.14) for laminar flow. This is one minor detail in which the formulation considered herein differs from the formulation used by Isaacs and Mills (1980), who effectively set $R_j = 0$ when $|\,h_0 - h_j\,|$ became smaller than a specified value.

A computer coding for the solution of pipe network problems requires a convenient way of calculating f for use in (11.15). Swamee and Jain (1976) obtained the following explicit approximation for f:

$$f = \frac{1.325}{\left[\ln\left(\dfrac{\epsilon/D}{3.7} + 5.74\,Re^{-0.9} \right) \right]^2} \quad \text{for } 10^{-6} \le \frac{\epsilon}{D} \le 10^{-2} \tag{11.16}$$

$$\text{and } 5000 \le Re \le 10^8$$

Values of f computed from (11.16) are within one per cent of values computed from the following Colebrook implicit equation that was used to construct the Moody diagram in Fig. 7.18:

$$f = \frac{1.325}{\left[\ln\left(\dfrac{\epsilon/D}{3.7} + \dfrac{2.51}{Re\sqrt{f}} \right) \right]^2} \tag{11.17}$$

Equations (11.14)–(11.16) do not cover the transition zone $2000 < Re < 5000$. The computer program given at the end of this chapter uses (11.14) for $0 \le Re \le 2000$ and (11.15)–(11.16) for $Re > 2000$.

Example 11.6

The problem shown in Fig. 11.5 b has the following data:
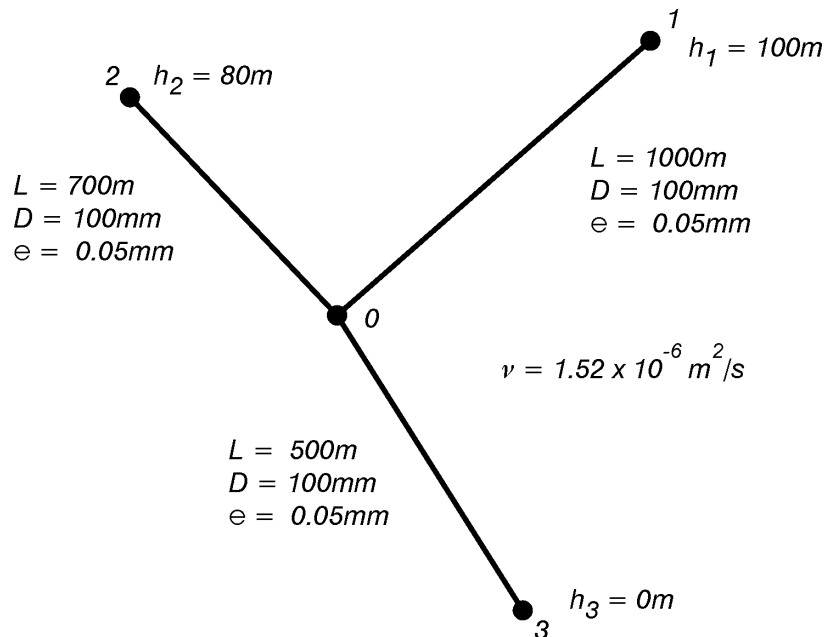
Use Eq. (11.13) to calculate h_0 and the flow rate in each of the three pipes.

Solution: Values of R_j for each of the three pipes are as follows:

$$R_1 = 0.0158 \qquad \text{for } 0 \leq Re \leq 2000$$

$$= \frac{0.000348}{\sqrt{f_1 \, | h_0 - h_1 |}} \qquad \text{for } Re > 2000$$

$$R_2 = 0.0226 \qquad \text{for } 0 \leq Re \leq 2000$$

$$= \frac{0.000416}{\sqrt{f_2 \, | h_0 - h_2 |}} \qquad \text{for } Re > 2000$$

$$R_3 = 0.0317 \qquad \text{for } 0 \leq Re \leq 2000$$

$$= \frac{0.000492}{\sqrt{f_3 \, | h_0 - h_3 |}} \qquad \text{for } Re > 2000$$

The relative roughness is the same for all pipes.

$$\frac{\epsilon}{D} = 0.0005$$

Reynolds numbers for each pipe are given by the following expression:

$$Re_j = 8.38 \times 10^6 \, | Q_j |$$

Since $Q_0 = 0$, $h_1 = 100$ m, $h_2 = 80$ m, and $h_3 = 0$ m, Eq. (11.13) reduces to

$$h_0 = \frac{100\,R_1 + 80\,R_2}{R_1 + R_2 + R_3}$$

Values of Q_j from the previous cycle are used to compute Re_j and f_j, which means that guessed values for f_j must be used for the first cycle. The following table summarizes the remaining calculations:

Cycle	h_0 m	f_1	f_2	f_3	Q_1 (m^3/s)	Q_2	Q_3
1	50.0	0.017	0.017	0.017	-0.0189	-0.0207	0.0267
2	58.0	0.0194	0.0192	0.0187	-0.0162	-0.0141	0.0274
3	59.9	0.0197	0.0200	0.0187	-0.0157	-0.0132	0.0278
4	60.6	0.0197	0.0201	0.0187	-0.0156	-0.0129	0.0280
5	60.9	0.0198	0.0202	0.0187	-0.0155	-0.0128	0.0281
6	61.0	0.0198	0.0202	0.0187	-0.0154	-0.0128	0.0281
7	61.0	0.0198	0.0202	0.0187	-0.0154	-0.0128	0.0281

Since no change occurs in the calculated results from cycle 6 to cycle 7, the final answers are

$$h_0 = 61.0 \text{ m}$$

$$Q_1 = -0.0154 \text{ m}^3/\text{s} \quad \text{(inflow)}$$

$$Q_2 = -0.0128 \text{ m}^3/\text{s} \quad \text{(inflow)}$$

$$Q_3 = 0.0281 \text{ m}^3/\text{s} \quad \text{(outflow)}$$

Despite the fact that the solution ceased to change after six cycles, continuity is not satisfied exactly at the junction.

$$Q_1 + Q_2 + Q_3 = -0.0001 \neq 0$$

This error, which is about 0.4 per cent of the flow rate Q_3, can be reduced by retaining more significant figures in the calculations.

Pipe Network Computer Program

The listing for a computer program that uses (11.13) - (11.16) to solve pipe network problems is shown in Fig. 11.7. The program has been designed to require a minimum amount of input data, with definitions for the input data variables shown in comment statements at the beginning. The piezometric head must be specified for at least one node, which is a requirement for uniqueness. (If h is not specified for at least one node, then the same arbitrary constant can be added to h at all nodes without changing the flow rate through any of the pipes. This is because the flow rate through each pipe depends only upon the difference between values of h at its two ends, and the arbitrary additive constant cancels when calculating this difference.) The external flow rate, Q_0, must be specified at all nodes for which h is not specified. Thus, either Q_0 or h, but not both, must be specified for every node in the network. An example of the use of this program for a network with 13 nodes and 18 pipes is shown in Figs. 11.8 - 11.9. Input data for this problem is printed in the first 32 lines of the output data shown in Fig. 11.9. Units of metres and seconds have been used for all variables in this example.

The program makes no allowance for pumps inserted in a network. However, a pump is easily included by placing nodes in the pipe immediately before and after the pump, as shown in Fig. 11.10. Then specification of an outflow and inflow with the same magnitudes at the upstream and downstream nodes, respectively, allows calculation of h at each node. The difference in these two values of h can be computed for the specified flow rate, and repeating this calculation for a number of different flow rates allows a system curve to be plotted on the pump characteristic curve. The intersection of the system and characteristic curves gives the operating point for the system.

Colebrook and White (1937) found that commercial pipe roughness heights generally increase linearly with time as the result of corrosion and deposition. The rate at which roughness increases with time can be determined for any given pipe only by measuring the friction factor, f, at two different times. This means that prediction of ϵ for a pipe often requires an educated guess. It also means that it is unrealistic to expect extremely accurate predictions from any pipe flow calculation.

```
C THIS CALCULATES SOLUTIONS FOR STEADY FLOW THROUGH PIPE NETWORKS
C Heads, H(I), are specified and external flows cannot be specified at nodes
C 1 through NH. External node flow rates, Q0(I), are specified and heads are
C unknown at nodes NH+1 through NQ. Other variable definitions follow:
C               NP = number of pipes
C               ERRA = allowable error
C               V = kinematic viscosity
C               H(I) = head at node I for I = 1 through NH
C               Q0(I) = external flow at node I for I = NH+1
C                       through NQ (outflows positive,
C                       inflows negative)
C If K = pipe number, then
C               L(K) = pipe length
C               D(K) = pipe diameter
C               E(K) = pipe roughness height
C               I1(K),I2(K) = node numbers at each pipe end
C Use a consistent set of units for all variables.
        REAL L
        DIMENSION H(100),Q0(100),L(100),D(100),E(100),I1(100),I2(100),
       1 N(100),ID(100,6),RL(100,6),RT(100,6),Q(100),F(100)
        OPEN(UNIT=1,FILE='INPUT.DAT',STATUS='OLD')
        OPEN(UNIT=2,FILE='OUTPUT.DAT',STATUS='NEW')
C
C Data is entered and written out.
C
        READ(1,*) NH,NQ,NP,ERRA,V
        WRITE(2,1000) NH,NQ,NP,ERRA,V
 1000   FORMAT(lX,'NH=',I3,2X,'NQ=',I3,2X,'NP=',I3,2X,'ERRA=',F9.6,
       1 2X,'V=',lPE10.2)
        DO 100 I=1,NH
        READ(1,*) J,H(I)
        WRITE(2,2000) J,H(I)
 2000   FORMAT(lX,'J=',I3,2X,'H=',F10.3)
  100   CONTINUE
        NH1=NH+1
        DO 150 I=NH1,NQ
        READ(1,*) J,Q0(I)
        WRITE(2,2500) J,Q0(I)
 2500   FORMAT(lX,'J=',I3,2X,'Q0=',F12.7)
  150   CONTINUE
        DO 200 I=1,NP
        READ(1,*) R,L(I),D(I),E(I),I1(I),I2(I)
        WRITE(2,3000) R,L(I),D(I),E(I),I1(I),I2(I)
 3000   FORMAT(1X,'R=',I3,2X,'L=',F6.0,2X,'D=',F6.3,2X,'E=',F8.5,
       1 2X,'I1=',I3,2X,'I2=',I3)
  200   CONTINUE
C
C Variables are initialised and connectivity is determined.
C
        G=9.806
        PI=3.141593
        DO 300 I=NH1,NQ
        N(I)=0
        H(I)=0.
  300   CONTINUE
        DO 400 K=1,NP
        F(R)=0.02
        N(Il(K))=N(Il(K))+1
        N(I2(K))=N(I2(K))+1
        ID(Il(K),N(Il(K)))=K
        ID(I2(K),N(I2(K)))=K
  400   CONTINUE
```

Figure 11.7 A computer program that solves pipe network problems.

```
C
C Coefficients are calculated
C
      DO 500 I=NH1,NQ
      NJ=N(I)
      DO 500 J=1,NJ
      K=ID(I,J)
      RL(I,J)=PI*G*D(K)**4/(V*L(K)*128.)
      RT(I,J)=SQRT(2.*G*D(K)/L(K))*PI*D(K)**2/4.
  500 CONTINUE
C
C The solution is calculated by iteration.
C
   10 ERRC=0.
      DO 600 I=NH1,NQ
      SUM1=-Q0(I)
      SUM2=0.
      NJ=N(I)
      DO 700 J=l,NJ
      K=ID(I,J)
          IF(I.EQ.Il(K)) THEN
              J1=I2(K)
          ELSE
              Jl=Il(K)
          ENDIF
      RE=4.*RT(I,J)*SQRT(ABS(H(I)-H(Jl))/F(K))/(PI*V*D(R))
          IF(RE.GT.2000) THEN
              C=RT(I,J)/SQRT(F(K)*ABS(H(I)-H(Jl)))
              SUM1=SUMl+C*H(J1)
              SUM2=SOM2+C
          ELSE
              C=RL(I,J)
              SUM1=SUMl+C*H(J1)
              SUM2=SOM2+C
          ENDIF
  700 CONTINUE
      A =SUM1/SUM2
      ERRC=ERRC+(H(I)-A)**2
      H(I)=A
  600 CONTINUE
      DO 750 K=1,NP
      C=SQRT(2.*G*D(K)*ABS(H(Il(K))- (I2(K)))/(F(K)*L(K)))
      RE=C*D(K)/V
          IF(RE.GT.2000) THEN
              Q(K)=C*PI*D(K)**2/4.
              F(K)=1.325/(ALOG(E(K)/(3.7*D(K))+5.74/RE**0.9))**2
          ELSE
              C=PI*G*D(K)**4/(V*L(K)*128.)
              Q(K)=C*(ABS(H(I1(K))-H(I2(K))))
          ENDIF
  750 CONTINUE
      ERRC=SQRT(ERRC)
      IF(ERRC.GT.ERRA) GO TO 10
C
C The solution is written out.
C
      DO 800 I=1,NQ
      WRITE(2,4000) I,H(I)
 4000 FORMAT(lX,'H(',I3,')=',Fl0.3)
  800 CONTINUE
      DO 900 K=l,NP
      WRITE(2,5000) K,Q(K)
 5000 FORMAT(lX,'Q(',I3,')=',Fl2.7)
  900 CONTINUE
      END
```

Figure 11.7 A computer program that solves pipe network problems, (continued).
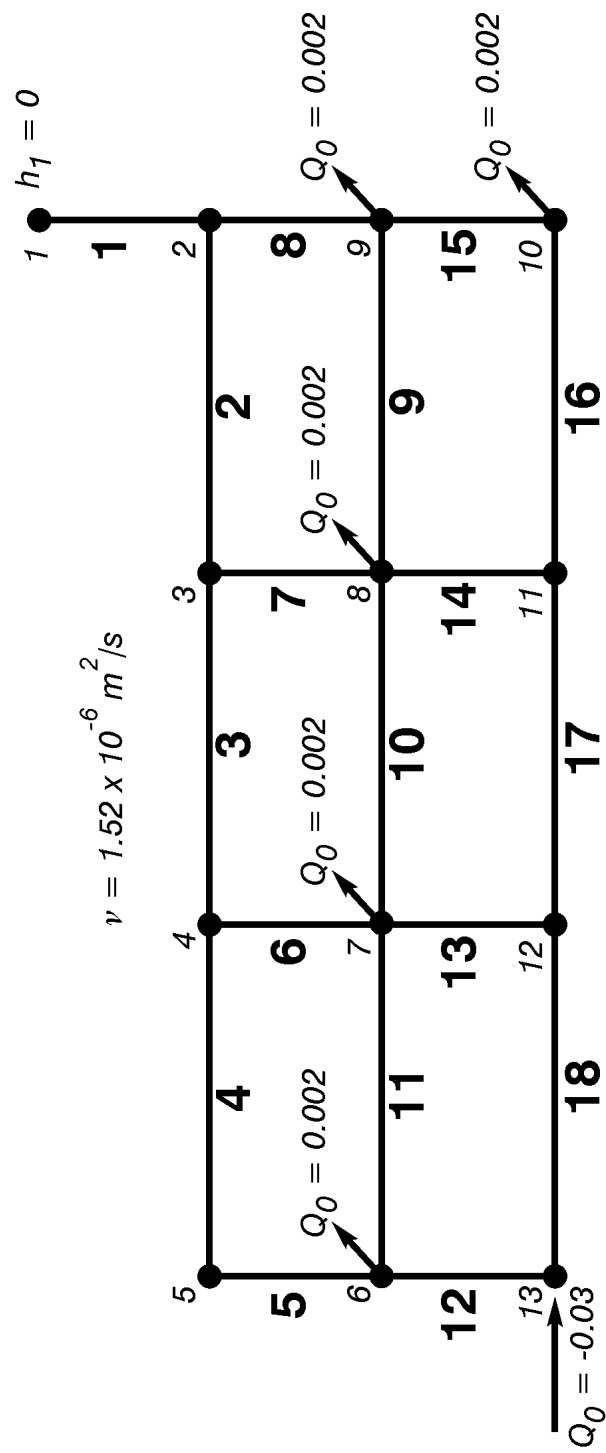
Figure 11.8 The pipe network used for a computer solves example. Units of metres and seconds have been used for all variables.

```
NH= 1 NQ= 13 NP= 18 ERRA= 0.000100 V= 1.52E-06
J=  1  H=     0.000
J=  2  Q0=   0.0000000
J=  3  Q0=   0.0000000
J=  4  Q0=   0.0000000
J=  5  Q0=   0.0000000
J=  6  Q0=   0.0020000
J=  7  Q0=   0.0020000
J=  8  Q0=   0.0020000
J=  9  Q0=   0.0020000
J= 10  Q0=   0.0020000
J= 11  Q0=   0.0000000
J= 12  Q0=   0.0000000
J= 13  Q0=  -0.0300000
K=  1  L=   50.  D= 0.100  E= 0.00010  I1=   1     I2=  2
K=  2  L=  100.  D= 0.100  E= 0.00010  I1=   2     I2=  3
K=  3  L=  100.  D= 0.100  E= 0.00010  I1=   3     I2=  4
K=  4  L=  100.  D= 0.100  E= 0.00010  I1=   4     I2=  5
K=  5  L=   50.  D= 0.100  E= 0.00010  I1=   5     I2=  6
K=  6  L=   50.  D= 0.100  E= 0.00010  I1=   4     I2=  7
K=  7  L=   50.  D= 0.100  E= 0.00010  I1=   3     I2=  8
K=  8  L=   50.  D= 0.100  E= 0.00010  I1=   2     I2=  9
K=  9  L=  100.  D= 0.100  E= 0.00010  I1=   9     I2=  8
K= 10  L=  100.  D= 0.100  E= 0.00010  I1=   8     I2=  7
K= 11  L=  100.  D= 0.100  E= 0.00010  I1=   7     I2=  6
K= 12  L=   50.  D= 0.100  E= 0.00010  I1=   6     I2= 13
K= 13  L=   50.  D= 0.100  E= 0.00010  I1=   7     I2= 12
K= 14  L=   50.  D= 0.100  E= 0.00010  I1=   8     I2= 11
K= 15  L=   50.  D= 0.100  E= 0.00010  I1=   9     I2= 10
K= 16  L=  100.  D= 0.075  E= 0.00010  I1=  10     I2= 11
K= 17  L=  100.  D= 0.075  E= 0.00010  I1=  11     I2= 12
K= 18  L=  100.  D= 0.075  E= 0.00010  I1=  12     I2= 13
H(  1)=      0.000
H(  2)=      3.537
H(  3)=      5.798
H(  4)=      7.835
H(  5)=      9.283
H(  6)=     10.007
H(  7)=      7.872
H(  8)=      5.804
H(  9)=      4.300
H( 10)=      4.351
H( 11)=      5.817
H( 12)=      8.008
H( 13)=     14.048
Q(  1)=      0.0199846
Q(  2)=      0.0110251
Q(  3)=      0.0104352
Q(  4)=      0.0087135
Q(  5)=      0.0087140
Q(  6)=      0.0017234
Q(  7)=      0.0005931
Q(  8)=      0.0089600
Q(  9)=      0.0088906
Q( 10)=      0.0105191
Q( 11)=      0.0106966
Q( 12)=      0.0214111
Q( 13)=      0.0035476
Q( 14)=      0.0009684
Q( 15)=      0.0020705
Q( 16)=      0.0040710
Q( 17)=      0.0050406
Q( 18)=      0.0085888
```

Figure 11.9 Output data for the pipe network example shown in Fig. 11.8.
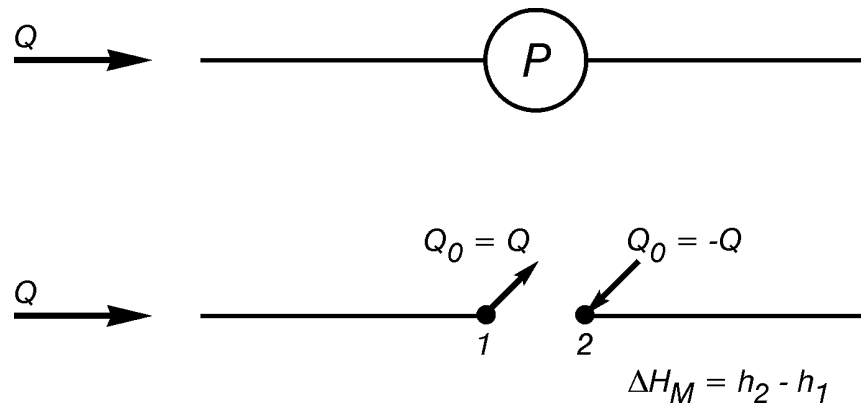
Figure 11.10 A method for including a pump in a pipe network problem.

References

Albertson, M.L., Barton, J.R. and D.B. Simons (1960). *Fluid mechanics for engineers*, Prentice-Hall, Englewood Cliffs, N.J., pp. 281-297.

Colebrook, C.F. and C.M. White (1937). The reduction of carrying capacity of pipes with age, *J. Inst. Civ. Eng. Lond.*, Vol. 7, pp. 99-118.

Isaacs, L.T. and K.G. Mills (1980). Linear theory methods for pipe network analysis, *ASCE J. Hyd. Div.*, Vol. 106, No. HY7, pp. 1191-1201.

Linsley, R.K. and J.B. Franzini (1955). *Elements of hydraulic engineering*, McGraw-Hill, New York, Ch. 12.

Streeter, V.L. and E.B. Wylie (1981). *Fluid Mechanics* (First SI metric edition), McGraw-Hill Ryerson, New York, Ch. 9.

Swamee, P.K. and A.K. Jain (1976). Explicit equations for pipe-flow equation, *ASCE J. Hyd. Div.*, Vol. 102, No. HY5, pp. 657-664.

Varga, R.S. (1962). *Matrix iterative analysis*, Prentice Hall, Englewood Cliffs, N.J. pp. 23, 73.

Chapter 12

Steady Open Channel Flow

Channelled flows with a free surface are known as open channel flows. Examples include flows in rivers, canals and drainage ditches. These flows are of traditional importance for civil engineers who work in the areas of water supply, flood control, hydropower, irrigation and drainage.

The study of steady flow in open channels can be divided into consideration of three separate types of flow. The first flow type is described as *rapidly varied*. In this flow changes in depth and velocity occur over relatively short lengths of channel. Typical control volume lengths are less than about ten channel depths, and example applications include flow beneath sluice gates, over weirs, spillways and humps and between side-wall constrictions and expansions. Since control volumes in these flows are relatively short, calculations usually neglect channel resistance and slope. However, energy losses from flow separation and turbulence are included when considering applications such as hydraulic jumps and sudden channel expansions.

The second type of flow is described as *gradually varied*. This flow has changes in depth and velocity that occur over relatively long lengths of channel. Typical control volume lengths are more than 100 channel depths. This means that channel resistance and slope play dominant roles and must be included in gradually varied flow calculations.

The third type of flow is described as *uniform*. It would probably be more accurate to describe this flow as fully developed rather than uniform since this is flow in which the free surface is parallel to the channel bottom and velocity distributions remain unchanged from one cross section to the next. This type of flow is seldom encountered in practice. However, approximations for energy losses that are used in gradually varied flow calculations are obtained from uniform flow equations. This means that uniform flow concepts are extremely important when studying gradually varied flow, even though examples of truly uniform flow are not common.

Rapidly Varied Flow Calculations

Rapidly varied flow calculations make use of three equations: the continuity equation, the Bernoulli or energy equation and the momentum equation. These are the same basic tools that were used in Chapter 4 except that the forms of these equations are a little more specialised. Initially we will consider flow in channels with rectangular cross sections, and changes that must be made when cross sections have more general shapes will be discussed later.

Variable definitions for rapidly varied flow in open channels are shown in Fig. 12.1. In rectangular channels it is convenient to define a flow rate per unit width, q, by

$$q = Uy \qquad \textbf{(12.1)}$$

in which $U(x)$ = flux velocity and $y(x)$ = flow depth. Thus, if the channel width, B, changes with distance, x, along the channel, the continuity equation takes the form

$$Q = q_1 B_1 = q_2 B_2 \tag{12.2}$$

in which Q is the constant flow rate and the subscripts 1 and 2 denote cross sections at two different values of x in the same flow.
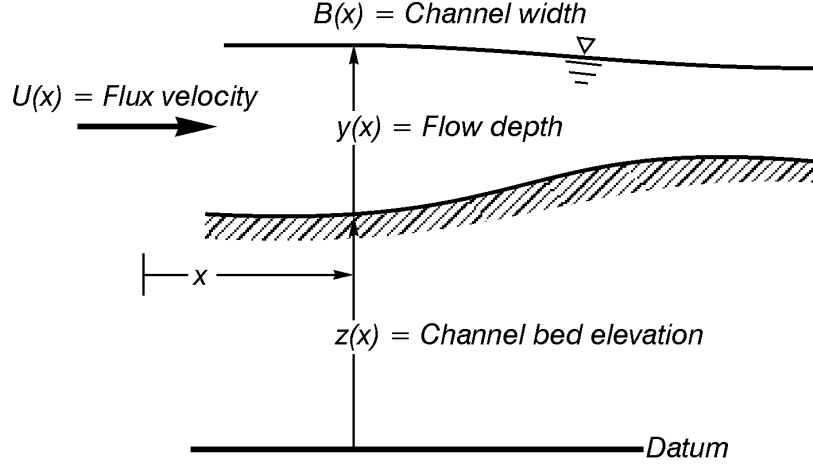
Figure 12.1 Definitions of variables used for rapidly varied flow in open channels.

It is also convenient to define a specific energy function, E, as

$$E = y + \frac{U^2}{2g} = y + \frac{q^2}{2g y^2} \tag{12.3}$$

This definition allows the Bernoulli or energy equation to be written in the form

$$z_1 + E_1 = z_2 + E_2 + E_L \tag{12.4}$$

in which z = channel bed elevation above an arbitrarily chosen horizontal datum plane, E_L = head loss and cross section 2 is downstream from cross section 1. The definition of E in (12.3) differs from an earlier use of this same letter in Eq. (4.13) by a factor of ρg. This switch in notation is excused on the grounds that the choice of notation in (12.3) is standard in most open channel flow texts.

In many applications both E and q in (12.3) are known numbers, and (12.3) must be solved for y. The resulting cubic equation may have two real positive roots. In other words, the solution of (12.3) for y is not unique until additional information is inserted into the problem for each application. This is one of the considerations that makes open channel flow calculations both challenging and interesting.

The best way to study solutions of (12.3) is to consider E as a function of y, with q a specified constant, rather than trying to calculate y as a function of E. (E is a single-valued function of y, whereas y is a multiple-valued function of E.) As $y \to \infty$, E has the asymptotic behaviour $E \sim y$, and, as $y \to 0$, $E \sim q^2/(2gy^2)$. Thus E becomes positively infinite as y approaches both zero and infinity. This means that E must have a minimum for some value of y in the range $0 < y < \infty$, as shown in Fig. 12.2.
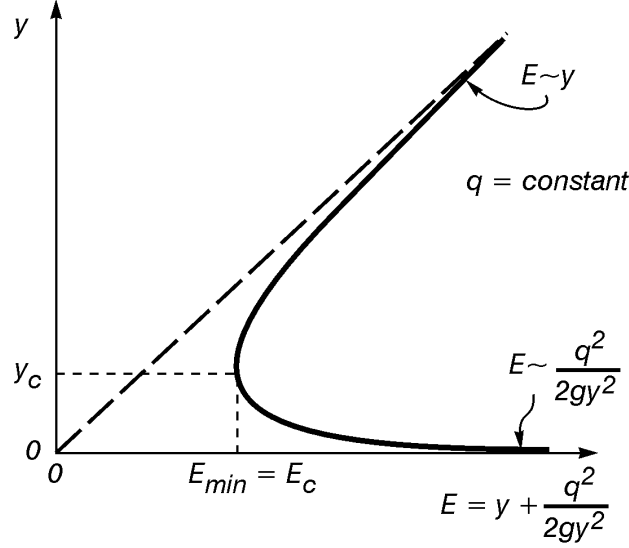
Figure 12.2 Behaviour of the specific energy function.

The value of y that makes $E(y)$ a minimum is called **_critical depth_** and is denoted by y_c, and the corresponding value of $E(y_c)$ is denoted by E_c. Since the derivative of (12.3) is given by

$$\frac{dE(y)}{dy} = 1 - \frac{q^2}{gy^3} \tag{12.5}$$

the requirement that $E(y)$ be a minimum at $y = y_c$ becomes

$$\frac{q^2}{gy_c^3} = 1 \tag{12.6}$$

Equation (12.6) gives critical depth as

$$y_c = \left(\frac{q^2}{g} \right)^{1/3} \tag{12.7}$$

Equation (12.6) also allows us to plot a generalized specific energy diagram, valid for all values of q, by eliminating q from (12.3) and (12.6) to obtain

$$\left(E/y_c\right) = \left(y/y_c\right) + \frac{1}{2\left(y/y_c\right)^2} \tag{12.8}$$

Equation (12.8) is plotted in Fig. 12.3. This generalized plot is useful in obtaining numerical solutions of rapidly varied flow problems. Equation (12.8) also shows that the minimum value of E at $y = y_c$ is given by

$$E_c = \frac{3}{2} y_c \tag{12.9}$$

Generally, flows in which $y > y_c$ are called **subcritical**, and flows in which $y < y_c$ are called **supercritical**. (Sometimes the terms "tranquil" or "streaming" are used to denote subcritical flow, and the terms "rapid" or "shooting" are used to denote supercritical flow. We will not use these terms.)

A relatively simple illustration of the use of the specific energy concept and Fig. 12.3 is provided by flow beneath the sluice gate shown in Fig. 12.4. We would expect on physical grounds to be able to calculate both upstream and downstream depths if q and the gate opening, y_G, are specified. Since the channel bottom is horizontal and energy losses are negligible, the Bernoulli equation gives

$$E\left(y_1\right) = E\left(y_2\right) \tag{12.10}$$

Equation (12.10) contains the two unknowns y_1 and y_2. A second equation with these same two unknowns is provided by the contraction coefficient relationship given in Chapter 6.

$$\frac{y_2}{y_G} = C_c \tag{12.11}$$

in which C_c is a function of y_G/y_1. Since C_c changes slowly with y_G/y_1, a previous estimate for y_1 can be used in (12.11) to calculate y_2, which in turn can be used in (12.10) to obtain an improved estimate for y_1. Several cycles of this method of successive approximation are usually sufficient to obtain reasonably accurate values for y_1 and y_2. Some examples follow.

The figure plots y/y_c (vertical axis, 0 to 3) against E/y_c (horizontal axis, 0 to 5). An inset box reads:

RECTANGULAR CROSS SECTIONS

$E = y + \dfrac{q^2}{2gy^2}$ Q = Flow rate (m^3/s)

$y_c = (q^2/g)^{1/3}$ B = Channel width (m)

$q = Q/B$ $g = 9.81 \ m/s^2$
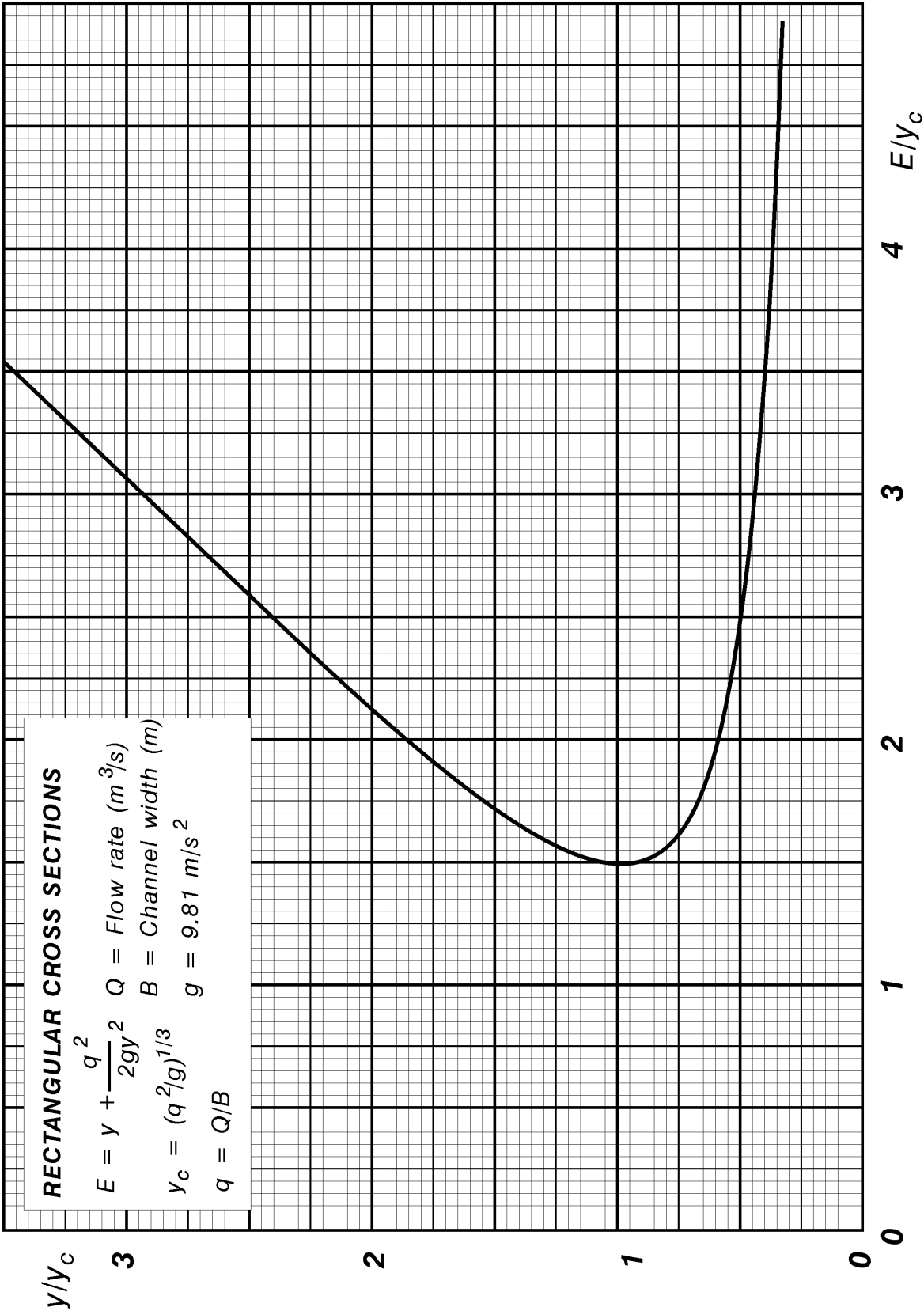
Figure 12.3 A generalized plot of the specific energy function.
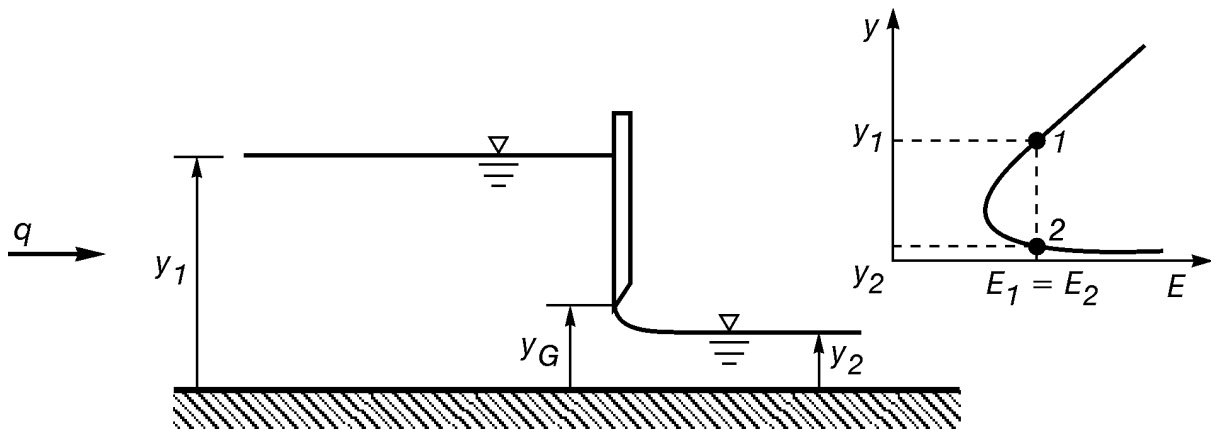
Figure 12.4 Use of specific energy for flow beneath a sluice gate.

Example 12.1

A sluice gate in a rectangular channel has a gate opening $y_G = 0.5$ m. Calculate y_1 and y_2 if $Q = 8$ m^3/s and $B = 4$ m.

Solution: Since $q = Q/B = 8/4 = 2$ m^2/s, critical depth is

$$y_c = \left(\frac{q^2}{g}\right)^{1/3} = \left(\frac{2^2}{9.81}\right)^{1/3} = 0.742 \text{ m}$$

The iterative process will be started by assuming that $C_c \approx 0.600$. Then $y_2 = 0.600\,y_G = 0.600\,(0.5) = 0.300$ m and

$$E_2 = y_2 + \frac{q^2}{2g\,y_2^2} = 0.3 + \frac{2^2}{2\,(9.81)\,(0.3)^2} = 2.57 \text{ m}$$

$$\therefore \;\; E_2/y_c = 2.57/0.742 = 3.46$$

Since flow at cross section 1 must be subcritical with $E_1 = E_2$, use of the larger value of y/y_c for $E_1/y_c = 3.46$ in Fig. 12.3 gives

$$y_1/y_c = 3.40$$

$$\therefore \quad\quad y_1 = 3.40\,y_c = 3.40\,(0.742) = 2.52 \text{ m}$$

Now we must check to see if the correct value of C_c was used initially. Since $y_G/y_1 = 0.5/2.52 = 0.200$, the contraction coefficient relationship given in Chapter 6 for flow beneath a sluice gate gives $C_c = 0.600$, which agrees exactly with our starting value. Hence, our final answers are

$$y_1 = 2.52 \text{ m}$$
$$y_2 = 0.300 \text{ m}$$

In most cases we would not be quite as lucky in our initial estimate for C_c, and one or two additional iterations might be required.

Example 12.2

Discuss the solution behaviour as y_1 decreases in Fig. 12.4.

Solution: Since $E_1 = E_2$, points 1 and 2 in the specific energy diagram must lie along the same vertical line. Thus, as y_1 decreases, y_2 must increase. This process continues until points 1 and 2 coincide at $y_1 = y_2 = y_c$. Since $C_c = 1$ when $y_G/y_1 = 1$ (this obvious result is outside the range of y_G/y_1 for which values of C_c are given in Chapter 6), we also see that $y_G = y_c$ at this critical point. Further decreases in y_1 will cause the flow to pass beneath the sluice gate without touching its lower edge. In this case points 1 and 2 will coincide and will be on the supercritical branch of the specific energy diagram in Fig. 12.4.

Example 12.3

Explain how y/y_c can be calculated by iteration from

$$\left(E/y_c\right) = \left(y/y_c\right) + \frac{1}{2\left(y/y_c\right)^2}$$

when $\left(E/y_c\right)$ is specified.

Solution: Some algebraic clutter can be eliminated by replacing $\left(E/y_c\right)$ and $\left(y/y_c\right)$ with E and y, respectively, to obtain

$$E = y + \frac{1}{2y^2}$$

For subcritical flow $\left(y > 1\right)$, the last term is relatively small. This suggests an iterative process in which the equation

$$y = E - \frac{1}{2y^2}$$

is solved by placing the last estimate for y in the right side to calculate the next estimate for y. Since convergence is fastest when a good starting value is used for y, it is suggested that E be used for the first approximation for y. An example for $E = 3.5$ is shown below, and convergence for larger values of E will be faster.

E = 3.50	
cycle	y
0	3.500
1	3.459
2	3.458
3	3.458

For supercritical flow $(y < 1)$, the first term on the right is relatively small. This suggests an iterative process in which the equation

$$y = 1 \Big/ \sqrt{2(E - y)}$$

is solved by placing the last estimate for y in the right side to calculate the next estimate for y. The first approximation for y should be $1 \big/ \sqrt{2E}$. An example for $E = 3.5$ is shown below, and convergence for larger values of E will be faster.

E = 3.50	
cycle	y
0	0.378
1	0.400
2	0.402
3	0.402

Newton's method provides a second approach to this problem. This method defines a function $f(y)$ by

$$f(y) = y + \frac{1}{2y^2} - E$$

The first derivative of $f(y)$ is

$$f'(y) = 1 - \frac{1}{y^3}$$

The first two terms of a Taylor's series expansion about $y = y_0$ are

$$f(y) = f(y_0) + f'(y_0)(y - y_0) + \cdots$$

If the series is truncated after the first two terms, and if $f(y)$ is set equal to zero, we obtain the following formula for y:

$$y = y_0 - \frac{f(y_0)}{f'(y_0)}$$

The last approximation for y is substituted in the right side for y_0 to calculate the next approximation for y.

Rates of convergence for these different methods are compared in the following table:

E	Starting Value for y	Final Answer for y	Number of Cycles for Convergence		
			Newton's Method	$y = E - \dfrac{1}{2y^2}$	$y = \dfrac{1}{\sqrt{2(E-y)}}$
1.55	1.550	1.207	3	10	—
1.55	0.568	0.838	4	—	11
2.00	2.000	1.855	2	3	—
2.00	0.500	0.597	3	—	4
3.00	3.000	2.942	1	2	—
3.00	0.408	0.442	2	—	2
4.00	4.000	3.968	1	2	—
4.00	0.354	0.371	2	—	2

In all cases, rates of convergence decrease as $E \rightarrow 1.50$ and increase as E becomes larger. Newton's method has a slightly more complicated iteration formula. On the other hand, Newton's method converges at a much faster rate for small values of E, and the same iteration formula is used for both subcritical and supercritical flow. There is not much difference in convergence rates for either of the methods when E is greater than about two.

Flow over a hump and the corresponding specific energy diagram are shown in Fig. 12.5. Since the hump has a maximum elevation of Δz, the Bernoulli equation becomes

$$E_1 = E_2 + \Delta z = E_3 \tag{12.12}$$

in which cross sections 1, 2 and 3 are upstream, on top of and downstream, respectively, from the hump. Equation (12.12) shows that $E_1 = E_3$ and $E_1 - E_2 = \Delta z$, a result which is shown graphically in the specific energy diagram of Fig. 12.5. If the approaching flow is subcritical $(y_1 > y_c)$, then the specific energy diagram shows that $y_2 < y_1$ and $y_1 = y_3$. If the approaching flow is supercritical $(y_1 < y_c)$, then the same diagram shows that $y_2 > y_1$ and $y_1 = y_3$.

One of the most interesting results for the flow in Fig. 12.5 occurs when Δz is allowed to increase. Then points 1 and 3 remain fixed in the specific energy diagram and point 2 moves leftward. This process continues until critical depth occurs at 2 and $y_2 = y_c$. Since point 2 can move no further leftward, any additional increase in Δz causes point 1 to move rightward. When the approaching flow is subcritical, y_1 increases and raises water levels upstream from the hump.

When the approaching flow is supercritical, y_1 suddenly increases to its subcritical value and creates a hydraulic jump upstream from the hump. At first glance, moving point 1 rightward when $y_1 < y_c$ causes y_1 to decrease. However, supercritical flow velocities are faster than the speed of a small wave or disturbance in still water.[*] This means that any disturbance or change in water level is rapidly swept downstream, and water levels in supercritical flow cannot be controller or changed from a downstream point. Therefore, the only possibility when point 1 moves rightward in Fig. 12.5 is to have subcritical flow form upstream from the hump, which sends a shock or surge in the upstream direction. This surge will eventually come to rest and become a hydraulic jump if the upstream channel is long enough. Thus, in either case moving point 1 rightward increases y_1, and the flow is said to be "choked".
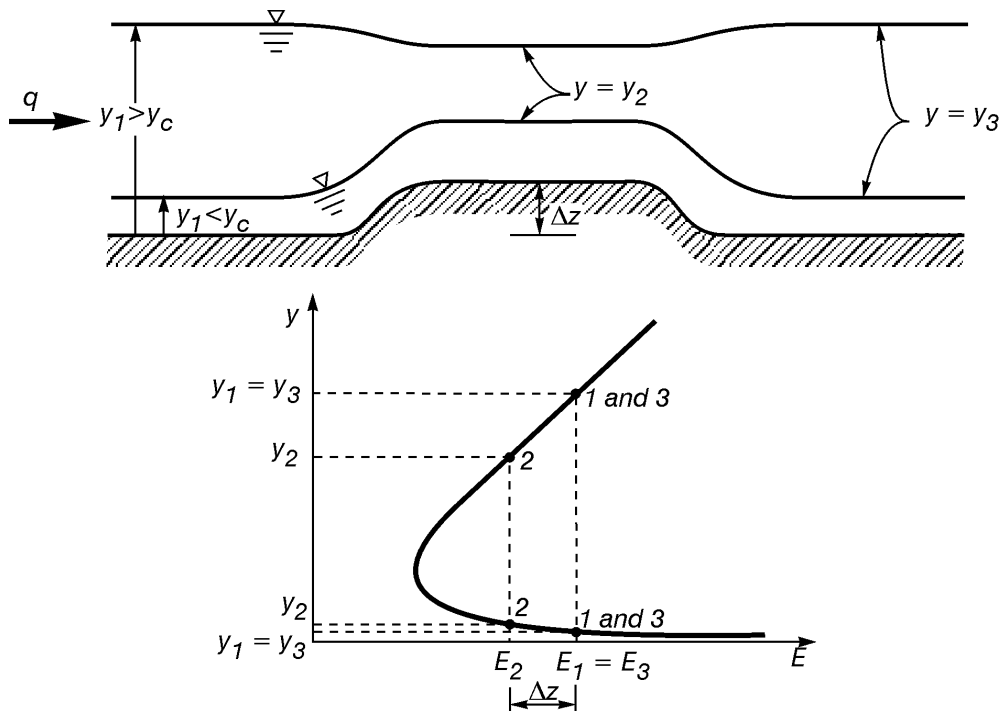

Figure 12.5 Supercritical and subcritical flow over a hump.

When the hump is sufficiently high to choke the flow, water levels at 3 may be either supercritical or subcritical. For example, a downstream sluice gate can be used to ensure subcritical flow at 3, and flows at cross sections 1, 2 and 3 are subcritical, critical or subcritical and subcritical, respectively. If no downstream control raises the water level at 3, then these

---

[*]   Since supercritical flow has $y < y_c$, Eq. (12.6) shows that supercritical flow is characterized by the requirement that $q^2/(gy^3) > 1$. Since $q = Uy$, this is equivalent to $U^2/gy > 1$ or

$$U > \sqrt{gy}$$

The theory of shallow water waves shows that the speed of an unbroken wave in still water is given by $\sqrt{gy}$. Thus, velocities in supercritical flow are greater than the wave speed of a disturbance. Likewise, consideration of Eq. (12.6) and $q = U_c y_c$ shows that critical conditions occur at a point where the flow velocity and wave speed are equal.

flows become subcritical, critical and supercritical, respectively. A sketch of these possibilities is shown in Fig. 12.6, in which (a) curve A results if the downstream depth is less than y_1, (b) curve B results if the downstream depth exactly equals y_1 and (c) curve C results if the downstream depth exceeds y_1. When curve A occurs, a hydraulic jump may or may not form further downstream from the hump. Curve C occurs when a downstream control completely submerges the hump. Flow downstream from a hump will be discussed again in the section on gradually varied flow.
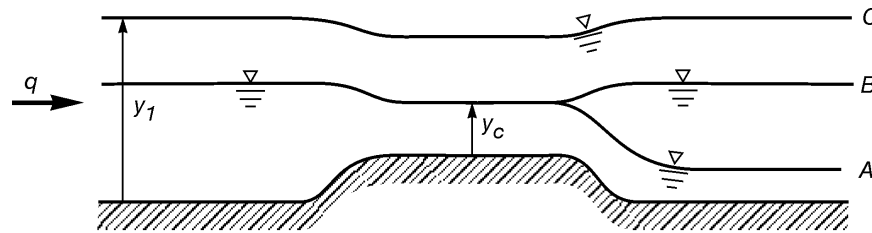

Figure 12.6 Choked flow over a hump.

Changes in cross section width, B, cause q to change according to Eq. (12.2). In this case Eq. (12.8) and Fig. 12.3 can still be used provided that different values for y_c are calculated at each cross section by using q_1 and q_2 in (12.7). However, a qualitative understanding of flow behaviour is best obtained from a dimensional plot of (12.3) for values of $q = q_1$ and $q = q_2$. If $q_2 > q_1$ (a constriction), then (12.3) shows that the curve for q_2 will lie to the right of the curve for q_1, as shown in Fig. 12.7.
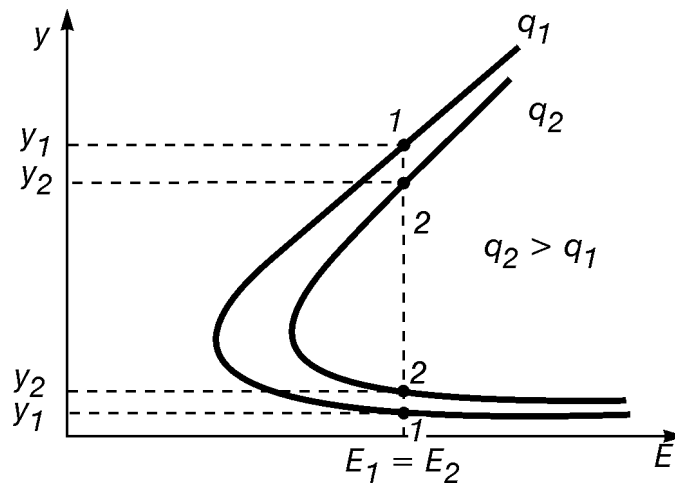
Figure 12.7 A plot of Eq. (12.3) for two different values of q.

If we consider the case in which a horizontal channel of width B_1 narrows to a width B_2, then $q_2 > q_1$ since $B_2 < B_1$. The different possibilities for this case are shown with dashed lines in Fig. 12.7. Since the Bernoulli equation requires $E_1 = E_2$, all operating points lie along the same vertical dashed line. If y_1 is subcritical, then $y_2 < y_1$; if y_1 is supercritical, then $y_2 > y_1$. If the constriction is narrowed further, then q_2 increases and the specific energy curve for q_2 moves rightward. This process continues until point 2 lies on the point of minimum E, where $y_2 = y_c$.

Any additional decrease in B_2 after critical conditions have been reached causes the vertical dashed line to move rightward with $y_2 = y_c$. In this case the flow becomes choked. If the approaching flow is subcritical, y_1 is increased and raises water levels upstream from the constriction. If the approaching flow is supercritical, then flow immediately upstream from the constriction suddenly becomes subcritical and sends a surge in the upstream direction. Depths downstream from the constriction are determined from the same considerations that are used in discussing flow downstream from a hump.

Non-rectangular Cross Sections

The extension of specific energy calculations to non-rectangular cross sections is straightforward. However, computational details are more difficult because relationships between area and depth are more complicated and because the flow rate per unit width, q, no longer has a meaning. This means that the specific energy must be calculated from

$$E = y + \frac{U^2}{2g} = y + \frac{Q^2}{2gA^2}$$

(12.13)

in which $A = A(y)$. Thus, plots of E versus y can be made and used in calculations, and the resulting curves and the solutions obtained from these curves will be similar to the corresponding results for rectangular cross sections. The more complicated relationship between area and depth makes it much more difficult to obtain a closed form solution for critical depth, and this usually makes it impractical to construct a generalized specific energy plot like the one shown in Fig. 12.3 for rectangular cross sections. This means that it is usually necessary to make dimensional plots of (12.13), like the plot shown in Fig. 12.8 for a trapezoidal cross section. The interpretation and use of dimensional specific energy diagrams for non-rectangular cross sections is straightforward once the principles for rectangular cross sections have been mastered.

Uniform Flow Calculations

Fully developed flow in an open channel is described as uniform. This is flow on a sloping channel bottom in which the free surface is parallel to the channel bottom and velocity distributions do not change with distance along the channel. Truly uniform flow conditions can be approached only in prismatic channels with very large ratios of length to depth. Nevertheless, uniform flow approximations are important because they are routinely used to estimate energy losses in gradually varied flows.

The free body diagram for a control volume of length Δx in uniform open channel flow is shown in Fig. 12.9. Pressure forces on end sections of the control volume have identical magnitudes and are not shown since they cancel out when summing forces. The pressure force exerted by the channel bottom on the control volume has also been omitted since we are only interested in forces parallel to the channel bottom. Since momentum fluxes at the two end sections have identical magnitudes, the momentum equation requires that the summation of forces parallel to the channel bottom vanish:

$$Q = 5\ m^3/s$$

$$A = 2y(2+y)m^2$$

$$E = y + \frac{1}{2(9.81)}\left[\frac{5}{2y(2+y)}\right]^2 m$$

$E_c = 0.704m$ at $y_c = 0.500m$

$E(m)$
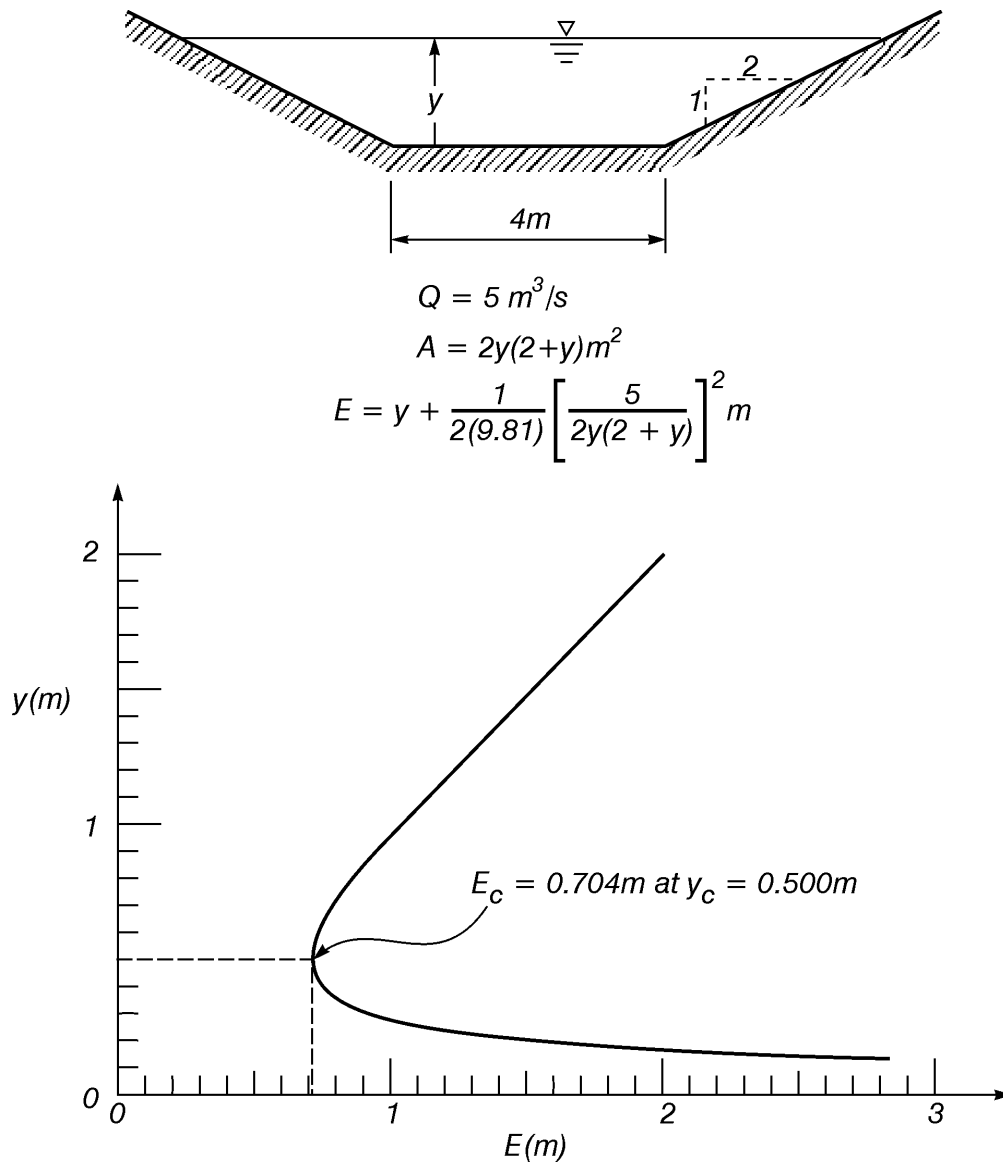
Figure 12.8 The dimensional specific energy diagram for a trapezoidal cross section.

$\rho g A \Delta x$

A = Cross sectional area
P_w = Wetted perimeter
τ = Channel bed shear

Δx

$\tau P_w \Delta x$
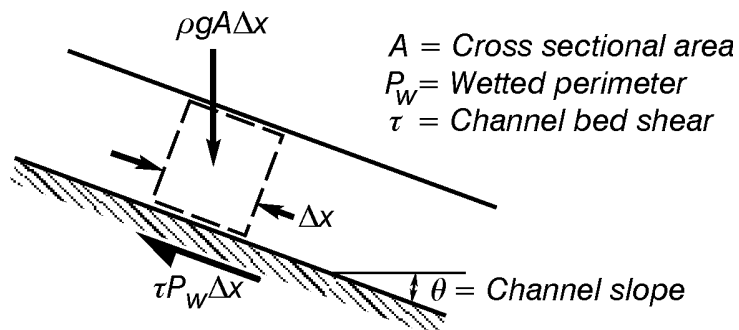
θ = Channel slope

Figure 12.9 The free body diagram for a control volume of length Δx in uniform flow.

$$\rho g A \, \Delta x \sin \theta \; - \; \tau P_w \, \Delta x \; = \; 0 \tag{12.14}$$

in which ρ = fluid mass density, g = gravitational constant, A = cross sectional area, Δx = control volume length, θ = channel bed slope, τ = channel bed shear stress and P_w = wetted perimeter of the cross section. Dividing (12.14) by Δx and using Eqs. (7.47) and (7.51) leads to the following expression for the flux velocity, $U \, (= Q / A)$:

$$U \; = \; \sqrt{\frac{8}{f} \, g R S_0} \tag{12.15}$$

in which $S_0 = \sin \theta$ = channel slope, f = Darcy-Weisbach friction factor and the hydraulic radius, R, is defined as the ratio of the cross sectional area to wetted perimeter.

$$R \; = \; \frac{A}{P_w} \tag{12.16}$$

The Bernoulli sum, H, for flow in a sloping channel is

$$H \; = \; E \; + \; z \tag{12.17}$$

in which E = specific energy [defined by (12.3) when slopes are small enough to allow $\cos \theta \approx 1$ and $\sin \theta \approx \tan \theta \approx \theta$] and z = channel bottom elevation. Since energy losses cannot be ignored when ratios of control volume length to flow depth are large, the Bernoulli sum decreases with x. In uniform flow E is constant, and differentiation of (12.17) gives

$$\frac{dH}{dx} \; = \; 0 \; + \; \frac{dz}{dx} \tag{12.18}$$

But $dz/dx = -\sin \theta = -S_0$, and $dH/dx = -S_f$ in which S_f is called the friction slope. Thus, (12.18) shows that the friction slope in uniform flow is given by

$$S_f \; = \; -\frac{dH}{dx} \; = \; S_0 \tag{12.19}$$

and elimination of S_0 from (12.15) and (12.19) gives

$$S_f \; = \; -\frac{dH}{dx} \; = \; \frac{f}{8} \frac{U^2}{g R} \tag{12.20}$$

Equation (12.20) has been derived for uniform open channel flow on a slope. ***However, it is also used as an approximation for*** S_f ***in gradually varied flow for both horizontal and sloping channels***.

In some applications the ratio of flow depth to channel width is small. Calculation of the hydraulic radius for a rectangular channel gives

$$R = \frac{A}{P_w} = \frac{By}{B + 2y} = \frac{y}{1 + 2(y/B)} \tag{12.21}$$

When $2(y/B)$ is small, (12.21) can be expanded in the following power series:

$$R = y\left[1 - 2(y/B) + 4(y/B)^2 - \cdots\right] \tag{12.22}$$

Thus, when $2(y/B)$ is less than 0.1, we can approximate R with the flow depth.

$$R \approx y \quad \text{for} \quad 2(y/B) < 0.1 \tag{12.23}$$

The error in (12.23) is about ten per cent when $2(y/B) = 0.1$, which leads to an error of about five per cent when used in (12.15) to calculate U.

Values of f in (12.15) and (12.20) are given by the Moody diagram shown in Fig. 7.18. Since the hydraulic radius of a circular pipe is given by $D/4$, both the Reynolds number and relative roughness in the Moody diagram are computed by replacing D with $4R$:

$$Re = \frac{UD}{\nu} = \frac{U(4R)}{\nu} \tag{12.24}$$

$$\frac{\epsilon}{D} = \frac{\epsilon}{4R} \tag{12.25}$$

in which R is calculated from (12.16). Values of ϵ for some different surfaces have been published in an ASCE task force report (1963) and are given in Table 12.1

Table 12.1 Values of ϵ in mm for some different surfaces.

0.15	Concrete class 4 (monolithic construction, cast against oiled steel forms with no surface irregularities).
0.30	Very smooth cement-plastered surfaces, all joints and seams hand-finished flush with surface.
0.49	Concrete cast in lubricated steel moulds, with carefully smoothed or pointed seams and joints.
0.61	Wood-stave pipes, planed-wood flumes, and concrete class 3 (cast against steel forms, or spun-precast pipe). Smooth trowelled surfaces. Glazed sewer pipes.
1.52	Concrete class 2 (monolithic construction against rough forms or smooth-finished cement-gun surface, the latter often termed gunite or shot concrete). Glazed brickwork.
2.44	Short lengths of concrete pipe of small diameter without special facing of butt joints.
3.05	Concrete class 1 (precast pipes with mortar squeeze at the joints). Straight uniform earth channels.
4.27	Roughly made concrete conduits.
6.10	Rubble masonry.
3.05 to 9.14	Untreated gunite.

For many years engineers have used an empirical equation known as the Manning equation to calculate velocities in uniform open channel flow. Because this equation is not dimensionally homogeneous, it has different forms for different systems of units. In metre-second units it has the form

$$U = \frac{1}{n} R^{2/3} S_0^{1/2} \tag{12.26}$$

and in foot-second units it changes to

$$U = \frac{1.49}{n} R^{2/3} S_0^{1/2} \tag{12.27}$$

in which n is the dimensionless Manning surface roughness coefficient. It is generally agreed that Mannings equation holds only in fully rough turbulent flow, where f depends upon relative roughness but not upon the Reynolds number. On the other hand, Eq. (12.15) is dimensionally correct, so that its form does not change with the system of units, and it holds for flows in which f depends upon both relative roughness and Reynolds number. Consequently, we will prefer the use of (12.15).

Despite the shortcomings of the Manning equation, a great deal of information exists about choices for n in open channel flows. [For example, Chow (1959) and Henderson (1966).] For this reason, many engineers continue to use the Manning equation. Values for f can be calculated from n by using the following equation with foot-second units:

$$n = 1.49 \, R^{1/6} \sqrt{\frac{f}{8g}} \qquad\qquad \textbf{(12.28)}$$

When metre-second units are used, this equation changes to

$$n = R^{1/6} \sqrt{\frac{f}{8g}} \qquad\qquad \textbf{(12.29)}$$

Equations (12.28) - (12.29) have been obtained by equating the expressions for U in (12.15) and (12.26) - (12.27).

Example 12.4

Calculate the uniform flow velocity and discharge in the trapezoidal canal shown in Fig. 12.8 if $y = 2$ m, $S_0 = 1{:}2000$ and $\epsilon = 0.49$ mm.

Solution: The area and wetted perimeter for a depth of 2 m are

$$A = 2y(2 + y) = 2(2)(2 + 2) = 16 \text{ m}^2$$

$$P_w = 4 + 2y\sqrt{5} = 4 + 2(2)\sqrt{5} = 12.9 \text{ m}$$

This leads to the following value for the hydraulic radius:

$$R = \frac{A}{P_w} = \frac{16}{12.9} = 1.24 \text{ m}$$

Thus, Eq. (12.15) gives

$$U = \sqrt{\frac{8}{f} \, gR\,S_0} = \sqrt{\frac{8}{f}(9.81)(1.24)\left(\frac{1}{2000}\right)} = \frac{0.221}{\sqrt{f}}$$

In general, f depends upon Re and ϵ/D, and this equation must be solved by successive approximation. We will start by calculating

$$\epsilon/D = \epsilon/(4R) = 0.49 \times 10^{-3} \big/ (4 \times 1.24) = 0.0001$$

If the flow is completely turbulent with a rough boundary, Fig. 7.18 gives $f = 0.012$ and $U = 0.221 \big/ \sqrt{0.012} = 2.02$ m/s. At 10°C, this gives a Reynolds number of

$$Re = \frac{U(4R)}{\nu} = \frac{(2.02)(4 \times 1.25)}{1.31 \times 10^{-6}} = 7.65 \times 10^6$$

This leads to a revised value of $f = 0.0123$ from Fig. 7.18 and a slightly changed value for U.

$$U = 0.221 \Big/ \sqrt{0.0123} = \boxed{1.99 \text{ m/s}}$$

Since $Re = 7.53 \times 10^6$, Fig. 7.18 shows that the next cycle would give the same values for f and U. Finally, the discharge is

$$Q = UA = (1.99)(16) = \boxed{31.8 \text{ m}^3/\text{s}}$$

Example 12.5

Calculate the uniform flow depth in the trapezoidal canal shown in Fig. 12.8 if $Q = 20 \text{ m}^3/\text{s}$, $S_0 = 1:2000$ and $\epsilon = 0.49$ mm.

Solution: The unknown depth appears in A, P_w (and, thus R) and also in f since f depends upon both the Reynolds number and relative roughness. Thus, the uniform flow equation, (12.15), cannot be solved directly for y. Therefore, it is better to specify values for y and calculate corresponding values for Q. Then interpolation gives an estimate for y corresponding to $Q = 20 \text{ m}^3/\text{s}$. The results for this example are summarized in the following table:

y (m)	A (m^2)	P_w (m)	R (m)	U (m/s)	Q (m^3/s)
1.3	8.58	9.81	0.874	1.61	13.8
1.5	10.5	10.7	0.981	1.73	18.2
1.6	11.5	11.2	1.03	1.79	20.6

Linear interpolation gives

$$\boxed{y = 1.58 \text{ m}}$$

Gradually Varied Flow Calculations

In gradually varied flow, where changes in depth and velocity occur over distances greater than about 100 flow depths, the effects of both channel slope and energy losses must be taken into account. Mathematical solutions for this type of flow are obtained from a simultaneous solution of the continuity and momentum equations. Probably the easiest way to derive the momentum equation is to differentiate the Bernoulli sum

$$H = z + y + \frac{U^2}{2g} \tag{12.30}$$

with respect to x to obtain

$$\frac{dH}{dx} = \frac{dz}{dx} + \frac{dy}{dx} + \frac{U}{g}\frac{dU}{dx} \tag{12.31}$$

Setting $dz/dx = -S_0$ and $dH/dx = -S_f$ in (12.31) gives a general form of the momentum equation for gradually varied flow in an open channel:

$$\boxed{\frac{dy}{dx} + \frac{U}{g}\frac{dU}{dx} = S_0 - S_f} \tag{12.32}$$

Equation (12.32) holds for any cross sectional geometry, and s_f in (12.32) is usually approximated with the friction slope for uniform flow on a slope given by (12.20).

The qualitative behaviour of solutions of (12.32) is investigated most easily for a relatively shallow flow in a prismatic channel for which the ratio of flow depth to channel width is small. Under these conditions, (12.23) shows that the hydraulic radius is approximated with the flow depth and (12.20) becomes

$$S_f = \frac{f}{8}\frac{U^2}{gy} \tag{12.33}$$

It is also convenient to introduce the definition of normal depth, y_n, as the depth calculated from (12.15) if uniform flow existed in the channel:

$$U_n = \sqrt{\frac{8}{f}\,g\,y_n\,S_0} \tag{12.34}$$

in which U_n = velocity for the corresponding uniform flow depth, y_n. Eliminating $8g/f$ between (12.33) and (12.34) gives

$$S_f = S_0\frac{y_n}{y}\frac{U^2}{U_n^2} = S_0\left(\frac{y_n}{y}\right)^3 \tag{12.35}$$

in which the continuity equation $q = Uy = U_n\,y_n$ has been used to replace $(U/U_n)^2$ with $(y_n/y)^2$. Finally use of $U = q/y$ allows the convective acceleration term to be calculated in the following form:

$$\frac{U}{g}\frac{dU}{dx} = \frac{q}{gy}\frac{d}{dx}\left(\frac{q}{y}\right) = -\frac{q^2}{gy^3}\frac{dy}{dx} = -\left(\frac{y_c}{y}\right)^3\frac{dy}{dx} \tag{12.36}$$

in which the definition of critical depth given by (12.6) has been used to eliminate q^2/g. Substituting (12.35) and (12.36) into (12.32) gives an ordinary differential equation for the gradual variation of depth in a shallow open channel.

$$\frac{dy}{dx} = S_0 \, \frac{1 - \left(y_n/y\right)^3}{1 - \left(y_c/y\right)^3} = S_0 \, \frac{y^3 - y_n^3}{y^3 - y_c^3} \qquad \textbf{(12.37)}$$

Equation (12.37) was first integrated in closed form by Bresse in 1860. Although the integration is fairly straightforward, we will give neither the details nor the results. This is because most engineers calculate numerical solutions of (12.32), and these numerical solutions can be calculated for both prismatic and non-prismatic channels with cross sections of any form. It is important, however, to obtain a qualitative understanding of the way in which solutions of (12.37) behave. This qualitative behaviour is obtained most easily from a direct study of (12.37) rather than from plots of the integral of (12.37).

Solutions of (12.37) have behaviours that depend upon the magnitude of y compared with the magnitudes of y_n and y_c. Since the straight lines $y = y_n$ and $y = y_c$ divide the solution domain into three distinct regions, a sloping channel has three different solution regions that are denoted by subscripts 1, 2 and 3 in going from the top, to the middle and to the bottom, respectively. Furthermore, we must consider slopes that are mild $\left(y_n > y_c\right)$, steep $\left(y_n < y_c\right)$, adverse (y_n non-existent) and horizontal $\left(y_n = \infty\right)$. Solutions for these various slopes are denoted with the letters M, S, A and H, respectively. This classification should become clear as each possibility is discussed.

A mild slope is characterized by the requirement $y_n > y_c$. The straight lines $y = y_n$ and $y = y_c$ are shown in Fig. 12.10 with dashed lines that are parallel to the channel bottom. The solution for a mild slope when $y_n < y < \infty$ is denoted by M_1 in Fig. 12.10. In this region the right side of (12.37) is positive. Thus, $dy/dx > 0$ in region one and approaches S_0 as $y \to \infty$, which shows that the solution for y is asymptotic to a horizontal line as $y \to \infty$. As $y \to y_n$ from within region one, $dy/dx \to 0$. In region two, where $y_c < y < y_n$, the right side of (12.37) is negative. Thus, dy/dx is negative for region two and approaches zero and negative infinity as $y \to y_n$ and $y \to y_c$, respectively. This solution is denoted by M_2 in Fig. 12.10. Finally, region three has $0 < y < y_c$. In this case the right side of (12.37) is positive. When $y \to 0$, dy/dx is a finite positive number. When $y \to y_c$, dy/dx becomes positively infinite. This solution is denoted by M_3 in Fig. 12.10. Solution curve behaviour for a steep slope is determined in the same way, and the result is shown in Fig. 12.10.

The solution behaviour for an adverse slope $\left(S_0 < 0\right)$ cannot be determined from (12.37) since y_n is not defined. Since critical depth can still be calculated from (12.7), the convective acceleration term can be replaced with (12.36). The friction slope can be approximated with (12.33), in which U can be replaced with q/y. Thus, (12.32) can be written for an adverse slope in the form
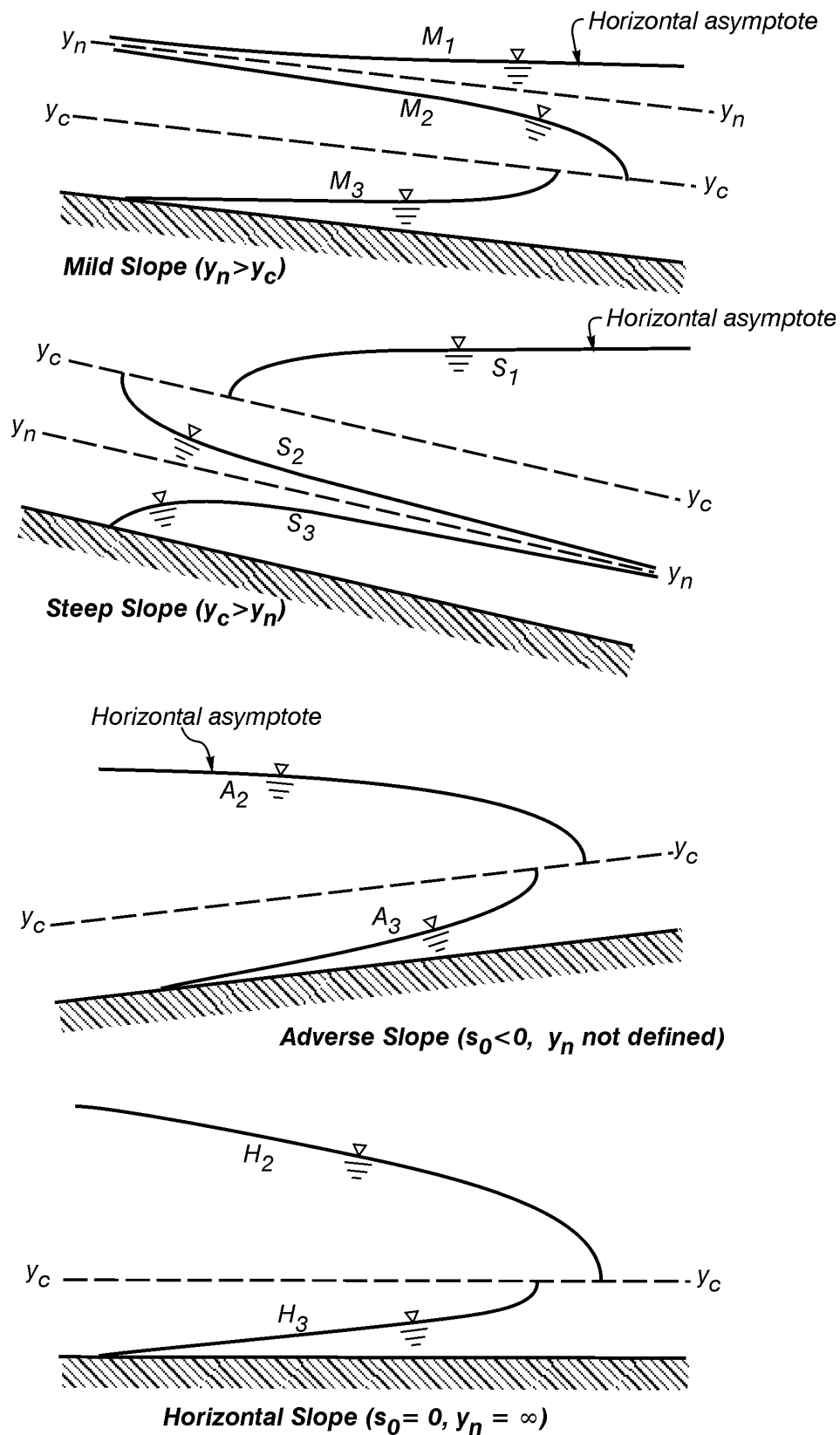
Figure 12.10 Gradually varied flow solution behaviour for relatively shallow flow in open channels.

$$\frac{dy}{dx} = \frac{S_0 - \dfrac{fq^2}{8gy^3}}{1 - \left(y_c/y\right)^3}$$

(12.38)

in which $S_0 < 0$. The right side of (12.38) is negative when $y_c < y < \infty$ and approaches S_0 as $y \to \infty$. When $y \to y_c$ through values of y greater than y_c, dy/dx approaches negative infinity. The curve for this region, which is defined to be region two, is labelled A_2 in Fig. 12.10. Similar reasoning gives the curve labelled A_3 when $0 < y < y_c$. Solutions for the horizontal slope are also determined from (12.38) after setting $S_0 = 0$. These curves are labelled H_2 and H_3 in Fig. 12.10.

It is now possible to summarize the results shown in Fig. 12.10. Since a finite normal depth exists only for positive slopes, there are three possible solutions for mild and steep slopes but only two solutions for adverse and horizontal slopes. Normal depth is approached asymptotically at the upstream end of mild slopes and at the downstream end of steep slopes, and horizontal asymptotes are approached in all cases as y becomes infinite. Finally, all solutions have an infinite slope as $y \to y_c$. When these facts are remembered, it becomes easy to sketch qualitatively correct solution behaviours for the different cases. There is no need to memorize the results, however, since they are all summarized concisely in Fig. 12.10.

Flow Controls

A flow control is defined to be any point along an open channel where a unique relationship exists between flow rate and depth. One example is the sluice gate considered in Example 12.1, where specification of a flow rate and gate opening allowed upstream and downstream depths to be calculated. Another example occurs for flow over either a weir or spillway, in which case specification of Q determines an upstream depth. A free overfall, shown in Fig. 12.11a, becomes a flow control if the approaching flow is subcritical. Then critical depth occurs at the overfall.[*] Critical depth does not occur at the overfall, however, if the approaching flow is supercritical. In that case the overfall is not a flow control. A final example, shown in Fig. 12.11b, occurs at a point where a channel slope changes from mild to steep, in which case critical depth occurs at the point where the slope changes. In all of these cases subcritical and supercritical flow occur upstream and downstream, respectively, from the control unless another downstream control drowns all or part of the control under consideration.

A channel constriction or rise in channel bottom elevation becomes a flow control only if the flow is choked so that critical depth occurs at the constriction or on top of the rise. A hydraulic jump is not a flow control since specification of Q determines a relationship between y_1 and y_2 but is not sufficient to determine values for these depths. Henderson (1966) gives a detailed discussion of flow controls.

---

[*]   Experiments show that critical depth actually occurs a distance of $3y_c$ to $4y_c$ upstream from the brink. This distance is usually ignored in gradually varied flow calculations, and critical depth is assumed to occur at the brink.
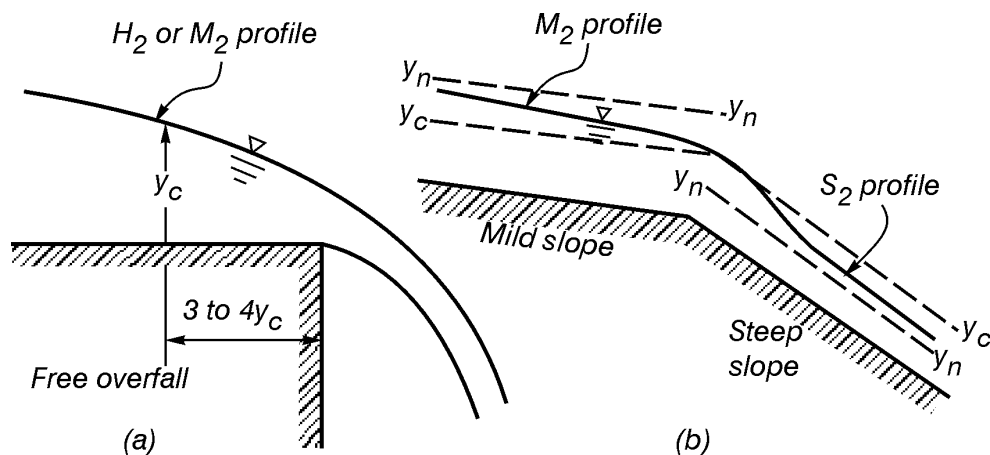
Figure 12.11 Flow controls (a) at a free overall and (b) at a change in channel slope.

Gradually varied flow calculations must, in general, start at a flow control and proceed in the upstream direction for subcritical flow and in the downstream direction for supercritical flow. Flow controls are important because they fix the flow depth, and, therefore, provide an initial condition to fix the integration constant when integrating the first-order differential equation for gradually varied flow. Since subcritical and supercritical flow generally exist upstream and downstream, respectively, from a flow control, gradually varied flow profiles are calculated by integrating in both the upstream and downstream direction from flow controls. When a flow control exists at both ends of a channel reach, the resulting flow profiles can be joined only by inserting a hydraulic jump somewhere along the reach. However, a hydraulic jump can always move upstream to submerge all or part of an upstream control, or sometimes it can move downstream to eliminate a downstream flow control. Examples will be shown in the following section.

Flow Profile Analysis

Flow profile analysis uses the free surface behaviours shown in Fig. 12.10 together with additional information about flow controls to predict free surface flow profiles in open channel flows. Every problem generally has a number of different possible profiles, and a final unique solution for any given problem ultimately depends upon specific values for y_n, y_c, flow control depths, depths calculated from rapidly varied flow equations and from integrations of (12.32) or (12.37) for gradually varied flow. *However, the final numerical solution of a particular problem should not be attempted until a flow profile analysis has been used to examine the different possibilities*.

Our first example will consider flow in a horizontal channel downstream from a hump when the hump chokes the flow, as shown in Fig. 12.12. We will assume that the downstream channel terminates with a free overfall. Since the flow immediately downstream from the hump is likely to be supercritical, Fig. 12.10 shows that an H_3 profile will extend downstream until critical depth is reached at a finite distance from the hump. We assume initially that the overfall brink occurs well downstream from this point, which means that critical depth occurs at the overfall brink and that an H_2 profile extends upstream from this point. Thus, the overfall also acts as a flow control, and the supercritical profile downstream from the hump and the subcritical profile

upstream from the overfall can be joined only with a discontinuity in depth given by the hydraulic jump equation calculated in Example 4.7:

$$\frac{y_2}{y_1} = \frac{1}{2}\left(-1 + \sqrt{1 + 8F_1^2}\right)$$

(12.39)

in which the upstream Froude number is given by

$$F_1 = \frac{U_1}{\sqrt{gy_1}} = \frac{q}{\sqrt{gy_1^3}}$$

(12.40)

By starting at the point where y_c occurs in the H_3 profile, depths in the H_3 profile can be inserted for y_1 in (12.39) -(12.40) to calculate corresponding values for y_2, which are shown with dots in Fig. 12.12. The intersection of this curve with the H_2 curve is the point where the gradually varied flow equations and the hydraulic jump solution are satisfied simultaneously, and it is at this point where the jump will stabilize.
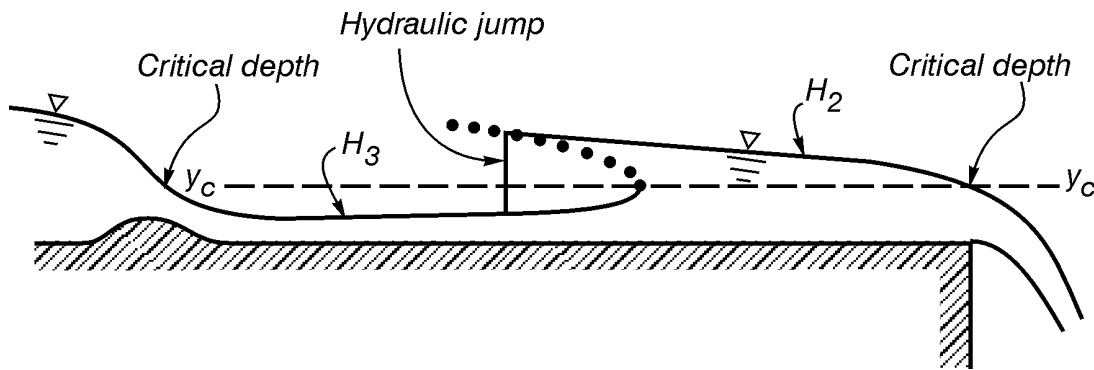

Figure 12.12 The flow profile downstream from a hump in a horizontal channel. The hump chokes the upstream flow, and the downstream channel terminates with a free overfall.

The flow profile shown in Fig. 12.12 is not unique, but it can be used to arrive at other possible profiles. For example, shortening the distance between the overfall and hump lowers the H_2 profile and causes the intersection of the H_2 profile with the curve calculated from (12.39) - (12.40) to move downstream. If this channel reach is shortened sufficiently to place the overfall brink upstream from the point where critical depth occurs in the H_3 profile, the jump will be swept over the brink. Then supercritical flow with an H_3 profile extends along the entire reach. In this case the overfall no longer acts as a flow control. At the other extreme, lengthening the channel reach causes the jump to move upstream by raising the elevation of the H_2 profile. If the channel reach becomes long enough, the jump will move upstream to the hump. In this case the jump will remain at the hump as a drowned hydraulic jump if the H_2 depth at this point is less than the depth just upstream from the hump. If the H_2 depth equals the depth upstream from the hump, curve B in Fig. 12.6 will result. Finally, if the H_2 depth at the hump exceeds the depth immediately upstream from the hump, curve C in Fig. 12.6 will occur. In this case, critical depth no longer occurs on the hump, and the hump ceases to act as a flow control.
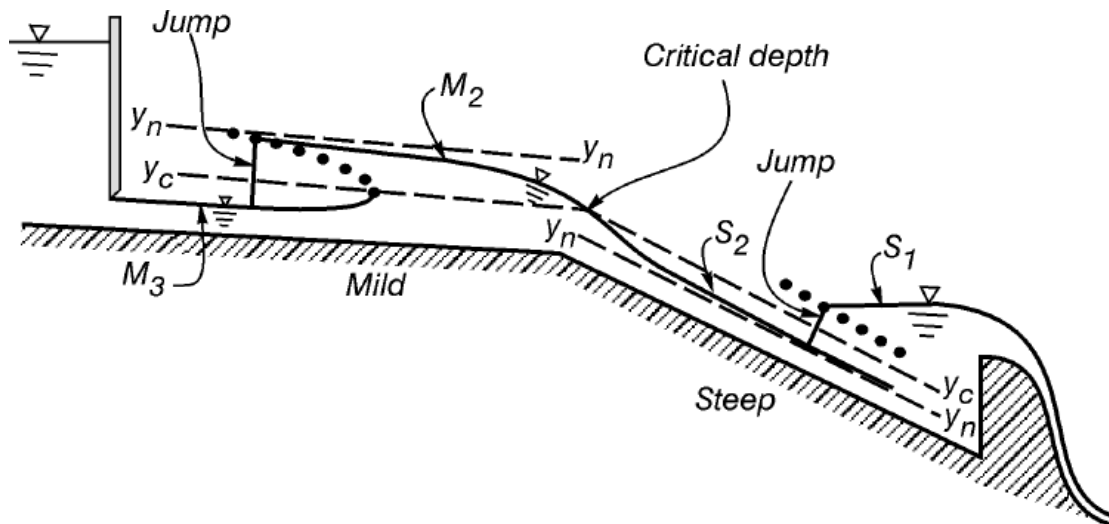
Figure 12.13 A possible flow profile for two consecutive reaches.

In more general problems flow profiles must be considered for two or more reaches joined together. Figure 12.13 shows a mild reach $\left(y_n > y_c\right)$ joined to a steep reach $\left(y_n < y_c\right)$ with a sluice gate at the upstream end of the mild reach and a weir at the downstream end of the steep reach. Flow profiles are shown in Fig. 12.13 for the case in which flow controls exist at the sluice gate, the change in channel slope and the weir. Values of y_2 calculated from (12.39) - (12.40) are shown again with dots, and hydraulic jumps occur in each reach at the intersection of these curves with subcritical flow profiles. As in the previous example, the remaining possible profiles can be obtained by modifications of the channel and profile geometry shown in Fig. 12.13. For example, lengthening the mild reach will force the first jump upstream, and shortening the mild reach allows the jump to move downstream. It is also possible to shorten the mild reach enough to sweep the jump over the change in channel slope, in which case an M_3 profile extends over the full length of the reach and the change in channel slope ceases to act as a flow control. Lowering the sluice gate will also move the jump downstream, and raising the gate allows the jump to move upstream. Likewise, lowering or raising the weir causes the jump on the steep slope to move downstream or upstream, respectively, and it may be possible to raise the weir enough to drown the flow control at the change in channel slope.

The problems considered so far have assumed that flow rates are given. A more difficult problem occurs when the flow rate is an unknown that must be calculated as part of the solution. An example of this occurs when two reservoirs at different elevations are joined with a sloping channel, as shown in Fig. 12.14. Free surface elevations in both reservoirs are given, and the unknowns are the flow rate per unit width, q, and the free surface profile in the open channel. Since q is unknown, critical and normal depths cannot be calculated directly. This means that a method of successive approximation must be used to obtain the final solution.
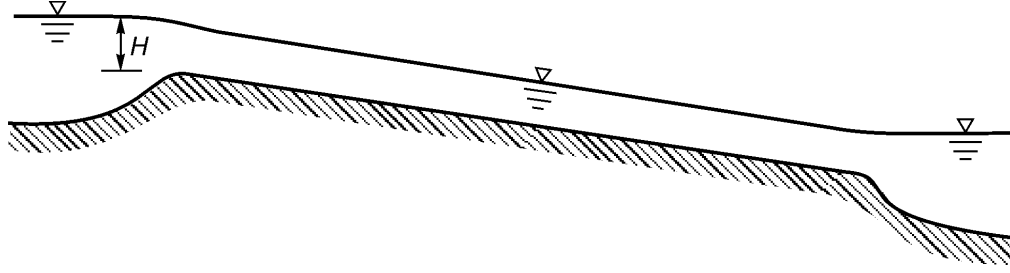
Figure 12.14 Two reservoirs joined with a sloping channel.

Since critical and normal depths are unknown, the solution of this problem can be started by assuming that the channel slope is steep. If the channel is steep, then critical depth must occur at the upstream end of the channel with an S_2 curve extending downstream. If the downstream reservoir surface is high enough, then an S_1 curve extends upstream from the lower end of the channel. In this case the S_1 and S_2 curves are joined with a hydraulic jump at the point where the S_1 and S_2 depths satisfy (12.39) - (12.40), as shown in Fig. 12.15. Raising or lowering the downstream reservoir surface will cause the jump to move upstream or downstream, respectively. If the downstream reservoir surface falls below the value of y_2 calculated from (12.39) - (12.40) at the downstream channel end, then the jump will be swept into the reservoir.
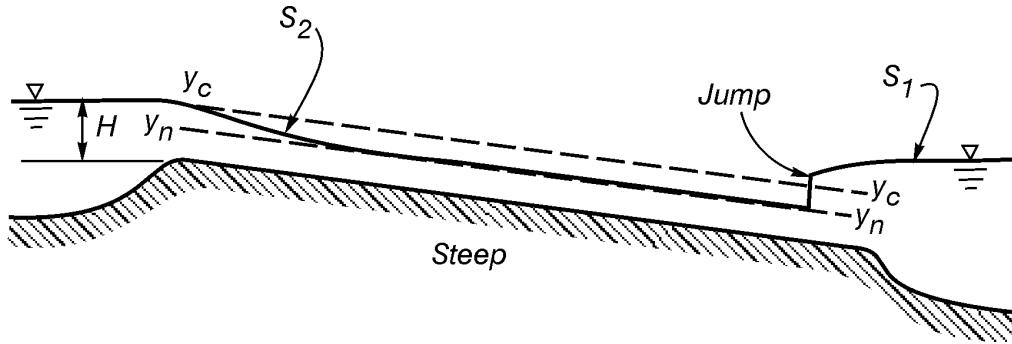

Figure 12.15 The free surface profile for Fig. 12.14 when the channel slope is steep.

An application of the Bernoulli equation at the upstream channel end in Fig. 12.15 gives

$$H = y_c + \frac{q^2}{2gy_c^2} \tag{12.41}$$

The simultaneous solution of (12.6) and (12.41) for y_c and q gives

$$y_c = \frac{2}{3}H \tag{12.42}$$

$$q = \sqrt{\frac{8}{27}gH^3} \tag{12.43}$$

The value of q in (12.43) can be used to calculate a normal depth from

$$q = y_n \sqrt{\frac{8}{f} g y_n S_0} \qquad (12.44)$$

If y_n calculated from (12.44) is less than y_c calculated from (12.42), then the channel is confirmed to be steep and (12.42) - (12.43) give the correct solution. In this case, the free surface profiles shown in Fig. 12.15 can be calculated without further difficulty.

If the value of y_n calculated from (12.44) exceeds the value of y_c calculated from (12.42), then the channel slope is mild and (12.41 - (12.43) are invalid. Possible free surface profiles for a mild slope are shown in Fig. 12.16, with either an M_1 or M_2 profile extending upstream from the downstream reservoir. In this case an assumed value of q can be used to calculate corresponding values for y_c, y_n and free surface coordinates in the open channel. Then the free surface coordinate at the upstream end of the channel can be used to calculate H from the Bernoulli equation.

$$H = y + \frac{q^2}{2g y^2} \qquad (12.45)$$

After H has been calculated from (12.45) for a number of assumed values of q, a plot of H versus q can be prepared and used to calculate the particular value of q that will occur for any specified value of H.
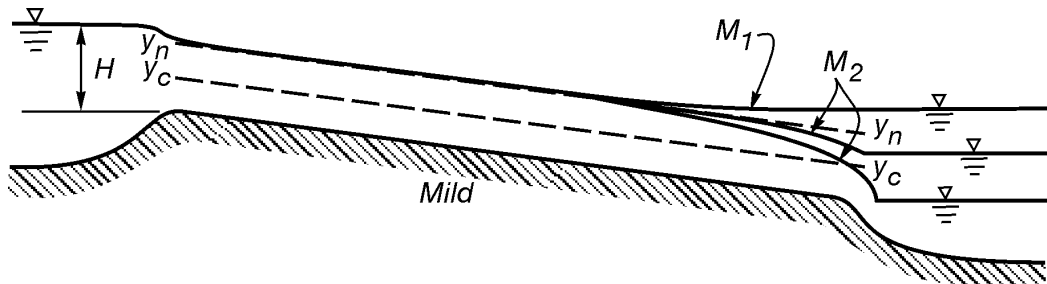

Figure 12.16 Free surface profiles for Fig. 12.14 when the channel slope is mild.

It becomes apparent from an examination of Fig. 12.16 that all free surface profiles for a mild slope approach normal depth asymptotically at the upper end of the channel. Therefore, if the channel is long enough, the procedure just outlined becomes equivalent to the simultaneous solution of (12.44) and (12.45) [after replacing y in (12.45) with y_n]. In this case it is convenient to specify y_n and calculate q and H from (12.44) and (12.45), respectively, to obtain a plot of H versus q. This procedure is considerably easier than the first procedure given for a mild slope since it does not require calculation of a free surface profile for every assumed value of q. However, one or two free surface profiles should be calculated for the channel to ensure that the channel reach is long enough to allow uniform flow to be approached at the upstream end of the channel.

Example 12.6

A rectangular open channel serves as an outlet for a reservoir. Calculate a dimensionless relationship between the outflow per unit width, q, and reservoir free surface elevation, H, if the channel is long enough to ensure that any downstream control creates a negligible backwater effect at the reservoir outlet.

Solution: When the channel slope is steep, Eq. (12.43) gives the outflow discharge.

$$\frac{q}{\sqrt{gH^3}} = \sqrt{\frac{8}{27}} \quad \text{when} \quad y_n < y_c$$

Solution of Eq. (12.44) for y_n and use of the previous equation for q gives

$$y_n = \left(\frac{fq^2}{8g\,S_0} \right)^{1/3} = \left(\frac{fH^3}{27\,S_0} \right)^{1/3}$$

Substituting this expression for y_n and Eq. (12.42) for y_c in the inequality $y_n < y_c$ gives

$$y_n < y_c \quad \text{when} \quad \frac{f}{S_0} < 8$$

This shows that the channel can be made steep by either increasing S_0 or decreasing f.

When the channel slope is mild, flow at the reservoir outlet can be influenced by non-uniform flow that results from a downstream control (i.e. a backwater effect). If we assume that the channel is long enough to have a negligible backwater effect at the reservoir outlet, then uniform flow exists in the channel immediately downstream from the outlet and Eq. (12.44) gives the following expression for the flow depth:

$$\frac{y_n}{H} = \left(\frac{1}{8} \frac{q^2}{gH^3} \frac{f}{S_0} \right)^{1/3}$$

Setting $y = y_n$ in the Bernoulli equation, Eq. (12.45), gives a second relationship.

$$1 = \frac{y_n}{H} + \frac{1}{2} \frac{q^2}{gH^3} \frac{1}{\left(y_n/H \right)^2}$$

Elimination of the parameter y_n/H between these two equations gives a relationship between $q/\sqrt{gH^3}$ and f/S_0 for a mild slope when $y_n > y_c$. However, the numerical solution of these equations is achieved most easily by calculating $q/\sqrt{gH^3}$ from the second equation for an assumed value of y_n/H. Then the assumed value of y_n/H and calculated value of $q/\sqrt{gH^3}$ can be used in the first equation to compute f/S_0. The result of this calculation is shown in the following plot. Applications of this plot under the most general circumstances must proceed by trial and error since f depends upon both Reynolds number and relative roughness.
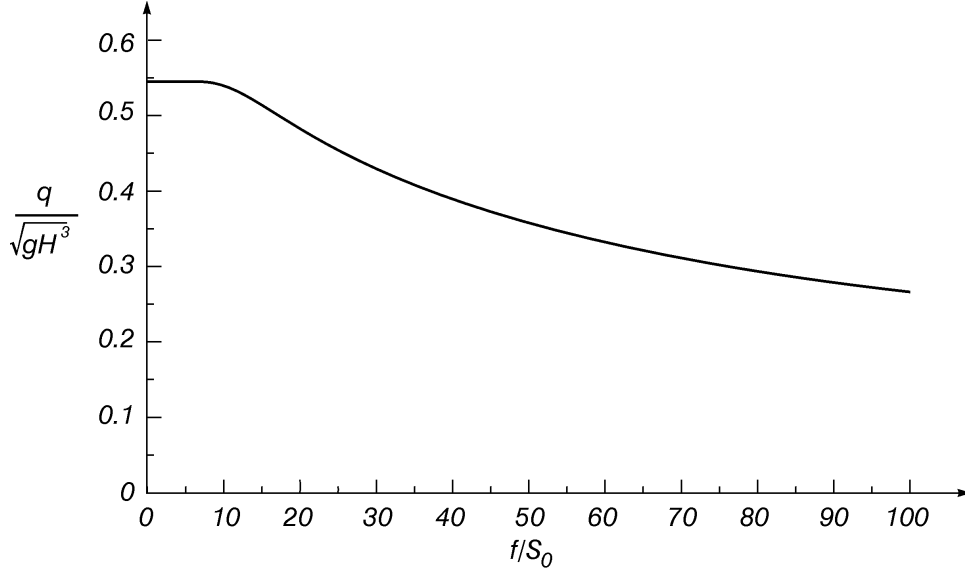
Numerical Integration of the Gradually Varied Flow Equation

The numerical integration of (12.32) is carried out most conveniently by rewriting it in the form

$$\frac{dE}{dx} = S_0 - S_f \tag{12.46}$$

in which E is defined, for the most general case, by (12.13). There are two basic ways in which (12.46) is integrated to calculate free surface coordinates. The first way, which can only be used for prismatic channels with constant slopes, specifies E (and, therefore, y) at two different cross sections and uses (12.46) to calculate the x distance between these two cross sections. Thus, if E_1 and E_2 are specific energies at $x = x_1$ and $x = x_2$, respectively, an application of the trapezoidal rule to integrate (12.46) gives

$$x_2 - x_1 = \frac{\left(E_2 - E_1\right)}{2}\left[\frac{1}{\left(S_0 - S_f\right)_1} + \frac{1}{\left(S_0 - S_f\right)_2}\right] \tag{12.47}$$

in which the sign of $x_2 - x_1$ determines whether cross section 2 is upstream or downstream from cross section 2. The second method, which can be used for both prismatic and non-prismatic channels with either constant or variable slopes, specifies the distance $x_2 - x_1$ between two cross sections and integrates (12.46) to calculate E and the depth at cross section 2. For example, a second-order Runge-Kutta method uses the known value of E_1 at $x = x_1$ to get a first approximation for E_2:

$$E_2^{(1)} = E_1 + \left(S_0 - S_f\right)_1\left(x_2 - x_1\right) \tag{12.48}$$

This first approximation for E_2 gives corresponding values for $y_2^{(1)}$ and $\left(S_0 - S_f\right)_2^{(1)}$, and the second and final approximation for E_2 is given by

$$E_2^{(2)} = E_1 + \frac{\left(x_2 - x_1\right)}{2}\left[\left(S_0 - S_f\right)_1 + \left(S_0 - S_f\right)_2^{(1)}\right]$$ **(12.49)**

Again, $\left(x_2 - x_1\right)$ has a sign determined by the relative positions of cross sections 1 and 2. Computational accuracy is increased with (12.47) by decreasing $\left(E_2 - E_1\right)$, which increases the number of steps required to calculate a profile for a specified channel length. Computational accuracy is increased with (12.48) - (12.49) by decreasing $\left(x_2 - x_1\right)$, which also increases the number of steps required to calculate a profile for a specified channel length.

Example 12.7

The trapezoidal canal in Fig. 12.8 has $Q = 5$ m^3/s, $S_0 = 1:2000$, $\epsilon = 0.49$ mm and $y_c = 0.500$ m. Use two equal steps in depth to calculate the distance between cross sections that have depths of $y = 0.90$ and 1.00 m.

Solution: A calculation like the one illustrated in Example 12.5 gives $y_n = 0.74$ m for $Q = 5$ m^3/s. Since $y_c < y_n$, the slope is mild. Since all values of y in this calculation are greater than y_n, we expect an M_1 curve in which depths go from $y = 1.00$ to 0.95 to 0.90 m in the upstream direction.

Figure 12.8 shows that $E = 1.03$, 0.98 and 0.94 m when $y = 1.00$, 0.95 and 0.90 m, respectively. Corresponding values for S_f at these depths are calculated from Eq. (12.20):

$$S_f = \frac{f}{8}\frac{U^2}{gR} = \frac{f}{8}\frac{(Q/A)^2}{gR}$$

Calculations for S_f are summarized in the following table:

Cross Section	1	2	3
y (m)	1.00	0.95	0.90
A (m^2)	6.00	5.61	5.22
R (m)	0.708	0.680	0.650
Re	1.80×10^6	1.85×10^6	1.90×10^6
$\epsilon/(4R)$	0.00017	0.00018	0.00019
f	0.0140	0.0141	0.0141
S_f	0.000175	0.000210	0.000254

Since $S_0 = 1/2000 = 0.00050$, application of (12.47) gives

$$x_3 - x_1 = \frac{(E_2 - E_1)}{2}\left[\frac{1}{(S_0 - S_f)_1} + \frac{1}{(S_0 - S_f)_2}\right] + \frac{(E_3 - E_2)}{2}\left[\frac{1}{(S_0 - S_f)_2} + \frac{1}{(S_0 - S_f)_3}\right]$$

$$= -\frac{0.05}{2}\left[\frac{1}{0.000325} + \frac{1}{0.000290}\right] - \frac{0.04}{2}\left[\frac{1}{0.000290} + \frac{1}{0.000246}\right]$$

$$= \boxed{-313 \text{ m}}$$

The negative sign indicates that cross section 3 is upstream from cross section 1, which is to be expected for an M_1 curve.

Example 12.8

Rework the previous example by using two equally spaced steps in x to calculate y_3 at $x = -313$ m if $y_1 = 1.00$ m at $x_1 = 0$.

Solution: From Example 12.7 we have $(x_2 - x_1) = -313/2 = -157$ m, $(S_0 - S_f)_1 = 0.000325$ and $E_1 = 1.03$ m. Therefore, Eq. (12.48) gives the following first approximation for E_2:

$$E_2^{(1)} = E_1 + (S_0 - S_f)_1(x_2 - x_1) = 1.03 + (0.000325)(-157) = 0.98 \text{ m}$$

The corresponding value for y_2 is found from Fig. 12.8 to be $y_2^{(1)} = 0.95$m, which leads to $(S_0 - S_f)_2^{(1)} = 0.00050 - 0.000210 = 0.000290$. The final approximation for E_2 is now calculated from Eq. (12.49).

$$E_2^{(2)} = E_1 + \frac{(x_2 - x_1)}{2}\left[(S_0 - S_f)_1 + (S_0 - S_f)_2^{(1)}\right] = 1.03 - \frac{157}{2}[0.000325 + 0.000290] = 0.98 \text{ m}$$

The corresponding value for y_2 is found from Fig. 12.8 to be $y_2^{(2)} = 0.95$ m, which leads to $(S_0 - S_f)_2^{(2)} = 0.000290$.

Repetition of this process for the second step in x gives the following results:

$$E_3^{(1)} = E_2 + (S_0 - S_f)_2(x_3 - x_2) = 0.98 + 0.000290(-157) = 0.93 \text{ m}$$

$$y_3^{(1)} = 0.88 \quad \text{and} \quad (S_0 - S_f)_3^{(1)} = 0.00050 - 0.000273 = 0.000227$$

$$E_3^{(2)} = E_2 + \frac{(x_3 - x_2)}{2}\left[(S_0 - S_f)_2 + (S_0 - S_f)_3^{(1)}\right] = 0.98 - \frac{157}{2}[0.000290 + 0.000227] = 0.94 \text{ m}$$

$$y_3^{(2)} = \boxed{0.90 \text{ m}}$$

This happens to agree exactly with the value of y_3 that was used in Example 12.7. In general we would expect these values to be close but not necessarily identical.

Gradually Varied Flow in Natural Channels

Gradually varied flow in natural channels can be calculated with the one-dimensional flow approximations used in this chapter only when flow is subcritical. This is because standing waves always occur in irregular channels containing supercritical flow, and this causes the flow to become highly two and three-dimensional. Since channel cross sections used in the integration have x coordinates that are fixed by the natural geometry of the channel, subcritical flow integrations must be carried out in the upstream direction by using Eqs. (12.48) - (12.49). However, these equations are usually modified to include a term for local losses at sharp bends or sudden expansions. Furthermore, since the channel slope varies irregularly, the channel slope and flow depth terms in E are combined to give the vertical elevation, z, of the free surface above an arbitrarily chosen fixed datum. Thus, Eqs. (12.48) - (12.49) take the following form:

$$H_2^{(1)} = H_1 - \left(S_f\right)_1 \left(x_2 - x_1\right) + H_L \tag{12.50}$$

$$H_2^{(2)} = H_1 - \frac{\left(x_2 - x_1\right)}{2}\left[\left(S_f\right)_1 + \left(S_f\right)_2^{(1)}\right] + H_L \tag{12.51}$$

in which H_L = local head loss, $\left(x_2 - x_1\right) < 0$ since cross section 2 is upstream from cross section 1 and H is defined as

$$H = z + \frac{(Q/A)^2}{2g} \tag{12.52}$$

Equations (12.50) - (12.51) are applied in the same way that (12.48) - (12.49) were used in Example 12.8 except that Eq. (12.52) and field measurements must be used to prepare a plot of H versus z for each channel cross section. Henderson (1966) points out that little generalized information is available for values of H_L, and river engineers commonly use values that have been measured in past floods.

References

Chow, V.T. (1959) *Open-channel hydraulics*, McGraw-Hill Book Co., New York, pp. 115-123.

Henderson, F.M. (1966) *Open channel flow*, MacMillan Publishing Co., New York, pp. 96-101, p. 141, ch. 6.

Report (1963) ASCE task force on friction factors in open channels, *Proc. Am. Soc. Civil Engrs*, vol. 89, no. HY2, pp. 97-143.

Chapter 13

Unsteady Pipe Flow

In unsteady flow variables such as velocity and pressure change with time at a fixed point. An important example of unsteady flow that will be considered in this chapter is concerned with the movement of relatively large pressure waves through a pipe when a valve is closed rapidly, a phenomenon known as waterhammer. We will treat these flows as one-dimensional. However, the addition of time as a second independent variable means that all dependent variables are functions of both x and t. As a result, these problems are described with partial rather than ordinary differential equations. In this chapter we will learn to solve these partial differential equations by using a very general and powerful technique that is known as the method of characteristics.

The Equations of Unsteady Pipe Flow

We will only consider flow in constant diameter pipes. However, pressures in these flows often become so large that elastic effects in both the fluid and pipe walls must be included in an analysis. Thus, the control volume shown in Fig. 13.1 has a cross sectional area, A, and mass density, ρ, that change with both x and t. For this reason longitudinal pressure forces include pressure forces on both end sections and a third force exerted by the diverging pipe walls on the flow. The remaining longitudinal forces include a component of the fluid weight and a tangential shear force along the pipe walls. The pipe centreline makes an angle θ with the horizontal.
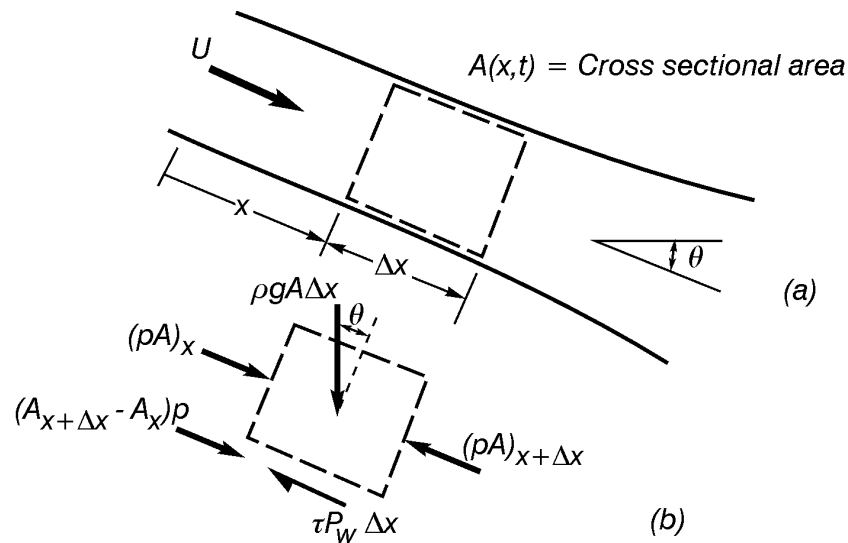

Figure 13.1 The control volume and free body diagram for unsteady flow in a pipe.

The control volume form of the continuity equation states that the sum of the net mass flux out through the control volume boundaries and the time rate of increase of mass within the control volume must vanish.

$$\left(\rho A\, U\right)_{x\,+\,\Delta x} - \left(\rho A\, U\right)_{x} + \frac{\partial\left(\rho A\, \Delta x\right)}{\partial t} = 0 \tag{13.1}$$

Since x and t are independent variables, Δx is treated as a constant when differentiating with respect to t. Therefore, division of (13.1) by Δx and letting $\Delta x \rightarrow 0$ gives

$$\frac{\partial\left(\rho A\, U\right)}{\partial x} + \frac{\partial\left(\rho A\right)}{\partial t} = 0 \tag{13.2}$$

Expansion of the first term in (13.2) gives

$$\rho A\, \frac{\partial U}{\partial x} + U\, \frac{\partial\left(\rho A\right)}{\partial x} + \frac{\partial\left(\rho A\right)}{\partial t} = 0 \tag{13.3}$$

and use of the definition of the material derivative puts (13.3) in a relatively simple form.

$$\frac{\partial U}{\partial x} + \frac{1}{\rho A}\, \frac{D\left(\rho A\right)}{Dt} = 0 \tag{13.4}$$

Changes in ρA occur in the flow only as a result of changes in pressure, p. Thus, we define

$$\frac{1}{\rho A}\, \frac{d\left(\rho A\right)}{dp} = \frac{1}{\rho c^{2}} \tag{13.5}$$

Use of the chain rule and Eq. (13.5) gives

$$\frac{1}{\rho A}\, \frac{D\left(\rho A\right)}{Dt} = \frac{1}{\rho A}\, \frac{d\left(\rho A\right)}{dp}\, \frac{Dp}{Dt} = \frac{1}{\rho c^{2}}\, \frac{Dp}{Dt} \tag{13.6}$$

and allows Eq. (13.4) to be written in its final form.

$$\rho c^{2}\, \frac{\partial U}{\partial x} + U\, \frac{\partial p}{\partial x} + \frac{\partial p}{\partial t} = 0 \tag{13.7}$$

Later in this chapter we will show that c is the celerity or speed of a pressure wave in the flow, (i.e. c is the speed of sound in the fluid). Wylie and Streeter (1982) give expressions for c for various types of conduits. The most important of these expressions for our purposes is the following result for an elastic conduit with thin walls:

$$c = \sqrt{\frac{E_{f}/\rho}{1 + \dfrac{E_{f}}{E_{p}}\, \dfrac{D}{T}}} \tag{13.8}$$

in which E_f = fluid bulk modulus of elasticity, E_p = pipe material modulus of elasticity, D = pipe diameter and T = pipe wall thickness. Equation (13.8) shows that c can be increased either by stiffening the pipe walls or by increasing the pipe wall thickness relative to the pipe diameter. For water at 15°C in a steel pipe, c decreases from 1,464 m/s when D/T = 0 to 1,017 m/s when D/T = 100.

The momentum equation can be derived by using the free body diagram shown in Fig. 13.1b. In this case the dashed lines become system volume boundaries. Since the mass of fluid within the system volume does not change with time (by definition of a system volume, as explained in Chapter 2), Newton's second law states that the resultant of all external forces on the system volume equals the product of its mass and acceleration.

$$(pA)_x - (pA)_{x+\Delta x} + (A_{x+\Delta x} - A_x)p + \rho g A \Delta x \sin\theta - \tau P_w \Delta x = \rho A \Delta x \frac{DU}{Dt} \qquad \textbf{(13.9)}$$

Dividing by $\rho A \Delta x$ and letting $\Delta x \to 0$ gives

$$-\frac{1}{\rho A} \frac{\partial(pA)}{\partial x} + \frac{p}{\rho A} \frac{\partial A}{\partial x} + g\sin\theta - \frac{\tau}{\rho A / P_w} = \frac{DU}{Dt} \qquad \textbf{(13.10)}$$

Expansion of the derivative in the first term and use of (7.47), (7.51) and $A/P_w = D/4$ puts (13.10) in the following form:

$$\boxed{-\frac{1}{\rho} \frac{\partial p}{\partial x} + g\sin\theta - \frac{f}{2D}|U|U = \frac{DU}{Dt} = U\frac{\partial U}{\partial x} + \frac{\partial U}{\partial t}} \qquad \textbf{(13.11)}$$

in which the absolute value sign in the third term has been used to ensure that the tangential wall shear force is always in a direction opposite to the direction of motion. This is necessary because pressure waves and velocities in water hammer problems invariably oscillate in direction.

Simplification of the Equations

Equations (13.7) and (13.11) contain a few terms that are relatively small. While it is not incorrect to retain these terms, their presence complicates both the calculation and interpretation of solutions. Furthermore, these terms are likely to make contributions to the end result that are of the same order as errors introduced by inaccurate estimates for c and f. For these reasons, we will scale terms in (13.7) and (13.11) and discard several terms that are found to be relatively small.

The problem in Fig. 13.2 is useful for estimating magnitudes of terms in (13.7) and (13.11). As in Chapter 5, the symbol $\sim$ will be used to denote "of the order of". Thus, since flow in the pipe has a constant initial velocity U_0 that is reduced to zero at the downstream pipe end when the valve is suddenly closed, we have the estimate $U \sim U_0$. Since c is the speed of a pressure wave in the flow, a characteristic time is given by $\Delta t \sim L/c$. Changes in ρ and c are relatively small in these problems, and this allows us to treat ρ and c as constants in Eqs. (13.7) and (13.11).
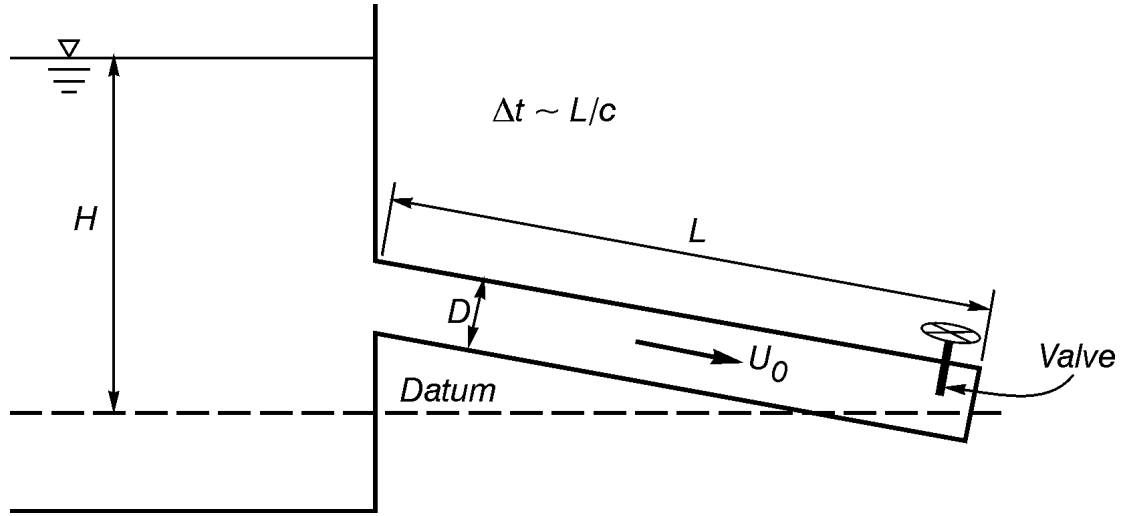
Figure 13.2 A problem used to estimate magnitudes of terms in Eqs. (13.7) and (13.11).

If Δp is the maximum change in pressure created by suddenly closing a valve at the downstream end of the pipe, then terms in Eq. (13.7) have the following orders of magnitude:

$$\rho c^2 \, \frac{U_0}{L} \; + \; U_0 \, \frac{\Delta p}{L} \; + \; \frac{\Delta p}{L/c} \; \sim \; 0 \tag{13.12}$$

Since $\partial p / \partial t$ is unlikely to be small in (13.7), division of (13.12) by $\Delta p /(L/c)$ gives an estimate for each of the first two terms relative to $\partial p / \partial t$.

$$\frac{\rho c \, U_0}{\Delta p} \; + \; \frac{U_0}{c} \; + \; 1 \; \sim \; 0 \tag{13.13}$$

But $c \sim 1400$ m/s and, in most problems, we would expect that U_0 would not exceed 50 m/s. Thus, the second term is unlikely to be more than four per cent of the third term, and the first and third terms must have the same order of magnitude. Thus, Eq. (13.13) gives the following estimate for Δp:

$$\Delta p \; \sim \; \rho c \, U_0 \tag{13.14}$$

When we eventually solve the problem in Fig. 13.2, we will find that the estimate given by (13.14) is extremely close.

The easiest way to appreciate the size of the pressure increase given by (13.14) is to divide both sides of (13.14) by ρg to obtain

$$\Delta h \sim \frac{c\, U_0}{g} \tag{13.15}$$

in which Δh is the maximum increase in piezometric head. Since $c \sim 1400$ m/s and $g = 9.81$ m/s, Δh is very large for any reasonably large value of U_0. For example, if $H = 10$ m, if friction and local losses are neglected and if the valve is completely open before being suddenly closed, then $U_0 = \sqrt{2gH} = 14$ m/s and $\Delta h \sim 2000$ m. In dimensionless terms, this gives $\Delta h / H \sim 200$. This massive pressure increase can be large enough to burst a pipe and is the reason for using the term waterhammer to describe the phenomenon.

The preceding analysis showed that the second term in (13.7) can be neglected and also provided an estimate for the maximum pressure rise created by suddenly closing a valve at the downstream end of the pipe. A similar analysis of Eq. (13.11) gives

$$\frac{c\, U_0}{L} + g\, \sin\theta + \frac{f}{2D}\, U_0^2 \sim U_0\, \frac{U_0}{L} + \frac{U_0}{L/c} \tag{13.16}$$

in which (13.14) has been used to provide an estimate for Δp. Since $\partial U / \partial t$ is unlikely to be small, division of (13.16) by $U_0 / (L/c)$ gives an estimate for each term relative to $\partial U / \partial t$.

$$1 + \frac{gL}{c\, U_0}\, \sin\theta + \frac{f}{2}\, \frac{L}{D}\, \frac{U_0}{c} \sim \frac{U_0}{c} + 1 \tag{13.17}$$

Equation (13.17) shows that the convective acceleration term, $U\, \partial U / \partial x$, should be dropped since it has the same relative magnitude as the term $U\, \partial p / \partial x$ that was dropped in (13.7). The friction term can be neglected only when

$$\frac{f}{2}\, \frac{L}{D}\, \frac{U_0}{c} << 1 \tag{13.18}$$

Since (13.18) is not always true, we will retain the friction term but note that it can be neglected when (13.18) is satisfied. Equation (13.17) also shows that the gravitational term $g\, \sin\theta$ can probably be neglected in most problems. However, we will choose to retain this term and then absorb it by changing the dependent variables from p and U to h and U.

The governing equations, (13.7) and (13.11), now have the following simpler forms:

$$\rho c^2\, \frac{\partial U}{\partial x} + \frac{\partial p}{\partial t} = 0 \tag{13.19}$$

$$-\frac{1}{\rho}\, \frac{\partial p}{\partial x} + g\, \sin\theta - \frac{f}{2D}\, |U|\, U = \frac{\partial U}{\partial t} \tag{13.20}$$

in which ρ and c are treated as constants. If z is measured upward from an arbitrarily chosen horizontal datum, the piezometric head defined by Eq. (2.22) becomes

$$h = \frac{p}{\rho g} + z \tag{13.21}$$

in which $z(x)$ = elevation of the pipe centreline above datum. Since $\partial z(x)/\partial t = 0$, (13.21) allows (13.19) to be rewritten in the form

$$c^2 \frac{\partial U}{\partial x} + g \frac{\partial h}{\partial t} = 0 \tag{13.22}$$

Since $\sin \theta = -\partial z(x)/\partial x$, (13.21) allows (13.20) to be rewritten in the following simpler form:

$$g \frac{\partial h}{\partial x} + \frac{\partial U}{\partial t} = -\frac{f}{2D} |U| U \tag{13.23}$$

Second-order equations with U or h as their unknown can be obtained from (13.22)-(13.23). For example, differentiating (13.23) with respect to x and using (13.22) to eliminate $\partial U/\partial x$ gives

$$c^2 \frac{\partial^2 h}{\partial x^2} - \frac{\partial^2 h}{\partial t^2} = \frac{f|U|}{D} \frac{\partial h}{\partial t} \tag{13.24}$$

In a similar way, differentiating (13.23) with respect to t and using (13.22) to eliminate $\partial h/\partial t$ gives

$$c^2 \frac{\partial^2 U}{\partial x^2} - \frac{\partial^2 U}{\partial t^2} = \frac{f|U|}{D} \frac{\partial U}{\partial t} \tag{13.25}$$

Equations (13.24) and (13.25) are a nonlinear form of an equation known as the wave equation. If these equations are linearized by replacing $|U|$ with a constant, say U_0, then standard solution techniques such as separation of variables (Fourier series) or Laplace transform methods can be used to obtain solutions. However, the method of characteristics offers a number of important advantages over these other techniques. These advantages include closed-form solutions that are easily interpreted when friction is neglected together with a technique that can be used to obtain accurate and stable numerical solutions when the nonlinear friction term is included. Therefore, the remainder of this chapter will be concerned exclusively with the use of characteristics to solve (13.22) - (13.23).

The Method of Characteristics

The method of characteristics is based upon the idea of a directional derivative, which was introduced in Chapter 1. If a dependent variable, ϕ, is a function of the two independent variables x and t, then a curve in the (x, t) plane can always be described parametrically as a function of arc length, s, along its path.

$$x = x(s)$$
$$t = t(s)$$

(13.26 a, b)

This means that along this curve ϕ takes on the values $\phi[x(s), t(s)]$, and the derivative of ϕ with respect to s is calculated from the chain rule of differential calculus.

$$\frac{d\phi}{ds} = \frac{\partial \phi}{\partial x}\frac{dx}{ds} + \frac{\partial \phi}{\partial t}\frac{dt}{ds}$$

(13.27)

Since dx/ds and dt/ds are the direction cosines of the unit tangent to the curve, Eq. (13.27) is a two-dimensional form of Eq. (1.44).

An alternative form for a directional derivative can be obtained by solving (13.26 b) for $s = s(t)$ and substituting the result into (13.26 a) to obtain

$$x = x[s(t)] = x(t)$$

(13.28)

The function ϕ now takes on the values of $\phi[x(t), t]$ along the curve, and the derivative of ϕ along this curve is given by

$$\frac{d\phi}{dt} = \frac{dx}{dt}\frac{\partial \phi}{\partial x} + \frac{\partial \phi}{\partial t}$$

(13.29)

We will choose to use (13.29) when using the method of characteristics to solve problems because dx/dt has the physical interpretation of a velocity. However, we could just as easily use (13.27), in which s may or may not be chosen as arc length, or we could instead solve (13.26 a) for $s = s(x)$ and use $t = t[s(x)] = t(x)$ to calculate

$$\frac{d\phi}{dx} = \frac{\partial \phi}{\partial x} + \frac{dt}{dx}\frac{\partial \phi}{\partial t}$$

(13.30)

Our choice of (13.29) is quite arbitrary. We will call the curve given by Eq. (13.28) a "characteristic curve". Some examples will now be used to show how (13.29) can be used to integrate partial differential equations.

Example 13.1

Solve the following problem by using the method of characteristics:

$$\frac{\partial \phi}{\partial x} + e^t \frac{\partial \phi}{\partial t} = 0 \qquad \text{for} \qquad -\infty < x < \infty \quad \text{and} \quad 0 < t < \infty$$

$$\phi(x, 0) = e^{-x^2} \qquad \text{for} \qquad -\infty < x < \infty$$

Solution: The first step is to divide the differential equation by e^t so that $\partial \phi / \partial t$ has a coefficient of unity.

$$e^{-t} \frac{\partial \phi}{\partial x} + \frac{\partial \phi}{\partial t} = 0$$

Equation (13.29) shows that this partial differential equation is equivalent to the simultaneous solution of two ordinary differential equations along a characteristic curve:

$$\frac{d\phi}{dt} = 0 \quad \text{along the curve} \quad \frac{dx}{dt} = e^{-t}$$

Integration of these two equations gives

$$\phi = K_1 \quad \text{along} \quad x + e^{-t} = K_2$$

The next step is to make qualitatively correct sketches of the (x, t) plane and a typical characteristic curve. It is usually easier to obtain characteristic curve geometry from the differential equation ($dx/dt = e^{-t}$ in this case) than from its integral ($x + e^{-t} = K_2$ in this case).
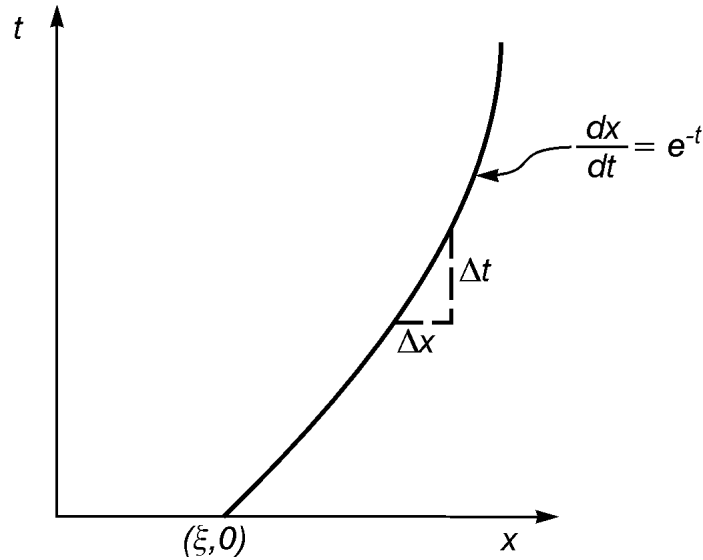
The characteristic curve originates from the point $(x, t) = (\xi, 0)$, where $\phi = e^{-\xi^2}$ from the initial condition given in the problem statement. Thus, K_1 and K_2 may be evaluated at this point to obtain

$$\phi = e^{-\xi^2} \quad \text{along} \quad x + e^{-t} = \xi + 1 \quad \text{for} \quad -\infty < \xi < \infty$$

This allows ϕ to be calculated at every point along the characteristic curve, and by allowing ξ to take on all values in the range $-\infty < \xi < \infty$ we are able to calculate a value for ϕ at every point in the solution domain $-\infty < x < \infty$ and $0 \le t < \infty$. This will be called the parametric form of the solution, with ξ as a parameter.

The non-parametric form of the solution is obtained by eliminating ξ from the two equations that hold along the characteristic curve. In this case, the characteristic curve gives $\xi = x + e^{-t} - 1$, from which we obtain

$$\phi = e^{-\left(x + e^{-t} - 1\right)^2} \quad \text{for} \quad -\infty < x + e^{-t} - 1 < \infty$$

The solution for ϕ obviously satisfies the correct initial condition at $t = 0$, and it is not difficult to show that it also satisfies the partial differential equation. The inequality shows that the solution holds only in the region covered by characteristic curves that pass through points where initial data for ϕ was specified. (In this case, initial data was specified along the entire x axis. Since the characteristic curves passing through the x axis cover the entire solution domain, the solution for ϕ holds everywhere within this region.) In practice it is easier and more informative to omit the inequality and, instead, indicate in a drawing of the (x, t) plane the region in which the solution holds.

$$\phi = e^{-\left(x + e^{-t} - 1\right)^2} \quad \text{for} \quad -\infty < x < \infty \quad \text{and} \quad 0 \le t < \infty$$
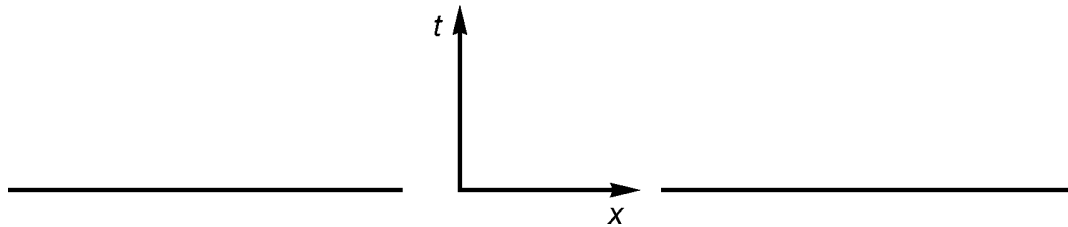
Example 13.2

Use characteristics to solve the following problem:

$$5 \frac{\partial \phi}{\partial x} + \frac{\partial \phi}{\partial t} = 1 \qquad \text{for} \quad 0 < x < \infty \quad \text{and} \quad 0 < t < \infty$$

$$\phi(x, 0) = 0 \qquad \text{for} \quad 0 < x < \infty$$

$$\phi(0, t) = \frac{1}{1 + t} \qquad \text{for} \quad 0 < t < \infty$$

Solution: Since the coefficient of $\partial\phi/\partial t$ is unity, Eq. (13.29) shows that the following two ordinary differential equations hold along a characteristic curve:

$$\frac{d\phi}{dt} = 1 \quad \text{along the curve} \quad \frac{dx}{dt} = 5$$

Integration of these two equations gives

$$\phi - t = K_1 \quad \text{along} \quad x - 5t = K_2$$

The characteristic curves are straight lines with a slope of 5. A sketch of the (x, t) plane follows:
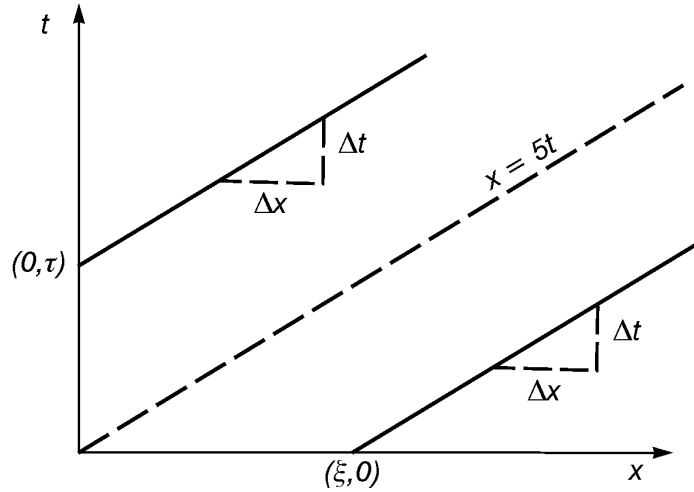
The solution domain covers the entire first quadrant. However, the characteristic curves passing through the positive x axis, where K_1 and K_2 can be calculated from the given initial condition, only cover the portion of this solution domain that lies below the characteristic curve passing through the coordinate origin $(x = 5t)$. Because of this, the boundary condition along the positive t axis is required so that the solution can be calculated in the region above the curve $x = 5t$.

Along the characteristic curve that intersects the x axis at $(\xi, 0)$ we obtain

$$\boxed{\phi - t = 0 \quad \text{along} \quad x - 5t = \xi \quad \text{for} \quad 0 < \xi < \infty}$$

Elimination of the parameter ξ gives

$$\boxed{\phi = t}$$

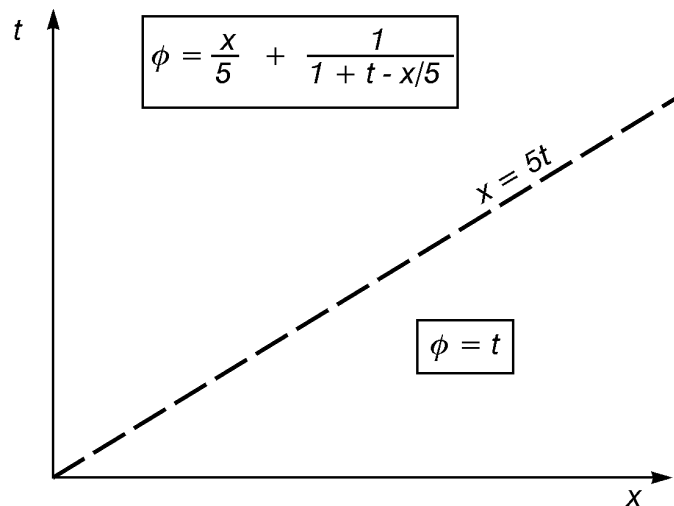in the region between $x = 5t$ and the positive x axis.

Along the characteristic curve that intersects the t axis at $(0, \tau)$ we obtain

$$\boxed{\phi - t = \frac{1}{1 + \tau} - \tau \quad \text{along} \quad x - 5t = -5\tau \quad \text{for} \quad 0 < \tau < \infty}$$

Elimination of the parameter τ gives

$$\boxed{\phi = t + \frac{1}{\left(1 + t - x/5\right)} - \left(t - x/5\right)}$$

in the region between $x = 5t$ and the positive t axis. A sketch of the solution domain and the final form of the solution follows:

Again, it is easy to see that the boundary and initial conditions are satisfied, and a bit more work would show that the partial differential equation is also satisfied.

Example 13.3

Use characteristics to solve the following problem:

$$-5 \frac{\partial \phi}{\partial x} + \frac{\partial \phi}{\partial t} = 1 \quad \text{for} \quad 0 < x < \infty \quad \text{and} \quad 0 < t < \infty$$

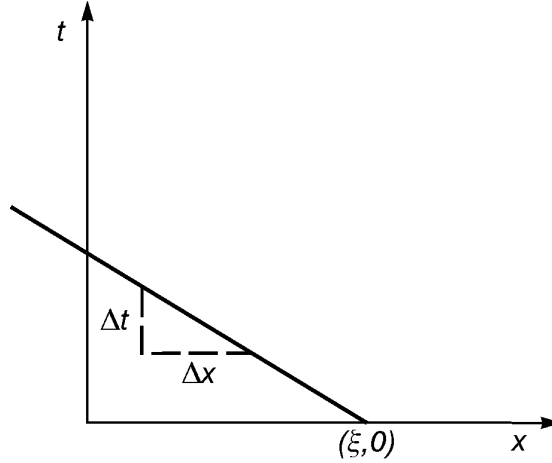$$\phi(x, 0) = 0 \quad \text{for} \quad 0 < x < \infty$$

Solution: The characteristic form of the partial differential equation follows:

$$\frac{d\phi}{dt} = 1 \quad \text{along the curve} \quad \frac{dx}{dt} = -5$$

Integration of these equations gives

$$\phi - t = K_1 \quad \text{along} \quad x + 5t = K_2$$

The characteristic curves are straight lines with a slope of -5. A sketch of the (x, t) plane follows:

The solution domain again consists of the first quadrant. However, because the characteristics have a negative slope, characteristics passing through the positive x axis cover the entire solution domain. Therefore, only the initial condition along the positive x axis is needed to calculate a solution in the first quadrant.

Along the characteristic curve that intersects the x axis at $(\xi, 0)$ we obtain

$$\boxed{\phi - t = 0 \quad \text{along} \quad x + 5t = \xi \quad \text{for} \quad 0 < \xi < \infty}$$

The non-parametric form of the solution is

$$\boxed{\phi = t}$$

which is valid throughout the entire solution domain.

The previous three examples illustrate a number of important points that can be generalized. We will state these points without proofs.

1.   Any equation or set of equations that can be solved by using characteristics is defined to be hyperbolic. All linear first-order equations with a single unknown can be solved using characteristics and, therefore, are hyperbolic.

2.   Hyperbolic equations allow discontinuities in either the dependent variable or its derivatives to be carried from a boundary into a solution domain along a characteristic. (See the discontinuity in ϕ that occurs along the characteristic $x = 5t$ in Example 13.2.) Only hyperbolic equations have this property. Since numerical methods usually approximate dependent variables with polynomials, hyperbolic problems with discontinuous boundary or initial conditions can be solved accurately with numerical techniques only by integrating along, rather than across, characteristics. This suggests that accurate numerical solutions of these problems can be obtained only by using the method of characteristics.

3.   The geometry of the characteristics determines which boundary and initial conditions must be used to obtain a unique solution. For example, a single first-order equation in one unknown requires that the dependent variable, ϕ, be specified at one, and only one, point on each and every characteristic within its solution domain. (In Example 13.2, the positive sloping characteristics required that data be specified along both the positive x and positive t axes to calculate a solution in the first quadrant. In Example 13.3, the negative sloping characteristics meant that data specified along only the positive x axis was sufficient to calculate a solution in the first quadrant. Specification of any more data, say along the positive t axis, would have over determined the solution.)

4.   The characteristic slope, dx/dt, gives the wave speed. This is the speed at which a disturbance or solution is carried through a solution domain.

One fascinating topic that has not been discussed is the occurrence of shocks within a solution domain. Shocks, which are often called surges by hydraulic engineers, occur only when coefficients of the highest derivatives in hyperbolic partial differential equations are functions of the dependent variable or its derivatives. (This causes characteristic curve slopes to vary with changes in the dependent variable.) Since coefficients of the derivatives of h and U in (13.22) - (13.23) are constants, shocks cannot occur in waterhammer problems. However, shocks do occur in unsteady open channel flow problems, which are not considered in this chapter. Stoker (1957) and Whitham (1974) give detailed discussions of shocks.

The ideas just discussed for a single first-order equation can sometimes be extended to solve two or more simultaneous first-order equations. For example, consider the following two equations:

$$\frac{\partial u}{\partial x} + \frac{\partial v}{\partial t} = 0$$

$$\frac{\partial v}{\partial x} + \frac{\partial u}{\partial t} = 0$$

(13.31 a, b)

We will look for a linear combination of these equations that contains derivatives along the same characteristic curve in the (x, t) plane. Multiplying (13.31 b) by an unknown parameter λ and adding the result to (13.31 a) gives

$$\frac{\partial u}{\partial x} + \frac{\partial v}{\partial t} + \lambda \left(\frac{\partial v}{\partial x} + \frac{\partial u}{\partial t} \right) = 0 \qquad\qquad \textbf{(13.32)}$$

This can be rearranged in the following form:

$$\lambda \left(\frac{1}{\lambda} \frac{\partial u}{\partial x} + \frac{\partial u}{\partial t} \right) + \left(\lambda \frac{\partial v}{\partial x} + \frac{\partial v}{\partial t} \right) = 0 \qquad\qquad \textbf{(13.33)}$$

Since we want all derivatives in (13.33) to be directional derivatives along the same curve in the (x, t) plane, (13.29) shows that we must choose λ so that

$$\frac{dx}{dt} = \frac{1}{\lambda} = \lambda \qquad\qquad \textbf{(13.34)}$$

Then (13.33) becomes

$$\lambda \frac{du}{dt} + \frac{dv}{dt} = 0 \quad \text{along} \quad \frac{dx}{dt} = \lambda \qquad\qquad \textbf{(13.35)}$$

Since (13.34) gives $\lambda^2 = 1$ and $\lambda = \pm 1$, we obtain two sets of equations from (13.35).

$$\frac{du}{dt} + \frac{dv}{dt} = 0 \quad \text{along} \quad \frac{dx}{dt} = 1$$

$$-\frac{du}{dt} + \frac{dv}{dt} = 0 \quad \text{along} \quad \frac{dx}{dt} = -1 \qquad\qquad \textbf{(13.36 a, b)}$$

Integration of (13.36) gives

$$u + v = K_1 \quad \text{along} \quad x - t = K_2$$

$$-u + v = K_3 \quad \text{along} \quad x + t = K_4 \qquad\qquad \textbf{(13.37 a, b)}$$

From this result we see that there are two families of characteristic curves for this problem. ***In general, the method of characteristics can be used to solve a problem only if the number of unknowns, the number of simultaneous differential equations and the number of families of characteristic curves are all identical***. The next example will show how (13.37 a, b) are used to solve a particular problem.

Example 13.4

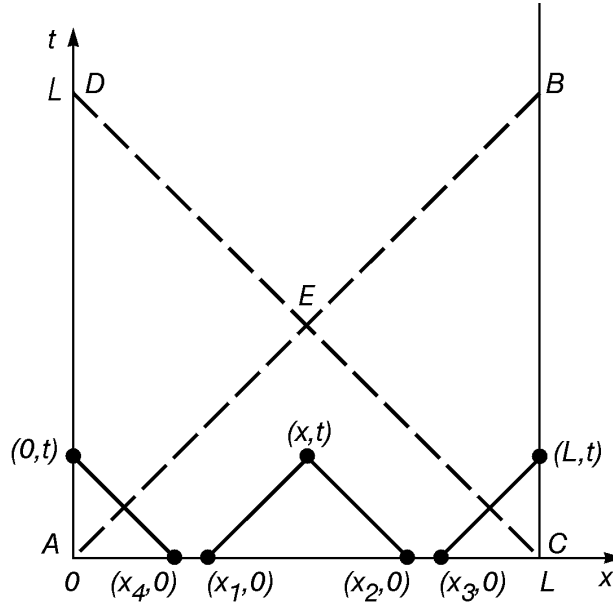We will use (13.37 a, b) to solve the following problem

$$\frac{\partial u}{\partial x} + \frac{\partial v}{\partial t} = 0 \quad \text{for} \quad 0 < x < L \quad \text{and} \quad 0 < t < \infty$$

$$\frac{\partial v}{\partial x} + \frac{\partial u}{\partial t} = 0 \quad \text{for} \quad 0 < x < L \quad \text{and} \quad 0 < t < \infty$$

$$u = x \quad \text{and} \quad v = 0 \quad \text{at} \quad t = 0 \quad \text{for} \quad 0 < x < L$$

$$u = 1 \quad \text{at} \quad x = 0 \quad \text{for} \quad 0 < t < \infty$$

$$v = 0 \quad \text{at} \quad x = L \quad \text{for} \quad 0 < t < \infty$$

Solution: Sketches of the (x, t) plane and some typical characteristics are shown below.

Since (13.37 a) and (13.37 b) apply along the characteristics originating from $(x_1, 0)$ and $(x_2, 0)$, respectively, we obtain

$$u + v = x_1 \quad \text{along} \quad x - t = x_1$$

$$-u + v = x_2 \quad \text{along} \quad x + t = x_2$$

in which K_1, K_2, K_3 and K_4 have been calculated from the given initial conditions for u and v at $t = 0$. Solution of these equations for u, v, x and t at the point where the two characteristics meet gives the parametric solution.

$$\boxed{\begin{array}{ll} u = \left(x_1 + x_2\right)/2 & v = \left(x_1 - x_2\right)/2 \\[2mm] x = \left(x_1 + x_2\right)/2 & t = \left(x_2 - x_1\right)/2 \end{array}}$$

By choosing x_1 and x_2 in the range $0 \le x_1 < x_2 \le L$, values for u, v, x and t can be calculated at every point within the triangle AEC. The non-parametric form of the solution is obtained by eliminating the parameters x_1 and x_2 to obtain

$$u = x \quad \text{and} \quad \text{v} = -t \quad \text{within } AEC$$

Thus, u and v must both be specified at $t = 0$ for $0 < x < L$ if a unique solution is to be calculated within AEC.

Application of (13.37 a) along the characteristic originating at $(x_3, 0)$ gives the parametric solution for u and t along BC.

$$u = x_3 \quad \text{along} \quad L - t = x_3$$

Elimination of the parameter x_3 gives the non-parametric form of the solution.

$$u = L - t \quad \text{along} \quad BC$$

From this result it becomes apparent that either u or v or some functional relationship between u and v must be specified as a boundary condition along $x = L$ if a unique solution is to be calculated along BC.

Application of (13.37 b) along the characteristic originating at $(x_4, 0)$ give the parametric solution for v and t along AD.

$$-1 + \text{v} = -x_4 \quad \text{along} \quad t = x_4$$

Elimination of the parameter x_4 gives the non-parametric form of the solution.

$$\text{v} = 1 - t \quad \text{along} \quad AD$$

Thus, either u or v or a functional relationship between u and v must be specified along the boundary $x = 0$ if a unique solution is to be calculated along AD.

The solution within AED can be obtained by using positive and negative sloping characteristics that originate from AD and AC, respectively. The solution within BEC can be obtained by using positive and negative sloping characteristics that originate from AC and BC, respectively. The solution in the region immediately above DEB can be calculated by using positive and negative sloping characteristics that originate from AD and BC, respectively. Thus, the solution for each region is used as a stepping stone to calculate the solution for another region.

In this particular problem the boundary and initial conditions specify u so that it is discontinuous at $x = t = 0$. Therefore, discontinuities in u and v can be expected to travel through the solution domain along the characteristic *AB*.

These discontinuities will then move back into the solution domain along the negative sloping characteristic that originates at *B*. From this we see that disturbances move through the solution domain with speeds given by the slopes of the characteristics, and the discontinuities in y and v that originated at $x = t = 0$ continue to travel through the entire solution domain for $0 < t < \infty$ along both positive and negative sloping characteristics. These discontinuities would make an accurate numerical solution of this problem virtually impossible to obtain with finite difference or finite element methods.

A Fourier series solution could be obtained since u and v can be shown to both satisfy the second-order wave equation.

$$\frac{\partial^2 u}{\partial x^2} = \frac{\partial^2 u}{\partial t^2} \quad \text{and} \quad \frac{\partial^2 v}{\partial x^2} = \frac{\partial^2 v}{\partial t^2}$$

However, the rate of convergence of a Fourier series is slowed considerably by discontinuities, and oscillations known as Gibbs phenomenon occur in Fourier series solutions near discontinuities. Kreyszig (1993) gives a brief discussion of Gibbs phenomenon.

Example 13.5

Under what conditions can the equation

$$A \frac{\partial^2 \phi}{\partial x^2} + B \frac{\partial^2 \phi}{\partial x \partial t} + C \frac{\partial^2 \phi}{\partial t^2} = 0$$

be solved by using characteristics?

Solution: The second-order equation can be rewritten as two simultaneous first-order equations by setting

$$u = \frac{\partial \phi}{\partial x} \quad \text{and} \quad v = \frac{\partial \phi}{\partial t}$$

Then the second-order equation becomes

$$A \frac{\partial u}{\partial x} + B \frac{\partial v}{\partial x} + C \frac{\partial v}{\partial t} = 0$$

A second equation is obtained from a compatibility condition.

$$\frac{\partial u}{\partial t} = \frac{\partial^2 \phi}{\partial t \partial x} = \frac{\partial}{\partial x}\left(\frac{\partial \phi}{\partial t}\right) = \frac{\partial v}{\partial x}$$

Multiply the second equation by λ and add to the first equation.

$$\lambda \left(\frac{\partial u}{\partial t} - \frac{\partial v}{\partial x} \right) + \left(A \frac{\partial u}{\partial x} + B \frac{\partial v}{\partial x} + C \frac{\partial v}{\partial t} \right) = 0$$

Rearranging terms gives

$$\lambda \left(\frac{A}{\lambda} \frac{\partial u}{\partial x} + \frac{\partial u}{\partial t} \right) + C \left(\frac{B - \lambda}{C} \frac{\partial v}{\partial x} + \frac{\partial v}{\partial t} \right) = 0$$

This equation will contain derivatives along the same curve in the (x, t) plane if we can choose λ so that

$$\frac{dx}{dt} = \frac{A}{\lambda} = \frac{B - \lambda}{C}$$

Then the equation takes the following form:

$$\boxed{\lambda \frac{du}{dt} + C \frac{dv}{dt} = 0 \quad \text{along} \quad \frac{dx}{dt} = \frac{A}{\lambda}}$$

Calculation of λ requires the solution of a quadratic equation

$$\frac{A}{\lambda} = \frac{B - \lambda}{C}$$

The solution for λ is

$$\boxed{\lambda = \left(B \pm \sqrt{B^2 - 4AC} \right) / 2}$$

Since there are two equations with two unknowns, u and v, the method of characteristics can be used only if there are two distinct families of characteristics. This requires that

$$\boxed{B^2 - 4AC > 0}$$

in which case the original second-order equation is said to be hyperbolic. The method of characteristics cannot be used if $B^2 - 4AC = 0$, in which case the equation is said to be parabolic, or if $B^2 - 4AC < 0$, in which case the equation is said to be elliptic.

The Solution of Waterhammer Problems

The method of characteristics will now be used to solve (13.22) - (13.23). Multiplying (13.22) by λ and adding the result to (13.23) gives

$$\lambda \left(c^2 \frac{\partial U}{\partial x} + \frac{\partial h}{\partial t} \right) + g \frac{\partial h}{\partial x} + \frac{\partial U}{\partial t} = - \frac{f}{2D} |U| U \tag{13.38}$$

Rearrangement of the terms in (13.38) gives the following result:

$$\left(\lambda c^2 \frac{\partial U}{\partial x} + \frac{\partial U}{\partial t} \right) + \lambda g \left(\frac{1}{\lambda} \frac{\partial h}{\partial x} + \frac{\partial h}{\partial t} \right) = - \frac{f}{2D} |U| U \tag{13.39}$$

Derivatives in (13.39) will be calculated along the same curve in the (x, t) plane if we choose λ so that

$$\frac{dx}{dt} = \lambda c^2 = \frac{1}{\lambda} \tag{13.40}$$

in which case (13.39) becomes

$$\frac{dU}{dt} + \lambda g \frac{dh}{dt} = - \frac{f}{2D} |U| U \quad \text{along} \quad \frac{dx}{dt} = \frac{1}{\lambda} \tag{13.41}$$

Equation (13.40) gives $\lambda = \pm 1/c$, and we obtain from this result and (13.41) the following equations:

$$\begin{array}{ll} \dfrac{d(U + gh/c)}{dt} = - \dfrac{f}{2D} |U| U \quad \text{along} \quad \dfrac{dx}{dt} = c \\[2mm] \dfrac{d(U - gh/c)}{dt} = - \dfrac{f}{2D} |U| U \quad \text{along} \quad \dfrac{dx}{dt} = - c \end{array} \tag{13.42 a, b}$$

When (13.18) is satisfied, friction losses can be neglected. In this case (13.42) can be integrated to obtain

$$\begin{array}{ll} U + gh/c = K_1 \quad \text{along} \quad x - ct = K_2 \\[2mm] U - gh/c = K_3 \quad \text{along} \quad x + ct = K_4 \end{array} \tag{13.43 a, b}$$

Since two equations with two unknowns, U and h, have given two families of characteristics, we see that the method of characteristics can be used to solve waterhammer problems. Furthermore, (13.42) furnishes the proof that velocity and pressure waves in these problems move with a speed given by c. Finally, since one family of characteristics has a positive slope and the other family has a negative slope, we see that a unique solution requires:

1   Specification of U and h at $t = 0$ for $0 < x < L$. (Initial conditions.)

2   Specification of U or h or one functional relationship between U and h at both $x = 0$ and $x = L$ for $0 < t < \infty$. (Boundary conditions.)

Equation (13.15) shows that H is likely to be a very small portion of the maximum change in h. Therefore, any initial or boundary condition which specifies a value of h that does not exceed H can often be replaced with the requirement $h = 0$. This approximation can always be checked at the end of any calculation by comparing the maximum calculated value of Δh with H to see if $H/\Delta h << 1$. Thus, the problem in Fig. 13.2 has an initial value for h that does not exceed H, and we will use the approximate initial condition $h = 0$ at $t = 0$ for $0 < x < L$. Likewise, the boundary condition at $x = 0$ specifies a value for h that does not exceed H, and we will use the approximate boundary condition $h = 0$ at $x = 0$ for $0 < t < \infty$. If the valve at $x = L$ is completely closed during a zero time interval, we will require that $U = 0$ at $x = L$ for $0 < t < \infty$.

Example 13.6

Solve the problem in Fig. 13.2 by neglecting friction and local losses. Use the following initial and boundary conditions:

$$U = U_0 \quad \text{and} \quad h = 0 \quad \text{at} \quad t = 0 \quad \text{for} \quad 0 < x < L$$

$$h = 0 \quad \text{at} \quad x = 0 \quad \text{for} \quad 0 < t < \infty$$

$$U = 0 \quad \text{at} \quad x = L \quad \text{for} \quad 0 < t < \infty$$

Solution: Sketches of the (x, t) plane and some typical characteristics are shown below.
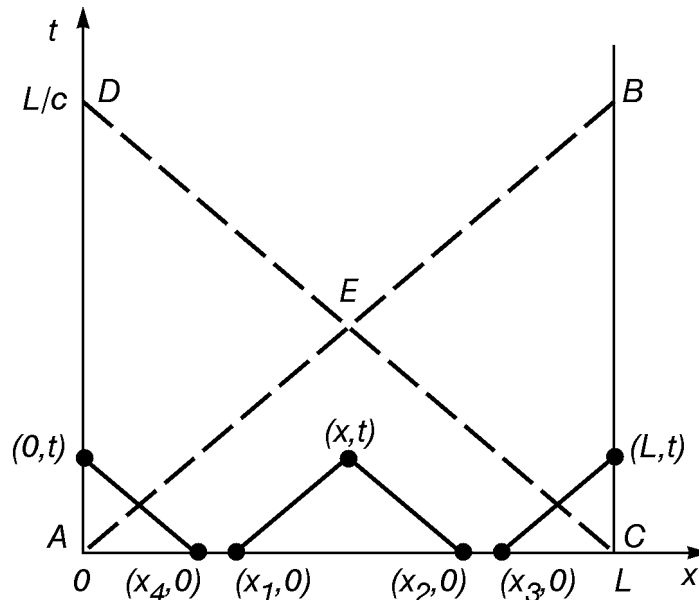
Equations (13.43 a) and (13.43 b) apply along the characteristic originating from $(x_1, 0)$ and $(x_2, 0)$, respectively. Use of the initial conditions to evaluate K_i gives

$$U + gh/c = U_0 \quad \text{along} \quad x - ct = x_1$$

$$U - gh/c = U_0 \quad \text{along} \quad x + ct = x_2$$

Simultaneous solution gives

$$\boxed{U = U_0 \quad \text{and} \quad h = 0 \quad \text{within } AEC}$$

Equation (13.43 a) applied along the characteristic originating from $(x_3, 0)$ gives

$$gh/c = U_0 \quad \text{along} \quad x - ct = x_3$$

Thus, we obtain the result

$$\boxed{h = \frac{c U_0}{g} \quad \text{along} \quad BC}$$

We note that this agrees exactly with the order of magnitude estimate given by (13.15) for the maximum change in piezometric head.

Equation (13.43 b) applied along the characteristic originating from $(x_4, 0)$ gives

$$\boxed{U = U_0 \quad \text{along} \quad ct = x_4}$$

Thus, the initial velocity does not change at $x = 0$ for $0 < t < L/c$.

Continuing in this way gives the solution shown in the following sketch of the (x, t) plane:
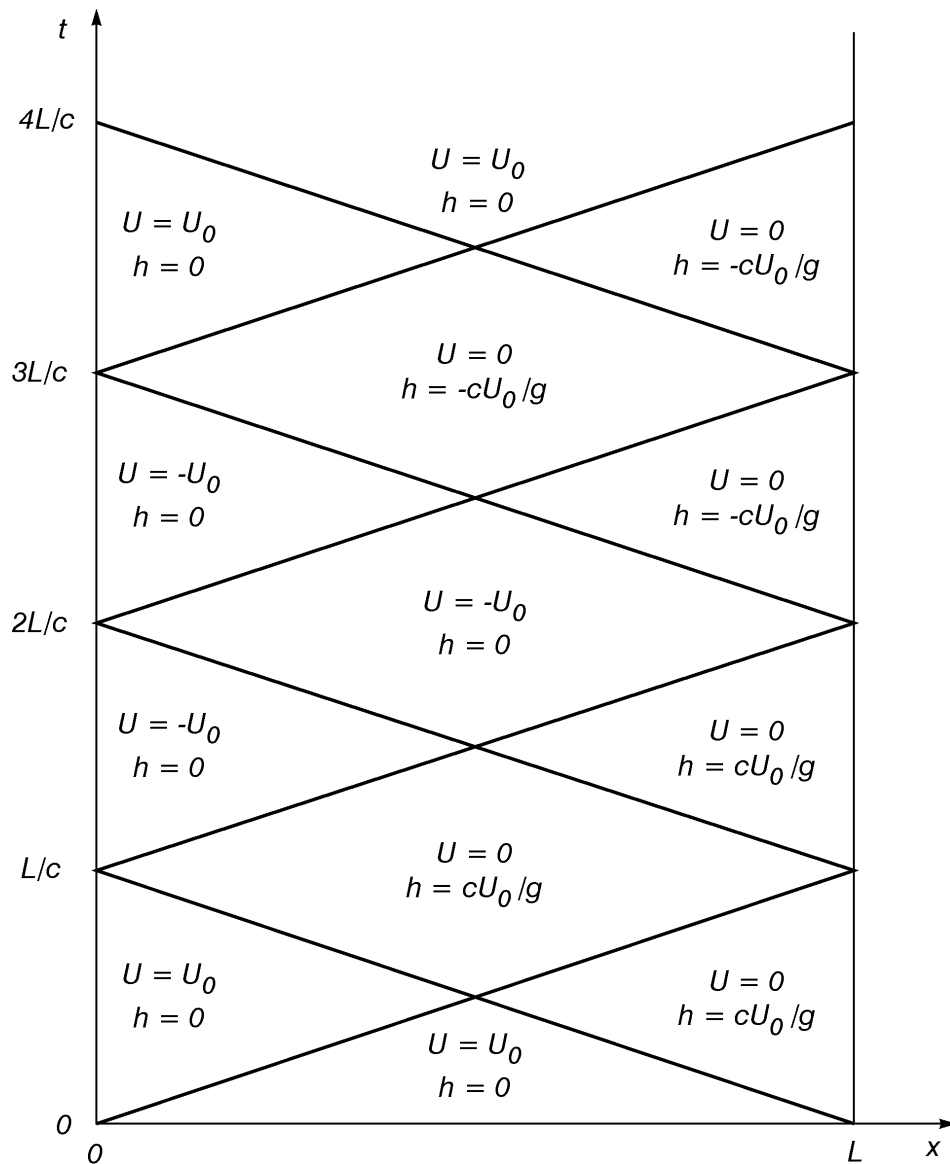
Plots of h versus t at $x = L$ and of U versus t at $x = 0$ show that the maximum piezometric head oscillates between cU_0/g and $-cU_0/g$ with a period of $4L/c$ and that the velocity at $x = 0$ oscillates between U_0 and $-U_0$ with the same period. These oscillations continue indefinitely since friction and local losses have been neglected.
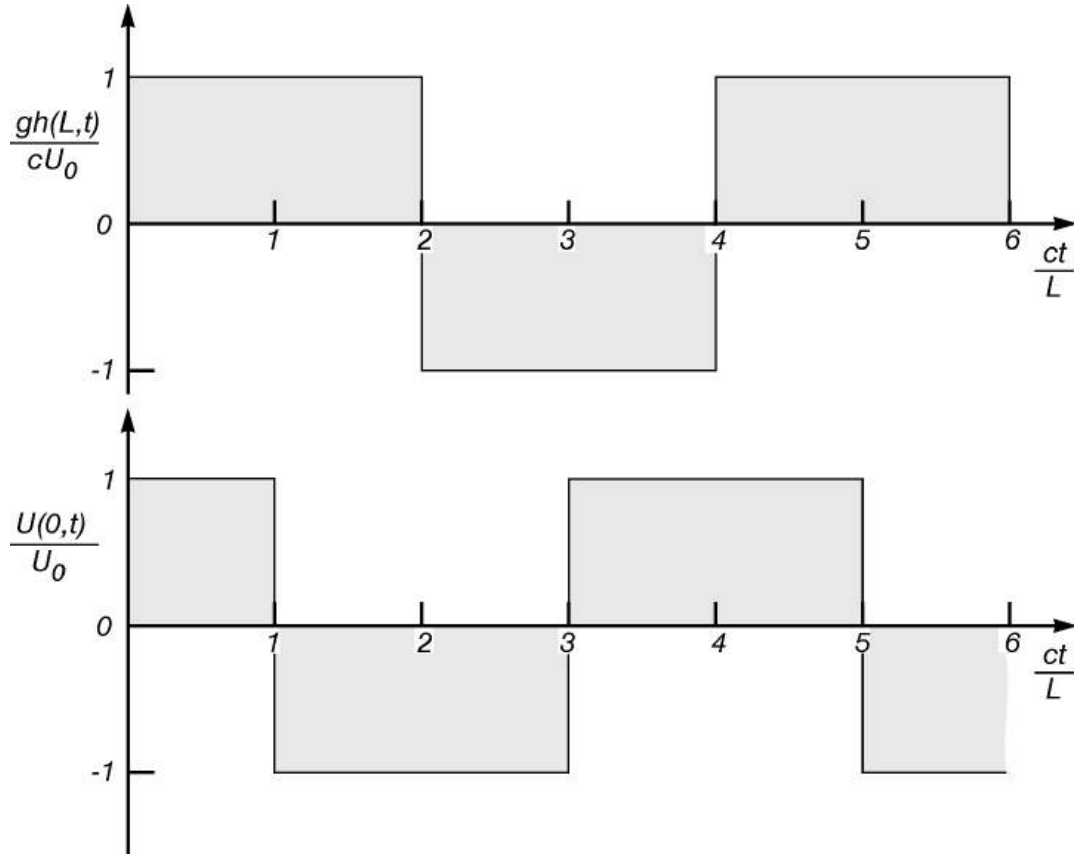
Numerical Solutions

Departures from the idealized assumptions made in working Example 13.6 usually make it necessary to obtain numerical solutions of (13.42). These departures include the effects of friction, finite valve closure times and systems with a number of different pipes. Whenever possible, the solution domain should be discretized with constant node spacings in the x and t directions with node spacings determined by the slope of the characteristic curves.

$$\Delta x = c \, \Delta t \tag{13.44}$$
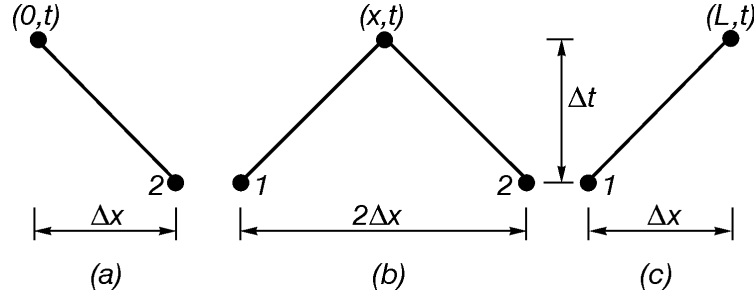
Figure 13.3 Characteristic line segments used for calculating numerical solutions.

At internal nodes, as in Fig. 13.3 b, Eqs (13.42) are approximated with

$$U + gh/c = \left(U + gh/c\right)_1 - \left(\frac{f}{2D}\,|U|\,U\right)_1 \Delta t = K_1$$

$$U - gh/c = \left(U - gh/c\right)_2 - \left(\frac{f}{2D}\,|U|\,U\right)_2 \Delta t = K_2$$

(13.45 a, b)

which can be solved for U and h at the node (x, t).

$$U = \left(K_1 + K_2\right)/2$$

$$h = c\left(K_1 - K_2\right)/(2g)$$

(13.46 a, b)

At the boundary node $(0, t)$ in Fig. 13.3 a, an approximate integral of (13.42 b)

$$U - gh/c = \left(U - gh/c\right)_2 - \left(\frac{f}{2D}\,|U|\,U\right)_2 \Delta t = K_2 \qquad \textbf{(13.47)}$$

is solved simultaneously with a boundary condition at $(0, t)$ to obtain U and h at $(0, t)$. At the boundary node (L, t) in Fig. 13.3 c, an approximate integral of (13.42 a).

$$U + gh/c = \left(U + gh/c\right)_1 - \left(\frac{f}{2D}\,|U|\,U\right)_1 \Delta t = K_1 \qquad \textbf{(13.48)}$$

is solved simultaneously with a boundary condition at (L, t) to obtain U and h at (L, t).

When more than one pipe occurs in a system, it is impossible to choose constant values for Δx and Δt that satisfy (13.44) everywhere. The usual procedure in this case is to choose constant values for Δx and Δt in all pipes. Then points 1 and 2 in Fig. 13.3, whose locations are found from (13.44), do not coincide with nodes, and linear interpolation along a horizontal line between nodes is used to calculate U and h (and, therefore, K_1 and K_2) for use in (13.45) - (13.48). If a discontinuity or steep gradient in U and h occurs between nodes, this interpolation process will smooth the solution and create artificial numerical diffusion. For this reason, (13.44) should be used to determine node spacings whenever possible.

Finite valve closure times are sometimes used to reduce peak pressures in pipes. When this is done, Δh may no longer be very large compared to H in Fig. 13.2. This means that $h = 0$ is no longer an acceptable approximation for a boundary condition at $x = 0$ or for an initial condition at $t = 0$. In this case the initial condition for h is calculated from the Bernoulli equation with, or without, a friction loss term. The most accurate form of the boundary condition at $x = 0$ is

$$h(0, t) = H - \frac{U^2}{2g} \quad \text{if} \quad U > 0$$
$$= H \quad\quad\quad \text{if} \quad U < 0 \tag{13.49}$$

This is because the flow behaves as flow into a pipe entrance when $U > 0$ and as flow in a submerged jet when $U < 0$. In practice, most analysts apparently set $h(0, t) = H$ for both cases, which is an acceptable approximation if $U^2/(2gH) << 1$.

For a finite closure time, the velocity upstream from the valve in Fig. 13.2 can be related to h by

$$U = \alpha\sqrt{gh} \tag{13.50}$$

in which α is an experimental coefficient that varies with the valve geometry. Thus, α will change with time as the valve is closed. [If datum is not chosen at the valve and the flow does not exit to the atmosphere at the valve, then h in (13.50) must be replaced with the change in h across the valve.] Introduction of (13.50) into (13.48) gives

$$\alpha\sqrt{gh} + gh/c = K_1 \tag{13.51}$$

which can be solved for h to obtain

$$h = \frac{c^2}{4g}\left[-\alpha + \sqrt{\alpha^2 + 4K_1/c}\right]^2 \tag{13.52}$$

At the junction of two different pipes, h and the flow rate are assumed to be continuous. Thus, the following simultaneous equations apply:

$$U_- + gh/c_- = K_1$$

$$U_+ - gh/c_+ = K_2 \qquad \qquad \textbf{(13.53 a, b, c)}$$

$$U_-A_- = U_+A_+$$

in which K_1 and K_2 are defined in (13.48) and (13.47) and U_+ and U_- are velocities on each side of the pipe junction as shown in Fig. 13.4. The solution of these equations is given by

$$U_- = \frac{K_1 c_- + K_2 c_+}{A_+ c_- + A_- c_+} A_+$$

$$U_+ = \frac{K_1 c_- + K_2 c_+}{A_+ c_- + A_- c_+} A_- \qquad \qquad \textbf{(13.54 a, b, c)}$$

$$h = \frac{K_1 A_- - K_2 A_+}{A_+ c_- + A_- c_+} \frac{c_+ c_-}{g}$$

A similar, but more involved, calculation can be made where three or more pipes meet by requiring continuity of flow rates and piezometric heads at the junction.

If a pump or valve is inserted in the middle of a pipeline, and if the pipes on either side of the pump or valve have different areas, then the relevant equations are

$$U_- + gh_-/c_- = K_1$$

$$U_+ - gh_+/c_+ = K_2 \qquad \qquad \textbf{(13.55 a, b, c)}$$

$$U_-A_- = U_+A_+$$

The characteristic geometry for (13.55) is shown in Fig. 13.4.
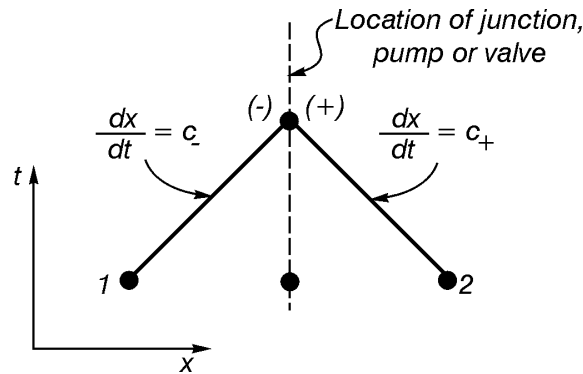
Figure 13.4 Characteristic geometry at the location of a pipe junction, pump or valve.

The three equations in (13.55) contain four unknowns: U_-, U_+, h_- and h_+. This system of equations is closed for a valve by requiring

$$U_- = \alpha(t)\sqrt{g\,|h_- - h_+|} \tag{13.56}$$

in which $\alpha(t)$ is an experimental coefficient that has the same sign as $\left(h_- - h_+\right)$. The system of equations is closed for a pump by using an experimental pump characteristic curve that plots Q versus the change in h across the pump. An extensive discussion of unsteady flow in pipes, together with computer program listings for some of the simpler cases, can be found in Wylie and Streeter (1982).

Pipeline Protection from Waterhammer

There are numerous ways to prevent pipelines from bursting as a result of waterhammer. One obvious way is to simply design pipes so that they are strong enough to withstand the expected changes in pressure. Changes in pressure can also be controlled by specifying equipment and operational procedures, such as minimum times for valve closures. Mechanical devices such as surge tanks, air chambers, reflux valves and pressure relief valves can be used in some applications. Discussions of many different possibilities are given by Wylie and Streeter (1982) and Stephenson (1989).

References

Kreyszig, E. (1993) *Advanced engineering mathematics*, seventh edition, John Wiley and Sons, New York, pp. 602-603.

Stephenson, D. (1989) *Pipeline design for water engineers*, Third revised and updated edition, Elsevier, New York, pp. 69-96.

Stoker, J.J. (1957) *Water waves*, Interscience Publishers, New York, ch. 10.

Whitham, G.B. (1974) *Linear and nonlinear waves*, John Wiley and Sons, New York.

Wylie, E.B. and V.L. Streeter (1982) *Fluid transients*, Corrected edition 1983, FEB Press, Ann Arbor, Michigan, 384 p.

Chapter 14

Unsteady Open Channel Flow

Unsteady flows in open channels occur frequently. Examples include waves moving across the free surfaces of lakes and reservoirs, changes in flow rates and water levels downstream from reservoir outlet works, sudden releases of water from burst dams and floods moving down rivers. Many of these problems can be modelled by assuming one-dimensional velocity distributions and pressure distributions that are hydrostatic along lines normal to the channel bottom. This leads to a set of partial differential equations known as the Saint-Venant equations. These equations are hyperbolic, so the method of characteristics can be used in their solution. However, the use of characteristics is considerably more difficult for flow in open channels than for flow in pipes. This is because the equations are nonlinear, so that the slope of the characteristic curves is not constant but is a function of the dependent variables. As a result, shocks or surges can appear spontaneously in these solutions, causing difficulties with numerical accuracy and stability.

In this chapter we will derive the Saint-Venant equations for unsteady flow in a prismatic rectangular channel. Then the method of characteristics will be used to show the types of boundary and initial conditions that must be imposed and to illustrate an effective numerical technique that is sometimes used to solve these equations. Finally, a simplification of the Saint-Venant equations known as the kinematic wave approximation will be introduced and used to discuss the problem of flood-wave movement down rivers in a process known as "flood routing".
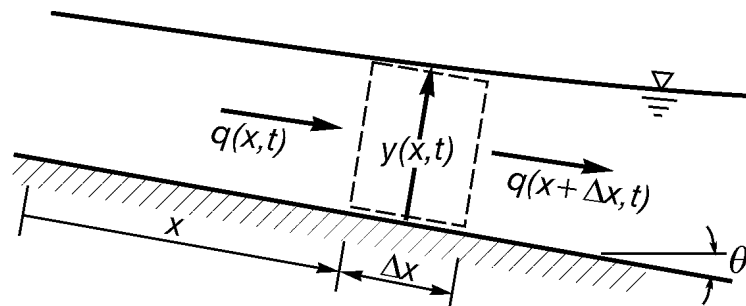
Figure 14.1 A control volume for unsteady flow in an open channel.

The Saint-Venant Equations

A control volume bounded by the free surface, the channel bottom and two surfaces normal to the channel bottom is shown with dashed lines in Figure 14.1. The two surfaces normal to the channel bottom are fixed, which means that fluid passes through them. The top boundary, however, moves in the vertical direction as the free surface geometry changes with time.

Let $q(x, t)$ be the flow rate per unit width. Since the continuity principle states that the difference between flow rates entering and leaving the control volume must be balanced by the rate at which fluid is stored within, we obtain

$$q(x, t) - q(x + \Delta x, t) = \frac{\partial(y \Delta x)}{\partial t} \tag{14.1}$$

Since x and t are independent variables, dividing (14.1) by Δx and putting all terms on the same side of the equation gives

$$\frac{q(x + \Delta x, t) - q(x, t)}{\Delta x} + \frac{\partial y}{\partial t} = 0 \tag{14.2}$$

Finally, letting $\Delta x \to 0$ gives the continuity equation for flow in a prismatic rectangular channel with zero lateral inflow.

$$\frac{\partial q}{\partial x} + \frac{\partial y}{\partial t} = 0 \tag{14.3}$$

Since $q = Uy$ in which U is the one-dimensional flux velocity, (14.3) can be written with U and y as its two unknowns.

$$\frac{\partial(Uy)}{\partial x} + \frac{\partial y}{\partial t} = 0 \tag{14.4}$$

Probably the simplest way to recover the momentum equation is to take the partial derivative of (6.22) with respect to x.

$$\frac{\partial h}{\partial x} + \frac{V}{g} \frac{\partial V}{\partial x} + \frac{1}{g} \frac{\partial^2 \phi}{\partial x \partial t} = \frac{\partial H}{\partial x} \tag{14.5}$$

If pressures are hydrostatic along any vertical line, then $h = z(x) + y(x, t)$ in which $z(x) =$ channel bed elevation and the channel slope, θ, has been assumed small enough to make the approximations $\cos \theta \approx 1$ and $\sin \theta \approx \tan \theta \approx \theta = S_0 =$ bed slope. Therefore, the first term in (14.5) can be rewritten as

$$\frac{\partial h}{\partial x} = \frac{dz}{dx} + \frac{\partial y}{\partial x} = -S_0 + \frac{\partial y}{\partial x} \tag{14.6}$$

in which the negative sign in front of S_0 indicates that z decreases with x when S_0 is positive. (i.e. θ is positive when the channel slopes downward in the direction of flow.) In one-dimensional flow the velocity magnitude, V, is given by the velocity component in the x direction, U. Since x and t are independent variables, the third term becomes

$$\frac{\partial^2 \phi}{\partial x \partial t} = \frac{\partial}{\partial t}\left(\frac{\partial \phi}{\partial x}\right) = \frac{\partial U}{\partial t} \tag{14.7}$$

in which use has been made of (6.14a). Finally, (12.20) allows us to rewrite the last term in (14.5) in terms of the friction slope.

$$\frac{\partial H}{\partial x} = -S_f \tag{14.8}$$

Then use of (14.6)–(14.8) in (14.5) and a bit of algebra gives the momentum equation for unsteady one-dimensional flow.

$$g\,\frac{\partial y}{\partial x} + U\,\frac{\partial U}{\partial x} + \frac{\partial U}{\partial t} = g\left(S_0 - S_f\right) \tag{14.9}$$

Equations (14.4) and (14.9) are known as the Saint-Venant equations of open channel flow. When the right side of (12.20) is used to approximate S_f, they contain U and y as their only unknowns.

Characteristic Form of the Saint-Venant Equations

Expansion of the first term in (14.4) gives

$$y\,\frac{\partial U}{\partial x} + U\,\frac{\partial y}{\partial x} + \frac{\partial y}{\partial t} = 0 \tag{14.10}$$

Multiplication of (14.10) by an unknown parameter, λ, and addition to (14.9) gives

$$\left(g + \lambda U\right)\frac{\partial y}{\partial x} + \lambda\frac{\partial y}{\partial t} + \left(U + \lambda y\right)\frac{\partial U}{\partial x} + \frac{\partial U}{\partial t} = g\left(S_0 - S_f\right) \tag{14.11}$$

which can be altered slightly to

$$\lambda\left[\frac{g + \lambda U}{\lambda}\,\frac{\partial y}{\partial x} + \frac{\partial y}{\partial t}\right] + \left[\left(U + \lambda y\right)\frac{\partial U}{\partial x} + \frac{\partial U}{\partial t}\right] = g\left(S_0 - S_f\right) \tag{14.12}$$

The directional derivative defined by (13.29) allows (14.12) to be rewritten as a set of simultaneous ordinary differential equations that hold along a characteristic curve in the (x, t) plane.

$$\lambda\,\frac{dy}{dt} + \frac{dU}{dt} = g\left(S_0 - S_f\right) \tag{14.13}$$

The time derivatives in (14.13) are calculated along characteristic curves that satisfy the differential equation

$$\frac{dx}{dt} = \frac{g + \lambda U}{\lambda} = U + \lambda y \tag{14.14}$$

The second of the two equations in (14.14) gives $\lambda = \pm\sqrt{g/y}$, and use of this result in (14.13)–(1.414) gives two equations for each of two separate and distinct families of characteristic curves in the (x, t) plane.

$$\frac{d(U + 2c)}{dt} = g\left(S_0 - S_f\right) \quad \text{along} \quad \frac{dx}{dt} = U + c$$

$$\frac{d(U - 2c)}{dt} = g\left(S_0 - S_f\right) \quad \text{along} \quad \frac{dx}{dt} = U - c \tag{14.15 a, b}$$

in which

$$c = \sqrt{g y} \tag{14.16}$$

Equations (14.15) show that c is the speed of a disturbance or wave when $U = 0$. These equations also show that, when $U \neq 0$, a disturbance travels with a speed of $U + c$ along one family of characteristics and with a speed $U - c$ along the other family of characteristics. When the flow is subcritical, with $U < c$, one wave travels downstream and another wave travels upstream. When the flow is supercritical, with $U > c$, dx/dt is positive for both families of characteristics and waves travel only in the downstream direction. Another way of stating this result is that conditions at a point in **subcritical** flow are influenced by boundary conditions **both upstream** and **downstream** from the point in question. On the other hand, conditions at a point in **supercritical** flow are influenced only by boundary conditions **upstream** from the point under consideration.
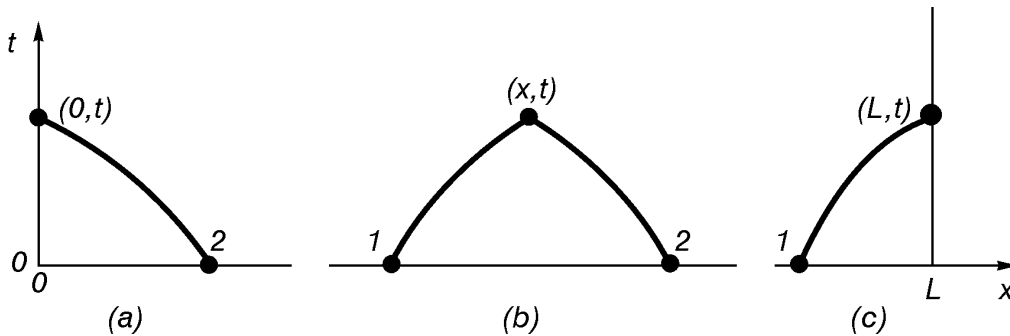
Figure 14.2 Segments of a characteristic grid for subcritical flow.

Numerical Solution of the Characteristic Equations

The numerical solution of (14.15) can be carried out with a closely spaced set of nodes along the characteristic curves. Figure 14.2 shows segments of a characteristic grid for **subcritical** flow. At an internal point, such as Fig. 14.2 b, Eqs. (14.15 a) and 14.15 b) can be integrated along the line segments joining point 1 to (x, t) and point 2 to (x, t), respectively, to obtain

$$\left(U + 2c\right) - \left(U_1 + 2c_1\right) = g \int_{t_1}^{t} \left(S_0 - S_f\right) dt \quad \text{along} \quad x - x_1 = \int_{t_1}^{t} \left(U + c\right) dt$$

$$\text{(14.17 a, b)}$$

$$\left(U - 2c\right) - \left(U_2 - 2c_2\right) = g \int_{t_2}^{t} \left(S_0 - S_f\right) dt \quad \text{along} \quad x - x_2 = \int_{t_2}^{t} \left(U - c\right) dt$$

Equations (14.17) are four equations to be solved for unknown values of U, c, x and t at the intersection of the two characteristic segments. A second-order Runge-Kutta scheme can be used to do this with the following two steps:

(1)   Approximate the integrals with

$$\int_{t_i}^{t} F \, dt \approx F_i \left(t - t_i\right)$$

Then solve the resulting linear equations for the first approximations $U^{(1)}$, $c^{(1)}$, $x^{(1)}$ and $t^{(1)}$.

(2)   Use the first approximations to improve the calculation of the integrals with

$$\int_{t_i}^{t} F \, dt \approx \frac{1}{2}\left[F_i + F^{(1)}\right]\left(t - t_i\right)$$

Then solve the linear equations for the second, and final, approximations for U, c, x and t.

People often continue this iteration process until solutions for U, c, x and t cease to change from one cycle to the next. However, this only increases the complexity of the calculation and not its accuracy since steps 1 and 2 are sufficient to obtain second order accuracy, which is the same accuracy as the trapezoidal rule that is used to approximate the integrals. Since all variables must be known at points 1 and 2, we see that both U and c must be prescribed for initial conditions at $t = 0$ along the full length of the channel.

At the upstream end of the channel, shown in Fig. 14.2 a, we have only the two equations (14.17 b). Since $x = 0$, these equations contain the three unknown values of U, c, and t on the boundary. Therefore, either U, c or one functional relationship between U and c must be prescribed at the upstream boundary. A similar situation exists at the downstream boundary, shown in Fig. 14.2 c. Since Eqs. (14.17 a) apply along the segment joining point 1 to (L, t), we see that U, c or one functional relationship between U and c must be prescribed at the downstream boundary.

In supercritical flow both families of characteristics have positive slopes. This means that U and c must be prescribed both for initial conditions along the entire channel length and for boundary conditions at the ***upstream*** boundary. This will be necessary and sufficient to calculate the solution everywhere else, including the downstream boundary at $x = L$. ***Therefore, no boundary conditions can be prescribed at a downstream boundary for supercritical flow***.

The method of characteristics shows how data must be prescribed to calculate solutions of the Saint-Venant equations. It also gives what is probably the most generally accurate and stable numerical method. However, Wylie and Streeter (1982) point out that the method is cumbersome to apply to slow transients since time steps tend to be small. The irregular spacing of nodes that is required for natural channel calculations also makes it difficult to obtain satisfactory solutions. Therefore, they recommend an implicit finite difference method for slow transients in natural river channels. Most commercially available computer programs use finite difference methods.

Since we are more interested in learning about the physics of fluid motion than in learning about commercially available computer software, we will use the remainder of this chapter to study an approximate method known as the kinematic wave approximation. This approximation will be used to discuss the movement of flood waves down rivers.
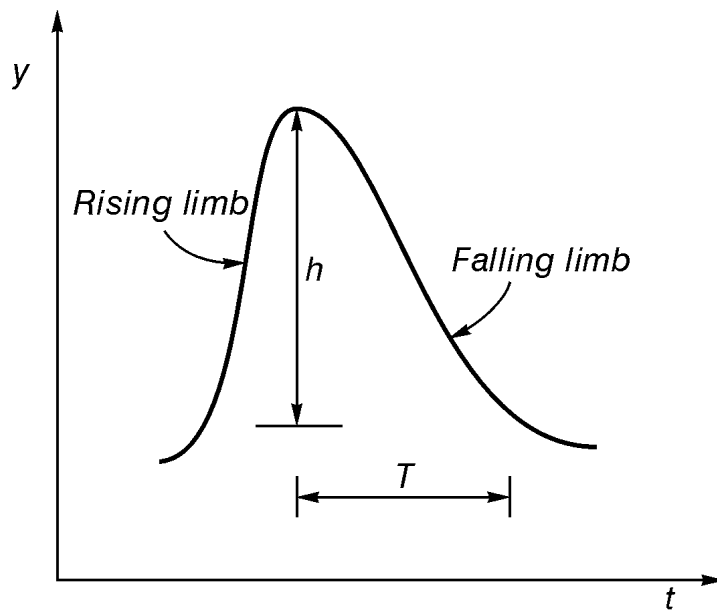
Figure 14.3 A typical depth hydrograph for a flood.

The Kinematic Wave Approximation

The usual engineering approach to flood data acquisition is to measure river depth or stage as a function of time at a fixed location along the river. River stages are then related to flow rates with a rating curve that has been obtained from previous measurements of flow rates and stages at that particular location. The resulting plot of flow versus time for a particular location and flood is called a hydrograph. The plot of depth versus time, which is not used as often but is more useful for this discussion, is called a depth hydrograph.

A typical depth hydrograph for a flood is shown in Fig. 14.3. In almost all instances, for reasons that we will discuss later, the rising limb of the hydrograph has a steeper slope than the falling limb. For scaling purposes, we will denote the maximum change in depth with h, and a time scale, T, will be chosen so that the ratio h/T gives an order of magnitude for the maximum value of $\partial y/\partial t$ on the **falling** limb. (The reason for concentrating on the falling rather than rising limb will be discussed later.) The value of T decreases as the river catchment area decreases and as the average channel slope increases. Thus, T can vary from as little as several hours for small steep catchments to weeks for large catchments with smaller slopes. For most applications T is probably of the order of one to ten days.

There is no obvious reference length for x in this problem. However, if we denote a reference length by L, and if both terms in the continuity equation (14.4) are assumed to be equally important, we obtain the estimate

$$\frac{U_0 h}{L} \sim \frac{h}{T} \tag{14.18}$$

in which U_0 is an estimate for the maximum velocity. From (14.18) we obtain an estimate for L.

$$L \sim U_0 T \tag{14.19}$$

Equation (14.19) shows that L is the distance travelled by a water particle moving at the maximum speed, U_0, during time T. In most problems L is very large. For example, if $U_0 \sim 1$ m/s and $T \sim 24$ hours, then $L \sim 86.4$ km.

Scaling terms in the momentum equation (14.9) gives

$$g\,\frac{h}{L} + \frac{U_0^2}{L} + \frac{U_0}{T} \sim g\left(S_0 - S_f\right) \tag{14.20}$$

If we use (14.19) to eliminate T and (12.20) and (12.23) to approximate S_f, Eq. (14.20) becomes

$$g\,\frac{h}{L} + \frac{U_0^2}{L} + \frac{U_0^2}{L} \sim g\,S_0 + \frac{f}{8}\,\frac{U_0^2}{h} \tag{14.21}$$

Division of (14.21) by $g\,S_0$ gives relative magnitudes of terms.

$$\frac{h}{L\,S_0}\left(1 + Fr^2 + Fr^2\right) \sim 1 + \frac{f}{8}\frac{U_0^2}{g\,h\,S_0} \tag{14.22}$$

in which Fr = maximum Froude number = $U_0/\sqrt{g\,h}$. In rivers Fr has an order that almost never exceeds one.

The kinematic wave approximation assumes that the free surface is nearly parallel to the channel bottom. In other words, the flow is approximated locally as uniform, and only the bed and friction slope terms in (14.9) are important. Thus, for a wide shallow channel, the kinematic wave approximation gives

$$S_0 = S_f = \frac{f}{8}\frac{U^2}{g\,y} \tag{14.23}$$

Equation (14.22) now shows that the kinematic wave approximation, Eq. (14.23), results from assuming that

$$\frac{f}{8}\frac{U_0^2}{g\,h\,S_0} \sim 1 \tag{14.24}$$

$$\frac{h}{L\,S_0} \ll 1 \tag{14.25}$$

If (14.19) and (14.24) are used to eliminate L and U_0, respectively, from (14.25), the requirement for validity of the kinematic wave approximation reduces to

$$T \gg \sqrt{\frac{f}{8}\frac{h}{g\,S_0^3}} \tag{14.26}$$

For a typical application we might set $f \sim 0.1$, $h \sim 2$ m, $g \sim 10$ m/s^2 and $S_0 \sim 1/300$. Then (14.26) requires that $T \gg 4.3$ minutes. If S_0 is reduced to $S_0 \sim 1/3000$, the requirement becomes $T \gg 2.3$ hours. Since most flood hydrographs have values of T that greatly exceed these values, we conclude that Eqs. (14.4) and (14.23) are likely to give an accurate description of flood wave movement in many, if not most, applications.

The Behaviour of Kinematic Wave Solutions

By solving (14.23) for U and substituting the result in (14.4) we obtain

$$\frac{3}{2} \sqrt{\frac{8}{f} \, g \, y \, S_0} \, \frac{\partial y}{\partial x} \; + \; \frac{\partial y}{\partial t} \; = \; 0 \qquad\qquad \textbf{(14.27)}$$

Since the coefficient of the first term in (14.27) is proportional to $U(y)$ calculated from (14.23), we obtain the following significant result:

$$\frac{3}{2} \, U(y) \, \frac{\partial y}{\partial x} \; + \; \frac{\partial y}{\partial t} \; = \; 0 \qquad\qquad \textbf{(14.28)}$$

Use of (13.29) now allows (14.28) to be rewritten in the equivalent form

$$\frac{dy}{dt} \; = \; 0 \qquad\qquad \textbf{(14.29)}$$

along the characteristic curves

$$\frac{dx}{dt} \; = \; \frac{3}{2} U(y) \qquad\qquad \textbf{(14.30)}$$

Equations (14.29)–(14.30) lead immediately to at least four very important observations:

(1)   Since (14.29) shows that y is constant along a characteristic, and since U depends only on y, Eq. (14.30) shows that all characteristics are straight lines with slopes that can be determined, once and for all, at each characteristic initial point.

(2)   Eq. (14.30) shows that disturbances move in the downstream direction only. Therefore, upstream backwater effects are neglected in the kinematic wave approximation.

(3)   A point of constant depth moves downstream with a speed equal to one and a half times the local flux velocity.

(4)   If y_2 and y_1 are two different depths in the flood wave, and if $y_2 > y_1$, then (14.30) shows that the point of greater depth moves downstream faster than the point of smaller depth. $\left[\text{Since } U\!\left(y_2\right) > U\!\left(y_1\right) \right].$
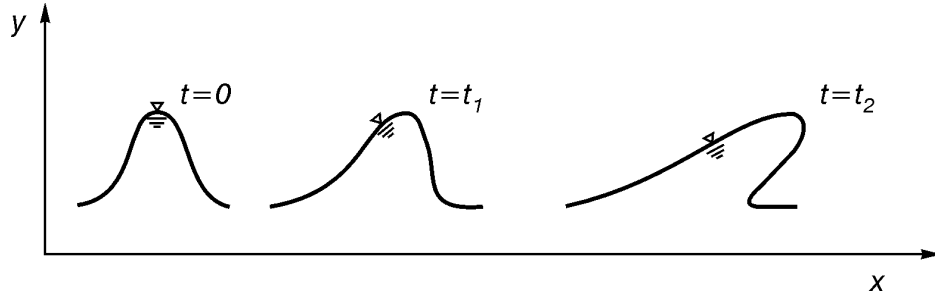
Figure 14.4 Development of a flood wave profile with time using the kinematic wave approximation.

The fourth observation shows why the rising limb of the flood hydrograph in Fig. 14.3 usually has a steeper slope than the falling limb. If, as shown in Fig. 14.4, the flood wave profile at $t = 0$ has a shape that is nearly symmetrical about its peak, then the front portion of the wave steepens and the trailing portion of the wave flattens since points of larger depth move downstream with a greater speed. If the channel is long enough, the front of the wave eventually develops an overhanging "nose" that gives, in some places, as many as three different values of y for the same values of x and t, as shown in Fig. 14.4 at $t = t_2$.
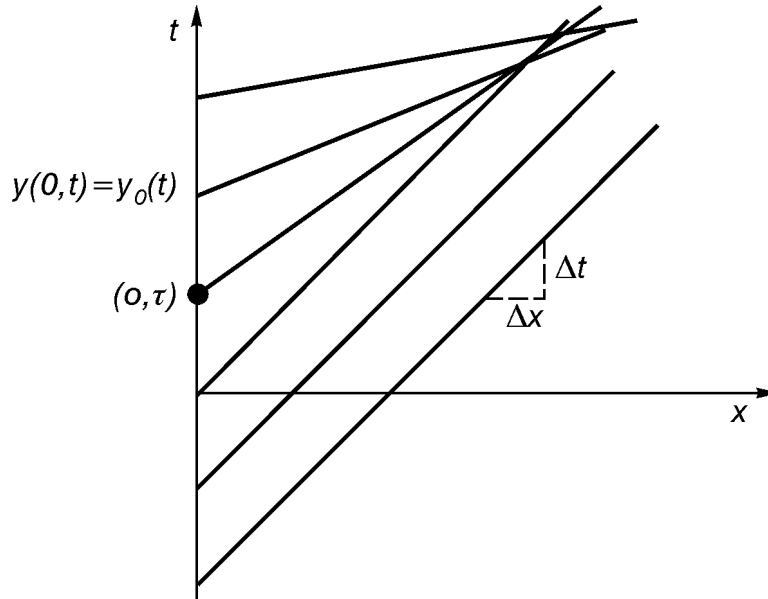
Figure 14.5 Characteristic curves in the (x, t) plane when $y_0(t)$ increases with t.

The multiple valued behaviour of the solution is also easy to see in the (x, t) plane by solving (14.29)–(14.30) subject to the boundary condition

$$y(0, t) = y_0(t) \quad \text{for} \quad -\infty < t < \infty \tag{14.31}$$

Then (14.29)–(14.30) give

$$y(x, t) = y_0(\tau) \quad \text{for} \quad -\infty < \tau < \infty \tag{14.32}$$

along the characteristic curve

$$x = \frac{3}{2} U\left[y_0(\tau)\right](t - \tau) \quad \text{for} \quad -\infty < \tau < \infty \tag{14.33}$$

in which $(0, \tau)$ is the initial point on a typical characteristic. When $y_0(\tau)$ increases with τ, the straight line characteristics have slopes that also increase with τ since these slopes are determined at $x = 0$ from $y_0(\tau)$. This means that a region will exist in the (x, t) plane where characteristics overlap each other, as shown in Fig. 14.5. Since each characteristic carries a different value of $y(x, t)$ along its path, it becomes obvious that the solution is multiple valued in the region of overlapping characteristics.

The solution for $y(x, t)$ is calculated from (14.32)–(14.33) for every point in the right half of the (x, t) plane in Fig. (14.5). This is done by choosing a numerical value for τ in the range $-\infty < \tau < \infty$. Then the constant value of y along the characteristic is given by (14.32), and the path of the characteristic is calculated from (14.33). The multiple valued nature of the solution presents no difficulty at all in this calculation.

The "nose" of the flood wave, shown in Fig. 14.4 at $t = t_2$, can be located from (14.32)–(14.33). Since the wave profile at $t = t_2$ is found by setting $t = t_2$ in (14.32)–(14.33) and letting τ take on a sufficient number of values in the range $-\infty < \tau < \infty$ to plot the solution near the nose, we see that $x(t, \tau)$ in (14.33) achieves a relative maximum at the nose when τ is varied and t is held constant. The mathematical requirement for locating this relative maximum is

$$\frac{\partial x(t, \tau)}{\partial \tau} = 0 \tag{14.34}$$

Substituting (14.33) into (14.34) gives

$$0 = \frac{3}{2} \frac{dU(y_0)}{dy} \frac{dy_0(\tau)}{d\tau} (t - \tau) - \frac{3}{2} U(y_0) \tag{14.35}$$

Equation (14.35) can be solved for t to obtain

$$t = \tau + \frac{U(y_0)}{U'(y_0)y_0'(\tau)} \tag{14.36}$$

Use of (14.23) to eliminate U from (14.36) gives

$$\boxed{t = \tau + 2\frac{y_0(\tau)}{y_0'(\tau)} \tag{14.37}}$$

Equation (14.37) gives the t coordinate of the nose in the (x, t) plane for any value of the parameter τ in the range $-\infty < \tau < \infty$. The x coordinate is calculated from (14.23), (14.33) and (14.37) in the form

$$x = 3 \, \frac{y_0(\tau)}{y_0^/(\tau)} \, \sqrt{\frac{8}{f} \, g \, y_0(\tau) S_0} \qquad\qquad (14.38)$$

Equation (14.38) gives a mathematical proof that a nose and, therefore, a multiple valued solution can occur only when $y_0^/(\tau) > 0$. When $y_0^/(\tau) < 0$, the x coordinate of the nose is negative and outside the region of physical interest.[*]

A multiple valued solution, of course, has no physical interest, and this behaviour is always prevented in kinematic wave solutions by inserting a vertical discontinuity, called a shock, in the wave profile. A sketch of a shock is shown with a dashed line in Fig. 14.6. A graphical solution for the shock location can be obtained by inserting the vertical dashed line so that the two cross hatched areas in Fig. 14.6 are equal. A numerical solution for the shock location is found by locating the first point where the shock forms. After this shock initial point is calculated, future positions of the shock are obtained by requiring conservation of mass across the moving shock.
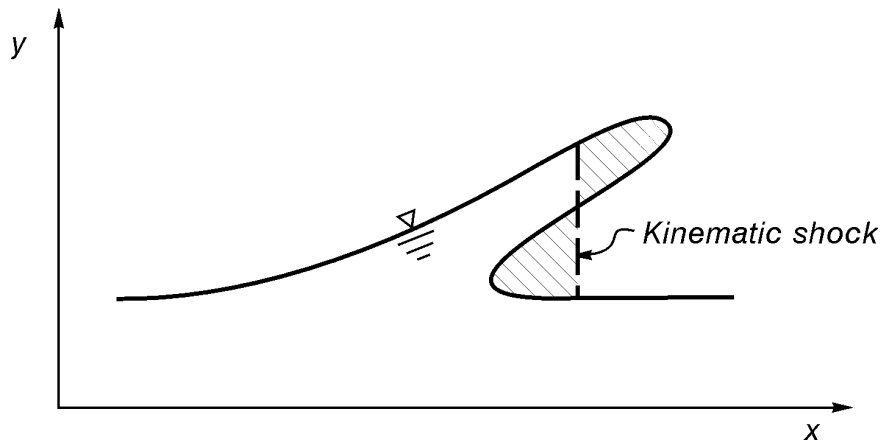
Figure 14.6 A shock used to keep a kinematic wave solution single valued.

The shock initial point is calculated from (14.37) by finding the value of τ that makes t a minimum. This is the first point at which the free surface tangent becomes vertical, and it is the point at which t in (14.37) is either an absolute or relative minimum. A relative minimum can be found from (14.37) by setting the derivative of t with respect to τ equal to zero. If a relative minimum does not occur, then an absolute minimum occurs and can be found by inserting values for τ and calculating corresponding values for t.

---

[*] Equations (14.37)–(14.38) give, in parametric form, what is known as the envelope of the characteristic curves (14.33). Hart (1957) gives a formal and easily understood introduction to the concept of an envelope of a family of curves.
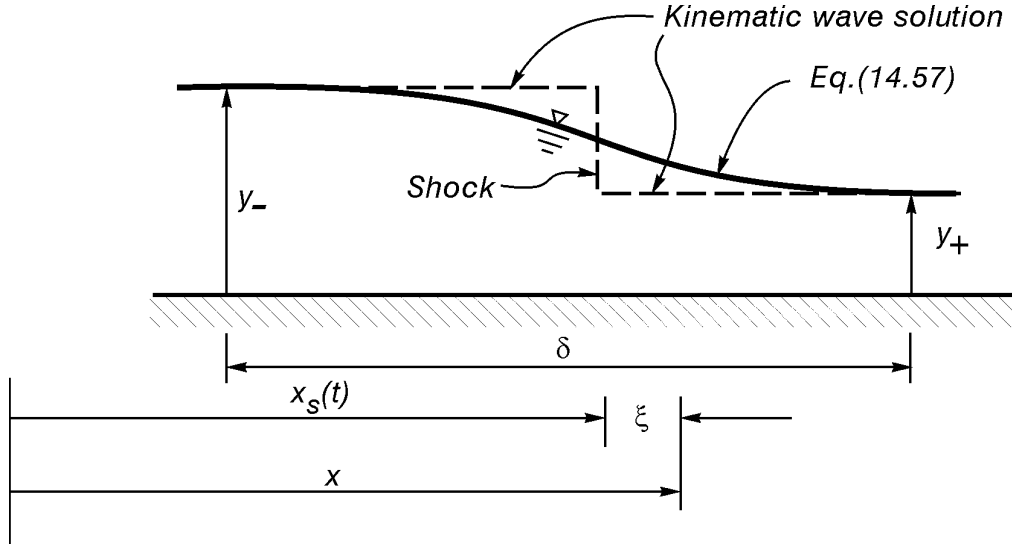
Figure 14.7 The free surface profile near a kinematic shock.

The differential equation that tracks the location of a shock can be obtained by rewriting (14.4) in a new system of coordinates that moves with the shock. If the kinematic shock location is denoted by $x = x_s(t)$, as shown in Fig. 14.7, the new system of coordinates is defined by

$$\xi = x - x_s(\tau)$$
$$\tau = t$$

(14.39 a, b)

in which the new time coordinate, τ, is unrelated to the parameter τ in (14.32)–(14.33). The chain rule shows that derivatives transform according to

$$\frac{\partial}{\partial x} = \frac{\partial}{\partial \xi} \frac{\partial \xi}{\partial x} = \frac{\partial}{\partial \xi}$$

$$\frac{\partial}{\partial t} = \frac{\partial}{\partial \xi} \frac{\partial \xi}{\partial \tau} \frac{\partial \tau}{\partial t} + \frac{\partial}{\partial \tau} \frac{\partial \tau}{\partial t} = -\dot{x}_s(\tau) \frac{\partial}{\partial \xi} + \frac{\partial}{\partial \tau}$$

(14.40 a, b)

in which a dot is used to denote differentiation with respect to τ. Thus, (14.4) has the following form in the moving system of coordinates:

$$\frac{\partial}{\partial \xi}\left[\left(U - \dot{x}_s(\tau)\right)y\right] + \frac{\partial y}{\partial \tau} = 0$$

(14.41)

Since a solution of (14.41) is to be calculated over the same range for τ that was used for t in the (x, t) coordinates, τ is scaled with T. Likewise, U and $\dot{x}_s$ are both scaled with U_0, and y is scaled with the change in y across the shock, which we will call h. However, ξ is scaled with a length, δ, that gives an order of magnitude for the shock length, as shown in Fig. 14.7. This means that terms in (14.41) have the following magnitudes:

$$\frac{U_0 h}{\delta} + \frac{h}{T} \sim 0 \tag{14.42}$$

Division of (14.42) by the first term and use of (14.19) to eliminate $U_0 T$ gives relative magnitudes.

$$1 + \frac{\delta}{L} \sim 0 \tag{14.43}$$

It is assumed in the kinematic wave approximation that $\delta/L \ll 1$. This means that (14.41) reduces to

$$\frac{\partial}{\partial \xi}\left[\left(U - \dot{x}_s\right)y\right] = 0 \tag{14.44}$$

Equation (14.44) shows that $\left(U - \dot{x}_s\right)y$ changes only with τ across a shock. This requirement gives

$$\left(U_- - \dot{x}_s\right)y_- = \left(U_+ - \dot{x}_s\right)y_+ \tag{14.45}$$

in which the subscripts + and - denote values of U and y immediately downstream and upstream, respectively, from the shock. [In fact, the kinematic wave approximation (14.23) gives no information that can be used to fix a value for δ, and a kinematic wave solution always sets $\delta = 0$ in (14.43).] A physical interpretation of (14.45) follows by writing velocities relative to the moving shock and noting that (14.45) requires that flow rates calculated relative to the moving shock be equal immediately upstream and downstream from the discontinuity in depth. This procedure was carried out earlier in Example 4.8.

Solution of (14.45) for $\dot{x}_s$ gives

$$\dot{x}_s(\tau) = \frac{U_+ y_+ - U_- y_-}{y_+ - y_-} \tag{14.46}$$

Equation (14.23) can be used to eliminate U from (14.46) to obtain

$$\frac{dx_s(t)}{dt} = \frac{y_+^{3/2} - y_-^{3/2}}{y_+ - y_-} \sqrt{\frac{8}{f} g S_0} \tag{14.47}$$

At the shock initial point, and also as $t \to \infty$, (14.47) has the indeterminate form $0/0$ as $y_- \to y_+$. However, l'Hospital's rule can be applied by fixing y_+ and letting $y_- \to y_+$. Therefore, fixing y_+ in (14.47), differentiating numerator and denominator with respect to y_- and setting $y_- = y_+$ gives the following finite result:

$$\frac{dx_s}{dt} \rightarrow \frac{3}{2} \, y_+^{1/2} \, \sqrt{\frac{8}{f} \, g \, S_0} = \frac{3}{2} \, U\left(y_+\right) \tag{14.48}$$

Numerical methods are almost always required to integrate (14.47) in a procedure that is sometimes referred to as "shock tracing".

Now it is easy to discuss why the maximum slope of the falling limb of the hydrograph was used to obtain the time scale, T, for the kinematic wave approximation. The rising limb becomes steeper and the falling limb becomes flatter as a flood wave moves downstream. This fact, together with Eq. (14.26) and the physical requirement that the free surface be nearly parallel to the channel bottom for the kinematic wave approximation to be applicable, suggests that the accuracy of approximation increases for the falling limb and decreases for the rising limb as a flood wave moves downstream. ***Therefore, for flows in which (14.26) is satisfied, the kinematic wave approximation gives an accurate approximation for the falling limb of the hydrograph but a relatively poor approximation for the rising limb***. In the next section we will rescale the Saint-Venant equations to obtain a more accurate approximation for the rising limb.

Solution Behaviour Near a Kinematic Shock

The existence of a shock in a kinematic wave solution does not mean that a shock necessarily occurs in either the physical problem or in the solution of the full set of the Saint-Venant equations. A shock forms in the kinematic wave solution because some terms that were neglected to obtain (14.23) become important close to the moving shock. The behaviour of the solution of the Saint-Venant equations near a kinematic shock can be obtained by rescaling these equations in a coordinate system that moves with the shock. This has already been done with Eqs. (14.39)–(14.40) to obtain (14.41) and (14.44)–(14.45) as δ/L becomes small. Applying the same transformation to (14.9) gives

$$g \, \frac{\partial y}{\partial \xi} + \left(U - \dot{x}_s\right) \frac{\partial U}{\partial \xi} + \frac{\partial U}{\partial \tau} = g \, S_0 - \frac{f}{8} \, \frac{U^2}{y} \tag{14.49}$$

in which S_f has been approximated with the right side of (14.23). Scaling terms in (14.49) with the same values that were used to obtain (14.44) $\left(\tau \sim T, \; U \sim U_0, \; \dot{x}_s \sim U_0, \; y \sim h = y_- - y_+, \; \xi \sim \delta\right)$ gives

$$g \, \frac{h}{\delta} + \frac{U_0^2}{\delta} + \frac{U_0}{T} \sim g \, S_0 + \frac{f}{8} \, \frac{U_0^2}{h} \tag{14.50}$$

Setting $T \sim L/U_0$ and dividing by $g \, S_0$ gives relative magnitudes.

$$\frac{h}{\delta \, S_0}\left(1 + \frac{U_0^2}{gh} + \frac{U_0^2}{gh} \, \frac{\delta}{L}\right) \sim 1 + \frac{f}{8} \, \frac{U_0^2}{ghS_0} \tag{14.51}$$

Since $\partial y/\partial \xi$ becomes infinite at the shock in the kinematic wave solution, it is evident that this term must become important near the shock. However, since $\delta/L \ll 1$ in problems described by the kinematic wave approximation, Eq. (14.51) suggests that the time derivative of U can be neglected in (14.49) to obtain

$$g \frac{\partial y}{\partial \xi} + \left(U - \dot{x}_s\right) \frac{\partial U}{\partial \xi} = g S_0 - \frac{f}{8} \frac{U^2}{y} \tag{14.52}$$

The time variable, $\tau = t$, appears in (14.44) and (14.52) only as a parameter. In other words, when considering the local behaviour of flow near a kinematic shock, depths and velocities change much more rapidly with respect to the spacial coordinate than with respect to time. Integration of (14.44) gives

$$\left(U - \dot{x}_s\right) y = F(\tau) = -\frac{y_+ y_-}{\sqrt{y_+} - \sqrt{y_-}} \sqrt{\frac{8}{f} g S_0} \tag{14.53}$$

in which $F(\tau)$ has been evaluated by using (14.47) and (14.23) either at a point ahead of the shock, where $y = y_+$, or at a point behind the shock, where $y = y_-$. [Either point is shown by (14.45) to give the same result.] Use of (14.47) and (14.53) to eliminate U and $\dot{x}_s$ from (14.52) gives, after some complicated algebra, the following differential equation for y:

$$\frac{\partial y}{\partial \xi} = \frac{\left(y - y_-\right)\left(y - y_+\right)\left(y - y_1\right)}{y^3 - \frac{8}{f} S_0 \, y_- \, y_+ \, y_1} S_0 \tag{14.54}$$

in which the depth y_1 is given by

$$y_1 = \frac{y_+ y_-}{\left(\sqrt{y_+} + \sqrt{y_-}\right)^2} \tag{14.55}$$

It is easy to show that y_1, y_+ and y_- satisfy the following inequalities:

$$y_1 < y_+ < y_- \tag{14.56}$$

The solution of (14.54) has been known for years among hydraulic engineers and applied mathematicians as the monoclinal rising flood wave. The equation can be integrated in closed form by separating variables and using partial fractions. The result is

$$\xi S_0 = D + y + A \ln\left(y_- - y\right) - B \ln\left(y - y_+\right) - C \ln\left(y - y_1\right) \tag{14.57}$$

in which D is an unknown function of τ and the remaining functions of τ are given by the following equations:

$$A = \frac{y_-^3 - \frac{8}{f} S_0 \, y_- \, y_+ \, y_1}{\left(y_- - y_+\right)\left(y_- - y_1\right)} \tag{14.58}$$

$$B = \frac{y_+^3 - \dfrac{8}{f} S_0 \, y_- \, y_+ \, y_1}{\left(y_- - y_+\right)\left(y_+ - y_1\right)} \tag{14.59}$$

$$C = \frac{\dfrac{8}{f} S_0 \, y_- \, y_+ \, y_1 - y_1^3}{\left(y_- - y_1\right)\left(y_+ - y_1\right)} \tag{14.60}$$

The qualitative solution behaviour is far easier to deduce from (14.54) than from (14.57). When $y_+ < y < y_-$, as in Fig. 14.7, the inequality (14.56) shows that the numerator on the right side of (14.54) is negative and vanishes at both $y = y_+$ and $y = y_-$. Therefore, when the denominator is positive for $y_+ < y < y_-$, the solution is a smooth curve joining the depths y_+ and y_- on each side of the kinematic shock, as shown in Fig. 14.7. On the other hand, when the denominator becomes negative for at least some values of y in the range $y_+ < y < y_-$, a smooth curve cannot be used to join y_+ and y_- across the shock. In this case, a shock can be expected to appear in the solution of the Saint-Venant equations. Since this requires that the denominator of (14.54) be negative for at least the smallest value of y in the range $y_+ < y < y_-$, a shock will occur in the solution of the Saint-Venant equations if

$$y_+^3 - \frac{8}{f} S_0 \, y_- \, y_+ \, y_1 < 0 \tag{14.61}$$

Equation (14.55) can be used to put (14.61) in the following more useful form:

$$\frac{8}{f} S_0 > \left(1 + \sqrt{\frac{y_+}{y_-}}\right)^2 \frac{y_+}{y_-} \tag{14.62}$$

Equation (14.62) shows that a shock will occur in the solution of the Saint-Venant equations if y_- is made large enough relative to y_+ to satisfy the inequality. It also shows that a shock can be created by either decreasing f or increasing S_0 sufficiently to satisfy (14.62).

Equation (14.57) can be used to obtain an estimate for the shock thickness, δ, in Fig. 14.7. If δ is taken as the difference between ξ at $y = y_+ + \epsilon\left(y_- - y_+\right)$ and ξ at $y = y_- - \epsilon\left(y_- - y_+\right)$ in which ϵ is a small positive constant, Eq. (14.57) gives

$$\delta S_0 = \left(\xi_+ - \xi_-\right)S_0 = \left(-1 + 2\epsilon\right)h + A \ln\left(\frac{1 + \epsilon}{\epsilon}\right) + B \ln\left(\frac{1 - \epsilon}{\epsilon}\right)$$
$$+ C \ln\left[\frac{\left(y_- - y_1\right) - \epsilon h}{\left(y_+ - y_1\right) + \epsilon h}\right] \tag{14.63}$$

in which $h = y_- - y_+ =$ change in depth across the kinematic shock. The leading term in the expansion of (14.63) for $\epsilon \ll 1$ is $(A + B)\ln(1/\epsilon)$, and arbitrarily choosing $\epsilon = 0.05$ gives the following estimate for δ:

$$\delta \sim 3 \, \frac{A + B}{S_0} \qquad\qquad \textbf{(14.64)}$$

The solution across the shock requires $\delta/L \ll 1$ for its validity, in which $L \sim U_0 T$.

Backwater Effects

Upstream backwater effects are neglected in the kinematic wave approximation because all characteristics have positive slopes that carry disturbances in the downstream direction only. For example, river and reservoir free surface elevations should be identical where a reservoir exists at the downstream end of a river. However, the kinematic wave solution determines all depths along the river from an upstream hydrograph, and this means that the river and reservoir free surfaces will not generally meet where the river enters the reservoir. This anomaly can be removed by rescaling the Saint-Venant equations to obtain a locally valid solution. In this case x_s in (14.39)–(14.40) is replaced with the constant x coordinate of the river end, and (14.44) and (14.52) reduce to

$$\frac{\partial(Uy)}{\partial\xi} = 0 \qquad\qquad \textbf{(14.65)}$$

$$g \, \frac{\partial y}{\partial\xi} + U \, \frac{\partial U}{\partial\xi} = g \, S_0 - \frac{f}{8} \, \frac{U^2}{y} \qquad\qquad \textbf{(14.66)}$$

in which the time variable, $\tau = t$, once again appears only as a parameter. These equations are identical with the equations that describe steady flow in gradually varied open channel flow. Thus, if $q(\tau)$ and $y_-(\tau)$ are the flow rate and depth calculated at the river exit from the kinematic wave approximation, the same manipulations that were used to obtain Eq. (12.37) can be used to put (14.65)–(14.66) in the form

$$\frac{\partial y}{\partial\xi} = \frac{y^3 - y_-^3}{y^3 - y_c^3} \, S_0 \qquad\qquad \textbf{(14.67)}$$

in which $y_c(\tau)$ is defined by

$$\frac{q^2(\tau)}{g y_c^3(\tau)} = 1 \qquad\qquad \textbf{(14.68)}$$

Equation (14.67) was integrated by Bresse in 1860 to obtain

$$\xi \, S_0 \;=\; y \;-\; \left[1 \;-\; \left(\frac{y_c}{y_-} \right)^2 \right] y_- \; \Phi \, (z) \tag{14.69}$$

in which the Bresse function, Φ, is given by

$$\Phi(z) \;=\; \frac{1}{6} \ln \left[\frac{z^2 + z + 1}{(z - 1)^2} \right] - \frac{1}{\sqrt{3}} \tan^{-1} \left(\frac{\sqrt{3}}{2z + 1} \right) \;+\; \kappa \tag{14.70}$$

with κ = integration constant and z defined by

$$z \;=\; \frac{y}{y_-} \tag{14.71}$$

The entire free surface profile can be calculated either by integrating (14.67) with one of the numerical techniques introduced in chapter 12 for steady gradually varied flow or by using (14.69)–(14.71). An estimate for the length, δ, of the backwater curve can be obtained by setting $y = y_- + h$ at $\xi = 0$ to evaluate κ and then setting $y = y_- + \epsilon h$ at $\xi = -\delta$ to calculate δ. The first order term for $\epsilon \ll 1$ is

$$\delta \, S_0 \;\sim\; \left[1 \;-\; \left(\frac{y_c}{y_-} \right)^3 \right] \frac{y_-}{6} \ln \left(\frac{1}{\epsilon^2} \right) \tag{14.72}$$

If we arbitrarily choose $\epsilon = 0.05$, Eq. (14.72) gives the following order of magnitude for δ:

$$\delta \;\sim\; \left[1 \;-\; \left(\frac{y_c}{y_-} \right)^3 \right] \frac{y_-}{S_0} \tag{14.73}$$

A Numerical Example

The kinematic wave approximation will be used to route the inflow depth hydrograph shown in Fig. 14.8 down a channel that has a friction factor $f = 0.1$ and a slope $S_0 = 1/300$. Equation (14.26) requires that

$$T \;\gg\; \sqrt{\frac{0.1}{8} \; \frac{2}{(9.81)(1/300)^3}} \quad \text{seconds} \tag{14.74}$$

Computing the right side of (14.74) and changing time units to hours gives the requirement

$$T \;\gg\; 0.073 \quad \text{hours} \tag{14.75}$$

Since T in Fig. 14.8 is about 10 hours, which is 140 times larger than the right side of (14.75), the kinematic wave approximation can be applied with confidence in this example.
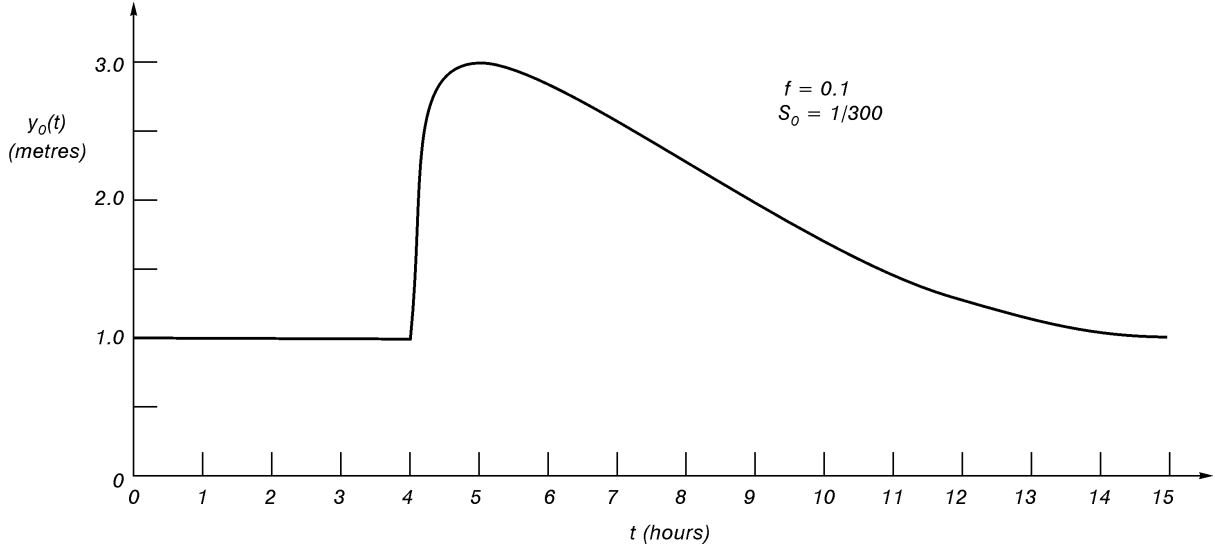
Figure 14.8 The inflow depth hydrograph used for a numerical example.

The only difficult part of a kinematic wave solution is the calculation of shock coordinates in the (x, t) plane. This requires that (14.37)–(14.38) be used to locate the shock initial point on a characteristic that passes through the point $(0, \tau_I)$, as shown in Fig. 14.9. Thereafter, shock path coordinates are calculated by using (14.32)–(14.33) along each of the two straight line characteristics that join $(0, \tau_-)$ to (x_s, t) and $(0, \tau_+)$ to (x_s, t) together with Eq. (14.47), which holds along the curved shock path. This means that five equations hold along three different curves in the (x, t) plane. The equations contain six variables: x_s, t, y_-, y_+, τ_- and τ_+. Any one of these variables may be chosen as independent, and the simultaneous solution of the five equations gives values for the remaining dependent variables.

The solution of the shock tracing problem in its most general form is difficult. However, two simplifications can often be made in the inflow hydrograph that make this problem easy to solve. These simplifications have been made in Fig. 14.8 and are (1) a constant inflow depth for values of t less than the time at which depths first start to increase on the rising limb of the hydrograph and (2) either a zero or negative curvature $\left[y_0''(t) \leq 0 \right]$ on the rising limb. Differentiation of (14.37) gives

$$\frac{dt}{d\tau} = 3 - 2 \frac{y_0(\tau)\, y_0''(\tau)}{\left[y_0'(\tau) \right]^2} \tag{14.76}$$
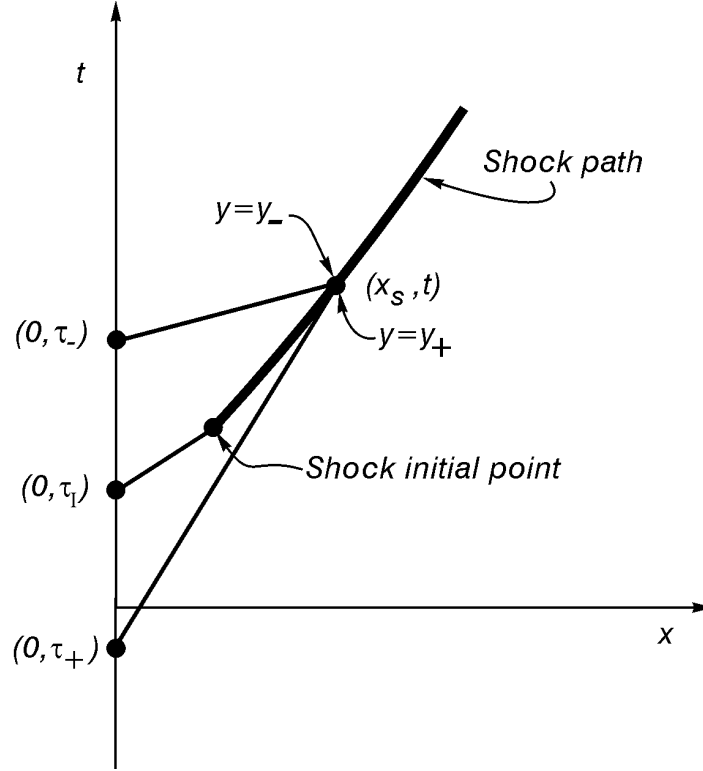
Figure 14.9 Different curves used for calculation of the shock path.

Equation (14.76) shows that $dt/d\tau > 0$ on the rising limb since $y_0''(\tau) \le 0$. Therefore, the minimum value of the right side of (14.37) is an absolute rather than relative minimum that occurs at the beginning of the interval along which Eq. (14.37) is applied. ***This means that the shock initial point, which is calculated by setting $\tau = \tau_I$ in (14.37)–(14.38), lies on the characteristic that passes through the point $(x, t) = (0, \tau_I)$ in which τ_I is the time at which $y_0'(t)$ changes from zero to a positive value.*** This is the point $x = 0$ and $t = 4$ hours for the example shown in Fig. 14.8. Setting $\tau = 4$ hours in (14.37)–(14.38) gives the following coordinates for the shock initial point:

$$t = 4 + 2 \frac{1}{(0.35/0.05)} = 4.29 \text{ hours}$$

(14.77 a, b)

$$x = 3 \frac{3600}{(0.35/0.05)} \sqrt{\frac{8}{0.1}(9.81)(1)(1/300)} = 2{,}495 \text{ metres}$$

Since the shock initial point lies on the characteristic that passes through the point $(0, \tau_I)$ in which τ_I is the value of τ where $y_0(\tau)$ first starts to increase from its initially constant value, and since values of τ_+ in Fig. 14.9 are less than τ_I, we see that y_+ in Fig. 14.9 is always equal to the constant initial value of $y_0(\tau)$. Therefore, a second advantage of using a simplified inflow hydrograph is that y_+ becomes a known constant. This reduces the shock tracing problem to the simultaneous solution of (14.32)–(14.33) along the characteristic joining $(0, \tau_-)$ to (x_s, t) with (14.47) along the shock path. These three equations contain the four variables x_s, t, y_- and τ_-. It will be convenient to choose τ_- as the independent variable when solving these equations.
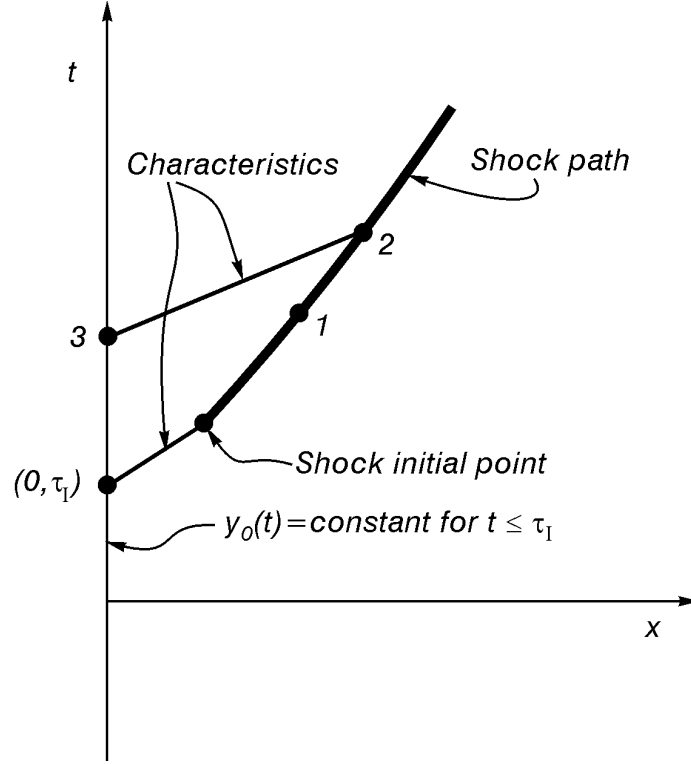
Figure 14.10 Curves used for calculation of the shock
path when using the simplified inflow hydrograph.

Curves used for calculation of the shock path when using the simplified inflow hydrograph are
shown in Fig. 14.10. The (x, t) coordinates and depths y_- and y_+ are known at point 1, and we
will obtain a set of equations that give a direct solution for these variables at point 2. The depth y_+
at points 1 and 2 equals the known constant initial value of $y_0(t)$. Since $y(x, t)$ is shown by
(14.32) to be constant along the characteristic joining points 2 and 3, and since $\tau_- = t_3$ has been
selected as the independent variable, the depth y_- at point 2 equals the known value y_3.
Therefore, dx_s/dt can be calculated from the right side of (14.47) at both points 1 and 2 and
these two values of dx_s/dt can be added to obtain

$$A = \left(\frac{dx_s}{dt}\right)_1 + \left(\frac{dx_s}{dt}\right)_2 \tag{14.78}$$

Then use of the trapezoidal rule to integrate (14.47) along the shock path gives

$$x_{s_2} - x_{s_1} = \frac{A}{2}\left(t_2 - t_1\right) \tag{14.79}$$

Equation (14.79) contains x_{s_2} and t_2 as its two unknowns, and a second equation with these
same two unknowns is obtained from (14.32)–(14.33).

$$x_{s_2} = \frac{3}{2} U_3\left(t_2 - t_3\right) \tag{14.80}$$

Since U is determined from (14.23) as a function of y, and since y is constant along a characteristic, U_3 is calculated from the known value of y_3. Elimination of x_{s_2} from (14.79)–(14.80) gives t_2.

$$t_2 = \frac{2x_{s_1} + 3U_3 t_3 - A t_1}{3U_3 - A} \tag{14.81}$$

The value of x_{s_2} can then be calculated from either (14.79) or (14.80). A Fortran computer program that calculates the entire shock path from a simplified inflow depth hydrograph is shown in Figs. 14.11–14.12. The computed shock path and characteristics are plotted as a solid line and dashed lines, respectively, in Fig. 14.13.

Values of y at any point (x, t) are calculated from (14.32)–(14.33) after the shock path has been obtained. In particular, the depth hydrograph for any specified value of x is calculated by solving (14.33) for t.

$$t = \tau + \frac{2}{3}\frac{x}{U\big[y_0(\tau)\big]} \tag{14.82}$$

Substituting any value of τ and the corresponding value of $y_0(\tau)$ in the right sides of (14.32) and (14.82) gives values of $y(x, t)$ and t for the specified value of x. Care must be taken, though, to set y equal to its constant initial value for values of t that are less than the time of arrival for the shock. Depth hydrographs for the numerical example are plotted in Fig. 14.14 for different values of x and shock arrival times, t_a.

A kinematic shock first appears at $x = 2.5$ km. The shock path, which is shown as a solid curve in Fig. 14.13, keeps the solution single valued by preventing characteristics from passing through it. Since all characteristics carry a constant value of $y(x, t) = y_0(\tau)$ in Fig. 14.9, and since $y_0(\tau) = $ constant for $\tau \le \tau_I$, the depth y_+ immediately downstream from the shock is always equal to the constant initial depth of one metre. Since characteristics meeting the upper side of the shock path carry the constant depth $y_0(\tau_-)$ for $\tau_- \ge \tau_I$ in Fig. 14.9, we see that the depth y_- immediately upstream from the shock will at first increase as $y_0(\tau_-)$ increases, then attain a maximum of $y_+ = 3$ metres at $\tau_- = 5$ hours and thereafter decrease as $y_0(\tau_-)$ decreases for $\tau_- > 5$ hours. If the inflow depth hydrograph ultimately approaches the same constant depth that existed before $y_0(\tau)$ started to increase, then the depth discontinuity across the shock will approach zero and the shock path will become asymptotic to a characteristic as time becomes infinite, as shown by Eq. (14.48). In this particular problem, Eq. (14.62) shows that a shock will not occur in the solution of the Saint-Venant equations since $8S_0/f = 0.267$, and the right side of (14.62) has a minimum value of 0.829 for $y_+ = 1$ and $y_- = 3$ metres.

A more accurate depth variation across the kinematic shock is plotted in Fig. 14.15 from Eq. (14.57) for $x_s = 13.3$ km. The function $D(\tau)$ in (14.57) was fixed by arbitrarily setting $y = 1.8$ metres at $\xi = 0$. An order of magnitude for the shock thickness is calculated from (14.64) to be $S_0 \delta \sim 3(A + B) = 16.9$ metres, which is very close to the value shown in Fig. 14.15. This gives a value of $\delta \sim 16.9(300)/1000 = 5.07$ km. The value of L computed from (14.19) and (14.24) is 82.3 km, which gives $\delta/L \sim 0.062$. Therefore, the assumption $\delta/L \ll 1$ that was used to obtain (14.57) is justified in this case.

_DSA1 1 4:[CIVL233]SHOCKTRACER.FOR;7

```
C THIS CALCULATES KINEMATIC WAVE SHOCK COORDINATES FOR A SIMPLIFIED INFLOW
C DEPTH HYDROGRAPH. It assumes a constant depth at X=0 for all values of
C time less than the time at which DY/DT changes from zero to a positive
C value. It also assumes a negative curvature for the rising limb of the
C hydrograph. Definitions for the input variables follow:
C      Y(I)=inflow depth (metres) at time TAU(I) (hours) for I=1,N
C      F=constant friction factor
C      S=constant channel slope
C The first value of Y(I) must be the constant initial depth, and the first
C value of TAU(I) must be the time at which DY/DT changes from zero to a
C positive value. Output variables include the shock coordinate, X, at
C time T.
C
       DIMENSION Y(100),TAU(100)
       OPEN(UNIT=1,FILE='INPUT.DAT',STATUS='OLD')
       OPEN(UNIT=2,FILE='OUTPUT.DAT',STATUS='NEW')
C
C Data is entered and written out.
C
       READ(1,*) N,F,S
       WRITE(2 1000) N,F,S
1000   FORMAT(iX,'N=',I3,2X,'F=',F7.4,2X,'S=',F10.7//2X,'I',3X,
      1 'TAU(hours)',2X,'Y(metres)')
       DO 100 I=1,N
       READ(1,*) J,TAU(I),Y(I)
       WRITE(2,3000) I,TAU(I),Y(I)
 100   CONTINUE
C
C The shock initial point is calculated.
C
       DYDT=(Y(2)-Y(l))/(TAU(2)-TAU(l))
       T=TAU(1)+2*Y(1)/DYDT
       X=3*(Y(l)/DYDT)*SQRT(8*9.81*Y(l)*S/F)*3600
       WRITE(2,2000) 1,TAU(l),Y(l),X,T
 2000  FORMAT(2X,'I',3X,'TAU(hours)',2X,'Y(metres)',2x,'X(metres)'
      1 5X,'T(hours)'//lX,I3,4X,F7.2,4X,F6.2,3X,E10.3,2X,E10.3)
       U=SQRT(8*9.81*Y(1)*S/F)*3600
       DXDT1=1.5*U
C
C The remaining shock coordinates
C
       DO 200 I=2,N
       U=SQRT(8*9.81*Y(I)*S/F)*3600
       DXDT2=(Y(I)**1.5-Y(1)**1.5)/(Y(I)-Y(1))
       DXDT2=DXDT2*SQRT(8*9.81*S/F)*3600
       A=DXDT1+DXDT2
       DXDT1=DXDT2
       T=(2*X+3*U*TAU(I)-A*T)/(3*U-A)
       X=1.5*U*(T-TAU(I))
       WRITE(2,3000) I,TAU(I),Y(I),X,T
3000   FORMAT(lX,I3,4X,F7.2,4X,F6.2,3X,E10.3,2X,E10.3)
 200   CONTINUE
       END
```

Figure 14.11 Computer program used to calculate the shock path for a simplified inflow hydrograph.

_DSA11 4:[CIVL233]0UTPUT.DAT;95

```
N= 31   F= 0.1000     S= 0.0033333
I    TAU(hours)  Y(metres)
 1      4.00        1.00
 2      4.05        1.35
 3      4.10        1 70
 4      4.15        1 93
 5      4.20        2.10
 6      4.25        2.27
 7      4.30        2.45
 8      4.35        2 56
 9      4.40        2 70
10      4.50        2.83
11      4.60        2.91
12      4 70        2.96
13      4.80        2.98
14      4.90        3.00
15      5.00        3.00
16      5 20        2 98
17      5 50        2 94
18      6.00        2.83
19      7.00        2.54
20      8.00        2.25
21      9 00        1 96
22     10 00        1 70
23     11.00        1.46
24     11 50        1.36
25     12 00        1.27
26     12 50        1 19
27     13 00        1 13
28     13.50        1.08
29     14.00        1.05
30     14.50        1.02
31     15.00        1.01
I TAU(hours)     Y(metres)    X(metres)    T(hours)

 1      4.00        1.00      0.250E+04    0.429E+01
 2      4.05        1.35      0.339E+04    0.438E+01
 3      4.10        1.70      0.434E+04    0.448E+01
 4      4.15        1.93      0.618E+04    0.466E+01
 5      4.20        2.10      0.815E+04    0.484E+01
 6      4.25        2.27      0.981E+04    0.500E+01
 7      4.30        2.45      0.112E+05    0.512E+01
 8      4.35        2.56      0.133E+05    0.530E+01
 9      4.40        2.70      0.148E+05    0.543E+01
10      4.50        2.83      0.195E+05    0.583E+01
11      4.60        2.91      0.246E+05    0.625E+01
12      4.70        2.96      0.300E+05    0.670E+01
13      4.80        2.98      0.359E+05    0.718E+01
14      4.90        3.00      0.417E+05    0.766E+01
15      5.00        3.00      0.480E+05    0.818E+01
16      5.20        2.98      0.615E+05    0.928E+01
17      5.50        2.94      0.827E+05    0.110E+02
18      6.00        2.83      0.123E+06    0.144E+02
19      7.00        2.54      0.233E+06    0.238E+02
20      8.00        2.25      0.401E+06    0.386E+02
21      9.00        1.96      0.701E+06    0.663E+02
22     10.00        1.70      0.129E+07    0.124E+03
23     11.00        1.46      0.288E+07    0.284E+03
24     11.50        1.36      0.453E+07    0.457E+03
25     12.00        1.27      0.779E+07    0.804E+03
26     12.50        1 19      0.154E+08    0.162E+04
27     13.00        1.13      0.325E+08    0.351E+04
28     13.50        1.08      0.883E+08    0.974E+04
```

Figure 14.12 Output from the computer program shown in Fig. 14.11 for the numerical example.
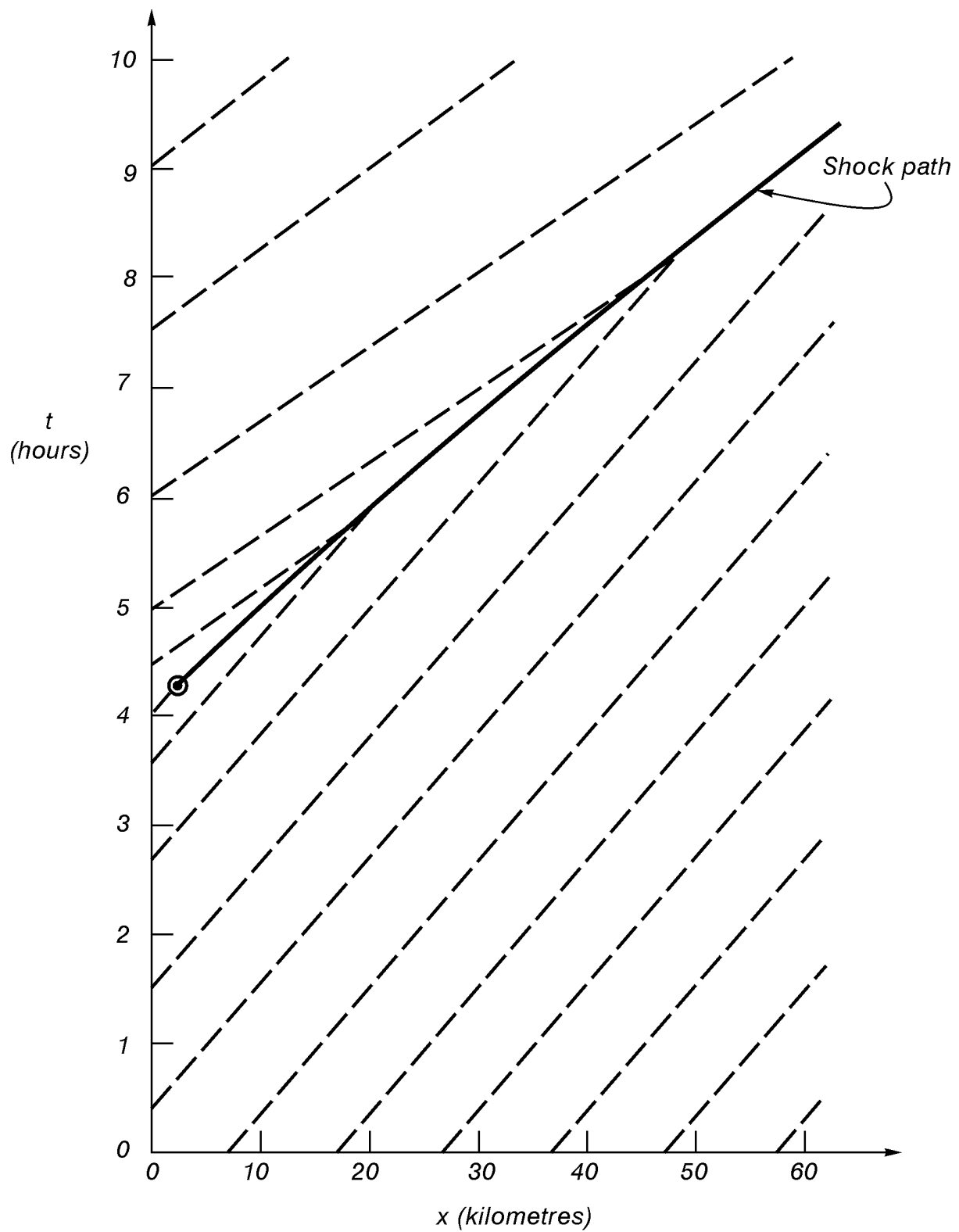
Figure 14.13 The shock path and characteristics for the numerical example.
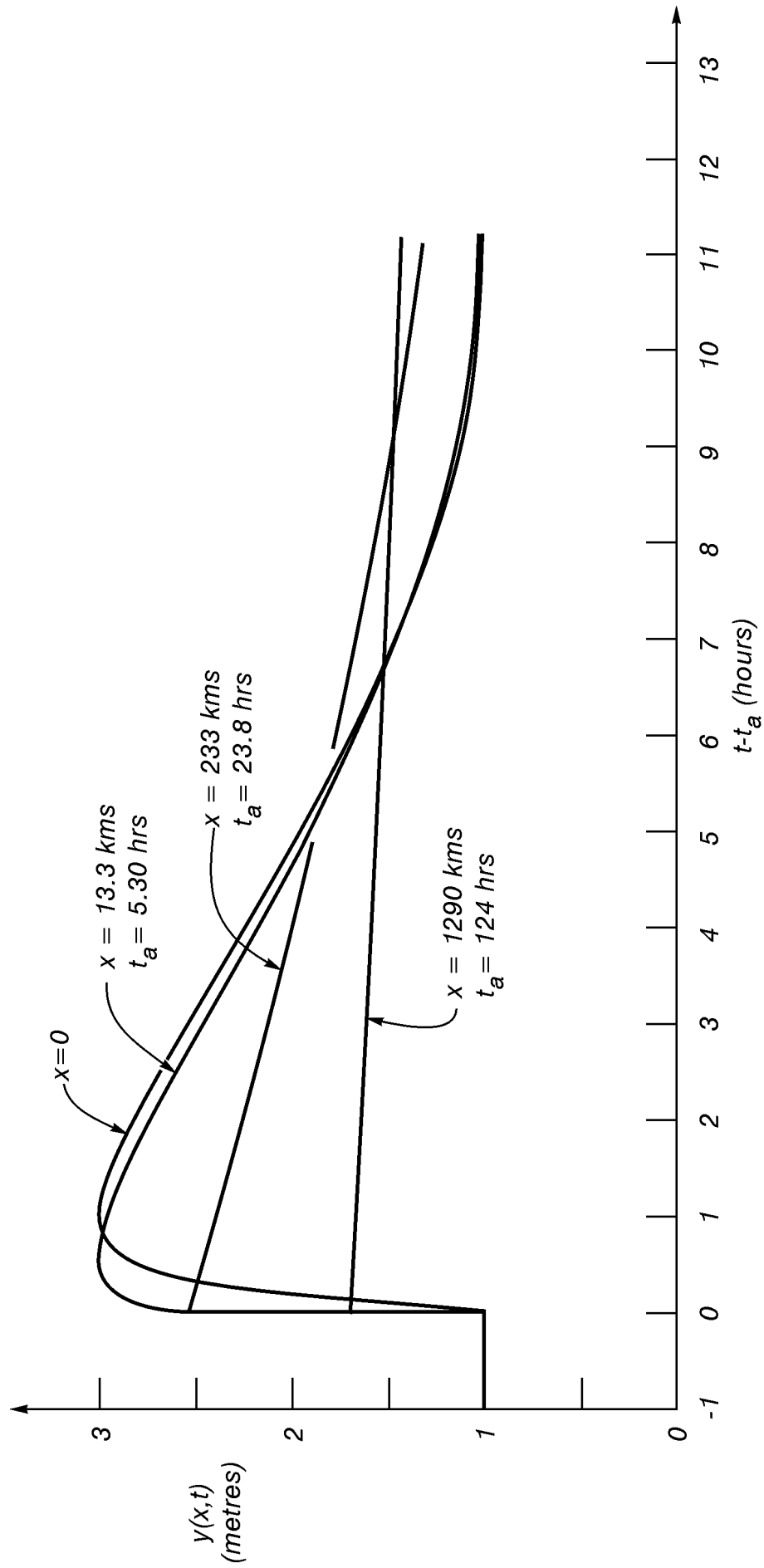
Figure 14.14 Depth hydrographs for different values of x and shock arrival times, t_a.
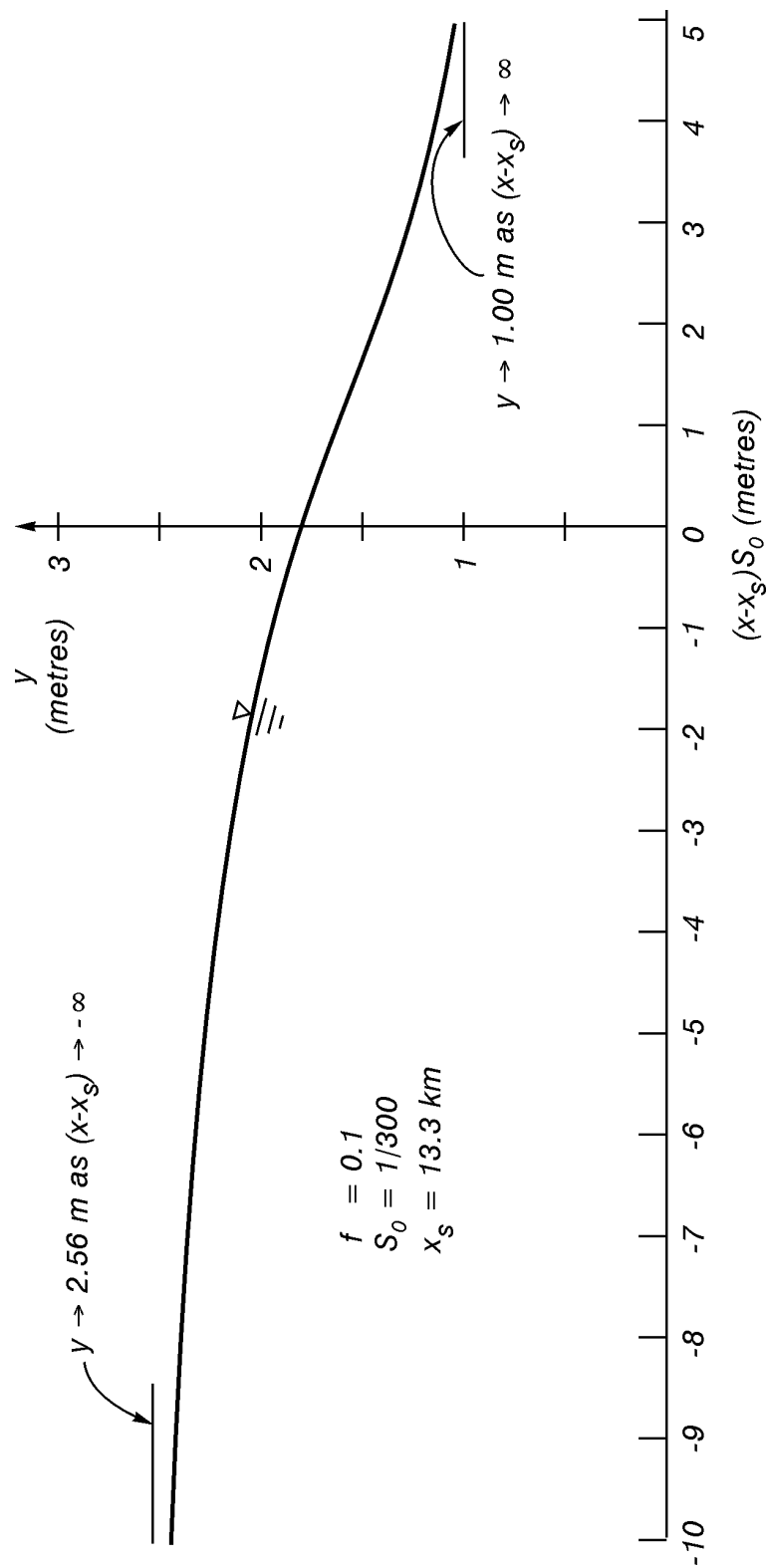
Figure 14.15 Depth variation across the shock at $x_s = 13.3$ km.

The kinematic wave approximation originated in a well known paper by Lighthill and Whitham (1955). Much of the material in this chapter, apart from scaling arguments and the discussion of backwater effects, can be found in a slightly different form in the book by Whitham (1974).

References

Hart, W.L. (1957) *Analytic geometry and calculus*, D.C. Heath and Co., Boston, pp. 576-579.

Lighthill, M.H. and G.B. Whitham (1955) On kinematic waves: I. Flood movement in long rivers; II. Theory of traffic flow on long crowded roads, *Proc. Roy. Soc. A*, Vol. 229, pp. 281-345.

Whitham, G.B. (1974) *Linear and nonlinear waves*, John Wiley and Sons, New York, pp. 80-91.

Wylie, E.G. and V.L. Streeter (1982) *Fluid transients*, FEB Press, Ann Arbor, Michigan, p. 294.

Appendix I

Physical Properties of Water and Air

WATER						
Temp. °C	Density kg/m^3 ρ =	Dynamic Viscosity N - s/m^2 $10^3\mu$ =	Kinematic Viscosity m^2/s $10^6\nu$ =	Surface Tension N/m $10^2\sigma$ =	Vapour Pressure (Absolute) N/m^2 $10^{-3}p$ =	Bulk Modulus of Elasticity N/m^2 $10^{-9}E$ =
0	1000	1.79	1.79	7.62	0.6	2.04
5	1000	1.52	1.52	7.54	0.9	2.06
10	1000	1.31	1.31	7.48	1.2	2.11
15	999	1.14	1.14	7.41	1.7	2.14
20	998	1.01	1.01	7.36	2.5	2.20
25	997	0.894	0.897	7.26	3.2	2.22
30	996	0.801	0.804	7.18	4.3	2.23
35	994	0.723	0.727	7.10	5.7	2.24
40	992	0.656	0.661	7.01	7.5	2.27
45	990	0.599	0.605	6.92	9.6	2.29
50	988	0.549	0.556	6.82	12.4	2.30
55	986	0.506	0.513	6.74	15.8	2.31
60	983	0.469	0.477	6.68	19.9	2.28
65	981	0.436	0.444	6.58	25.1	2.26
70	978	0.406	0.415	6.50	31.4	2.25
75	975	0.380	0.390	6.40	38.8	2.23
80	972	0.357	0.367	6.30	47.7	2.21
85	969	0.336	0.347	6.20	58.1	2.17
90	965	0.317	0.328	6.12	70.4	2.16
95	962	0.299	0.311	6.02	84.5	2.11
100	958	0.284	0.296	5.94	101.3	2.07
SEA WATER						
20	1024	1.07	1.04	7.3	2.34	2.30

Temp. °C	Density kg/m^3 ρ =	Dynamic Viscosity N - s/m^2 $10^3\mu$ =	Kinematic Viscosity m^2/s $10^6\nu$ =
-10	1.34	0.0164	12.3
0	1.29	0.0171	13.3
10	1.25	0.0176	14.2
20	1.20	0.0181	15.1
30	1.17	0.0185	15.9
40	1.13	0.0190	16.9
50	1.09	0.0195	17.9
60	1.07	0.0199	18.6
70	1.04	0.0204	19.7
80	1.01	0.0208	20.8
90	0.974	0.0213	21.8
100	0.946	0.0217	22.9

AIR
(Standard Atmospheric Pressure at Sea Level)

Appendix II

Properties of Areas
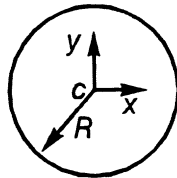
Circle

$$A = \pi R^2$$

$$I_x = I_y = \frac{1}{4} A R^2$$

$$I_{xy} = 0$$
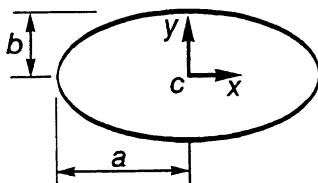
Ellipse

$$A = \pi a b$$

$$I_x = \frac{1}{4} A b^2 \quad , \quad I_y = \frac{1}{4} A a^2$$

$$I_{xy} = 0$$
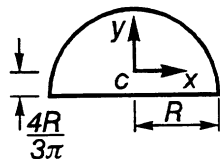
Semi-circle

$$A = \frac{1}{2} \pi R^2$$

$$I_x = \left(\frac{1}{4} - \frac{16}{9\pi^2} \right) A R^2 \quad , \quad I_y = \frac{1}{4} A R^2$$

$$I_{xy} = 0$$
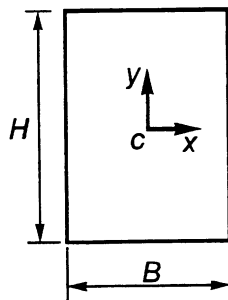
Rectangle

$$A = BH$$

$$I_x = \frac{1}{12} A H^2 \quad , \quad I_y = \frac{1}{12} A B^2$$

$$I_{xy} = 0$$
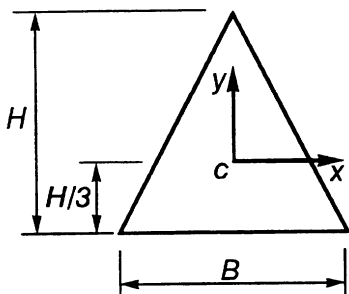
Isosceles Triangle

$$A = \frac{1}{2} BH$$

$$I_x = \frac{1}{18} A H^2 \quad , \quad I_y = \frac{1}{24} A B^2$$

$$I_{xy} = 0$$

INDEX